The measurement of reinstatement backfill properties

M.G Winter

The Measurement of Reinstatement Backfill Properties

MG Winter *BSc (Hons), FGS*

A Thesis submitted for the Degree of
Doctor of Philosophy
in the Faculty of Science, University of Durham

Work Funded by a British Gas plc
Engineering Research Award

Applied Mechanics Group
School of Engineering and Applied Science
Faculty of Science
University of Durham

September 1989

Abstract

The Horne Committee Report, published in 1985, identified the need for the reinstatement of service trench backfill to be performed to a higher and more reliable standard. This end was perceived as desirable, not only to improve road quality and safety, but also to increase the protection afforded to utility apparatus, thereby reducing the number of excavations required for its repair and replacement.

The replacement of existing method specifications with a performance specification, based on the testing of an appropriate property of the reinstated material, is one possible means of improving the quality of reinstatement works. The Clegg meter is finding increasing usage for the purpose of compaction measurement. This device is simple to use and measures the decceleration response of a mass in collision with the ground surface. The decelartaion response is characterised by the Impact Value. The sampled volume is, however, very small in relation to the volume of material compacted and, for full evaluation, each compacted layer must be individually tested prior to the placing of the subsequent layer.

The ideal test would be non-intrusive and operable from the final surface of the granular backfill; wave transmission velocity measurements are thus a potential technique. The propagation of sinusoidally excited Rayleigh-type surface waves is identified as the most promising method of measurement for reinstatement backfill quality. Experimental measurements of particle displacement at depth lend credence to the classical assumption that the depth of propagation of Rayleigh-type surface waves is equal to one-half the wavelength ($z = \lambda/2$).

Included in this thesis is a review of the salient aspects of reinstatement works and a presentation of the necessary theory of wave propagation. The experimental results presented relate to tests on two sand materials compacted using different levels of compactive effort in an above-ground laboratory based trench and also to tests conducted on a crushed limestone aggregate under field conditions. Results from a short programme of field-based case studies are also presented.

In addition to the surface wave velocity and Impact Value results, values for dry density and *CBR* are also presented. The data generally show a good correlation with compactive effort, whether defined simply as the number of passes/layer (N_p) or by a new parameter, the ratio of N_p to the mean layer thickness ($N_p/\overline{h}$). Sensitivity analyses indicate that the Impact Value is a more sensitive measure of the degree of compaction than are either the surface wave velocity or the dry density. Conversion of the surface wave velocity results to shear modulus values, using measured density values, gives a sensitivity to compactive effort that is broadly comparable to that of the Impact Value.

A novel technique for the analysis of Rayleigh-type surface wave attenuation data is presented. This allows the calculation of the material attenuation coefficient while obviating the need for potentially erroneous estimates as to the state of the attenuation curve, close to the source of vibration, to be made.

Acknowledgements

I would like to express my grateful thanks to my supervisors, Professor PB Attewell and Dr AR Selby at the University of Durham, for their constant guidance and support which has been so freely given during the last three years. Thanks are also due to Dr DJ Gunton of British Gas plc, Engineering Research Station (BG, ERS), the Research Visitor assigned to this project.

The technical support at the University of Durham, School of Engineering and Applied Science has at all times been excellent. I would in particular like to thank Messrs CB McEleavey, S Richardson, AG Swann and BP Scurr of the Applied Mechanics Laboratories. Also Mr TB Brown and both the mechanical and electrical workshop technicians whose manufacturing and repair skills have been greatly appreciated. Thanks are also due to Mr R Hardy of the University of Durham Department of Geological Sciences who operated the XRD and XRF equipment and greatly assisted with the interpretation of the Permian Sand mineralogy results.

The field work activities would have been more difficult without the assistance of Messrs BJ Smith, AJ Robinson, I Bell and D Boyes (BG, ERS) in locating possible field sites and organising plant and material deliveries. The bulk of the field work was carried out at the British Gas plc Northern, Blaydon Depot. Thanks are due to Mr D Robson for allowing me the use of the site and to Dr AH Kelly for permitting the use of on site laboratory space and facilities. Messrs BJ Smith (BG, ERS), D Harrison (British Gas plc Northern, Team Valley Depot), M Jackson and R Dickson (British Gas plc Northern, Stanley Depot) all assisted in locating a suitable site for the final case study at Acton Dean, Stanley, County Durham. Thanks are also due to Mrs S Row (BG, ERS) for allowing the use of the apparatus for determining the compactability of graded aggregates to BS 5835: Part 1 (1980).

Funding for this project was by British Gas plc as an Engineering Research Award sourced from the Engineering Research Station at Killingworth near Newcastle-Upon-Tyne and administered by Mr D Reay of British Gas plc Research and Development Head Quarters in London. I am most grateful for this generous funding.

I would like to make a special acknowledgement to the friends who have made my three years in Durham such a happy time, in particular to Becky, to whom I am also grateful for proof reading this thesis.

Statement of Copyright

Declaration

No material from this thesis has previously been submitted for a degree at this or any other university.

Table of Contents

Title Page i

Abstract ii

Acknowledgements iii

Statement of Copyright iv

Declaration iv

Table of Contents v

List of Tables xii

List of Figures xix

List of Plates xxviii

Notation xxix

1. INTRODUCTION AND SCOPE OF WORK 1

1.1 Introduction 1

1.2 Responsibility for reinstatement works 2

1.3 Economics and scale of reinstatement works 5

1.4 Summary and scope of work 7

2. COMPACTION THEORY, COMPACTION PLANT AND COMPACTION MEASUREMENT 15

2.1 Introduction 15

2.2 Compaction theory and laboratory measurement 15

2.2.1 Compaction theory 15

2.2.2 Laboratory determination of the dry density-moisture content relationship 17

2.3 Compaction plant 19

2.4 Methods of compaction measurement 20

2.4.1 The Clegg Meter 25

2.5 Summary 31

3. WAVE MECHANICS AND MEASUREMENT TECHNIQUES **38**

3.1 Introduction 38

3.2 Types of seismic wave 38

3.2.1 Body waves 39

3.2.2 Surface waves 40

3.2.4 Selected experimental wave transmission technique 41

3.3 Measurement techniques for Rayleigh-type surface waves 42

3.4 The mechanics of Rayleigh waves 45

3.4.1 The fundamental wave equation 46

3.4.2 Relationships between elastic wave velocities 47

3.4.3 Displacements due to Rayleigh waves and the effective depth of propagation 49

3.4.4 Attenuation of Rayleigh waves 52

3.4.5 Summary 52

3.5 Rayleigh-type surface wave velocity data 53

3.6 Summary 57

4. MATERIAL CLASSIFICATION AND COMPACTION TESTS **71**

4.1 Introduction and source of materials 71

4.2 Particle size distribution 72

4.3 Specific gravity and water absorption value 72

4.4 Dry density-moisture content relationships 74

4.4.1 Permian Sand (BS 1377, 1975: Test 12) 76

4.4.2 Sharp Sand (BS 1377, 1975: Test 12) 77

4.4.3 Wet-mix macadam (BS 1377, 1975: Test 12) 77

4.4.4 Wet-mix macadam (BS 5835: Part 1, 1980) 81

4.4.5 British Standard compaction tests: A comparison 85

4.4.6 The influence of compactive effort on the dry density-moisture content relationship 88

4.5 10% fines value: Wet-mix macadam 93

4.6 Flakiness index: Wet-mix macadam 95

4.7 Mineralogy: Permian Sand 96

4.8 Discussion and summary 97

5. EXPERIMENTAL PROCEDURE AND DATA ANALYSIS 115

5.1 Introduction 115

5.2 The laboratory based trench 118

5.3 Experimental procedure for the laboratory based trench 119

5.3.1 Filling the laboratory based trench 119

5.3.2 Surface wave velocity measurements 121

5.3.3 Surface wave attenuation measurements 123

5.3.4 Particle displacement at depth 124

5.3.5 CBR measurements 124

5.3.6 Emptying the laboratory based trench 124

5.4 The field trenches 125

5.5 Experimental procedure for the field trenches 125

5.5.1 Excavating the field trenches 125

5.5.2 Filling the field trenches 126

5.5.3 Surface wave velocity measurements 126

5.5.4 Surface wave attenuation measurements 126

5.6 Data analysis 126

5.6.1 Density, moisture content, Impact Value and CBR measurements 127

5.6.2 Surface wave velocity measurements 128

5.6.3 Surface wave attenuation measurements 129

5.6.4 Particle displacement at depth 130

5.7 Summary 131

6. EXPERIMENTAL RESULTS 144

6.1 Introduction and test programme 144

6.1.1 Introduction 144

6.1.2 Test programme 144

6.1.3 Determination of the wavelength of surface waves 146

6.2 Measurements on Permian Sand 146
6.2.1 Density, moisture content, Impact Value and CBR results 146
6.2.2 Surface wave velocity results 147
6.2.3 Derived shear modulus results 147
6.2.4 Surface wave attenuation results 147
6.2.5 Particle displacement at depth results 147
6.2.6 Summary 148
6.3 Measurements on Sharp Sand 148
6.3.1 Density, moisture content, Impact Value and CBR results 148
6.3.2 Surface wave velocity results 149
6.3.3 Derived shear modulus results 149
6.3.4 Surface wave attenuation results 149
6.3.5 Summary 149
6.4 Measurements on Wet-mix macadam 150
6.4.1 Density, moisture content and Impact Value results 150
6.4.2 Surface wave velocity results 150
6.4.3 Derived shear modulus results 150
6.4.4 Surface wave attenuation results 151
6.4.5 Summary 151
6.5 Measurements on Wet-mix macadam and Sharp Sand 151
6.5.1 Density, moisture content and Impact Value results 151
6.5.2 Surface wave velocity results 152
6.5.3 Derived shear modulus results 152
6.5.4 Surface wave attenuation rsults 152
6.5.5 Summary 153
6.6 Case studies 153
6.6.1 SEAS service trench 153
6.6.2 Blaydon demonstration trench 154
6.6.3 Salters Lane: Back-to-back tests—well/poorly compacted 154
6.6.4 Field trial: Acton Dean, Stanley, County Durham 155
6.6.5 Summary 156
6.7 Summary 157

7. INTERPRETATION AND DISCUSSION OF RESULTS 238

7.1 Introduction 238

7.2 Measurements on Permian Sand 241

7.2.1 Density, moisture content, Impact Value and CBR results 241

7.2.2 Surface wave velocity results 246

7.2.3 Derived shear modulus results 250

7.2.4 Surface wave attenuation results 252

7.2.5 Particle displacement at depth results 253

7.2.6 Summary 255

7.3 Measurements on Sharp Sand 257

7.3.1 Density, moisture content, Impact Value and CBR results 257

7.3.2 Surface wave velocity results 260

7.3.3 Derived shear modulus results 263

7.3.4 Surface wave attenuation results 264

7.3.5 Summary 265

7.4 Measurements on Wet-mix macadam 266

7.4.1 Density, moisture content and Impact Value results 267

7.4.2 Surface wave velocity results 270

7.4.3 Derived shear modulus results 272

7.4.4 Surface wave attenuation results 274

7.4.5 Summary 275

7.5 Measurements on Wet-mix macadam and Sharp Sand 277

7.5.1 Density, moisture content and Impact Value results 278

7.5.2 Surface wave velocity results 279

7.5.3 Derived shear modulus results 281

7.5.4 Surface wave attenuation results 281

7.5.5 Summary 281

7.6 Case studies 282

7.6.1 SEAS service trench 282

7.6.2 Blaydon demonstration trench 283

7.6.3 Salters Lane: Back-to-back tests—well/poorly compacted 284

7.6.4 Field trial: Acton Dean, Stanley, County Durham 285

7.6.5 Summary 286

7.7 Comparison of laboratory and field derived dry density and moisture content data with relationships derived from British Standard tests 287
7.8 Additional comments on surface wave velocity measurements 290
7.8.1 Shear strains due to surface waves 291
7.9 Summary 292

8. CONCLUSIONS AND RECOMMENDATIONS FOR FURTHER WORK 356
8.1 Conclusions 356
8.2 Recommendations for further work 361

References 364

A1. INTEGRATION TO FIND THE EFFECTIVE DEPTH OF PROPAGATION FOR RAYLEIGH-TYPE SURFACE WAVES A1-1
A1.1 Introduction A1-2
A1.2 Centroid of the area under the W function A1-3

A2. SOIL CLASSIFICATION AND COMPACTION TESTS: DETAILED DATA A2-1
A2.1 Particle size distribution data A2-2
A2.2 Dry density-moisture content data A2-3

A3. MATERIAL SPECIFICATIONS A3-1
A3.1 Sharp Sand: BS 882 (1983) A3-2
A3.2 Wet-mix macadam: Department of Transport (1986) A3-2

A4. MOISTURE CONTENT DETERMINATION AND CONTROL A4-1
A4.1 Moisture content determination by the microwave method A4-2
A4.2 Moisture content control A4-3

A5. THE ELECTRICALLY POWERED WACKER BS45Y VIBRATORY RAMMER A5-1

A6. DENSITY, MOISTURE CONTENT AND IMPACT VALUE MEASUREMENTS: DETAILED DATA **A6-1**

A6.1 Permian Sand: Tests TPS1 to TPS5 A6-2

A6.2 Sharp Sand: Tests TSS1 to TSS5 A6-12

A6.3 Wet-mix macadam: Tests WMM1 to WMM6 and WMM10 A6-22

A6.4 Wet-mix macadam and Sharp Sand: Tests WMM7 to WMM9 A6-29

A6.5 Case study data A6-32

A7. SURFACE WAVE VELOCITY MEASUREMENTS: DETAILED DATA **A7-1**

A7.1 Permian Sand: Tests TPS1 to TPS5 A7-2

A7.2 Sharp Sand: Tests TSS1 to TSS5 A7-10

A7.3 Wet-mix macadam: Tests WMM1 to WMM6 and WMM10 A7-15

A7.4 Wet-mix macadam and Sharp Sand: Tests WMM7 to WMM9 A7-22

A7.5 Case study data A7-25

A8. SURFACE WAVE ATTENUATION MEASUREMENTS: DETAILED DATA **A8-1**

A8.1 Permian Sand: Tests TPS3 to TPS5 A8-2

A8.2 Sharp Sand: Tests TSS1 to TSS5 A8-5

A8.3 Wet-mix macadam: Tests WMM1 to WMM6 and WMM10 A8-10

A8.4 Wet-mix macadam and Sharp Sand: Tests WMM7 to WMM9 A8-17

A9. PARTICLE DISPLACEMENT AT DEPTH MEASUREMENTS: DETAILED DATA FOR PERMIAN SAND TESTS TPS2 AND TPS3 **A9-1**

List of Tables

Table 1.1 - Guide to types of flexible road construction for reinstatement trenches in carriageways (after Department of Transport, 1974).

Table 1.2 - Types of roads and estimated mileages in Great Britain (after Department of Transport, 1974).

Table 1.3 - Utilities' current annual workload of excavations for the financial year 1982/83 (after Horne Committee, 1985: National Joint Utilities Group).

Table 1.4 - British Gas workload 1974/75 to 1988/89 (after Horne Committee, 1985: National Joint Utilities Group).

Table 3.1 - Relative energies of the seismic waves generated by a vertically oscillating circular footing at the surface of an elastic half-space with Poisson's ratio, $\nu = 0.25$ (after Miller and Pursey, 1955).

Table 3.2 - Elastic wave velocity ratios.

Table 3.3 - Attenuation factors with depth for the vertical and horizontal components of displacement of Rayleigh waves.

Table 4.1 - Analysis of particle size distributions for Permian Sand, Sharp Sand and Wet-mix-macadam and description to BS 5930 (1981).

Table 4.2 - Specific gravities (on an oven-dried basis) for Permian Sand, Sharp Sand and Wet-mix macadam; water absorption values for the Wet-mix macadam are also given.

Table 4.3 - Summary compaction data for Permian Sand, Sharp Sand and Wet-mix macadam.

Table 4.4 - Compactive effort data.

Table 4.5 - Flakiness index data.

Table 4.5 - Mineralogy of the Permian Sand.

Table 5.1 - Lissajous Figures.

Table 6.1 - Test programme for Permian Sand in the laboratory based trench ($w \approx w_{opt}$ for all tests).

Table 6.2 - Test programme for Sharp Sand in the laboratory based trench ($w \approx w_{opt}$ for all tests).

Table 6.3 - Test programme for Wet-mix macadam in the field.

Table 6.4 - Test programme for Wet-mix macadam and Sharp Sand in the field ($w \approx w_{opt}$ for all tests).

Table 6.5 - Transducer separation (d), phase angle (ϕ) data for Test TPS2A (f = 375 Hz; r = 0.979). The corresponding Lissajous Figures are also shown.

Table 6.6 - Transducer separation (d), phase angle (ϕ) data for Test WMM9 (f = 450 Hz; r = 1.000). The corresponding Lissajous Figures are also shown.

Table 6.7 - Summary compaction data for tests on Permian Sand (Tests TPS1 to TPS5).

Table 6.8 - Summary excavation data for tests on Permian Sand (Tests TPS1 to TPS5).

Table 6.9 - Summary surface wave velocity-depth profile data for tests on Permian Sand (Tests TPS1 to TPS5).

Table 6.10 - Summary shear modulus-depth data for tests on Permian Sand (Tests TPS1 to TPS5).

Table 6.11 - Summary surface wave attenuation data for tests on Permian Sand (Tests TPS1 to TPS5).

Table 6.12 - Summary compaction data for tests on Sharp Sand (Tests TSS1 to TSS5).

Table 6.13 - Summary excavation data for tests on Sharp Sand (Tests TSS1 to TSS5).

Table 6.14 - Summary surface wave velocity-depth profile data for tests on Sharp Sand (Tests TSS1 to TSS5).

Table 6.15 - Summary shear modulus-depth data for tests on Sharp Sand (Tests TSS1 to TSS5).

Table 6.16 - Summary surface wave attenuation data for tests on Sharp Sand (Tests TSS1 to TSS5).

Table 6.17 - Summary compaction data for tests on Wet-mix macadam (Tests WMM1 to WMM6 and WMM10).

Table 6.18 - Summary surface wave velocity-depth profile data for tests on Wet-mix macadam (Tests WMM1 to WMM6 and WMM10).

Table 6.19 - Summary shear modulus-depth data for tests on Wet-mix macadam (Tests WMM1 to WMM6 and WMM10).

Table 6.20 - Summary surface wave attenuation data for tests on Wet-mix macadam (Tests WMM1 to WMM6 and WMM10).

Table 6.21 - Summary subgrade data for Tests WMM1 to WMM10.

Table 6.22 - Summary compaction data for tests on Wet-mix macadam and Sharp Sand (Tests WMM7 to WMM9).

Table 6.23 - Summary surface wave velocity-depth profile data for tests on Wet-mix macadam and Sharp Sand (Tests WMM7 to WMM9).

Table 6.24 - Summary shear modulus-depth data for tests on Wet-mix macadam and Sharp Sand (Tests WMM7 to WMM9).

Table 6.25 - Summary surface wave attenuation data for tests on Wet-mix macadam and Sharp Sand (Tests WMM7 to WMM9).

Table 7.1 - Numerical sensitivities (S) and 'correlation sensitivities' (rS) of the parameters ρ_d, IV, CBR, $v_{Rz_{max}/2}$ and $G_{z_{max}/2}$ to compactive effort.

Table 7.2 - Ranges for maximum shear strains induced by surface wave propagation for tests on Permian Sand, Sharp Sand and Wet-mix macadam.

Table A1.1 - Values of the centroid, $\overline{z/\lambda}$, for corresponding values of Poisson's ratio.

Table A2.1 - Particle size distributions for Permian Sand, Sharp Sand and Wet-mix macadam.

Table A2.2 - Dry density-moisture content data for Permian Sand; BS 1377 (1975): Test 12.

Table A2.3 - Dry density-moisture content data for Sharp Sand; BS 1377 (1975): Test 12.

Table A2.4 - Dry density-moisture content data for Wet-mix macadam; BS 1377 (1975): Test 12. Data prior to the application of the correction for stone content.

Table A2.5 - Dry density-moisture content data for Wet-mix macadam; BS 1377 (1975): Test 12. Data after the application of the correction for stone content.

Table A2.6 - Dry density-moisture content data for Wet-mix macadam; BS 5835: Part 1 (1980).

Table A3.1 - Concrete Sand range of grading (from BS 882, 1983: Table 5).

Table A3.2 - Wet-mix macadam range of grading. Also shown are the gradings for Types 1 and 2 granular sub-base materials (from Department of Transport, 1986: Tables 8/2, 8/3 and 8/4).

Table A5.1 - Specifications for the Wacker BS45Y electrically powered vibratory rammer (Source: Wacker Great Britain Ltd).

Table A6.1 - Compaction data for Test TPS1 (6–30/3/87).

Table A6.2 - Excavation data for Test TPS1 (9–20/6/87).

Table A6.3 - Compaction data for Test TPS2 (2–23/7/87).

Table A6.4 - Excavation data for Test TPS2 (26/8–3/9/87).

Table A6.5 - Compaction data for Test TPS3 (22/9–5/10/87).

Table A6.6 - Excavation data for Test TPS3 (6–12/11/87).

Table A6.7 - Compaction data for Test TPS4 (17–18/11/87).

Table A6.8 - Excavation data for Test TPS4 (10–11/12/87).

Table A6.9 - Compaction data for Test TPS5 (4–16/1/88).

Table A6.10 - Excavation data for Test TPS5 (25–27/1/88).

Table A6.11 - Compaction data for Test TSS1 (8–17/2/88).

Table A6.12 - Excavation data for Test TSS5 (22/2/88).

Table A6.13 - Compaction data for Test TSS2 (25/2–15/3/88).

Table A6.14 - Excavation data for Test TSS5 (24/3/88).

Table A6.15 - Compaction data for Test TSS3 (13–21/4/88).

Table A6.16 - Excavation data for Test TSS5 (29/4–4/5/88).

Table A6.17 - Compaction data for Test TSS4 (9/5/88).

Table A6.18 - Excavation data for Test TSS5 (20/5/88).

Table A6.19 - Compaction data for Test TSS5 (24/5–3/6/88).

Table A6.20 - Excavation data for Test TSS5 (8–9/6/88).

Table A6.21 - Compaction data for Test WMM1 (13–15/9/88).

Table A6.22 - Compaction data for Test WMM2 (29–30/9/88).

Table A6.23 - Compaction data for Test WMM3 (7–14/10/88).

Table A6.24 - Compaction data for Test WMM4 (28–31/10/88).

Table A6.25 - Compaction data for Test WMM5 (8–10/11/88).

Table A6.26 - Compaction data for Test WMM6 (25–28/11/88).

Table A6.27 - Compaction data for Test WMM10 (18/1/89).

Table A6.28 - Compaction data for Test WMM7 (7–8/12/88).

Table A6.29 - Compaction data for Test WMM8 (14/12/88).

Table A6.30 - Compaction data for Test WMM9 (21/12/88).

Table A6.31 - Impact Value data for the Blaydon demonstration trench.

Table A6.32 - Compaction data for tests at Salters Lane (Tests SL1 and SL2).

Table A6.33 - Additional (detailed) Impact Value data Test SL1.

Table A6.34 - Compaction data for the case study at Acton Dean, Stanley, County Durham.

Table A7.1 - Surface wave velocity data for Test TPS1A (test completed 30/3/87).

Table A7.2 - Surface wave velocity data for Test TPS1B (test completed 29/4/87).

Table A7.3 - Surface wave velocity data for Test TPS1C (test completed 21/5/87).

Table A7.4 - Surface wave velocity data for Test TPS1D (test completed 17/6/87).

Table A7.5 - Surface wave velocity data for Test TPS2A (test completed 10/7/87).

Table A7.6 - Surface wave velocity data for Test TPS2B (test completed 25/7/87).

Table A7.7 - Surface wave velocity data for Test TPS2C (test completed 1/9/87).

Table A7.8 - Surface wave velocity data for Test TPS3A (test completed 5/10/87).

Table A7.9 - Surface wave velocity data for Test TPS3B (test completed 15/10/87).

Table A7.10 - Surface wave velocity data for Test TPS4 (test completed 8/12/87).

Table A7.11 - Surface wave velocity data for Test TPS5A (test completed 9/1/88).

Table A7.12 - Surface wave velocity data for Test TPS5B (test completed 20/1/88).

Table A7.13 - Surface wave velocity data for Test TSS1A (test completed 12/2/88).

Table A7.14 - Surface wave velocity data for Test TSS1B (test completed 21/2/88).

Table A7.15 - Surface wave velocity data for Test TSS2A (test completed 14/3/88).

Table A7.16 - Surface wave velocity data for Test TSS2B (test completed 23/3/88).

Table A7.17 - Surface wave velocity data for Test TSS3A (test completed 19/4/88).

Table A7.18 - Surface wave velocity data for Test TSS3B (test completed 24/4/88).

Table A7.19 - Surface wave velocity data for Test TSS4 (test completed 16/5/88).

Table A7.20 - Surface wave velocity data for Test TSS5A (test completed 27/5/88).

Table A7.21 - Surface wave velocity data for Test TSS5B (test completed 7/6/88).

Table A7.22 - Surface wave velocity data for Test WMM1 (test completed 16/9/88).

Table A7.23 - Surface wave velocity data for Test WMM2 (test completed 4/10/88).

Table A7.24 - Surface wave velocity data for Test WMM3 (test completed 17/10/88).

Table A7.25 - Surface wave velocity data for Test WMM4 (test completed 2/11/88).

Table A7.26 - Surface wave velocity data for Test WMM5 (test completed 11/11/88).

Table A7.27 - Surface wave velocity data for Test WMM6 (test completed 6/12/88).

Table A7.28 - Surface wave velocity data for Test WMM10 (test completed 20/1/89).

Table A7.29 - Surface wave velocity data for Test WMM7 (test completed 12/12/88).

Table A7.30 - Surface wave velocity data for Test WMM8 (test completed 15/12/88).

Table A7.31 - Surface wave velocity data for Test WMM9 (test completed 21/12/88).

Table A7.32 - Surface wave velocity data for the SEAS service trench: Test NSSEAS (test completed 30/8/87).

Table A7.33 - Surface wave velocity data for Test SL1 (test completed 13/6/89).

Table A7.34 - Surface wave velocity data for Test SL2 (test completed 14/6/89).

Table A7.35 - Surface wave velocity data for the case study at Acton Dean, Stanley, County Durham (test completed 8/8/89).

Table A8.1 - Attenuation data for Permian Sand (Test TPS3) at frequencies of 300 and 500 Hz.

Table A8.2 - Attenuation data for Permian Sand (Test TPS4) at frequencies of 300 and 500 Hz.

Table A8.3 - Attenuation data for Permian Sand (Test TPS5) at frequencies of 300 and 500 Hz.

Table A8.4 - Attenuation data for Sharp Sand (Test TSS1) at frequencies of 300 and 500 Hz.

Table A8.5 - Attenuation data for Sharp Sand (Test TSS2) at frequencies of 300 and 500 Hz.

Table A8.6 - Attenuation data for Sharp Sand (Test TSS3) at frequencies of 300 and 500 Hz.

Table A8.7 - Attenuation data for Sharp Sand (Test TSS4) at frequencies of 300 and 500 Hz.

Table A8.8 - Attenuation data for Sharp Sand (Test TSS5) at frequencies of 300 and 500 Hz.

Table A8.9 - Attenuation data for Wet-mix macadam (Test WMM1) at frequencies of 300 and 500 Hz.

Table A8.10 - Attenuation data for Wet-mix macadam (Test WMM2) at frequencies of 300 and 500 Hz.

Table A8.11 - Attenuation data for Wet-mix macadam (Test WMM3) at frequencies of 300 and 500 Hz.

Table A8.12 - Attenuation data for Wet-mix macadam (Test WMM4) at frequencies of 300 and 500 Hz.

Table A8.13 - Attenuation data for Wet-mix macadam (Test WMM5) at frequencies of 300 and 500 Hz.

Table A8.14 - Attenuation data for Wet-mix macadam (Test WMM6) at frequencies of 300 and 500 Hz.

Table A8.15 - Attenuation data for Wet-mix macadam (Test WMM10) at frequencies of 300 and 500 Hz.

Table A8.16 - Attenuation data for Wet-mix macadam (Test WMM7) at frequencies of 300 and 500 Hz.

Table A8.17 - Attenuation data for Wet-mix macadam (Test WMM8) at frequencies of 300 and 500 Hz.

Table A8.18 - Attenuation data for Wet-mix macadam (Test WMM9) at frequencies of 300 and 500 Hz.

Table A9.1 - Particle displacement at depth data for Test TPS2B at 450 Hz (λ = 0.388 m).

Table A9.2 - Particle displacement at depth data for Test TPS3B at 300 Hz (λ = 0.280 m).

Table A9.3 - Particle displacement at depth data for Test TPS3B at 150 Hz (λ = 0.810 m).

List of Figures

Figure 1.1 - Diagrammatic cross-section of reinstatement layers in a flexible road pavement (after Department of Transport, 1974).

Figure 1.2 - The British Gas perception of reinstatement works in the light of possible future legislation based on the Horne Report recommendations; (a) for small works and (b) for larger works (after Rhodes *et al* 1987).

Figure 2.1 - Idealised dry density-moisture content relationship. Compaction curves for three levels of compactive effort are shown with the lines of constant air voids for $A = 0,\ 5$ and 10%.

Figure 2.2 - Post-compaction dry densities, achieved by a variety of hand-held compactors on a sand material, regardless of the time and effort involved (after Reid, 1983).

Figure 2.3 - Dry density-moisture content envelope achieved by combining data achieved using a range of proprietry vibratory rammers; 300 mm layers, 10 passes/ layer; sand material (after Reid, 1983).

Figure 2.4 - Schematic diagram of the Clegg meter showing the salient features of construction and operation.

Figure 2.5 - Comparison between the Clegg (1977 and 1980) and Mathur and Coghlan (1987) relationships for California Bearing Ratio (CBR) in terms of the Impact Value (IV).

Figure 3.1 - Directional notation for the mutually perpendicular x, y and z axes with the corresponding particle displacements (u, v and w), velocities ($\dot{u}, \dot{v}$ and $\dot{w}$), and accelerations ($\ddot{u}, \ddot{v}$ and $\ddot{w}$). The arrows show the positive directions.

Figure 3.2 - Types of seismic wave; (a) Longitudinal body waves, (b) Transverse body waves, (c) Rayleigh surface waves and (d) Love surface waves.

Figure 3.3 - Displaced shape of an elastic half-space, at any instaneous time,aue to a sinusoidal output source.

Figure 3.4 - Dependence of the wave velocity ratios ($v_S/v_P, v_R/v_S = \alpha$ and v_R/v_P) upon the Poisson's ratio ν.

Figure 3.5 - Normalised curves showing the variation of the vertical and horizontal components of dynamic displacement with depth due to the propagation of a Rayleigh wave. Curves are shown for differing values of Poisson's ratio.

Figure 3.6 - Surface wave velocity-depth profiles for two silty clay sites showing the influence of moisture content on the surface wave velocity (after Jones, 1958).

Figure 3.7 - Surface wave velocity-depth profile for a pit filled with compacted wet-mix macadam overlying clay showing the use of the approximation for depth of propagation, $z = \lambda/2$ (after Abbiss, 1983).

Figure 3.8 - Surface wave velocity-depth profile for a flexible road pavement (after Huekelom and Foster, 1960).

Figure 3.9 - The influence of compaction on the surface wave velocity-depth profile for a sandy soil (after Jones, 1960).

Figure 3.10 - The influence of trafficking on the surface wave velocity-depth profile for a road sub-base construction (after Jones, 1960).

Figure 3.11 - Surface wave velocity-depth profiles for a road pavement construction showing the influence of the addition of further layers on top of the pre-existing construction (after Maxwell, 1960).

Figure 4.1 - Particle size distribution curves for Permian Sand (a) and Sharp Sand (b) with the grading envelope for BS 882 (1983) Concrete Sand Grading C.

Figure 4.2 - Particle size distribution curves for Wet-mix macadam (c) with the Department of Transport (1986) grading envelope for Wet-mix macadam.

Figure 4.3 - Particle size distribution curves for Permian Sand (a), Sharp Sand (b) and Wet-mix macadam (c).

Figure 4.4 - Dry density-moisture content relationships for Permian Sand compacted at 27, 54, 81, 108 and 135 blows/layer to BS 1377 (1975): Test 12. Curves of constant air voids (A = 0, 5 and 10%) are also shown.

Figure 4.5 - Dry density-moisture content relationships for Sharp Sand compacted at 27, 54 and 81 blows/layer to BS 1377 (1975): Test 12. Curves of constant air voids (A = 0, 5 and 10%) are also shown.

Figure 4.6 - Dry density-moisture content relationships for Wet-mix macadam compacted at 27, 54 and 81 blows/layer to BS 1377 (1975): Test 12. The curves are shown both corrected and uncorrected for the stone content of the material. Curves of constant air voids (A = 0, 5 and 10%) are also shown.

Figure 4.7 - The effect of scalping (particles retained on a 20 mm test sieve removed) on the particle size distribution of a stoney cohesive soil (after Barnes, 1987).

Figure 4.8 - The effect of scalping (d) (particles retained on a 19.05 mm test sieve removed) on the particle size distribution of Wet-mix macadam (c).

Figure 4.9 - Dry density-moisture content relationship for Wet-mix macadam compacted to BS 5835: Part 1 (1980). The dry density-moisture content relationship obtained using the BS 1377 (1975) form of analysis is also shown as are curves of constant air voids (A = 0, 5 and 10%).

Figure 4.10 - Relationships between the logarithm of compactive effort (CE) and maximum dry density ($\rho_{d_{max}}$) for Permian Sand, Sharp Sand and Wet-mix macadam. Levels of compactive effort for BS 1377 (1975): Tests 12, 13 and 14 are shown for comparison.

Figure 4.11 - Relationships between the logarithm of compactive effort (CE) and optimum moisture content (w_{opt}) for Permian Sand, Sharp Sand and Wet-mix macadam. Levels of compactive effort for BS 1377 (1975): Tests 12, 13 and 14 are shown for comparison.

Figure 5.1 - Graphical explanation of the principle of least squares regression analysis (after Kreyszig, 1983).

Figure 5.2 - Schematic diagram showing the apparatus for determining surface wave velocity-depth profiles.

Figure 5.3 - The generation of Lissajous figures by an oscilloscope in X-Y mode for a range of phase angles (ϕ): a) $\phi = 0$; b) $\phi = 0$; c) $\phi = \pi/4$; d) $\phi = \pi/2$ and e) $\phi = \pi$.

Figure 5.4 - Trench profile produced with the ERS narrow bucket (reproduced courtesy of British Gas plc, Engineering Research Station) compared to the required trench profile.

Figure 6.1 - Plot of transducer separation (d) against phase angle (ϕ) for Test TPS2A ($f = 375$ Hz; $r = 0.979$).

Figure 6.2 - Plot of transducer separation (d) against phase angle (ϕ) for Test WMM9 ($f = 450$ Hz; $r = 1.000$).

Figure 6.3 - Surface wave velocity-depth profile for Test TPS1A.

Figure 6.4 - Surface wave velocity-depth profile for Test TPS1B.

Figure 6.5 - Surface wave velocity-depth profile for Test TPS1C.

Figure 6.6 - Surface wave velocity-depth profile for Test TPS1D.

Figure 6.7 - Surface wave velocity-depth profile for Test TPS2A.

Figure 6.8 - Surface wave velocity-depth profile for Test TPS2B.

Figure 6.9 - Surface wave velocity-depth profile for Test TPS2C.

Figure 6.10 - Surface wave velocity-depth profile for Test TPS3A.

Figure 6.11 - Surface wave velocity-depth profile for Test TPS3B.

Figure 6.12 - Surface wave velocity-depth profile for Test TPS4.

Figure 6.13 - Surface wave velocity-depth profile for Test TPS5A.

Figure 6.14 - Surface wave velocity-depth profile for Test TPS5B.

Figure 6.15 - Attenuation data for Test TPS3 (frequency, $f = 300$ and 500 Hz).

Figure 6.16 - Attenuation data for Test TPS4 (frequency, $f = 300$ and 500 Hz).

Figure 6.17 - Attenuation data for Test TPS5 (frequency, $f = 300$ and 500 Hz).

Figure 6.18 - Normalised particle displacement-depth profile for Test TPS2B at 450 Hz (λ = 0.388 m).

Figure 6.19 - Normalised particle displacement-depth profile for Test TPS3B at 300 Hz (λ = 0.280 m).

Figure 6.20 - Normalised particle displacement-depth profile for Test TPS3B at 150 Hz (λ = 0.810 m).

Figure 6.21 - Surface wave velocity-depth profile for Test TSS1A.

Figure 6.22 - Surface wave velocity-depth profile for Test TSS1B.

Figure 6.23 - Surface wave velocity-depth profile for Test TSS2A.

Figure 6.24 - Surface wave velocity-depth profile for Test TSS2B.

Figure 6.25 - Surface wave velocity-depth profile for Test TSS3A.

Figure 6.26 - Surface wave velocity-depth profile for Test TSS3B.

Figure 6.27 - Surface wave velocity-depth profile for Test TSS4.

Figure 6.28 - Surface wave velocity-depth profile for Test TSS5A.

Figure 6.29 - Surface wave velocity-depth profile for Test TSS5B.

Figure 6.30 - Attenuation data for Test TSS1 (frequency, f = 300 and 500 Hz).

Figure 6.31 - Attenuation data for Test TSS2 (frequency, f = 300 and 500 Hz).

Figure 6.32 - Attenuation data for Test TSS3 (frequency, f = 300 and 500 Hz).

Figure 6.33 - Attenuation data for Test TSS4 (frequency, f = 300 and 500 Hz).

Figure 6.34 - Attenuation data for Test TSS5 (frequency, f = 300 and 500 Hz).

Figure 6.35 - Surface wave velocity-depth profile for Test WMM1.

Figure 6.36 - Surface wave velocity-depth profile for Test WMM2.

Figure 6.37 - Surface wave velocity-depth profile for Test WMM3.

Figure 6.38 - Surface wave velocity-depth profile for Test WMM4.

Figure 6.39 - Surface wave velocity-depth profile for Test WMM5.

Figure 6.40 - Surface wave velocity-depth profile for Test WMM6.

Figure 6.41 - Surface wave velocity-depth profile for Test WMM10.

Figure 6.42 - Attenuation data for Test WMM1 (frequency, f = 300 and 500 Hz).

Figure 6.43 - Attenuation data for Test WMM2 (frequency, f = 300 and 500 Hz).

Figure 6.44 - Attenuation data for Test WMM3 (frequency, f = 300 and 500 Hz).

Figure 6.45 - Attenuation data for Test WMM4 (frequency, f = 300 and 500 Hz).

Figure 6.46 - Attenuation data for Test WMM5 (frequency, f = 300 and 500 Hz).

Figure 6.47 - Attenuation data for Test WMM6 (frequency, f = 300 and 500 Hz).

Figure 6.48 - Attenuation data for Test WMM10 (frequency, f = 300 and 500 Hz).

Figure 6.49 - Surface wave velocity-depth profile for Test WMM7..

Figure 6.50 - Surface wave velocity-depth profile for Test WMM8.

Figure 6.51 - Surface wave velocity-depth profile for Test WMM9.

Figure 6.52 - Attenuation data for Test WMM7 (frequency, f = 300 and 500 Hz).

Figure 6.53 - Attenuation data for Test WMM8 (frequency, f = 300 and 500 Hz).

Figure 6.54 - Attenuation data for Test WMM9 (frequency, f = 300 and 500 Hz).

Figure 6.55 - Surface wave velocity-depth profile for Test NSSEAS.

Figure 6.56 - Surface wave velocity-depth profile for Test SL1.

Figure 6.57 - Surface wave velocity-depth profile for Test SL2.

Figure 6.58 - Surface wave velocity-depth profile for the case study at Acton Dean, Stanley, County Durham.

Figure 7.1 - Plot of the number of passes per layer (N_p) (logarithmic scale) against dry density (ρ_d) for tests on Permian Sand, Sharp Sand and Wet-mix macadam.

Figure 7.2 - Plot of the ratio of the number passes per layer to the mean layer thickness ($N_p/\overline{h}$) (logarithmic scale) against dry density (ρ_d) for tests on Permian Sand, Sharp Sand and Wet-mix macadam.

Figure 7.3 - Plot of the number of passes per layer (N_p) (logarithmic scale) against Impact Value (IV) for tests on Permian Sand, Sharp Sand and Wet-mix macadam.

Figure 7.4 - Plot of the ratio of the number passes per layer to the mean layer thickness ($N_p/\overline{h}$) (logarithmic scale) against Impact Value (IV) for tests on Permian Sand, Sharp Sand and Wet-mix macadam.

Figure 7.5 - Plot of the number passes per layer (N_p) (logarithmic scale) against CBR for tests on Permian Sand and Sharp Sand. Also shown (inset) is the relationship between log N_p and the product of CBR and moisture content ($wCBR$) for tests on Permian Sand.

Figure 7.6 - Plot of the ratio of the number passes per layer to the mean layer thickness ($N_p/\overline{h}$) (logarithmic scale) against CBR for tests on Permian Sand and Sharp Sand. Also shown is the relationship between log($N_p/\overline{h}$) and the product of CBR and moisture content ($wCBR$) for tests on Permian Sand.

Figure 7.7 - Plot of dry density (ρ_d) against IV for tests on Permian Sand, Sharp Sand and Wet-mix macadam.

Figure 7.8 - Plot of Impact Value (IV) against CBR for tests on Permian Sand and Sharp Sand. Clegg's (1980) relationship [$CBR = 0.07(IV)^2$] is shown for comparison.

Figure 7.9 - Surface wave velocity-depth profiles for Tests TPS1A and TPS1B. Layer logs are shown for the two tests.

Figure 7.10 - Surface wave velocity-depth profiles for Tests TPS1A and TPS1D. Layer logs are shown for the two tests.

Figure 7.11 - Surface wave velocity-depth profiles for Tests TPS1B and TPS1C. The layer log is shown for both tests.

Figure 7.12 - Surface wave velocity-depth profiles for Tests TPS1C and TPS1D. Layer logs are shown for the two tests.

Figure 7.13 - Surface wave velocity-depth profiles for Tests TPS2A and TPS2B. Layer logs are shown for the two tests.

Figure 7.14 - Surface wave velocity-depth profiles for Tests TPS2A and TPS2C. Layer logs are shown for the two tests.

Figure 7.15 - Surface wave velocity-depth profiles for Tests TPS2B and TPS2C. The layer log is shown for both tests.

Figure 7.16 - Surface wave velocity-depth profiles for Tests TPS3A and TPS3B. Layer logs are shown for the two tests.

Figure 7.17 - Surface wave velocity-depth profiles for Tests TPS5A and TPS5B. Layer logs are shown for the two tests.

Figure 7.18 - Surface wave velocity-depth profiles for Tests TPS1A, TPS2A, TPS3A and TPS5A (half depth).

Figure 7.19 - Surface wave velocity-depth profiles for Tests TPS1B, TPS2B, TPS3B, TPS4 and TPS5B (full depth).

Figure 7.20 - Plot of the number of passes per layer (N_p) (logarithmic scale) against the mean surface wave velocity ($v_{Rz_{\max}/2}$) for tests on the Permian Sand in both the half-full and the full trench.

Figure 7.21 - Plot of the ratio of the number of passes per layer to the mean layer thickness ($N_p/\overline{h}$) (logarithmic scale) against the mean surface wave velocity ($v_{Rz_{\max}/2}$) for tests on the Permian Sand in both the half-full and the full trench.

Figure 7.22 - Shear modulus-depth profiles for Tests TPS1A, TPS2A, TPS3A and TPS5A (half depth).

Figure 7.23 - Shear modulus-depth profiles for Tests TPS1B, TPS2B, TPS3B, TPS4 and TPS5B (full depth).

Figure 7.24 - Plot of the number of passes per layer (N_p) (logarithmic scale) against the mean shear modulus ($G_{z_{max}/2}$) for tests on the Permian Sand in both the half-full and the full trench.

Figure 7.25 - Plot of the ratio of the number of passes per layer to the mean layer thickness ($N_p/\overline{h}$) (logarithmic scale) against the mean shear modulus ($G_{z_{max}/2}$) for tests on the Permian Sand in both the half-full and the full trench.

Figure 7.26 - Surface wave velocity-depth profiles for Tests TSS1A and TSS1B. Layer logs are shown for the two tests.

Figure 7.27 - Surface wave velocity-depth profiles for Tests TSS2A and TSS2B. Layer logs are shown for the two tests.

Figure 7.28 - Surface wave velocity-depth profiles for Tests TSS3A and TS31B. Layer logs are shown for the two tests.

Figure 7.29 - Surface wave velocity-depth profiles for Tests TSS5A and TSS5B. Layer logs are shown for the two tests.

Figure 7.30 - Surface wave velocity-depth profiles for Tests TSS1A, TSS2A, TSS3A and TSS5A (half depth).

Figure 7.31 - Surface wave velocity-depth profiles for Tests TSS1B, TSS2B, TSS3B, TSS4 and TSS5B (full depth).

Figure 7.32 - Plot of the number of passes per layer (N_p) (logarithmic scale) against the mean surface wave velocity ($v_{Rz_{max}/2}$) for tests on the Sharp Sand in both the half-full and the full trench.

Figure 7.33 - Plot of the ratio of the number of passes per layer to the mean layer thickness ($N_p/\overline{h}$) (logarithmic scale) against the mean surface wave velocity ($v_{Rz_{max}/2}$) for tests on the Sharp Sand in both the half-full and the full trench.

Figure 7.34 - Shear modulus-depth profiles for Tests TSS1A, TSS2A, TSS3A and TSS5A (half depth).

Figure 7.35 - Shear modulus-depth profiles for Tests TSS1B, TSS2B, TSS3B, TSS4 and TSS5B (full depth).

Figure 7.36 - Plot of the number of passes per layer (N_p) (logarithmic scale) against the mean shear modulus ($G_{z_{max}/2}$) for tests on the Sharp Sand in both the half-full and the full trench.

Figure 7.37 - Plot of the ratio of the number of passes per layer to the mean layer thickness ($N_p/\overline{h}$) (logarithmic scale) against the mean shear modulus ($G_{z_{max}/2}$) for tests on the Sharp Sand in both the half-full and the full trench.

Figure 7.38 - Surface wave velocity-depth profiles for Tests WMM1, WMM2, WMM3 and WMM5 (nominal layer thickness, $h < 150$ mm).

Figure 7.39 - Surface wave velocity-depth profiles for Tests WMM4, WMM6 and WMM10 and WMM7, WMM8 and WMM9 (nominal layer thickness, $h < 200$ mm).

Figure 7.40 - Plot of the number of passes per layer (N_p) (logarithmic scale) against the mean surface wave velocity ($v_{Rz_{max}/2}$) for tests on the Wet-mix macadam.

Figure 7.41 - Plot of the ratio of the number of passes per layer to the mean layer thickness ($N_p/\overline{h}$) (logarithmic scale) against the mean surface wave velocity ($v_{Rz_{max}/2}$) for tests on the Wet-mix macadam.

Figure 7.42 - Shear modulus-depth profiles for Tests WMM1, WMM2, WMM3 and WMM5 (nominal layer thickness, $h < 150$ mm).

Figure 7.43 - Shear modulus-depth profiles for Tests WMM4 and WMM6 and WMM7, WMM8 and WMM9 (nominal layer thickness, $h < 200$ mm).

Figure 7.44 - Plot of the number of passes per layer (N_p) (logarithmic scale) against the mean shear modulus ($G_{z_{max}/2}$) for tests on the Wet-mix macadam.

Figure 7.45 - Plot of the ratio of the number of passes per layer to the mean layer thickness ($N_p/\overline{h}$) (logarithmic scale) against the mean shear modulus ($G_{z_{max}/2}$) for tests on the Wet-mix macadam.

Figure 7.46 - Surface wave velocity-depth profiles for Tests WMM7, WMM8 and WMM9 (tests with Wet-mix macadam and Sharp Sand layers).

Figure 7.47 - Shear modulus-depth profiles for Tests WMM7, WMM8 and WMM9 (tests with Wet-mix macadam and Sharp Sand layers).

Figure 7.48 - The increase of Impact Value (IV) with applied compactive effort (N_p) (Blaydon demonstration trench).

Figure 7.49 - The variation of Impact Value (IV) along the length of the trench for Test SL1 (Salters Lane).

Figure 7.50 - Surface wave velocity-depth profiles for Tests SL1 and SL2.

Figure 7.51 - Dry density-moisture content relationships for Permian Sand compacted at 27, 54, 81, 108 and 135 blows/layer to BS 1377 (1975): Test 12. Field dry density-moisture content data are plotted for comparison. Curves of constant air voids ($A = 0,\ 5$ and 10%) are also shown.

Figure 7.52 - Dry density-moisture content relationships for Sharp Sand compacted at 27, 54 and 81 blows/layer to BS 1377 (1975): Test 12. Field dry density-moisture content data are plotted for comparison. Curves of constant air voids ($A = 0,\ 5$ and 10%) are also shown.

Figure 7.53 - Dry density-moisture content relationships for Wet-mix macadam compacted at 27, 54 and 81 blows/layer to BS 1377 (1975): Test 12. The curves are shown both corrected (top three curves) and uncorrected (lower three curves) for the stone content of the material. Field dry density-moisture content data are plotted for comparison. Curves of constant air voids ($A = 0,\ 5$ and 10%) are also shown.

Figure 7.54 - Dry density-moisture content relationship for Wet-mix macadam compacted to BS 5835: Part 1 (1980). Field density-moisture content data are plotted for comparison. Curves of constant air voids (A = 0, 5 and 10%) are also shown.

Figure A1.1 - Centroid of the area under the W function, $\overline{z/\lambda}$, plotted as a function of Poisson's ratio.

Figure A3.1 - BS 882 (1983) grading envelopes for Concrete Sand Gradings C, M and F.

Figure A3.2 - Department of Transport (1986) grading envelopes for Type 2 (Clause 803), Type 1 (Clause 804) and Wet-mix macadam (Clause 805).

List of Plates

Plate 5.1 - The laboratory based trench showing the usage of the Clegg meter.

Plate 5.2 - Detailed view of the Clegg meter showing (from right to left) the hand held readout meter, the guide tube and the drop weight with handle and internally mounted accelerometer.

Plate 5.3 - The Wacker BS45Y electrically powered vibratory rammer in use in the laboratory based trench.

Plate 5.4 - The electromagnetic oscillator showing the circular plate and sprung mass arrangement which have been added to improve signal quality.

Plate 5.5 - The apparatus for surface wave velocity-depth profile measurement shown in use in the field.

Plate 5.6 - Oscilloscope trace of in-phase signals from two accelerometers (top) and the Lissajous Figure generated (bottom) for a phase angle of, $\phi = n\pi$ ($n = 0, 2, 4, 6, \ldots,$ etc).

Plate 5.7 - The JCB 3C excavator equipped with the ERS narrow bucket excavating one of the trenches for the field trials.

Plate 6.1 - The Bomag BG 100 vibratory roller narrow trench compactor.

Plate A5.1 - The specially modified Wacker BS45Y electrically powered vibratory rammer.

Notation

The following notations and abbreviations are used in this thesis.

A	Volume of air voids in soil, expressed as a percentage of total soil volume.
AIV	Aggregate Impact Value.
A_1	A constant.
$a_1, a_2, \ldots, a_n$	Particle size fractions.
a	A constant dependent upon the Poisson's ratio.
a	A constant.
BS	British Standard (Abbreviation).
B_1	A constant such that $B_1 = -2iA_1/(s^2 - p^2)$.
b	A constant dependent upon the Poisson's ratio.
CBR	California Bearing Ratio.
CE	Compactive Effort.
CMV	Compaction Meter Value (Abbreviation).
CRO	Cathode Ray Oscilloscope (Abbreviation).
$CSCP$	Corrected sum of cross products.
$CSSX$	Corrected sum of squares of x.
$CSSY$	Corrected sum of squares of y.
c	Intercept constant of a linear (or semi-logarithmic) regression line.
c	A constant dependent upon the Poisson's ratio.
DC	Direct Current.
D_c	Degree of compaction.
D_r	Relative density ($= I_D$).
d	Seperation of two measurement points on the x-axis.
d	A constant dependent upon the Poisson's ratio.
E	Young's modulus.
ERS	Engineering Research Station, British Gas plc (Abbreviation).
$\exp x$	Exponential of x (also represented as e^x).
F	Ratio of matrix material (< 19.05 mm) and the whole sample measured from the grading curve.
FI	Flakiness Index.
f	Frequency of a sinusoidal waveform.
G_s	Specific gravity of soil particles.
G_t	Specific gravity of soil particles ≥ 19.05 mm.
G	Shear modulus ($= \mu$, Lamé's second constant).
$G_{z_{\max}/2}$	Mean shear modulus of a shear modulus-depth profile.

g	Acceleration due to gravity ($= 9.81\ \mathrm{m/s^2}$).
H	Drop height for the rammer in BS 1377 (1975): Tests 12 and 13 and also for the Clegg meter drop weight.
H_0	Drop height of mass *(La Dynaplaque).*
H_r	Rebound height of mass *(La Dynaplaque).*
h	Thickness of a layer of compacted material.
$\overline{h}$	Mean thickness of a number of compacted layers.
I_D	Density index ($= D_r$).
IV	Impact Value.
i	$\sqrt{-1}$.
i	A counter.
j	The j^{th} determination, from a total of n determinations, of the parameters x and y.
j	The number of wavelength's separating the first and current measurement transducer—a counter.
K	A constant.
k	A constant.
$\ln x$	Natural logarithm (base e) of x.
$\log x$	Logarithm (base 10) of x.
MCA	Moisture Condition Apparatus (Abbreviation).
MCV	Moisture Condition Value (Abbreviation).
m	Slope constant of a linear (or semi-logarithmic) regression line.
m	Mass (as defined in the text).
m_{dry}	Dry mass of soil.
$m_{\mathrm{H_2O}}$	Mass of water required to be added to a known mass of soil to raise the moisture content from w_i to w_{req}.
m_{wet_i}	Initial wet mass of soil.
m_{wet_r}	Required wet mass of soil.
NDG	Nuclear (or Isotopic) Density Gauge (Abbreviation).
N_b	Number of blows applied to each layer of material in BS 1377 (1975): Test 12 and 13 laboratory compaction tests.
N_l	Number of layers in which material is compacted in BS 1377 (1975): Test 12 and 13 laboratory compaction tests.
N_p	Number of passes applied to each layer by compaction plant (parameter of compactive effort).
$N_p/\overline{h}$	Ratio of the number of passes to the mean layer thickness (parameter of compactive effort).
n	Number of determinations of a parameter x.
P	Rated electrical power of vibrating hammers used in BS 1377 (1975): Test 14 and BS 5835: Part 1 (1980) laboratory compaction tests.

PRD	Percentage Refusal Density test (Abbreviation).
PSD	Particle Size Distribution (Abbreviation).
PUSWA	Public Utilities Street Works Act 1950 (Abbreviation).
p	A constant.
Q_0	Amplitude of a sinusoidal vibration.
q	A constant.
R	Coefficient of energy restitution *(La Dynaplaque)*.
RSJ	Rolled Steel Joist (Abbreviation).
r	Regression correlation coefficient.
rms	Root mean square (Abbreviation).
S	Percentage numerical sensitivity of a parameter to increases in compactive effort.
SEM	Suitable Excavated Material (Abbreviation).
s	A constant.
t	Time.
U	Dynamic attenuation factor for the horizontal component of particle displacement of a Rayleigh wave with depth.
UK	United Kingdom (Abbreviation).
u	Particle displacement in the x-direction.
$\dot{\mathrm{u}}$	Particle velocity in the x-direction.
$\ddot{\mathrm{u}}$	Particle acceleration in the x-direction.
V	Volume.
V	Voltage.
v	Particle displacement in the y-direction.
$\dot{\mathrm{v}}$	Particle velocity in the y-direction.
$\ddot{\mathrm{v}}$	Particle acceleration in the y-direction.
v_0	Velocity on impact with the ground surface of a falling weight.
W	Dynamic attenuation factor for the vertical component of particle displacement of a Rayleigh wave with depth.
w	Particle displacement in the z-direction.
$\dot{\mathrm{w}}$	Particle velocity in the z-direction.
$\ddot{\mathrm{w}}$	Particle acceleration in the z-direction.
w	Moisture content.
w_A	Absorbed moisture content of soil particles.
w_i	Initial moisture content.
w_{mass}	Moisture content of the material including that ≥ 19.05 mm.
w_{matrix}	Moisture content of the material excluding that ≥ 19.05 mm.
w_{opt}	Optimum moisture content.
w_r	Residual moisture content.

w_{req}	Required moisture content.
XRD	X-Ray Diffractometry (Abbreviation).
XRF	X-Ray Fluorescence (Abbreviation).
x	Required force to give 10% fines.
x	Distance along the x-axis.
x	A parameter.
$\overline{x}$	Mean of the parameter x for n determinations.
$\overline{x}$	Centroid of the area under a curve measured along the x-axis.
y	Distance along the y-axis.
y	Mean percentage fines from two 10% fines tests at x kN force.
z	Distance along the z-axis.
z	Depth.
α	Ratio of the Rayleigh and Transverse wave velocities ($= v_R/v_S$).
α	Coefficient of material attenuation for a Rayleigh-type surface wave.
γ	Shear strain.
ϵ	Normal strain.
ϵ_1	Axial strain (unconfined compression test).
ϵ_v	Volumetric strain.
Λ	Lamé's first constant.
λ	Wavelength of a sinusoidal wave.
μ	Lamé's second constant ($= G$).
ν	Poisson's ratio.
π	3.141592654 . . .
ρ	Bulk density of soil.
ρ_d	Dry density of soil.
$\rho_{d_{\text{mass}}}$	Dry density of particles $\geq$ 19.05 mm.
$\rho_{d_{\text{matrix}}}$	Dry density of particles $<$ 19.05 mm.
$\rho_{d_{\text{max}}}$	Maximum dry density of soil.
$\rho_{d_{\text{min}}}$	Minimum dry density of soil.
ρ_w	Density of water ($= 1\,\text{Mg/m}^3$).
$\sigma_{x_{n-1}}$	Sample standard deviation for n determinations of the parameter x.
v_L	Velocity of Love waves.
v_P	Velocity of Longitudinal waves.
v_R	Velocity of Rayleigh waves.
$v_{Rz_{\text{max}}/2}$	Mean surface wave velocity of a surface wave velocity-depth profile.
v_S	Velocity of Transverse waves.
ϕ	Phase angle between two sinusoidal waveforms.
φ	Potential function.

ψ	Potential function.
ω	Angular velocity of a sinusoidal vibration ($= 2\pi f$).
d	Representation of a differential (*e.g.* dx/dy).
∂	Representation of a partial differential (*e.g.* $\partial x/\partial y$).
∇^2	Representation of the operator $\partial^2/\partial x^2 + \partial^2/\partial y^2 + \partial^2/\partial z^2$.
∞	Infinity.

CHAPTER 1

INTRODUCTION AND SCOPE OF WORK

1.1 Introduction

Road and footpath users are all familiar with utility and local highway authority roadworks and the subsequent frequently poor quality reinstatements where a hole or trench is filled with a number of layers of unbound and bound materials, and the surface is left either raised or depressed in relation to the surrounding pavement surface. Whilst it is undoubtably uncomfortable to drive over such reinstatements the effects can be far more serious. Drivers may be caused to swerve or even to lose control of their vehicles in an attempt to avoid a particularly bad pothole. Cyclists are at risk even more; they may be thrown from their machines by bumps or hollows in the road which would cause no more than a mild inconvenience to a motorist, or forced to swerve violently in order to avoid such a fate, possibly into the path of a larger vehicle. On footpaths, uneven reinstatements can cause pedestrians, especially elderly or handicapped people, to trip and fall with the consequential possibility of personal injury claims being lodged against the highway authority.

Discontinuities and bumps, introduced by reinstatements to the normally level pavement surface, may cause an increase of some two orders of magnitude in the ground borne vibrations transmitted by the gravitational impact of motorised vehicles. The effect of this as a fatiguing agent on building cracks may be severe.

Poor reinstatements also have an economic cost, in addition to the cost imposed on the community by accidents which may be attributed in whole or in part to poor quality examples of such works. Partial or complete re-excavation and subsequent reinstatement may be necessary either just at the surface level or including the lower layers in particularly bad cases. The cost of delays to traffic must, of course, be included in the overall costs to the community of utility roadworks.

The need for reinstatements to be performed to a higher standard has long been recognised, and was reinforced by the Horne Committee Report of 1985, not just to reduce the effects of the factors noted above but also to improve the level of protection afforded to the buried utility apparatus, thus increasing the service life of the apparatus and so necessitating fewer excavations for apparatus repair and

replacement purposes. The recommendations of the Horne Committee Report were excellently summarised by Horne (1986) in a more concise and readable form than the original wide-ranging report. The scale of public concern may be gauged, to some extent, by recent articles on reinstatement works and the state of Britain's roads in 'The Independent' and 'The Daily Telegraph' newspapers (Anon, 1988a and 1989a). The current legislation which controls the way in which reinstatements are carried out in the UK is considered, along with the Horne Committee Report and the economics and scale of reinstatement works, in the following sections.

1.2 Responsibility for reinstatement works

Currently the legal framework within which reinstatement works are carried out is dictated by the Public Utilities Street Works Act 1950, commonly known as PUSWA. This document is described in terms easily understandable to the layman by the Department of Transport (1973). The original legislation giving the public utilities the right to break open publicly maintainable highways dates back to the mid-nineteenth century. The principal nineteenth century statutes governing such operations were the Gasworks Clauses Act 1847, the Waterworks Clauses Act 1847, The Electricity Supply Act 1882, the Telegraph Act 1863 and the Public Health Act 1875. The Horne Committee (1985) in its review of PUSWA reports that: *'Although there has, of course, been much subsequent legislation affecting the utilities, their rights to break open the highway remain as contained in these nineteenth century enactments'.*

Dramatic increases in the volume of motor traffic, advances in highway engineering and developments in the utilities' services in the early part of the twentieth century effectively rendered the nineteenth century legislation obsolete. Unsuccessful attempts, between the years of 1925 and 1935, to remedy the problems inherent in the old legislation led to the formation of a Joint Committee of the Houses of Lords and Commons, chaired by Lord Carnock, which reported in 1939, its main recommendation being that a new code should be formed applying equally to all the utilities. This led eventually to the Public Utilities Street Works Act of 1950.

PUSWA provides a general code governing the exercise of the utilities' powers to break open streets and lay and maintain apparatus in them. Its main objects are described by the Department of Transport (1973) as:

i) *'to regulate the exercise of powers of undertakers for the protection of street authorities and other undertakers',*

ii) *'to protect undertakers whose apparatus may be affected by roadworks, and'*

iii) *'to enable powers exercisable in a street which is, or is prospectively, a maintainable highway to be exercised in controlled land'.*

Divided into four parts, PUSWA is described by the Horne Committee (1985) as an: *'undoubtedly complex Act; for instance, it provides for 39 different types of notices to be served, in various circumstances, and includes 14 different criminal offences'.* Part I of the Act contains the Street Works Code, which provides a uniform code governing works in the streets by the utilities whether under a power derived from the general Acts or from special enactments. Schedule 3 contains detailed provisions relating to the reinstatement of the road after the completion of the utilities' works[1]. Part II provides a similar code to govern the relations between utilities and authorities promoting roadworks which affect utility apparatus. Part III sets out procedures to be applied when works by one utility affect the apparatus of another utility. Part IV deals with enforcement, interpretation and application of the Act to Scotland and to London, and financial and general provisions.

A further complication is introduced into the operation of PUSWA by Section 16 of the Act; this allows for a highway authority and a utility to make an agreement modifying the provisions of the Act relating to reinstatements. A Model Agreement (Department of Transport, 1974) was drawn up by the PUSWA Conference[2], with the twin objectives of improving the standard of reinstatements carried out by the utilities and reducing the time taken by the highway authorities to carry out permanent reinstatements. With this came the recommendation that all highway authorities and utilities should enter into agreements of this form. The Model Agreement provides for highway authorities who elect to carry out the permanent reinstatement to become responsible, both physically and financially, for the interim restoration six months after completion of the utility's works—though the utility still has to pay for the permanent reinstatement when that is carried out. The

[1]Schedule 3 gives the highway authority the right to elect to carry out permanent reinstatements. Notice of election may be given either generally or for specific cases. Where the highway authority makes such an election, the utility is responsible for the interim restoration and the maintenance of the temporary reinstatement until the highway authority gives notice that it is about to undertake the permanent reinstatement. The highway authority is required to carry out the permanent reinstatement, *'as soon as is prudent and practicable'*, after the completion of the utilities works. The cost of the permanent reinstatement is payable by the utility.

[2]The PUSWA Conference consists of an *ad hoc* body bringing together the local highway authorities and the utilities, under the chairmanship of the Department of Transport.

Model Agreement also provides that, where the highway authority does not elect to carry out the permanent reinstatement, the utility should be responsible for the permanent reinstatement for two years after its completion (*cf.* six months in the Act).

In direct comparison to PUSWA, the Model Agreement provides increased protection for the highway authority in cases where they elect to leave the utility to carry out the permanent reinstatement, and increases the incentive for the highway authority to carry out the permanent reinstatement quickly where they elect to do that themselves. The Horne Committee Report (1985) states that the: *'overall effect is to increase the attractiveness to the highway authority of allowing the utilities to carry out permanent reinstatements'.* Despite the recommendations of the PUSWA Conference the Model Agreement has been far from universally adopted.

The Model Agreement also usefully provides a guide to the layers which should be used in reinstatement works in varying types of flexible road pavement construction (Table 1.1). Table 1.2 defines the types of road constructions (Types I to IV) described in Table 1.1 along with rough estimates of the mileage of each type, in Great Britain in 1974, while Figure 1.1 illustrates the geometrical relationship between the different layers in a road reinstatement. One important point must be made about the data contained in Table 2.1, which is that the clause numbers refer to the old 5th Edition of the Specification for Road and Bridge Works (Department of Transport, 1976) and not the new renamed 6th Edition—Specification for Highways Works (Department of Transport, 1986).

The Horne Committee, in addition to recommending new legislation to replace and greatly improve upon PUSWA while operating alongside a detailed national specification for reinstatement works, makes in its conclusions one recommendation (Recommendation Number 29) which is particularly relevant to the work presented later in this report. *'If sampling reveals that a reinstatement had not been done in accordance with the specification, then the highway authority should be able to charge its reasonable costs to the utility'.* Here we plainly see the Horne Committee advocating the formation of a performance (or end-result) specification as opposed to the more traditional method specification. This move can be seen as a more general trend within the highway engineering industry, especially since the recent publication of the 6th Edition of the Department of Transport, Specification for Highway Works and the associated Notes for Guidance in late 1986 (collectively known as

the Brown Book[3]). The essential difference, in compaction terms, between the old and new specifications is that the new specification ceases to use the method specification for bound granular materials, insisting instead on a fairly rigid perfomance (or end product) specification. Although this applies only to the compaction of bound materials (and the specification for the compaction of unbound granular materials remains largely unchanged—still being described in terms of the old method specification) moves are already afoot within the Department of Transport to apply a performance specification to unbound granular materials (Nutt, 1987). Possible means of achieving this end will be described in some detail in Section 2.3.

Calls for new legislation to replace PUSWA, based on the Horne Committee recommendations, are perhaps most strongly supported by consideration of the six-fold increase in the annual vehicle mileage for all types of motor vehicles and the two-fold increase between the enactment of PUSWA in 1950 and 1984 in the annual vehicle mileage for damaging heavy goods vehicles. This latter figure must, of course, be seen in the light of greatly increased lorry weights (19 to 38 tonne in the case of articulated lorries) and still more pertinently in the light of the increase in maximum permitted axle weights from 8 to 10.5 tonne over the same time period. British Gas (Rhodes *et al*, 1987) currently expect that legislation based on the Horne Report would lead to reinstatements being carried out as illustrated in Figures 1.2a and b, for small and larger reinstatement works, respectively. Permanent reinstatement is expected to be required within 6 months of the completion of the temporary, or interim, reinstatement. New legislation, to replace PUSWA, is expected to make the utilities fully responsible for both temporary and permanent reinstatement (Anon, 1989b) in line with Horne Committee recommendations. It has been reported (Anon,1989b) that the new legislation to replace PUSWA could not be fully implemented until the end of 1990 at the very earliest. However, as the new legislation is not expected to be announced until the autumn of 1989 (Anon, 1989c) this date is most likely extremely optimistic.

1.3 Economics and scale of reinstatement works

In the preceding section, the somewhat complex manner in which utility reinstatements are legislated was examined. Estimates of the total length of roads in Great

[3]The Brown Book is not intended to act as a specification for road reinstatement works but traditionally the old 5th Edition, or Blue Book, has acted as a basis for Local Authority specifications. There is no reason to suppose that the Brown Book will not fulfill a similar role in the future.

Britain vary between 210,000 km (Department of Transport, 1974) and 384,000 km (South, 1986). South's figure is estimated by the Central Statistics Office to be worth some £28,000 m. A commercial interest might aim to spend some 5% per annum on the maintenance of such a valuable stock holding. This is not currently the case. It is therefore seen as essential that the 3,000,000 openings per year[4] (South, 1986) which are made in our roads are reinstated to the highest possible standard; in fact the Horne Committee (1985) concluded that: *'the standard of reinstatements needs to be improved, and the gain in efficiency offered by the simplification of procedures offers scope for this without increasing overall costs'.* This view is put forward not only by impartial bodies such as the Horne Committee but also by the utilities themselves which, with an estimated total length of apparatus of 1,650,000 km buried below the roads and having a replacement cost of some £117,000 m[5] (Nitze, 1986), plainly have a vested interest in providing a structurally sound environment for their plant.

British Gas estimate that their expenditure on road works is of the order of £445 m per annum and, although such precise information regarding the expenditure of the other utilities was not available, the Horne Committee (1985) estimated that the expenditure on water and sewage is around £300 m per annum and, while expenditure by the electricity and telecommunications industries was not as great, the total expenditure by the four utilities was some £1,000 m per annum. Since highway authority expenditure on road maintanence was some £800 m in 1983/84[6], the portion of the total £1,000 m spent by the utilities on reinstatement works plainly supports a substantial industry.

Estimates of the amount of roadworks expenditure apportioned to reinstatement works vary by the utilities. The Horne Committee (1985) states that the utilities as a whole spend some £200 m per annum while Peters (1984) estimates that British Gas alone spent £186 m on reinstatement works in 1983/84. However, regardless of precise figures it is patently vital to the national interest that an industry of this

[4]This figure neglects those openings made by the highway authorities in pursuance of their own repairs to street lighting service cables, etc. It is further estimated (Anon, 1989d) that some 15,000 utility excavations are made annually in the 700 mile road network in Newcastle-Upon-Tyne.

[5]This figure includes gas, electric, telephone, water and public sewer services but excludes domestic service connections, which with a typical domestic consumer taking a service from each of the utilities indicates a further investment of £1,650 per residential dwelling; or an additional £27,000 m on the total system cost.

[6]This figure discounts expenditure on motorway maintenance as no utility apparatus is present beneath the carriageway.

size is managed efficiently and sympathetically with regard to the needs of both the road users and the utility customers.

The scale of reinstatement operations for the five major utilities is illustrated in Table 1.3. In the financial year 1982/83 a total of 18,307 km of new and replacement mains was installed, along with 1,664,000 new and replacement services, and 1,371,000 small openings were made in the carriageways of our roads. These figures may be expected to decrease in the future, due to factors such as subscriber saturation (in the case of British Telecom), curtailment of a massive mains replacement scheme (in the case of British Gas) and advances in trenchless mains replacement technology. This is illustrated by the more detailed figures for British Gas works (Table 1.4) over the period 1974–84, and projections for the year 1988/89. The assertion that the number of excavations in our roads will fall over the next few years is, however, open to some dispute. An increase in the number of excavations for the purpose of laying and repairing underground services could be caused by the implementation of a much needed sewer repair and replacement programme in many of our larger cities and also by the new phenomenon of competing private sector telecommunications and cable television industries. These factors already create a particular problem in the City of London where it is claimed that trenching has doubled during the last five years (Anon, 1988b).

1.4 Summary and scope of work

This chapter has examined in some detail the way in which reinstatement works have been administered over the years since the utilities were first granted the right to break open the public highways. In doing so particular attention has been paid to PUSWA 1950 which is the Parliamentary Act which currently controls the logistics of reinstatement works. Further detailed attention has been paid to the report of the Horne Committe which recommends the replacement of PUSWA with a new Act operating alongside a national specification for utility roadworks, and which would make some progress towards developing a performance specification for reinstatement works.

Fortunately, recent reports (Anon, 1988c) indicate that agreement between the highway authorities and public utilities on the implementation of the Horne Committee proposals may be close. Further reports are still more optimistic: *'The government's proposals for primary legislation are virtually complete'*, and that, *'Work*

is well advanced on the detailed technical material, such as the specifications for reinstatements', (Anon, 1988d). It has also been reported that the earliest possible date for full implementation of new legislation may be late 1990 (Anon, 1989b).

In Section 1.2 the economics and scale of utility roadworks as a whole and reinstatement works in particular were studied. The reported replacement cost of the utilities' buried services (£117,000 m) serves to illustrate the vested interest which the utilities have in the improvement of the structural integrity of reinstatement works, as well as the rather more obvious interest of the highway authority as the representative of the road user. The scale of reinstatement works may contract over the next few years due to such factors as subscriber saturation and advances in trenchless mains replacement techniques, or it may expand due to factors such as the implementation of sewer repair and replacement schemes and the competing private sector telecommunications and cable television industries. Either way the industry will still constitute a significant drain on utility resources. Smith (1983) presented an interesting review of both trenching and trenchless techniques relating to reinstatement works carried out by British Gas.

One possible means of improving reinstatement backfill quality is to base the acceptance, or rejection, of a completed reinstatement on some form of test which can be applied to the reinstated surface. Short of removing a cylindrical core from the completed profile, potential test methods may rely on either the testing of the surface of each layer as it is completed, using a device such as the Clegg meter to produce an Impact Value, or on the use of non-intrusive surface devices, such as the falling weight deflectometer, which are generally economically and geometrically unsuitable for the reinstatement environment. Plainly the current situation with respect to testing reinstatement quality is far from satisfactory. The characteristics of the ideal *in situ* test are summarised in Chapter 2, in which the theory and current practice of compaction are considered along with other potential means of reinstatement backfill control. Measurement of the transmission velocity of seismic waves is identified as one potential method of controlling the quality of the unbound layers. In Chapter 3 the transmission velocity of Rayleigh-type surface waves generated by a vertical oscillator with a sinusoidal output is identified as the most likely of the potential wave transmission techniques to be suitable. The theoretical behaviour of Rayleigh waves is examined in some detail in Chapter 3. Rayleigh-type surface

wave velocity measurement techniques used by previous workers are also examined in this Chapter 3, along with surface wave data for earth materials.

Early experimental trials of both the Clegg meter and the Rayleigh-type surface wave velocity measurement technique were carried out in a full-size laboratory based trench-type construction. Single material reinstatement-type environments were constructed in the trench using two sand materials, compactive effort being applied by the use of an electrically operated vibratory-rammer (Wacker BS45Y). Measurements of the dry density were also made. Extensive, carefully controlled field trials under realistic reinstatement trench conditions have also been conducted. A series of case studies on actual reinstatement works followed the field trials. Material properties and laboratory compaction characteristics are presented and discussed in Chapter 4. The experimental methods and data analysis techniques for both the experimental studies in the laboratory and in the field are discussed in Chapter 5.

Detailed experimental results are given in Chapter 6. These results are interpreted, in terms of compactive effort, and discussed in Chapter 7. Compactive effort is defined in two different ways:

i)the number of passes applied per layer (N_p) using the Wacker BS45Y vibratory-rammer, and

ii)the ratio of N_p to the mean layer thickness ($N_p/\overline{h}$).

In addition to the basic surface wave velocity measurements and the subsequent interpretation in terms of compactive effort, measurements of the surface wave attenuation characteristics of the compacted materials were made and the resulting attenuation coefficient interpreted in terms of compactive effort. Attempts were also made to determine dynamic displacement-depth profiles using buried accelerometers and the results obtained are compared with the theoretical, normalised forms presented in Chapter 3. Conclusions and recommendations for further work are made in Chapter 8.

A series of nine appendices include work which it was felt would distract the reader from the main text of this thesis and yet were believed to be of sufficient value to merit inclusion.

Table 1.1 - Guide to types of flexible road construction for reinstatement of trenches in carriageways (after Department of Transport, 1974).

Layer	Permitted materials	Specification clause number†	THICKNESS OF LAYERS FOR ROADS			
			Type I (mm)	Type II (mm)	Type III (mm)	Type IV (mm)
Wearing course	If existing surface is rolled asphalt:					
	Rolled asphalt	907	40	40	40	40
	If existing surface is not rolled asphalt:					
	Fine cold asphalt *or*	910	25	20	20	20
	Dense bitumen macadam	908	25	20	20	20
Base Course‡	If existing surface is rolled asphalt:					
	Dense tar macadam *or*	903	65	65	65	40
	Dense bitumen macadam *or*	904	65	65	65	40
	Rolled asphalt	902	65	65	65	40
	If existing surface is not rolled asphalt:					
	Single course tarmacadam *or*	906	75	60	60	60
	Single sourse bitumen macadam	905	75	60	60	60
Road Base	Rolled asphalt base *or*	812	130	110	90	—
	Dense tar or dense bitumen base *or*	810/811	160	160	100	—
	Cement bound granular *or*	806	NP*	NP	150	100
	Lean concrete *or*	807	NP	190	150	100
	Wet mix macadam *or*	808	240	200	160	100
	Dry bound macadam	809	240	200	160	100
Sub-Base	Granular sub-base 40 mm maximum size (Type 1) *or*	803	280	260	210	150
	Granular sub-base Type 2 *or*	804	280	260	210	150
	Cement bound granular *or*	806	280	260	210	150
	Lean concrete *or*	807	280	260	210	150
	Suitable excavated road pavement material complying with the reasonable requirements of the Engineer					

†Clause numbers refer to the Blue Book (Department of Transport, 1976) which has been recently superseded by the Brown Book (Department of Transport, 1986).
‡If a wearing course is laid the thickness of the base course may be reduced by the thickness of the wearing course.
*NP denotes that the specified material is not permitted to be used in the indicated type of road.

Table 1.2 - Types of roads and estimated mileages in Great Britain (after Department of Transport, 1974).

Road Type	Definition	Estimated Mileage
I	Trunk and principal dual-carriageway roads, about 50% of whose length within the area of any given highway authority is dual.	3,000
II	All other "A" roads, and roads with hot rolled asphalt surfacing (but there may be obvious exceptions to this criterion, for example when housing estate roads and *cul-de-sacs* are surfaced with hot rolled asphalt).	30,000
III	Roads not in types I and II which carry bus services.	15,000
IV	All other roads.	162,000

Table 1.3 - Utilities' current annual workload of excavations for the financial year 1982/83 (after Horne Committee, 1985: National Joint Utilities Group Evidence).

Utility	New and replacement mains (km)	New and replacement services (km)	Small openings† (number)
Electricity	4,000	200,000	210,000
Gas	5,457	767,000	544,000
Telecom	3,150	467,000	74,000
Water‡	3,200	230,000	536,000
Sewers‡	2,500	—	—
Total	**18,307**	**1,664,000**	**1,371,000**

†The figure for small openings in the water industry is for all openings. For the other utilities, there is probably a substantial degree of overlap between the number of service connections and the number of small openings.

‡England and Wales only.

Table 1.4 - British Gas workload 1974/75 to 1988/89 (after Horne Committee, 1985: National Joint Utilities Group Evidence).

Year	Mains laid (km)		Services laid (km)		Small holes
	New	Replacement	New	Replacement	(number)
1974/75	2,210	991	3,564	3,047	717,000
1979/80	3,065	2,449	5,394	4,220	665,000
1983/84	2,625	3,125	4,636	5,550	483,000
1988/89	2,000	2,214	4,000	4,600	403,000

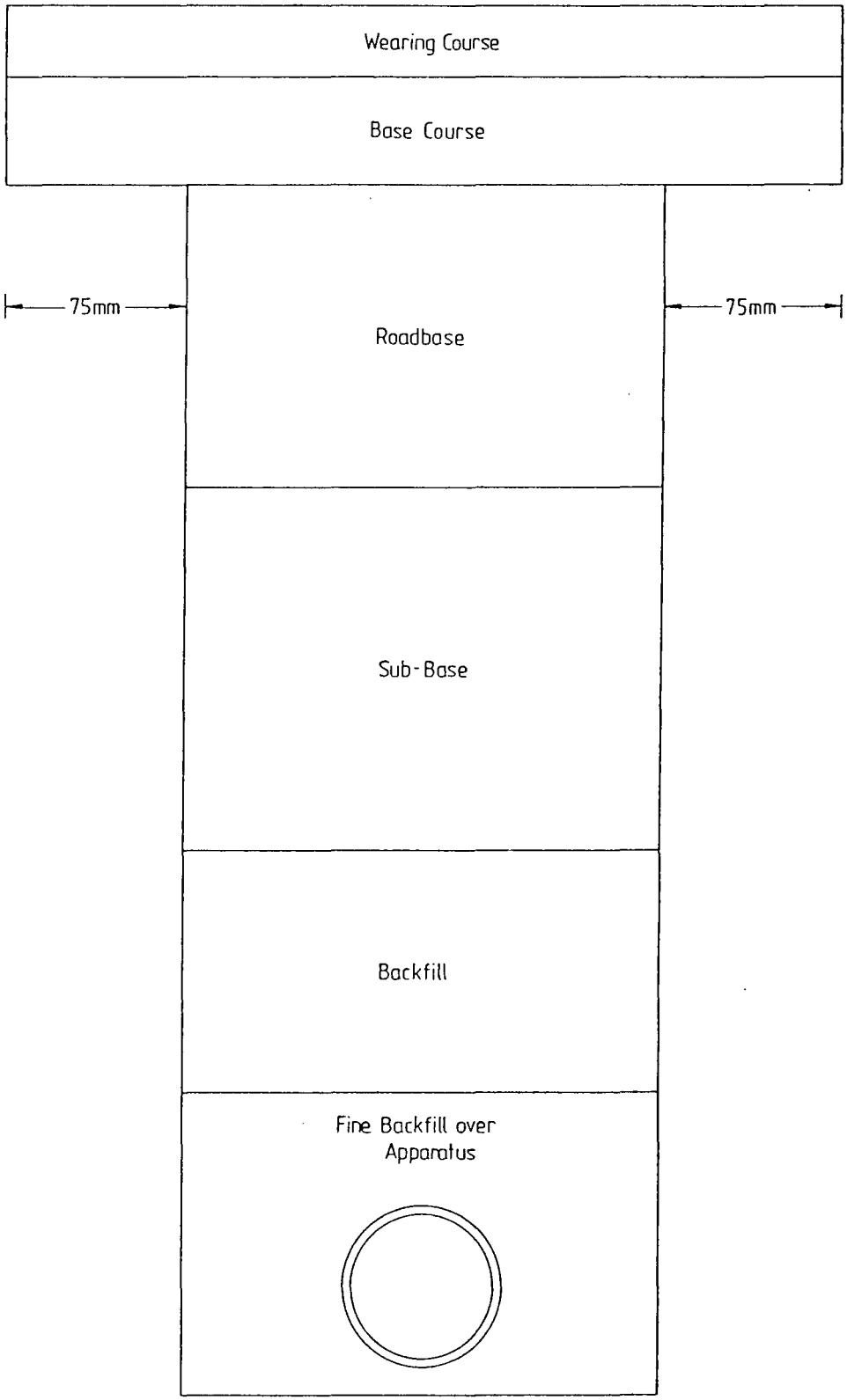

Figure 1.1 - Diagrammatic cross-section of reinstatement layers in a flexible road pavement (after Department of Transport, 1974).

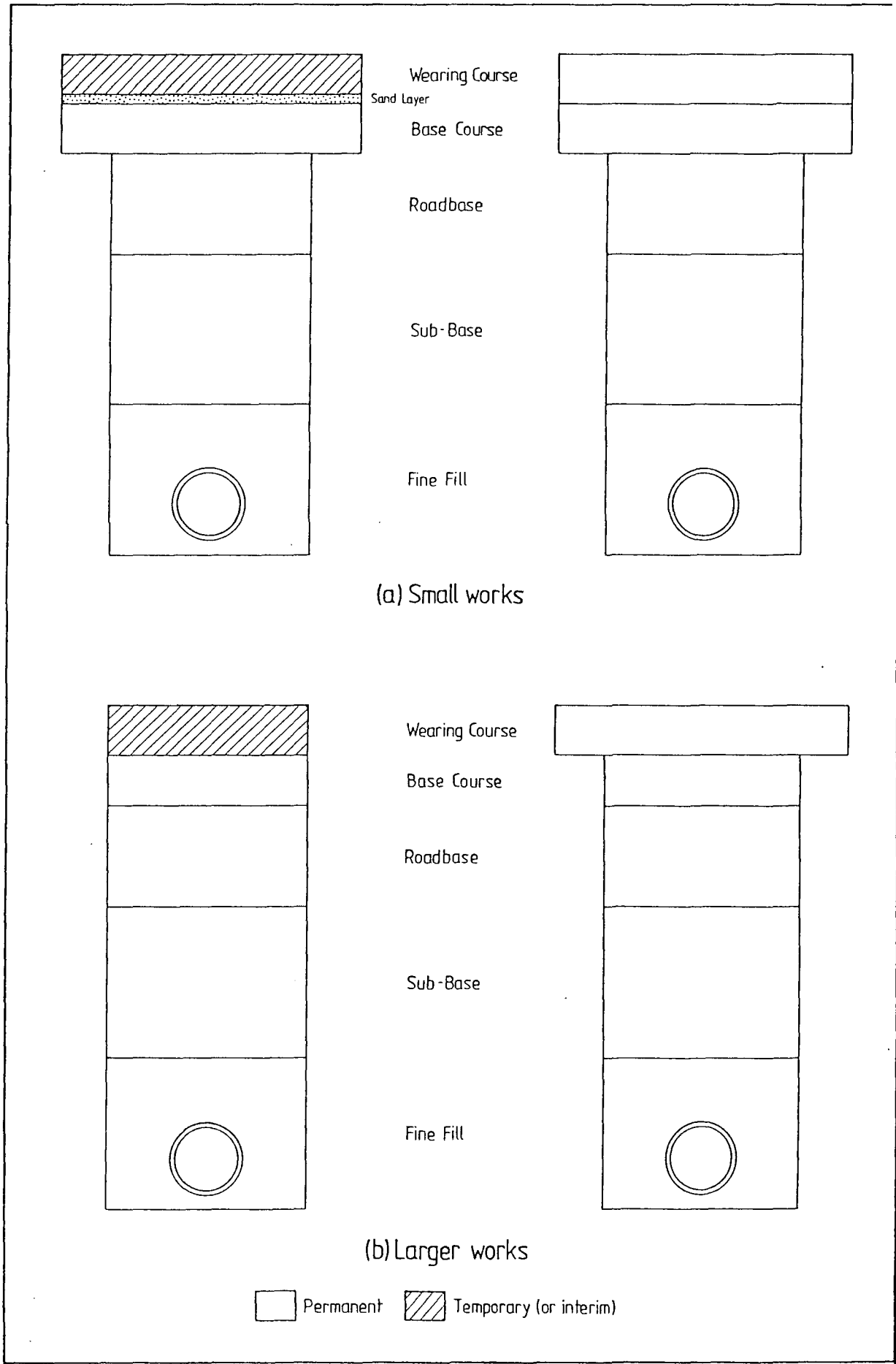

Figure 1.2 - The British Gas perception of reinstatement works in the light of possible future legislation based on the Horne Report recommendations; (a) for small works and (b) for larger works (after Rhodes *et al* 1987).

CHAPTER 2

COMPACTION THEORY, COMPACTION PLANT AND COMPACTION MEASUREMENT

2.1 Introduction

In this chapter the important areas of compaction theory and its corresponding laboratory measurement, as related to the determination of the dry density-moisture content relationship, are examined (Section 2.2). A brief examination of the study by Reid (1983) of the types of hand-held compaction plant available and their suitability and performance in terms of the reinstatement environment is given in Section 2.3. In Section 2.4 the current Department of Transport (1986) method and performance specifications for the compaction of road pavement materials are examined in the light of possible future trends. In Section 2.4 currently available methods of compaction measurement are described in relation to the potential performance of new works and also to the measurement of the stiffness and/or strength of existing road pavement structures. A number of devices and techniques are described in this section most proving to be inappropriate to the reinstatement environment. The Clegg meter, a device currently gaining increasing usage in the British Gas regions for the purpose of monitoring unbound reinstatement backfill quality during placement, is described in considerable detail in Section 2.4.1. This device has been used extensively to measure reinstatement backfill properties during the laboratory and field test programmes described in Chapter 6.

Section 2.5 summarises the work presented in this chapter.

2.2 Compaction theory and laboratory measurement

2.2.1 Compaction theory

In discussing the theory of compaction it is perhaps worthwhile detailing exactly what is meant by the term 'compaction' in soil mechanics. The Road Research Laboratory (1952) describes soil compaction as: *'the process whereby soil particles are constrained to pack more closely together through a reduction in the air voids, generally by mechanical means'.* The distinction can thus be made between the superficially similar process of consolidation, which may be seen as the process of

constraining the soil particles to pack more closely together through the expulsion of the pore water. A more fundamental approach to this distinction is to be had by considering, albeit at a very superficial level, the formulation of soil models to describe these phenomena; a model describing the behaviour of a soil undergoing compaction must describe the soil as a three-phase material (*i.e.* containing air and water voids and the soil particles), while one concerned with a soil undergoing consolidation need, in general, only describe the soil as a two-phase material (*i.e.* containing only water voids and the soil particles)[1].

As is hinted in the preceding definition, the level of compaction is generally measured in terms of the resulting dry density. Plainly the increase in dry density experienced by a given soil will depend upon the moisture content of the soil and on the amount of energy applied to the soil during compaction.

For any given compactive effort the relationship between the dry density and moisture content is far from simple. Figure 2.1 shows idealised dry density-moisture content relationships for three different compactive efforts with increasing energy, with lines of constant air content also shown—these assist in the explanation of the shape of the compaction curves. At low moisture contents the soil mass is stiff and difficult to compact due to the high degree of interparticular friction. As the moisture content is increased the soil flows with increasing ease, as the water acts as a lubricant resulting in decreasing levels of air voids and higher levels of dry density. As the moisture content is further increased a minimum value of air voids is reached, when all of the small, individual pockets of air within the pores of the soil become entrapped or surrounded by pore water, thus tending to prevent the particles from moving closer together. The total voids, however, continue to increase with the moisture content, and hence the resultant dry density of the soil decreases. At some point between these two extremes a maximum value of dry density is achieved at a moisture content which is described as optimum.

For increasing amounts of compactive effort the level of maximum dry density achieved will increase and the optimum moisture content will decrease[2], as is illustrated in Figure 2.1. However, it should be noted that a doubling of the compactive effort will not result in a doubling of the maximum dry density, as there is plainly

[1]Certain soil consolidation models, particularly those relating to the behaviour of gassy soils (such as some sea-bed sediments) will of necessity be three-phase in nature.

[2]The reasons for this effect are not entirely clear but are most likely associated with the higher compactive efforts overcoming interparticular friction more easily (*i.e.* at lower moisture contents).

a limiting value of dry density for any given soil (*e.g.* the density corresponding to tetrahedral packing in the case of a single sized granular material—Barnes, 1987). Data presented by Hogentogler (1938) from static pressure compaction tests indicated that the maximum dry density increases as a logarithmic function of the static compaction pressure, while the optimum moisture content decreases as a logarithmic function of the static compaction pressure.

2.2.2 Laboratory determination of the dry density-moisture content relationship

There are currently four British Standard tests for the determination of the dry density-moisture content relationship of soils and aggregates:

i) *BS 1377 (1975): Test 12—Determination of the dry density/moisture content relationship* (2.5 kg *rammer method):* The portion of the soil sample passing a 20 mm test sieve is compacted in three layers of approximately equal mass into a mould of dimensions 105 mm internal diameter, 115.5 mm internal effective height (1000 cm^3 volume) by means of a 2.5 kg drop-weight of 50 mm diameter circular face which is dropped from a height of 300 mm. 27 blows are applied to each layer.

ii) *BS 1377 (1975): Test 13—Determination of the dry density/moisture content relationship* (4.5 kg *rammer method):* This test is identical to Test 12 (see (i) above) except that the compactive effort applied to the soil is greater. This is achieved by increasing the height of fall of the rammer to 450 mm, the mass of the drop-weight to 4.5 kg and the number of layers to five.

iii) *BS 1377 (1975): Test 14—Determination of the dry density/moisture content relationship (vibrating hammer method):* The portion of the soil sample passing a 37.5 mm test sieve is compacted in three layers of approximately equal mass into a mould of dimensions 152 mm internal diameter, 127 mm internal effective height (*i.e.* a *CBR* test mould) by means of an electric vibrating hammer, having a rated power consumption of between 600 and 750 W and operating at a frequency of between 25 and 45 Hz. The vibrating rammer is fitted with a circular foot of 145 mm diameter which applies the compactive effort to the sample for a period of 60 seconds per layer.

iv) *BS 5835: Part 1 (1980)—Recommendations for testing aggregates (Compactibility test for graded aggregates):* The portion of the aggregate sample

passing a 37.5 mm test sieve is compacted in a single layer of dry mass between 2.4 and 2.6 kg into a mould of 150 mm internal diameter, by means of an electric vibrating hammer, having a rated power consumption of 900 W and operating at a frequency of around 33 Hz. The vibrating hammer is fitted with a special shank which applies the compactive effort to the sample, by means of an anvil placed on top of the sample, for a period of 180 ± 5 seconds. The effective height of the sample is measured after compaction by means of a depth gauge allowing the calculation of the volume of compacted material.

The above tests are all repeated for a sensible range of moisture contents and the base on to which the mould is securely mounted should have a high effective mass. Ray and Chapman (1954) indicate that an effective mass of at least 200 lb is desirable for (i) and (ii) above. In practice, however, the bases used for the above tests are generally bolted to concrete floors giving a very high effective mass for the base.

For the three tests to BS 1377 (1975) the bulk density (ρ) of the sample is calculated from the mass of compacted soil divided by the volume of the compaction mould; the moisture content (w) is determined by oven-drying a representative portion of the compacted material. The dry density (ρ_d) of the compacted soil is then simply calculated from the values of bulk density and moisture content [$\rho_d = 100\rho/(100 + w)$] . This method is described in more detail in Section 4.4.1.

For the BS 5835: Part 1 (1980) test the entire compacted sample is weighed and oven dried to determine the mass of dry aggregate and the mass of water contained in the aggregate after compaction. The volume of the compacted material having been measured (as in (iv) above) the dry density and moisture content may then be calculated directly from these results, as described in more detail in Section 4.4.4.

For each of the tests a smooth curve is drawn through the points (w, ρ_d) and the maximum dry density ($\rho_{d_{\max}}$) and corresponding optimum moisture content (w_{opt}) are determined. The lines representing zero, 5% and 10% air voids are then plotted for comparison, based on the specific gravity and water absorption value of the soil particles, as described in Section 4.4.1.

2.3 Compaction plant

Historically, a wide variety of methods has been used for compacting soil and road pavement materials. For instance Meehan (1967) presented a paper highlighting the inadequacies of elephants for use as 'compaction plant' in Asian countries. This was found to be largely due to the beasts' preference for re-tracing their own steps as opposed to stepping on the softer virgin ground between the older footprints.

Meehan's somewhat offbeat study plainly has little relevance to roadworks in the UK in the 1980's and still less to the compaction of trench backfill where the geometrical constraints preclude the use of large items of compaction plant. It is largely with these constraints in view that the discussion of compaction plant will proceed.

A detailed study of the performance of hand-held compaction plant has previously been undertaken by the British Gas Engineering Research Station (Reid, 1983) and it is proposed to present only a brief synopsis of that work here. The following is a summary of the basic characteristics of each of the hand-held compacters studied by Reid:

i) *Hand Rammer:* Performance is strongly operator dependent and will clearly decrease rapidly as the operator becomes tired.

ii) *Vibrating Plate:* These are generally considered unsuitable for work in all but the largest of trenches as the only machines to be produced of a suitably small scale are non-reversible, making handling in a reinstatement environment difficult.

iii) *Road Breaker-Tamper:* These can be either hydraulically or pneumatically powered. Operation of this plant requires the continual lifting and repositioning of the tamper foot (usually about 180 mm in diameter) to achieve compaction. This process is plainly physically tiring for the operator leading to progressively poorer compaction.

iv) *Pole-Tamper:* Similar criteria apply to this plant as for road breaker-tampers although the pole-tamper is lighter and less physically demanding.

v) *Vibratory Rammer:* These are self-advancing and extremely easy to steer and, although manhandling is often required to turn the plant at the end of the trench, the benefit of the excellent compaction characteristics of these machines usually outweighs this disadvantage.

Reid's studies of the relative performance of the varying types of compaction plant are expressed in terms of an achievable dry density of a sand material regardless of time and effort involved in achieving the results (Figure 2.2). Further considerations of the time, effort and cost involved in achieving these results led to the adoption of the vibratory rammer as the standard compaction plant used by British Gas in their reinstatement works, although pole tampers are often used to compact fill around pipes in narrow trenches and in other situations where access is restricted or damage to buried apparatus is a possibility. Figure 2.3, again drawn from Reid's 1983 report, shows the dry density-moisture content envelope obtained by massing the data from tests conducted over a range of moisture content's on the same sand material, with a variety of proprietory vibratory-rammers. The performance of these devices, on a given material at a given moisture content, is dependent upon the manufacturer's choice of blow energy, blow frequency and amplitude of the stroke in addition to the number of passes made by the operator. In the experimental work presented in Chapter 6 a specially constructed electrically driven version of the Wacker BS45Y vibratory rammer has been used to achieve the desired compaction levels.

In addition to the hand-held devices described above, the plant manufacturing company Bomag have recently released a new narrow vibrating roller, the Bomag BG100. This device incorporates advantages of large scale vibrating rollers, including the virtual absence of operator fatigue, by virtue of being controlled from a cab, while eliminating some of the disadvantages by operating from the existing road surface and dropping the vibrating roller into the trench, thus allowing easy insertion and removal for the compaction of the lower layers. Bomag claim that this machine is capable of compacting thicker trench backfill layers more quickly than can a conventional vibratory rammer (Anon, 1988e). A case study using the Clegg meter (see Section 2.4.1) to monitor the increase in the stiffness of the reinstated material during compaction by this machine is presented in Chapter 6.

2.4 Methods of compaction measurement

In general, civil engineering structures are designed on the basis of specification of the appropriate properties of the materials in use. In contrast, until recently, the design of flexible road pavements has been based almost entirely on experience. This experience was incorporated in a number of design procedures which, while being of

great value for the range of conditions which they encompass, are, like all empirical formulations, suspect when extrapolated outside their normal range. Perhaps the most widely accepted of these methods was the Road Note 29 method in which the thicknesses of the pavement construction layers were determined from the soil subgrade *CBR* value and the projected design life traffic loading on the completed structure (Road Research Laboratory, 1970).

As was seen in Section 1.2, the maximum axle weight allowed on British roads has steadily increased during the last 30 years; this, combined with the two-fold increase in the number of damaging heavy goods vehicle miles, has meant that in an increasing number of cases traditional design methods (*e.g.* Road Note 29; Road Research Laboratory, 1970) have become inappropriate. The design procedure which replaced the Road Note 29 method was based upon extensive full-size road experiments conducted at realistic traffic loadings, the results of research on mathematical modelling of pavement behaviour and also the simulated testing of road materials and pavements used to re-analyse the behaviour of the full-scale experiments and was described by Powell *et al* (1984). The design procedure described by Powell *et al* (1984) is often referred to as the LR 1132 design procedure. The work contained within LR 1132 has more recently been combined with the latest Transport and Road Research Laboratory research findings related to concrete (rigid) pavement design to create new design standards for road design (Department of Transport, 1987 and Scottish Development Department, 1987) in the UK.

Concurrent with the introduction of the LR 1132 document was a swing of support among the highway engineering community, away from the old method specification of the Blue Book (Department of Transport, 1976) towards the performance, or end result, specification. This resulted in the inclusion of some performance specifications in the latest edition of the 'Specification for Highways Works', or the Brown Book (Department of Transport, 1986). The Brown Book introduces performance specification only for the bound base course layer, leaving the method specification for unbound materials essentially unchanged (Nutt, 1987). A mean Percentage Refusal Density (PRD)[3] of 93% must be achieved with no absolute minimum for individual cores (Anon, 1987a); as a spread of ±2% of the PRD is typical, contractors must aim for 95% of the PRD (Powell and Leech, 1987). The minimum turn around time for the PRD test is around 33 hours (Loveday, 1987) and as such

[3]The PRD test is described in full detail in the Brown Book, Clause 927 (Department of Transport, 1986).

the specification allows the use of Nuclear (or Isotopic) Density Gauges (NDG) to reduce the likelihood of the failure of material which has already been overlayed (see below). As the PRD test is extremely slow and requires the cutting of cores of 150 mm diameter it is plainly far from ideal for controlling the compaction of the bound layers in reinstatement works.

Although the foregoing paragraph relates to the performance specification of bound materials, which is outside the scope of the research presented here, it is worthwhile to continue this exploration of compaction measurement methods with reference to testing techniques applied to both the bound and unbound layers in a road structure. Similarly, large-scale devices used to test existing full-scale road structures in order to estimate their potential for further service which, at least in their present form, are geometrically inappropriate to the reinstatement environment, will be examined to a limited extent. It is to be hoped that, by studying such techniques and apparatus, a broader understanding of the range of possible approaches to the more specific problem of compaction control in the unbound granular layers of a reinstatement environment may be achieved.

Perhaps the most obvious parameter which is used for compaction measurement is the dry density attained by the compacted material. Such measurement may be achieved by one of the sand replacement methods detailed in BS1377 (1975) [Test 15(A, B and C)] or by the use of an NDG. The former methods are cumbersome and slow, and require the further reinstatement of an excavated hole of a similar size to that required for the PRD test. The NDG uses the 'back scatter' technique, detecting scattered gamma photons beamed back from a caesium source and rebounding back through compacted pavement layers of maximum 100 mm thickness. Six Geiger-Müller detectors in the sensing unit pick up the rebounded photons. The use of these devices may, at the discretion of the Engineer, allow the reduction of the frequency of PRD testing from the usual rate of one test per 1000 m^2. These devices are easily portable by the operator, although roller mounted NDGs which are claimed to be capable of taking density readings every one to two seconds are currently being introduced by plant manufacturers (Anon, 1987b). Taking a typical roller speed to be, say, 7 km/hour this would equate to one reading every 2 to 4 m, a much higher reading rate than could be economically achieved by a single operator using the traditional portable device. Apart from requiring a high capital outlay[4]

[4]The cost of a portable Nuclear (or Isotopic) Density Gauge is around £7, 000 at 1987 prices.

the NDG requires highly trained and licensed operators. This of course neglects the damage that could be caused to the public image of a utility by advertising their use of isotopic sources, however low the potential radiation exposure levels may be, in the shopping and residential streets of our cities and towns.

On site measurement of the *CBR* value is a further potential measurement technique. This is unfortunately difficult, time consuming and costly to achieve, requiring a heavy vehicle to provide a reaction to the applied load; in addition it is impractical to test at levels much below the surrounding road surface level (say 300 to 400 mm). Laboratory measurements are often used to assess the *CBR* values which a properly compacted material may potentially achieve.

The Falling Weight Deflectometer measures the transient deflections (along a 2.4 m radial length) caused by the impact of a weight, dropped from a fixed height, with the road surface. Using prior knowledge of the road construction and layered elastic theory, Young's modulus values of the structure are computed. The fully vehicle mounted system has a cost, at 1987 prices, of around £90, 000 and is plainly economically unsuitable for the testing of individual reinstatements. The major use of this device would appear to be in assessing the remaining life and repair needs of significant lengths of pavements, the need for repair in some instances being influenced by the presence of sub-standard reinstatements.

The use of the Clegg meter for assessment of reinstated material is rapidly spreading in the British Gas regions. This device measures the retardation of a falling weight on impact with a reinstated surface and will be discussed in greater detail in Section 2.4.1.

It has already been noted that the Department of Transport (1986) has introduced a performance specification for bound granular materials. Nutt (1987) states: *'The Department is examining the possibility of applying end product tests to all earth works compaction'*, and presumably to the compaction of unbound granular pavement materials. *'The most promising method currently appears to be the Dynaplate ("La Dynaplaque") a French machine for measuring the elastic recovery of the soil'. 'La Dynaplaque'*, or The Dynaplate, characterises subgrade materials by means of the coefficient of energy restitution (Benoist and Schaeffner, 1982). The coefficient of energy restitution is defined as the ratio of the rebound height of a mass, dropped onto a circular plate *via* a set of springs, to the height from which the mass was dropped (*i.e.* coefficient of energy restitution, $R = H_r/H_0$). Although

suitable for the evaluation of full scale road construction works this device is vehicle mounted and too large in its current form for use in the reinstatement environment.

A further *in situ* dynamic test apparatus is under joint development by the geotechnical engineering consultants Geotechnics and Loughborough University (Anon, 1988f). This device is similar in principle to the Clegg Meter (see Section 2.4.1) and has been used to investigate the effects of drop-height (0–600 mm), hammer diameter (50–300 mm) and hammer mass (5–20 kg) on the results of the peak decelerations and time period of impulse measured in impact tests on granular materials (Boyce *et al*, 1989).

Compaction meters, which record the Compaction Meter Value (CMV), have been commercially available in Sweden since 1978 (Forssblad, 1982). Control is achieved by mounting an accelerometer on the central bearing of a vibrating drum roller, the signals from which are analysed with respect to the first harmonics of the vibration. When the material is soft and uncompacted the signal returned by the accelerometer is regular and sinusoidal with little or no harmonics. As the stiffness of the material is increased during the compaction process the signal becomes distorted with increasing harmonics with increasing stiffness. The readout presented to the operator is of an index scale representing an increased proportion of harmonics in the analysed signal from the accelerometer. Extensive *in situ* calibrations for each material are necessary to establish an acceptable CMV which is known to relate to an acceptable value of a parameter such as dry density. At least one major plant manufacturer (Sakai) states that their compaction meters are not suitable for controlling the compaction of silts, clays and bituminous materials. Clearly, vibrating drum rollers are unsuitable for use in the lower layers of a reinstatement where unbound granular materials, suitable for test by such devices, will be encountered.

The practice of fitting vibrating drum rollers with compaction meters has not been widely practised in the UK until very recently. The Brown Book, however, in addition to giving a performance specification for the compaction of bound granular materials, insists that vibrating drum rollers be fitted with devices that enable an engineer to read the frequency of vibration and the speed of travel at which the plant is operating. The major plant manufacturers Bomag see the requirements of the Brown Book as major motivating factors to plant manufacturers to develop and improve devices such as the compaction meter (Ferris, 1987).

2.4.1 The Clegg meter

Øverby (1982) describes the Clegg meter as essentially consisting of a modified compaction hammer fitted with a piezoelectric accelerometer. The output from this transducer is fed into a peak-hold meter where necessary filtering ensures that the peak reflects the retardation due to the soil's characteristics.

Studies of dynamic soil properties using falling weights fitted with accelerometers to monitor impact retardations and impact times were undertaken by Forssblad (1965) and later by Orrje and Broms (1970). Measurement of 'impact bearing capacity' by dropping weights on to plates such as those used for conventional, static plate bearing tests (Asai, 1960), and using a mechanical procedure for measuring the displacements, provided some interesting comparisons between the impact (dynamic) and static bearing capacities of soils. Later in the Sixties an attempt was made to modify the *CBR* procedure by dropping a 4.5 kg mass on a *CBR* plunger (Savage, 1963). In this case the height of drop was adjusted to give 25.4 mm (1 inch) penetration and this parameter was used as an indicator of strength.

It was not until later that experiments were carried out with accelerometers attached to laboratory compaction hammers. The heavy 4.5 kg hammer was found to be the most satisfactory for base course materials (Clegg, 1976). This work led to the development of the Clegg meter described in detail below and illustrated in Figure 2.4.

Some doubt exists as to whether the Impact Value determined by the Clegg meter is a measure of the stiffness or the strength of compacted materials. Clegg in his 1980 paper (see Section 2.4.1.3) states that the Clegg meter may be used to, *'observe stiffness differences'*, while in his 1983a and 1983b paper's Clegg describes the use of the Clegg meter to determine 'Target Strengths' for compacted materials in terms of the Impact Value (see Section 2.1.4.5). The indications are that the Impact Value is most likely a measure of both stiffness and strength in varying proportions depending on the state of the compacted material under test. With 'weak' or poorly compacted materials large penetrations of the drop weight are observed and the Impact Value is most likely to be predominantly a measure of strength. In contrast, with 'strong' or well compacted materials, small penetrations of the drop weight

are observed and the Impact Value is most likely to be predominantly a measure of stiffness.

Care must be taken when assessing Clegg meter-derived Impact Value results, because some research workers have used an alternative device manufactured in Italy. This device differs from the standard device, distributed in the UK by Trevor Deakin Consultants Ltd of Bath, in two ways. Firstly, under identical test conditions, the Italian device yields different values of the Impact Value from the standard device, and, secondly, the conversion recommended for the interpretation of Impact Values in terms of *CBR* values differs for the Italian device (see Equation 2.1; Section 2.4.1.4). Boyes and Robinson (1987) report that for a situation in which the standard device indicates a *CBR* value of 65%, the Italian device indicates *CBR* = 256%. Boyes and Robinson further report that Dawson and Thom (1988) are among the research workers to have used the Italian version of the Clegg meter in order to obtain relationships between Dynamic Cone Penetrometer readings and Impact Value.

2.4.1.1 Construction

The Clegg meter consists of a standard 4.5 kg laboratory compaction hammer with an internally mounted piezoelectric accelerometer and a rigid handle attached to the top face of the drop-weight. The method of attachment of the handle is such as to minimise the effect of resonance on the accelerometer output (Clegg, 1976). A circumferential mark inscribed on the drop-weight lines up with the top of the plastic guide tube to indicate the height of drop, which is around 450 mm as for the British Standard 4.5 kg rammer compaction test (BS 1377, 1975: Test 13)[5]. In addition to controlling the drop-height, the guide tube, as its name suggests, acts as a guide to ensure that for successive drops the drop-weight strikes the same area of the soil surface. The base of the guide tube is recessed and rests on the ground only around its perimeter, thus avoiding the application of any surcharge where the hammer strikes the ground surface. A detachable coaxial cable connects the accelerometer within the drop-weight to the hand-held processing and recording instrument. A centrally-located automatic reset button discharges the previous signal as well as acting as an on/off switch. The box contains the necessary solid state circuits to

[5]Drop weights of different mass are available for the Clegg meter (500 g, 2.5 kg and 20 kg). these being described in more detail by Clegg (1985).

adjust and filter the incoming signal and remove unwanted frequencies resulting from resonance of the accelerometer and drop-weight and crushing and displacement of individual soil particles. The output is fed to a digital display which indicates the Impact Value, IV (*n.b.* $1\,IV = -10\,\mathrm{g}$; Clegg, 1977). Two 9 V dry cells provide the power necessary to drive the electronic circuits. For transport purposes a pin secures the hammer in the guide tube, so allowing the complete instrument (with the readout meter clipped to a bracket on the guide tube) to be carried by the handle which forms an integral part of the guide tube.

2.4.1.2 Calibration

Field calibration of the Clegg meter, as distinct from its initial electronic calibration, is facilitated by a plastic ring supplied with the instrument. This ring is placed on a solid surface such as a concrete floor and the hammer dropped as in a normal test. The Impact Value so recorded must be checked from time to time. During the experimental work presented in Chapter 6 such calibrations were carried out prior to the commencement of each test (*i.e.* approximately every forty determinations of the Impact Value).

2.4.1.3 Operation and test mechanism

The operation of the Clegg meter is simple and, although ideally a two man operation, a single operator can work at a satisfactory rate. The operation of the device is as follows:

i)loose material is removed from the surface to be tested,

ii)the instrument is placed in position and the guide tube held vertical and in position by the operator's foot,

iii)the hammer is raised so that the circumferential mark on the hammer surface and the top of the guide tube coincide to within ± 10 mm,

iv)the reset button on the readout meter is held in the down position,

v)the hammer is dropped, the Impact Value recorded and the reset button released,

vi)steps (iii) to (v) are repeated five times, and

vii)the Impact Value, IV, is taken to be the average of the fourth and fifth readings at any given test point.

Early reports on the Clegg meter (Clegg, 1976) indicated that the Impact Value should be taken when a reasonably steady value of the impact reading was observed, or, alternatively, when sufficient readings had been obtained to establish an increasing or decreasing trend; not more than six blows were recommended. However, in his 1980 paper Clegg recommends that the operator takes the reading from the fourth blow as the Impact Value. The present author's experience with the Clegg meter indicates that taking the mean of the fourth and fifth readings as the Impact Value yields more consistent results, by halving the effect of erroneous readings, while not significantly altering the mean of a number of separate determinations compared to Clegg's 1980 recommendation. This effect is especially pertinent for materials with low *CBR* value (*i.e.* materials of uniform grading).

The mean of the fourth and fifth impact readings has been taken as the Impact Value for the experimental data presented in Chapter 6.

With respect to the mechanism of the impact, Clegg (1980) states: *'The fact that the Impact Value increases with successive blows appears to be inconvenient but in some respects it is essential to the technique. Should the surface be so strong that there is virtually elastic rebound from the first blow it is more difficult to observe stiffness differences. The desirable mechanism appears to be that a wad of compacted material is projected into the body of the material. The first one or two blows flatten and compact. Too many blows pulverise and loosen the immediate surface or may continue to densify the material'.* Thus, taking the Impact Value to be either the fourth reading or the mean of readings from the fourth and fifth blows, the above undesirable effects should be avoided.

The depth to which the underlying soil affects Impact Value is of patent importance. Mathur and Coghlan (1987) indicate that the depth of underlying material which influences the Impact Value is at least 300 mm, although it is important to note the large differences in the stiffnesses of the two bases ('soft soil' and concrete) which were chosen for comparison.

2.4.1.4 Relationships with other parameters

Tentative relationships between Dynamic Cone Penetrometer readings in mm/blow and the Impact Value have been developed from experimental data by both Øverby (1982) and Dawson and Thom (1988), and in addition Øverby also developed a relationship between Benkelman Beam deflections and the Impact Value.

Clegg's original research concentrated on observations in relation to different materials at varying densities and moisture contents (Clegg, 1976), pavement performance observations and compaction control (Clegg, 1977). However, evidence began to accumulate that a correlation with *CBR* would be obtained. In his 1980 paper Clegg presented the following relationship:

$$CBR = 0.07(IV)^2 \qquad (2.1).$$

This was a development of an earlier relationship published in Clegg's 1977 paper ($CBR = 2.5IV - 25$ for $CBR > 30\%$). Lees and Bindra (1982) claimed to have substantiated this earlier relationship although their paper included no evidence to support their claim. Mathur and Coghlan (1987) while in agreement with the general form of Equation 2.1 ($CBR = K.IV^2$) show that the value of the constant K may vary for different types of material. Their results indicate that K varies between 0.062 for a 'Well graded silty gravel (GW–GM)' and 0.08 for an 'Inorganic clay of low plasticity (CL)'.

Clegg (1983a) developed a theoretical equivalent to the empirical relationship, between Impact Value and California Bearing Ratio, given by Equation 2.1. Clegg observed that the deceleration-time response of the drop-hammer on impact with the ground surface could be approximated to a sine wave with a duration of one-half of a full wavelength. Integrating this curve, and assuming that at zero time (just prior to impact) the velocity of the drop-hammer could be simply calculated from Equations of Motion (*i.e.* $v_0 = \sqrt{2\,gH} = \sqrt{2 \times 9.81 \times 0.45} = 2.971$ m/s) the velocity-time curve was derived. Further integration of the velocity-time curve gave the penetration-time response for the impact. The force-time relationship was evaluated by considering Newton's second law of motion (force = mass × acceleration). The force-time and penetration-time responses were combined to give a force-penetration curve and by comparing this curve to those given for the purpose of evaluating the *CBR* value from static force-penetration data (BS 1377, 1975: Form S) a value of *CBR* was obtained (at 1 mm penetration) equivalent to a particular value of peak retardation. Repeating this procedure for a number of curves of different peak retardation values, a theoretical relationship was derived between the Impact Value and *CBR* value:

$$CBR = 0.10(IV)^2 \qquad (2.2).$$

The various relationships obtained for the *CBR* value in terms of the Impact Value by Clegg (1977, 1980 and 1983a) and Mathur and Coghlan (1987) are shown in Figure 2.5.

2.4.1.5 The practical value of the Clegg meter

The Clegg meter is currently gaining increasing usage for reinstatement evaluation with the utilities. Although the Clegg meter represents a significant advance in compaction evaluation, some problems associated with its use are as follows:

i)the Impact Value is highly sensitive to the presence of large stones at, or near, the surface and is markedly increased in such a situation,

ii)the volume of material tested is small in relation to the volume of compacted material and considerable uncertainty exists with regard to the depth of underlying material which affects the Impact Value, and

iii)testing should be carried out at the surface of each compacted layer; thus each layer must be individually tested prior to the placement of the next layer. Also the effect of the placement of the subsequent layer is neglected.

Clegg (1983b) demonstrates the potential of the Clegg meter for identifying areas of poor compaction by very rapidly 'scanning' large areas, on a uniform grid, and plotting contours of constant Impact Value. The area which Clegg examined was around 2000 m^2 and was covered on a 10 m grid with around 250 tests which were claimed to have been completed by one person in around a half day. Similar data, although one-dimensional, was also presented by Yoder *et al* (1982).

In his 1983a and 1983b papers Clegg also discusses the use of the Impact Value to determine a 'target strength' in order to control compaction. Comparing dry density-moisture content relationships for a Laterite Gravel and a Fine Crushed Rock, Clegg showed that a similar Impact Value-moisture content relationship could be obtained, from tests in a *CBR* compaction mould, with the maximum Impact Value occurring at a moisture content corresponding to around 98–99% of maximum dry density. Clegg suggested that the maximum Impact Value so achieved could be used in the field as a target also to be achieved during the compaction of materials as road sub-bases. Impact Value-moisture content data are also given by Freer-Hewish (1982) although the data presented by this author is in the form of iso-Impact Value contours and as such the point of maximum Impact Value, corresponding to any given level of compactive effort, is not determinable (see also Toll *et al*, 1987).

Detailed procedures for the use of the Clegg meter are given by Clegg (1985).

2.5 Summary

In this chapter the generally accepted mechanisms which govern the compaction of granular materials have been studied and the four current British Standard laboratory test methods for determining the dry density-moisture content relationship have been identified and described (Section 2.2).

The suitability of hand-held compaction plant for usage in the reinstatement environment has been discussed in the light of Reid's 1983 study. The vibratory rammer was identified by Reid as the most suitable type of compaction plant for the compaction of unbound granular materials in the reinstatement environment (Section 2.3).

Several of the methods of compaction evaluation and control that are currently, or may soon be, available to the highway engineer have been examined (Section 2.4). Some of these lend themselves equally to usage in the reinstatement environment (*e.g.* the Clegg meter) and to the full-scale highway construction environment; most however do not. The Clegg meter has been examined in considerable detail in Section 2.4.1 and has been used extensively in the experimental work described in Chapter 6. The foregoing discussion has naturally been selective, because a complete review of the possible methods of compaction measurement and control would indeed be a large task; the interested reader is referred to Kennedy (1982). The current Specification for Highways Works (Department of Transport, 1986) implements method specifications for the compaction of unbound materials; the current trend in Highway Enginering is, however, towards performance specifications. It is hoped that the range of possible approaches to the solution of the control of reinstatement backfill quality by performance specification have been highlighted. The current situation regarding reinstatement backfill quality control can be seen to be far from ideal. The characteristics of the ideal *in situ* test, on which a performance specification might be based, can be summarised as follows:

i)a minimum of disturbance should be caused to the reinstated material,

ii)it should be possible to carry out the test from the surface of the reinstated unbound granular layers,

iii)it should be possible to define the properties of the reinstated material as a function of depth, and

iv)the test procedure should be simple and quick.

The measurement of seismic wave transmission velocity is a potential measurement technique which may satisfy the above requirements. The various seismic wave transmission techniques available, with excitation of either transient or sinusoidal form, are discussed further in Chapter 3.

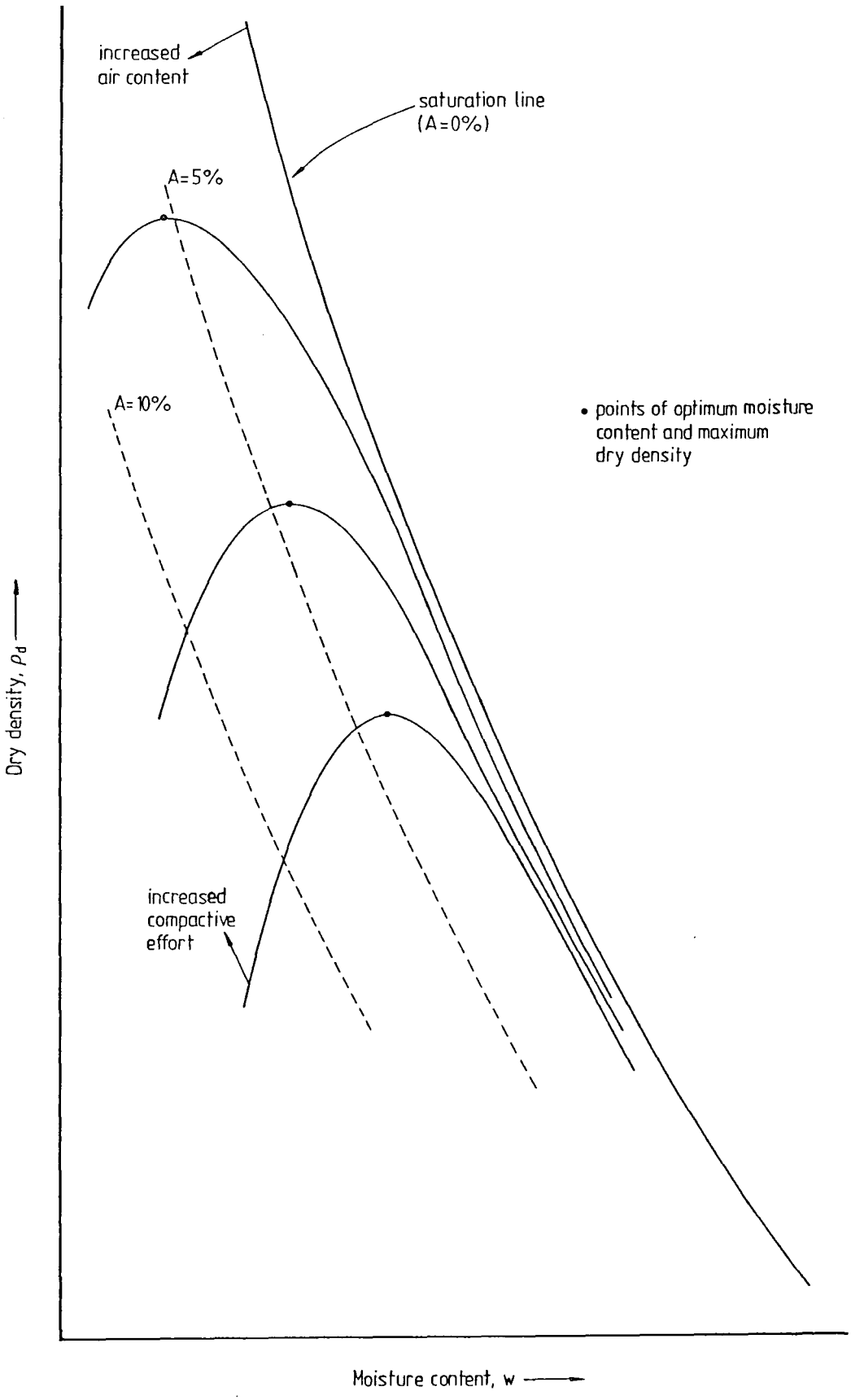

Figure 2.1 - Idealised dry density-moisture content relationship. Compaction curve for three levels of compactive effort are shown with the lines of constant air void for $A = 0$, 5 and 10%.

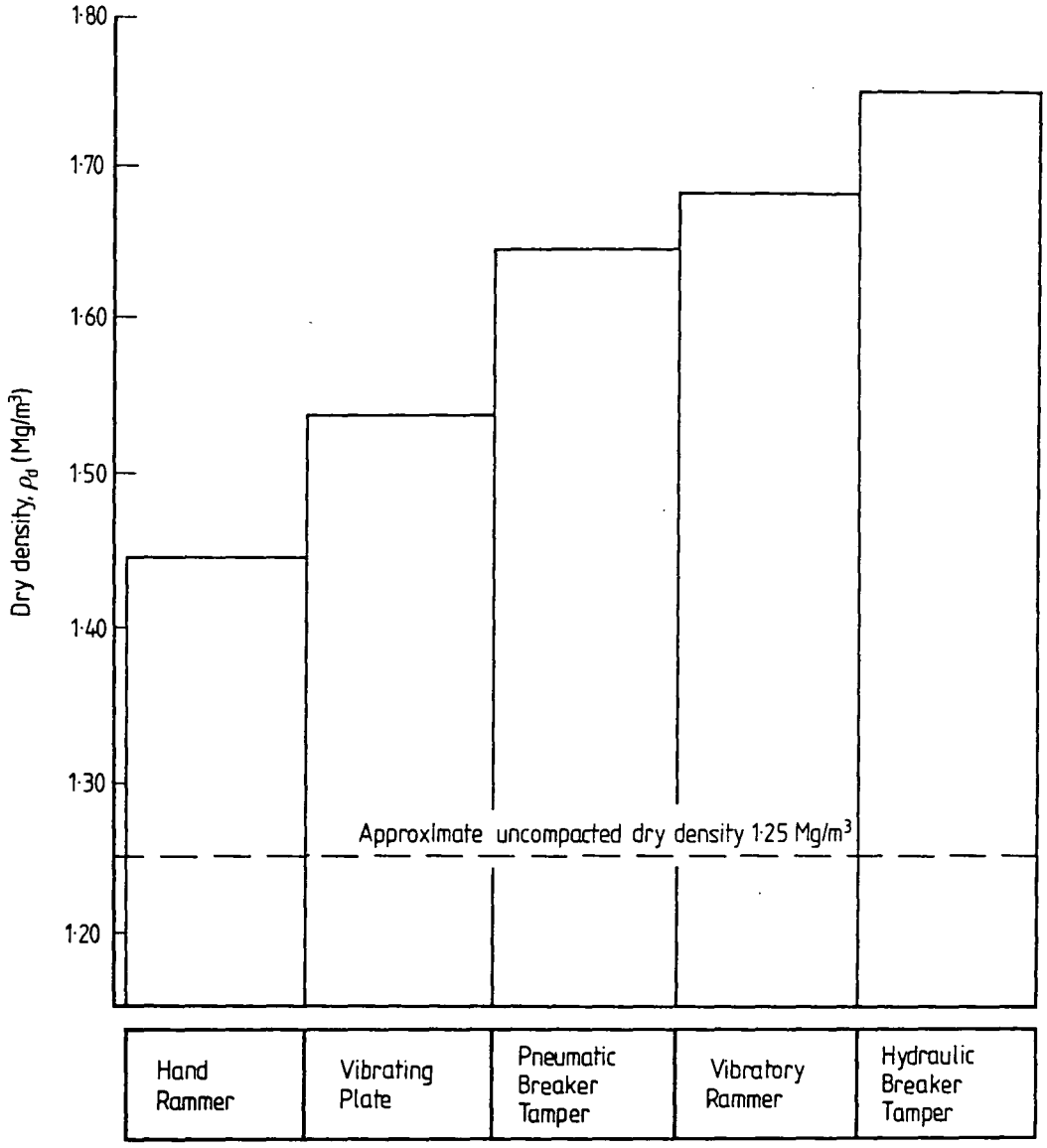

Figure 2.2 - Post-compaction dry densities, achieved by a variety of hand-held compactors on a sand material, regardless of the time and effort involved (after Reid, 1983).

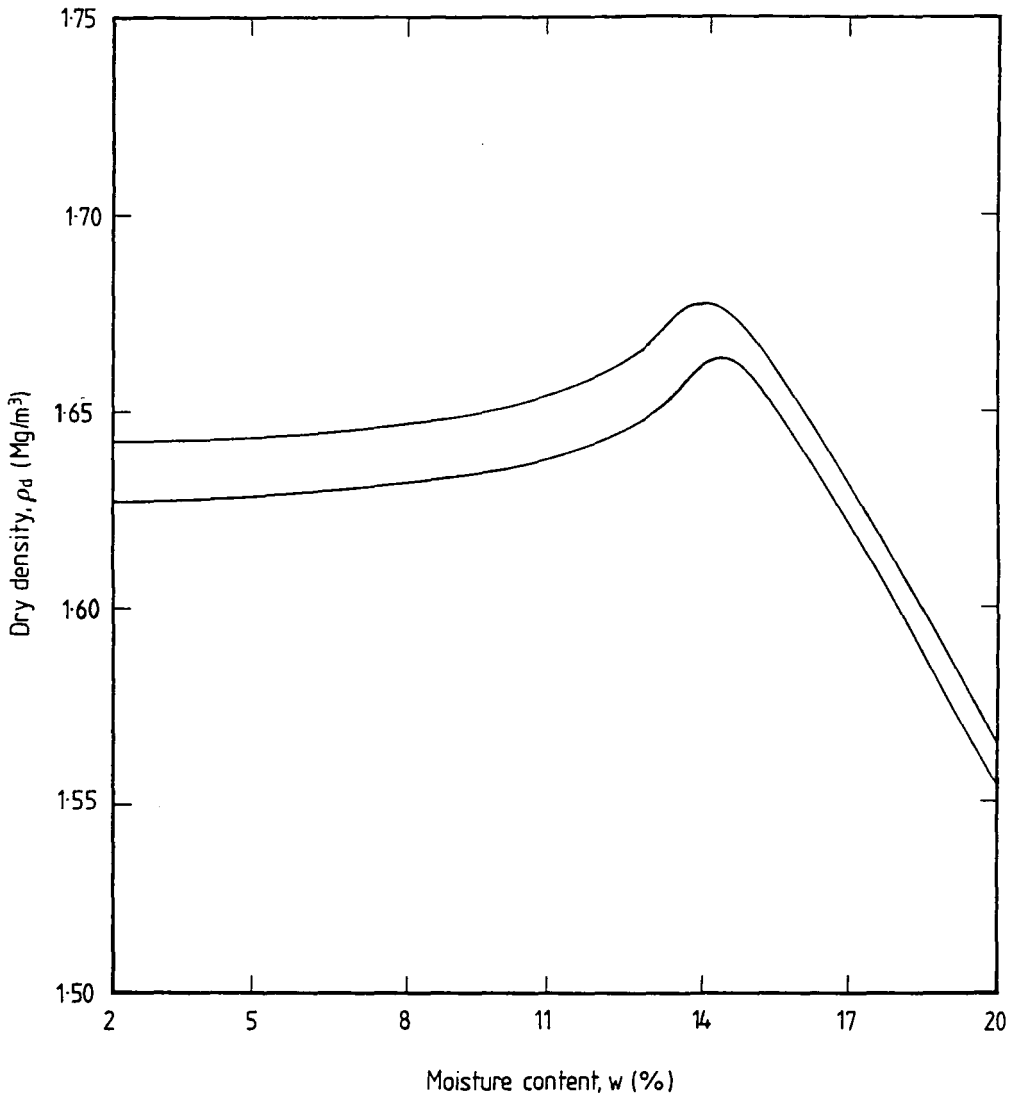

Figure 2.3 - Dry density-moisture content envelope achieved by combining data achieved using a range of proprietry vibratory rammers; 300 mm layers, 10 passes/ layer; sand material (after Reid, 1983).

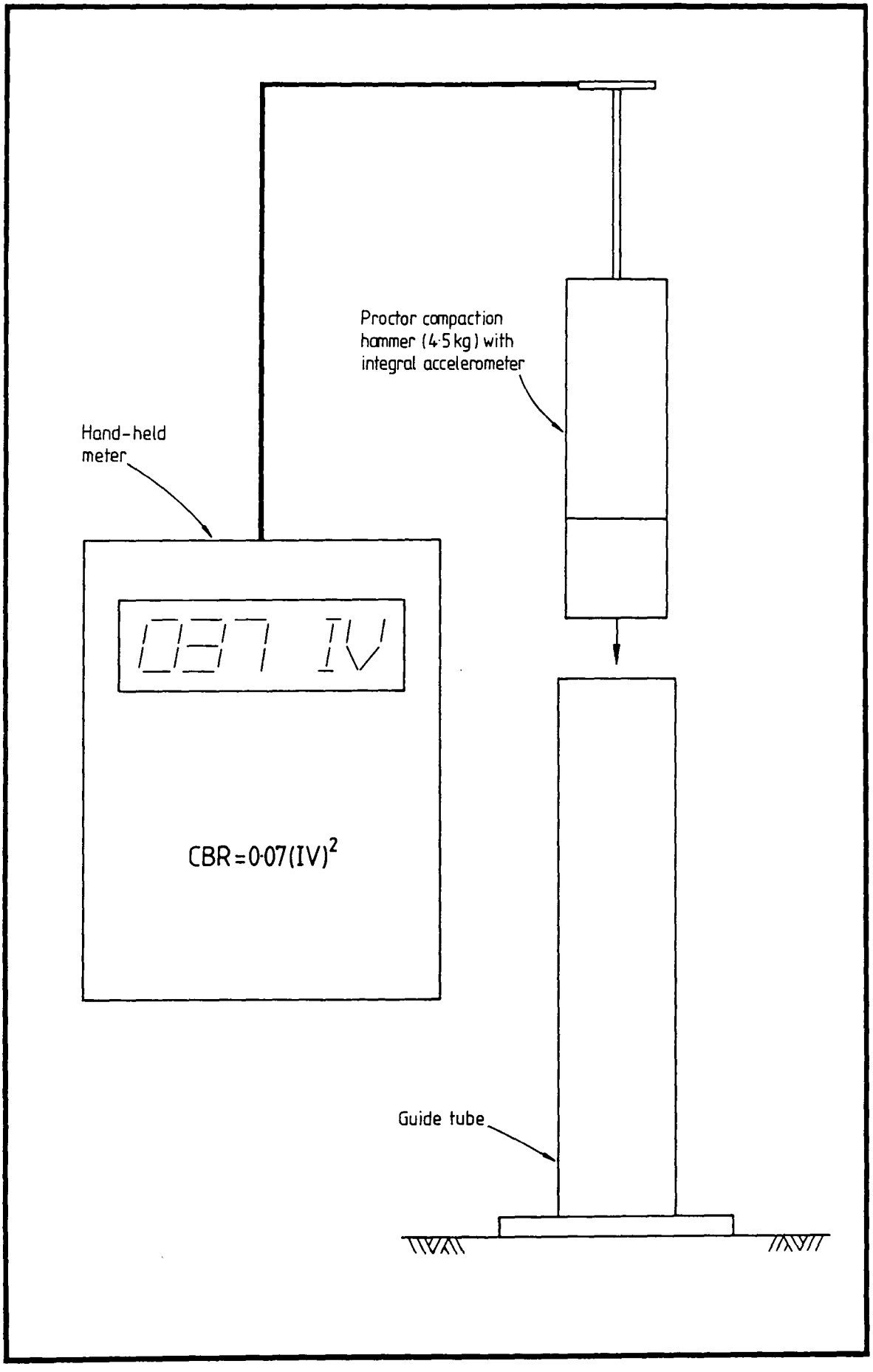

Figure 2.4 - Schematic diagram of the Clegg meter showing the salient features of construction and operation.

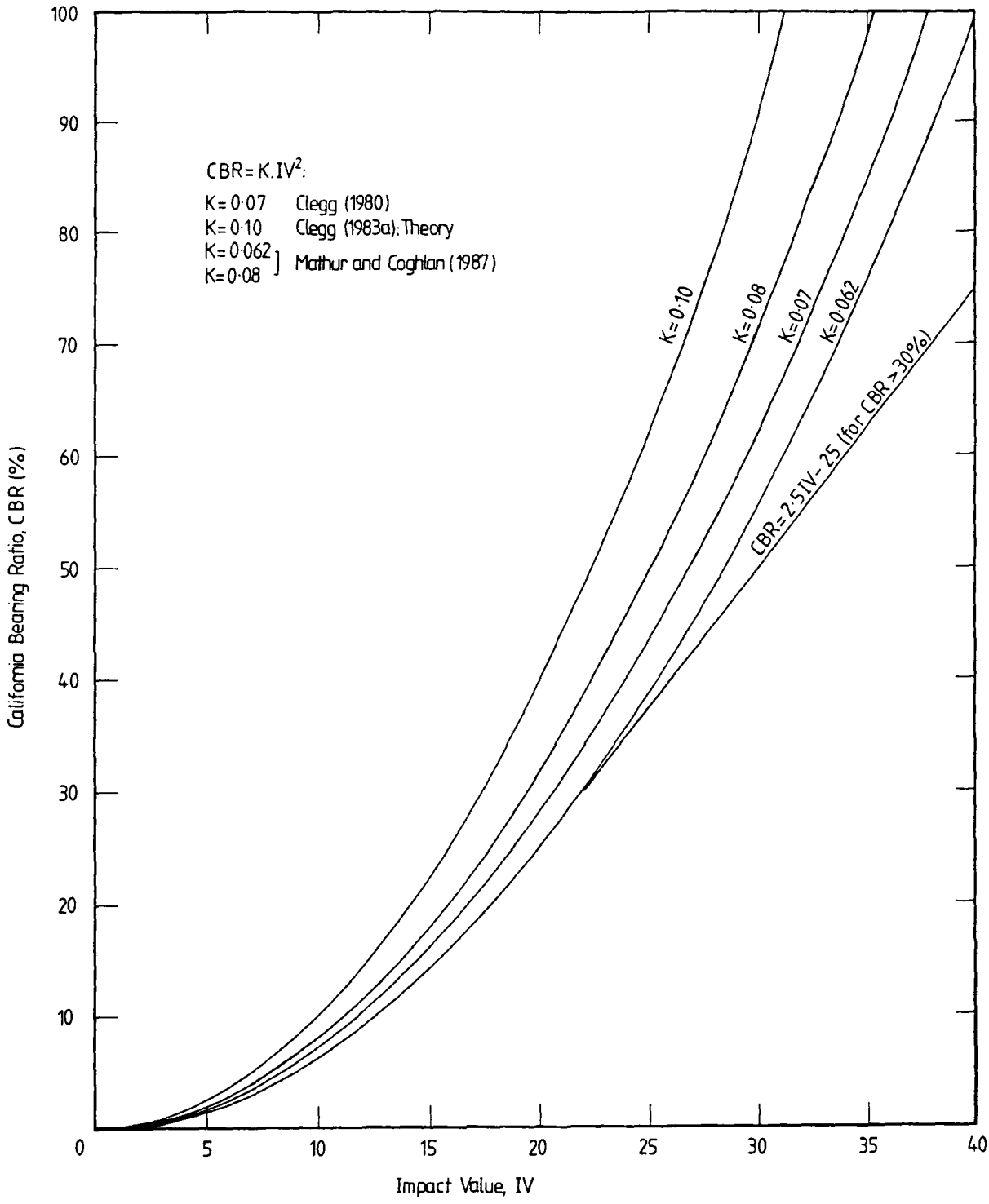

Figure 2.5 - Comparison between the Clegg (1977 and 1980) and Mathur and Coghlan (1987) relationships for California Bearing Ratio (CBR) in terms of the Impact Value (IV).

CHAPTER 3

WAVE MECHANICS AND MEASUREMENT TECHNIQUES

3.1 Introduction

In this chapter the various seismic wave types available for measurement purposes are described (Section 3.2). The detailed techniques used by previous research workers for the selected sinusoidally excited Rayleigh-type surface wave propagation method are discussed in Section 3.3, while in Section 3.4 emphasis is placed upon the presentation of the relevant theory pertaining to Rayleigh waves. Finally a review of the Rayleigh-type surface wave velocity data obtained by previous workers is presented in Section 3.5.

The term "Rayleigh wave" is used when considering theoretical aspects of pure Rayleigh waves while the term "Rayleigh-type surface wave" is used when considering experimentally generated Rayleigh waves which may be corrupted by such factors as boundary conditions. The term "Surface wave velocity" is used to annotate graph axes and in the text of Chapters 6 and 7 in place of the term "Rayleigh-type surface wave velocity", purely for the sake of brevity.

Throughout this chapter and the remainder of this thesis the directional notation illustrated in Figure 3.1 is used; x, y and z are the mutually perpendicular directions (z is vertical) from the source of any waveform and u, v and w are the corresponding particle displacements in these directions. It follows, therefore, that $\dot{u}, \dot{v}$ and $\dot{w}$ are the corresponding particle velocities and $\ddot{u}, \ddot{v}$ and $\ddot{w}$ the corresponding particle accelerations.

3.2 Types of seismic wave

In selecting a technique suitable for the measurement of the wave velocity of material compacted in a reinstated excavation, from the ground surface as a function of depth, it is immediately apparent that there is a variety of techniques available which may be drawn from the field of Engineering Geophysics. There are essentially four wave types which may be propagated due to a seismic disturbance, either transient or sinusoidal, in elastic, isotropic, homogeneous ground. The four wave types may be grouped into two categories:

i)Body waves, which propagate as spherical wave fronts from the source, may be either;

a)Longitudinal (or P-) waves, or

b)Transverse (or S-) waves,

i)Surface waves, which travel at shallow depths along the ground surface (*i.e.* as a cylindrical front), may be either;

c)Rayleigh waves, or

d)Love waves.

These waves are described further in the following sections.

3.2.1 Body waves

3.2.1.1 Longitudinal waves

These are also known as primary, compression or irrotational waves.

Consider plane waves travelling in the direction of the x-axis (Figure 3.1). Longitudinal waves cause the particles of the medium to vibrate back and forth in the direction of propagation, *i.e.* the x-direction (Figure 3.2a). The regions labelled A are regions of compression and as a result the density of the material is slightly greater here. The parts of the figure indicated by B are regions of rarefaction and they represent regions of decreased density. Waves of this type can be propagated in media having volume elasticity, *i.e.* all types of media.

The velocity of propagation, v_P, of a longitudinal wave is given by

$$v_P = \sqrt{\frac{\Lambda + 2G}{\rho}} \tag{3.1}$$

where:

Λ is Lamé's first constant,

G is the shear modulus ($= \mu$ or Lamé's second constant), and

ρ is the density.

The velocity of propagation of longitudinal waves is faster than that of any of the other wave types.

3.2.1.2 Transverse waves

These are also known as secondary, shear or equivoluminal waves.

Consider, again, plane waves travelling in the direction of the x-axis (Figure 3.1). For transverse waves the particles vibrate in a direction perpendicular to that of propagation. In practice the motion due to transverse waves is resolved into components parallel to and perpendicular to the ground surface which are known as SH- and SV-waves, respectively. Figure 3.2b shows the particle motions induced by the propagation of the horizontal component of a transverse wave (SH-wave). The velocity of transverse waves varies between 40% and 70% of the longitudinal wave velocity through the same medium. A unique characteristic of these waves is that they have no regions of rarefaction. In other words, there are no local fluctuations in density such as may occur in other types of wave. Waves of this type can be propagated in media only where there is shear elasticity, *i.e.* in solids only. The velocity of propagation, v_S, of a transverse wave is given by

$$v_S = \sqrt{\frac{G}{\rho}} \qquad (3.2).$$

3.2.2 Surface waves

3.2.2.1 Rayleigh waves

Rayleigh waves are the resultant waveform of a significant portion of the energy dissipated from a vertical, sinusoidal oscillation at the surface of a semi-infinite elastic medium (Table 3.1). Nettleton (1940) describes the particle motion as a: *'combination of longitudinal and vertically polarised transverse vibration'*. A retrograde elliptical motion of the medium is thus produced, with the major axis of the ellipse almost perpendicular to the surface and the minor axis almost parallel to the surface and the direction of propagation. Barkan (1962) presented experimental data which went some way towards confirming the retrogressive, elliptical particle motion due to Rayleigh waves. The mode of propagation for Rayleigh waves is illustrated in Figure 3.2c. The amplitude of the motion decreases exponentially as the depth below the surface increases (Section 3.4.3). At a depth of one wavelength below the surface the amplitude of vibration is generally less than 10% of that at the surface giving rise to the relation, $z = \lambda/2$; where z is the depth of propagation and λ is the wavelength. This approximation is discussed further in Sections 3.3 and 3.4.3.

The velocity of propagation of a Rayleigh wave, v_R, is given by

$$v_R = f\lambda \tag{3.3}$$

where f is the frequency of the vertical, sinusoidal oscillation.

This relation is developed in Section 3.4.1. The Rayleigh wave velocity will be shown to approximate to within 10% of the shear wave velocity making estimates of elastic moduli a relatively simple matter (Section 3.4.2).

3.2.2.2 Love waves

Love waves have been described as horizontally polarised sinusoidally excited transverse waves trapped in a superficial layer overlying a semi-infinite elastic solid and propagated by multiple total reflections (Ewing *et al*, 1957). The velocity of propagation of Love waves depends on the wavelength and varies between that of transverse waves in the surface layers (approached as $\lambda \rightarrow 0$) and that of transverse waves in the lower layers (approached as $\lambda \rightarrow \infty$). The mode of propagation for Love waves is illustrated in Figure 3.2d.

Although the theory for Love waves is marginally more tractable than that for Rayleigh waves comparative experiments by Jones (1960) indicated that there appears to be no convenient relation for the depth of propagation of Love waves as there is for Rayleigh waves.

The velocity of propagation of Love waves, v_L, is given by

$$v_L = f\lambda \tag{3.4}.$$

3.2.4 Selected experimental wave transmission technique

In most geotechnical environments Gibson-type soil formations are encountered, in which stiffness and strength increase with depth below the surface. In the case of a reinstated excavation in a road pavement it is possible that the reverse of the Gibson-type formation may be found, as the upper layers of the structure are designed to be more stiff than the lower layers in order to spread the applied stresses efficiently. Transverse waves, in particular those which are horizontally polarised, are particularly suited to measurements on Gibson-type soil formations. Kurzeme (1972) adopted an unusual method of generating horizontally polarised shear waves (SH-waves)—a sinusoidal excitation by a torsionally driven exciter. Abbiss (1983)

notes that: *'where a high velocity layer overlies a layer with a lower velocity the high velocity zone may be missed out altogether with a consequent error in the depths for subsequent layers'.* Longitudinal wave propagation techniques may be similarly ruled out due to the strong dependence of the resultant modulus on the Poisson's ratio (Equation 3.15—Section 3.4.2). The Poisson's ratio is a notoriously difficult parameter to measure reliably.

Transient source excitations in general are more difficult to handle experimentally than are sinusoidal source excitations. Again quoting Abbiss (1983): *'if a material exhibits viscoelastic properties then the pulse velocities will differ from the velocities of continuous wave derivations which correspond to the elastic case'.* Some research has been carried out on transiently excited Rayleigh-type surface waves, in particular for the purpose of obtaining data for liquefaction studies (Stokoe and Nazarian, 1985). Appraisal of the data so acquired was by spectral analysis of the resulting time-domain records. Sinusoidal wave propagation techniques are described for Rayleigh-type (vertical polarisation) and Love-type (horizontal polarisation) surface waves in some detail by Jones (1958). The convenient relation for the depth of propagation of Rayleigh waves (Section 3.2.2.1) led to the sinusoidal wave propagation technique, similar to that described by Huekelom and Foster (1960), being adopted for use in the experimental work presented in Chapter 6. The following section examines the basic sinusoidal excitation Rayleigh-type surface wave propagation technique and also some of the variations of the technique used by previous workers.

3.3 Measurement techniques for Rayleigh-type surface waves

Several research workers have used the propagation of sinusoidal, vertical surface waves, believed to approximate to Rayleigh waves, to measure the transmission velocity of earth and road pavement materials as a function of depth. The basic requirements of the method are;

i)a vertical oscillating source to apply a sinusoidal loading to the ground surface at a known frequency,

ii)a fixed reference point at which the applied waveform is monitored (either a transducer or the oscillator, in (i) above, may be used),

iii)a transducer which may be moved along a radial axis from the oscillator, and

iv)means of measuring the separation of the reference point and transducer, in (iii) above, and the phase angle between the two signals monitored at these points.

The theory governing the propagation of Rayleigh waves will be examined in some detail in Section 3.4, but for the time being it is sufficient to note the results of this theory relevant to the measurement technique under discussion here. The Rayleigh wave velocity is given by Equation 3.3 ($v_R = f\lambda$) while the wavelength is given by the straight line equation (see Section 3.4.1):

$$\lambda = \frac{2\pi}{\phi} d \tag{3.5}$$

where:

ϕ is the phase angle between the signals monitored at a fixed reference point and a second point on the same radial axis from the vertical source of oscillation, normally plotted on the y-axis, and

d is the separation distance between the above two points, normally plotted on the x-axis.

From Equation 3.3 it can be seen that in order to determine the Rayleigh wave velocity both the frequency of the input signal and the resulting wavelength must be measured. The input frequency is usually controlled by means of a power amplifier with some form of digital counter to allow fine-tuning of the frequency. Equation 3.5 demonstrates that by successively measuring the separations and corresponding phase angles between the signals at two points on a radial axis it is possible to estimate the wavelength (from the slope of the straight line plot of d against ϕ) and thus describe the velocity of propagation[1]. There are two distinct approaches which may be taken to measuring the wavelength; either the separation of the reference points may be fixed and the phase angle measured or the phase angle fixed and the corresponding separation of the reference points measured. Most previous workers have adopted the former approach. However the measurement of absolute phase angles was shown by Gent (1985) to lead to uncertainties in the interpretation, particularly as there may be no indication of the number of whole wavelengths between the two reference points. More simply, a measured phase angle of, say, 0.1π radians may indicate a true phase angle of 0.1π, 2.1π, 4.1π radians, ..., etc., depending

[1]A full proof of Equations 3.3 and 3.5 is presented in Section 3.4.1.

upon the number of whole wavelengths between the reference point and measurement point. Many workers taking the latter approach have used a single transducer to monitor the waveform (these include Nijboer and van der Poel, 1953; Jones, 1958 and 1960; Fry, 1963 and 1965; Maxwell and Fry, 1967). The oscillating source is taken as the first reference point and the original sine-wave signal from the oscillator suppressed so that all that remains is a spike once every cycle. This signal is added to the sine-wave signal from the transducer and, thus, when displayed on the screen of a Cathode Ray Oscilloscope (CRO), a sine-wave signal appears with a spike once every cycle. Moving the transducer away from the oscillator on a radial axis the points can be found where the spike corresponds to the peaks and troughs of the sine-wave (*i.e.* $\phi = 0,\ \pi,\ 2\pi,\ 3\pi,\ 4\pi, \ldots$, etc.) and plotted with the corresponding measured separations to give an estimate of the wavelength from the slope of the resulting straight line plot.

It has been observed (Jones, 1960 and Gent, 1985) that at positions close to the oscillator (< 1 m) the measured wavelength is somewhat less than that measured further from the oscillator on the same axial radius. This may possibly be due to the presence of poorly damped longitudinal and transverse body waves close to the source.

This problem is simply solved by using a second transducer, placed at a distance of 1 m or greater from the oscillator, as a first reference point. This approach has been used by both Bergström and Linderholm (1946) and Abbiss (1983). Bergström and Linderholm also describe a simple technique for measuring the phase angle between the two signals received by the transducers. Applying one signal to the horizontal deflecting plates of a CRO and the other to the vertical plates a Lissajous Figure is displayed on the screen. The shape of the Lissajous Figure is related to the phase angle between the two signals. This technique is discussed in more detail in Section 5.3.2.2, in the context of the experimental work presented in Chapter 6.

With the two transducers at the same point on a radius and about 1 m from the oscillator a reference condition exists at which the phase angle between the two signals and the separation of the two transducers are both zero. Stepping out one transducer from the other on a radial axis, then measuring the separations at increments of the phase angle of π radians, and then plotting the (d, ϕ) data pairs, then an estimate of the wavelength is obtained.

In order to derive an estimate of the depth of propagation z it is necessary to resort to the estimate used by Abbiss (1981) amongst others. Summarising: for a layer of depth h and velocity v_{R_1}, overlying a semi-infinite elastic half-space with velocity v_{R_2} if $\lambda/2 < h$ ($\lambda/2$ is half the wavelength) then the phase velocity tends towards v_{R_1} and if $\lambda/2 > h$ then the phase velocity tends towards v_{R_2} with a transition at $\lambda/2 \approx h$. Thus the rule

$$z = \lambda/2 \tag{3.6}$$

may be adopted to describe the depth of propagation for Rayleigh-type surface waves. This relation is examined in further detail in Section 3.4.3. A cautionary note regarding the reliability of the $z = \lambda/2$ approximation was given by Klomp and Dorman (1964) and may be simply summarised as follows: for roads with thick bound layers overlying the unbound layers the $z = \lambda/2$ relation is inapplicable, a relation of the form $z = \lambda/k$ where k is a constant less than 2 being more appropriate. The experimental work presented in Chapter 6 takes full account of this effect; all determinations of Rayleigh-type surface wave velocity being made from the surface of the unbound layers.

3.4 The mechanics of Rayleigh waves

The techniques for analysing Rayleigh-type surface wave velocity data presented by Jones (1962) and used extensively by Jones (1958, 1960 and 1963), Coghill (1967), Metcalf (1967), Guillemin and Gramsammer (1972), Rao (1972) and Martinček and Kadlečik (1982) and summarised by Jones *et al* (1967) are described by Djärf (1982) as being based on Lamb's analysis (Lamb, 1917) for wave propagation in an elastic plate. Djärf (1982) states: *'According to this analysis the wave propagation velocity at a given frequency depends not only upon the elastic parameters but also on the wavelength and thickness of the plate'.* This form of analysis is rather complex, requiring very detailed interpretation. There is a great deal of empirical data which suggests that the simple form of analysis used by several previous research workers (Heukelom and Foster, 1960; Maxwell and Joseph, 1967; Lutton, 1974; Abbiss, 1981 and 1983) based on the assumption that the effective depth of propagation (z) of a Rayleigh-type surface wave is equal to one-half the wavelength ($\lambda/2$) may be applied to tests on soil strata. This assumption was obtained by matching Rayleigh-type surface wave velocity-depth profiles to core logs (Ballard, 1963). Some of this

empirical evidence will be examined in Section 3.5 and the $z = \lambda/2$ relation will be given further credence by a consideration, in Section 3.4.3, of the way in which the vertical component of displacement due to a Rayleigh wave attenuates with depth below the surface.

3.4.1 The fundamental wave equation

It was shown by Miller and Pursey (1955) that the seismic waves generated by a vertically oscillating circular footing at the surface of an elastic half-space were predominately Rayleigh waves (Table 3.1). It would be expected, therefore, that a vertical transducer located at the surface of the half-space would sense the vertical component of the Rayleigh wave. The displaced shape of the half-space surface at any instant in time due to a sinusoidal source could be represented by a sine-curve (Figure 3.3). The distance between any two successive peaks (or troughs) is equivalent to one wavelength of the Rayleigh wave (λ). The time variation of the vertical displacement at any point on a radial axis from the vertical oscillator can be expressed as

$$\mathrm{w}(t) = Q_0 \sin \omega t \tag{3.7}$$

where:

Q_0 is the amplitude of vibration (*i.e.* the maximum value of w),

ω is the angular velocity of vibration ($= 2\pi f$), and

t is the instantaneous time.

At any other point on the same radial axis from the vertical oscillator the variation of the vertical displacement can be expressed as

$$\mathrm{w}(t) = Q_0 \sin (\omega t - \phi) \tag{3.8}$$

where ϕ is a phase angle. Plainly, the particle motion at a distance x from the source will lag behind that at the source by $\omega x/v_R$ radians. Equation 3.8 then becomes

$$\mathrm{w}(t) = Q_0 \sin (\omega t - \phi) = Q_0 \sin \left(\omega t - \omega \frac{x}{v_R}\right) = Q_0 \sin \left(\omega t - \frac{2\pi f x}{v_R}\right) \tag{3.9}.$$

However, at the source $x = 0$ and thus $\phi = 0$ at a distance of $x = \lambda$ from the source,

$$\phi = \frac{2\pi f \lambda}{v_R} \tag{3.10}$$

and $\phi = 2\pi$ so Equation 3.10 becomes

$$v_R = f\lambda \qquad (3.3\text{bis}).$$

It can be seen from Equation 3.3 that v_R can be computed from the measured value of λ at any input frequency f. This is often referred to as the Fundamental Wave Equation.

Now from Equation 3.3; $f/v_R = 1/\lambda$, and from Equation 3.9 $\phi = 2\pi f x/v_R$, so $\phi = 2\pi x/\lambda$. When the phase angle is that observed between two signals monitored by accelerometers, neither of which is located at the position $x = 0$, then the transducer separation, d, may be simply substituted for x giving:

$$\lambda = \frac{2\pi}{\phi} d \qquad (3.5\text{bis}).$$

3.4.2 Relationships between elastic wave velocities

From consideration of the differential equations, in terms of displacements, for an elastic medium, Timeshenko and Goodier (1970) (the same result was also obtained by Prakash, 1982) obtained the equations of small body motion based on the assumption of no body forces[2] but with the inertia forces added:

$$\begin{aligned}
(\Lambda + G)\frac{\partial \epsilon_v}{\partial x} + G\nabla^2 \mathrm{u} - \rho\frac{\partial^2 \mathrm{u}}{\partial t^2} &= 0 \\
(\Lambda + G)\frac{\partial \epsilon_v}{\partial y} + G\nabla^2 \mathrm{v} - \rho\frac{\partial^2 \mathrm{v}}{\partial t^2} &= 0 \\
(\Lambda + G)\frac{\partial \epsilon_v}{\partial z} + G\nabla^2 \mathrm{w} - \rho\frac{\partial^2 \mathrm{w}}{\partial t^2} &= 0
\end{aligned} \qquad (3.11)$$

where:

ϵ_v is the volumetric strain, and

∇^2 represents the operator:

$$\nabla^2 = \frac{\partial^2}{\partial x^2} + \frac{\partial^2}{\partial y^2} + \frac{\partial^2}{\partial z^2}$$

Considering the two cases of the deformation consisting entirely of dilation (longitudinal waves) and then, in turn, shearing distortion and rotation (transverse

[2] *Body forces* are those forces which are distributed over the volume of a body, such as gravitational forces, magnetic forces, or, in the case of a body in motion, inertia forces. In contrast, *surface forces* are those forces distributed over the surface of a body, such as the pressure of one body on another, or hydrostratic pressure.

waves), Timeshenko and Goodier (1970) found that the resulting equations were of the form

$$\frac{\partial \psi^2}{\partial t^2} = a^2 \nabla^2 \psi \tag{3.12}$$

where ψ is u, v or w as appropriate and

$$a = \sqrt{\frac{\Lambda + 2G}{\rho}} \tag{3.13}$$

for the case of waves of dilation and

$$a = \sqrt{\frac{G}{\rho}} \tag{3.14}$$

for the case of waves of distortion. It can be shown that a is equal to either the longitudinal wave velocity, v_P, or the transverse wave velocity, v_S, in Equations 3.13 and 3.14 respectively. Thus, as $G = E/[2(1+\nu)]$ and $\Lambda = E\nu/[(1+\nu)(1-2\nu)]$ then

$$v_P = \sqrt{\frac{\Lambda + 2G}{\rho}} = \sqrt{\frac{E(1-\nu)}{\rho(1+\nu)(1-2\nu)}} \tag{3.15}$$

and

$$v_S = \sqrt{\frac{G}{\rho}} = \sqrt{\frac{E}{2\rho(1+\nu)}} \tag{3.16}.$$

The ratio v_S^2/v_P^2 is thus given by

$$\frac{v_S^2}{v_P^2} = \frac{(1-2\nu)}{2(1-\nu)} \tag{3.17}.$$

The solution of a similar relationship for the Rayleigh wave and shear wave velocities (v_R/v_S) is somewhat more complex. Rayleigh (1885) gave the theory for surface waves on the free surface of a semi-infinite elastic solid, showing that the motion became negligible at a distance of a few wavelengths from the free surface. Rayleigh's definition of a Rayleigh wave was essentially a simple harmonic wave train travelling in the x-direction such that:

i)the disturbance is independent of the y-coordinate, and

ii)the disturbance decreases rapidly with distance from the free surface.

Waves satisfying the second condition are called surface waves.

Ewing *et al* (1957) showed that the Rayleigh Wave Equation can be reduced to

$$\frac{v_R^2}{v_S^2}\left[\frac{v_R^6}{v_S^6} - 8\frac{v_R^4}{v_S^4} + v_R^2\left(\frac{24}{v_S^2} - \frac{16}{v_P^2}\right) - 16\left(1 - \frac{v_S^2}{v_P^2}\right)\right] = 0 \qquad (3.18).$$

Substituting Equation 3.17 into Equation 3.18, re-arranging and putting $v_R/v_S = \alpha$,

$$\alpha^6 + 8\alpha^4 + 8\left(3 - \frac{1-2\nu}{1-\nu}\right)\alpha^2 - 16\left(1 - \frac{1-2\nu}{2(1-\nu)}\right) = 0 \qquad (3.19).$$

The above equation is a cubic in α^2. For a given value of Poisson's ratio, the proper value of α^2 can be determined.

Clearly the determination of the α ratio is somewhat complex. A good approximation was given by Filipczynski *et al* (1966):

$$\alpha = \frac{0.87 + 1.12\nu}{1 + \nu} \qquad (3.20).$$

Table 3.2 tabulates the three wave velocity ratios (v_S/v_P, $v_R/v_S = \alpha$ and v_R/v_P) comparing the Rayleigh and Filipczynski equations. The differences between the Rayleigh and Filipczynski determinations of α are too small to be usefully illustrated in Figure 3.4 where the three wave velocity ratios are compared in graphical form. The data for the value of $\alpha = v_R/v_S$ are those determined by Knopoff (1952).

3.4.3 Displacements due to Rayleigh waves and the effective depth of propagation

In Section 3.4.2 the Rayleigh surface wave measurement techniques were described and the assertion that the depth of propagation of the wave approximates to one-half the wave length (*i.e.* $z = \lambda/2$) was made. In this section this assertion will be justified by consideration of the theoretical dynamic displacement-depth profile caused by a Rayleigh surface wave propagated in an elastic half-space. Using the directional notation of Figure 3.1 for dynamic displacements u and w in the x and z directions respectively (v = 0 in the y direction for a Rayleigh wave according to Rayleigh's 1885 definition):

$$\mathrm{u} = \frac{\partial\varphi}{\partial x} + \frac{\partial\psi}{\partial z} \qquad (3.21)$$

and

$$\mathrm{w} = \frac{\partial \varphi}{\partial x} - \frac{\partial \psi}{\partial z} \tag{3.22}$$

where φ and ψ are two potential functions. It can be shown (Das, 1983) that for a sinusoidal wave travelling in the positive z-direction, the solutions for φ and ψ are

$$\varphi = \left(A_1 e^{-qz}\right) e^{i(\omega t - px)} \tag{3.23}$$

and

$$\psi = \left(B_1 e^{-sz}\right) e^{i(\omega t - px)} \tag{3.24}$$

where A_1 and B_1 are constants such that $B_1 = -2iA_1/\left(s^2 - p^2\right)$,

i is $\sqrt{-1}$,

q^2 is given by $p^2 - (\omega^2/v_P^2)$,

s^2 is given by $p^2 - (\omega^2/v_S^2)$, and

p is $2\pi/\lambda$.

Substituting the relations for φ, ψ and B_1, in terms of A_1, into Equations 3.21 and 3.22:

$$\mathrm{u} = A_1 pi \left(-e^{-qz} + \frac{2qs}{s^2 + p^2} e^{-sz}\right) e^{i(\omega t - px)} \tag{3.25}$$

and

$$\mathrm{w} = A_1 q \left(-e^{-qz} + \frac{2p^2}{s^2 + p^2} e^{-sz}\right) e^{i(\omega t - px)} \tag{3.26}.$$

From the above two equations it is clear that the rate of attenuation of displacement in the x-direction (u) with depth z will depend on the term in the parentheses, U, where

$$\mathrm{U} = -e^{-qz} + \frac{2qs}{s^2 + p^2} e^{-sz} = -e^{-(q/p)(pz)} + \left[\frac{2(q/p)(s/p)}{s^2/p^2 + 1}\right] e^{-(s/p)(pz)} \tag{3.27}.$$

Similarly, the rate of attenuation of the displacement in the z-direction (w) with depth will depend upon

$$\mathrm{W} = -e^{-qz} + \frac{2p^2}{s^2 + p^2} e^{-sz} = -e^{-(q/p)(pz)} + \left[\frac{2}{s^2/p^2 + 1}\right] e^{-(s/p)(pz)} \tag{3.28}.$$

However, from the definitions of q and p we have

$$\frac{q^2}{p^2} = 1 - \frac{\omega^2}{p^2 v_P^2} = 1 - \frac{v_R^2}{v_P^2} = 1 - \frac{v_S^2}{v_P^2} \times \frac{v_R^2}{v_S^2} = 1 - \frac{(1 - 2\nu)}{2(1 - \nu)}\alpha^2 \tag{3.29}$$

and from the definitions of s and p we have

$$\frac{s^2}{p^2} = 1 - \frac{\omega^2}{p^2 v_S^2} = 1 - \frac{4\pi^2 f^2}{4\pi^2 v_S^2/\lambda^2} = 1 - \frac{v_R^2}{v_S^2} = 1 - \alpha^2 \qquad (3.30).$$

Equations 3.28 and 3.29 can be represented in a much simplified form

$$\mathrm{U} = -e^{-\mathrm{a}(pz)} + \mathrm{b}\, e^{-\mathrm{c}(pz)} \qquad (3.31)$$

$$\mathrm{W} = -e^{-\mathrm{a}(pz)} + \mathrm{d}\, e^{-\mathrm{c}(pz)} \qquad (3.32)$$

where a, b, c and d are constants dependent upon the Poisson's ratio such that

$\mathrm{a} = q/p,$

$\mathrm{b} = 2(q/p)(s/p)/(s^2/p^2 + 1),$

$\mathrm{c} = s/p,$ and

$\mathrm{d} = 2/(s^2/p^2 + 1).$

The values of a, b, c and d have been evaluated for values of Poisson's Ratio in the range $0 < \nu \leq 0.5$ and presented in the form of Equations 3.31 and 3.32 in Table 3.3. The results of these equations are plotted in Figure 3.5 for the range $0 \leq z/\lambda \leq 2.0$ for the various values of the Poisson's ratio. The data are normalised to the dynamic attenuation factor at the surface of the elastic half-space (*i.e.* U_z / $\mathrm{U}_{z=0}$ and W_z / $\mathrm{W}_{z=0}$ for the horizontal and vertical components respectively).

The shape of the curves presented in Figure 3.5 tends to add weight to the experimental assumption that $z = \lambda/2$. This relationship is investigated further in Appendix 1. In Appendix 1 the equation defining the attenuation of the vertical component of displacement with depth (Equation 3.32) has been integrated to find the centroid of the area under the curve for values of Poission's Ratio, $\nu = 0.1, 0.2, 0.3, 0.4$ and 0.5. The value of the centroid is assumed to approximate to the depth at which the Rayleigh wave has a median energy from the vertical component of displacement. The results of this analysis are given in Table A1.1, illustrated in Figure A1.1, and may be summarised as follows:

$$\text{for } 0 < \nu \leq 0.5 \text{ then } 0.406 < \overline{z/\lambda} \leq 0.609.$$

In short, this analysis indicates that the effective depth of propagation (z) of Rayleigh waves is between 0.406λ and 0.609λ compared to the assumption that the depth of propagtion is 0.5λ which, in the light of this evidence, may be seen as a convenient average approximation relating to material having a Poisson's Ratio of around 0.3.

3.4.4 Attenuation of Rayleigh waves

The attenuation of the vertical component of displacement due to a Rayleigh wave, with horizontal distance from the source of excitation, is generally considered to compose two components; geometrical damping and material damping (Richart *et al*, 1970). The geometrical component of damping, or attenuation, of Rayleigh waves can be expressed as:

$$\mathrm{w} = \mathrm{w}_1 \sqrt{\frac{x_1}{x}} \tag{3.33}$$

where:

x_1 is the distance from the source to a point of known amplitude,

x is the distance from the source to any point on the same radial axis as x_1,

w_1 is the amplitude of the vertical component of the Rayleigh wave at a distance x_1 from the source, and

w is the amplitude of the vertical component of the Rayleigh wave at a distance x from the source.

The material component of attenuation is attributed to energy loss due to imperfect elasticity. Bornitz (1931) gave an expression for Rayleigh wave attenuation accounting for both geometrical and material damping:

$$\mathrm{w} = \mathrm{w}_1 \sqrt{\frac{x_1}{x}} \exp[-\alpha(x - x_1)] \tag{3.34}$$

where α is the coefficient of material attenuation (in m^{-1}). Barkan (1962) presented a considerable amount of Rayleigh wave attenuation data with calculated values of the coefficient of material attenuation varying between 0.04 and 0.12 m^{-1} depending upon soil type. These data are summarised in tabular form by Das (1983).

3.4.5 Summary

In this section a number of important aspects of the mechanics of the theoretical propagation of Rayleigh waves, as defined by Lord Rayleigh in 1885, have been described:

i)The Fundamental Wave Equation describing the velocity of a sinusoidal waveform ($\upsilon_R = f\lambda$) was derived. This relationship will be extensively used in the interpretation of the results presented in Chapter 6.

ii)The ratios between the three basic elastic wave types were derived (v_S/v_P and v_R/v_S) and the third ratio (v_R/v_P) was calculated for completeness. The most important point to be drawn from this work is that the Rayleigh wave velocity approximates to within about 10% of the transverse wave velocity for the possible range of Poisson's ratio, thus

$$v_R = \alpha v_S = \alpha\sqrt{\frac{G}{\rho}} \tag{3.35}$$

where α lies in the range $0.875 < \alpha \leq 0.955$ (for the Rayleigh Wave Equation) corresponding to the range $0 < \nu \leq 0.5$ for Poisson's ratio.

iii)The dynamic displacements induced in an elastic half-space by a sinusoidally propagated Rayleigh wave were also studied. Normalised displacement-depth profiles were presented for the range $0 < \nu \leq 0.5$ for Poisson's ratio. These tend to confirm the usual assumption that the Rayleigh wave is predominately propagated in a surface layer of depth approximately equal to one wavelength so justifying the experimental assumption that the depth of propagation of a surface wave is equal to one-half of the wavelength (*i.e.* $z = \lambda/2$).

iv)Bornitz's (1931) equation describing the attenuation of the vertical component of displacement due to a Rayleigh wave, with horizontal distance from the source of excitation, was given in Section 3.4.4.

3.5 Rayleigh-type surface wave velocity data

In this section surface wave velocity data published by various authors will be examined. Much of this data was originally published in terms of imperial units and has been converted to standard metric units to provide a more direct comparison to the experimental data presented in Chapter 6. Some of the data, particularly that sourced from Jones (1958) and (1960), has been re-interpreted from a velocity-wavelength format to a velocity-depth format using the approximation for depth of propagation, $z = \lambda/2$, again to provide more direct comparisons. Each data set presented in this section has been selected to illustrate a particular effect in relation to the propagation of Rayleigh-type surface waves in either the ground or in road pavement structures.

A significant amount of the experimental data presented in Chapter 6 is for sands. The surface wave velocity for sands is generally reported as being between 115 and 180 m/s (Huekelom and Foster, 1960; Woods and Richart, 1967) and

although shear (transverse) wave velocities have been assigned much greater values, between 250 and 850 m/s (Dowding, 1985), these are thought to be for relatively deep strata.

The influence of moisture content on the surface wave velocity in a reinstatement environment is obviously of some importance. Jones (1958) presents velocity-wavelength profiles for two sites consisting of silty clay. The first is described as firm and dry (Site A) and the second as soft and wet (Site B). The wavelength has been reinterpreted in terms of the depth of propagation ($z = \lambda/2$) and the resulting surface wave velocity-depth profiles illustrated in Figure 3.6. The surface wave velocity differs appreciably between the two sites. However, at very long wavelengths, the velocity profiles approach each other, possibily due to underlying gravel allowing drainage of the silty clay.

The variation of surface wave velocity values for clays is perhaps best illustrated by the work of Abbiss (1983) who reports values between 100 and 250 m/s at depths between 0 and 12 m for Boulder Clay and velocities between 75 and 100 m/s for depths between 0 and 5 m for London Clay. Experiments performed under contract to the British Gas Engineering Research Station by Abbiss tend to confirm the generally accepted approximation for the depth of propagation of a surface wave ($z = \lambda/2$). The test site used by Abbiss consisted of a large 1 m deep pit filled with compacted Wet-mix macadam overlying a clay material. The surface wave velocity-depth profile is based upon the $z = \lambda/2$ approximation and a distinct break in the profile is noted at the Wet-mix macadam/clay interface (Figure 3.7).

The use of the surface wave velocity-frequency curve as an aid to the interpretation of the surface wave velocity-depth profile is shown in Figure 3.8 using data from Huekelom and Foster (1960) for a flexible road pavement of construction as shown in the log. These data also tend to confirm the approximation for the depth of propagation of a surface wave.

The influence on the surface wave velocity-depth profile of compaction of earth materials has been demonstrated by Jones (1960) and by Maxwell (1960). Jones carried out testing on a sandy soil both before and after compaction with a roller of an unspecified type and number of passes (Figure 3.9). Jones' original velocity-wavelength curves have been reinterpreted in terms of the $z = \lambda/2$ approximation. The most significant effects of the compaction process are confined to a surface layer

of approximately 200 mm thickness, the increase in velocity being steadily reduced until at a depth of 1.5 m the increase is negligible.

Jones (1960) also presented data showing the changes occurring in the surface wave velocity-depth profile of a road pavement sub-base structure as a result of vehicle induced stresses. These data are presented in Figure 3.10 and again Jones' original velocity-wavelength curves have been converted to surface wave velocity-depth profiles using the $z = \lambda/2$ approximation. Data were obtained at about 3, 13 and 18 months after completion of the road construction. The increases in surface wave velocity were attributed to compaction of the sand sub-base by the relatively high stresses generated below this construction. It is interesting to note that the greatest increment occurred during the warm summer months, possibly due to the lower effective elastic moduli of the bound surface layers causing the stress levels in the sub-base to be higher than in the colder periods of the year.

Depth profiles showing the influence of vehicle induced stresses on the dynamic Young's modulus (determined from the surface wave velocity) were given by Maxwell (1960) and although these data are not presented here similar conclusions to those from the data presented in Figure 3.10 may be drawn. Maxwell also showed the effect of the addition of further layers on top of an existing subgrade and road construction (Figure 3.11). The test dated 8/5/58 was carried out while the surface was at Point 1 on the log. The other tests were carried out after the addition of a 280 mm layer of unbound base course material (surface at Point 2 on the log) and a further 60 mm of bituminous binder (surface at Point 3 on the log). Plainly the curves are not coincident although there is generally good agreement between the three. The slight divergence between the curve obtained in May 1958 and those obtained in August 1958, between the depths 0.9 and 1.9 m is thought to be due to a wetting and subsequent drying which took place between these two dates. There is no evidence to suggest that compactive effort applied to the new layers during August has had any effect on the lower layers first tested in May.

With respect to the maximum depth of propagation which may be achieved using the Rayleigh-type surface wave velocity propagation technique, Ballard and McLean (1975) state: *'Practically, the test is limited by the availability of large vibrators and site access', ..., 'In addition accuracy and definition generally tend to decrease in direct proportion to depth of penetration'.* Despite this limitation Fry (1965), using a large counter-rotating eccentric mass mechanical vibrator, achieved

maximum depths of propagation of around 90 feet (27.3 m) through 'Topsoil', overlying Vesicular Basalt, overlying Dense Basalt. The experimentally derived depths of propagation were used to predict the depth of transition between the three material types and agreed well with borehole logs.

Attempts to relate the modulus derived from plate load tests to that derived from Rayleigh-type surface wave velocity measurements were made by Andersson (1975) and by Kasianchuk and Argue (1972). The latter authors obtained reasonable linear correlations between the stresses required to generate 0.1 inch (2.54 mm) deflection, based upon the moduli determined by the two experimental methods. Inevitably, due to the strain-dependent nature of the elastic properties of soils, the low strain Rayleigh-type surface wave velocity tests yielded higher moduli values than did the high strain plate load tests.

Strains developed by seismic waves are of obvious interest if the moduli determined from wave velocity and density measurements are to be used for design purposes. The normal strain, ϵ, developed by a longitudinal wave, propagated in the x-direction, can be shown to be (Prakash, 1981):

$$\epsilon = \dot{u}/v_P \tag{3.36}$$

Similarly, the shear strain, γ, developed by a shear wave, also propagated in the x-direction, may be given by:

$$\gamma = \dot{v}/v_S \text{ and } \gamma = \dot{w}/v_S \tag{3.37}$$

for horizontally polarised (SH) and vertically polarised (SV) shear waves, respectively (Hoadley, 1985 and White, 1965). For the vertical component of a Rayleigh wave the developed shear strain is given by:

$$\gamma = \dot{w}/v_R \tag{3.38}.$$

In the above equations $\dot{u}$, $\dot{v}$ and $\dot{w}$ are peak particle velocities. Seed and Idriss (1970) estimated, from Equation 3.38, that for sinusoidally propagated Rayleigh waves γ was of the order of $5 \times 10^{-4}\%$.

Useful reviews of wave propagation techniques are given by Jones and Whiffen (1960), Nijboer (1967), Gazetas and Yegian (1979), Miller and Odum (1986) and Anon (1988g).

3.6 Summary

This chapter has reviewed 'Wave mechanics and measurement techniques' with particular reference to the Rayleigh-type surface wave propagation technique used extensively in the experimental work presented in Chapter 6.

In Section 3.2 the four basic types of seismic wave were identified and described; reasons for selecting the Rayleigh-type surface wave propagation technique for the measurement of elastic properties were also given. Section 3.3 reviewed the detailed experimental techniques used by previous workers in determining Rayleigh-type surface wave velocities. The convenient approximation for the effective depth of propagation of a sinusoidally excited Rayleigh-type surface wave, $z = \lambda/2$, was also identified. Section 3.4 reviewed relevant theory relating to the mechanics of Rayleigh wave propagation and in particular a simple analysis, presented in detail in Appendix 1, lends further weight to the $z = \lambda/2$ assumption. A more detailed summary of the mechanics of Rayleigh waves was given in Section 3.4.5. Section 3.5 reviewed Rayleigh-type surface wave velocity data obtained by previous workers. This section presented and discussed a series of data sets which were carefully selected from the available data, each to illustrate a particular point in relation to the propagation of Rayleigh-type surface wave in either the ground or in road pavement structures.

Table 3.1 - Relative energies of the seismic waves generated by a vertically oscillating circular footing at the surface of an elastic half-space with Poisson's ratio, $\nu = 0.25$ (after Miller and Pursey, 1955).

Wave type	Percentage of total energy
Longitudinal wave	6.9
Transverse wave	25.8
Surface (Rayleigh) wave	67.4

Table 3.2 - Elastic wave velocity ratios.

Poisson's ratio ν	$v_S/v_P = \sqrt{(1-2\nu)/2(1-\nu)}$	$\alpha = v_R/v_S$		v_R/v_P
		Rayleigh	Filipczynski	
0	0.707	0.875	0.870	0.619
0.100	0.667	0.893	0.893	0.596
0.200	0.612	0.912	0.912	0.558
0.250	0.577	0.919	0.920	0.530
0.300	0.535	0.928	0.928	0.496
0.333	0.500	0.933	0.932	0.466
0.400	0.408	0.943	0.941	0.385
0.500	0	0.955	0.953	0

Table 3.3 - Attenuation factors with depth for the vertical and horizontal components of displacement of Rayleigh waves.

Poisson's ratio ν	Attenuation factor U in the x direction with depth z	Attenuation factor W in the z direction with depth z
0	$-\exp(-0.7856pz) + 0.6162\exp(-0.4841pz)$	$-\exp(-0.7856pz) + 1.6202\exp(-0.4841pz)$
0.10	$-\exp(-0.8035pz) + 0.6015\exp(-0.4501pz)$	$-\exp(-0.8035pz) + 1.6631\exp(-0.4501pz)$
0.20	$-\exp(-0.8295pz) + 0.5825\exp(-0.4102pz)$	$-\exp(-0.8295pz) + 1.7119\exp(-0.4102pz)$
0.25	$-\exp(-0.8476pz) + 0.5785\exp(-0.3943pz)$	$-\exp(-0.8476pz) + 1.7310\exp(-0.3943pz)$
0.30	$-\exp(-0.8683pz) + 0.5682\exp(-0.3726pz)$	$-\exp(-0.8683pz) + 1.7562\exp(-0.3726pz)$
0.40	$-\exp(-0.9229pz) + 0.5530\exp(-0.3328pz)$	$-\exp(-0.9229pz) + 1.8005\exp(-0.3328pz)$
0.50	$-\exp(-1.0000pz) + 0.5452\exp(-0.2966pz)$	$-\exp(-1.0000pz) + 1.8382\exp(-0.2966pz)$

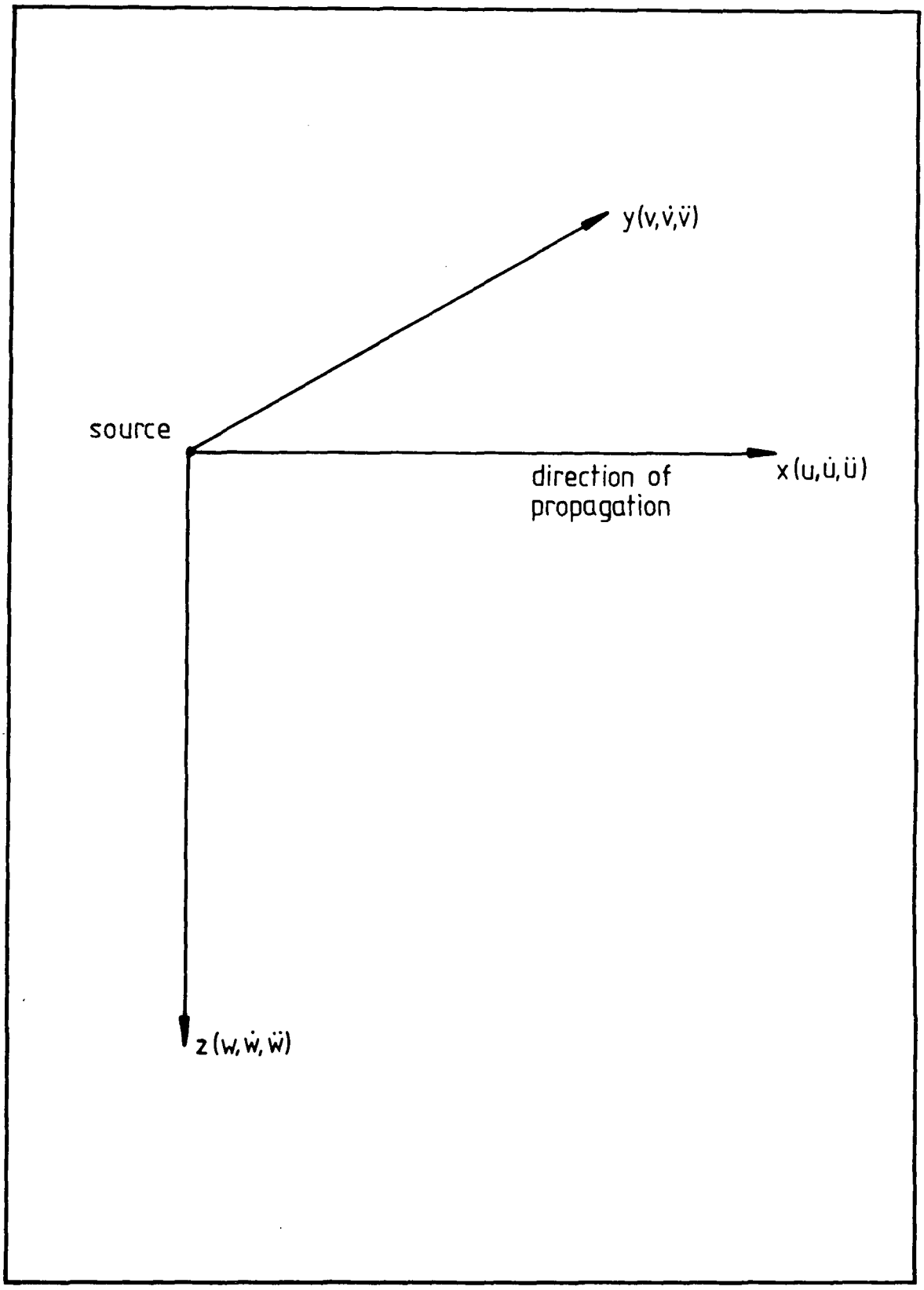

Figure 3.1 - Directional notation for the mutually perpendicular x, y and z axes with the corresponding particle displacements (u, v and w), velocities ($\dot{u}, \dot{v}$ and $\dot{w}$), and accelerations ($\ddot{u}, \ddot{v}$ and $\ddot{w}$). The arrows show the positive directions.

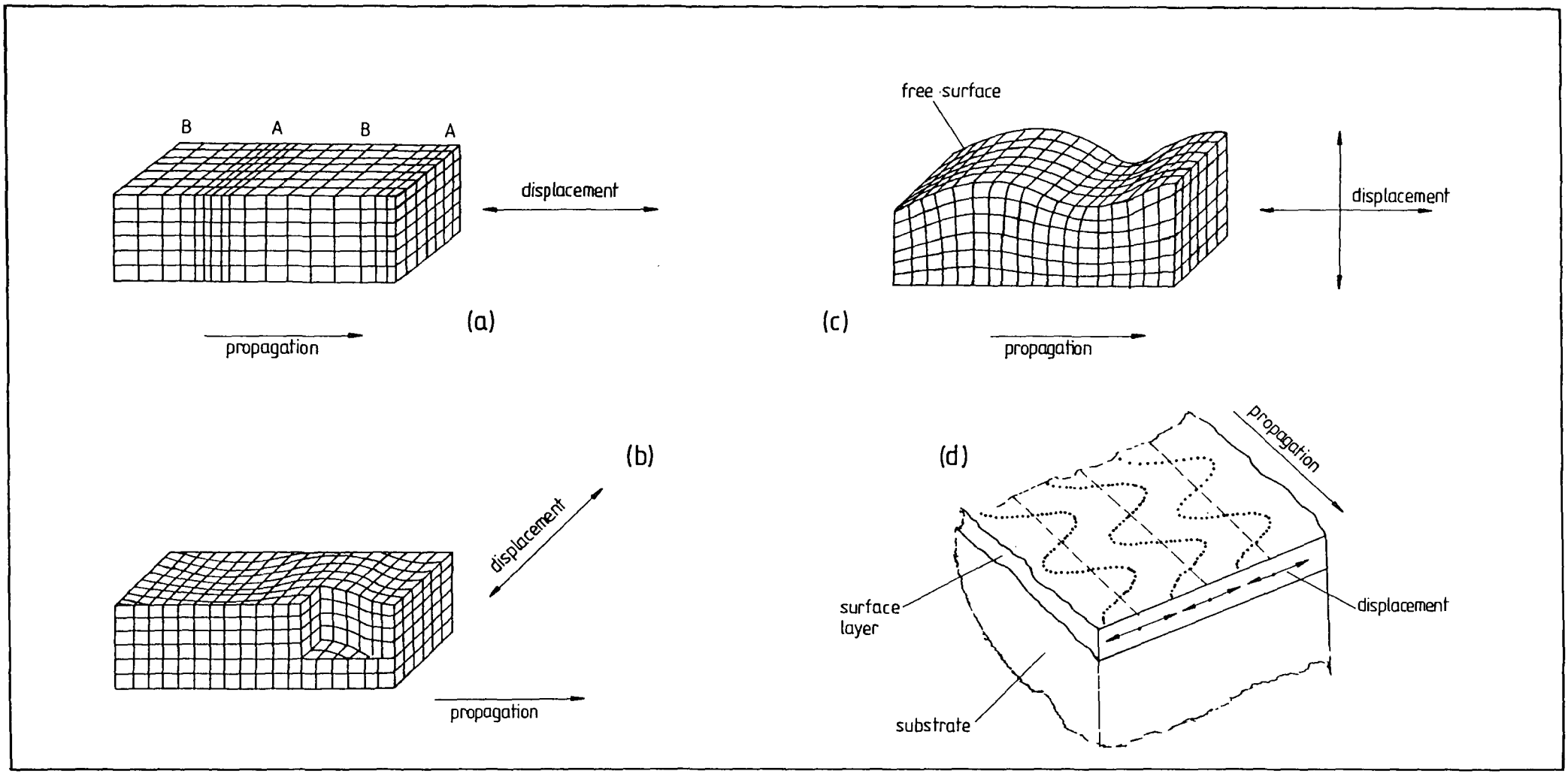

Figure 3.2 - Types of seismic wave; (a) Longitudinal body waves, (b) Transverse body waves, (c) Rayleigh surface waves and (d) Love surface waves.

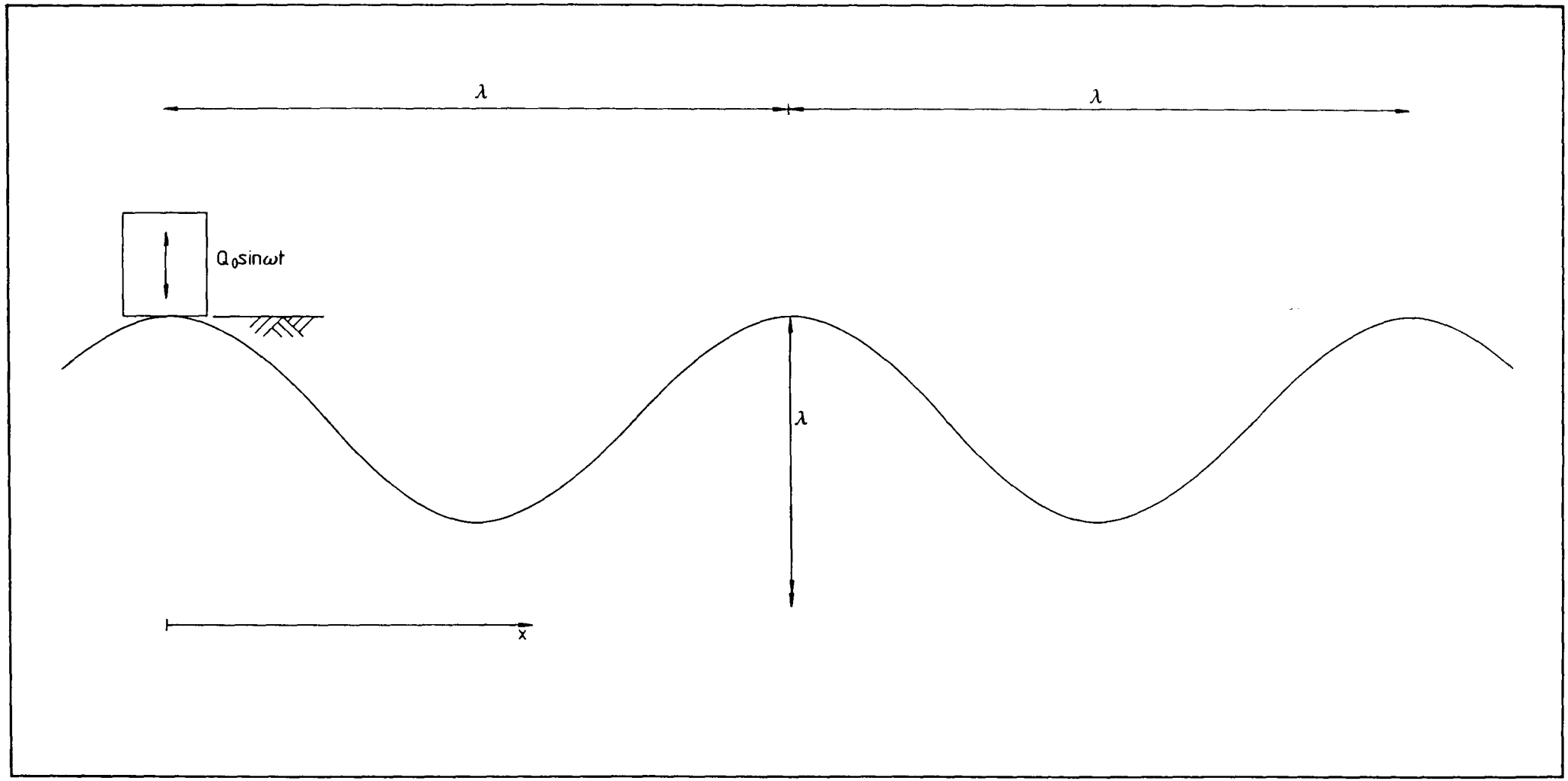

Figure 3.3 - Displaced shape of an elastic half-space, at any instaneous time, due to a sinusoidal output source.

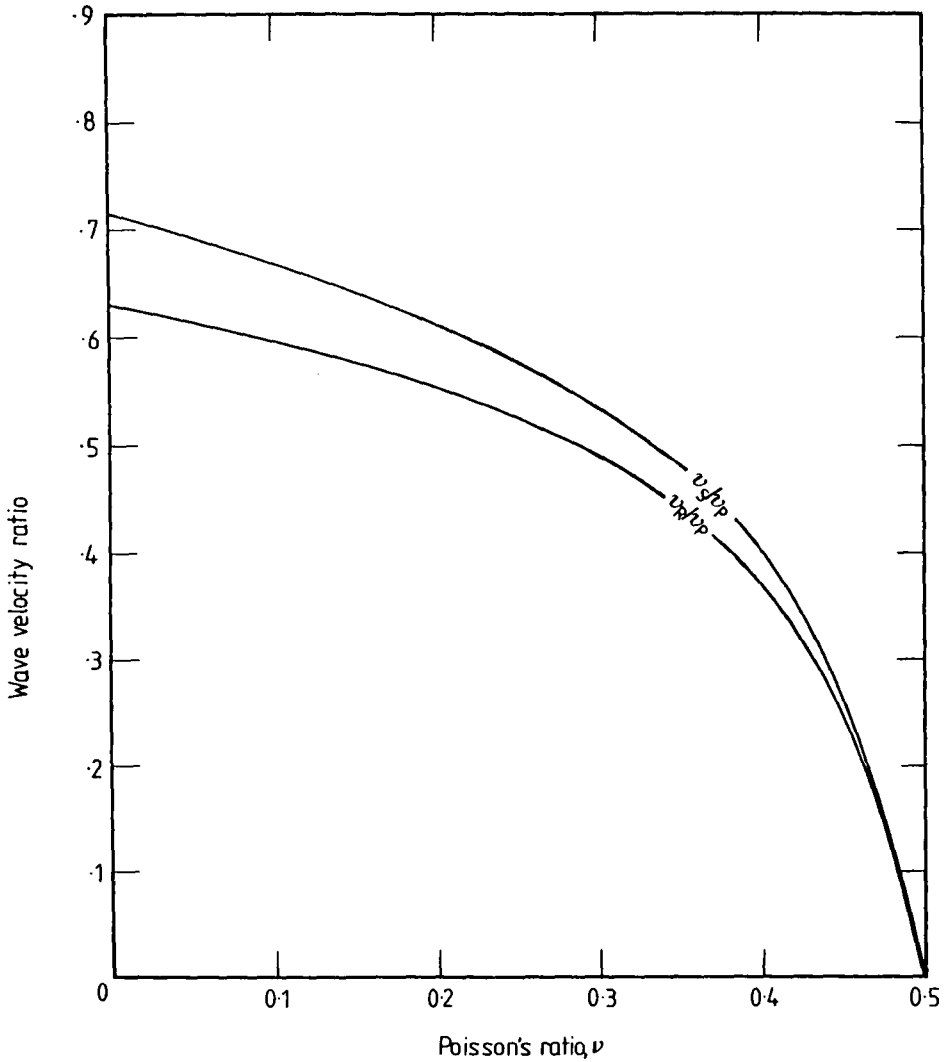

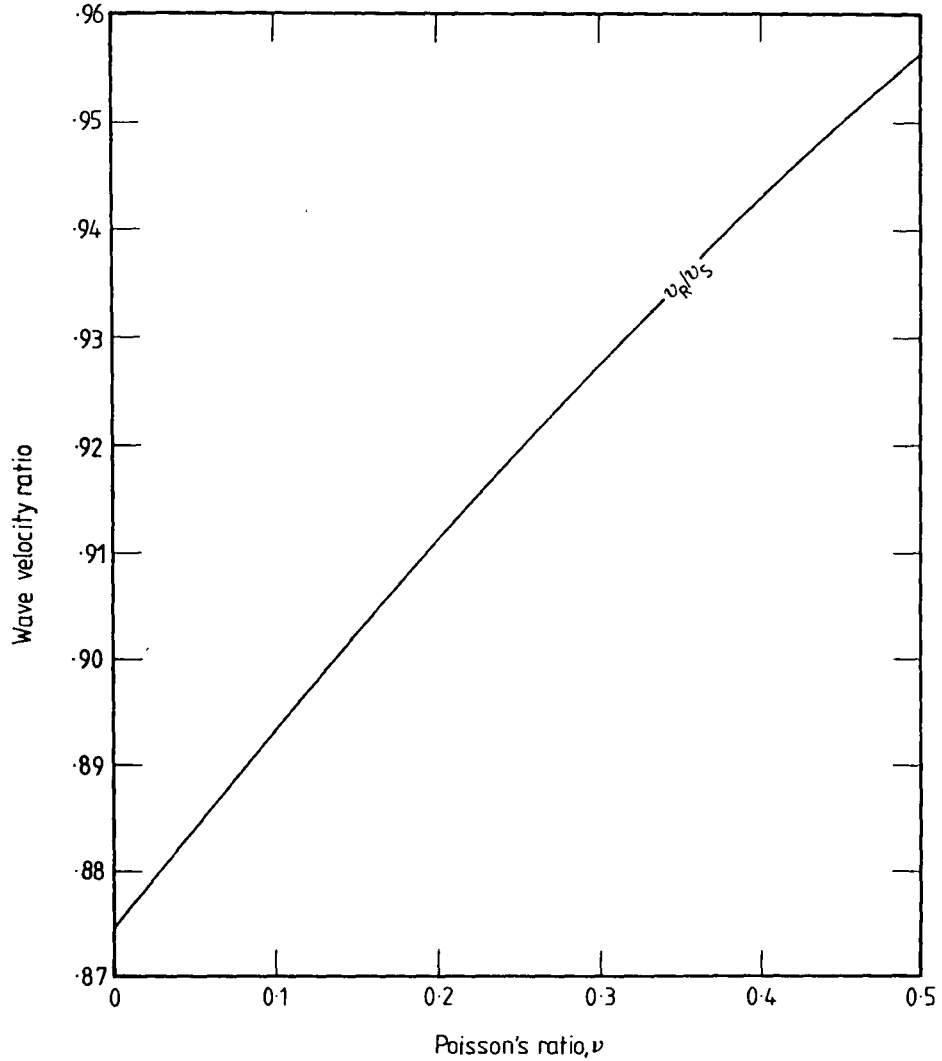

Figure 3.4 - Dependence of the wave velocity ratios (v_S/v_P, $v_R/v_S = \alpha$ and v_R/v_P) upon the Poisson's ratio ν.

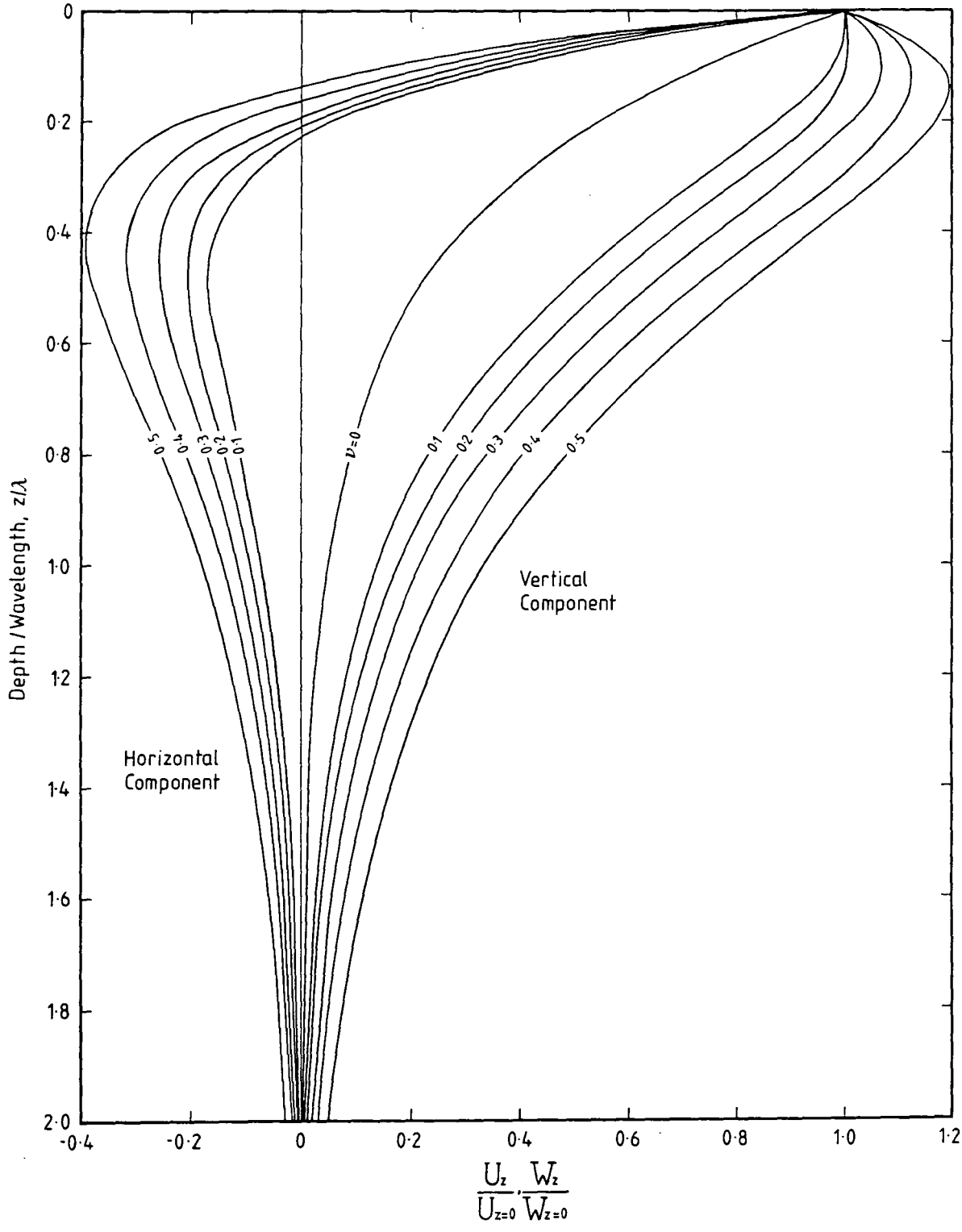

Figure 3.5 - Normalised curves showing the variation of the vertical and horizontal components of dynamic displacement with depth due to the propagation of a Rayleigh wave. Curves are shown for differing values of Poisson's ratio.

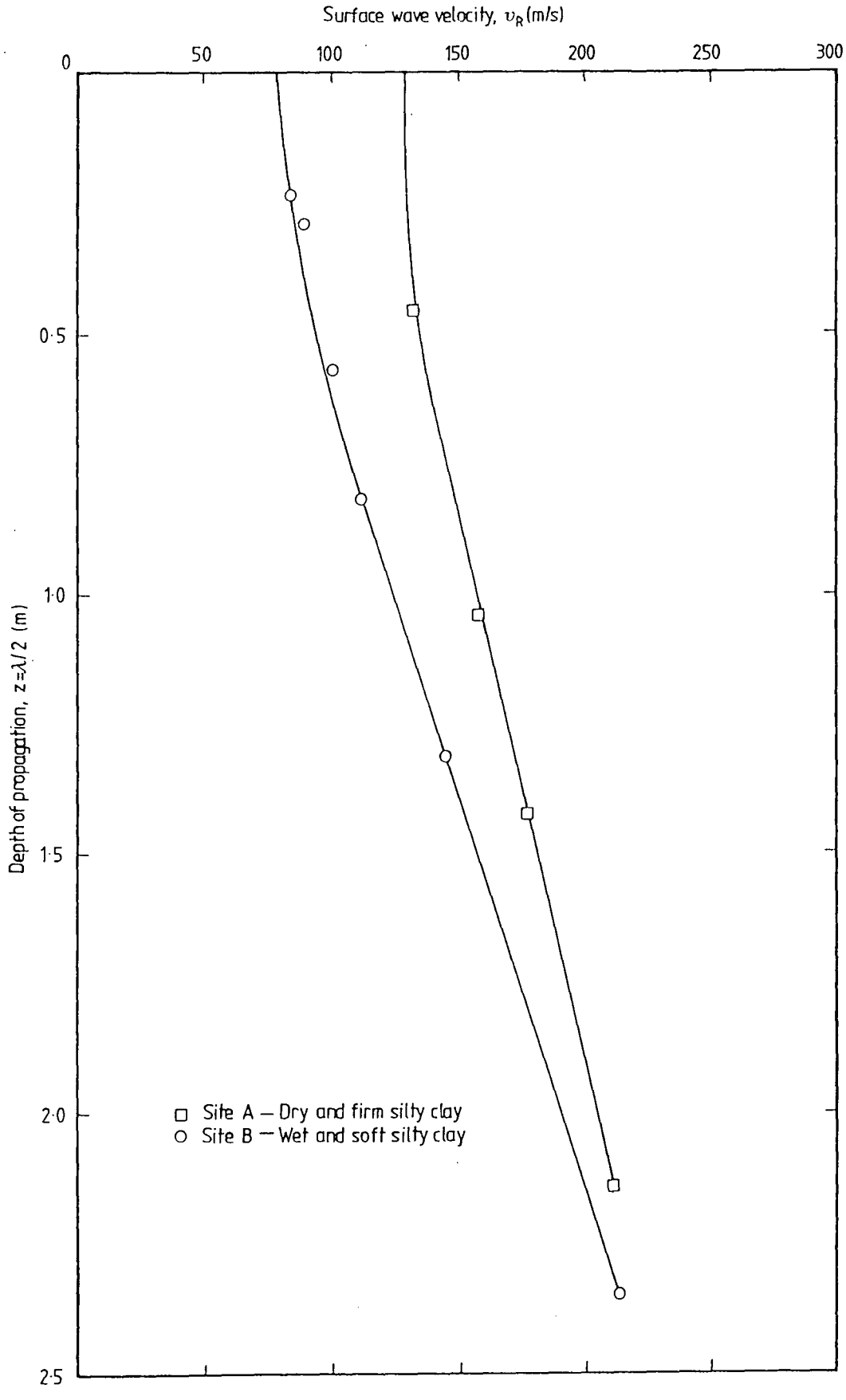

Figure 3.6 - Surface wave velocity-depth profiles for two silty clay sites showing the influence of moisture content on the surface wave velocity (after Jones, 1958).

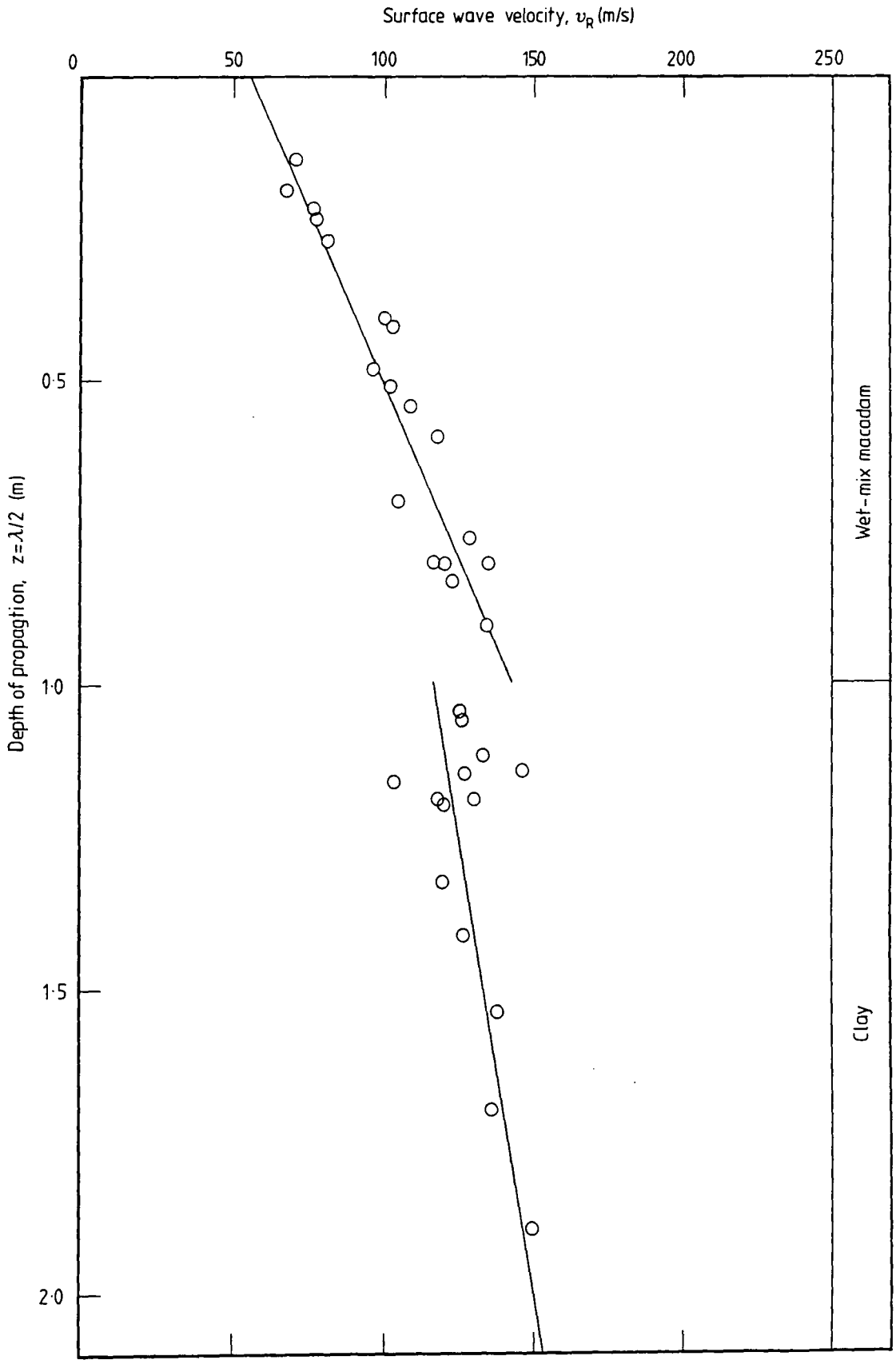

Figure 3.7 - Surface wave velocity-depth profile for a pit filled with compacted wet-mix macadam overlying clay showing the use of the approximation for depth of propagation, $z = \lambda/2$ (after Abbiss, 1983).

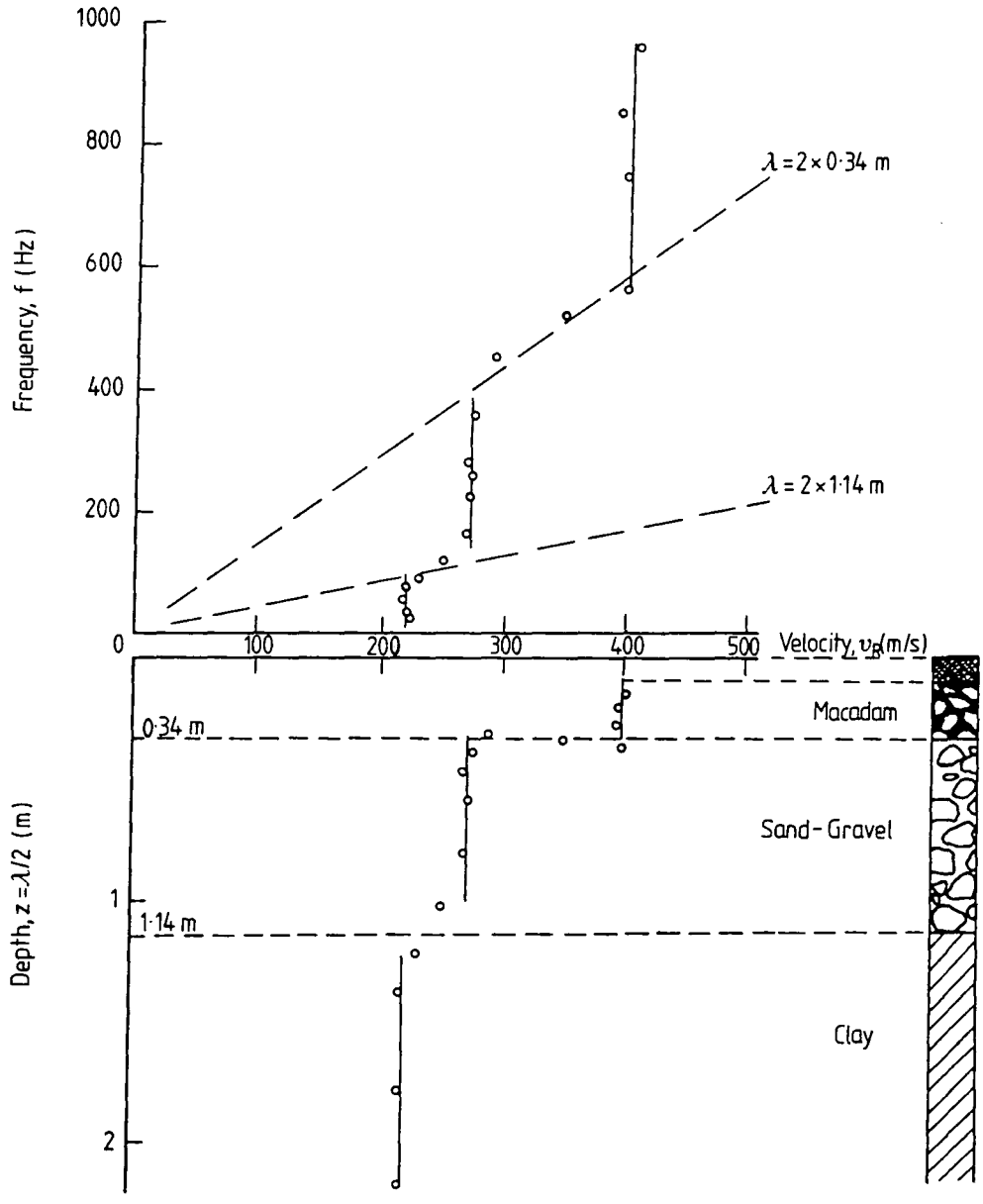

Figure 3.8 - Surface wave velocity-depth profile for a flexible road pavement (after Huekelom and Foster, 1960).

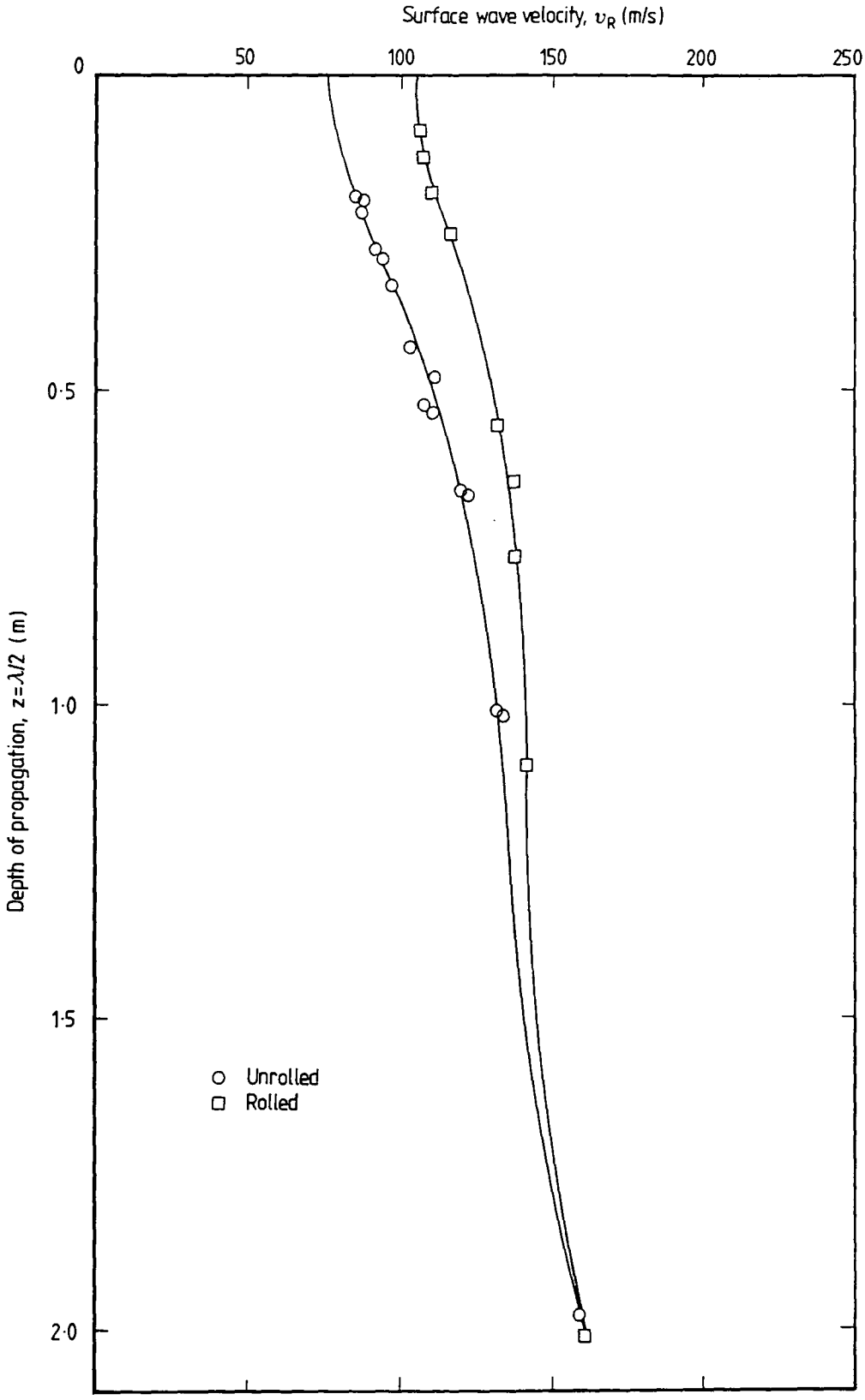

Figure 3.9 - The influence of compaction on the surface wave velocity-depth profile for a sandy soil (after Jones, 1960).

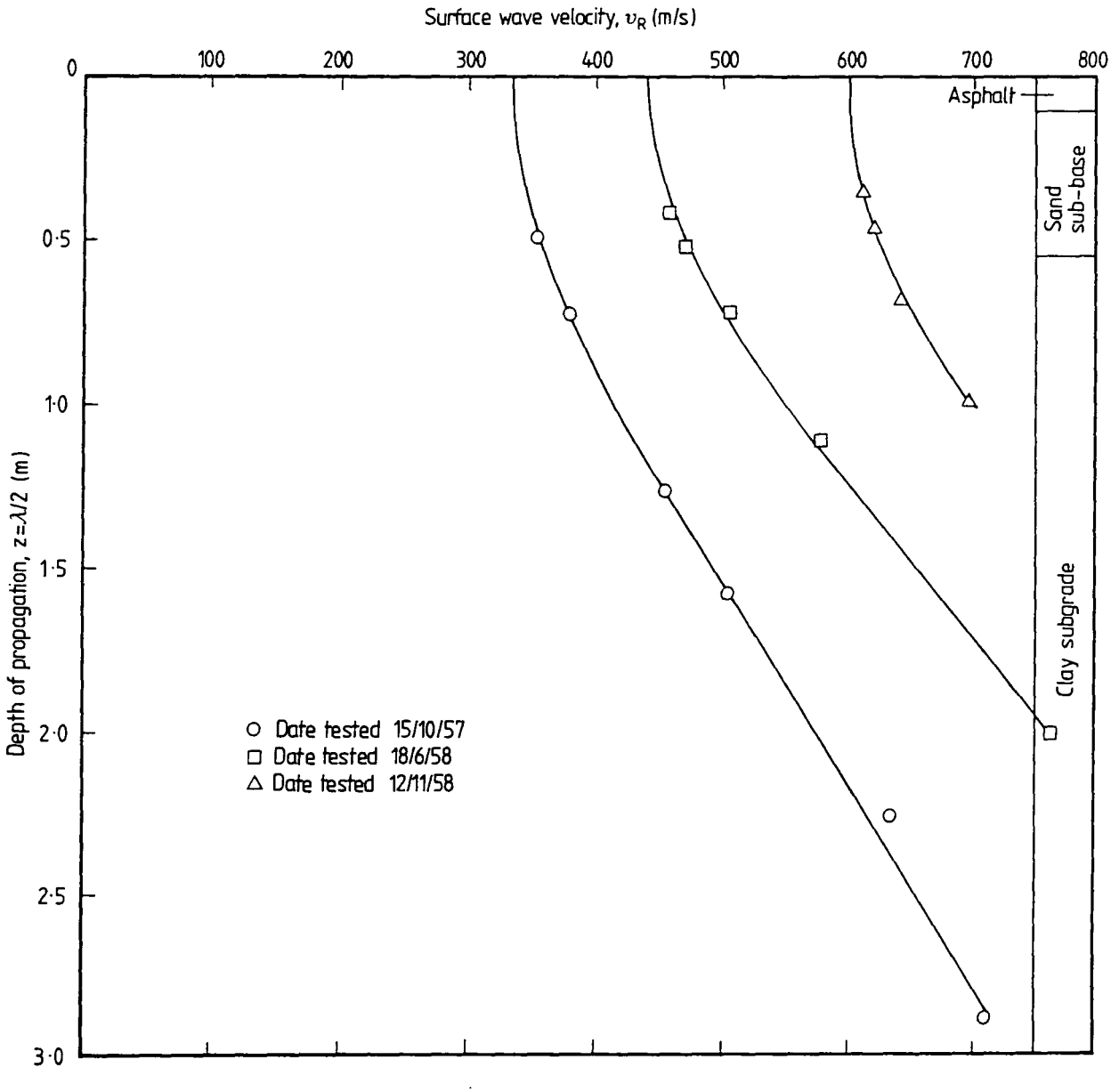

Figure 3.10 - The influence of trafficking on the surface wave velocity-depth profile for a road sub-base construction (after Jones, 1960).

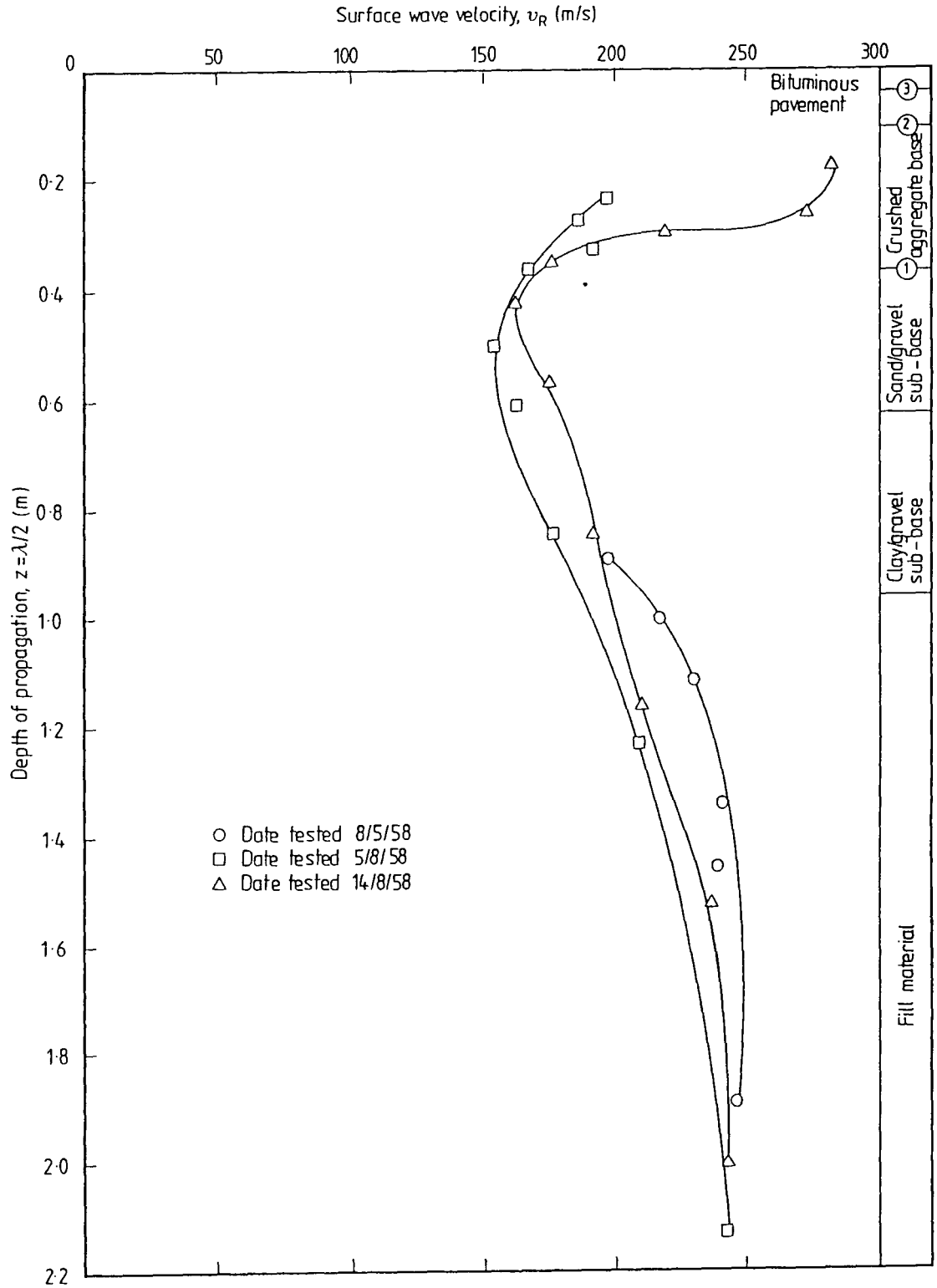

Figure 3.11 - Surface wave velocity-depth profiles for a road pavement construction showing the influence of the addition of further layers on top of the pre-existing construction (after Maxwell, 1960).

CHAPTER 4

MATERIAL CLASSIFICATION AND COMPACTION TESTS

4.1 Introduction and source of materials

This chapter details basic soil classification and compaction tests carried out on the Permian Yellow Sand and Sharp Sand used in the tests carried out in the laboratory based trench (Sections 6.2 and 6.3) and also similar tests carried out on the crushed rock Wet-mix macadam used for the field trials (Sections 6.4 and 6.5). Detailed data are presented in Appendix 2.

All samples for testing were taken and reduced, from material stockpiles, using the quartering technique and riffle-boxes, as appropriate, in accordance with the procedures detailed in BS 812: Part 102 (1984).

The Permian Yellow Sand is excavated from the Hepplewhite Quarries, Old Quarrington Quarry at Bowburn, County Durham. The identification of this material has been carried out by mineralogical analysis and is reported in Section 4.7. The Sharp Sand, sourced from the Tilcon quarry at Scorton near Catterick in Yorkshire, is a river terrace gravel and consists of around 60% Carboniferous Limestone, 25% Sandstone, 10% dolomitised Carboniferous Limestone and 5% Siltstone and Basalt. The Wet-mix macadam is sourced from the North Tyne Roadstone quarry at Moot Law, near Stamfordham in Northumberland and has been identified by the Department of Geological Sciences at the University of Durham as a Carboniferous Limestone with no evidence of dolomitisation.

Section 4.2 presents the particle size distribution determinations for the three materials, Section 4.3 presents specific gravity and water absorption value data while Section 4.4 presents the results of an extensive programme to determine the dry density-moisture content relationships for the three materials. The Sharp Sand is shown to fall within the grading envelope for Concrete Sand Grading C (BS 882, 1983) and the Wet-mix macadam is similarly shown to fall within the grading envelope for this material specified by the Department of Transport (1986). Details of tests, additional to the particle size distribution determination, necessary to confirm that the Wet-mix macadam conforms to the Department of Transport (1986) specification are presented in Sections 4.5 (10% fines value) and 4.6 (Flakiness index).

The detailed specifications for both Concrete Sand and Wet-mix macadam are reproduced, in Appendix 3, from BS 882 (1983) and Department of Transport (1986) respectively.

4.2 Particle size distribution

Particle Size Distribution's (PSD) were determined to BS 1377 (1975), Test 7(A), 'Standard method by wet sieving' for the three materials. Detailed results are presented in Appendix 2.1. Figure 4.1 shows the particle size distribution for the Permian Sand and Sharp Sand along with the BS 882 (1983) Grading C particle size distribution envelope for Concrete Sand. The Sharp Sand tested conforms to the British Standard for Concrete Sand Grading C, while examination of Appendix 3 (Figure A3.1) indicates that the Permian Sand falls on the fine side of even the fine Concrete Sand Grading F. Figure 4.2 shows the particle size distribution for the Wet-mix macadam along with the Department of Transport (1986) grading envelope for Wet-mix macadam. The Wet-mix macadam tested falls within the allowable particle size range for this material. Figure 4.3 simply compares the three materials tested.

Classification of the Permian Sand, Sharp Sand and the Wet-mix macadam to BS 5930 (1981); the British Soil Classification System is possible solely on the basis of the particle size distributions given in Figure 4.3. The resulting classifications are developed in Table 4.1 and may be abbreviated to SWF, SW and GWF for the Permian Sand and Sharp Sand and Wet-mix macadam, respectively. It should be noted, however, that the classification system is designed for the description of naturally occuring soils. As a result the crushed rock Wet-mix macadam is described by the British Soil Classification System as a gravel. Of far more practical use is its identification as a material conforming to the Department of Transport (1986) specification for Wet-mix macadam which, as noted above, will be confirmed in Sections 4.5 and 4.6.

4.3 Specific gravity and water absorption value

All values of specific gravity are oven-dry basis values, as opposed to saturated and surface dried basis or apparent relative density values. The material used in the determinations was oven-dried prior to test for twenty-four hours.

Four specific gravity determinations were made on both the Permian Sand and the Sharp Sand. Two of these determinations were made strictly in accordance with BS 1377 (1975): Test 6(B), 'Method for fine grained soils' while a further two determinations were made in accordance with BS 812: Part 2 (1975), Section 5.5, 'Method for aggregate 10 mm nominal size and smaller'. Material from the full particle size range was used for both types of test. The values of the mean and standard deviation of the specific gravities for each sand are given in Table 4.2. No appreciable differences were found between the results from the two test types as is indicated by the low values of the standard deviation. The values of specific gravity are used in the calculation of the constant air voids lines, shown on the dry density-moisture content plots, using Equation 4.7 (Sections 4.4.1 and 4.4.2).

The water absorption values of the two sand materials were assumed to be negligible. This assumption is lent weight by the mineralogy of the Permian Sand (80% quartz; see Section 4.7) and by information from the suppliers (Tilcon) in the case of the Sharp Sand.

The larger particles contained in the Wet-mix macadam are unsuitable for use in the small pycnometer used to contain the particles in BS 1377 (1975): Test 6(B). Determination of the specific gravity of the Wet-mix macadam was achieved by splitting a sample into three fractions and testing each fraction individually using the tests detailed in BS 812: Part 2 (1975), Section 5.4, 'Method for aggregate between 40 mm and 5 mm nominal size' (fractions passing 40 mm and retained on 19.05 mm test sieves and passing 19.05 mm and retained on 4.76 mm test sieves) and BS 812: Part 2 (1975), Section 5.5, 'Method for aggregate 10 mm size and smaller' (fraction passing a 4.76 mm test sieve). The mean and standard deviation from two tests on each fraction are given in Table 4.2. The weighted specific gravity was then calculated using the method given in BS 5835: Part 1 (1980) as

$$\begin{aligned} G_s &= \frac{100}{a_1/G_{s_1} + a_2/G_{s_2} + a_4/G_{s_4}} \\ &= \frac{100}{34.9/2.71 + 29.9/2.70 + 35.2/2.70} \\ &= 2.70 \end{aligned} \tag{4.1}$$

where:

a_1, a_2 and a_4 are the concentrations of the size fractions, defined in Table 4.2, in the bulk sample, from Figure 4.2 and

G_{s_1}, G_{s_2} and G_{s_4} are the specific gravities of the size fractions a_1, a_2 and a_4, respectively, from Table 4.2.

The values of water absorption, w_A, were also determined using the test methods given in Sections 5.4 and 5.5 of BS 812: Part 2 (1975). For these tests the material passing a 75 μm test sieve was removed due to the difficulty in the determination of the saturated surface dry condition of such fine material. The water absorption value of the material passing a 75 μm test sieve was assumed to be the same as that of the material passing 4.76 mm and retained on 75 μm test sieves. The mean and standard deviation of the water absorption values of the two fractions are given in Table 4.2, and the weighted water absorption value calculated in similar fashion to the weighted specific gravity, from

$$\begin{aligned} w_A &= \frac{100}{a_1/w_{A_1} + a_2/w_{A_2} + a_3/w_{A_3} + a_5/w_{A_5}} \\ &= \frac{100}{34.9/0.5 + 29.9/0.8 + 28.2/1.3 + 7.0/1.3} \\ &= 0.8 \end{aligned} \tag{4.2}$$

where:

a_1, a_2, a_3 and a_5 are the concentrations of the size fractions, defined in Table 4.2, in the bulk sample, from Figure 4.2 and

$w_{A_1}, w_{A_2}, w_{A_3}$ and w_{A_5} are the water absorption values of the size fractions a_1, a_2, a_3 and a_5, respectively, from Table 4.2.

The values of specific gravity and water absorption are used in the calculation of the constant air voids lines, shown on the dry density-moisture content plots, using Equation 4.7 (Sections 4.4.3 and 4.4.4). The water absorption value is also used in the calculation of the correction for stone content of the material used in the determination of the dry density moisture content relationship to BS 1377 (1975): Test 12 (Section 4.4.3.1).

4.4 Dry density-moisture content relationships

Determinations of dry density-moisture content relationships were carried out to BS 1377 (1975): Test 12, '2.5 kg rammer method', using a Farnell electric, automatic ramming machine with automatic blow counter. Tests were conducted using the standard 27 blows per layer for each of three layers and additionally at 54 and 81 blows per layer ($N_b = 27, 54, 81$) in order to assess the influence of increased

compactive effort on the resulting values of maximum dry density ($\rho_{d_{max}}$) and optimum moisture content (w_{opt}) obtained for the materials under test. Such tests were conducted on the Permian Sand (Section 4.4.1), Sharp Sand (Section 4.4.2) and the Wet-mix macadam (Section 4.4.3). Additional tests were carried out on the Permian Sand at 108 and 135 blows per layer by a different operator (McCulloch, 1987) in order to make a crude assessment of the operator dependability of this test.

The standard method requires that material with large sized particles, such as the Wet-mix macadam, has the particles retained on a 20 mm test sieve removed. This process is often referred to as scalping. The effect of scalping on the dry density-moisture content relationship obtained is discussed in Section 4.4.3.1 and corrections are made to counteract the effect of scalping and so indicate the nature of the dry density-moisture content relationship of the bulk material.

In addition to the tests carried out to BS 1377 (1975): Test 12 tests have been carried out to BS 5835: Part 1 (1980), the current British Standard for the determination of the dry density-moisture content relationship of an aggregate, on the Wet-mix macadam (Section 4.4.4).

Detailed results for these tests are presented in Appendix 2.2.

For tests carried out to BS 1377 (1975): Test 12 results include bulk density (ρ), moisture content (w), dry density (ρ_d) and the degree of compaction (D_c), defined as

$$D_c = \frac{\rho_d}{\rho_{d_{max}}} \qquad (4.3).$$

This parameter should not be confused with the relative density (D_r), which is defined as

$$D_r = \frac{\rho_{d_{max}}}{\rho_d} \times \frac{\rho_d - \rho_{d_{min}}}{\rho_{d_{max}} - \rho_{d_{min}}} \times 100\% \qquad (4.4.).$$

This parameter is discussed in more detail by Lambe and Whitman (1979) and methods for the determination of the relative density are given by Head (1980).

Detailed test results, presented in Appendix 2.2 for the BS 5835: Part 1 (1980) tests on Wet-mix macadam, include the nominal moisture content, initial moisture content (w_i) and the residual moisture content (w_r) as well as dry density based on the BS 5835 method of interpretation and dry density determined following a procedure which mirrors the BS 1377 method of interpretation.

The methods of obtaining the dry density-moisture content data are described in Section 4.4.1 (BS 1377, 1975: Test 12) and Section 4.4.4 (BS 5835: Part 1, 1980).

In all compaction tests separate batches were used, each batch being compacted once only.

In Section 4.4.5 comparisons are made between the methods used for the determination of the dry density-moisture content relationship contained in BS 1377 (1975): Test 12, BS 5835: Part 1 (1980) and BS 1377: Part 4 (1988)[1].

Section 4.4.6 assesses the relationship between compactive effort (CE), defined as the energy input per unit volume, and the maximum dry density ($\rho_{d_{\max}}$) and also the optimum moisture content (w_{opt}).

4.4.1 Permian Sand (BS 1377, 1975: Test 12)

As stated earlier, determinations of the dry density-moisture content relationship were carried out to BS 1377 (1975): Test 12, using the standard 27 blows per layer, and also at 54, 81, 108 and 135 blows per layer ($N_b = 27, 54, 81, 108, 135$). Detailed data are presented in Appendix 2.2. For each moisture content the bulk density (ρ) was first determined (in Mg/m^3) from

$$\rho = \frac{m_2 - m_1}{V} \tag{4.5}$$

where:

m_1 is the mass of the mould and base plate (g),

m_2 is the mass of the mould, baseplate and compacted soil (g), and

V is the volume of the mould (cc).

The moisture content (w) was then measured using the microwave oven-drying method described in Appendix 4.1, thus allowing the calculation of the dry density (ρ_d) using

$$\rho_d = \frac{100\rho}{100 + w} \tag{4.6}.$$

A smooth curve was then drawn through the points for each level of compactive effort (Figure 4.4). The lines corresponding to 0, 5 and 10% air voids are plotted for comparison using Equation 4.7 in which the water absorption value (w_A) is assumed to be zero and the specific gravity was taken from Table 4.2.

$$\rho_d = \rho_w \frac{100 - A}{100/G_s + (w - w_A)} \tag{4.7}$$

[1]BS 1377 (1988) is a British Standard draft for discussion document and contains proposals for the update of the current British Standard (BS 1377, 1975) in nine parts; Part 4 contains proposals for compaction related tests for soils.

where:

ρ_w is the density of water ($= 1\,\mathrm{Mg/m^3}$), and

A is the volume of air voids in the soil, expressed as a percentage of the total volume of the soil.

The maximum dry density and optimum moisture content were then measured from each of the dry density-moisture content relationships. These data are presented in Table 4.3.

4.4.2 Sharp Sand (BS 1377, 1975: Test 12)

Determinations of the dry density-moisture content relationship were carried out to BS 1377 (1975): Test 12, using the standard 27 blows per layer and also at 54 and 81 blows per layer ($N_b = 27, 54, 81$). Detailed data are presented in Appendix 2.2.

The data were derived as described in Section 4.4.1 and are plotted as Figure 4.5 with the lines representing 0, 5 and 10% air voids being based on Equation 4.7. The water absorption value is assumed to be zero and the specific gravity was taken from Table 4.2.

The values of maximum dry density and optimum moisture content for each of the dry density-moisture content relationships are presented in Table 4.3.

4.4.3 Wet-mix macadam (BS 1377, 1975: Test 12)

Determinations of the dry density-moisture content relationship were carried out to BS 1377 (1975): Test 12, using the standard 27 blows per layer and also at 54 and 81 blows per layer ($N_b = 27, 54, 81$), on the material passing a 19.05 mm (3/4″) test sieve (a 20 mm test sieve, as specified in BS 1377 (1975) was not available). Detailed data are presented in Appendix 2.2.

The data were derived as described in Section 4.4.1 and are plotted as Figure 4.6 with the lines representing 0, 5 and 10% air voids being based on Equation 4.7. The weighted water absorption value and weighted specific gravity were taken as calculated from the data presented in Table 4.2 ($w_A = 0.8\%$ and $G_s = 2.70$), using Equations 4.1 and 4.2. Figure 4.6 also shows the dry density-moisture content relationships for the bulk material, corrections having been made to both the dry density and moisture content to allow for the material retained on the 19.05 mm test sieve. The derivation of these relationships will be described in Section 4.4.3.1.

The values of maximum dry density and optimum moisture content for each of the dry density-moisture content relationships, before and after the correction for stone content is applied, are presented in Table 4.3.

It will be observed that the position of the constant air voids lines implies that the compacted material has negative air voids when compacted at moisture contents at or above the optimum. Obviously a negative value of the air voids corresponds to an impossible state.

The reasons for this apparent phenomenon are relatively simple. BS 1377 (1975): Test 12 recommends compaction of the soil in three layers of approximately equal mass. The use of an extension collar prevents the excess material from the third layer spilling out of the compaction mould. This excess material should not exceed a height of 6 mm above the top of the mould and should be struck off using a straight edge. This is a simple operation for medium- or fine-grained soils. However, coarse-grained soils, such as the Wet-mix macadam, present something of a problem as individual particles can be up to 20 mm in diameter so presenting a dilema for the operator when levelling the compacted surface. Should he remove the particles and fill the resulting void with fine material or push the individual particles into the mass of the material. In this instance the latter coarse of action was followed. An additional effect was noted during the striking-off operation; as the straight edge was drawn across the excess material, at water contents around or above optimum, the fine material simply 'slipped' under the straight restoring its original form after the passage of the straight edge. The physical effect of these phenomena is, in both cases, to increase the density calculated, either because the material has been artificially compacted by the pushing in of the larger particles partially present in the excess material or because the volume of the compacted sample is actually larger than the volume of the compaction mould due to the excess material which is not struck off with the straight edge.

Simple calculations suggest that a volume of compacted material 3% greater than the volume of the compaction mould would return all of the points in Figure 4.6 to a situation of positive air voids. This volume error corresponds to a uniform height of excess material above the top face of the compaction mould of $\approx$ 3 mm. This rather large amount of excess material does not correspond to visual observations made during the tests but will be taken as an equivalent error and deemed to include both the error in density of the compacted material caused by the excess material not

being fully struck off at the end of each test and the effect of small stones being pushed into the body of the material. The effect of this potential error in the volume of the compacted material will be discussed further in Section 4.4.6.

4.4.3.1 Stone content and the effect of scalping

The removal of coarse particles from soil samples to accommodate standard laboratory apparatus is an accepted and necessary part of testing practice. BS 1377 (1975): Test 12 requires that the portion of material retained on a 20 mm test sieve be removed prior to test. As noted earlier, in Section 4.4.3, a 19.05 mm test sieve was used in the prepartion of the Wet-mix macadam samples because a 20 mm test sieve was not available.

The effect of scalping prior to compaction of stony cohesive soils was observed by Barnes (1987). The particle size distributions of such materials cover a wide range of particle sizes, from 125 mm (cobbles) down to silt and clay sized particles ($<$ 60 μm). The effects of the removal of particles retained on a 20 mm test sieve from such materials may be considerable. Figure 4.7 shows idealised grading curves for Barnes' (1987) test specimens ($<$ 20 mm) prepared from samples ($<$ 125 mm) each with 30% passing 2 mm, as an example. The significant effect is that samples ($<$ 125 mm) which have coarser grading curves yield test specimens ($<$ 20 mm) with finer grading curves. The grading curves are labelled 'A', 'B', 'C', ..., 'G' to allow this effect to be observed more easily.

The effect of the removal of the material retained on a 19.05 mm test sieve from the Wet-mix macadam under consideration here is not so dramatic. Figure 4.8 shows the particle distribution curves for Wet-mix macadam prior to scalping and also after scalping. Although not illustrated, the application of a 20 mm scalping correction to the Department of Transport (1986) grading envelope for Wet-mix macadam does not result in a reversal of the coarse and fine limits. There is, a translation of the envelope to the left on the particle size distribution chart and, of course, a convergence of the coarse and fine limits of the grading envelope at 100% passing 20 mm.

From the above, it can be seen that the properties of test specimens may differ significantly from those of the *in situ* samples which they purport to represent as a result of discarding the coarse particles from the laboratory test specimens.

A correction to calculate the mass material dry density-moisture content relationship from the matrix (test specimen) dry density-moisture content relationship is reported in some detail by Head (1980) and is essentially as follows:

$$\rho_{d_{\text{mass}}} = \left[\frac{G_t}{(1-F)\rho_{d_{\text{matrix}}} + FG_t}\right] \rho_{d_{\text{matrix}}} \tag{4.8}$$

where:

G_t is the specific gravity of the stones passing 40 mm and retained on 19.05 mm test sieves (size fraction a_1) given in Table 4.2 ($G_t = 2.71$),

F is the ratio of the matrix material to the whole sample measured from the grading curve (from Figure 4.8; $F = 0.66$),

$\rho_{d_{\text{matrix}}}$ is the dry density of the matrix material, as tested, and

$\rho_{d_{\text{mass}}}$ is the dry density of the mass of the material including the stones.

The moisture content of the material as a whole will differ from that of the matrix, owing to the presence of the stones. The stones themselves may absorb a certain amount of moisture, which may be removed by the normal drying procedure. As the absorbed moisture does not alter the volume of the stones, then it can be shown that the moisture content of the mass material (w_{mass}) is given by

$$w_{\text{mass}} = Fw_{\text{matrix}} + (1-F)w_A \tag{4.9}$$

where w_{matrix} is the moisture content of the matrix, and w_A is the water absorption value (moisture content in the saturated surface dry condition) of the stones. The water absorption value of the stones passing 40 mm and retained on 19.05 mm test sieves (size fraction a_1) is given in Table 4.2 ($w_A = 0.5\%$).

The correction procedure assumes that the proportion of stones in the mass material is not large, *i.e.* less than 25% by total dry mass (or $F \geq 75\%$). From Figure 4.8 F is equal to 66% and the limits of the basic assumption of the correction procedure are violated. However, in the absence of any alternative procedure, that reported by Head (1980) has been used to obtain a cautious estimate of the true dry density-moisture content relationships for the Wet-mix macadam.

Head (1980) states: *'If the percentage of stones is quite large'*, presumably greater than 25%, *'there may not be sufficient matrix material completely to fill the voids between the stones, and this could be an unstisfactory fill for many purposes'*. It is interesting to note that the Department of Transport (1986) grading

envelope for Wet-mix macadam requires between 20 and 40% of particles to be greater than 20 mm, as such material conforming to the specification for wet-mix macadam will rarely conform to the assumptions of the correction described above. Head's comments may, perhaps, be more applicable to the stony cohesive type soils discussed by Barnes (1987), the somewhat more gap-graded nature of the particle size distribution curve allowing the stones to act as individual elements within the silt/clay matrix. In contrast, the uniform grading of the Wet-mix macadam allows different sized particles to interlock more effectively, thus causing the mix to act as a whole rather than as a discrete matrix/stone arrangement.

The recommendation that in cases where $F < 75\%$ the dry density-moisture content relationship be determined in a larger compaction mould (Head, 1980) has been effected in Section 4.4.4, using the current British Standard for the determination of the dry density-moisture content relationship for coarse aggregate (BS 5835: Part 1, 1980). The larger mould used in this test can accommodate particles of up to 37.5 mm and as such only 4% of the dry mass of material need be removed in the prepartion of the test specimens (Figure 4.2), so negating the necessity for the application of corrections for stone content.

The values of the corrected maximum dry density $\rho_{d_{\max}}$ and corrected optimum moisture content w_{opt} obtained from Figure 4.6 are given in Table 4.3, values being given also for the Wet-mix macadam matrix material. Detailed data, corrected for the stone content, are given in Appendix 2.2.

4.4.4 Wet-mix macadam (BS 5835: Part 1, 1980)

The BS 5835: Part 1 (1980) compactability test for aggregates is essentially the same as the BS 1377 (1975): Test 14, 'Vibrating hammer method', but modified to prevent the loss of fine aggregate during compaction. The development of the BS 5835: Part 1 (1980) test was instigated as a result of work reported by Pike (1972) on the compactability of aggregates using BS 1377 (1975): Test 14. The modified test, which was first described by Pike and Acott (1975), involves the compaction of five samples of aggregate, each of mass 2.5 ± 0.1 kg, at each of the moisture contents required to define the dry density-moisture content relationship. Compaction of each sample is carried out in a mould of 150 mm nominal diameter with a filter arrangement set in the base, this arrangement being designed to prevent the loss of fines during compaction (see Section 4.4.5). Filter papers (Whatman grade 113) are

also placed top and bottom of the roughly levelled sample surface which is carefully mixed to the required moisture content before being stored in a sealed water-tight container for at least 12 hours, prior to compaction, to ensure thorough wetting. The compactive effort is applied by the impact of a 900 W (33.3 Hz) vibrating hammer for 180 ± 5 seconds on an anvil which is fitted with two 'O'-rings to achieve a water-tight seal between the compaction mould and anvil. A loading frame positions the hammer and mould and provides a downward force of 450 ± 10 N to the top of the hammer. The test apparatus is enclosed in a noise-reducing cabinet during operation of the vibrating hammer.

Six batches, each of nominal mass 2.55 to 2.60 kg, were prepared by careful riffling for wetting to each of the required moisture contents (nominal moisture contents $= 0, 1, 2 \ldots 8\%$). After a 24 hour storage period five were removed for testing at the British Gas plc, Engineering Research Station, Soils Laboratory and the sixth used to determine the initial moisture content (w_i) by the normal oven-drying procedure. The compaction mould, base, filter system and anvil were carefully cleaned prior to the compaction of each batch and two new filter papers were used for each batch.

The compacted sample volume was obtained by measuring the height of the compacted sample, as determined from the difference between depth-gauge measurements from the top of the compaction mould and the top of the compaction anvil (with all filters in place and compacted for 5 seconds with the vibrating hammer) and a similar measurement after the compaction of each batch. The volume is then simply the product of the compacted sample height and the known cross-sectional area of the compaction mould.

The combined mass of the compaction mould, base, anvil and sample is great (*circa* 27 kg) and as such it would not normally be possible to determine accurately the bulk density of the compacted material from the mass of the mould, baseplate, anvil and compacted soil and the volume of compacted sample and the mass of the clean mould, baseplate and anvil prior to the test (Equation 4.5). The availability of a large capacity balance (60000 ± 1 g) meant that such a BS 1377 (1975) style of analysis was possible. This form of analysis includes, in the calculation for bulk density, water and very fine material forced through the filter arrangement into the baseplate. This allowed a comparison of the results obtained from the BS 1377

(1975) style of analysis with those obtained from the, perhaps more rigorous, style given in BS 5835: Part 1 (1980).

The residual moisture content (w_r), after compaction, was determined by oven-drying the entire sample complete with the two filter papers. Corrections were applied during calculation of the moisture content and dry density as follows:

i)Corrections to the mass of water contained in the bulk sample for

a)the loss of dry mass of two filter papers on oven-drying (= 0.8 g), and,

b)the mass of water contained in two filter papers when saturated (= 12.9 g). This correction was only applied when the filter papers were observed to be wet on extraction of the sample from the compaction mould ($w_i \geq 5\%$), and,

ii)Corrections to the dry mass of the sample for

c)the mass of two oven-dry filters (= 3.7 g).

Thus, the residual moisture content is given by:

$$w_r = \frac{m_2 - m_3 + 0.8 - 12.9}{m_3 - m_1 - 3.7} \times 100\% \tag{4.10}$$

where:

m_1 is the mass of the moisture content tin (g),

m_2 is the mass of the moisture content tin and the wet sample (g), and

m_3 is the mass of the moisture content tin and the dry sample (g).

The dry density was then calculated from Equation 4.6. These results are plotted with those for the BS 5835: Part 1 (1980) style of analysis in Figure 4.9. Detailed results are given in Appendix 2.2.

For the BS 5835: Part 1 (1980) form of analysis the dry density was calculated directly from the mass of dry material ($m_3 - m_1 - 3.7$; in Equation 4.10) divided by the volume of the compacted sample. The residual moisture content is calculated from the oven-drying of the whole sample as described for Equation 4.10.

The dry density-moisture content relationship is plotted, with the relationship obtained from the BS 1377 (1975) form of analysis described above, in Figure 4.9. The essential differences between the two forms of analysis will be discussed in Section 4.4.5. Curves of constant air content are also shown in Figure 4.9, based on

Equation 4.7, with weighted specific gravity and water absorption values taken from Table 4.2. Although BS 5835: Part 1 (1980) specifies that density values should be quoted in units of kg/m^3, units of Mg/m^3 are used here to ease comparison of the data with that from tests carried out to BS 1377 (1975). Detailed data are presented in Appendix 2.2. Values of maximum dry density and optimum moisture content are given in Table 4.3.

Due to the compactive effort being applied to the whole surface area of the sample in this test, disruption of adjacent areas to the compaction area does not occur as in BS 1377 (1975): Test 12, and so relatively high densities occur when the compacted material is compacted in a nominally dry condition. As water is added and the demand for absorbed water is satisfied a thin film of water forms on the particle surfaces tightly held by surface tension forces acting as displacers and causing lower dry densities to be achieved. This displacing effect continues with increased moisture content until a "pessimum" moisture content is reached at which a minimum dry density is recorded. In this case, from Figure 4.9, the pessimum moisture content is 2.2%.

Further increase in moisture content yields sufficient free (not absorbed) water to lubricate the particles allowing the material to flow more easily and thus causing higher dry densities to be achieved until the maximum dry density is reached at the optimum moisture content (Pike, 1972). As the moisture content is further increased a minimum value of air voids is reached when all of the small, individual pockets of air within the compacted material become entrapped, or surrounded by pore water thus tending to prevent the particles from moving closer together. The total voids, however, continue to increase with the moisture content and hence the resultant dry density of the soil decreases (see Section 2.1). As may be inferred from the comparison of the initial and residual moisture contents, plotted in Figure 4.9, the practical consequence of the compaction of material at these moisture contents in the BS 5835: Part 1 (1980) compaction mould is the driving-out of water from the sample through the filter system into the hollow baseplate and to some extent out of the system through the air-bleed hole in the baseplate. This caused the observed low values of the residual moisture content compared to the initial moisture content.

Pike (1972), using the BS 1377 (1975): Test 14, 'Vibrating hammer test', did not characterise this latter portion of the dry density-moisture content relationship, presenting only the convex downwards portion of the curve. Although it is notoriously

difficult to relate the results of laboratory compaction tests to the field condition, in a quantitative sense, the vibrating hammer tests (BS 1377, 1975: Test 14 and BS 5835: Part 1, 1980) are likely to represent more closely the behaviour of material under field compaction conditions than do the drop-weight tests (BS 1377, 1975: Tests 12 and 13) if only for the simple reason that field compacting usually involves the use of vibratory plant, such as the vibratory rammer used in the experimental work presented in Chapter 6. Certainly observations during field compaction of the Wet-mix macadam, and informally communicated experience of research workers at the British Gas Engineering Research Station, indicates that the optimum moisture content determined from the BS 5835: Part 1 (1980) test relates more closely to the field optimum than do the values from drop-weight tests (see Table 4.3).

4.4.5 British Standard compaction tests: A comparison

The principle that for, *'a given amount of compaction, there exists for each soil'*, ..., *'a moisture content termed the "optimum moisture content" at which a maximum dry density is obtained'*, is of fundamental importance to all problems relating to soil compaction. The foregoing quote is derived from Markwick (1945). This basic principle appears to have been deduced independently by both Proctor (1933) and Kelso (1934–35). In his paper, which is now around 45 years old, Markwick described a standard compaction test which, apart from a few minor modifications, is essentially the same as the current BS 1377 (1975): Test 12.

In the years since 1945, BS 1377 (1975): Test 13 has been introduced. This test is essentially a 'heavy compaction' version of Test 12 (see Section 2.2.2). As a result of the increasing usage of vibratory compaction plant for field compaction a further test was introduced in the 1967 revision of BS 1377. This test is now designated as Test 14 in BS 1377 (1975) (see Section 2.2.2). Test 14 is recommended for use with granular soils. In applying this test to the determination of the dry density-moisture content relationship of graded aggregates Pike (1972) generally found the test to be incapable of defining the post-optimum portion of the curve. The test developed by Pike and Acott (1975), and produced later as a British Standard test (BS 5835: Part 1, 1980), was specifically designed for the determination of the dry density-moisture content relationship of graded aggregates.

Several problems have been observed during the course of the experimental work on granular materials, presented in this section, relating to the compaction tests described in BS 1377 (1975):

i)The areas occupied by the rammers, used to apply the compactive effort in Tests 12 and 13, are small and, as such, a blow applied to one part of the surface may cause disruption within the specimen without causing any increase in the density.

ii)Tests 12 and 13 require the removal of material retained on a 20.0 mm test sieve prior to test. As was demonstrated in Section 4.4.3.1 (Figure 4.7) this can mean, in terms of the particle size distribution, that the test specimen bears little relation to the sample removed from the ground or material stockpile.

iii)During tests at high moisture contents the construction of the compaction mould used for Tests 12 and 13 and the *CBR* mould used for Test 14 means that water and fines may be forced out of the specimen during the compaction process and may 'leak' from the moulds. Leakage may be either from between the baseplate and mould, or in some cases, from between the collar and mould. In either case the leaked material is difficult to clean from the mould prior to weighing the specimen and mould to determine the density. This may result in an overestimate of the density.

iv)Excess material is required to be removed from the top of the compacted specimen (Tests 12 and 13) prior to weighing the specimen and mould to determine the density. With coarse granular materials, especially at higher moisture contents, this 'striking-off' process may be impossible to achieve as the wet surface material is simply forced under the straight edge to return to its original shape after the passage of the straight edge.

v)A dilemma may be presented to the operator during the striking-off process as large particles often protude into the excess material while being firmly embedded in the compacted specimen. Either of two courses of action may be followed; the large particles may be completely removed and the resulting voids filled with fine material or the large particles may be forced into the specimen. In the tests reported on the Wet-mix macadam (Section 4.4.3) the latter course of action was followed and the resulting increase in density,

combined with the effect described in (iv) above is believed to have produced an equivalent volume of around 3% (Figure 4.6).

The above observations must, of course, be tempered with the knowledge that the BS 1377 (1975): Tests 12 and 13 are not intended for use with graded aggregates.

Most of the problems noted above are eliminated by the experimental apparatus and procedure of the BS 5835: Part 1 (1980) test designed for use with graded aggregates. These can be treated in a point by point manner as above:

i)The full area of the specimen is occupied by the compaction anvil thus preventing the 'de-compaction' of areas adjacent to the area of compaction.

ii)Larger particle sizes may be retained in the test specimen than for BS 1377 (1975): Tests 12 and 13; only materials retained on a 37.5 mm test sieve need be removed. Although graded aggregates, as defined by the Department of Transport (1986); see Appendix 3, may contain particles of up to 50 mm (Wet-mix macadam) or even 75 mm (Types 1 and 2), this represents a significant stride forward compared to the two BS 1377 tests.

iii)The problem which may be created by the BS 1377 (1975): Tests 12, 13 and 14 by water being forced out of the specimen during the compaction process is overcome by the use of a purpose designed drainage system, within the baseplate, and the requirement to remove the entire sample from the compaction mould, prior to weighing, in order to calculate the density.

iv)Removal of excess material from the top of the compacted specimen is not required for the BS 5835: Part 1 (1980) test as the volume is measured rather than being controlled as for BS 1377 (1975): Tests 12 and 13. This comment may also be applied to BS 1377 (1975): Test 14.

v)As (iv) above.

Just one cautionary note is relevant to the BS 5835: Part 1 (1980) test:— as a result of the requirement for five compaction tests to be carried out at each moisture content the time required for both specimen preparation and testing is significantly greater than that for the BS 1377 (1975) tests. However, the much reduced scatter in the data derived from the BS 5835 test (Figure 4.9) compared to the data derived from the BS 1377: Test 12 (Figure 4.6) may be due partly to the five tests constituting a more representative sample than is provided by the single test.

As may be inferred from the foregoing discussion the test described in BS 5835: Part 1 (1980) has a number of advantages over the more traditional tests described in BS 1377 (1975). The current 1975 edition of BS 1377 is soon to be updated with a new edition. Study of the draft for discussion document relating to compaction tests (BS 1377: Part 4, 1988) is disappointing in as much as the old Tests 12, 13, and 14 appear to be little changed and have certainly not benefited from the use of the principles of the BS 5835: Part 1 (1980) test.

In its favour the new draft standard for compaction related tests (BS 1377, 1988: Part 4) is much more detailed and more clearly laid out than its predecessor (BS 1377, 1975: Tests 12, 13 and 14). The draft standard also gives test methods for the determination of the maximum dry density (by vibratory compaction under water) and the minimum dry density (by free fall) of sand and gravel materials for which difficulty in obtaining an optimum moisture content at a maximum dry density may be experienced (Clause 4). This allows the calculation of the relative density, D_r, from Equation 4.4[2]. Clause 5 gives a standard method for the determination of the Moisture Condition Value (MCV), using the Moisture Condition Apparatus (MCA). This test is described in detail by Parsons and Bowden (1979) and is generally used to determine the moisture suitability of soils prior their compaction.

4.4.6 The influence of compactive effort on maximum dry density and optimum moisture content

Compaction results, in particular the maximum dry density and optimum moisture content data, require a framework for their proper interpretation. One way of achieving this is to consider the compactive effort (CE) applied to the material. For that purpose the compactive effort may be defined as the energy applied per unit volume of material. Thus, for tests to BS 1377 (1975): Test 12, compactive effort is defined as

$$CE = \frac{m\,\mathrm{g}H N_l N_b}{V} \qquad [\mathrm{J/m^3}] \tag{4.11}$$

where:

m is the mass of the rammer (= 2.5 kg),

g is the acceleration due to gravity (= 9.81 m/s),

H is the drop-height of the rammer (= 0.300 m),

[2]The relative density, D_r, is described as the density index, I_D, in BS 1377 (1988): Part 4 (i.e. $I_D = D_r$).

N_l is the number of compacted layers (= 3),

N_b is the number of blows applied to each layer with the rammer (=variable), and

V is the volume of the mould (= 944×10^{-6} m^3).

This yields a value of 631 kJ/m^3 for N_b of 27. In contrast, for the BS 5835: Part 1 (1980) test compactive effort is defined as

$$CE = \frac{Pt}{V} \qquad [\mathrm{J/m^3}] \tag{4.12}$$

where:

P is the power output of the vibrating hammer (= 900 W),

t is the time for which the vibrating hammer is allowed to compact the aggregate (= 180 seconds), and

V is the average volume of the samples compacted at the maximum dry density (= 1085×10^{-6} m^3).

It should be noted that in this test the volume of the compacted material is measured, and not constrained, as in BS 1377 (1975): Tests 12 and 13.

Equation 4.12 yields a value of compactive effort, CE = 149309 kJ/m^3. However, this figure relates to the total rated electrical input power of the vibrating hammer. In calculating the compactive effort for the vibrating hammer used in the BS 1377 (1975): Test 14 compaction test Head (1980) assumes that 50% of the electrical input power is converted into mechanical energy of which half is absorbed by the operator holding the vibrating hammer. Making assumptions along similar lines for the BS 5835: Part 1 (1980) test—that 50% of the electrical input is converted into mechanical energy and that half of that energy is absorbed by the resulting vibration of the mass-hanger arrangment and the vibrating hammer itself, and that half of the energy remaining is used in overcoming friction between the compaction anvil 'O'-rings and the compaction pot[3]—Equation 4.12 then becomes

$$CE = \frac{Pt}{8V} \qquad [\mathrm{J/m^3}] \tag{4.13}$$

thus giving CE = 18664 kJ/m^3. This figure appears to be somewhat more realistic than the value from Equation 4.12 for the total electrical input power, in comparison to the compactive efforts calculated for the three BS 1377 (1975) tests.

[3]The reduction factor relating to the friction between the compaction anvil 'O'-rings and the compaction pot is purely nominal and friction may well reduce the calculated energy by a greater amount than is actually the case. However, in the absence of any evidence as to the numerical value of the actual energy applied to the compacted soil the estimate may be seen as adequate, provided that it is fully recognised that it is an estimate.

Figure 4.10 shows the compactive effort (logarithmic scale) plotted against the maximum dry density for the three materials, Permian and Sharp Sands and Wet-mix macadam (corrected for stone content and also uncorrected). Figure 4.12 is a similar plot dealing with the data for the optimum moisture content. Hogentogler (1938) fitted straight lines to similar data for static compaction.

The values of compactive effort have also been calculated for BS 1377 (1975): Test 13, '4.5 kg rammer method', and BS 1377 (1975): Test 14, 'Vibrating hammer method' (see Table 4.4). These are marked for comparative purposes on the plots of the logarithm of compactive effort against maximum dry density and optimum moisture content (Figures 4.10 and 4.11). BS 1377 (1975): Tests 12 and 13 specify the use of a mould of 1000 cm^3 volume but it should be noted that the mould used for Test 12 determinations of the dry density-moisture content relationship was slightly under-sized. The volume of the mould used for testing purposes is 944 cm^3 (or $1/30\,ft^3$) which complies with the forerunner of the current standard; BS 1377 (1967) Tests 11 and 12. The comparative values of compactive effort calculated for Tests 12 and 13, illustrated in Figures 4.10 and 4.11, are based on the 1000 cm^3 mould complying with the requirements of BS 1377 (1975): Tests 12 and 13.

Consideration of the relationships between compactive effort and both maximum dry density and optimum moisture content (Figures 4.10 and 4.11, respectively) for the Permian Sand gives:

$$\rho_{d_{\max}} = 1.466 + 0.126 \log CE \qquad (r = 0.999) \tag{4.14}$$

for the maximum dry density (Figure 4.10), and

$$w_{\text{opt}} = 18.12 - 2.46 \log CE \qquad (r = 0.989) \tag{4.15}$$

for the optimum moisture content (Figure 4.11), for $N_b = 27, 54, 81$. As noted earlier, the two determinations at higher compactive efforts ($N_b = 108, 135$) were carried out by a different operator (McCulloch, 1987) and exhibit higher levels of maximum dry density than would be predicted by simple extrapolation of Equation 4.14 and similarly lower levels of optimum moisture content than would be predicted from Equation 4.15. Straight lines between the two points for $N_b = 108, 135$ yield:

$$\rho_{d_{\max}} = 1.589 + 0.103 \log CE \tag{4.17}$$

for the maximum dry density (Figure 4.10), and

$$w_{\text{opt}} = 19.92 - 3.09 \log CE \tag{4.18}$$

for the optimum moisture content (Figure 4.11), for $N_b = 108, 135$. Sherwood (1970) gave an assessment of the mean and standard deviation from 36 determinations by 36 operators of the maximum dry density and optimum moisture content to BS 1377 (1975): Test 12 ($N = 27$) on a Clayey Sand ($\overline{\rho}_{d_{\max}} = 1.79\,\text{Mg/m}^3, \sigma_{\rho_{d_{\max}\,n-1}} = 0.029\,\text{Mg/m}^3, \overline{w}_{\text{opt}} = 15.0\%$ and $\sigma_{w_{\text{opt}\,n-1}} = 0.98\%$). These standard deviations are superimposed on the data points for Permian Sand ($N_b = 81, 108$) and when extrapolated parallel to the appropriate regression lines it can be seen that the observed variations, which are here assigned to the tests having been conducted by two different operators, are well within the limits described by Sherwood (1970) for both the maximum dry density (Figure 4.10) and the optimum moisture content (Figure 4.11).

From the data for the Sharp Sand the relationships between compactive effort and both maximum dry density and optimum moisture content are:

$$\rho_{d_{\max}} = 1.271 + 0.167 \log CE \qquad (r = 1.000) \tag{4.19}$$

for the maximum dry density (Figure 4.10), and

$$w_{\text{opt}} = 25.69 - 4.25 \log CE \qquad (r = 0.973) \tag{4.20}$$

for the optimum moisture content (Figure 4.11), for $N_b = 27, 54, 81$.

A similar treatment of the data for Wet-mix macadam matrix material (passing a 19.05 mm test sieve) gives relationships between compactive effort and both maximum dry density and optimum moisture content as follows:

$$\rho_{d_{\max}} = 1.641 + 0.216 \log CE \qquad (r = 0.983) \tag{4.21}$$

for the maximum dry density (Figure 4.10), and

$$w_{\text{opt}} = 14.47 - 2.05 \log CE \qquad (r = 0.989) \tag{4.22}$$

for the optimum moisture content (Figure 4.11), for $N_b = 27, 54, 81$.

Similarly for the Wet-mix macadam mass material:

$$\rho_{d_{\max}} = 1.957 + 0.152 \log CE \qquad (r = 0.971) \tag{4.23}$$

for the maximum dry density (Figure 4.10), and

$$w_{\text{opt}} = 9.36 - 1.23 \log CE \qquad (r = 0.989) \tag{4.24}$$

for the optimum moisture content (Figure 4.11), for $N_b = 27, 54, 81$.

In Section 4.4.3 it was noted that the dry density-moisture content relationships for Wet-mix macadam, determined to BS 1377 (1975): Test 12 ($N_b = 27, 54, 81$) and illustrated in Figure 4.6, corresponded to the impossible state of negative air voids at moisture contents at or above optimum. Possible explanations were proposed for this effect and it was suggested that if the volume of the compacted material was some 3% greater than the volume of the compaction mould this apparent error would be fully accounted for. Applying this error to the matrix material (< 19.05 mm) gives a relationship between compactive effort and maximum dry density as follows:

$$\rho_{d_{\max}} = 1.642 + 0.193 \log CE \qquad (r = 0.987) \tag{4.25}$$

for $N_b = 27, 54, 81$. Applying the correction for stone content given by Equation 4.8 (Section 4.4.3.1) gives a relation for the mass material corrected for the possible 3% volume error:

$$\rho_{d_{\max}} = 1.979 + 0.130 \log CE \qquad (r = 0.967) \tag{4.26}$$

for $N_b = 27, 54, 81$. The effect of the 3% equivalent volume error on the calculated compactive effort was found to be negligible and the correction has not been used in the determination of Equations 4.25 and 4.26. These data are plotted in Figure 4.10.

Plainly, volume errors such as those described above have no influence on the moisture content as determined from the compacted sample and thus corrections were not made to the relationships between compactive effort and optimum moisture content.

The fit of the single determination of maximum dry density and optimum moisture content to BS 5835: Part 1 (1980) with the above data is of some considerable importance. The sharply differing mode of compaction (vibrating hammer as opposed to drop weight) may go some way to explaining the lack of fit of this point to the BS 1377 (1975): Test 12 based determinations. The means of determining the level of compactive effort requires the assumption that apparently arbitrary amounts of energy are lost, as a result of converting the electrical energy of the vibrating hammer into mechanical energy, in vibrating the mass-hanger arrangement and overcoming the friction between the compaction anvil 'O'-rings and the compaction pot. These correction factors are applied following similar principles to

those used by Head (1980) to calculate compactive effort for the BS 1377 (1975): Test 14 'Vibrating hammer method'.

Logic would suggest that the maximum dry density data for the mass material corrected for the 3% equivalent error in volume should most likely fit with the data from the BS 5835: Part 1 (1980) test. From Figure 4.10 this is clearly not the case. The best-fit line through the data for the matrix material (< 19.05 mm) has been extrapolated to illustrate the lack of fit which the BS 5835: Part 1 (1980) data exhibits with the mass material data. Although a best-fit straight line could be applied to the matrix material data with a high value of the regression correlation coefficient resulting ($r \approx 0.98$), there is no reason to expect a correlation to exist between these data.

For the data relating to the optimum moisture content determination to BS 5835: Part 1 (1980), a fit with the data to BS 1377 (1975): Test 12 corrected for the stone content (mass material) would appear most likely. Applying Sherwood's (1970) value for $\sigma_{w_{\mathrm{opt}_{n-1}}}$ and extrapolating with increasing compactive effort parallel to Equation 4.24 shows that the value determined using the BS 5835: Part 1 (1980) method lies well within the range of values that might be expected if determined to BS 1377 (1975): Test12, with increased compactive effort ($N_b \approx 800$), dependent upon the operator.

In the foregoing paragraphs an approach, similar to that of Hogentogler (1938), yields good best-fit log-linear straight lines (regression correlation coefficient, r, generally ≥ 0.97) between compactive effort and both maximum dry density and optimum moisture content for the dynamic compaction data presented here.

4.5 10% Fines value: Wet-mix macadam

Normally, tests to determine the 10% fines value and the associated Aggregate Impact Value (AIV) are conducted on samples of aggregate in a surface-dry condition passing 14 mm and retained on 10 mm test sieves as specified in BS 812: Part 3 (1975), Sections 8 and 6, respectively. The Department of Transport (1986) specification for Wet-mix macadam requires the aggregate to be tested as detailed in the British Standard except that the material be tested in a saturated surface-dried condition, after having been soaked in water at room temperature for 24 hours without previously having been oven dried. It is this modified procedure that has been followed in obtaining the results presented in this section.

The 10% fines value gives a measure of the resistance of an aggregate to crushing and which is applicable to both weak and strong aggregates. The test requires an aggregate sample, prepared as described above, to be placed in a mould of 154 mm diameter in three equal layers each of which is manually tamped 25 times using a steel tamping rod. The quantity of material used is that required to give a total depth of sample of around 100 mm. The sample is then loaded steadily over a period of 10 minutes to a terminal load as determined from Equation 4.27:

$$\text{Required force, } x \text{ (kN)} = \frac{4000}{AIV} \tag{4.27}$$

where AIV is the Aggregate Impact Value.

The Aggregate Impact Value, used to determine the required load for the 10% fines test, gives a relative measure of the resistance of an aggregate to sudden shock or impact. It is determined, like the 10% fines value, from tests on the fraction passing 14 mm and retained on 10 mm test sieves. The mass of sample required is determined using a measure which is filled in three layers, each layer being manually tamped 25 times, with the surplus aggregate removed such that the cylindrical tamping rod may be rolled across the top of the measure without any impedence to its passage. Any obvious voids at the surface are then filled with some of the surplus aggregate previously removed. The sample is then placed in a metal cup of 102 mm diameter and 50 mm depth. The sample is then tamped a further 25 times and the cup is clamped into position in the aggregate impact test machine (see BS 812: Part 3, 1975; Figure 1). Fifteen blows are then applied to the sample using the impact testing machine, each blow being delivered at an interval of not less than 1 second. The Aggregate Impact Value is then determined by sieving the sample on a 2.36 mm test sieve and calculated as the percentage fines:

$$\text{Percentage fines } (AIV) = \frac{m_2}{m_1} \times 100\% \tag{4.28}$$

where:

m_1 is the initial mass of sample (g), and

m_2 is the mass of the fraction passing the 2.36 mm test sieve (g).

The Aggregate Impact Value was found to be 18% from the average of two tests for the Wet-mix macadam. The required load, calculated from Equation 4.27, for the 10% fines value test was thus determined to be 222 kN.

After loading, the material was sieved on a 2.36 mm test sieve and the percentage fines, calculated as for the aggregate impact value test (Equation 4.28), recorded as 13.8%. This value lies outside the 7.5 to 12.5% limits required for the calculation of the 10% fines value in Section 8 of BS 812: Part 3 (1975). The required load was re-calculated as 175 kN, from

$$\text{Force required to produce 10\% fines} = \frac{14x}{y+4} \tag{4.29}$$

where:

x is the required force (kN), and

y is the mean percentage fines from two tests at x kN force.

Previous experience with this test procedure indicated that the required load calculated above (175 kN) may have been somewhat low for this material. As the object of the calculation is to determine a load which will give a fines value close to 10% (within the range 7.5 to 12.5%) the load was increased to 200 kN. Two further tests were carried out to determine y (in Equation 4.29 above) using the 200 kN load and the mean percentage fines from these two tests was 11.3%. Thus, from Equation 4.29, the force required to produce 10% fines is 180 kN (to the nearest 10 kN), which is significantly higher than the 50 kN minimum specified by the Department of Transport (1986) for material conforming to the specification for Wet-mix macadam.

4.6 Flakiness index: Wet-mix Macadam

The method of determination of the flakiness index of a coarse aggregate is given in BS 812: Section 105.1 (1985).

Aggregate particles are defined as flaky when they have a thickness (smallest dimension) of less than 0.6 of their nominal size, the nominal size being defined as the mean of the limiting sieve apertures used for determining the size fraction in which the sample occurs. The flakiness index of an aggregate is found by separating the flaky particles, *i.e.* those which pass the apertures of a standard thickness gauge (see BS 812: Section 105.1, 1985; Figure 1 and Table 4.5), and expressing their

mass as a percentage of the mass of the sample tested. The test is not applicable to material passing a 6.30 mm test sieve or to material retained on a 63.0 mm test sieve.

The flakiness index (FI) was calculated for each of the particle size fractions specified in BS 812: Section 105.1 (1985), and tabulated along with the particle size fractions required and corresponding thickness gauge slot sizes, in Table 4.5. The overall value of the flakiness index is calculated from the percentage of the sum of the masses passing each thickness gauge slot (m_3) relative to the sum of the masses of each of the specified particle size fractions (m_2):

$$FI = \frac{m_3}{m_2} \times 100\% \qquad (4.30).$$

The fraction passing 63 mm and retained on 50.0 mm was not present in the Wet-mix macadam tested while the fraction passing 50.0 mm and retained on 37.5 mm tested had a total mass representing less than 5% of the original total mass of the specified size fractions (m_1) (Table 5.7) and was rejected for calculation purposes as specified in BS 812: Section 105.1 (1985). The flakiness index is thus calculated as 20%.

The Department of Transport (1986) state that material conforming to the specification for Wet-mix macadam must have a flakiness index of less than 35. Clearly the Wet-mix macadam under examination here conformed to this specification.

4.7 Mineralogy of the Yellow Permian Sand

The qualitative mineralogy of the Yellow Sand used in the laboratory based trench was determined from an air-dried and ground ($< 150\ \mu$m) sample by random powder X-Ray Diffractometry (XRD). The sample used was obtained by riffling some 10 kg of the bulk material down to a mass of 20 g, which after homogenisation was air-dried for 48 hours before grinding. X-Ray Fluorescence (XRF) was also carried out on pelletised samples to determine the quantitative chemical structure of the sand and so assist in the interpretation of the XRD results. Detailed XRF results (chemical analysis) are not presented in this thesis. Quartz content was determined by comparison of the areas of the x-ray peaks with those of artificially prepared standards of known quartz content. Calcite and Potassium Feldspar contents were determined by assuming reasonable values for the CaO and K_2O contents, respectively, and comparing these to the measured values of the sample as a whole. Kaolinite content was

determined by examination of the XRD peaks of a glycolated sample and checked by difference. Some small quantities of Illite were detected, although the amount represented much less than 1%. Around 30% of Illitic mixed-layer clay mineral was estimated to be expandable from comparison of the XRD peak areas of glycolated and un-glycolated samples[4]. Results are presented in Table 4.6.

The Durham Yellow Sands are believed to be Basal Permian Sands and have been described in previous mineralogical investigations (Hodge, 1932; Smith and Pattison, 1970) as having 10–20% total Feldspars in the whole of the loose outcrop, with the Quartz grains generally tending to be less than 1 mm diameter. The results presented here are generally supportive of the material being a Durham Yellow Sand.

4.8 Discussion and summary

In this chapter the important task of the classification of the materials used in the experimental work presented in Chapter 6 has been described. The materials were classified by means of the particle size distribution (Section 4.2) and the procedure given in BS 5930 (1981). Additionally, by means of the particle size distribution, the Sharp Sand has been identified as conforming to the BS 882 (1983) definition of Concrete Sand (Grading C). The particle size distribution of the Permian Sand falls on the fine side of the grading envelopes for Concrete Sands. The mineralogy of the Permian Sand was determined (Section 4.7) in order to explain the apparent cementing of this material with time; this effect will be discussed further in Chapter 7. The Wet-mix macadam material used in the experimental work was found to fall within the Department of Transport (1986) grading envelope for Wet-mix macadam. Tests to determine the 10% fines value and the Flakiness index (Sections 4.5 and 4.6 respectively) of the Wet-mix macadam were also necessary to confirm the materials adherance to the Department of Transport (1986) specification.

Values of specific gravity and the water absorption value were determined for each of the three materials and are reported in Section 4.3. These determinations were made simply in order that the lines of constant air voids could be plotted for comparison with the dry density-moisture content relationships.

[4]It has long been recognised that the separation of illite and smectite must frequently be purely arbitrary, with, in general, expanding material being called smectite and non-expanding material being called illite. According to Grim (1968) *'many minerals described in the literature as illites are undoubtably mixed-layer structures of micas and expandable components'*.

Dry density-moisture content relationships are reported in Section 4.4. Most of the tests were carried out to BS 1377 (1975): Test 12 with the notable addition of repeat determinations of the dry density-moisture content relationships at higher levels of compactive effort, defined as the energy input per unit volume. Results for the Permian Sand were presented in Section 4.4.1 (Figure 4.4) while results for the Sharp Sand were presented in Section 4.4.2 (Figure 4.5). The results for Wet-mix macadam were presented in two different forms; firstly before the application of a correction for the stone content in Section 4.4.3 (Figure 4.6) and secondly after the correction of the stone content in Section 4.4.3.1 (Figure 4.6). Standard soils tests often require the scalping, or removal of large particles, prior to testing. This effect often means that the specimens tested bear little relation to the bulk properties of the material and is discussed, in the context of the compaction tests carried out on the Wet-mix macadam, in Section 4.4.3.1. The data shown in Figure 4.6 indicate that the Wet-mix macadam, after compaction at high moisture contents, has negative air voids—an impossible state. This effect is attributed to the unsuitability of the BS 1377 (1975): Test 12 for the determination of the dry density-moisture content relationship of graded aggregates. A further test was carried out to the current British Standard for the determination of the dry density-moisture content relationship for graded aggregates, the results of which are presented in Section 4.4.4 (Figure 4.9). The differences between the BS 1377 (1975) test and the BS 5835: Part 1 (1980) test are discussed in Section 4.4.5 and it is concluded that the BS 5835 is eminently more suitable for the determination of the dry density-moisture content relationship of graded aggregates and that the test incorporates a number of innovations which could usefully be incorporated in the imminent new edition of BS 1377.

The values of maximum dry density and optimum moisture content were interpreted in terms of the logarithm of compactive effort in Section 4.4.6 (Figures 4.10 and 4.11). From the limited data available for Permian Sand, performed by a different operator, it was concluded that the estimates of operator errors in the determination of both maximum dry density and optimum moisture content (Sherwood, 1970), determined to BS 1377 (1975): Test 12, were of the correct magnitude. The maximum dry density determined to BS 5835: Part 1 (1980) was shown to bear little relation to the values determined to BS 1377 (1980): Test 12. In contrast the optimum moisture content data determined by the two procedures showed good aggreement.

Table 4.1 - Analysis of particle size distribution for Permian Sand, Sharp Sand and Wet-mix macadam and description to BS 5930 (1981).

Parameter	Permian Sand	Sharp Sand	Wet-mix macadam
Gravel (%)	1	27	76
Sand (%)	92	72	17
Silt/Clay (%)	7	1	7
Description	Well graded sand with fines	Well graded sand	Well graded gravel (crushed rock) with fines
Class	SWF	SW	GW

Table 4.2 - Specific gravities (on an oven-dried basis) for Permian Sand, Sharp Sand and Wet-mix macadam; water absorption values for the Wet-mix macadam are also given.

Material	$\overline{G}_s/\sigma_{G_{sn-1}}$	$\overline{w}_A/\sigma_{w_{An-1}}$
Permian Sand	2.60/0.007	—/—
Sharp Sand	2.52/0.023	—/—
Wet-mix macadam:		
a_1 : 40 mm > particle size $\geq$ 19.05 mm	2.71/0.008	0.5/0.08
a_2 : 19.05 mm > particle size $\geq$ 4.76 mm	2.70/0.020	0.8/0.01
a_3 : 4.76 mm > particle size $\geq$ 75 μm	—/—	1.3/0.13
a_4 : 4.76 mm > particle size	2.70/0.010	—/—
a_5 : 75 μm > particle size	—/—	Assumed = 1.3

Table 4.3 - Summary compaction data for Permian Sand, Sharp Sand and Wet-mix macadam.

Material	Number of blows per layer N_b	Maximum dry density $\rho_{d_{max}}$ (Mg/m^3)	Optimum moisture content w_{opt} (%)
Permian Sand	27	1.82	11.2
BS 1377 (1975): Test 12	54	1.86	10.6
	81	1.88	10.0
	108	1.94	9.4
	135	1.95	9.1
Sharp Sand	27	1.74	13.7
BS 1377 (1975): Test 12	54	1.79	12.8
	81	1.82	11.6
Wet-mix macadam			
BS 1377 (1975): Test 12	27	2.24	8.7
$<$ 19.05 mm	54	2.32	8.2
	81	2.34	7.7
Wet-mix macadam			
BS 1377 (1975): Test 12	27	2.38	5.9
Corrected for material	54	2.44	5.6
$\geq$ 19.05 mm	81	2.45	5.3
Wet-mix macadam			
BS 5835: Part1 (1980)	—	2.37	4.6

Table 4.4 - Compactive effort data.

British Standard Test	Mass of rammer m (kg)	Drop height H (m)	Number of blows per layer N_b	Number of layers N_l	Power output P (W)	Period of application t (seconds)	Volume of sample V (m^3)	Compactive effort CE (kJ/m^3)
BS 1377 (1975): Test12	2.5	0.3	27	3	—	—	944×10^{-6}	631
Under-size mould as used	2.5	0.3	54	3	—	—	944×10^{-6}	1263
in testing programme	2.5	0.3	81	3	—	—	944×10^{-6}	1894
(BS 1377, 1967: Test11)	2.5	0.3	108	3	—	—	944×10^{-6}	2525
	2.5	0.3	135	3	—	—	944×10^{-6}	3157
BS 1377 (1975): Test12 Full size mould	2.5	0.3	27	3	—	—	1000×10^{-6}	596
BS 1377 (1975): Test13	4.5	0.45	27	5	—	—	1000×10^{-6}	2682
BS 1377 (1975): Test14†	—	—	—	3	600	60	2300×10^{-6}	11739
	—	—	—	3	750	60	2300×10^{-6}	14674
BS 5835: Part 1 (1980)	—	—	—	1	900	180	1085×10^{-6}	18664

†BS 1377: Test 14 allows the compacted height of the specimen to vary between 127 and 133 mm. For simplicity of calculation the value of compactive effort was based on a compacted specimen height of 127 mm (*i.e.* the full height of the *CBR* mould).

Table 4.5 - Flakiness index data.

Aggregate size fraction BS test sieve nominal aperture size		Thickness gauge slot width†	Mass of original fraction	Mass of final fraction	Mass passing thickness gauge slots	Flakiness index
100% passing (mm)	100% retained (mm)	(mm)	m_1 (g)	m_2 (g)	m_3 (g)	FI (%)
63.0	50.0	33.9 ± 0.3	—	—	—	—
50.0	37.5	26.3 ± 0.3	291	—	—	—
37.5	28.0	19.7 ± 0.3	3335	3335	565	17
28.0	20.0	14.4 ± 0.15	4152	4152	732	18
20.0	14.0	10.2 ± 0.15	4359	4359	726	17
14.0	10.0	7.2 ± 0.1	3014	3014	685	23
10.0	6.3	4.9 ± 0.1	1134	1134	556	49
			$\sum = 13285$	$\sum = 15994$	$\sum = 3264$	20

†This dimension is equal to 0.6 times the mean sieve size.

Table 4.6 - Mineralogy of the Permian Sand.

Mineral	
Quartz	80%
Potassium Feldspar	15%
Calcite	3%
Kaolinite	2%
Illite	$\ll 1\%^{\dagger}$

†Approximately 30% of the Illite present is estimated to be expandable.

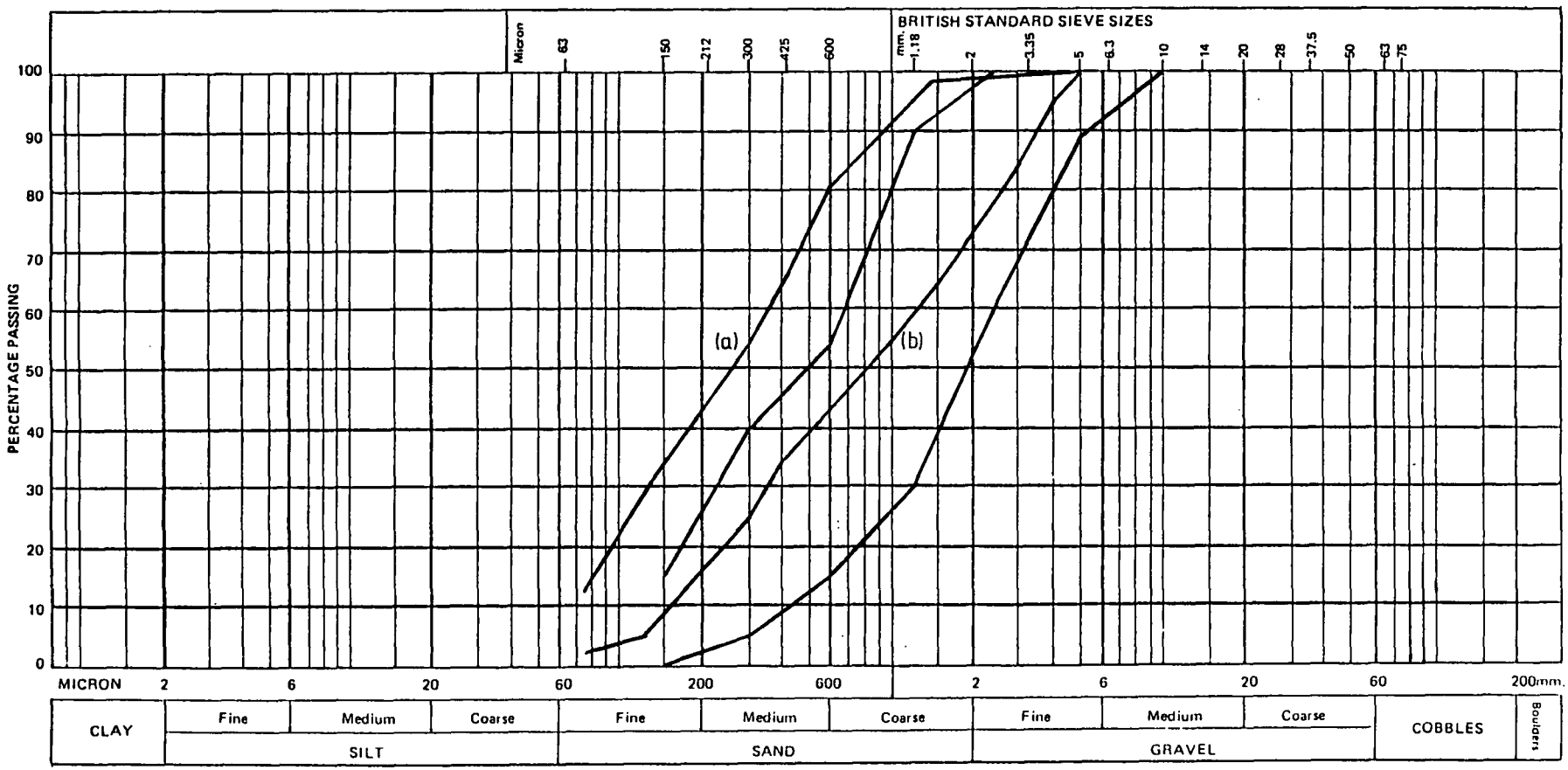

Figure 4.1 - Particle size distribution curves for Permian Sand (a) and Sharp Sand (b) with the grading envelope for BS 882 (1983) Concrete Sand Grading C.

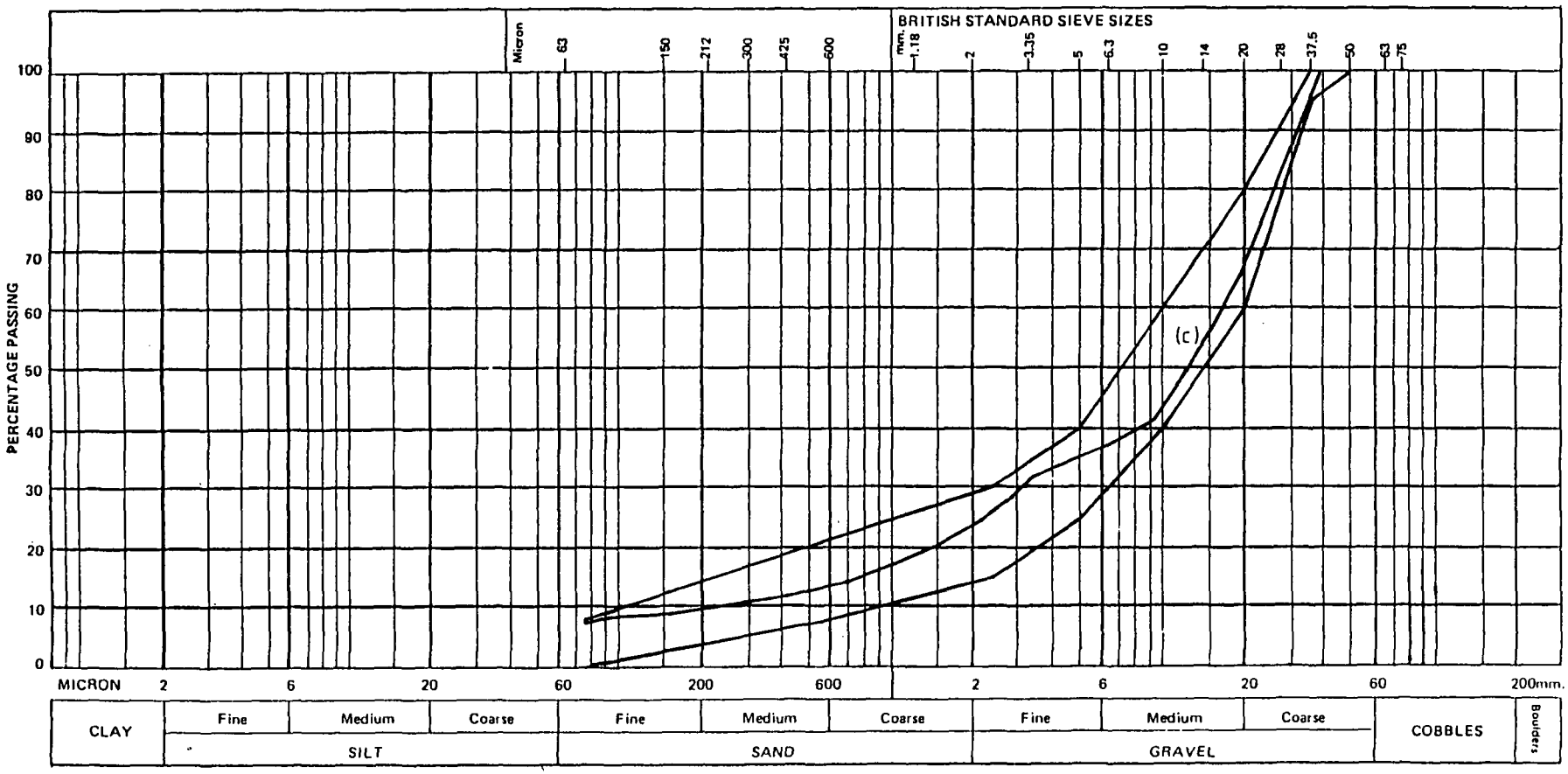

Figure 4.2 - Particle size distribution curves for Wet-mix macadam (c) with the Department of Transport (1986) grading envelope for Wet-mix macadam.

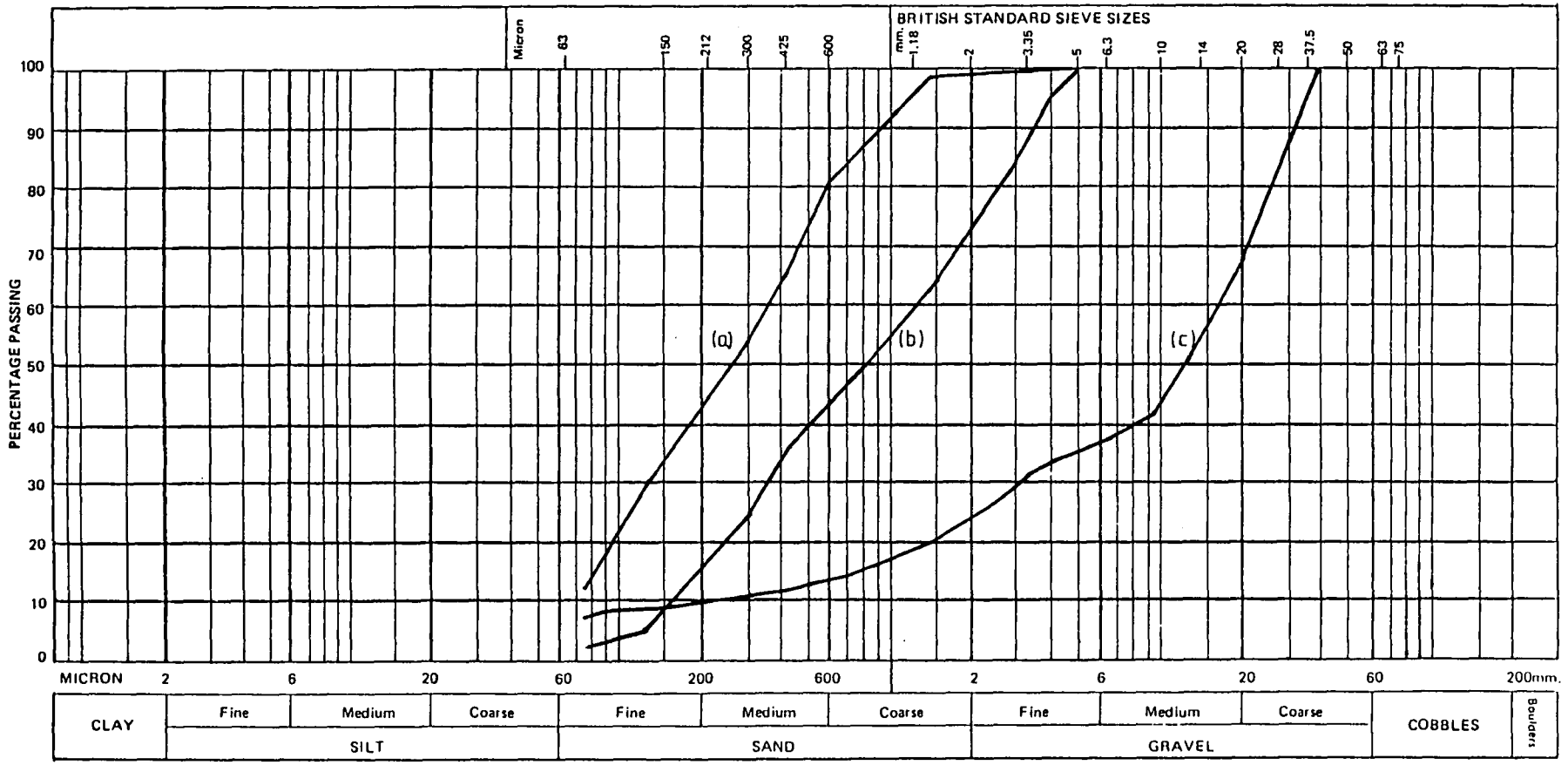

Figure 4.3 - Particle size distribution curves for Permian Sand (a), Sharp Sand (b) and Wet-mix macadam (c).

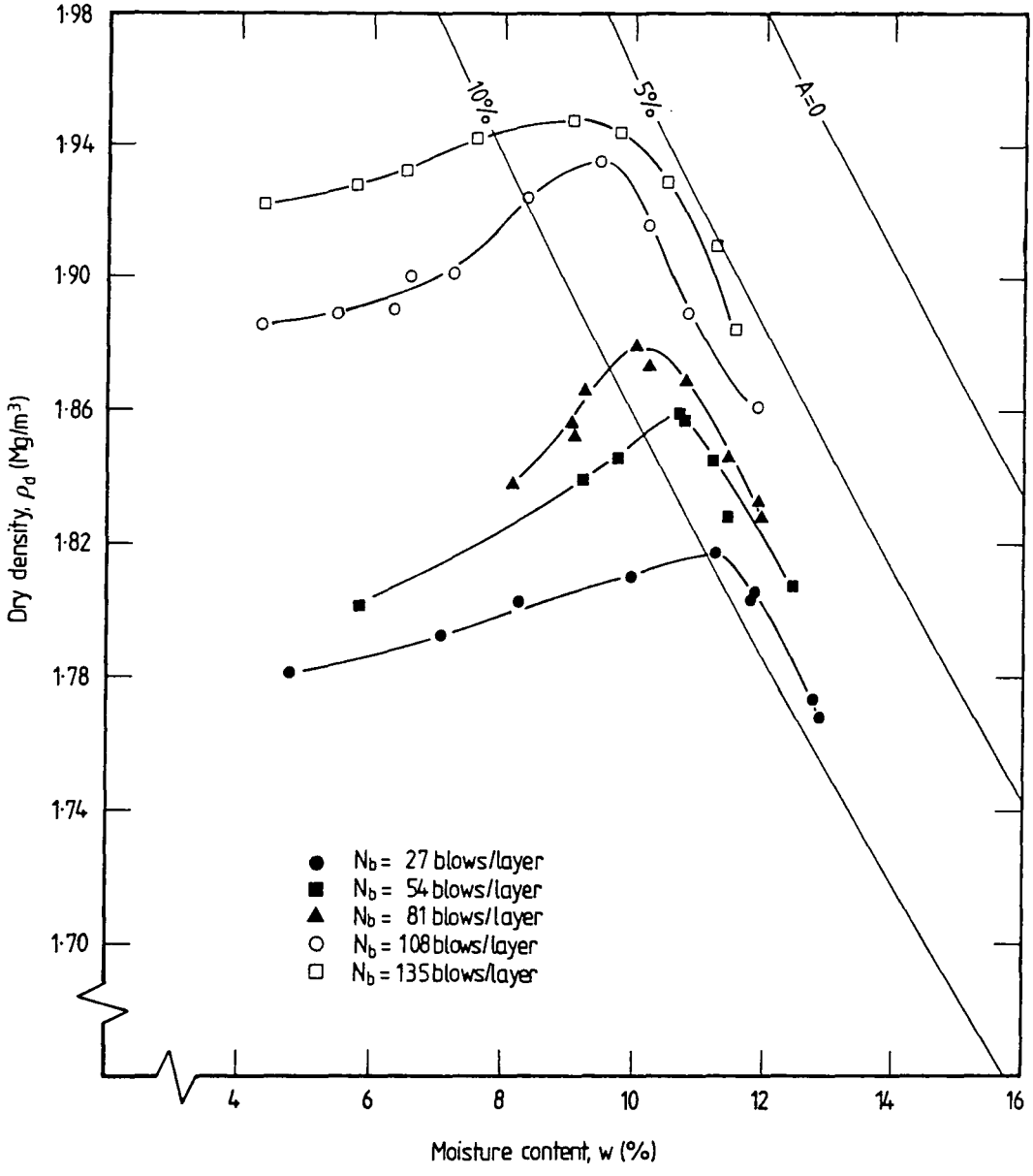

Figure 4.4 - Dry density-moisture content relationships for Permian Sand compacted at 27, 54, 81, 108 and 135 blows/layer to BS 1377 (1975): Test 12. Curves of constant air voids (A = 0, 5 and 10%) are also shown.

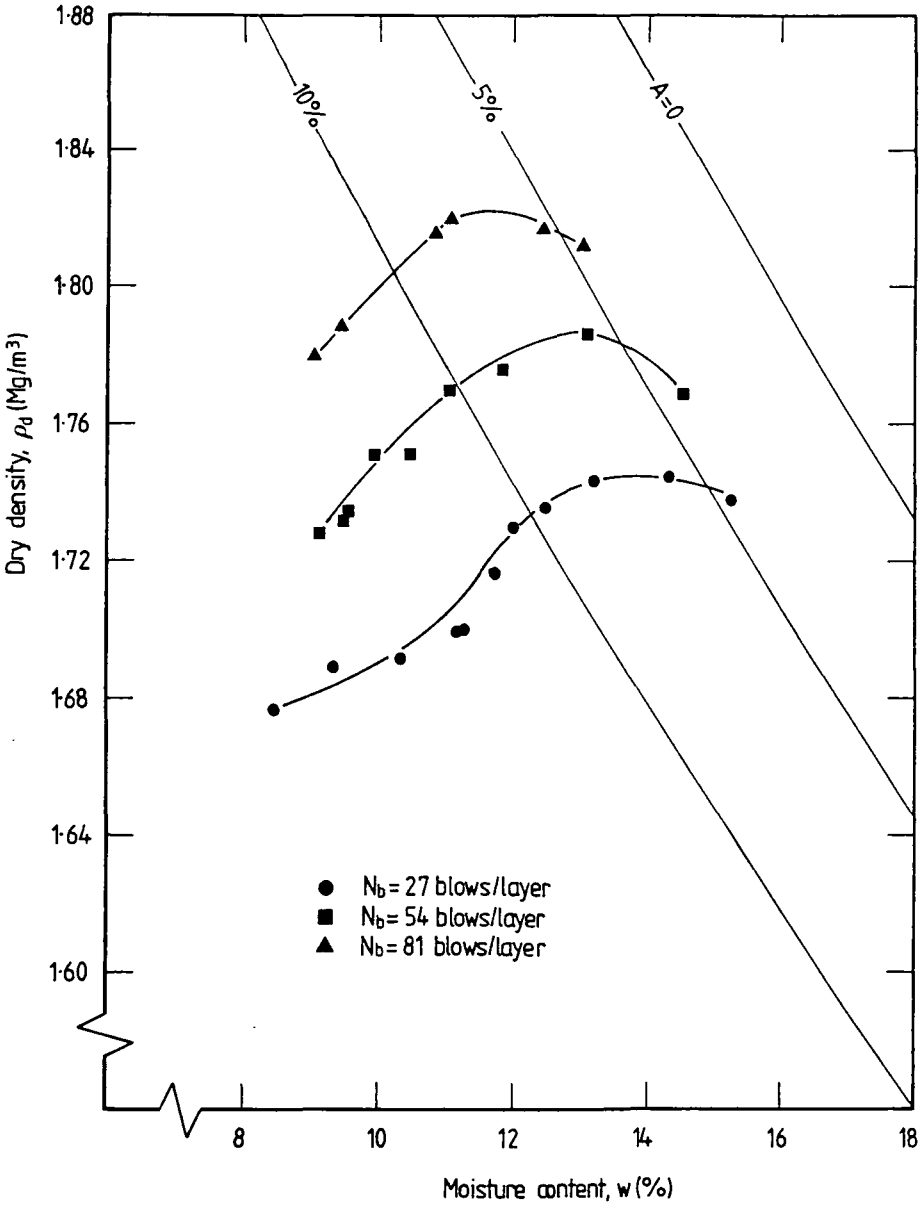

Figure 4.5 - Dry density-moisture content relationships for Sharp Sand compacte at 27, 54 and 81 blows/layer to BS 1377 (1975): Test 12. Curves of constant a voids ($A = 0$, 5 and 10%) are also shown.

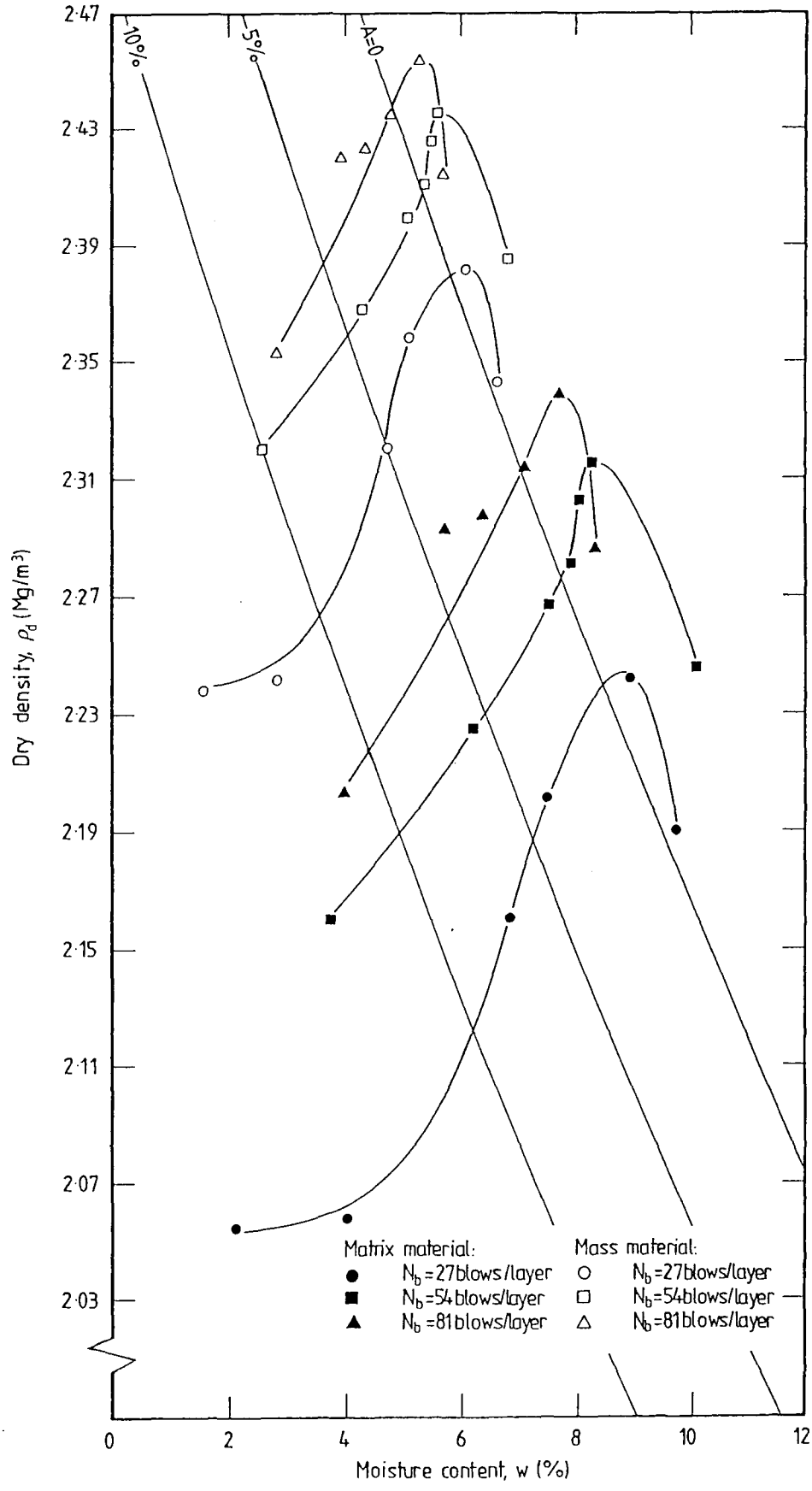

Figure 4.6 - Dry density-moisture content relationships for Wet-mix macadam compacted at 27, 54 and 81 blows/layer to BS 1377 (1975): Test 12. The curves are shown both corrected and uncorrected for the stone content of the material. Curves of constant air voids (A = 0, 5 and 10%) are also shown.

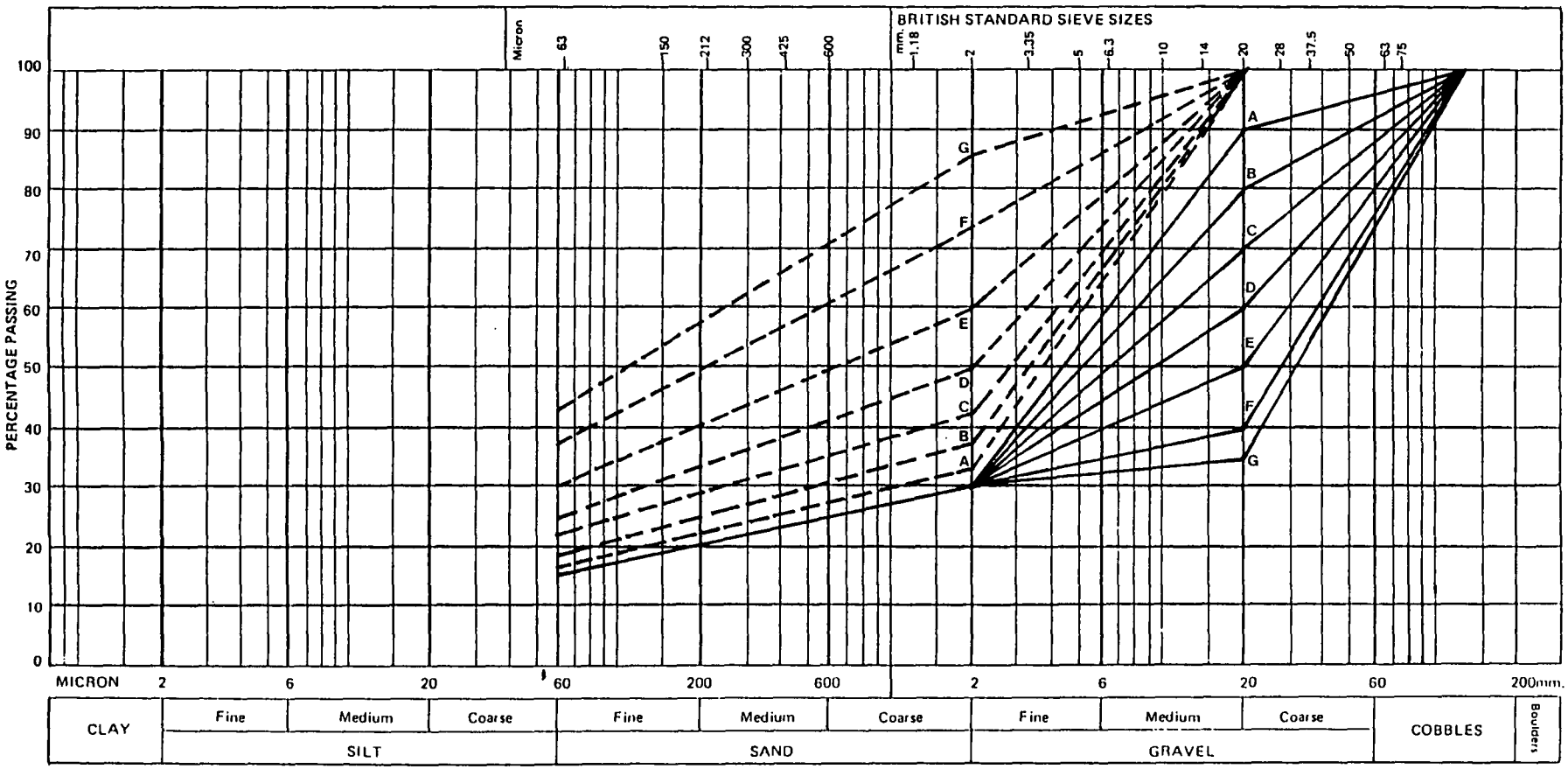

Figure 4.7 - The effect of scalping (particles retained on a 20 mm test sieve removed) on the particle size distribution of a stoney cohesive soil (after Barnes, 1987).

——— Before scalping

– – – – – – – After scalping

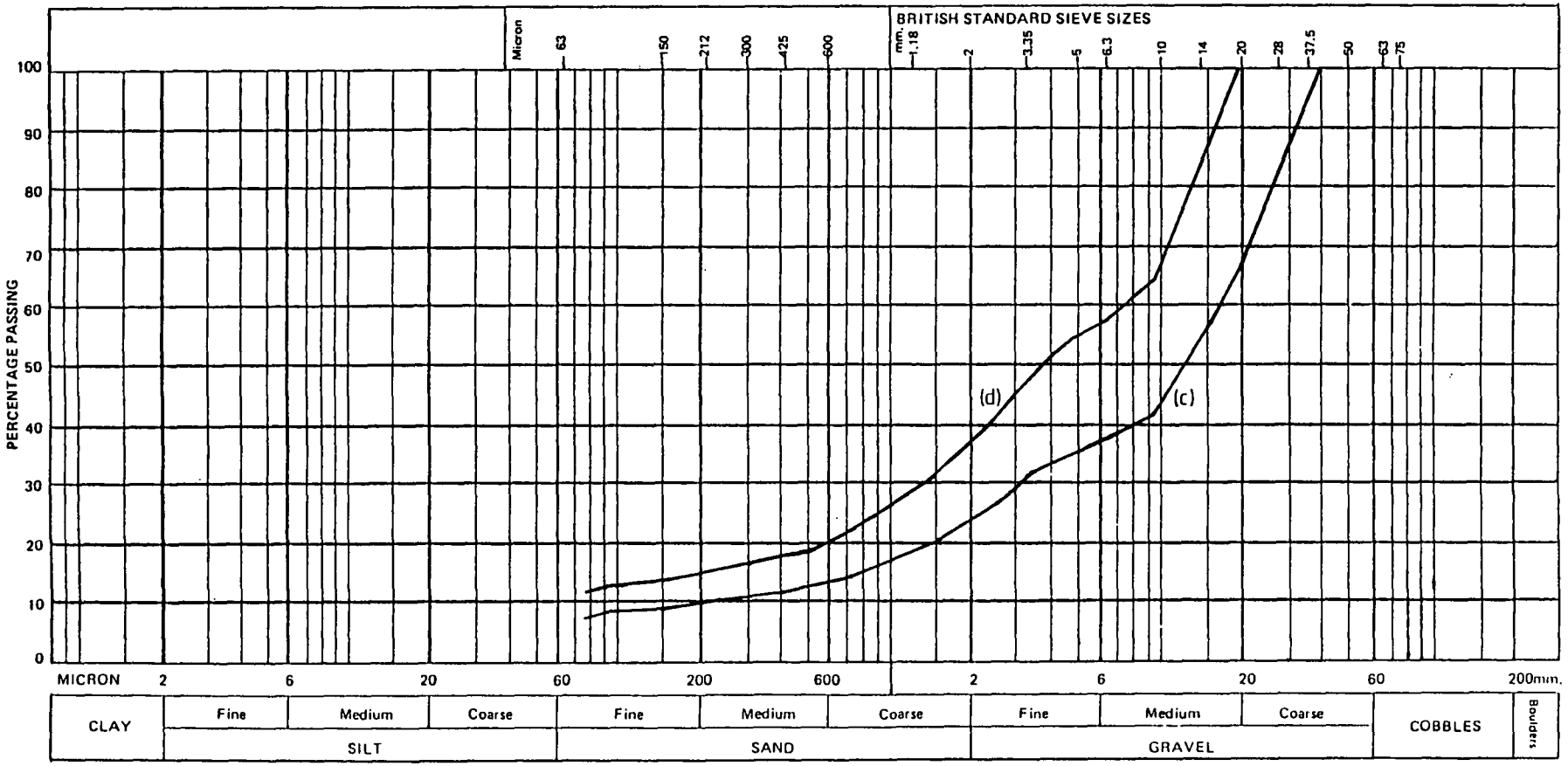

Figure 4.8 - The effect of scalping (d) (particles retained on a 19.05 mm test sieve removed) on the particle size distribution of Wet-mix macadam (c).

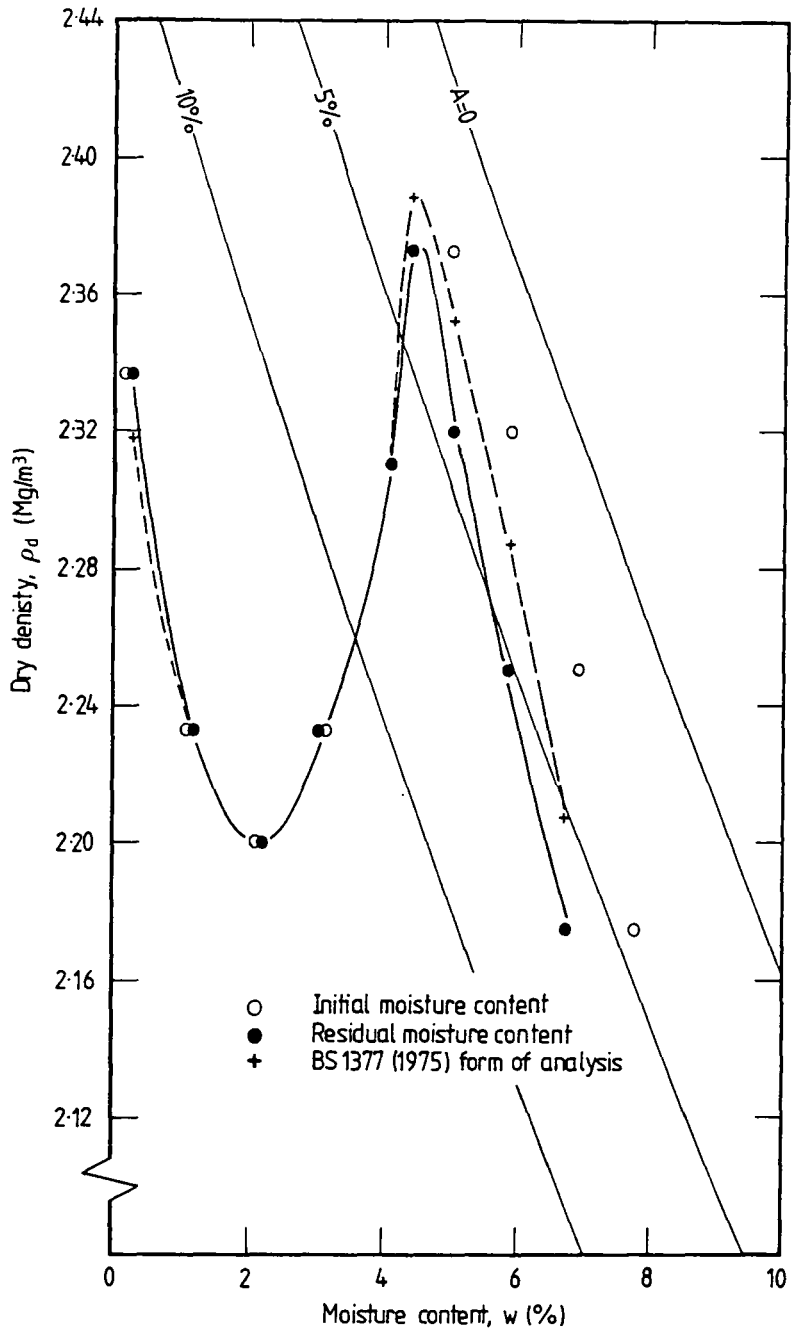

Figure 4.9 - Dry density-moisture content relationship for Wet-mix macadam compacted to BS 5835: Part 1 (1980). The dry density-moisture content relationship obtained using the BS 1377 (1975) form of analysis is also shown as are curves of constant air voids (A = 0, 5 and 10%).

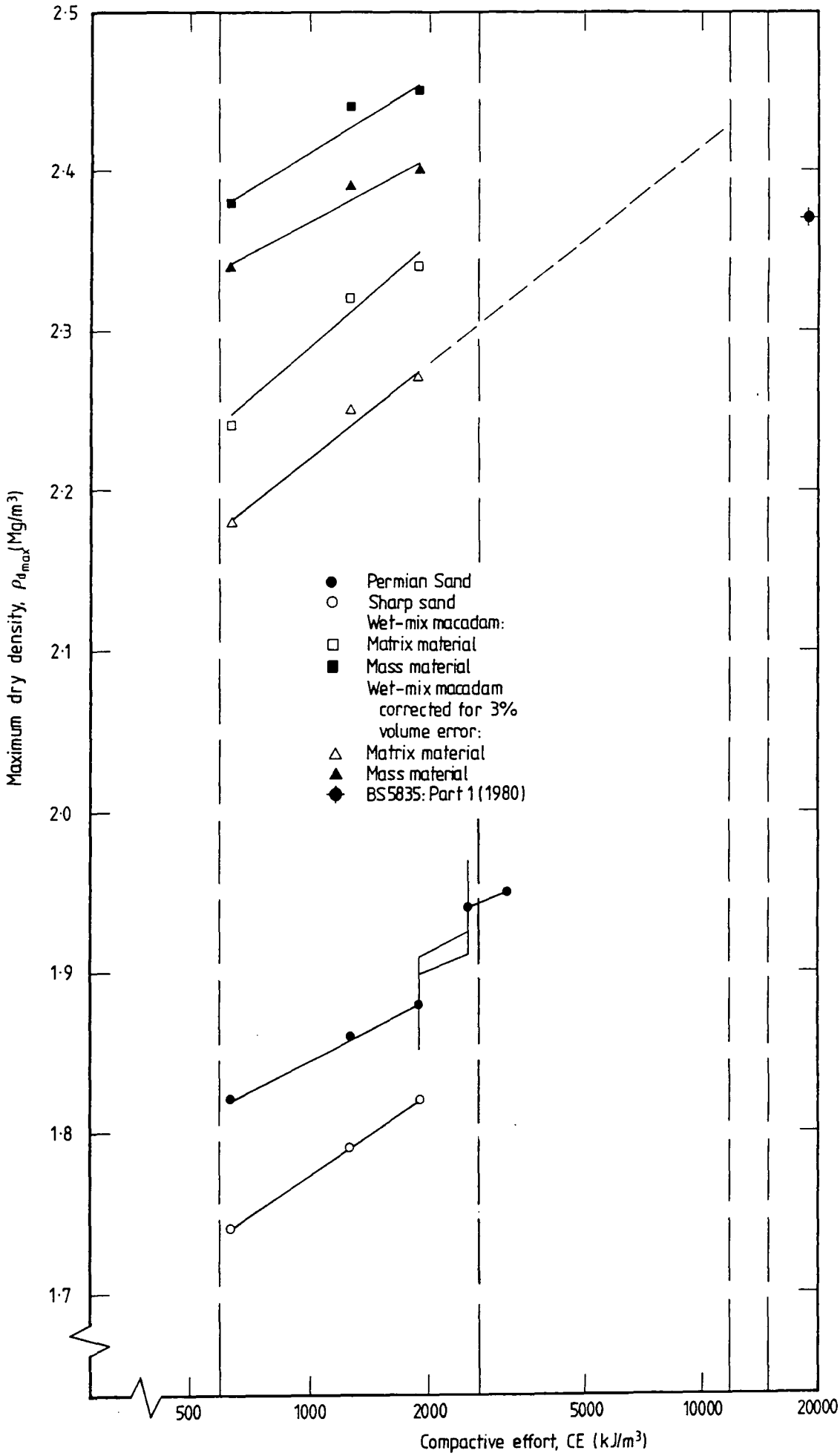

Figure 4.10 - Relationships between the logarithm of compactive effort (CE) and maximum dry density ($\rho_{d_{max}}$) for Permian Sand, Sharp Sand and Wet-mix macadam. Levels of compactive effort for BS 1377 (1975): Tests 12, 13 and 14 are shown for comparison.

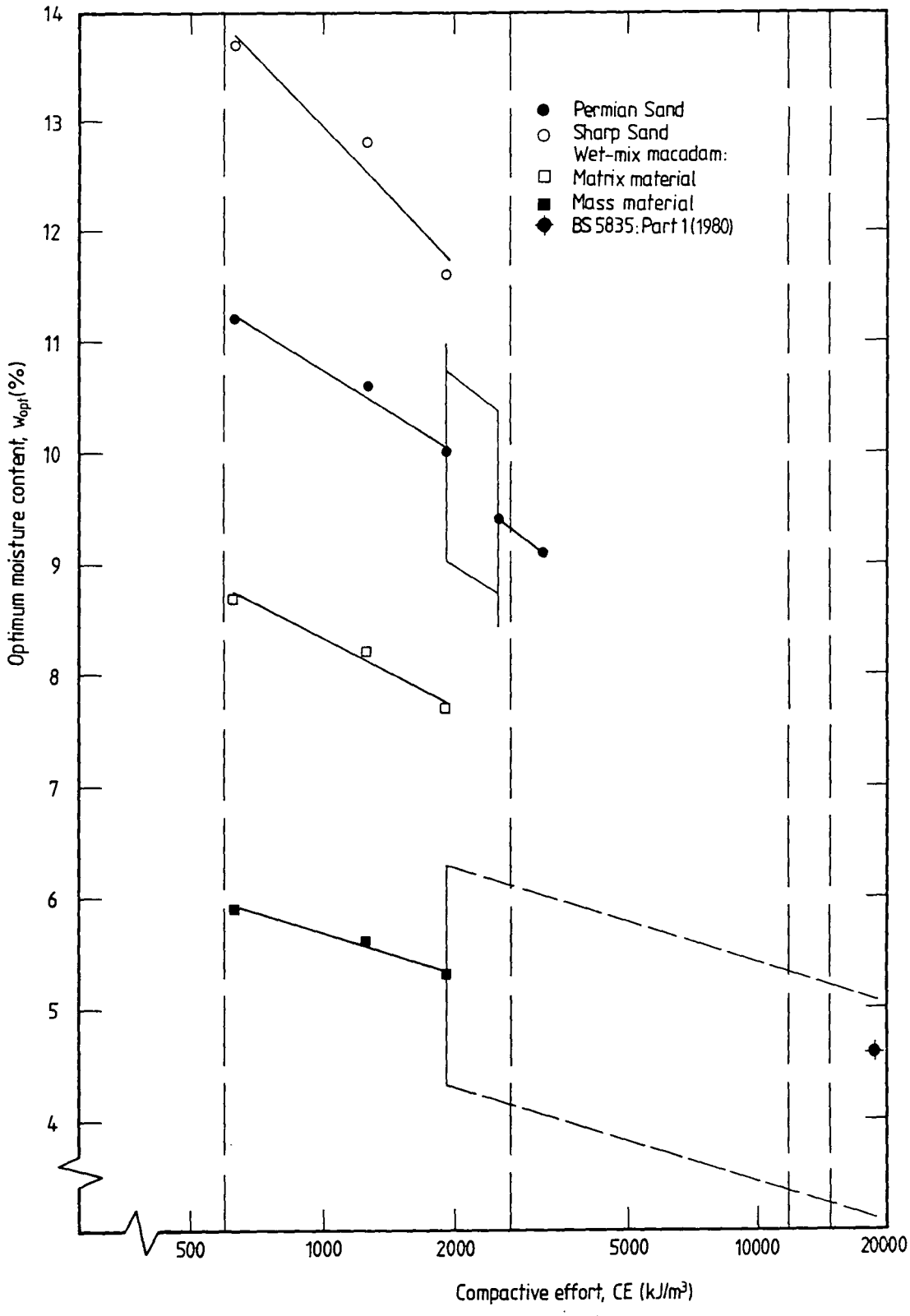

Figure 4.11 - Relationships between the logarithm of compactive effort (CE) and optimum moisture content (w_{opt}) for Permian Sand, Sharp Sand and Wet-mix macadam. Levels of compactive effort for BS 1377 (1975): Tests 12, 13 and 14 are shown for comparison.

CHAPTER 5

EXPERIMENTAL PROCEDURES AND DATA ANALYSIS

5.1 Introduction

In order to assess the dependence of a dependent variable upon an independent variable it is necessary to control, or assess, the independent variable(s) with a high degree of reliability and also to measure the dependent variable with a sufficiently high degree of accuracy. This argument is applied to all the various branches of science. It was with this basic maxim in mind that the decision to build a laboratory based 'trench' was made, in order to improve the control of both the level of compaction and moisture content of the compacted trench material, and also to standardise the boundary conditions imposed by the trench. Proper analysis of such laboratory derived data should allow a more confident interpretation of field data which is more representative of the complex situation encountered in a real reinstatement environment.

In this chapter the procedures used for filling, compacting and measuring the basic properties of each layer of material placed in the laboratory based trench are described, as are the techniques used for measuring the surface wave velocity-depth profile (on both the half-full and full trench), surface wave attenuation and the dynamic vibration-depth profiles. The procedure for emptying the trench so as to minimise the possibility of damage to buried apparatus and to allow further measurements on the compacted material is also described. Methods of excavation, filling and measurement used for the trenches in the extensive field trials are also discussed.

Methods of data analysis are also described in this chapter.

In order to achieve the simple analysis of the experimental data described above, a Casio *fx*-6000G programmable calculator has been utilised for performing regression analyses. A program for this purpose, utilising the calculator's tabulation memories, is built into the basic device; a graphics capability allows a visual assessment of the scatter of the experimental data by the operator without the need for laborious plotting. The use of such a device allows the speedy analysis of experimental data, so permitting the operator to identify any dubious data points and

This situation is encountered in Chapter 6 with both surface wave velocity-depth data and surface wave attenuation data (the forms of analysis for these two data types are given in Sections 5.6.2 and 5.6.3, respectively). The example relating to the surface wave velocity-depth profile (Test WMM5) with $r = -0.100$ in particular exhibits a low level of visually observed scatter comparable to that of similar tests with values of r of around 0.9. In this test the slope of the linear regression line is close to zero (or the surface wave velocity-depth profile is close to the vertical).

As is seen from the above discussion the value of the regression correlation coefficient (r) must be treated with great caution when the slope of the regression line is close to zero. It also follows that the same cautionary note must be applied to the value of the level of significance. In Chapters 6 and 7 values of the regression correlation coefficient are quoted extensively for linear regression analyses and in a small number of cases the slope of the regression line tends towards zero and the quoted values of r must be treated with caution.

5.2 The laboratory based trench

The laboratory based trench was an above ground timber construction of 0.3 m (internal width), 1.0 m (internal height) and 4.0 m (external length). The trench boundaries were constructed of 16 mm shuttering plywood, with external vertical timber stiffeners (75 mm × 50 mm) at the ends and at 0.5 m intervals along the length of the trench. Each pair of stiffeners was restrained by a 10 mm diameter steel tie-bar running across the width of the trench, below the trench floor. For additional external lateral support two timber beams (125 mm × 75 mm) were placed at one-third the internal trench height, one either side of the trench. These were restrained by two 10 mm tie-bars, one at either end of the trench. In addition two 178 mm × 102 mm × 21.54 kg/m RSJs were placed at two-thirds the internal trench height, these being supported on triangular blocks attached to the vertical cantilevers and restrained by four 10 mm tie-bars, two at either end. The RSJ's gave additional lateral support to the trench walls and also provided a walkway for the operator to use when filling, compacting material and emptying the trench. The walkway was also used to provide the reaction to the loads applied to the soil surface during the measurement of *CBR* values. The ends of the trench each had five removable gates to assist the emptying and filling operations, described in Sections 5.3.1 and 5.3.5, respectively. Plate 5.1 shows the laboratory based trench with the Clegg meter

which is described in detail in Section 2.4.1. A detailed view of the Clegg meter is given in Plate 5.2. Prior to use the internal faces of the trench were painted with two coats of waterproof varnish. The trench dimensions were chosen to be typical of a British Gas reinstatement.

5.3 Experimental procedure for the laboratory based trench

5.3.1 Filling the laboratory based trench

There were two basic objectives to be achieved when filling the laboratory based trench:

i)to compact the material in layers applying a known amount of compactive effort to each layer placed at a consistent moisture content, and

ii)to obtain data to aid the interpretation of the surface wave velocity measurements (*e.g.* moisture content and Impact Value).

The procedure for filling the trench may thus be described in terms of these two objectives.

A known mass (m_{wet_i}) of material was placed in the trench, to the required depth (generally 100–120 mm) as defined by the Department of Transport, 1986 (Clause 612, sub-Clauses 4–10, Table 6/4) with an allowance of around 25–50% for surcharge, where the Surcharge was defined as

$$\text{Surcharge} = \left(1 - \frac{\text{compacted layer thickness}}{\text{uncompacted layer thickness}}\right) \times 100\% \qquad (5.6).$$

In order to achieve the required moisture content control, random samples were taken from the loosely placed material and the average moisture content determined by the microwave oven-drying method described in Appendix 4.1. The mass of water necessary to achieve the required moisture content, $m_{\mathrm{H_2O}}$, was determined by

$$m_{\mathrm{H_2O}} = m_{\mathrm{wet}_i}\left[\frac{w_{\mathrm{req}} + 1}{w_i + 1} - 1\right] \qquad (5.7)$$

where:

w_r is the required moisture content, and

w_i is the initial moisture content.

Equation 5.7 is derived from basic principles in Appendix 4.2.

The required mass of water was added gradually to the loose material, this having first been 'bevelled' at the trench ends and walls and scored to around three-quarters depth to aid full absorption of the water. This process was further aided by allowing the wetted soil to stand for around half an hour. Aluminium density rings (nominal dimensions 50 mm internal diameter and 25 mm height) were buried close to the surface of the wet material in order to enable the determination of the bulk and dry density and moisture content of the compacted material on excavation (Section 5.3.5).

For tests in which particle displacement-depth profiles (Section 5.3.4) were determined, vertically orientated accelerometers were buried at a position 1.3 m from one end of the trench. These were first firmly mounted on brackets (constructed from aluminium angle section) so that the accelerometers remained vertical during placement of the subsequent layer, then carefully wrapped in cling-film (for protection against moisture ingress) and attached to micro-dot output cables which were passed through grommeted holes in the trench walls. This arrangement was then carefully placed in position and packed with fine sand for mechanical protection against the compaction process.

Compaction was achieved using the electrically driven Wacker BS45Y vibratory-rammer described in Appendix 5. The first pass was applied with the foot of the rammer adjacent to one wall of the trench and the second with the foot adjacent to the opposite trench wall. Subsequent passes were applied in a similar manner, except in the case when an odd number of passes were to be applied; then the final pass was applied centrally so as to achieve as even a degree of compaction as possible across the trench width. The vibratory-rammer is shown in use, in the laboratory based trench, in Plate 5.3.

Random samples were taken at this stage to determine the moisture content of the material in the compacted condition. The Impact Value (IV) was determined from five drops of the Clegg meter drop-weight at each of five reference points along the length of the trench (Section 5.6.1). The Clegg meter was calibrated, using the supplied plastic ring (Section 2.4.1.2), prior to commencement of each test.

The next layer was then placed in a similar manner. Placing of the surface accelerometer for particle displacement-depth profile determinations was achieved

by excavating a small hollow in which the accelerometer was placed before the excavated material was carefully replaced and hand compacted around it. The surface wave velocity-depth profile was determined when the trench was half-full, as well as when the trench was completely full.

5.3.2 Surface wave velocity measurements

For this work methods similar to those discussed in Section 3.3 were used, isolating the most desirable characteristics of the various systems utilised by previous researchers.

5.3.2.1 Apparatus

An electro magnetic oscillator was used to apply a sinusoidal vertical displacement to the soil surface of the form

$$\mathrm{w}(t) = Q_0 \sin \omega t \qquad (3.8\text{bis}).$$

This was fitted with a 285 mm diameter stainless steel base plate to improve the contact between the vibrator base and the soil surface, and a nominal 10 kg sprung-mass arrangement (plus 3.8 kg for the support arrangement) to improve the shape and stability of the observed sine-wave. The Ling Dynamic Systems oscillator, with these modifications, is illustrated in Plate 5.4. The oscillator was powered by a Ling Dynamic Systems PA100 power amplifier with variable frequency control. Monitoring of the applied sine-wave was achieved using two Brüel and Kjær (Type 8306—height 57 mm, diameter 49 mm and mass 500 g) very high sensitivity, low frequency (0.1 Hz to 1 kHz) seismic grade piezoelectric accelerometers; the in-built charge amplifiers of these devices were powered by a two-channel Farnell L30BT stabilised power supply rated at +28 V ac. The accelerometers were fitted with 10 mm deep base plates to raise the input/output cables from the damp soil surface. Frequency measurement was achieved by applying the output of one of the accelerometers to an AMF Venner 7735 digital counter. Phase angle measurement was carried out by monitoring the Lissajous Figures produced by the two accelerometer signals on the screen of a Hitachi V-212 cathode ray oscilloscope in X-Y mode (as described below). The apparatus described above is illustrated in schematic form in Figure 5.2 and shown in use in the field, in Plate 5.5.

5.3.2.2 Procedure

The experimental procedure described below and the corresponding data analysis techniques, described in Section 5.6.2, are central to the surface wave velocity measurement technique.

Prior to the measurement of the surface wave velocity profile the oscillator was placed on a bed of Permian Sand which was carefully levelled so as to optimise the contact between the oscillator baseplate and the soil surface. The 10 kg sprung mass arrangement was then attached to the vibrating core of the oscillator. The first accelerometer was placed on the surface of the compacted material at a point about one metre distant from the oscillator and a spike was pushed into the adjacent surface to which a measuring tape was attached so that the spacing (d) between the two accelerometers could be easily measured.

The desired excitation frequency was first set using the crude scale on the power amplifier, then checked using the digital counter and similarly fine-tuned to the precise frequency required.

The Lissajous Figures used to determine the accelerometer spacings, at which given phase differences existed between the signals monitored by the two accelerometers, are generated by applying one signal to the horizontal deflecting plates of the oscilloscope cathode ray tube and the other to the vertical deflecting plates. The effect of this is to cause the X-axis to reflect the amplitude of the signal applied to the horizontal plates and the Y-axis to reflect the amplitude of the signal applied to the vertical plates. Figure 5.3 illustrates the generation of Lissajous Figures from two sinusoidal waveforms of equal maximum amplitude for phase differences of $\phi = 0, \pi/4, \pi/2$ and π radians [1]. In practice the generation of Lissajous Figures from two signals is achieved by simply switching the oscilloscope to the X-Y mode position on the time scale control knob. The generation of Lissajous Figures is described in more detail by Robertson (1954).

Figure 5.3 shows Lissajous Figures for sine waves of equal maximum amplitude. When measuring the wavelength of the waves propagated in the ground, attenuation effects mean that the amplitude of the two signals is not equal (although some control over the amplitude can be achieved by altering the amplification which is applied by

[1] In the normal time-trace mode each signal is applied to the vertical plates to produce a two-dimensional trace of the signal with time on the X-axis and amplitude on the Y-axis. An internally generated horizontal magnetic force field causes the variation with time and is independent of the amplitude of the signal.

the oscilloscope's internal circuitry to the signals). Due to distortion of the elliptical Lissajous Figures, at $\phi = \pi/4$ and $3\pi/4$, and the circular Lissajous Figure, at $\phi = \pi/2$, the only phase angles which were found to provide Lissajous Figures which could be reliably interpreted regardless of the relative amplitudes of the two signals were the in-phase and out-of phase conditions ($\phi = 0, \pi, 2\pi, 3\pi, 4\pi, \ldots$, etc). These conditions are illustrated in Table 5.1 which also gives the corresponding separation of the accelerometers in terms of the number of wavelengths separating the two signals forming the Lissajous Figure.

With the two accelerometers placed adjacent to one another ($d = 0$) the first in-phase Lissajous Figure ($\phi = 0$) was found. Typical oscilloscope traces, for the X-Y mode and the more usual time-trace mode, for the $\phi = 0$ condition are illustrated in Plate 5.6.

One accelerometer was then stepped-out, in small increments (*circa* 5 mm), from the other along the centreline of the trench, away from the oscillator. Subsequent values of the in-phase and out-of-phase accelerometer separations (*i.e.* corresponding to values of $\phi = 0, \pi, 2\pi, 3\pi, 4\pi, \ldots$, etc.) were recorded. This procedure was repeated for values within the frequency range 50 Hz $\leq f \leq$ 1 kHz such that the full depth of the trench was examined.

5.3.3 Surface wave attenuation measurements

Surface wave attenuation measurements were achieved using essentially the same equipment as that described in Section 5.3.2 for surface wave velocity measurements. Throughout the measurement programme for surface wave attenuation, measurements were made at two frequencies of 300 and 500 Hz. Values of the sine-wave rms voltage (in mV) at the trench surface were obtained at 0.15 m intervals, by stepping a Brüel and Kjær (Type 8306) accelerometer along the trench centreline, using a Fluke 8000A digital multimeter. These measurements were taken between positions 0.19 and either 2.90 m (laboratory based trench tests) or 2.60 m (field trench tests) from the centre of the oscillator baseplate The second accelerometer was placed adjacent to the oscillator baseplate and used to monitor the input signal frequency and quality using the digital counter and oscilloscope, respectively. The method of data analysis is described in Section 5.6.3.

5.3.4 Particle displacement at depth

The measurement of vertical particle acceleration at depth was achieved using DJ Birchall accelerometers (Types A/20—height 16.6 mm, 14.2 mm flat-to-flat and mass 17.5 g—and A/21—height 19.0 mm, 25.4 mm flat-to-flat and mass 80.0 g) and a specially constructed Birchall modular system (Type PC/04/4/PS). This device consisted of a power supply unit (RM/04), an earthed, eleven input selector unit (IS/04/11), and a charge amplifier (CA/04/H) with a dual scale dial which allowed the calibration of each transducer to be set, in pC/g, so that a direct output of acceleration (in units of g = 9.81 m/s^2) could be displayed on an auto-ranging digital display unit (DD/04). This system also had the facility to output a signal directly to a cathode ray oscilloscope (or a digital voltmeter) to allow examination of the waveform.

Values of acceleration were read directly from the digital display unit and converted to displacement values as described in Section 5.6.4.

5.3.5 CBR measurements

Prior to emptying the laboratory based trench, the California Bearing Ratio (*CBR*) of the compacted material was determined at the central point of the soil surface. Field *CBR* apparatus was used to provide a constant penetration rate of 1 mm/min. The applied load was measured by means of a proving ring integral with the loading column and the penetration rate was measured using a dial gauge attached to the loading column (below the proving ring) and referenced to the top of the trench. Surcharge weights were not used on the compacted surface. The RSJ's along either side of the trench carried the load frame of the apparatus and provided a reaction to the applied load.

5.3.6 Emptying the laboratory based trench

Excavation of the compacted material was carried out with extreme caution so as to avoid damaging the buried accelerometers and associated cables and density rings. The filled density rings were struck level, using a large spatula, and weighed before and after drying, to constant weight, and the results analysed as described in Section 5.6.1.1. The Impact Value was measured during excavation at depth intervals of around 100–150 mm.

The surface wave velocity profile was determined, for tests TPS1 and TPS2, after the excavated surface has been carefully levelled at around half the full-depth of the trench.

5.4 The field trenches

A total of ten individual field trenches were excavated, reinstated and measured, in addition to the case studies on utility trenches, at the British Gas plc, Northern Region, Blaydon Depot. The excavations were through a concrete slab which varied in thickness from 170 to 280 mm overlying a 100 mm layer of hardcore, over silty clay with pockets of fine clinker. Care was taken to ensure that the total thickness of material placed in any trench was not sufficient to reach the bottom of the concrete slab thus eliminating the possibility of creating a 'faster' path for the Rayleigh-type surface waves to travel, in preference to the reinstated material.

The convenient location of 'circuit-protected', 240 V (50 Hz), outdoor electricity supply points at the Blaydon Depot meant that the electrically driven Wacker BS45Y vibratory rammer and the electronic apparatus, described in Section 5.3.2.1, could be used without the need for separate power generators.

5.5 Experimental procedure for the field trenches

5.5.1 Excavating the field trenches

Prior to excavation the concrete slab was saw-cut to give the required horizontal dimension of each trench (4.60 m long by 0.30 m wide) to allow easy removal of the concrete. The saw-cut concrete, hardcore and underlying silty clay were removed using a JCB 3C excavator fitted with a narrow bucket designed by the British Gas plc Engineering Research Station (ERS). The narrow bucket normally produces a slope sided trench profile (Figure 5.4). Alternate jacking-up of the hydraulic legs of the JCB 3C allowed excavation of vertical trench walls. The ends of the trenches were hand excavated to achieve the full 4.60 m trench length. The depth of trench required was dependent upon the number and thickness of layers to be placed and also upon the thickness of the concrete pad. Depths specified to the excavator operator varied between 0.8 and 0.9 m and with the use of a simple horizontal, adjustable profile board the operators obtained a depth accuracy generally around ± 20 mm. This was close to the smallest increment measurable using the adjustable profile board. The JCB 3C fitted with the ERS narrow bucket is illustrated in Plate 5.7.

5.5.2 Filling the field trenches

The filling of the field trenches followed essentially the same pattern as that of the laboratory based trench (Section 5.3.1), with the following exceptions:

i)The materials used to fill the field trenches were placed and compacted at their delivery moisture content. After each test the material stock pile was turned, using the JCB 3C, to reverse any trends in moisture movement and care was taken to ensure that material from the surface of the stockpile was discarded as this material was generally found to be surface dry. The moisture content of the placed material was measured from three random samples taken from the area where the placed material had been removed from the stockpile.

ii)Due to the large particle size of the Wet-mix macadam used in the field trials, and the difficulty of re-excavation, the density rings used for the determination of the dry density of material compacted in the laboratory based trench were deemed unsuitable for use in the field. The dry density was determined using the procedures laid down in BS 1377 (1975): Test 15(A), 'Determination of the dry density on the site; Sand replacement method suitable for fine- and medium-grained soils (small pouring cylinder method)'.

All determinations of moisture content were made using the microwave oven-drying method described in Appendix 4.1.

5.5.3 Surface wave velocity measurements

Surface wave velocity measurements were made using the same procedures as described earlier (Section 5.3.2) for tests in the laboratory based trench.

5.5.4 Surface wave attenuation measurements

Surface wave attenuation measurements were made using the same procedures as described earlier (Section 5.3.3) for tests in the laboratory based trench.

5.6 Data analysis

Simple approaches to data analysis, using a hand-held programmable, graphics calculator (Section 5.1) meant that the operator could analyse data as it was recorded, significantly aiding the understanding of the physical processes involved.

5.6.1 Density, moisture content, Impact Value and CBR measurements

5.6.1.1 Density and moisture content

The methods used to determine the dry density in the laboratory based and field trenches differed: density rings were used in the laboratory based trench and this technique is described in full below. The BS 1377 (1975): Test 15(B) Sand replacement method was used in the field trenches and as this technique is generally well understood no further comment is deemed necessary, except that the entire excavated sample was used to determine the moisture content by the microwave oven-drying technique described in Appendix 4.1.

For tests conducted in the laboratory based trench, measurements of the bulk and dry densities and the moisture content of the compacted material were made at the end of each suite of tests using the buried density rings described in Sections 5.3.1 and 5.3.5. These were of a known volume, V (nominal dimensions were 50 mm internal diameter and 25 mm height) and known mass, m_3. After careful excavation, excess material was cleaned from the external face of the ring and the top and bottom faces were carefully struck flat and parallel using a straight edge. The mass of the wet soil and ring was recorded as m_1 and the mass of the dry soil and ring was recorded, after oven-drying to constant weight[2], as m_2. The bulk density was calculated, in Mg/m^3, from

$$\rho = \frac{m_1 - m_3}{V} \tag{4.5bis}$$

the moisture content from

$$w = \frac{m_1 - m_2}{m_2 - m_3} \times 100\% \tag{4.6bis}$$

and the dry density from

$$\rho_d = \frac{100\rho}{100 + w} \tag{4.7bis}.$$

The depth of these measurements was taken to be the depth of the top surface of the layer where the density rings were placed prior to compaction of that layer.

5.6.1.2 Impact value

The Impact Value, IV, was determined at five central positions along the length of the trench for each layer immediately after compaction (and also during excavation

[2]As the density rings were metal (aluminium) it was not possible to dry the excavated material to constant weight using the microwave oven-drying technique described in Appendix 4.1. A conventional thermal oven was used for this purpose.

for tests conducted in the laboratory based trench), and five readings of IV were taken at each position. The Impact Value for each position was taken as the average of the readings from the fourth and fifth drops at that position, while the Impact Value for the layer was taken as the averages of the IV values at the five positions.

From these results the California Bearing Ratio could be estimated using the empirical relation proposed by Clegg (1980):

$$CBR = 0.07(IV)^2 \qquad (2.1\text{bis}).$$

5.6.1.3 California Bearing Ratio, CBR

Measurements of the California Bearing Ratio, CBR, were made after each laboratory based trench test was completed, prior to excavation. Due to the cumbersome nature of the apparatus only one determination was made per test, at the central position of the compacted surface. Analysis of the load-penetration data was achieved by means of the standard curves presented in BS1377 (1975): Form S. CBR values were estimated for 2.5 and 5.0 mm penetration and the greater of the two values taken to be the CBR. This value was compared to the indirect estimate of CBR from the Impact Value (Section 5.6.1.2). CBR measurements were not made in the field.

5.6.2 Surface wave velocity measurements

At each measurement frequency (or depth of measurement), the raw separation-phase angle (d, ϕ) data pairs were analysed using the linear regression program built into the Casio *fx*-6000G programmable calculator. The graphics capability of the device allowed the operator visually to assess the scatter of the data points in addition to calculating the value of the regression correlation coefficient. The wavelength for each frequency was determined from

$$\lambda = \frac{2\pi}{\phi} d \qquad (3.6\text{bis})$$

and the wave propagation velocity was calculated from

$$v_R = f\lambda \qquad (3.3\text{bis}).$$

The depth of propagation of the wave, z, was taken to be $\lambda/2$. A velocity-depth relationship of the straight line form:

$$v_R = c + mz \qquad (5.8)$$

was calculated for each set of data (where c and m are the intercept and slope of the linear regression line, respectively).

5.6.3 Surface wave attenuation measurements

In Section 3.4.4 it was seen that the attenuation of the vertical component of Rayleigh waves can be broken down into the components attributable to geometrical and material damping, the total attenuation being the product of the two components:

$$\mathrm{w} = \mathrm{w}_1 \sqrt{\frac{x_1}{x}} \exp\left[-\alpha(x - x_1)\right] \qquad (3.35\text{bis}).$$

The sine wave rms voltage data (V in mV) measured as described in Sections 5.3.3 and 5.5.4 were converted to peak-to-peak values ($V \times 2\sqrt{2}$) and then to peak-to-peak acceleration values, using the accelerometer voltage sensitivity constant ($= 991\,\mathrm{mV/ms^{-2}}$). Direct conversion to peak-to-peak displacement data (w in m) from the original single peak rms voltage data (V in mV) was achieved using

$$\mathrm{w} = \frac{2\sqrt{2}V}{991 \times 4\pi^2 f^2} = 2.854 \times 10^{-3} \frac{V}{4\pi^2 f^2} \qquad (5.9).$$

In order to obtain an estimate of the material attenuation coefficient (α), the usual procedure (Section 3.4.4) is to estimate values of (x_1, w_1) close to the source of oscillation and fit the experimental data to Equation 3.35. This technique was simply evaluated by selecting such values of (x_1, w_1) and plotting curves with various values of α with the experimental data. Two conclusions were drawn from this simple study:

i) that the value of α could not be simply estimated from such a technique due to the considerable scatter of the experimental data, and

ii) that the position of the resulting attenuation curve and consequently the estimated value α were strongly dependent upon the original estimate of (x_1, w_1).

The considerable scatter of the experimental data (observed in (i) above) was noted to be especially pronounced close to the source of vibration where estimates of (x_1, w_1) were to be made. Thus, a more reliable means of determining the value

of α without relying on potentially dubious estimates of (x_1, w_1) was sought. Re-arrangement of Equation 3.35 yields

$$\frac{\mathrm{w}}{\mathrm{w}_1}\sqrt{\frac{x}{x_1}} = \exp\left[-\alpha(x - x_1)\right]$$

and taking logarithms of both sides

$$\ln\left[\frac{\mathrm{w}}{\mathrm{w}_1}\sqrt{\frac{x}{x_1}}\right] = -\alpha(x - x_1)$$

and again, re-arranging,

$$\ln\left[\mathrm{w}\sqrt{x}\right] = \alpha x_1 + \ln\left[\mathrm{w}_1\sqrt{x_1}\right] - \alpha x \qquad (5.10).$$

Equation 5.10 is of the straight line form

$$y = c + mx$$

where:

y $= \ln\left[\mathrm{w}\sqrt{x}\right]$,

c $= \alpha x_1 + \ln\left[\mathrm{w}_1\sqrt{x_1}\right]$, the intercept,

m $= -\alpha$, the slope, and

x $= x$ in Equation 5.10.

Simple linear regression procedures could then be applied to the data in order to evaluate the values of c and m $= -\alpha$. This technique has the advantage over the more traditional technique that there is no requirement to estimate (x_1, w_1), these values being a part of the calculated intercept constant.

5.6.4 Particle displacement at depth

The raw peak-to-peak amplitude values of vertical acceleration ($\ddot{\mathrm{w}}$ in g), as determined in Section 5.3.4, were converted to peak-to-peak displacement values (w in m) using the equation

$$\mathrm{w} = \frac{\ddot{\mathrm{w}}\mathrm{g}}{4\pi^2 f^2} \qquad (5.11).$$

The ratio of the particle displacement at depth z to the particle displacement at depth $z = 0$ was then determined (w_z / $\mathrm{w}_{z=0}$) and plotted against the ratio of depth to wavelength. The wavelength for the frequency under consideration is obtained from the power regression curves obtained for the frequency-wavelength relationship from the wave velocity profile determination. These plots are compared to the theoretical curves for the displacement factors (W_z / $\mathrm{W}_{z=0}$) derived in Section 3.4.3.

5.7 Summary

In this chapter, apparatus, experimental procedures and methods for data analysis are described. In Section 5.1 the use of a simple hand-held programmable graphics calculator to perform linear regression analyses is described. This device was used to achieve speed and simplicity of data analysis in the field, allowing the operator to assess the results before leaving site (for field tests) and repeat any tests which gave dubious results to either confirm or re-evaluate any relationships so derived.

Section 5.2 describes the laboratory based trench which was used for the initial trials of the surface wave velocity measurement method. Section 5.3 describes the experimental procedures used for tests in the laboratory based trench, including filling and emptying procedures, and surface wave velocity and surface wave attenuation measurements. The section dealing with the experimental procedures for obtaining surface wave velocity data includes a detailed description of the use of Lissajous Figures for the purpose of determining the relationship between phase angle and separation of two sinusoidal signals.

Section 5.4 describes the field trenches used for the field trials at the British Gas plc Northern, Blaydon Depot. Section 5.5 describes the experimental procedures used during the field trials. In general these were the same as those used for tests in the laboratory based trench; certain aspects did, however, differ from those described in Section 5.3 and these are highlighted in this section.

Data analysis procedures are described in Section 5.6 for density, moisture content, Impact Value, *CBR*, surface wave velocity, surface wave attenuation and particle displacement at depth measurements. The section dealing with the analysis of surface wave attenuation data presents a novel technique for analysing such data which does not require the estimation of initial values of the particle displacement amplitude at a given distance from the source of vibration (x_1, w_1).

Table 5.1 - Lissajous Figures.

Lissajous Figure	Phase difference ϕ (radians)	Number of wavelengths between accelerometers λ
/	0	0
\	π	$\lambda/2$
/	2π	λ
\	3π	$3\lambda/2$
/	4π	2λ
\	5π	$5\lambda/2$
⋮	⋮	⋮
etc.	etc.	etc.

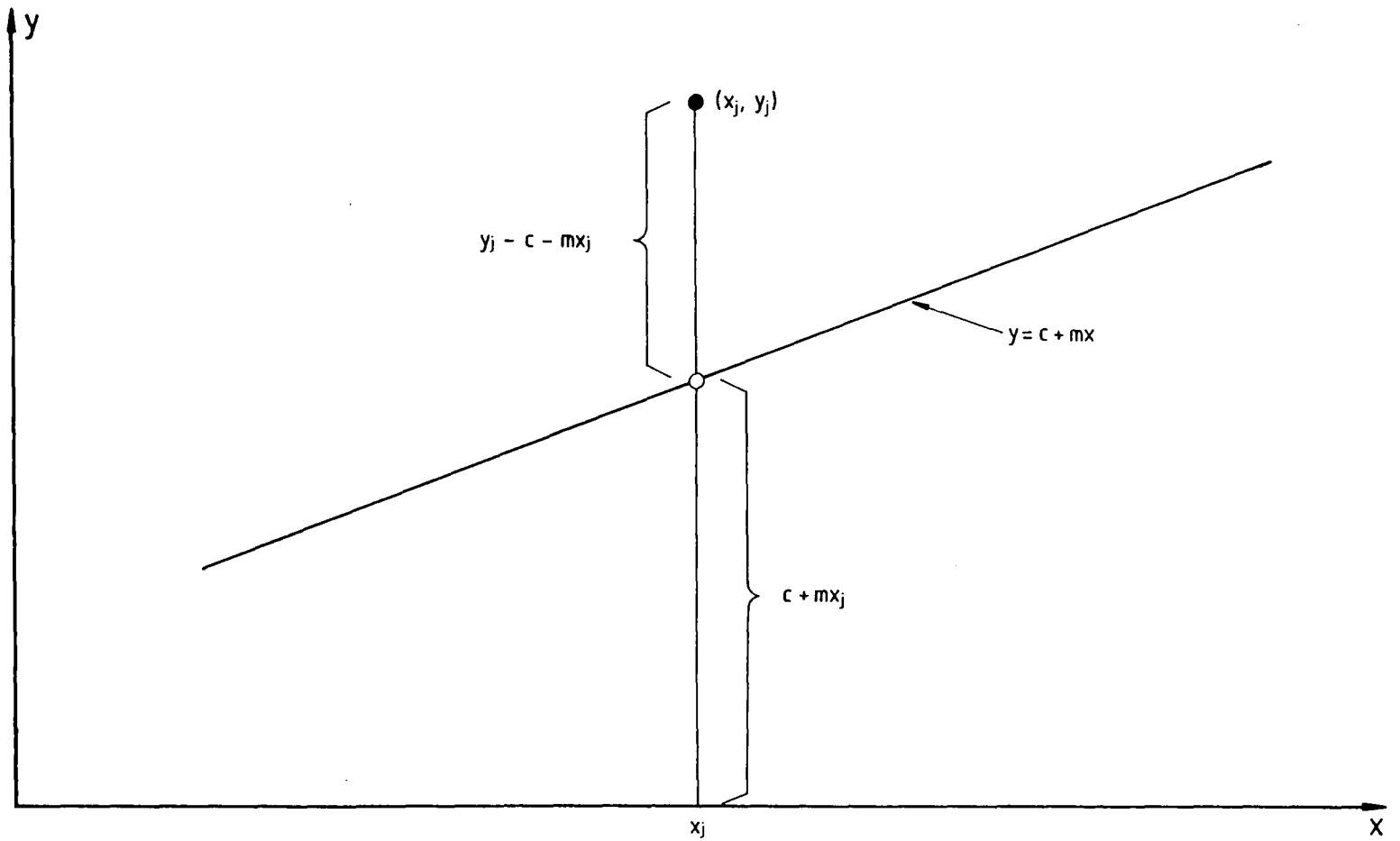

Figure 5.1 - Graphical explanation of the principle of least squares regression analysis (after Kreyszig, 1983).

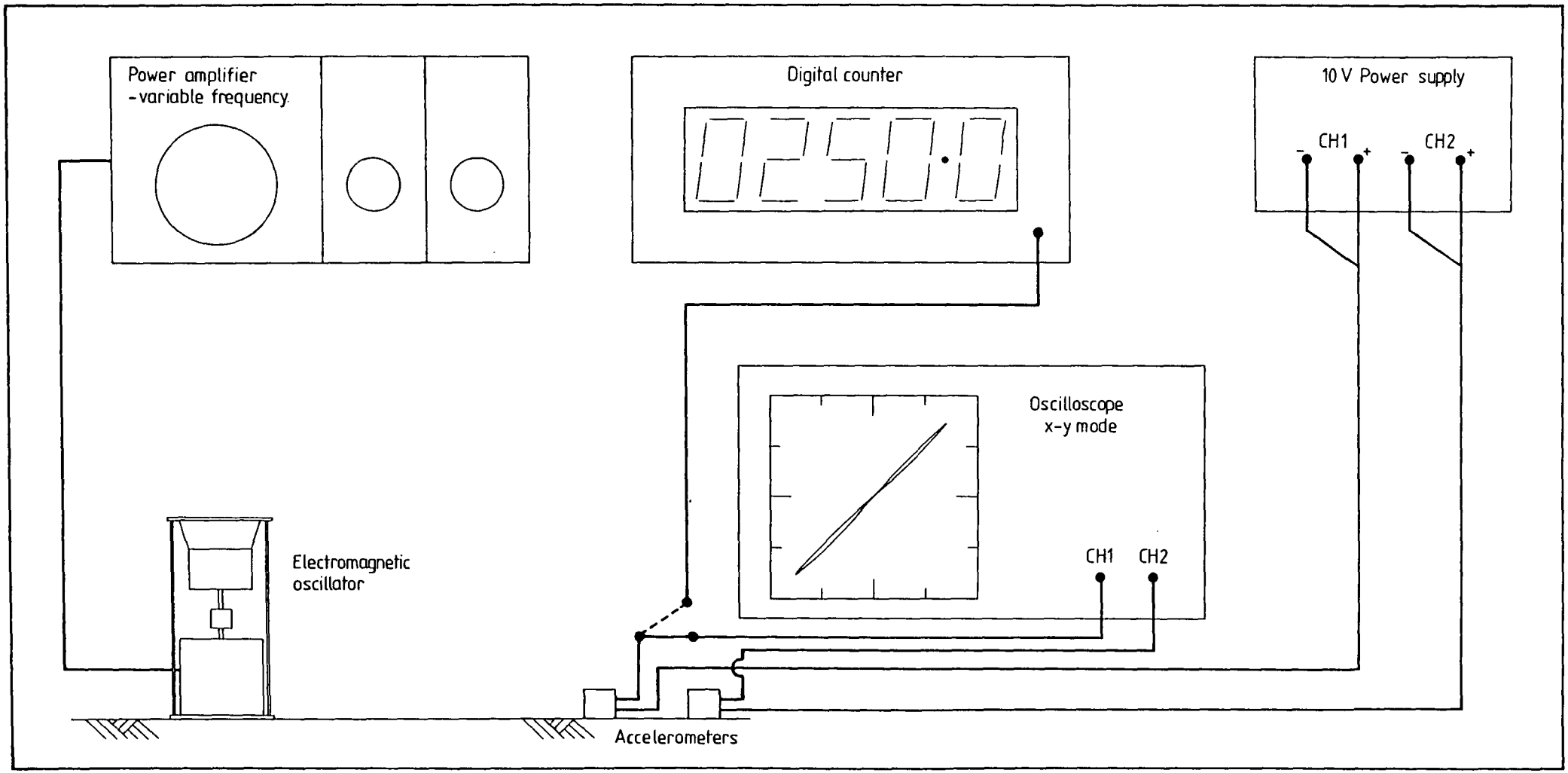

Figure 5.2 - Schematic diagram showing the apparatus for determining surface wave velocity-depth profiles.

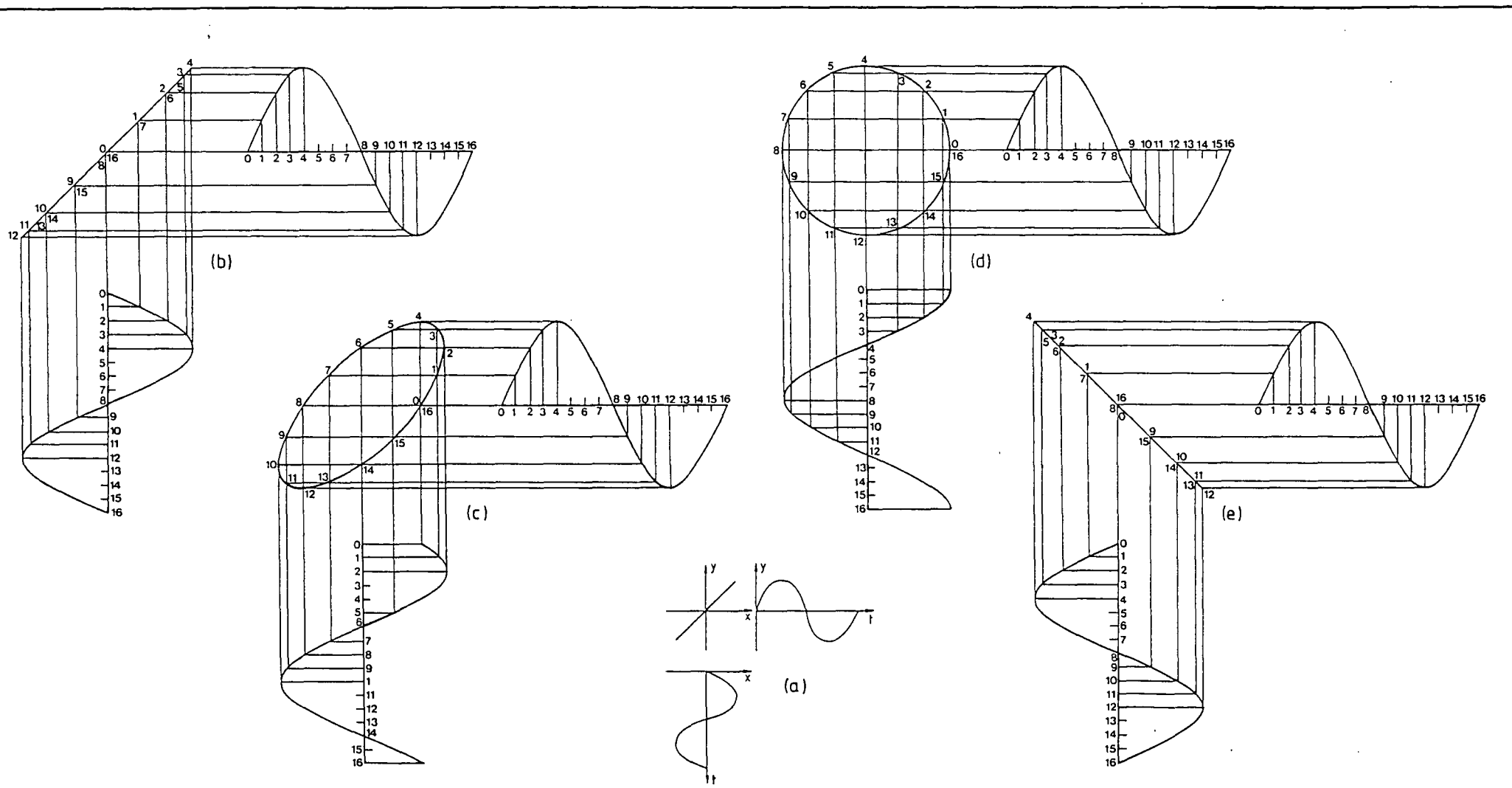

Figure 5.3 - The generation of Lissajous figures by an oscilloscope in X-Y mode for a range of phase angles (ϕ): a) $\phi = 0$; b) $\phi = 0$; c) $\phi = \pi/4$; d) $\phi = \pi/2$ and

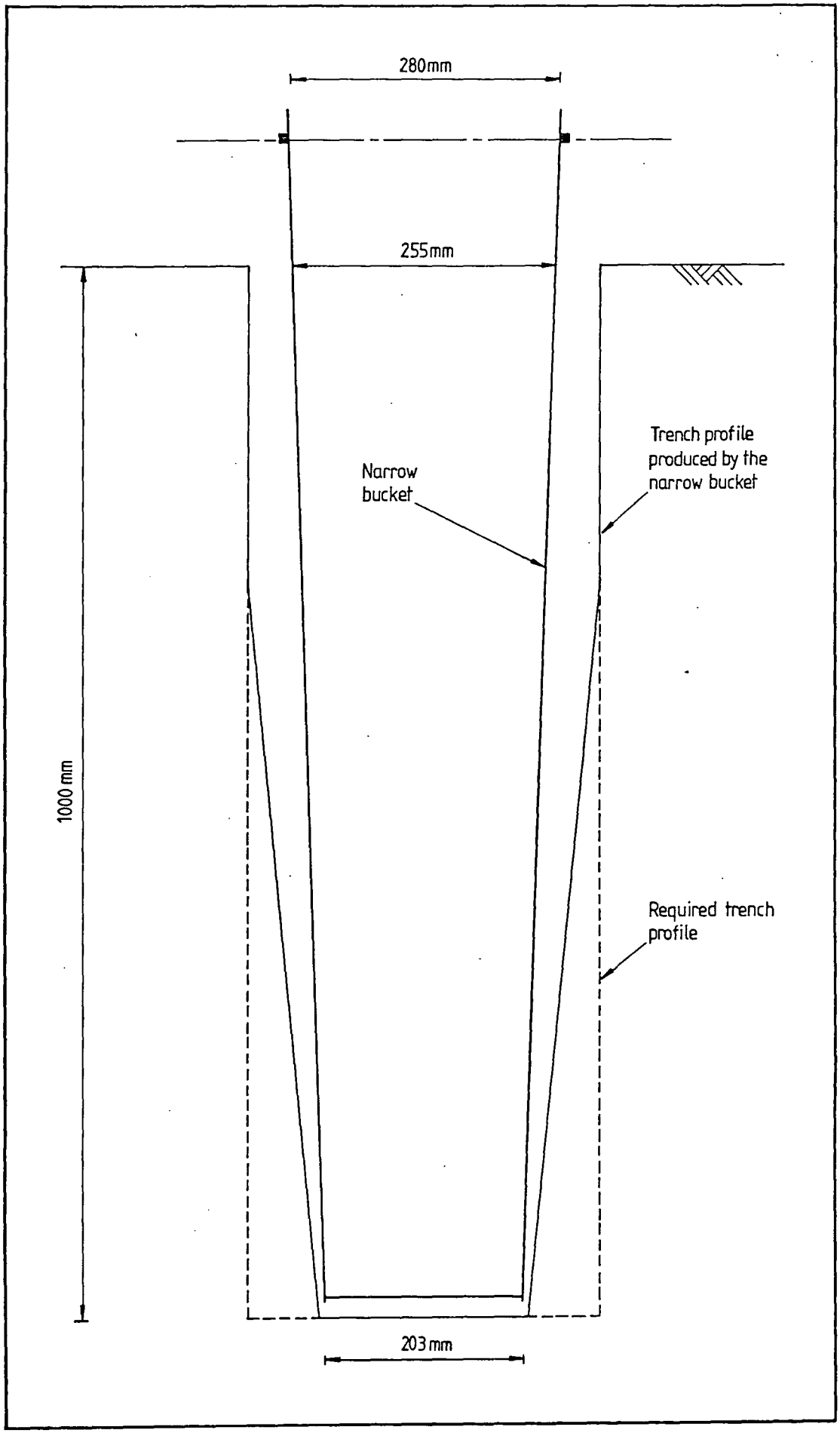

Figure 5.4 - Trench profile produced with the ERS narrow bucket (reproduced courtesy of British Gas plc, Engineering Research Station) compared to the required trench profile.

Plate 5.1 - The laboratory based trench showing the usage of the Clegg meter.

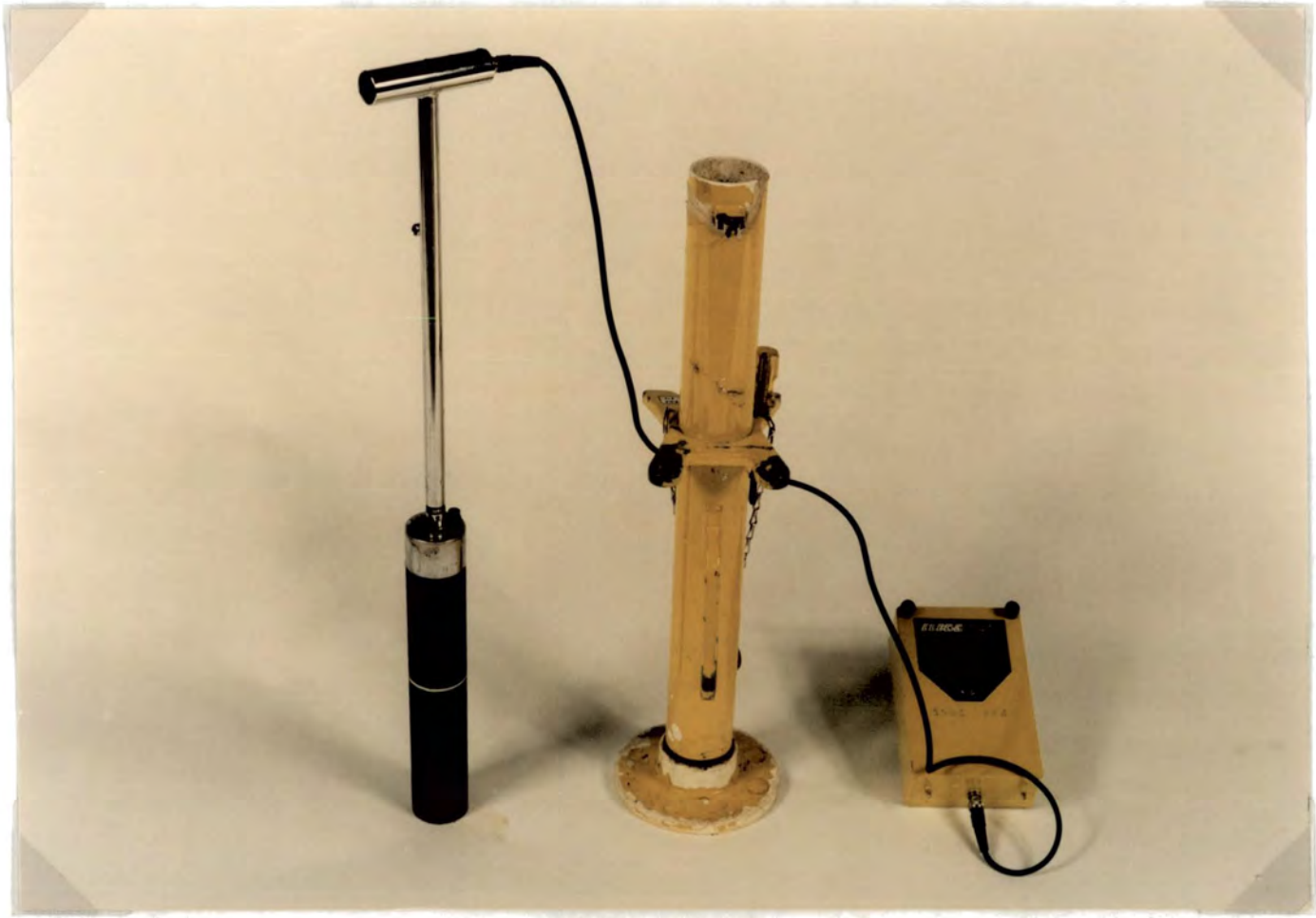

Plate 5.2 - Detailed view of the Clegg meter showing (from right to left) the hand held readout meter, the guide tube and the drop weight with handle and internally mounted accelerometer.

Plate 5.3 - The Wacker BS45Y electrically powered vibratory rammer in use in the laboratory based trench.

Plate 5.4 - The electromagnetic oscillator showing the circular plate and sprung mass arrangement which have been added to improve signal quality.

Plate 5.5 - The apparatus for surface wave velocity-depth profile measurement shown in use in the field.

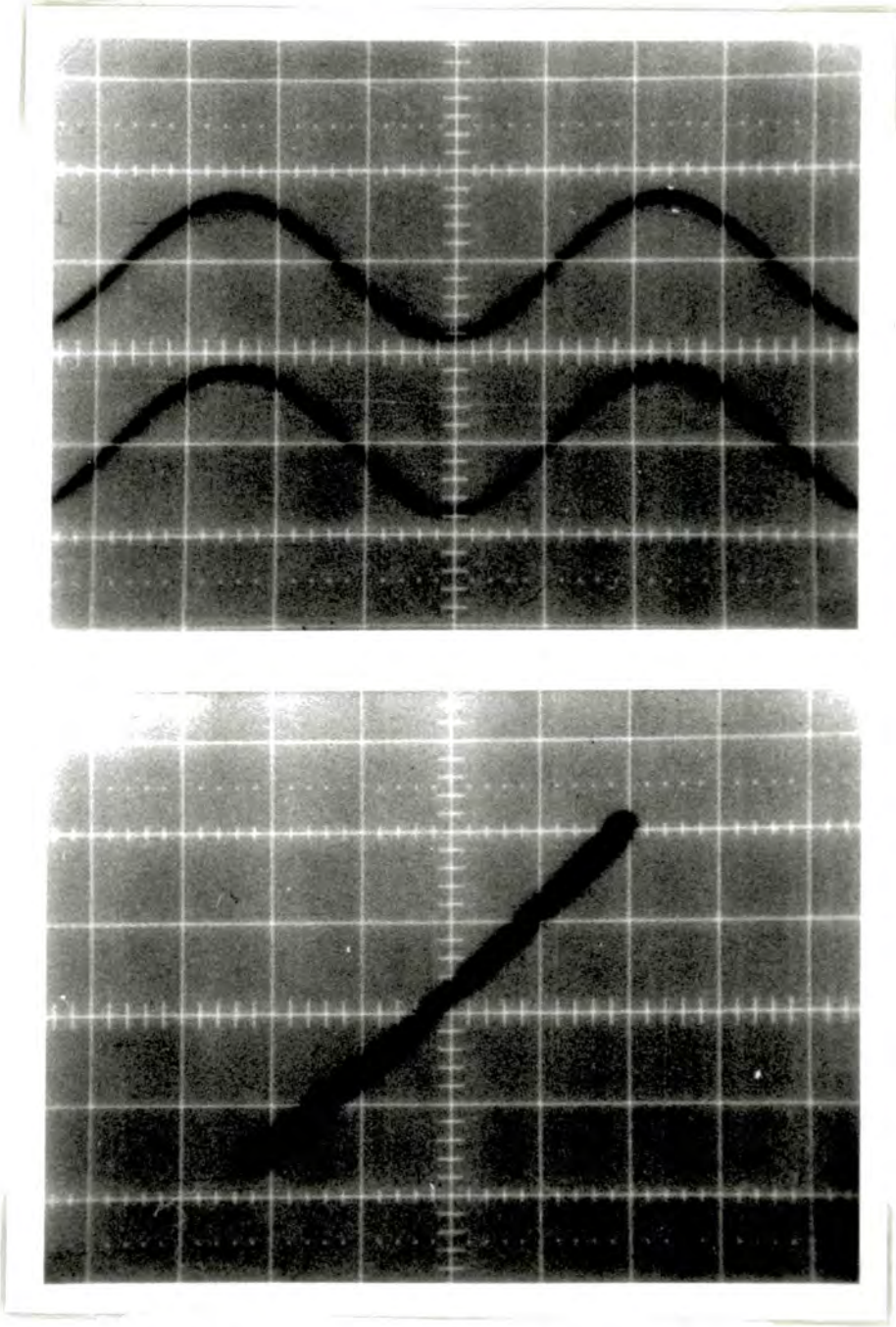

Plate 5.6 - Oscilloscope trace of in-phase signals from two accelerometers (top) and the Lissajous Figure generated (bottom) for a phase angle of, $\phi = n\pi$ ($n = 0, 2, 4, 6, \ldots$, etc).

Plate 5.7 - The JCB 3C excavator equipped with the ERS narrow bucket excavating one of the trenches for the field trials.

CHAPTER 6

EXPERIMENTAL RESULTS

6.1 Introduction and test programme

6.1.1 Introduction

This chapter has been designed to act as a vehicle for the presentation of experimental results in a structured format. Discussion and interpretation of the results presented are given in Chapter 7. The results presented in this chapter are derived from tests conducted in the laboratory based trench (Section 5.2), from field trials at the British Gas Blaydon Depot (Section 5.4) and also a series of some five case studies.

Detailed data from these tests are presented in Appendices 6 to 9 and these data used to construct a series of data summary statements presented in tabular form in this chapter. The detailed data presented in the appendices are also used to construct an extensive series of figures, mainly concerning surface wave velocity and surface wave attenuation measurements, which are also presented in this chapter. The tabulated data summaries include, in each case, values of the two parameters of compactive effort (N_p and $N_p/\overline{h}$) and are used to construct the figures which are presented with the discussion of the results in Chapter 7. Numerical values of the mean and sample standard deviation of the parameter x for n determinations ($\overline{x}/\sigma_{x_{n-1}}$) are presented, as appropriate, in the tabulated data summaries. The mean and sample standard deviation are defined as:

$$\overline{x} = \frac{\sum x}{n} \text{ and } \sigma_{x_{n-1}} = \sqrt{\frac{\sum x^2 - (\sum x)^2/n}{n-1}} \text{ respectively} \qquad (6.1).$$

These values were calculated using the inbuilt statistics package of the Casio *fx*-6000G programmable calculator described in Section 5.1. The range $\overline{x} \pm \sigma_{x_{n-1}}$ includes approximately 68% of the data.

6.1.2 Test programme

In order to ease identification of and reference to an individual test or group of tests a coding system has been introduced. Either two or three characters are used to identify the material used in each test as follows:

PS refers to tests on Permian Sand[1],

SS refers to tests on Sharp Sand[1], and

WMM refers to tests on Wet-mix macadam.

The prefix, 'T', is used to refer to tests conducted in the laboratory based trench, while a numerical suffix is used to refer to the test number within a given suite of tests on a specific material. A further suffix is used to refer to individual tests within a test suite; *e.g.* for tests on the half-full laboratory based trench the suffix 'A' is used and for tests on the full laboratory based trench the suffix 'B' is used. Further suffices, 'C' and 'D', are used to refer to additional tests carried out on the Permian Sand for when the trench was full, Test TPS1 (suffix is 'C'), and half-full (during excavation), Tests TPS1 and TPS2 (suffices are 'D' and 'C' respectively).

From the foregoing it can be seen, for example, that for the second test on Permian Sand, when the trench was full, the test code is 'TPS2B' and that for the third test on Wet-mix macadam the test code is 'WMM3'.

A further complication is introduced to the coding system by the tests carried out during the Blaydon field trials with layers of both Wet-mix macadam and Sharp Sand. These are generally coded in the same manner as the single material tests on Wet-mix macadam (*i.e.* Tests WMM7, WMM8 and WMM9). When referring to the specific materials in these tests a further suffix in parentheses is used, so that a reference to the sand layers of Test WMM7 is coded 'WMM7(SS)' and similarly a reference to the Wet-mix macadam layers of the same test is coded 'WMM7(WMM)'.

Individual layers are identified by roman numerals, the numbering beginning at 'I' for the first (or lowest) layer, placed at the bottom of the trench.

Details of the test programmes, for the laboratory based trench, on Permian Sand and Sharp Sand are given in Tables 6.1 and 6.2, respectively. Results are reported in Sections 6.2 and 6.3. Details of the test programmes for the field trials on Wet-mix macadam and Wet-mix macadam with Sharp Sand are given in Tables 6.3 and 6.4, respectively. Results are reported in Sections 6.4 and 6.5. Details of tests in the case study work are given in Section 6.6.

---

[1]In preliminary reports of the results presented here (Winter and Selby, 1988 and 1989) the codings 'BS' and 'CS' were used to refer to the Permian Sand and Sharp Sand respectively.

6.1.3 Determination of the wavelength of surface waves

The experimental procedure for determining the wavelength from accelerometer spacing-phase angle (d, ϕ) data was described in Section 5.3.3 while the corresponding method of data analysis was described in Section 5.6.2. Two sample sets of such data are presented in this section; the raw d, ϕ data, with the corresponding Lissajous Figures, are given in Tables 6.5 and 6.6 for Tests TPS2A ($f = 375$ Hz) and WMM9 ($f = 450$ Hz), respectively. The data points are plotted, ϕ against d, in Figures 6.1 and 6.2. The excellent fit of both data sets to the calculated best-fit regression lines should be observed because the two chosen examples represent the 'worst' and the 'best' fits of the data to linear regression lines of the form of Equation 3.6. Regression correlation coefficients, r, are 0.979 (Test TPS2A; $f = 375$ Hz) and 1.000 (Test WMM9; $f = 450$ Hz).

6.2 Measurements on Permian Sand

6.2.1 Density, moisture content, Impact Value and CBR results

Detailed moisture content and Impact Value data for tests conducted on Permian Sand in the laboratory based trench (Tests TPS1 to TPS5) at the time of compaction are given in Appendix 6.1 (Tables A6.1, A6.3, ..., A6.9). These tables also include details of the individual layer thicknesses and the measured percentage surcharge for each layer. Details of the BS45Y vibratory rammer (*i.e.* petrol or electrically driven) used for compaction are also given and a statement is made to identify which layers were compacted with the extension leg fitted to the vibratory rammer. These data are summarised in mean/sample standard deviation form in Table 6.7.

Detailed moisture content, bulk and dry density and Impact Value data for tests conducted on Permian Sand in the laboratory based trench (Tests TPS1 to TPS5) at the time of excavation are also given in Appendix 6.1 (Tables A6.2, A6.4, ..., A6.10). These tables also include details of the depth of sampling for the moisture content, bulk and dry density, and the depth of testing for the Impact Value determinations. These data are summarised, with *CBR* values, in mean/sample standard deviation form in Table 6.8.

6.2.2 Surface wave velocity results

Surface wave velocity-depth profile measurements on the Permian Sand compacted in the laboratory based trench (Tests TPS1 to TPS5) were conducted on both the half-full and full trench (test code suffices 'A' and 'B' respectively). Additionally, determinations of the surface wave velocity-depth profile were made, after allowing the Permian Sand to dry out for a period of some 3 weeks, (test code suffix 'C') and for the half-full trench during excavation (test code suffix 'D') for Test TPS1 and on the half-full trench during excavation (test code suffix 'C') for Test TPS2. Detailed data are presented in Appendix 7.1 (Tables A7.1, A7.2, ..., A7.12) and are plotted as surface wave velocity-depth profiles in Figures 6.3, 6.4, ..., 6.14. The individual layers are shown as layer logs on the depth (z) axis of each of these figures. Values of the intercept and slope of the surface wave velocity-depth profile, along with the regression correlation coefficients are summarised in Table 6.9.

6.2.3 Derived shear modulus results

The mean bulk density for each test (Table 6.8) together with the surface wave velocity-depth data were used to calculate the shear modulus-depth relationship from Equation 3.3. Detailed shear modulus (G) data are not presented. Values of the intercept and slope of the shear modulus-depth profile are summarised in Table 6.10.

6.2.4 Surface wave attenuation results

Surface wave attenuation measurements on Permian Sand compacted in the laboratory based trench were conducted on the full trench only (Tests TPS3B, TPS4 and TPS5B) at frequencies of 300 and 500 Hz. Detailed distance-displacement amplitude (w, x) data are presented in Appendix A8.1 (Tables A8.1, A8.2 and A8.3) and are plotted with the best-fit regression line determined from Equation 5.10 in Figures 6.15, 6.16 and 6.17. Values of the intercept $\left(\alpha x_1 + \ln\left[\mathrm{w}_1 \sqrt{x_1}\right]\right)$ and the slope, or the material attenuation coefficient (α), along with the regression correlation coefficients are given in Table 6.11.

6.2.5 Particle displacement at depth results

Results for the particle displacement at depth due to a surface wave were achieved using buried accelerometers, as described in Section 5.3.4, as part of Tests TPS2B

and TPS3B. Three representative data sets, analysed as described in Section 5.6.4, are given in Tables A9.1, A9.2 and A9.3. These data are plotted in a similar normalised form to that of Figure 3.6 in Figures 6.18, 6.19 and 6.20. Figure 3.6 plots the normalised vertical dynamic attenuation factor (W_z / $W_{z=0}$) on the y-axis while Figures 6.18, 6.19 and 6.20 have the actual normalised vertical displacements (w_z / $w_{z=0}$) on the y-axis. The normalised depth is represented by the depth upon wavelength (z/λ) on the x-axis.

6.2.6 Summary

Detailed data, summary data and plots based on detailed data (where appropriate) have been presented for density, moisture content, Impact Value and *CBR* (Section 6.2.1), surface wave velocity (Section 6.2.2), surface wave attenuation (Section 6.2.3) and particle displacement at depth (Section 6.2.4) for tests performed on the Permian Sand compacted in the laboratory based trench.

Additionally, the summary data for surface wave velocity and bulk density allowed the calculation of shear modulus data which has also been presented in summary form.

6.3 Measurements on Sharp Sand

6.3.1 Density, moisture content, Impact Value and CBR results

Detailed moisture content and Impact Value data for tests conducted on Sharp Sand in the laboratory based trench (Tests TSS1 to TSS5) at the time of compaction are given in Appendix 6.2 (Tables A6.11, A6.13, ..., A6.19). These tables also include details of the individual layer thicknesses and the measured percentage surcharge for each layer. A statement is made to identify which layers were compacted with the extension leg fitted to the vibratory rammer. These data are summarised in mean/sample standard deviation form in Table 6.12.

Detailed moisture content, bulk and dry density and Impact Value data for tests conducted on Sharp Sand in the laboratory based trench (Tests TSS1 to TSS5) at the time of excavation are also given in Appendix 6.2 (Tables A6.12, A6.14, ..., A6.20). These tables also include details of the depth of sampling, for the moisture content, bulk and dry density, and the depth of testing for the Impact Value determinations.

These data are summarised, with *CBR* values, in mean/sample standard deviation form in Table 6.13.

6.3.2 Surface wave velocity results

Surface wave velocity-depth profile measurements on the Sharp Sand compacted in the laboratory based trench (Tests TSS1 to TSS5) were conducted on both the half-full and full trench (test code suffices 'A' and 'B' respectively). Detailed data are presented in Appendix 7.2 (Tables A7.13, A7.14, ..., A7.21) and are plotted as surface wave velocity-depth profiles in Figures 6.21, 6.22, ..., 6.29. The individual layers are shown as layer logs on the depth (z) axis of each of these figures. Values of the intercept and slope of the surface wave velocity-depth profile along with the regression correlation coefficients are summarised in Table 6.14.

6.3.3 Derived shear modulus results

The mean bulk density for each test (Table 6.13) together with the surface wave velocity-depth data were used to calculate the shear modulus-depth relationship from Equation 3.3. Detailed shear modulus (G) data are not presented. Values of the intercept and slope of the shear modulus-depth profile are summarised in Table 6.15.

6.3.4 Surface wave attenuation results

Surface wave attenuation measurements on Sharp Sand compacted in the laboratory based trench were conducted on the full trench only (Tests TPS1B, TPS2B, TPS3B, TPS4 and TPS5B) at frequencies of 300 and 500 Hz. Detailed distance-displacement amplitude (w, x) data are presented in Appendix A8.2 (Tables A8.4, A8.5, ..., A8.8) and are plotted with the best-fit regression line determined from Equation 5.10 in Figures 6.30, 6.31, ..., 6.34. Values of the intercept $\left(\alpha x_1 + \ln\left[w_1 \sqrt{x_1}\right]\right)$ and the slope, or the material attenuation coefficient (α), along with the regression correlation coefficients are given in Table 6.16.

6.3.5 Summary

Detailed data, summary data and plots based on detailed data (where appropriate) have been presented for density, moisture content, Impact Value and *CBR* (Section 6.3.1), surface wave velocity (Section 6.3.2) and surface wave attenuation

(Section 6.3.3) for tests performed on the Sharp Sand compacted in the laboratory based trench.

Additionally, the summary data for surface wave velocity and bulk density allowed the calculation of shear modulus data which have also been presented in summary form.

6.4 Measurements on Wet-mix macadam

6.4.1 Density, moisture content and Impact Value results

Detailed moisture content, Impact Value together with bulk and dry density data for tests conducted on Wet-mix macadam in the field trials (Tests WMM1 to WMM6 and WMM10) at the time of compaction are given in Appendix 6.3 (Tables A6.21, A6.22, ..., A6.27). These tables also include details of individual layer thicknesses and the measured percentage surcharge for each layer. A statement is made to identify those layers which were compacted with the extension leg fitted to the vibratory rammer. These data are summarised in mean/sample standard deviation form in Table 6.17.

6.4.2 Surface wave velocity results

Surface wave velocity-depth profile measurements on the Wet-mix macadam compacted in the Blaydon field trial trenches (Tests WMM1 to WMM6 and WMM10) were conducted on the full trench only. Detailed data are presented in Appendix 7.3 (Tables A7.22, A7.23, ..., A7.28) and are plotted as surface wave velocity-depth profiles in Figures 6.35, 6.36, ..., 6.41. The individual layers are shown as layer logs on the depth (z) axis of each of these figures. It should be noted that the scales of both the axes of these plots have been expanded, compared to the plots derived from tests in the laboratory based trench. Values of the intercept and slope of the surface wave velocity-depth profiles along with the regression correlation coefficients are summarised in Table 6.18.

6.4.3 Derived shear modulus results

The mean bulk density for each test (Table 6.17) together with the surface wave velocity-depth data were used to calculate the shear modulus-depth relationship from Equation 3.3. Detailed shear modulus (G) data are not presented. Values

of the intercept and slope of the shear modulus-depth profile are summarised in Table 6.19.

6.4.4 Surface wave attenuation results

Surface wave attenuation measurements were conducted on the Wet-mix macadam compacted in the Blaydon field trial trenches (Tests WMM1 to WMM6 and WMM 10) at frequencies of 300 and 500 Hz. Detailed distance-displacement amplitude (w, x) data are presented in Appendix A8.3 (Tables A8.9, A8.10, ..., A8.15) and are plotted with the best-fit regression line determined from Equation 5.10 in Figures 6.42, 6.43, ..., 6.48. Values of the intercept $\left(\alpha x_1 + \ln\left[w_1 \sqrt{x_1}\right]\right)$ and the slope, or the material attenuation coefficient (α), along with the regression correlation coefficient are given in Table 6.20.

6.4.5 Summary

Detailed data, summary data and plots based on detailed data (where appropriate) have been presented for density, moisture content and Impact Value (Section 6.4.1), surface wave velocity (Section 6.4.2) and surface wave attenuation (Section 6.4.3) for tests performed on the Wet-mix macadam compacted in the Blaydon field trial trenches.

Additionally, the summary data for surface wave velocity and bulk density allowed the calculation of shear modulus data which have also been presented in summary form.

Measurements relating to the subgrade below the Wet-mix macadam compacted in the field trial trenches are presented in Table 6.21

6.5 Measurements on Wet-mix macadam and Sharp Sand

6.5.1 Density, moisture content and Impact Value results

Detailed moisture content, Impact Value and bulk and dry density data for tests conducted on Wet-mix macadam and Sharp Sand constructions in the field trials (Tests WMM7 to WMM9) at the time of compaction are given in Appendix 6.4 (Tables A6.28, 6.29 and A6.30) These tables also include details of individual layer thicknesses and the measured percentage surcharge for each layer. A statement is made to identify those layers which were compacted with the extension leg fitted to

the vibratory rammer. These data are summarised, for each of the two materials, in mean/sample standard deviation form in Table 6.22.

6.5.2 Surface wave velocity results

Surface wave velocity-depth profile measurements on the Wet-mix macadam and Sharp Sand constructions compacted in the Blaydon field trial trenches (Tests WMM7 to WMM9) were conducted on the full trench only. Detailed data are presented in Appendix 7.4 (Tables A7.29, A7.30 and A7.31) and are plotted as surface wave velocity-depth profiles in Figures 6.49, 6.50 and 6.51. The individual layers are shown as layer logs on the depth (z) axis of each of these figures. It should be noted that the scales of both the axes of these plots have been expanded, compared to the plots derived from tests in the laboratory based trench. Values of the intercept and slope of the surface wave velocity-depth profile along with the regression correlation coefficient are summarised, for both materials, along with the regression correlation coefficient in Table 6.23.

6.5.3 Derived shear modulus results

The mean bulk density for each test (Table 6.22) together with the surface wave velocity-depth data were used to calculate the shear modulus-depth relationship from Equation 3.3. Detailed shear modulus (G) data are not presented. Values of the intercept and slope of the shear modulus-depth profile are summarised, for both materials, in Table 6.24.

6.5.4 Surface wave attenuation results

Surface wave attenuation measurements were conducted on the Wet-mix macadam and Sharp Sand constructions compacted in the Blaydon field trial trenches (Tests WMM7, WMM8 and WMM 9) at frequencies of 300 and 500 Hz. Detailed distance-displacement amplitude (w, x) data are presented in Appendix A8.4 (Tables A8.16, A8.17 and A8.18) and are plotted with the best-fit regression line determined from Equation 5.10 in Figures 6.52, 6.53 and 6.54.. Values of the intercept $\left(\alpha x_1 + \ln\left[\mathrm{w}_1 \sqrt{x_1}\right]\right)$ and the slope, or the material attenuation coefficient (α) are presented, along with the regression correlation coefficients in Table 6.25.

6.5.5 Summary

Detailed data, summary data and plots based on detailed data (where appropriate) have been presented for density, moisture content and Impact Value (Section 6.5.1), surface wave velocity (Section 6.5.2) and surface wave attenuation (Section 6.5.3) for tests performed on the Wet-mix macadam and Sharp Sand constructions compacted in the Blaydon field trial trenches.

Additionally, the summary data for surface wave velocity and bulk density allowed the calculation of shear modulus data which have also been presented in summary form.

Data relating to the subgrade below the Wet-mix macadam and Sharp Sand in the field trial trenches are presented in Table 6.21

6.6 Case studies

In this section the test results of a series of some five case studies are reported. Two of these relate to genuine utility service trenches (Sections 6.6.1 and 6.6.4), one test presents only the increase of the measured Impact Value with increased compactive effort (Section 6.6.2) and two tests were designed, with the assistance of the British Gas plc Engineering Research Station, to evaluate the differences between a 'well compacted' and a 'poorly compacted' trench (Section 6.6.3).

In addition to the experimental results, detailed information on the location and circumstance, of each case study are reported in this section.

6.6.1 SEAS service trench

A single determination of the surface wave velocity-depth profile, after reinstatement of the unbound layers, was made in a water service trench located between the 'old' School of Engineering and Applied Science building (North SEAS) and the 'new' South SEAS building (Test NSSEAS). Trench dimensions were approximately 0.4 m in width with an average depth of 2.2 m over the length tested. Trench construction was of 0.40 m of fine-fill (sand), used to bed and protect two water service pipes, while the remainder of the construction consisted of crushed rock (Dolomite) Type 2 granular material (specified to Department of Transport, 1986; see also Appendix 3) in layers with a nominal compacted layer thickness of 0.300 m, with a final layer consisting of residual Type 2 material of diameter less than 25 mm. Compactive

effort was applied with a vibrating plate compactor for the lower layers of the trench and a ten-tonne roller for the upper layers of the trench; in both cases the level of compactive effort applied was unknown. At the surface of the trench construction, immediately after testing, the moisture content was 9.44% and the mean Impact Value, $\overline{IV}$, was measured as 20.0, with sample standard deviation, $\sigma_{IV_{n-1}} = 3.69$.

The best-fit to the surface wave velocity-depth data (Table A7.32) appears to be two linear regression lines of the form of Equation 5.8 as follows:

$$v_R = 216.7 - 80.5z \quad (r = -0.953) \qquad \text{for } 0 \leq z < 0.6\,\text{m} \tag{6.2}$$

and

$$v_R = 195.1 - 17.5z \quad (r = -0.941) \qquad \text{for } z \geq 0.6\,\text{m} \tag{6.3}$$

The data are illustrated along with the relationships defined by Equations 6.2 and 6.3 in Figure 6.55.

6.6.2 Blaydon demonstration trench

During the period spent conducting field trials at the British Gas Northern Region Blaydon Depot (Tests WMM1 to WMM10) an exhibition was held at the site, by British Gas, in order to demonstrate technology relevant to the gas industry to their engineers. At the exhibition, plant manufacturers Bomag demonstrated their BG 100 vibratory roller (see Section 2.3 and Plate 6.1). This opportunity was taken to obtain Impact Value data as successive passes were applied to a single layer of gravel Type 2 granular material (specified to Department of Transport, 1986; see also Appendix 3); the uncompacted depth of the material was some 0.5 m, and the trench width was around 0.35 m. Impact Value measurements were taken at $N_p = 1, 2, 4, 7, 14$ and 20. Detailed data are presented in Appendix 6.5 (Table A6.31) and will be further discussed in Chapter 7.

6.6.3 Salters Lane: Back-to-back tests—well/poorly compacted

Two tests were conducted at the British Gas Engineering Research Station (ERS) Salters Lane test site. These were carried out on Wet-mix macadam, from the Moot Law quarry (as for Tests WMM1 to WMM10), at the delivery moisture content which aproximates to the optimum moisture content, determined to BS 5835: Part 1 (1980) (Chapter 4). The trench was excavated to dimensions 4.60 m in length by 0.93 m deep by 0.37 m in width. Both tests were conducted in the same trench,

the second test being conducted after completion and subsequent excavation of the first test. Filling, compaction and excavation was undertaken by labourers under contract to the ERS. These tests were specified as follows:

SL1 Four layers, of nominal layer thickness 200 mm, compacted with eight passes per layer from a BS45Y petrol driven vibratory rammer. This test corresponded to the British Gas specification for a 'well compacted' trench.

SL2 A single layer, almost filling the trench, compacted with twelve passes from a BS45Y petrol driven vibratory rammer. This test corresponds to a 'poorly compacted' trench.

Detailed compaction data for the two trenches are given in Appendix 6.5 (Table A6.32). Prior to compaction of Test SL1 the underlying clay subgrade was observed to have a small amount of standing water at one end of the trench. This was noted to influence the measured Impact Values along the length of the trench, for the first two layers (Layers I and II). Detailed Impact Value data for each layer of this test are presented in Table A6.33 and will be discussed in Chapter 7.

Detailed surface wave velocity-depth data are presented in Appendix 7.5 (Tables A7.33 and A7.34 for Tests SL1 and SL2, respectively) and are plotted as surface wave velocity-depth profiles in Figures 6.56 and 6.57. The surface wave velocity depth profiles of the form of Equation 5.8 are

$$v_R = 154.8 + 103.5z \quad (r = 0.747) \tag{6.4}$$

and

$$v_R = 86.7 + 127.8z \quad (r = 0.987) \tag{6.5}$$

For Tests SL1 and SL2, respectively.

6.6.4 Field trial: Acton Dean, Stanley, County Durham

This test was organised with the cooperation of the British Gas plc Northern Region Team Valley and Stanley Depots.

The test was conducted on the compacted unbound layers of a footpath reinstatement and the job was carried out by a British Gas reinstatement gang from the Stanley Depot, in Acton Dean, Stanley. The excavation was for the purpose of placing a new 90 mm (internal diameter) plastic gas main in an area previously not served by British Gas. This was achieved by excavating, placing the pipe and

backfilling in runs of approximately 5 m. Trench width was approximately 300 mm at footpath level, tapering to around 230 mm at the full depth of 650 mm. The excavated unbound material was used for the subsequent reinstatement as this material was considered to be Suitable Excavated Material (SEM). The definition of SEM will be discussed in Chapter 7.

Samples for the determination of the compacted moisture content were not removed from site because the excavated material varied considerably. A heavy clay was excavated from the subgrade level with hardcore (of predominantly stone, broken brick and crushed furnace slag) above the subgrade. Inspection of the excavated material and the trench walls indicated that the bound materials of the footpath had been laid directly on top of the hardcore.

Impact Values were recorded at six approximately equi-distant points, along the 5 m run under test, for each of three layers (compacted with $N_p = 2$ of a Wacker BS65Y vibratory rammer—this is a slightly heavier and more powerful version of the BS45Y used in the other tests presented in this chapter). Impact Value results are presented in Table A6.34. Surface wave velocity results are presented in Table A7.35. The resulting surface wave velocity-depth profile for the compacted material (Figure 6.58) is given by

$$v_R = 131.9 + 139.5z \quad (r = 0.881) \qquad (6.6).$$

The subgrade surface wave velocities are expressed in mean/sample standard deviation form (as for Tests WMM1 to WMM10—Table 6.21) as $v_R = 182.3$ m/s and $\sigma_{v_{Rn-1}} = 1.0$ m/s.

6.6.5 Summary

The results from five case studies have been presented and the circumstances and other pertinent and backgroud information supplied in this section. Detailed interpretation and discussion of the experimental results will be presented in Chapter 7.

6.7 Summary

In this chapter experimental results have been presented in both graphical form, as figures, and numerical form, as tabulated data summaries. Careful and thorough cross-reference has also been made to the more detailed experimental data presented in Appendices 6 to 9.

The format of the text of this chapter has been constrained to agree, closely, with that of the following chapter (Chapter 7) in which the experimental results are further interpreted and discussed.

The test programme is described in detail in Section 6.1.2, along with a detailed description of the coding system used to identify and distinguish individual tests. Two sample data sets of d, ϕ data used to determine the wavelength of surface waves (Equation 3.5) are presented in Section 6.1.3.

Results presented are for tests conducted on Permian Sand (Section 6.2) and Sharp Sand (Section 6.3) in the laboratory based trench and include density, moisture content, Impact Value, CBR, surface wave velocity, derived shear modulus and surface wave attenuation. The results for tests on Permian Sand also include a limited experimental study of the nature of vertical particle displacement at depth due to the propagation of Rayleigh-type surface waves. Tests conducted on Wet-mix macadam in the field trenches, at the British Gas plc Northern Region Blaydon Depot, are presented in Section 6.4 and further test results which combine layers of Wet-mix macadam with layers of Sharp Sand and, in two cases a gas pipe, are presented in Section 6.5. The results presented for these tests include density, moisture content, Impact Value, surface wave velocity, derived shear modulus and surface wave attenuation. In addition the results from a series of five case studies are presented in Section 6.6.

Table 6.1 - Test programme for Permian Sand in the laboratory based trench ($w \approx w_{opt}$ for all tests).

Test No	Number of blows per layer N_p	Nominal layer thickness (mm)	Buried Accelerometers	Number of layers	Comments (Depth in mm)
TPS1A	5	≤ 150	No	4	Half-full (480)
TPS1B	5	≤ 150	No	8	Full (895)
TPS1C	5	≤ 150	No	8	Full (895)
TPS1D	5	≤ 150	No	4	Half-full (440)
TPS2A	10	≤ 150	No	4	Half-full (450)
TPS2B	10	≤ 150	Yes	8	Full (850)
TPS2C	10	≤ 150	No	4	Half-full (450)
TPS3A	2	≤ 150	Yes	4	Half-full (500)
TPS3B	2	≤ 150	Yes	8	Full (870)
TPS4	5	≤ 300	No	3	Full (820)
TPS5A	8	≤ 150	No	4	Half-full (470)
TPS5B	8	≤ 150	No	7	Full (800)

Table 6.2 - Test programme for Sharp Sand in the laboratory based trench ($w \approx w_{opt}$ for all tests).

Test No	Number of blows per layer N_p	Nominal layer thickness (mm)	Number of layers	Comments (Depth in mm)
TSS1A	5	≤ 150	4	Half-full (470)
TSS1B	5	≤ 150	8	Full (860)
TSS2A	10	≤ 150	4	Half-full (470)
TSS2B	10	≤ 150	7	Full (790)
TSS3A	2	≤ 150	4	Half-full (500)
TSS3B	2	≤ 150	8	Full (910)
TSS4	5	≤ 300	3	Full (800)
TSS5A	8	≤ 150	4	Half-full (480)
TSS5B	8	≤ 150	8	Full (890)

Table 6.3 - Test programme for Wet-mix macadam in the field.

Test No	Number of blows per layer N_p	Nominal layer thickness (mm)	Number of layers	Comments (Depth in mm)
WMM1	5	≤ 150	5	$w \approx w_{opt}$ (640)
WMM2	10	≤ 150	5	$w \approx w_{opt}$ (610)
WMM3	2	≤ 150	5	$w \approx w_{opt}$ (700)
WMM4	5	≤ 200	2	$w \approx w_{opt}$ (430)
WMM5	8	≤ 150	5	$w \approx w_{opt}$ (610)
WMM6	10	≤ 200	3	$w \approx w_{opt}$ (570)
WMM10	10	≤ 200	3	$w \approx 0\%$ (580)

Table 6.4 - Test programme for Wet-mix macadam and Sharp Sand in the field ($w \approx w_{opt}$ for all tests).

Test No (Material)	Number of blows per layer N_p	Nominal layer thickness (mm)	Number of layers	Comments (Depth in mm)
WMM7(WMM)	8	≤ 200	2	— (380)
(SS)	6	≤ 150	2	— (680)
WMM8(WMM)	8	≤ 200	2	— (380)
(SS)	3 & 4	≤ 150	2	Plastic Pipe(680)
WMM9(WMM)	8	≤ 200	2	— (380)
(SS)	3 & 4	≤ 150	2	Steel Pipe (690)

Table 6.5 - Transducer separation (d), phase angle (ϕ) data for Test TPS2A (f = 375 Hz; r = 0.979). The corresponding Lissajous Figures are also shown.

Lissajous Figure	Transducer separation d (m)	Phase angle ϕ (radians)
\	0.020	π
/	0.215	2π
\	0.325	3π
/	0.620	4π
\	0.890	5π
/	1.335	6π

Table 6.6 - Transducer separation (d), phase angle (ϕ) data for Test WMM9 (f = 450 Hz; r = 1.000). The corresponding Lissajous Figures are also shown.

Lissajous Figure	Transducer separation d (m)	Phase angle ϕ (radians)
/	0.020	0
\	0.175	π
/	0.350	2π
\	0.515	3π
/	0.670	4π
\	0.850	5π
/	0.995	6π
\	1.190	7π
/	1.320	8π

Table 6.7 - Summary compaction data for tests on Permian Sand (Tests TPS1 to TPS5).

Test No	N_p	$\overline{h}/\sigma_{h_{n-1}}$ (m)	$N_p/(\overline{h}+\sigma_{h_{n-1}})$	$N_p/\overline{h}$ (m^{-1})	$N_p/(\overline{h}-\sigma_{h_{n-1}})$	Surcharge Mean/SD (%)	$\overline{w}/\sigma_{w_{n-1}}$ (%)	$\overline{IV}/\sigma_{IV_{n-1}}$
TPS1	5	0.112/0.022	37.31	44.64	55.56	26.06/8.81	10.06/1.79	6.88/0.81
TPS2	10	0.106/0.026	75.78	94.34	125.00	33.88/7.75	10.79/1.73	6.52/1.12
TPS3	2	0.109/0.025	14.93	18.35	23.81	26.64/4.46	12.20/1.34	3.39/0.46
TPS4	5	0.273/0.023	16.89	18.32	20.00	31.67/5.77	11.58/2.14	3.00/0.76
TPS5	8	0.114/0.022	58.82	70.18	86.96	32.99/6.39	11.27/1.42	5.34/1.00

Table 6.8 - Summary excavation data for tests on Permian Sand (Tests TPS1 to TPS5).

Test No	N_p	$\overline{h}/\sigma_{h_{n-1}}$ (m)	$N_p/(\overline{h}+\sigma_{h_{n-1}})$	$N_p/\overline{h}$ (m^{-1})	$N_p/(\overline{h}-\sigma_{h_{n-1}})$	$\overline{IV}/\sigma_{IV_{n-1}}$	CBR (%)	$\overline{IV}/\sigma_{IV_{n-1}}$ At Surface	$\overline{\rho}/\sigma_{\rho_{n-1}}$ (Mg/m^3)	$\overline{w}/\sigma_{w_{n-1}}$ (%)	$\overline{\rho}_d/\sigma_{\rho_{d_{n-1}}}$ (Mg/m^3)
TPS1	5	0.112/0.022	37.31	44.64	55.56	13.60/1.78	20.0	—/—	1.893/0.061	6.20/1.77	1.785/0.047
TPS2	10	0.106/0.026	75.78	94.34	125.00	11.41/2.87	10.1	8.5/0.41	2.087/0.073	10.24/1.99	1.891/0.043
TPS3	2	0.109/0.025	14.93	18.35	23.81	8.49/0.83	10.0	8.3/0.58	1.960/0.080	9.36/2.21	1.793/0.038
TPS4	5	0.273/0.023	16.89	18.32	20.00	6.55/1.10	6.3	7.2/0.65	2.050/0.098	8.60/3.28	1.861/0.040
TPS5	8	0.114/0.022	58.82	70.18	86.96	10.84/2.03	8.7	8.8/1.44	1.994/0.120	9.27/2.18	1.815/0.058

Table 6.9 - Summary surface wave velocity-depth profile data for tests on Permian Sand (Tests TPS1 to TPS5).

Test No	N_p	$\overline{h}/\sigma_{h_{n-1}}$ (m)	$N_p/(\overline{h}+\sigma_{h_{n-1}})$	$N_p/\overline{h}$ (m^{-1})	$N_p/(\overline{h}-\sigma_{h_{n-1}})$	Intercept c (m/s)	Slope m (s^{-1})	r
TPS1A	5	0.112/0.022	37.31	44.64	55.56	71.8	233.8	0.996
TPS1B						66.3	254.6	0.995
TPS1C						130.7	138.4	0.977
TPS1D						131.9	246.3	0.983
TPS2A	10	0.106/0.026	75.78	94.34	125.00	106.9	340.4	0.994
TPS2B						148.2	108.7	0.870
TPS2C						83.0	383.0	0.983
TPS3A	2	0.109/0.025	14.93	18.35	23.81	57.1	204.2	0.990
TPS3B						68.3	190.2	0.984
TPS4	5	0.273/0.023	16.89	18.32	20.00	79.8	157.4	0.984
TPS5A	8	0.114/0.022	58.82	70.18	86.96	127.8	276.2	0.923
TPS5B						97.2	196.1	0.949

Table 6.10 - Summary shear modulus-depth data for tests on Permian Sand (Tests TPS1 to TPS5).

Test No	N_p	$\overline{h}/\sigma_{h_{n-1}}$ (m)	$N_p/(\overline{h}+\sigma_{h_{n-1}})$	$N_p/\overline{h}$ (m^{-1})	$N_p/(\overline{h}-\sigma_{h_{n-1}})$	Intercept c (MPa)	Slope m (MPa/m)
TPS1A	5	0.112/0.022	37.31	44.64	55.56	9.8	113.2
TPS1B						8.3	173.7
TPS1C						32.3	100.9
TPS1D						32.9	173.5
TPS2A	10	0.106/0.026	75.78	94.34	125.00	23.8	222.8
TPS2B						45.8	88.2
TPS2C						14.4	270.5
TPS3A	2	0.109/0.025	14.93	18.35	23.81	6.4	78.7
TPS3B						9.1	112.6
TPS4	5	0.273/0.023	16.89	18.32	20.00	13.1	93.2
TPS5A	8	0.114/0.022	58.82	70.18	86.96	32.6	212.3
TPS5B						18.8	137.4

Table 6.11 - Summary surface wave attenuation data for tests on Permian Sand (Tests TPS1 to TPS5).

Test No	N_p	$\overline{h}/\sigma_{h_{n-1}}$ (m)	$N_p/(\overline{h}+\sigma_{h_{n-1}})$	$N_p/\overline{h}$	$N_p/(\overline{h}-\sigma_{h_{n-1}})$ (m^{-1})	Frequency = 500 Hz			Frequency = 300 Hz		
						Intercept c	Slope $m=-\alpha$ (m^{-1})	r	Intercept c	Slope $m=-\alpha$ (m^{-1})	r
TPS3B	2	0.109/0.025	14.93	18.35	23.81	−15.068	−0.461	−0.465	−13.369	−0.275	−0.413
TPS4	5	0.273/0.023	16.89	18.32	20.00	−17.247	−0.603	−0.491	−14.605	−0.218	−0.313
TPS5B	8	0.114/0.022	58.82	70.18	86.96	−17.818	−0.174	−0.294	−14.319	−0.285	−0.350

Note: Intercept, $c = \alpha x_1 + \ln\left[w_1 \sqrt{x_1}\right]$.

Table 6.12 - Summary compaction data for tests on Sharp Sand (Tests TSS1 to TSS5).

Test No	N_p	$\overline{h}/\sigma_{h_{n-1}}$ (m)	$N_p/(\overline{h}+\sigma_{h_{n-1}})$	$N_p/\overline{h}$ (m^{-1})	$N_p/(\overline{h}-\sigma_{h_{n-1}})$	Surcharge Mean/SD (%)	$\overline{w}/\sigma_{w_{n-1}}$ (%)	$\overline{IV}/\sigma_{IV_{n-1}}$
TSS1	5	0.108/0.018	39.68	46.30	55.56	30.91/4.07	8.98/0.63	5.20/0.49
TSS2	10	0.113/0.017	76.92	88.50	104.17	29.57/4.21	9.44/0.52	6.74/0.46
TSS3	2	0.114/0.021	14.82	17.54	21.51	25.06/6.39	10.54/0.77	3.49/0.75
TSS4	5	0.267/0.021	17.36	18.73	20.33	25.30/3.52	9.81/1.60 13	5.23/0.31
TSS5	8	0.111/0.020	61.07	72.07	87.91	28.58/4.65	10.04/0.74	5.99/0.57

Table 6.13 - Summary excavation data for tests on Sharp Sand (Tests TSS1 to TSS5).

Test No	N_p	$\overline{h}/\sigma_{h_{n-1}}$ (m)	$N_p/(\overline{h}+\sigma_{h_{n-1}})$	$N_p/\overline{h}$ (m^{-1})	$N_p/(\overline{h}-\sigma_{h_{n-1}})$	$\overline{IV}/\sigma_{IV_{n-1}}$	CBR (%)	$\overline{IV}/\sigma_{IV_{n-1}}$ At Surface	$\overline{\rho}/\sigma_{\rho_{n-1}}$ (Mg/m^3)	$\overline{w}/\sigma_{w_{n-1}}$ (%)	$\overline{\rho}_d/\sigma_{\rho_{d_{n-1}}}$ (Mg/m^3)
TSS1	5	0.108/0.018	39.68	46.30	55.56	8.22/1.93	4.5	6.6/1.12	1.790/0.065	10.95/2.14	1.610/0.033
TSS2	10	0.113/0.017	76.92	88.50	104.17	10.85/2.69	6.6	8.0/0.71	1.862/0.057	7.78/2.16	1.727/0.031
TSS3	2	0.114/0.021	14.82	17.54	21.51	5.82/1.51	5.2	4.6/0.25	1.718/0.071	7.52/2.17	1.600/0.051
TSS4	5	0.267/0.021	17.36	18.73	20.33	6.58/1.08	6.9	7.7/0.29	1.806/0.041	7.63/1.56	1.679/0.016
TSS5	8	0.111/0.020	61.07	72.07	87.91	9.80/2.69	7.6	7.8/0.29	1.900/0.043	8.38/1.42	1.752/0.018

Table 6.14 - Summary surface wave velocity-depth profile data for tests on Sharp Sand (Tests TSS1 to TSS5).

Test No	N_p	$\overline{h}/\sigma_{h_{n-1}}$ (m)	$N_p/(\overline{h}+\sigma_{h_{n-1}})$	$N_p/\overline{h}$ (m^{-1})	$N_p/(\overline{h}-\sigma_{h_{n-1}})$	Intercept c (m/s)	Slope m (s^{-1})	r
TSS1A	5	0.108/0.018	39.68	46.30	55.56	56.7	237.9	0.995
TSS1B						56.7	274.4	0.998
TSS2A	10	0.113/0.017	76.92	88.50	104.17	70.4	261.6	0.993
TSS2B						106.8	185.2	0.995
TSS3A	2	0.114/0.021	14.82	17.54	21.51	70.5	183.8	0.991
TSS3B						76.7	180.8	0.981
TSS4	5	0.267/0.021	17.36	18.73	20.33	67.4	215.5	0.992
TSS5A	8	0.111/0.020	61.07	72.07	87.91	51.3	265.4	0.993
TSS5B						75.1	226.8	0.990

Table 6.15 - Summary shear modulus-depth data for tests on Sharp Sand (Tests TSS1 to TSS5).

Test No	N_p	$\overline{h}/\sigma_{h_{n-1}}$ (m)	$N_p/(\overline{h}+\sigma_{h_{n-1}})$	$N_p/\overline{h}$ (m^{-1})	$N_p/(\overline{h}-\sigma_{h_{n-1}})$	Intercept c (MPa)	Slope m (MPa/m)
TSS1A	5	0.108/0.018	39.68	46.30	55.56	5.8	95.9
TSS1B						5.8	171.6
TSS2A	10	0.113/0.017	76.92	88.50	104.17	9.2	128.5
TSS2B						21.2	124.1
TSS3A	2	0.114/0.021	14.82	17.54	21.51	8.5	73.5
TSS3B						10.1	98.8
TSS4	5	0.267/0.021	17.36	18.73	20.33	8.2	119.6
TSS5A	8	0.111/0.020	61.07	72.07	87.91	5.0	116.0
TSS5B						10.7	151.7

Table 6.16 - Summary surface wave attenuation data for tests on Sharp Sand (Tests TSS1 to TSS5).

Test No	N_p	$\overline{h}/\sigma_{h_{n-1}}$ (m)	$N_p/(\overline{h}+\sigma_{h_{n-1}})$	$N_p/\overline{h}$ (m^{-1})	$N_p/(\overline{h}-\sigma_{h_{n-1}})$	Frequency = 500 Hz			Frequency = 300 Hz		
						Intercept c	Slope $m=-\alpha$ (m^{-1})	r	Intercept c	Slope $m=-\alpha$ (m^{-1})	r
TSS1B	5	0.108/0.018	39.68	46.30	55.56	−17.131	−0.296	−0.648	−14.403	−0.202	−0.356
TSS2B	10	0.113/0.017	76.92	88.50	104.17	−17.753	−0.186	−0.291	−14.501	−0.156	−0.267
TSS3B	2	0.114/0.021	14.82	17.54	21.51	−17.595	−0.140	−0.191	−14.670	−0.157	−0.214
TSS4	5	0.267/0.021	17.36	18.73	20.33	−17.582	−0.095	−0.235	−14.204	−0.424	−0.556
TSS5B	8	0.111/0.020	61.17	72.07	87.91	−17.137	−0.376	−0.370	−14.363	−0.049	−0.175

Note: Intercept, $c = \alpha x_1 + \ln\left[w_1 \sqrt{x_1}\right]$.

Table 6.17 - Summary compaction data for tests on Wet-mix macadam (Tests WMM1 to WMM6 and WMM10).

Test No	N_p	$\overline{h}/\sigma_{h_{n-1}}$ (m)	$N_p/(\overline{h}+\sigma_{h_{n-1}})$ (m^{-1})	$N_p/\overline{h}$ (m^{-1})	$N_p/(\overline{h}-\sigma_{h_{n-1}})$ (m^{-1})	Surcharge Mean/SD (%)	$w/\sigma_{w_{n-1}}$ (%)	$\overline{IV}/\sigma_{IV_{n-1}}$	Density data		
									$\overline{\rho}/\sigma_{\rho_{n-1}}$ (Mg/m^3)	$\overline{w}/\sigma_{w_{n-1}}$ (%)	$\overline{\rho}_d/\sigma_{\rho_{d_{n-1}}}$ (Mg/m^3)
WMM1	5	0.128/0.018	34.25	39.06	45.46	20.00/0.00	5.31/0.41	19.18/2.35	2.086/0.069	4.45/0.38	1.997/0.066
WMM2	10	0.122/0.016	72.46	81.97	94.34	22.62/3.06	5.00/0.26	24.86/3.27	2.258/0.039	4.36/0.43	2.164/0.040
WMM3	2	0.140/0.017	12.74	14.29	16.26	12.32/3.23	4.84/0.82	12.76/0.72	1.972/0.143	4.35/0.47	1.890/0.133
WMM4	5	0.215/0.021	21.19	23.26	25.77	10.50/3.54	5.54/0.33	19.35/3.61	2.069/0.057	4.29/0.44	1.984/0.046
WMM5	8	0.122/0.030	52.63	65.57	86.96	21.38/7.25	5.04/0.30	23.28/0.89	2.168/0.081	4.03/0.83	2.084/0.064
WMM6	10	0.190/0.010	50.00	52.63	55.57	20.83/4.15	6.14/0.36	21.80/1.31	2.156/0.124	4.80/0.64	2.058/0.125
WMM10	10	0.193/0.012	48.78	51.81	55.25	10.83/3.00	0.55/0.00	12.37/1.89	—/—	—/—	—/—

Table 6.18 - Summary surface wave velocity-depth profile data for tests on Wet-mix macadam (Tests WMM1 to WMM6 and WMM10).

Test No	N_p	$\overline{h}/\sigma_{h_{n-1}}$ (m)	$N_p/(\overline{h}+\sigma_{h_{n-1}})$	$N_p/\overline{h}$ (m^{-1})	$N_p/(\overline{h}-\sigma_{h_{n-1}})$	Intercept c (m/s)	Slope m (s^{-1})	r
WMM1	5	0.128/0.018	34.25	39.06	45.46	118.1	99.1	0.980
WMM2	10	0.122/0.016	72.46	81.97	94.34	236.8	206.7	0.992
WMM3	2	0.140/0.017	12.74	14.29	16.26	113.0	44.5	0.808
WMM4	5	0.215/0.021	21.19	23.26	25.77	144.4	62.2	0.708
WMM5	8	0.122/0.030	52.63	65.57	86.96	177.4	−2.8	−0.100
WMM6	10	0.190/0.010	50.00	52.63	55.57	140.5	143.8	0.984
WMM10	10	0.193/0.012	48.78	51.81	55.25	176.4	−45.7	−0.274

Table 6.19 - Summary shear modulus-depth data for tests on Wet-mix macadam (Tests WMM1 to WMM6 and WMM10).

Test No	N_p	$\overline{h}/\sigma_{h_{n-1}}$ (m)	$N_p/(\overline{h}+\sigma_{h_{n-1}})$	$N_p/\overline{h}$ (m^{-1})	$N_p/(\overline{h}-\sigma_{h_{n-1}})$	Intercept c (MPa)	Slope m (MPa/m)
WMM1	5	0.128/0.018	34.25	39.06	45.46	29.1	61.9
WMM2	10	0.122/0.016	72.46	81.97	94.34	126.6	279.9
WMM3	2	0.140/0.017	12.74	14.29	16.26	25.2	22.6
WMM4	5	0.215/0.021	21.19	23.26	25.77	43.1	40.6
WMM5	8	0.122/0.030	52.63	65.57	86.96	68.2	-2.1
WMM6	10	0.190/0.010	50.00	52.63	55.57	42.6	112.5
WMM10	10	0.193/0.012	48.78	51.81	55.25	—	—

Table 6.20 - Summary surface wave attenuation data for tests on Wet-mix macadam (Tests WMM1 to WMM6 and WMM10).

Test No	N_p	$\overline{h}/\sigma_{h_{n-1}}$ (m)	$N_p/(\overline{h}+\sigma_{h_{n-1}})$	$N_p/\overline{h}$	$N_p/(\overline{h}-\sigma_{h_{n-1}})$ (m^{-1})	Frequency = 500 Hz			Frequency = 300 Hz		
						Intercept c	Slope $m=-\alpha$ (m^{-1})	r	Intercept c	Slope $m=-\alpha$ (m^{-1})	r
WMM1	5	0.128/0.018	34.25	39.06	45.46	−15.981	−1.267	−0.868	−14.630	−0.688	−0.680
WMM2	10	0.122/0.016	72.46	81.97	94.34	−16.342	−1.926	−0.915	−14.740	−0.726	−0.758
WMM3	2	0.140/0.017	12.74	14.29	16.26	−17.650	−1.590	−0.870	−14.191	−1.438	−0.841
WMM4	5	0.215/0.021	21.19	23.26	25.77	−15.946	−1.617	−0.863	−14.315	−0.592	−0.812
WMM5	8	0.122/0.030	52.63	65.57	86.96	−16.816	−1.483	−0.909	−14.935	−0.754	−0.690
WMM6	10	0.190/0.010	50.00	52.63	55.57	−17.162	−1.433	−0.914	−14.515	−0.800	−0.699
WMM10	10	0.193/0.012	48.78	51.81	55.25	−17.995	−1.181	−0.821	−15.641	−1.255	−0.941

Note: Intercept, $c = \alpha x_1 + \ln\left[w_1 \sqrt{x_1}\right]$.

Table 6.21 - Summary subgrade data for Tests WMM1 to WMM10.

Test No	Depth below top of concrete pad (m)	$\overline{IV}/\sigma_{IV_{n-1}}$	$v_R/\sigma_{v_{Rn-1}}$ (m/s)
WMM1	0.900	0.6/0.89	127.6/ 3.3
WMM2	0.880	1.9/1.56	134.5/ 3.4
WMM3	0.940	5.1/0.55	137.8/ 3.4
WMM4	0.830	7.9/1.14	126.9/ 2.7
WMM5	0.860	—/—	128.2/ 4.7
WMM6	0.860	5.1/0.82	132.6/15.1
WMM7	0.910	2.9/1.52	124.1/ 1.6
WMM8	0.900	2.9/1.60	111.6/15.1
WMM9	0.900	4.8/0.76	—/—
WMM10	0.920	—/—	159.8/ 9.5

Table 6.22 - Summary compaction data for tests on Wet-mix macadam and Sharp Sand (Tests WMM7 to WMM9).

Test No (Material)	N_p	$\overline{h}/\sigma_{h_{n-1}}$ (m)	$N_p/(\overline{h}+\sigma_{h_{n-1}})$ (m^{-1})	$N_p/\overline{h}$ (m^{-1})	$N_p/(\overline{h}-\sigma_{h_{n-1}})$ (m^{-1})	Surcharge Mean/SD (%)	$w/\sigma_{w_{n-1}}$ (%)	$\overline{IV}/\sigma_{IV_{n-1}}$	Density data $\overline{\rho}/\sigma_{\rho_{n-1}}$ (Mg/m^3)	$\overline{w}/\sigma_{w_{n-1}}$ (%)	$\overline{\rho}_d/\sigma_{\rho_{d_{n-1}}}$ (Mg/m^3)
WMM7(WMM)	8	0.190/0.000	42.11	42.11	42.11	20.80/0.00	4.95/1.06	23.15/1.77	2.130/0.119	4.62/0.49	2.036/0.104
(SS)	6	0.150/0.000	40.00	40.00	40.00	16.70/0.00	7.70/0.23	5.85/0.35	—/—	8.49/0.89	—/—
WMM8(WMM)	8	0.190/0.000	42.11	42.11	42.11	20.80/0.00	5.23/0.34	21.60/0.14	2.134/0.026	4.00/0.43	2.052/0.016
(SS)	3 & 4	0.150/0.085	—	—	—	18.70/0.71	7.72/0.06	3.55/0.07	1.842/0.163	7.78/1.22	1.709/0.172
WMM9(WMM)	8	0.190/0.000	42.11	42.11	42.11	20.80/0.00	4.62/1.03	22.75/1.48	2.141/0.027	3.75/0.47	2.064/0.016
(SS)	3 & 4	0.150/0.092	—	—	—	16.80/1.98	7.32/0.28	4.50/1.13	1.819/0.149	7.42/0.33	1.692/0.134

Table 6.23 - Summary surface wave velocity-depth profile data for tests on Wet-mix macadam and Sharp Sand (Tests WMM7 to WMM9).

Test No	N_p	$\overline{h}/\sigma_{h_{n-1}}$ (m)	$N_p/(\overline{h}+\sigma_{h_{n-1}})$	$N_p/\overline{h}$ (m^{-1})	$N_p/(\overline{h}-\sigma_{h_{n-1}})$	Intercept c (m/s)	Slope m (s^{-1})	r
WMM7(WMM)	8	0.190/0.000	42.11	42.11	42.11	48.9	552.1	0.958
(SS)	6	0.150/0.000	40.00	40.00	40.00	179.4	−44.3	−0.466
WMM8(WMM)	8	0.190/0.000	42.11	42.11	42.11	64.2	364.9	0.999
(SS)	3 & 4	0.150/0.085	—	—	—	140.6	−11.4	−0.157
WMM9(WMM)	8	0.190/0.000	42.11	42.11	42.11	116.7	188.7	0.992
(SS)	3 & 4	0.150/0.092	—	—	—	206.6	−114.4	−0.985

Table 6.24 - Summary shear modulus-depth data for tests on Wet-mix macadam and Sharp Sand (Tests WMM7 to WMM9).

Test No	N_p	$\overline{h}/\sigma_{h_{n-1}}$ (m)	$N_p/(\overline{h}+\sigma_{h_{n-1}})$	$N_p/\overline{h}$ (m^{-1})	$N_p/(\overline{h}-\sigma_{h_{n-1}})$	Intercept c (MPa)	Slope m (MPa/m)
WMM7(WMM)	8	0.190/0.000	42.11	42.11	42.11	5.1	361.7
(SS)	6	0.150/0.000	40.00	40.00	40.00	—	—
WMM8(WMM)	8	0.190/0.000	42.11	42.11	42.11	8.8	208.0
(SS)	3 & 4	0.150/0.085	—	—	—	36.4	-5.7
WMM9(WMM)	8	0.190/0.000	42.11	42.11	42.11	29.2	123.3
(SS)	3 & 4	0.150/0.092	—	—	—	77.6	-69.6

Table 6.25 - Summary surface wave attenuation data for tests on Wet-mix macadam and Sharp Sand (Tests WMM7 to WMM9).

Test No	N_p	$\overline{h}/\sigma_{h_{n-1}}$ (m)	$N_p/(\overline{h}+\sigma_{h_{n-1}})$	$N_p/\overline{h}$	$N_p/(\overline{h}-\sigma_{h_{n-1}})$	Frequency = 500 Hz			Frequency = 300 Hz		
			(m^{-1})			Intercept c	Slope $m=-\alpha$ (m^{-1})	r	Intercept c	Slope $m=-\alpha$ (m^{-1})	r
WMM7	8	0.190/0.000	42.11	42.11	42.11	−16.624	−1.705	−0.884	−14.774	−0.677	−0.733
WMM8	8	0.190/0.000	42.11	42.11	42.11	−17.287	−1.670	−0.898	−14.287	−1.055	−0.846
WMM9	8	0.190/0.000	42.11	42.11	42.11	−16.321	−1.990	−0.907	−14.484	−0.441	−0.590

Note: Intercept, $c = \alpha x_1 + \ln\left[w_1 \sqrt{x_1}\right]$.

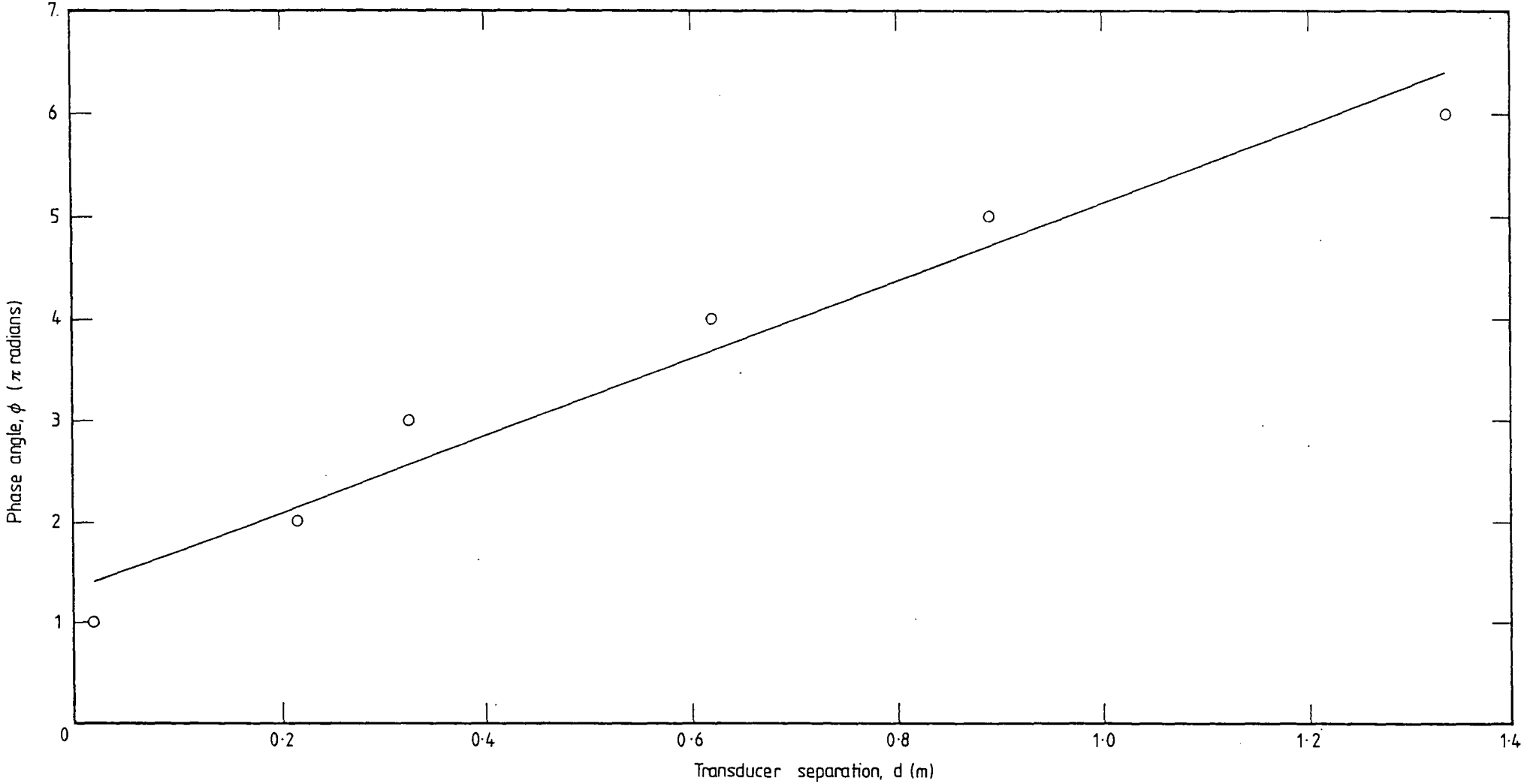

Figure 6.1 - Plot of transducer separation (d) against phase angle (ϕ) for Test TPS2A ($f = 375$ Hz; $r = 0.979$).

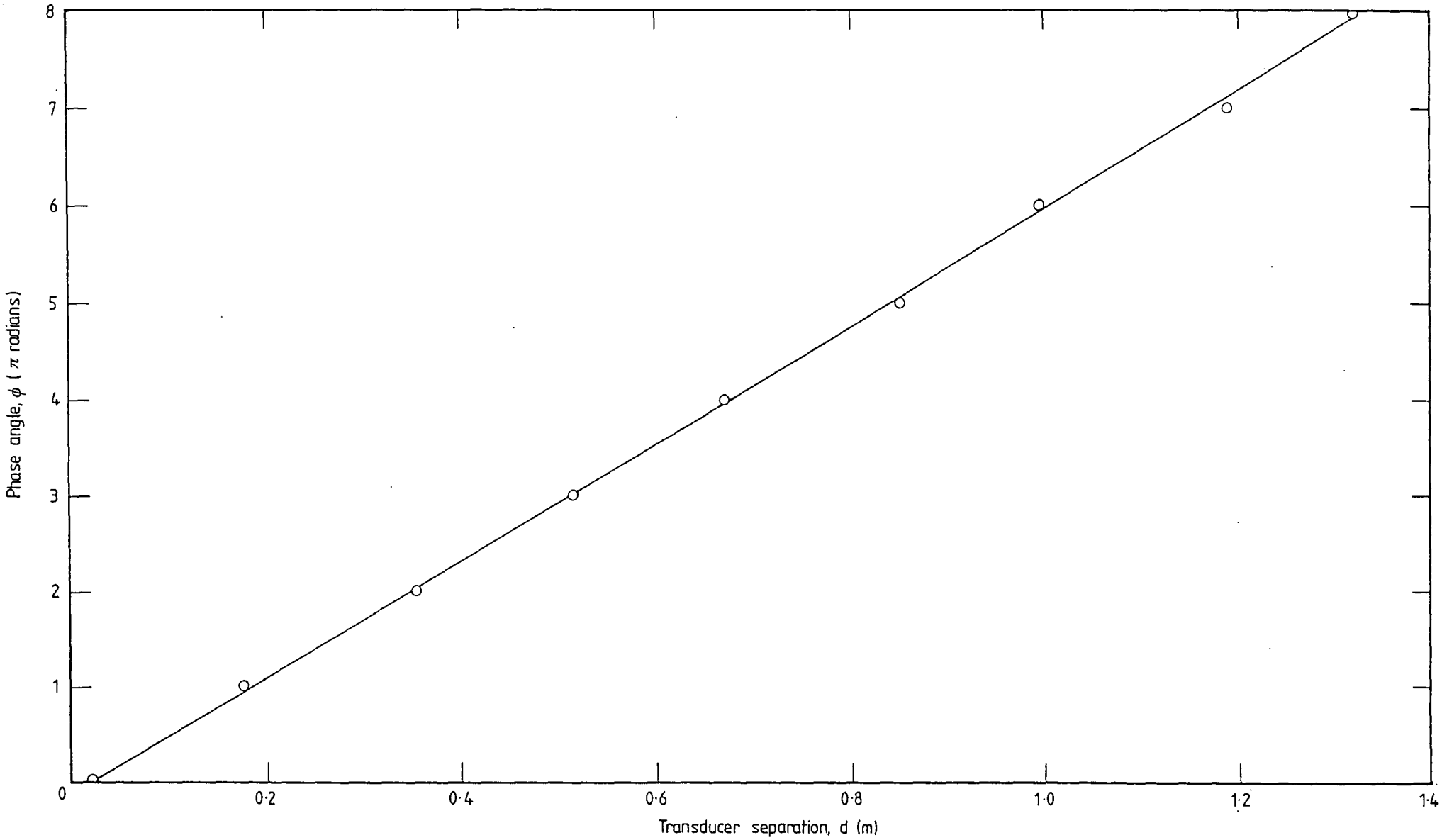

Figure 6.2 - Plot of transducer separation (d) against phase angle (ϕ) for Test WMM9 ($f = 450$ Hz; $r = 1.000$)

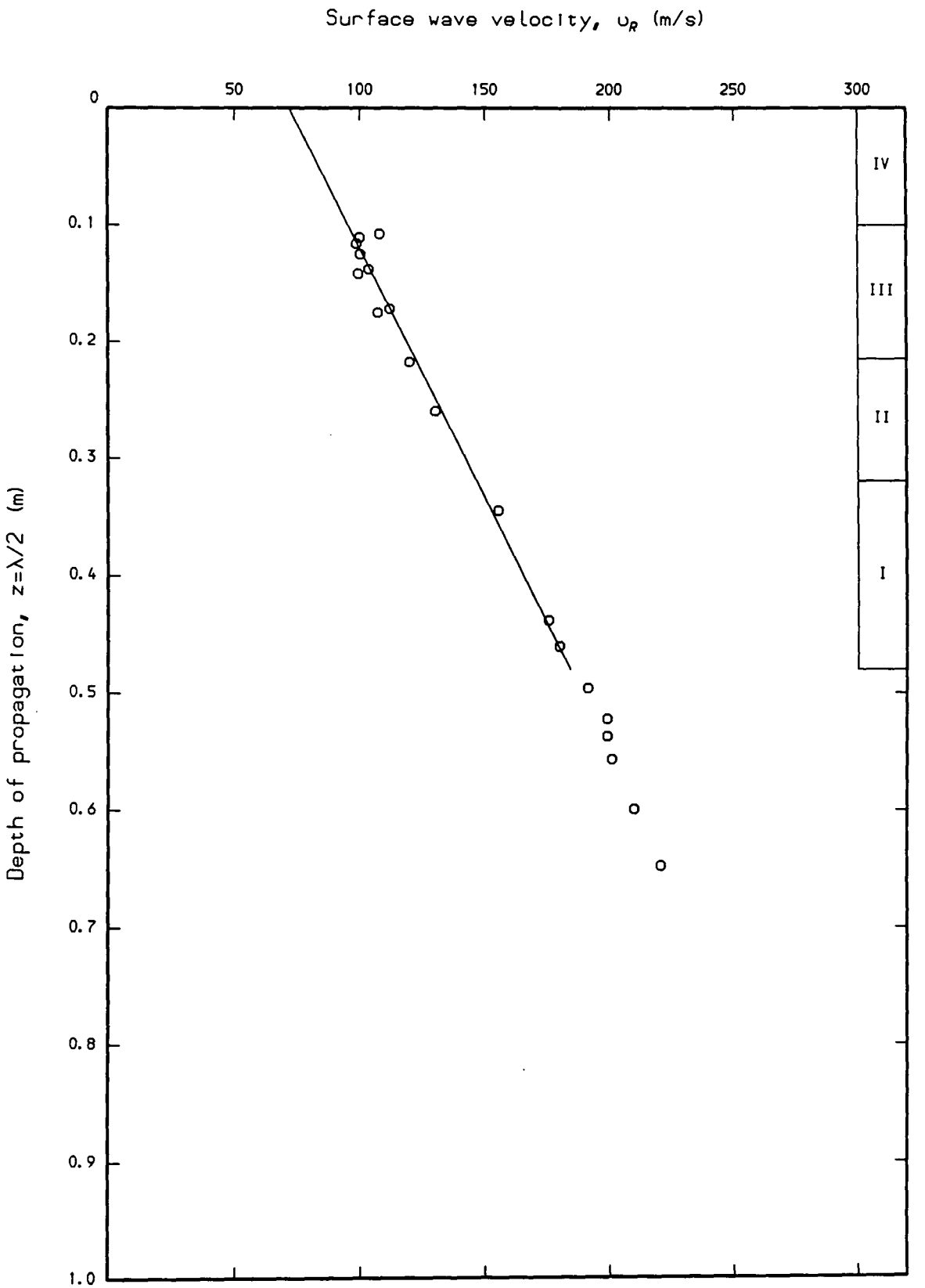

Figure 6.3 - Surface wave velocity-depth profile for Test TPS1A.

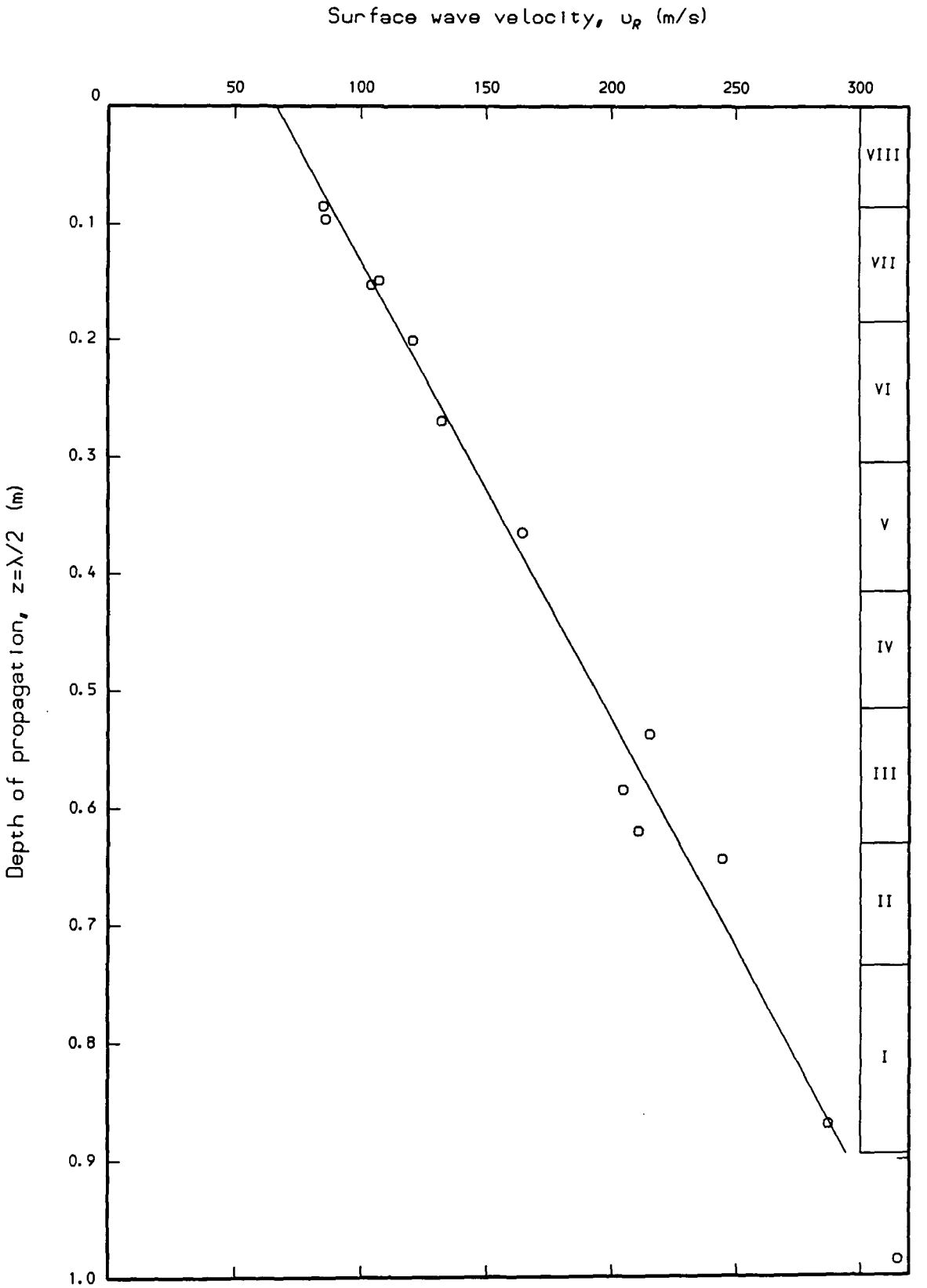

Figure 6.4 - Surface wave velocity-depth profile for Test TPS1B.

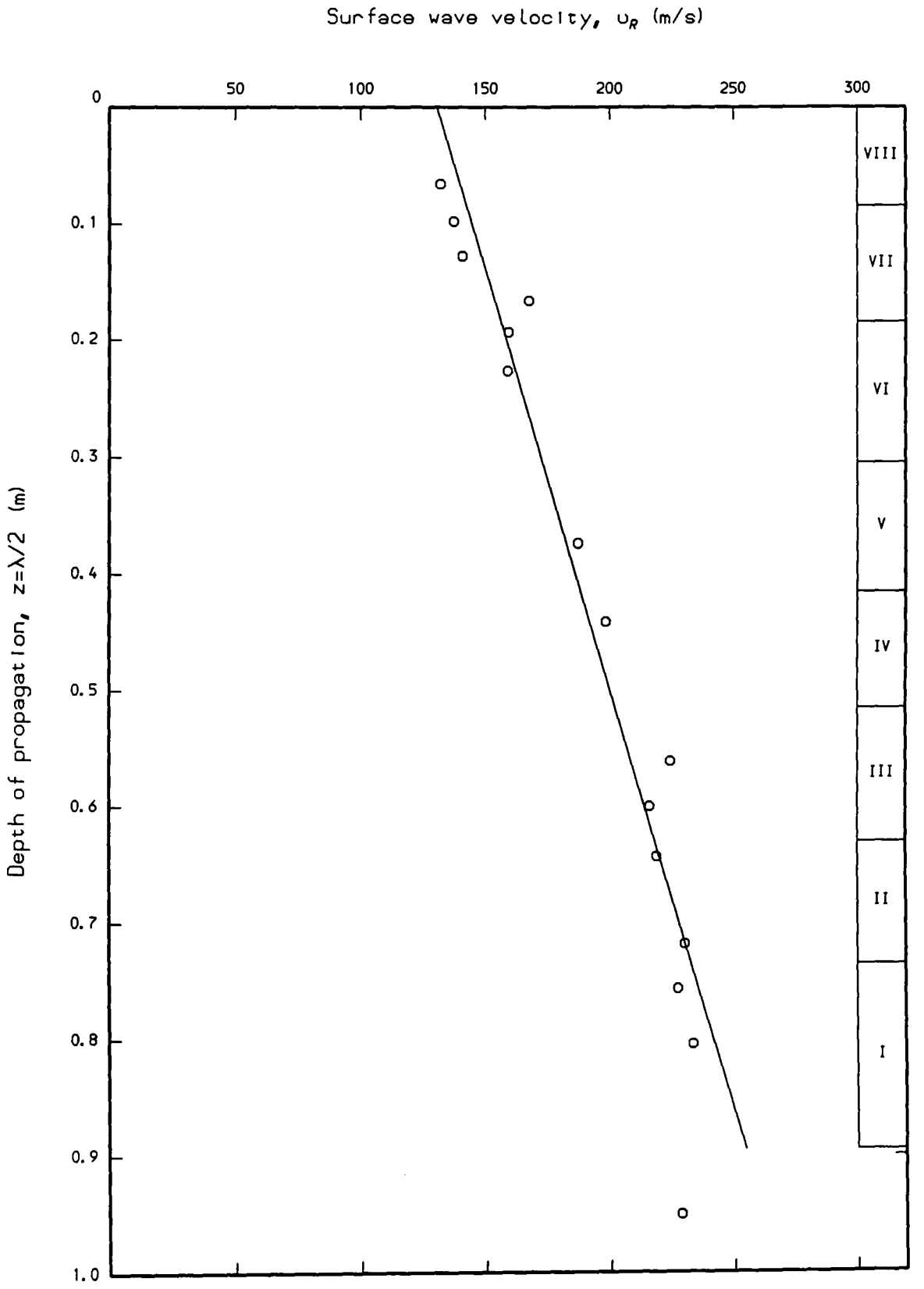

Figure 6.5 - Surface wave velocity-depth profile for Test TPS1C.

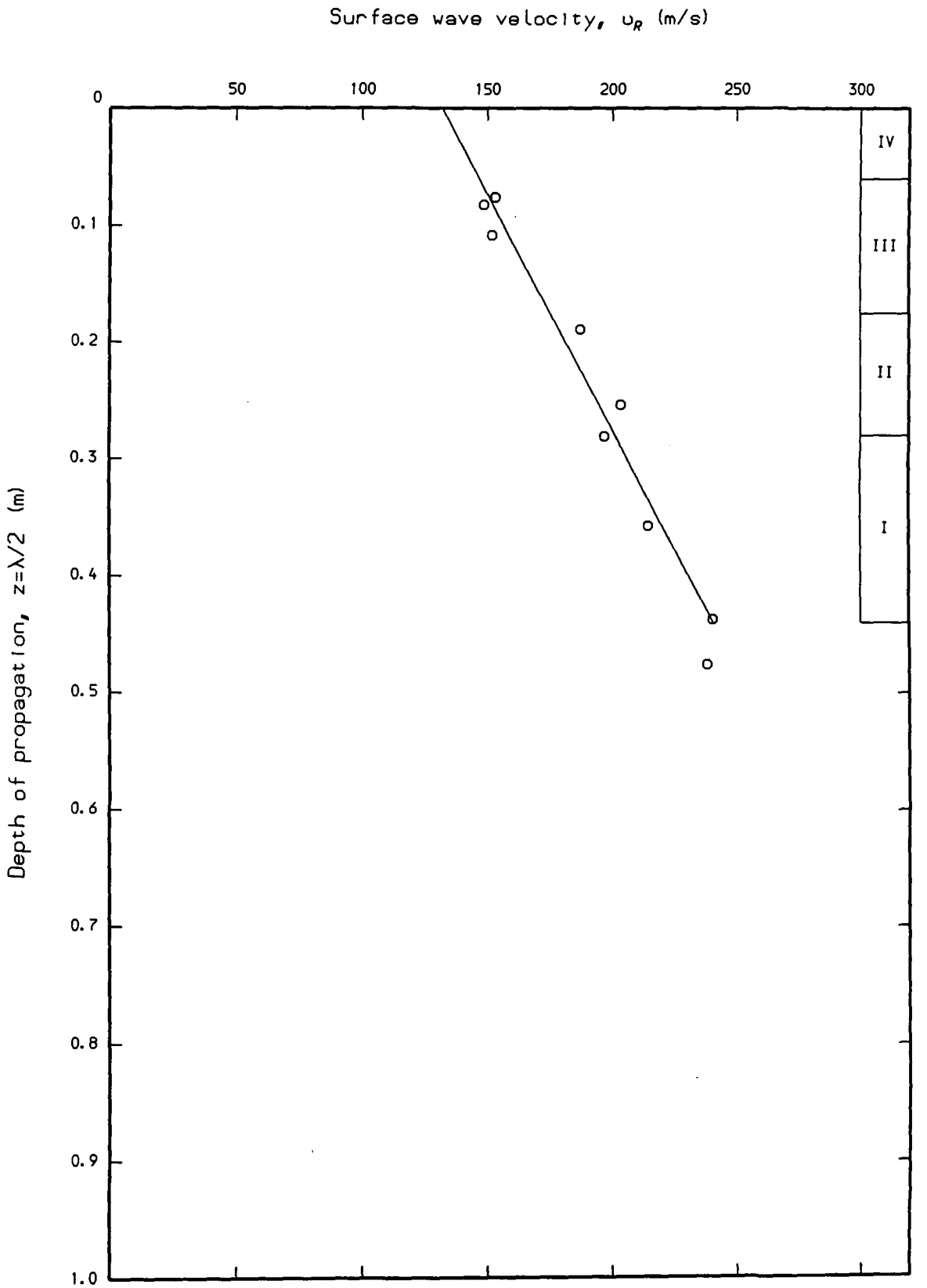

Figure 6.6 - Surface wave velocity-depth profile for Test TPS1D.

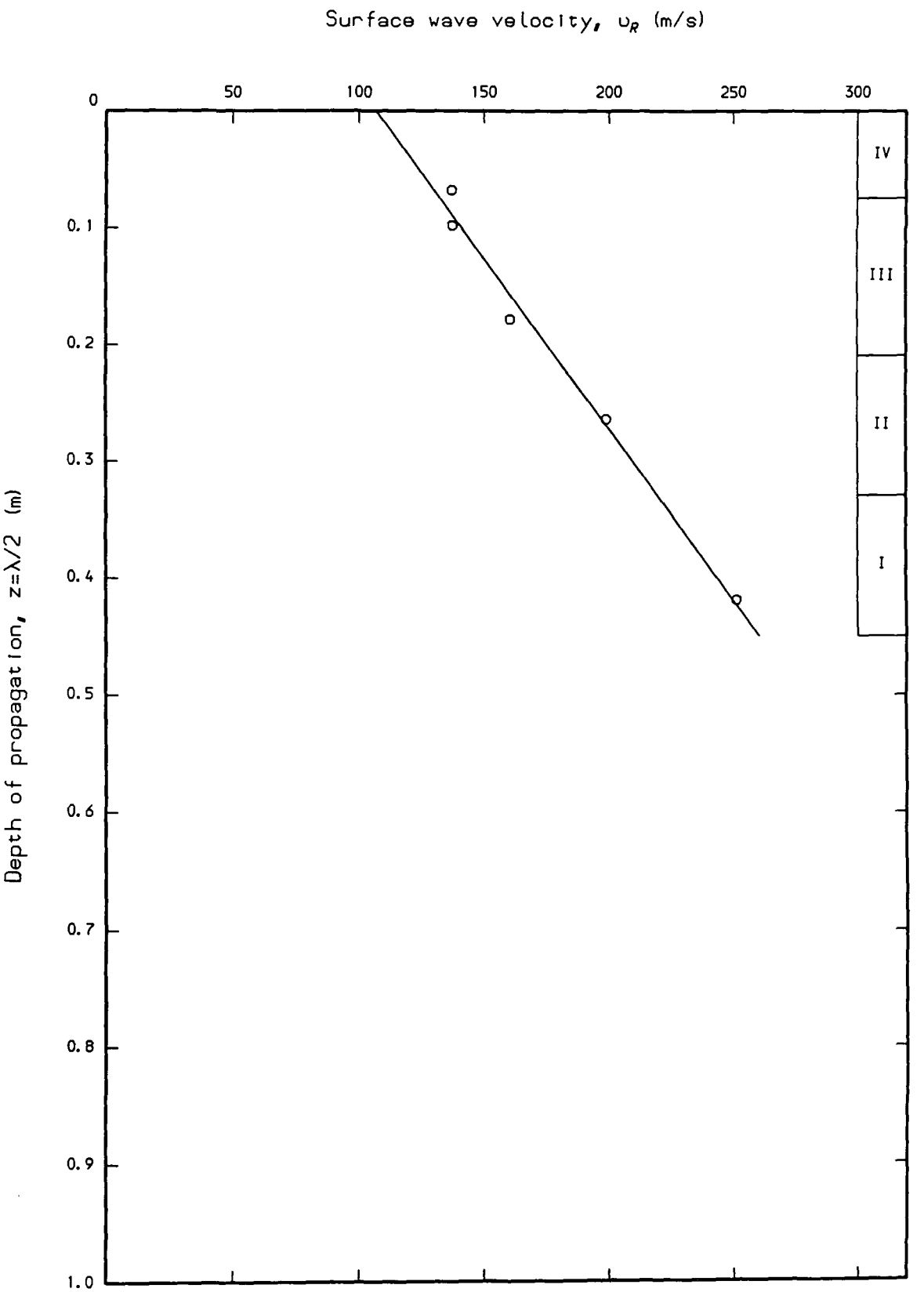

Figure 6.7 - Surface wave velocity-depth profile for Test TPS2A.

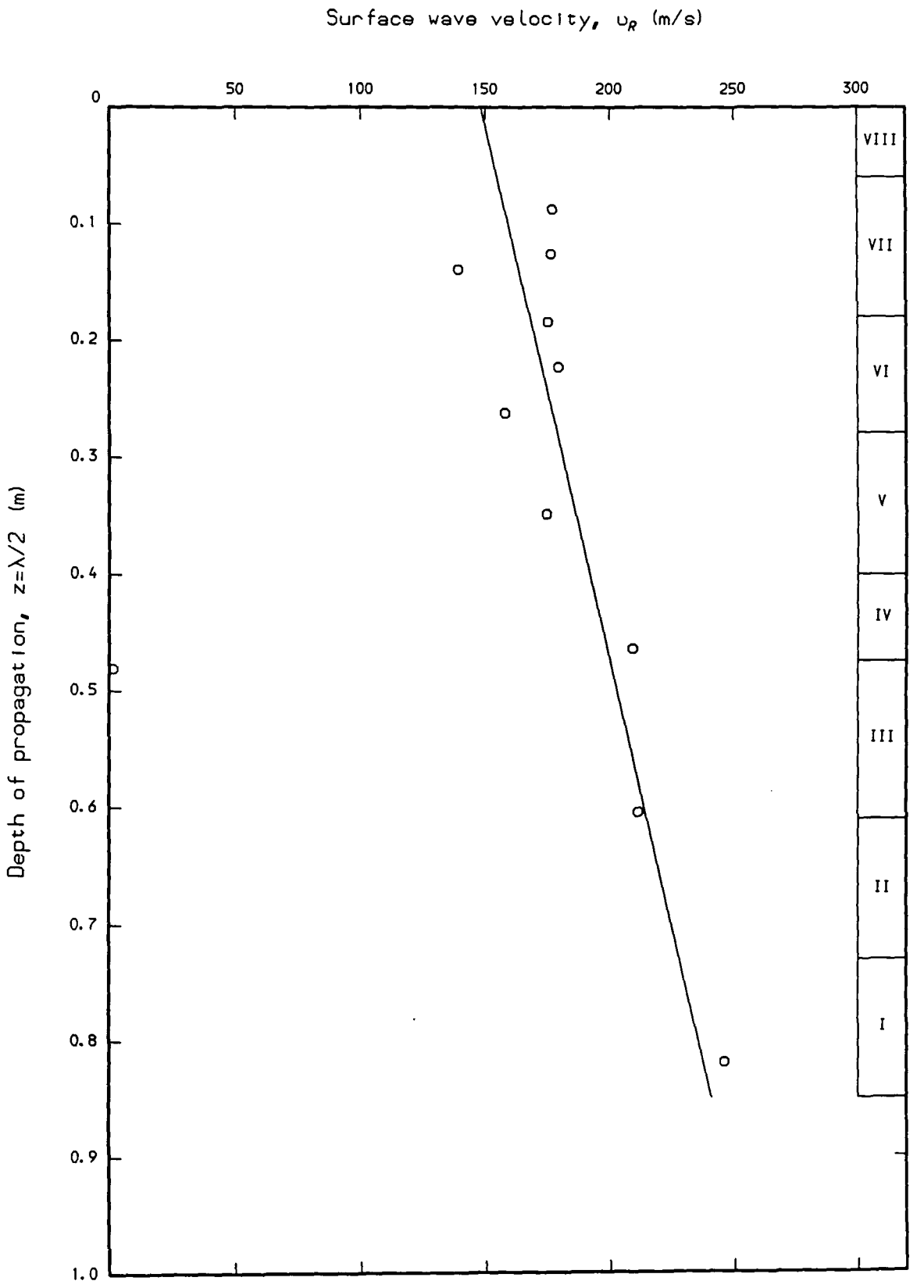

Figure 6.8 - Surface wave velocity-depth profile for Test TPS2B.

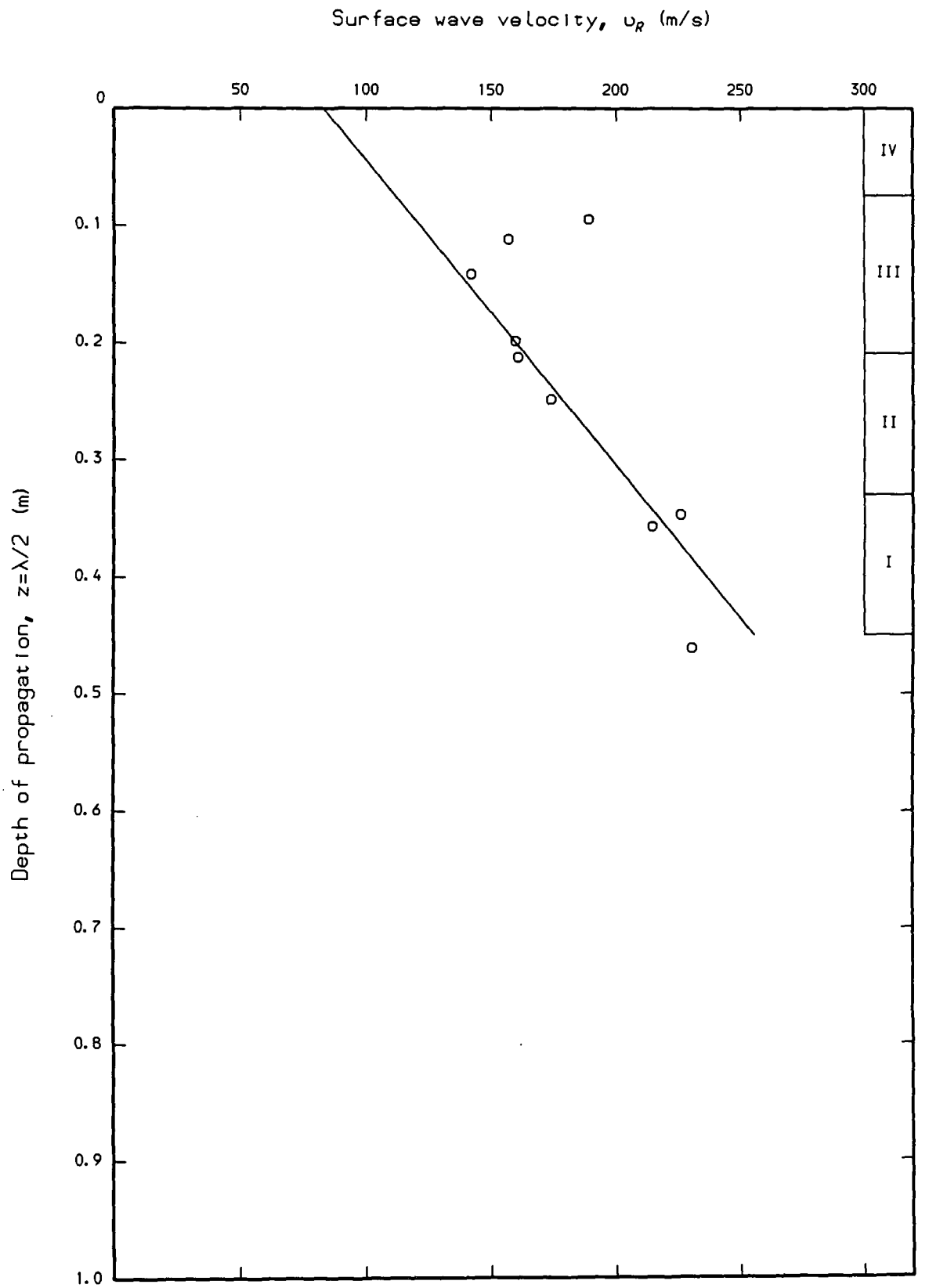

Figure 6.9 - Surface wave velocity-depth profile for Test TPS2C.

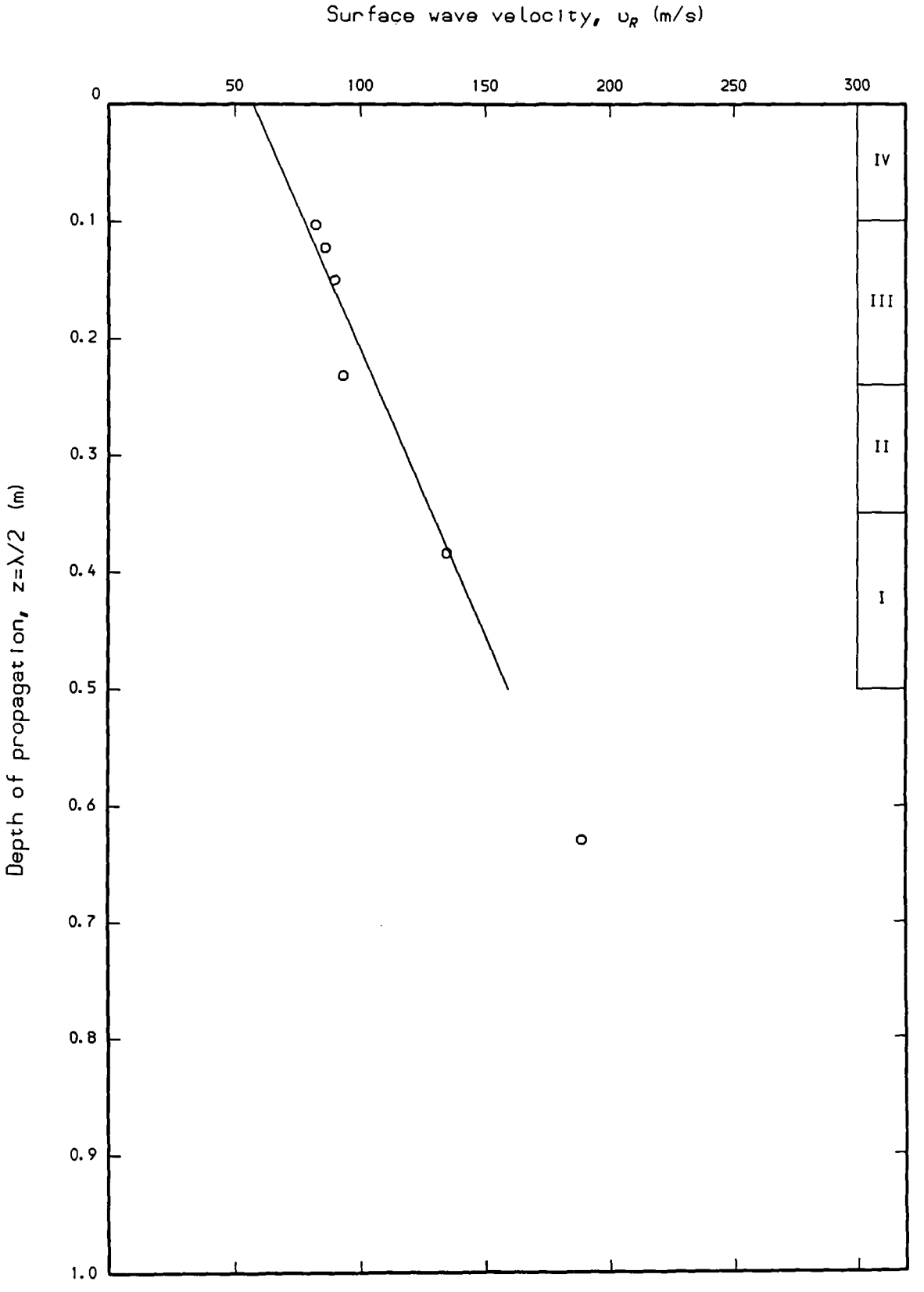

Figure 6.10 - Surface wave velocity-depth profile for Test TPS3A.

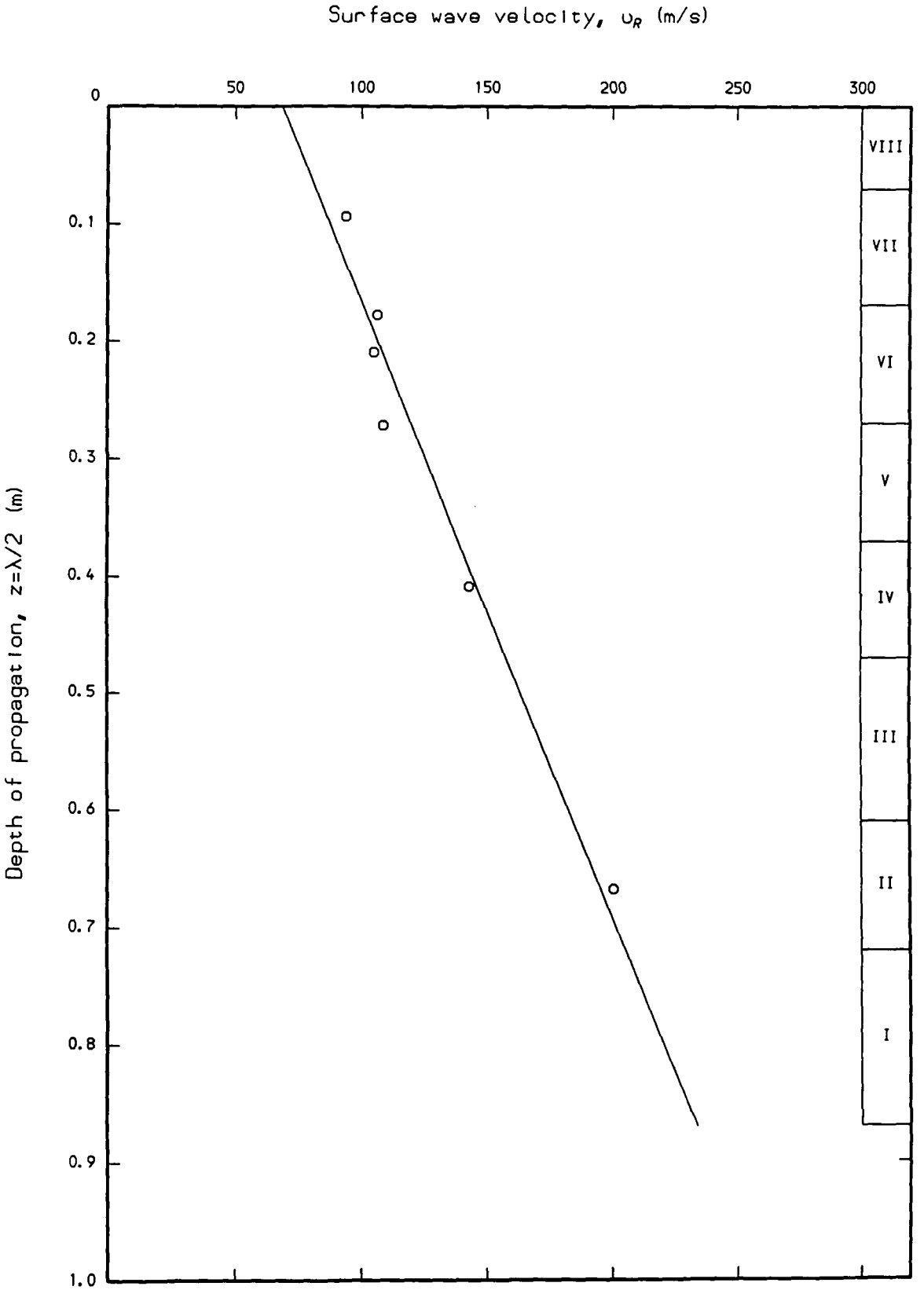

Figure 6.11 - Surface wave velocity-depth profile for Test TPS3B.

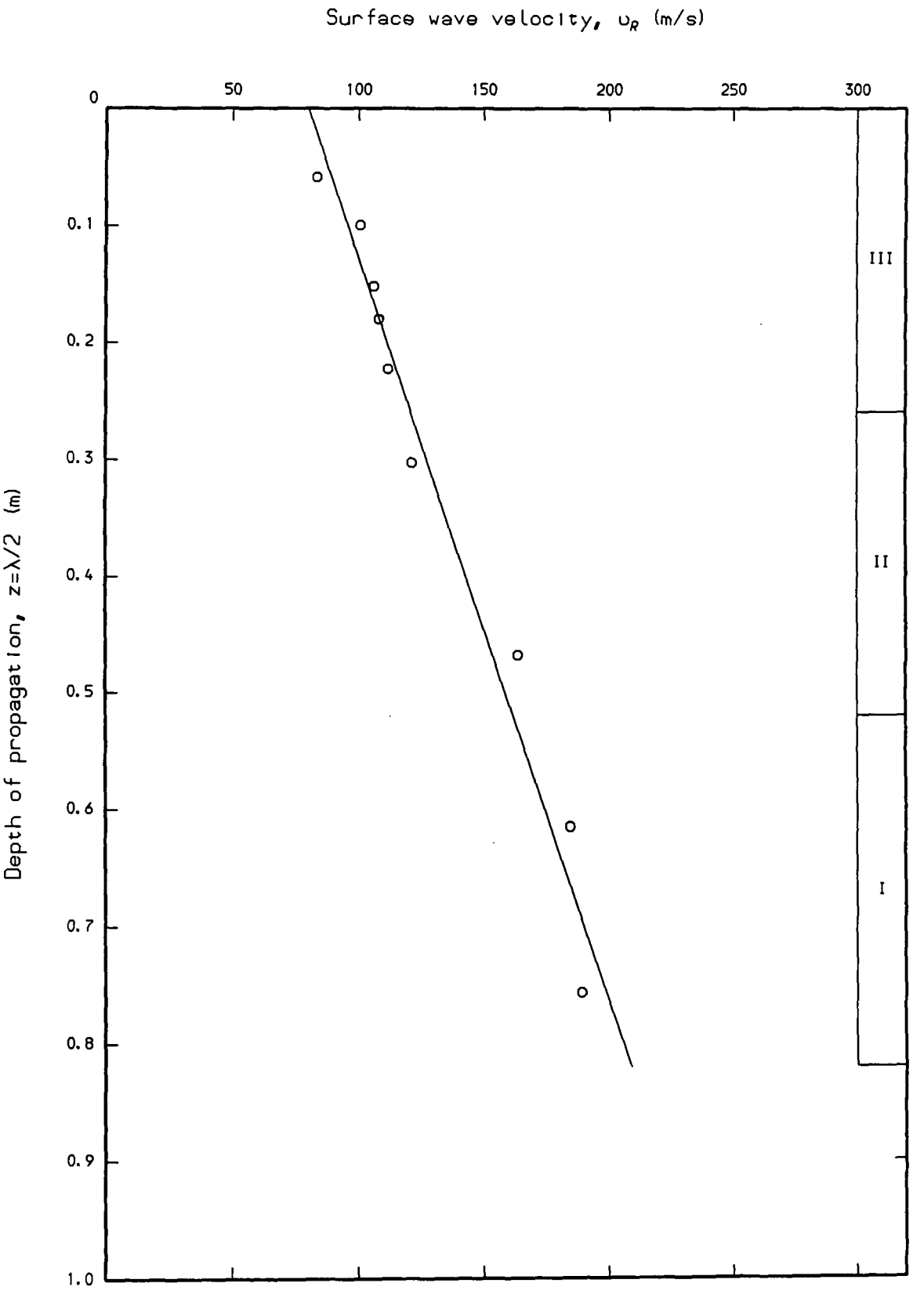

Figure 6.12 - Surface wave velocity-depth profile for Test TPS4.

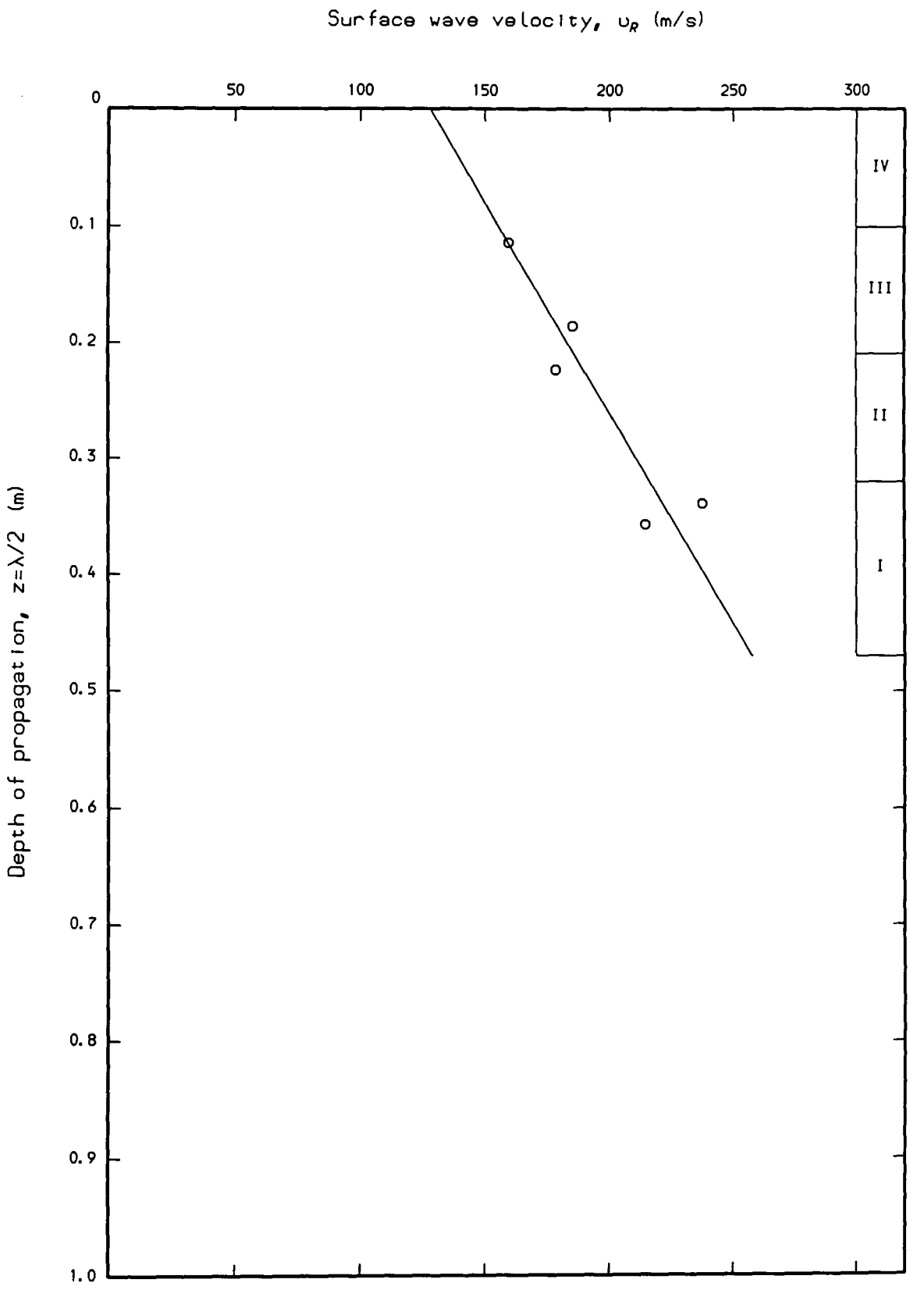

Figure 6.13 - Surface wave velocity-depth profile for Test TPS5A.

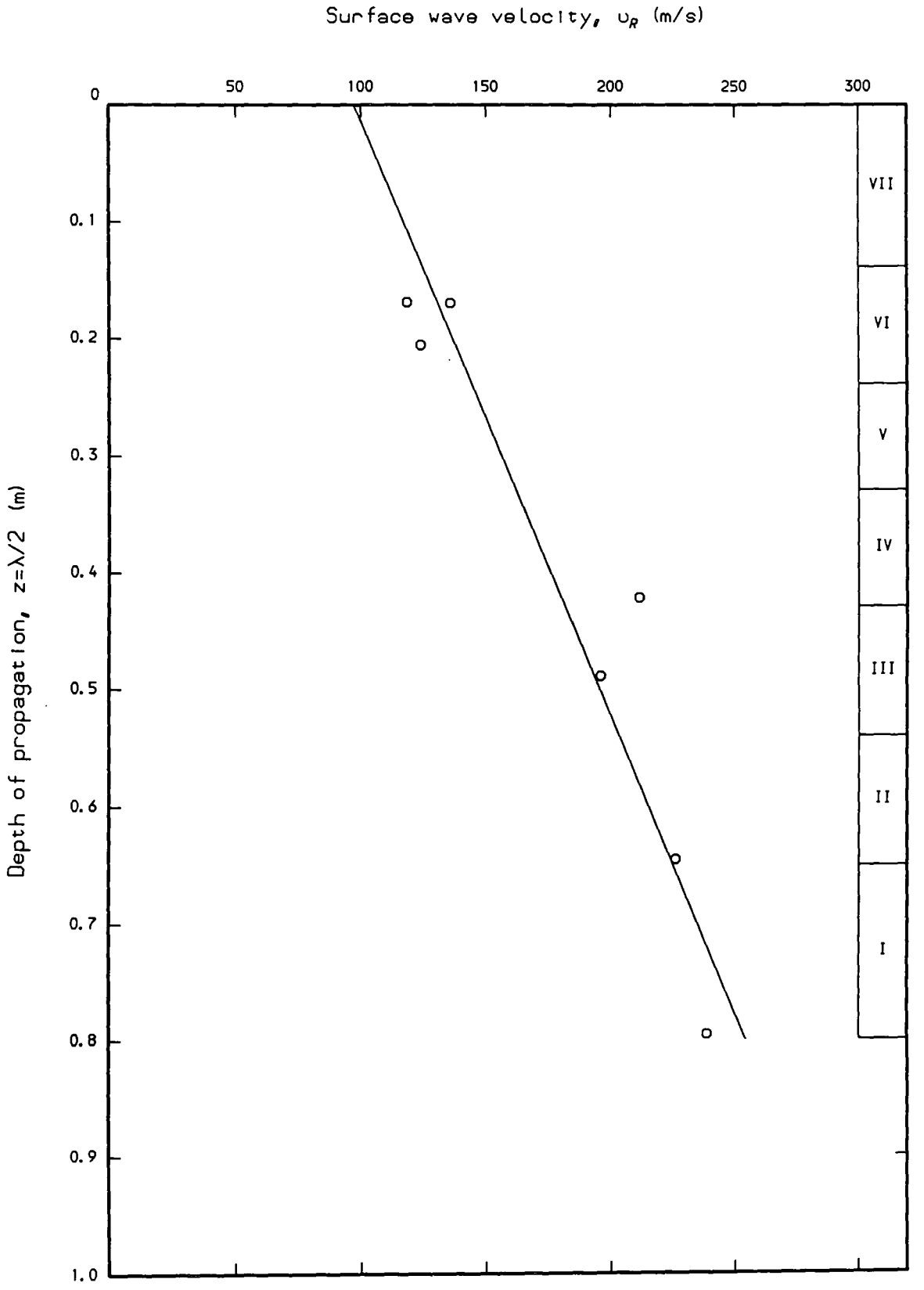

Figure 6.14 - Surface wave velocity-depth profile for Test TPS5B.

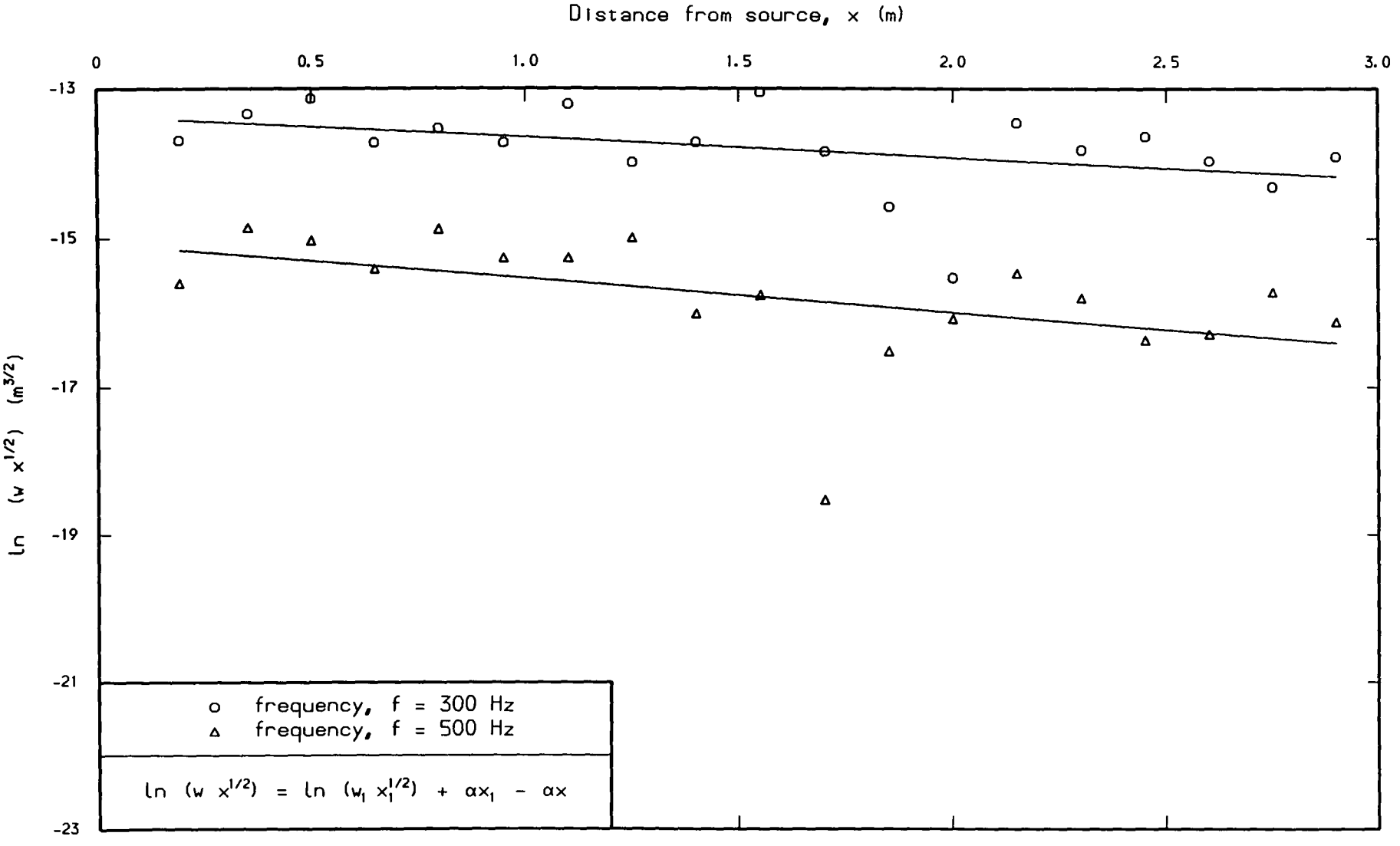

Figure 6.15 - Attenuation data for Test TPS3 (frequency, f = 300 and 500 Hz).

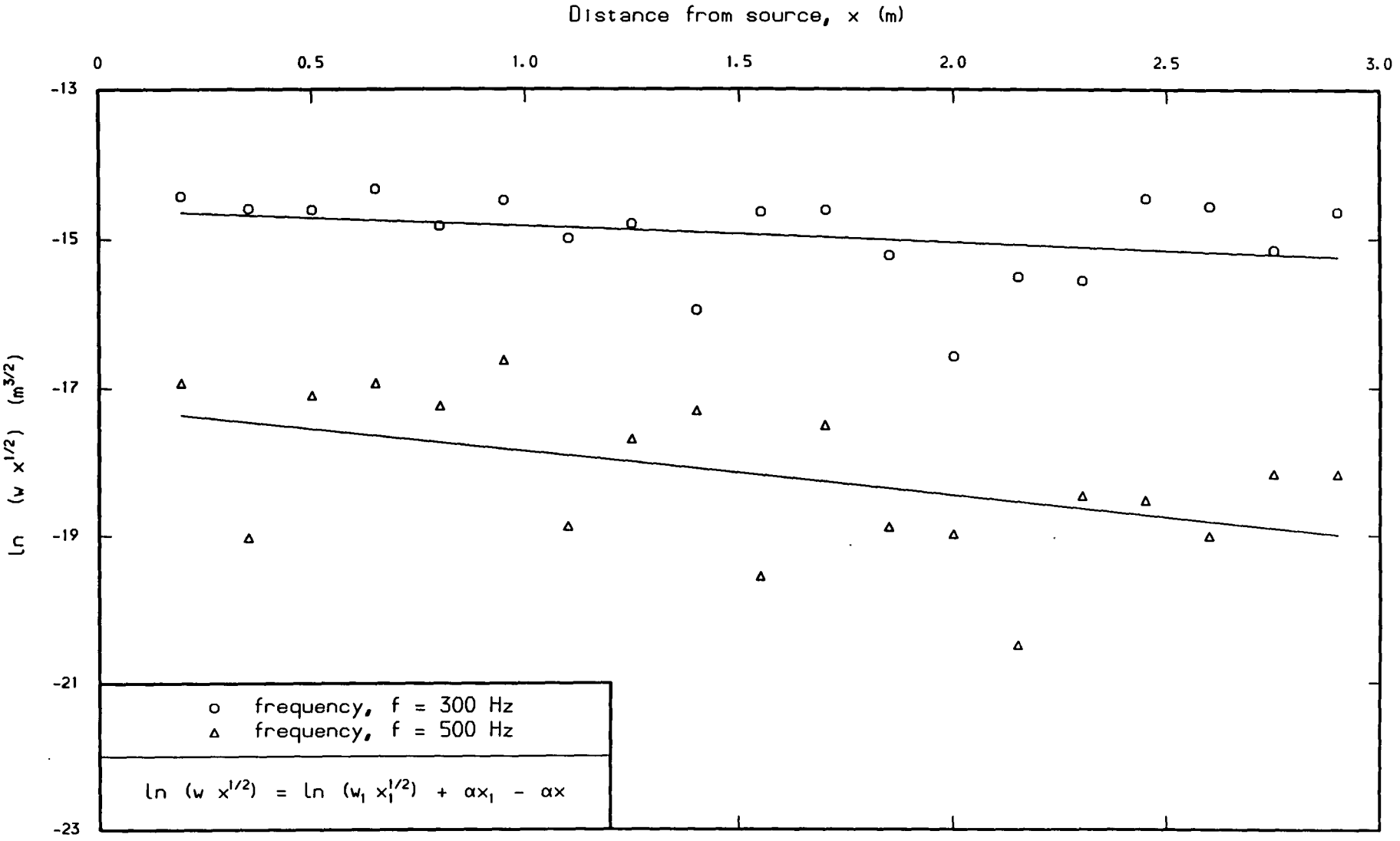

Figure 6.16 - Attenuation data for Test TPS4 (frequency, f = 300 and 500 Hz).

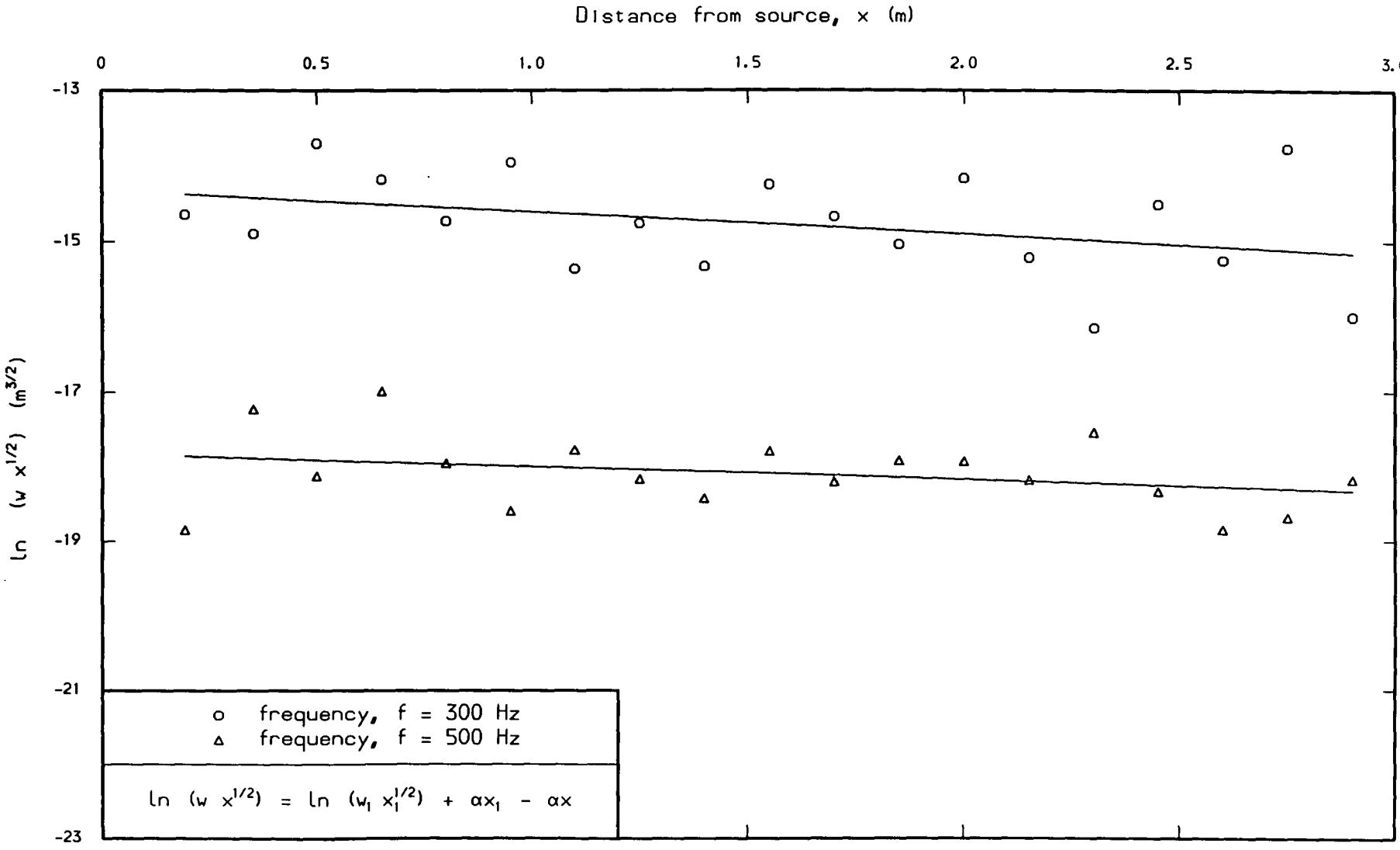

Figure 6.17 - Attenuation data for Test TPS5 (frequency, f = 300 and 500 Hz).

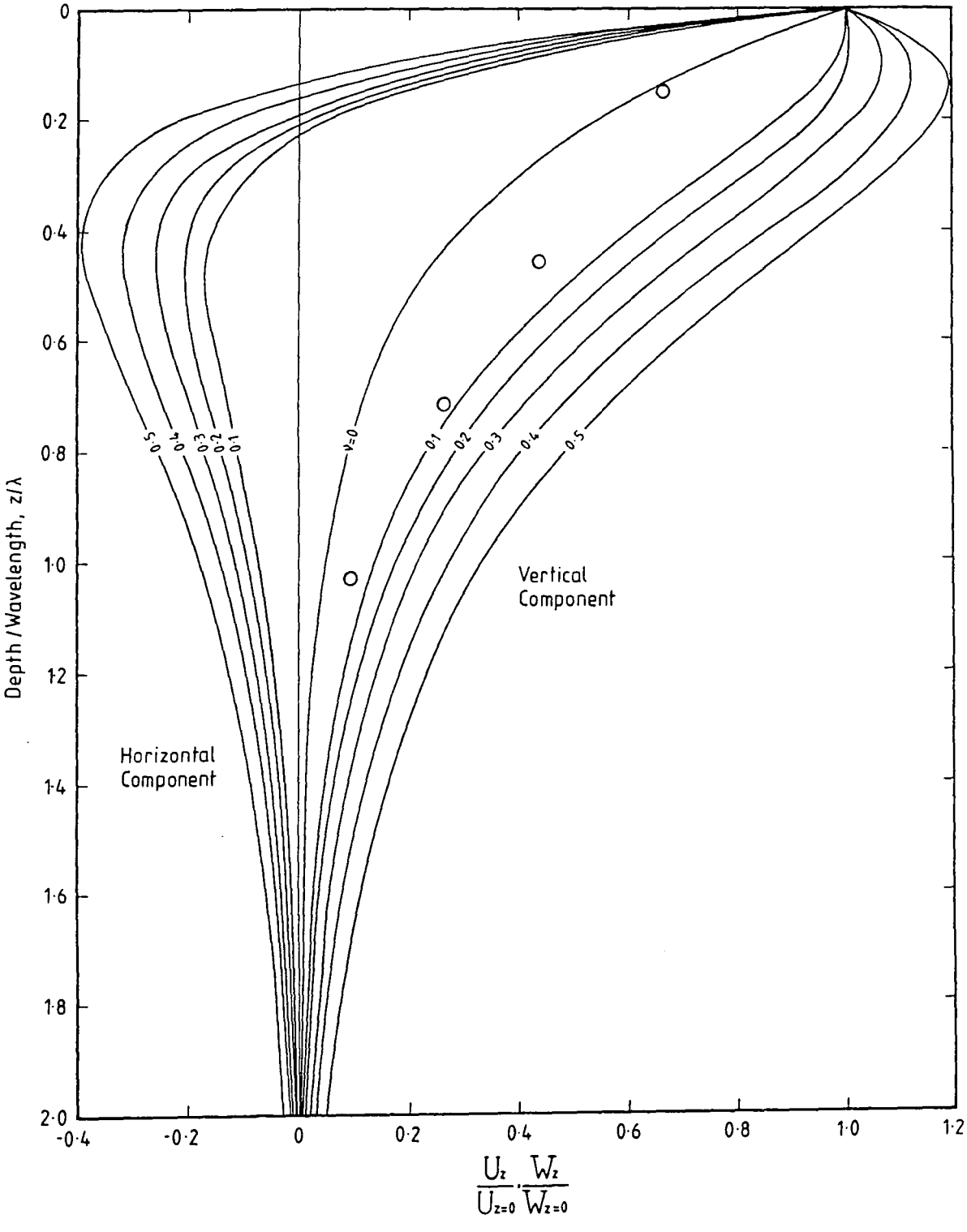

Figure 6.18 - Normalised particle displacement-depth profile for Test TPS2B at 450 Hz ($\lambda = 0.388$ m).

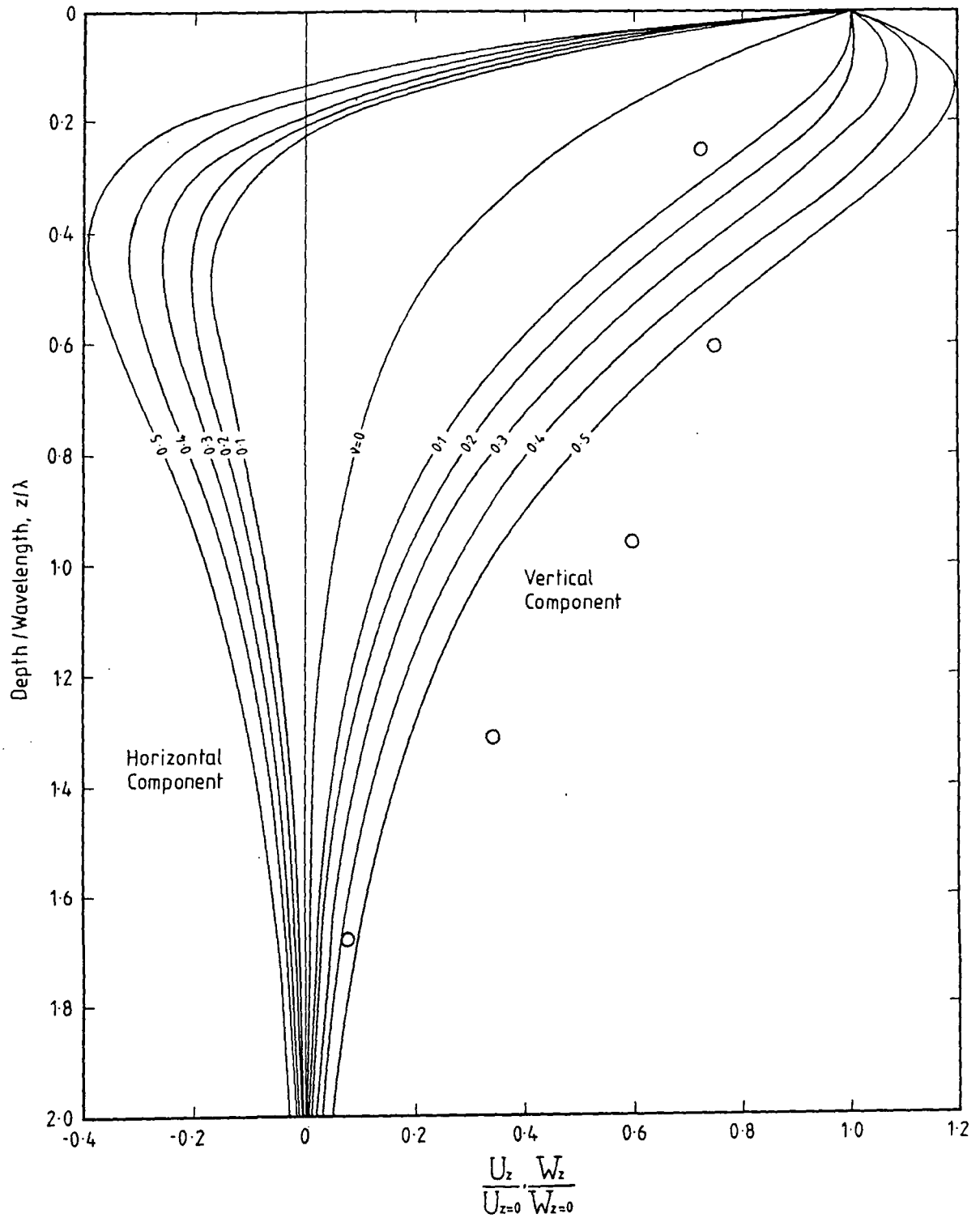

Figure 6.19 - Normalised particle displacement-depth profile for Test TPS3B at 300 Hz ($\lambda = 0.280$ m).

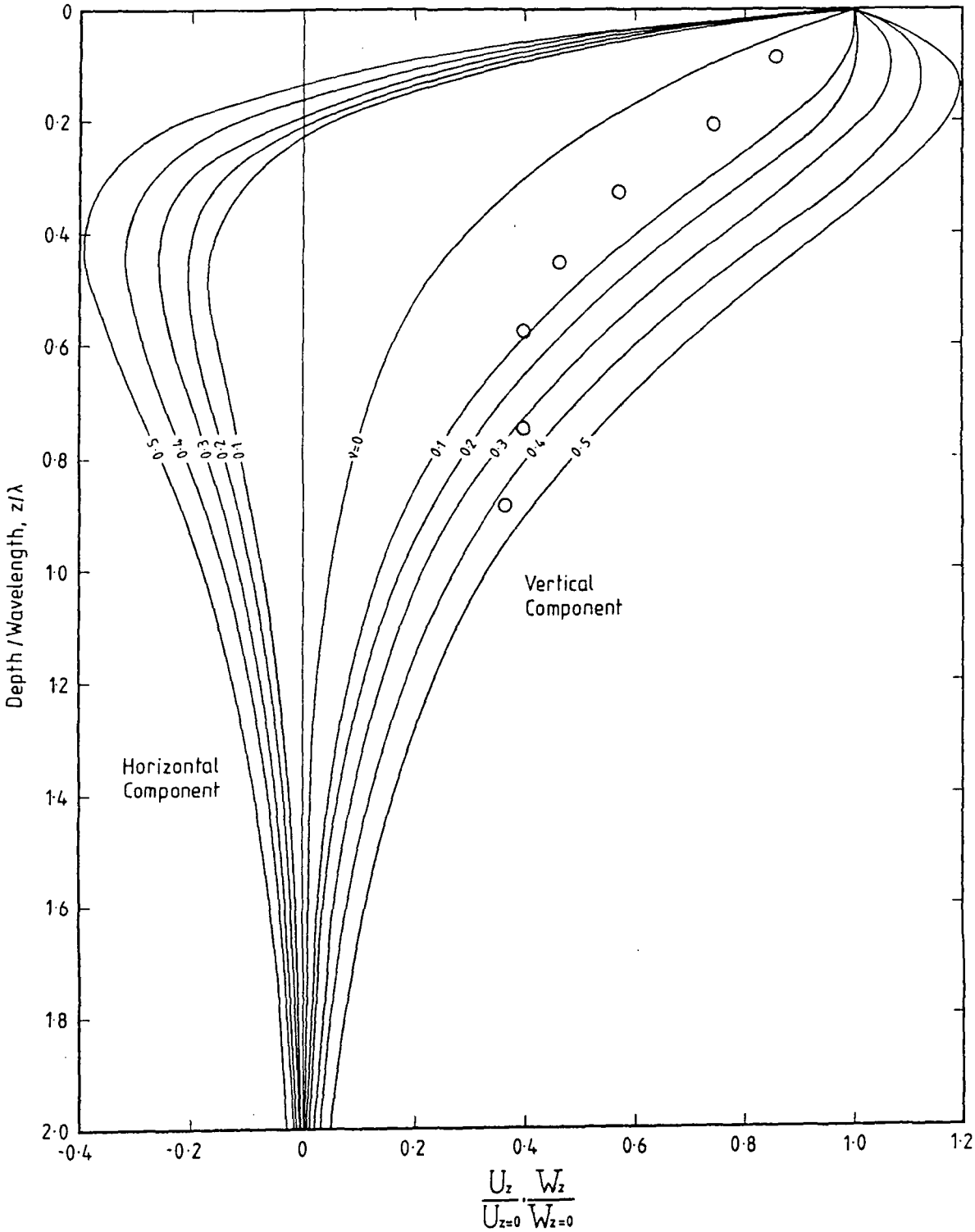

Figure 6.20 - Normalised particle displacement-depth profile for Test TPS3B at 150 Hz ($\lambda = 0.810$ m).

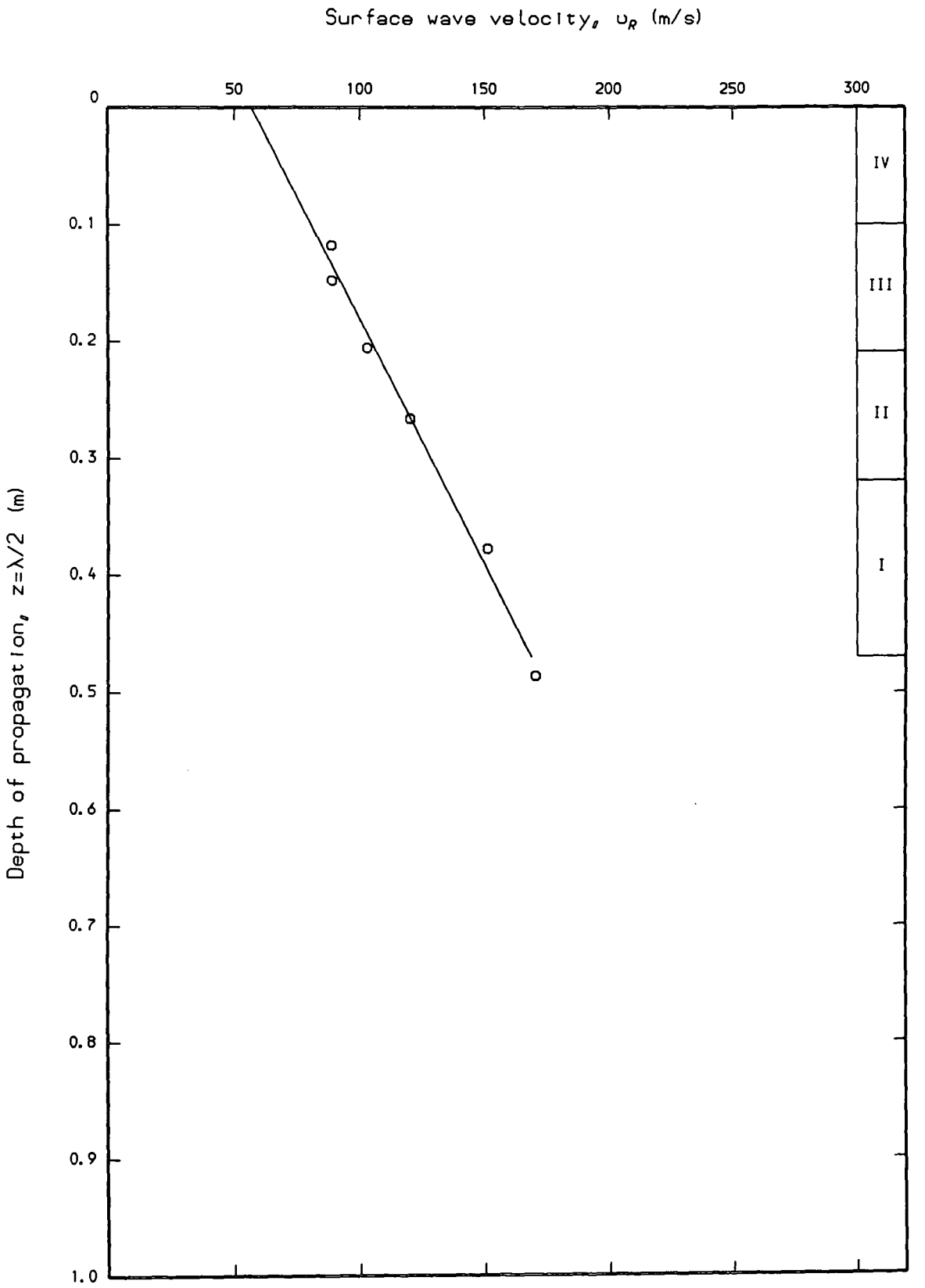

Figure 6.21 - Surface wave velocity-depth profile for Test TSS1A.

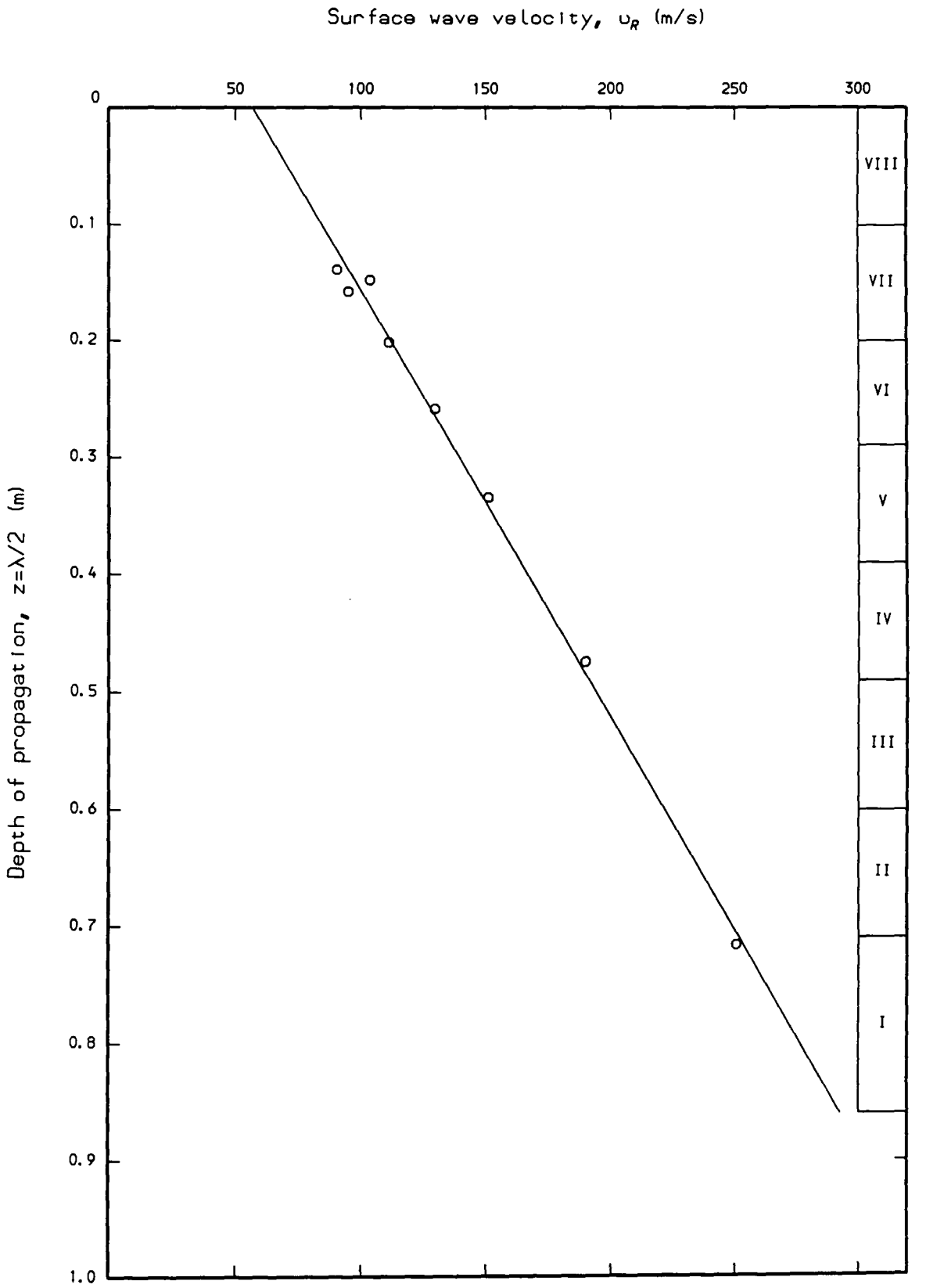

Figure 6.22 - Surface wave velocity-depth profile for Test TSS1B.

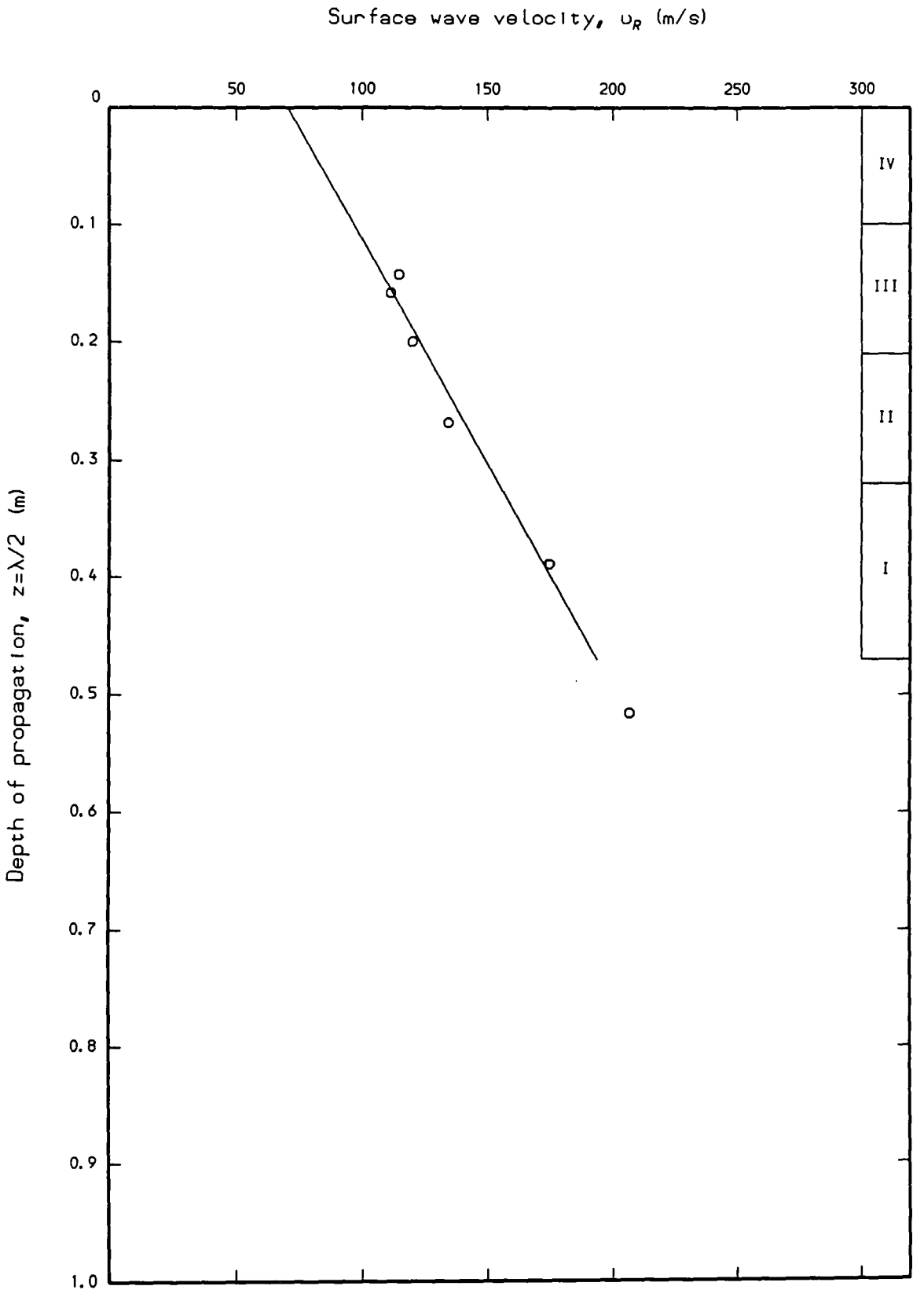

Figure 6.23 - Surface wave velocity-depth profile for Test TSS2A.

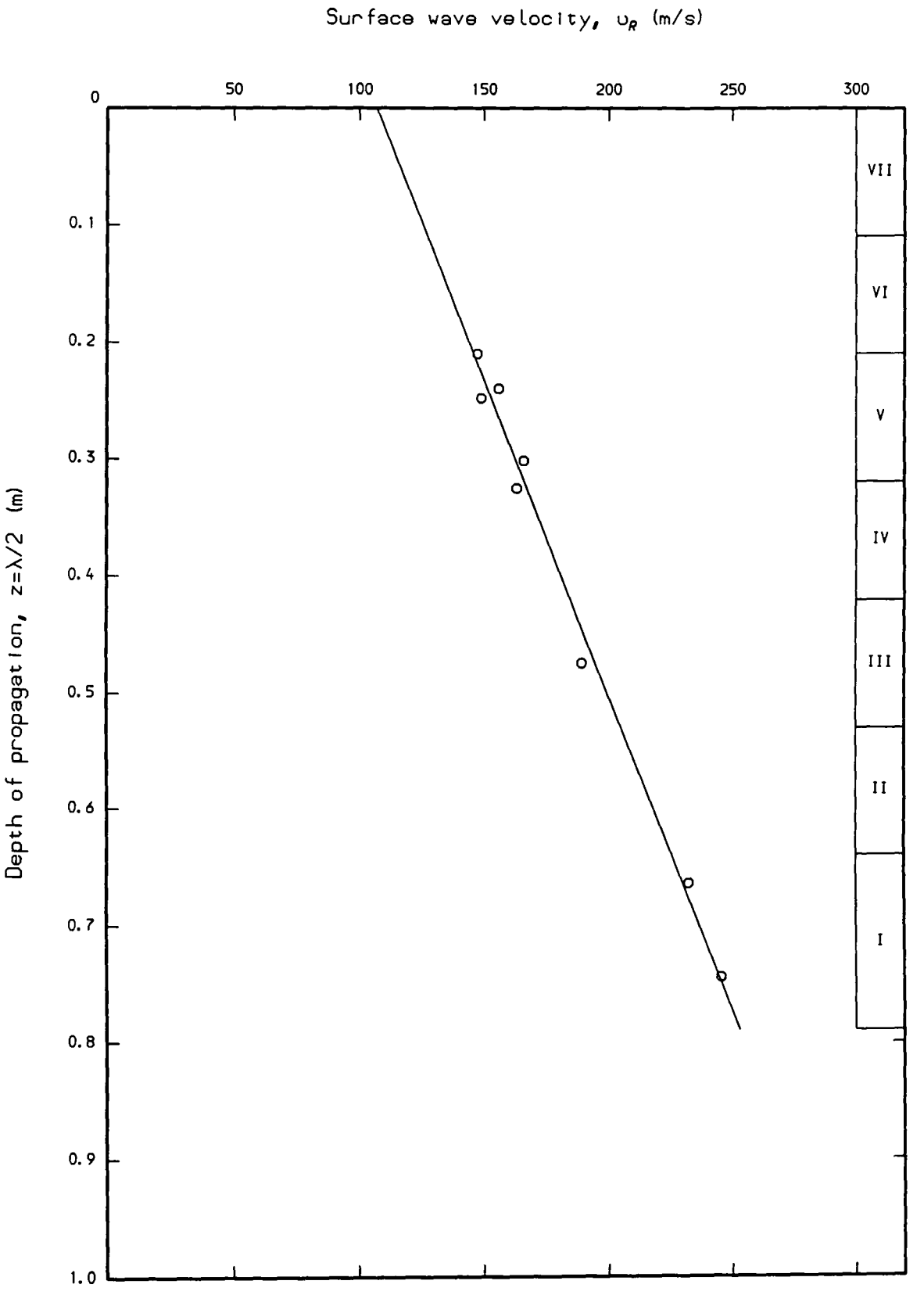

Figure 6.24 - Surface wave velocity-depth profile for Test TSS2B.

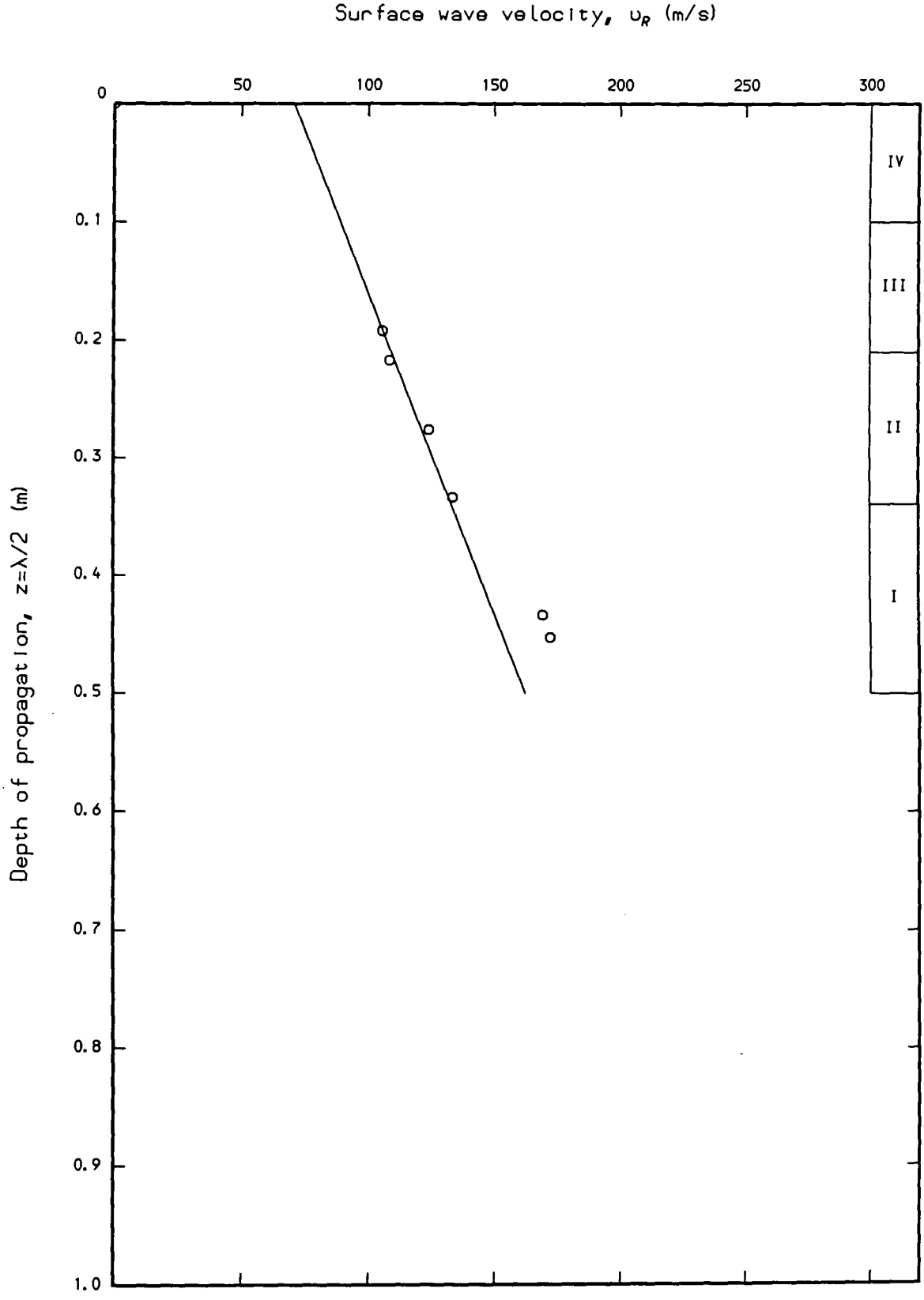

Figure 6.25 - Surface wave velocity-depth profile for Test TSS3A.

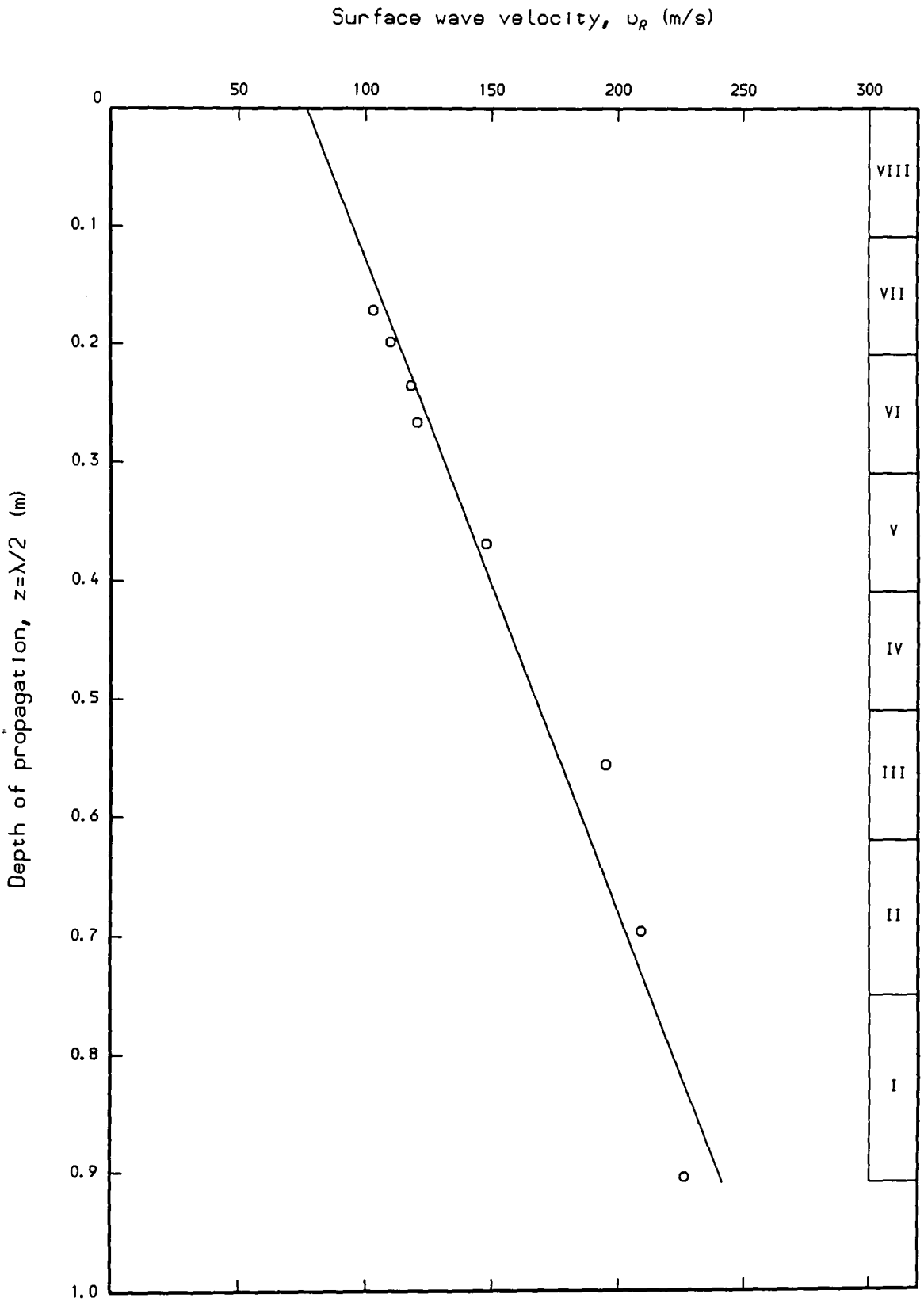

Figure 6.26 - Surface wave velocity-depth profile for Test TSS3B.

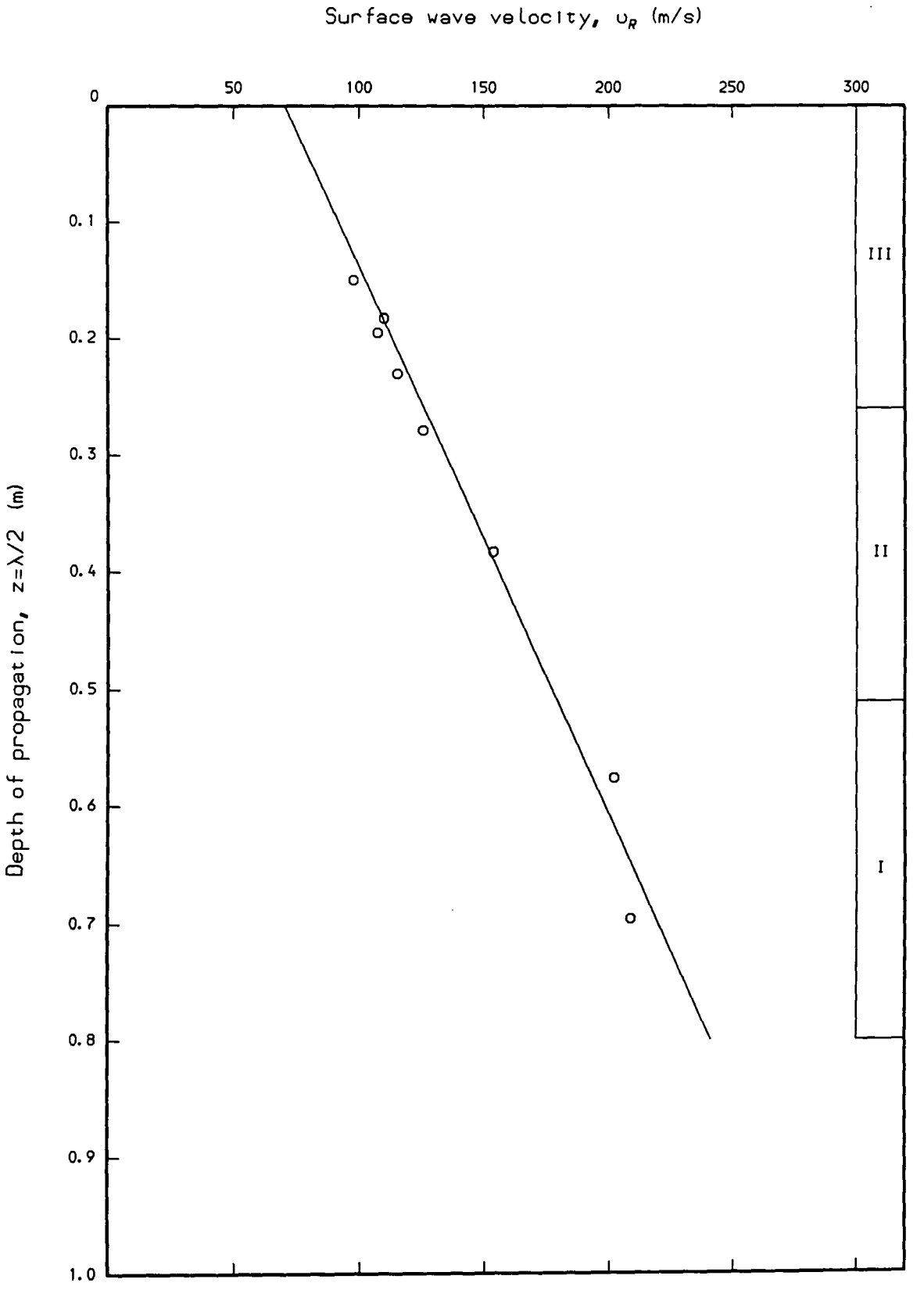

Figure 6.27 - Surface wave velocity-depth profile for Test TSS4.

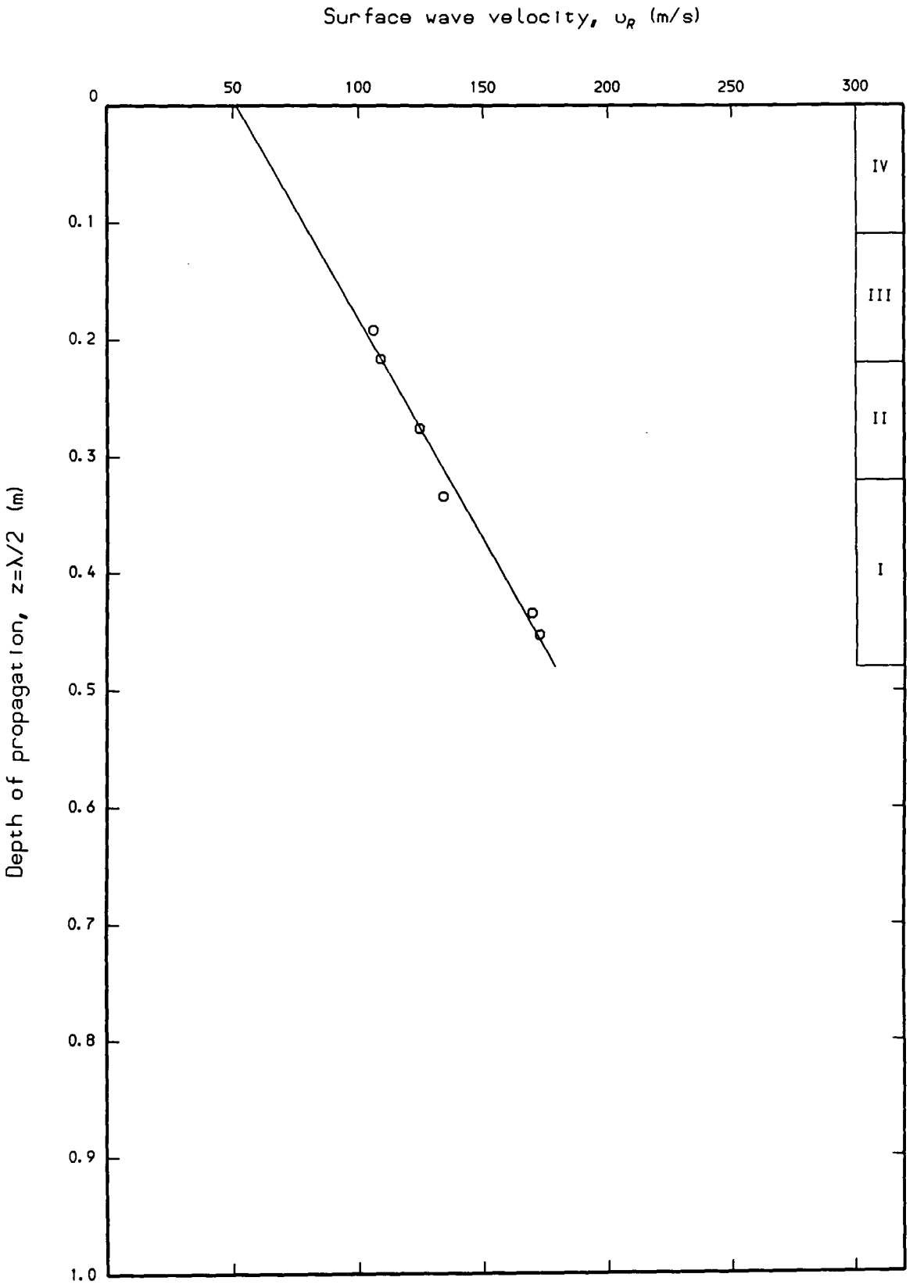

Figure 6.28 - Surface wave velocity-depth profile for Test TSS5A.

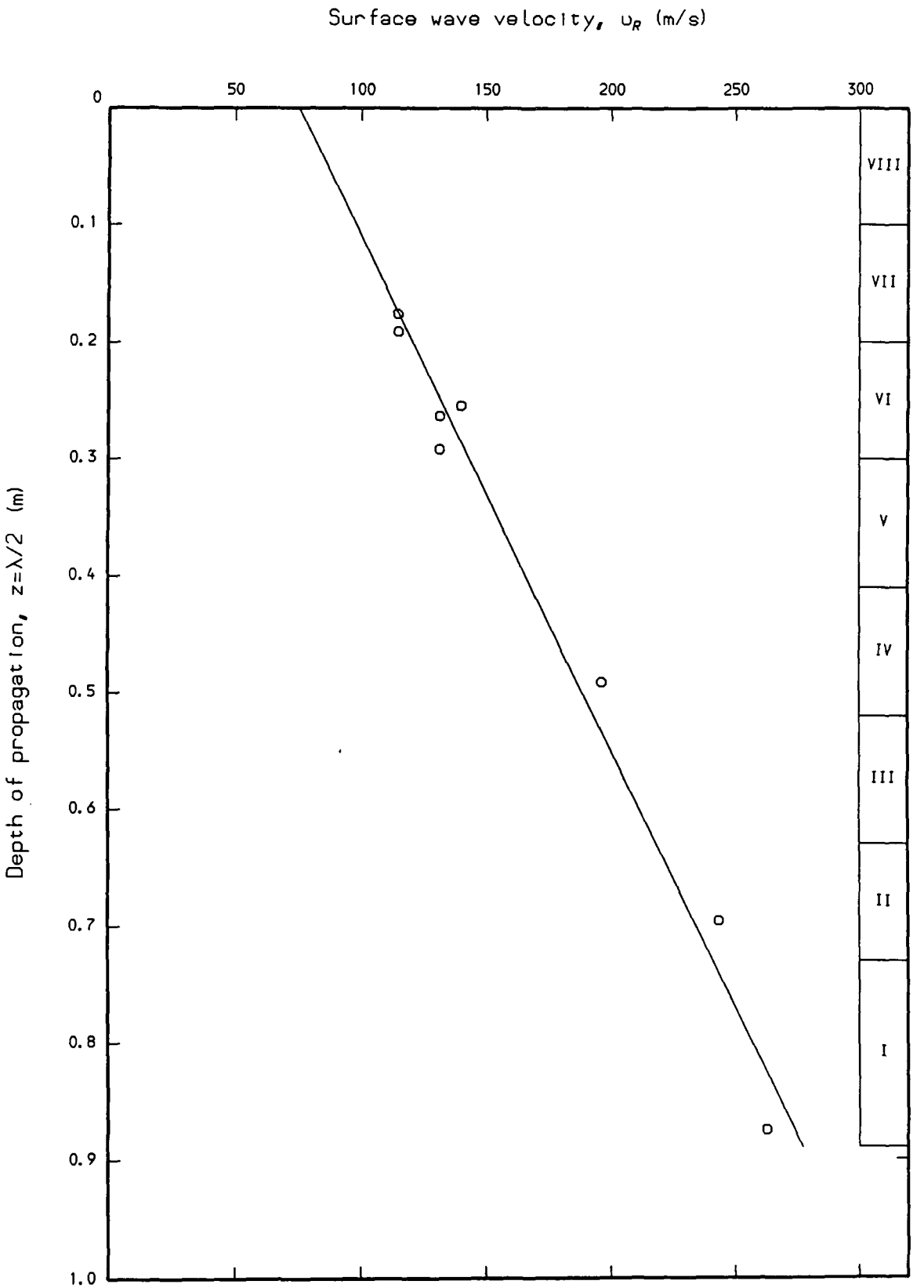

Figure 6.29 - Surface wave velocity-depth profile for Test TSS5B.

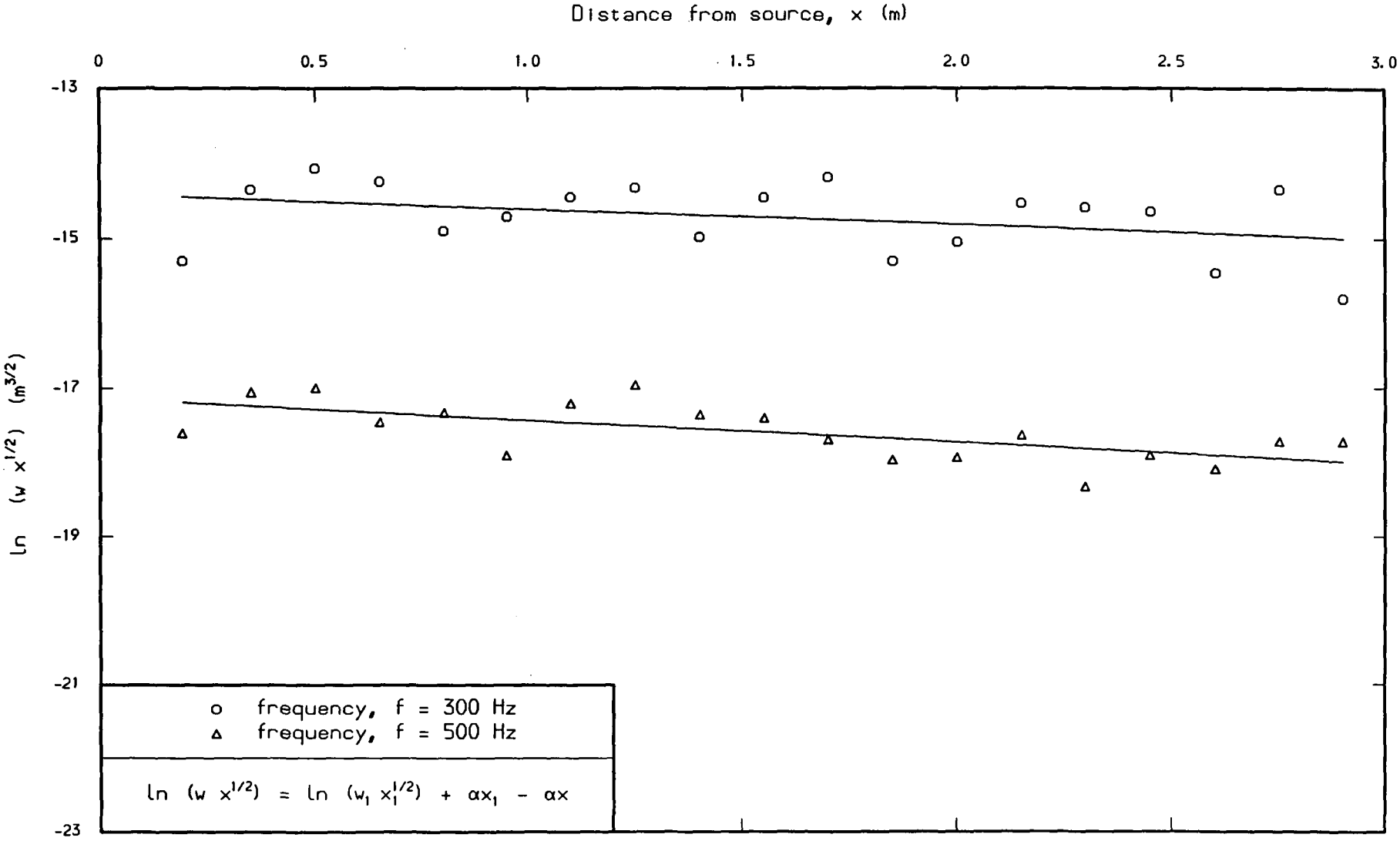

Figure 6.30 - Attenuation data for Test TSS1 (frequency, f = 300 and 500 Hz).

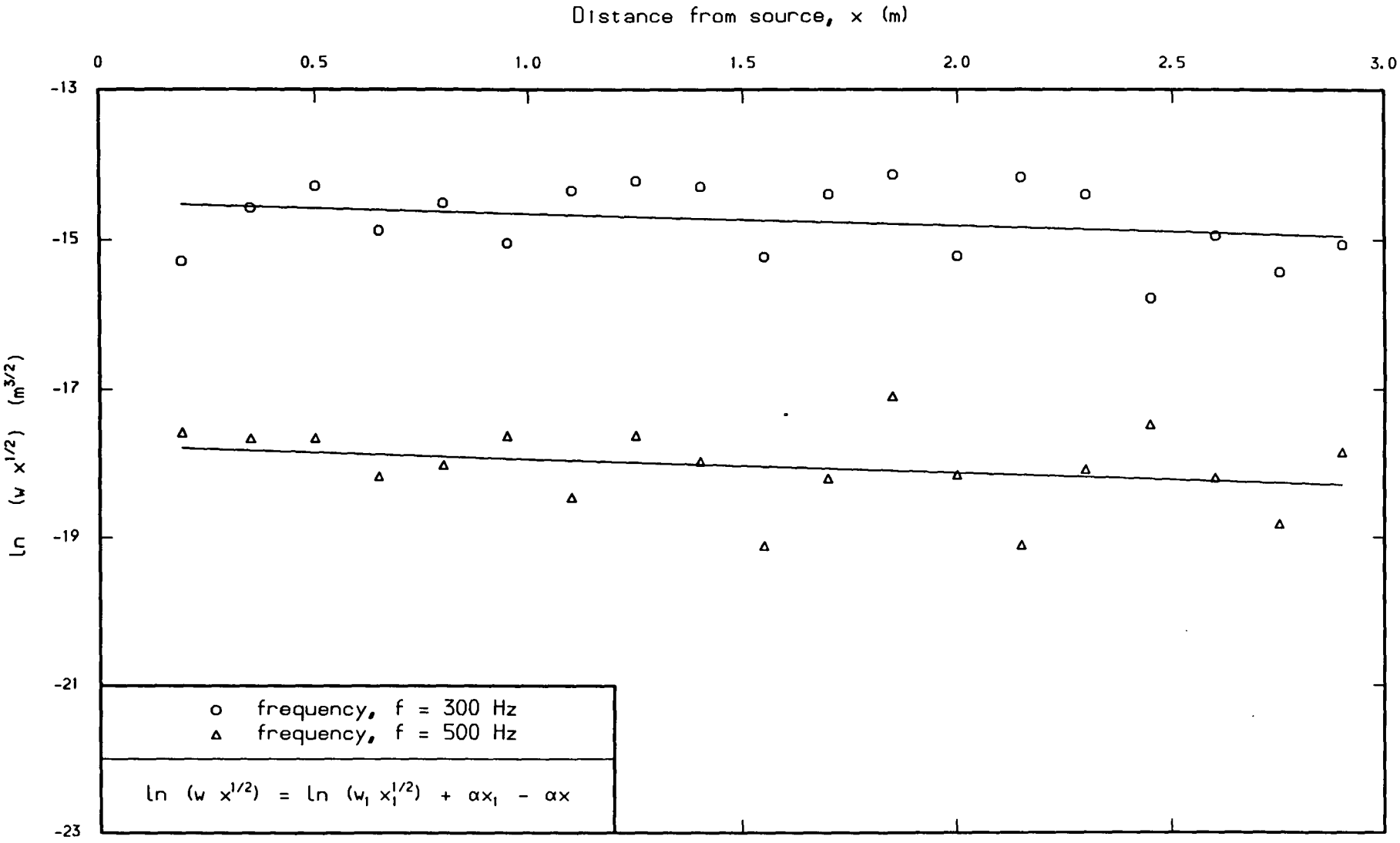

Figure 6.31 - Attenuation data for Test TSS2 (frequency, f = 300 and 500 Hz).

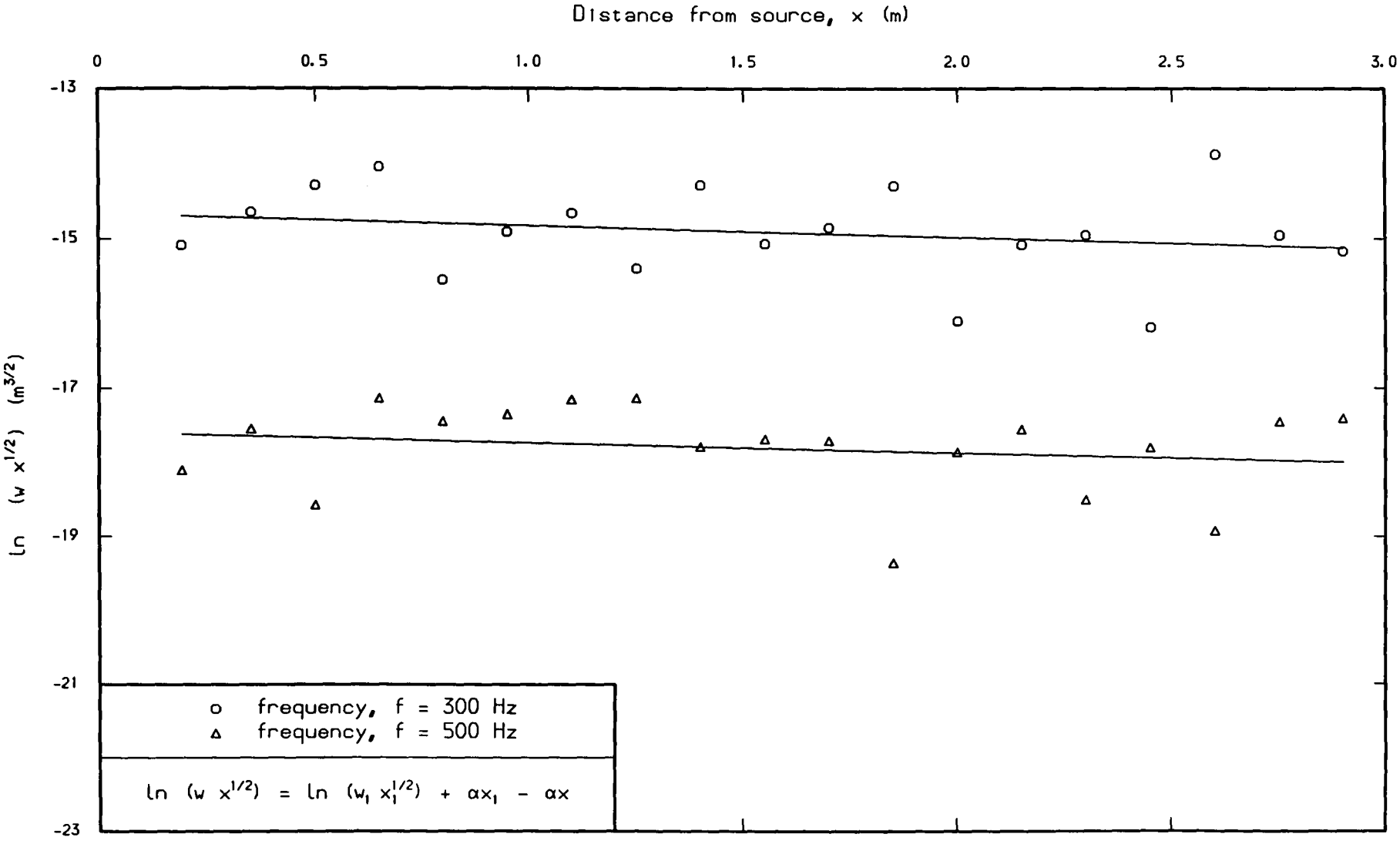

Figure 6.32 - Attenuation data for Test TSS3 (frequency, f = 300 and 500 Hz).

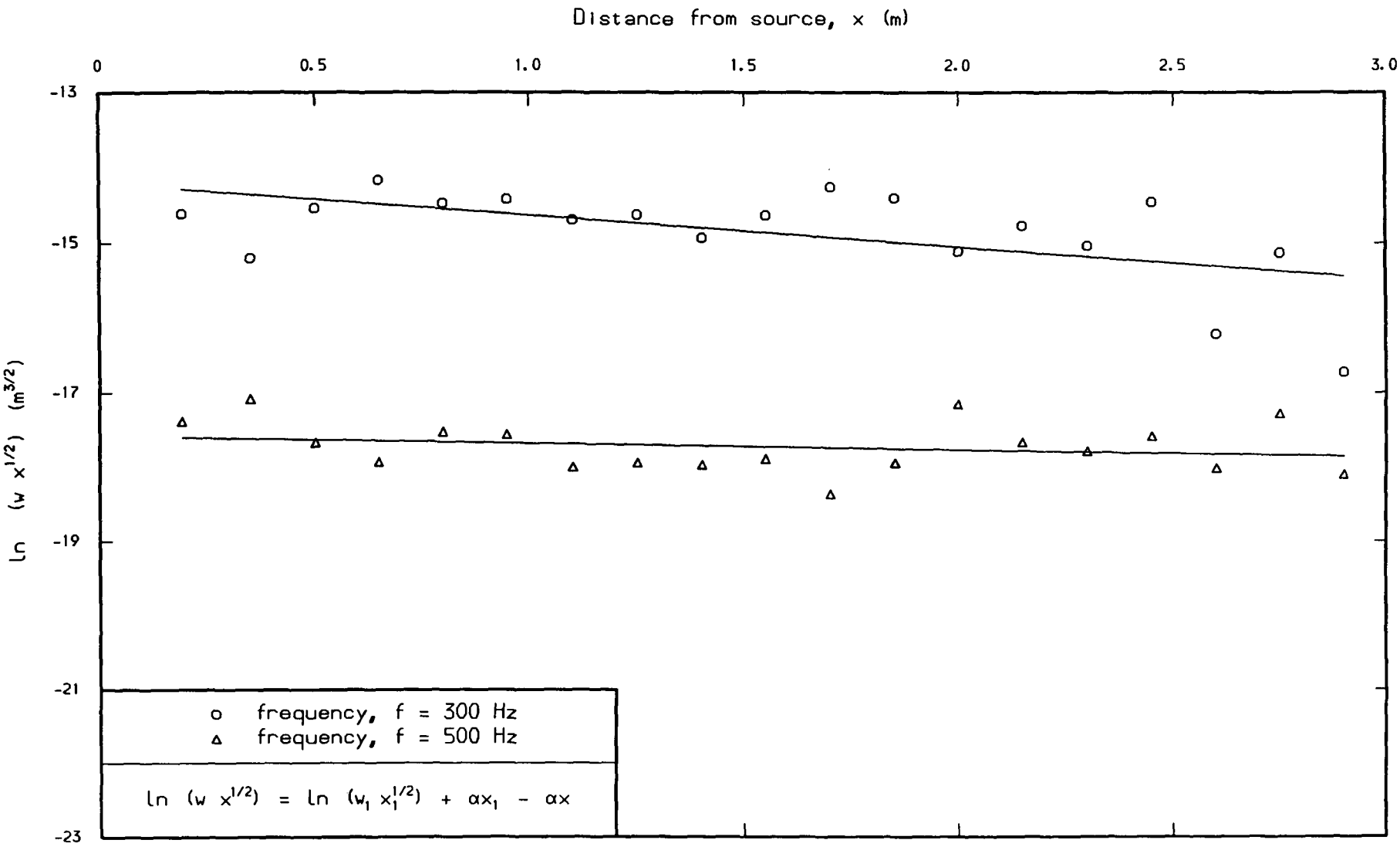

Figure 6.33 - Attenuation data for Test TSS4 (frequency, f = 300 and 500 Hz).

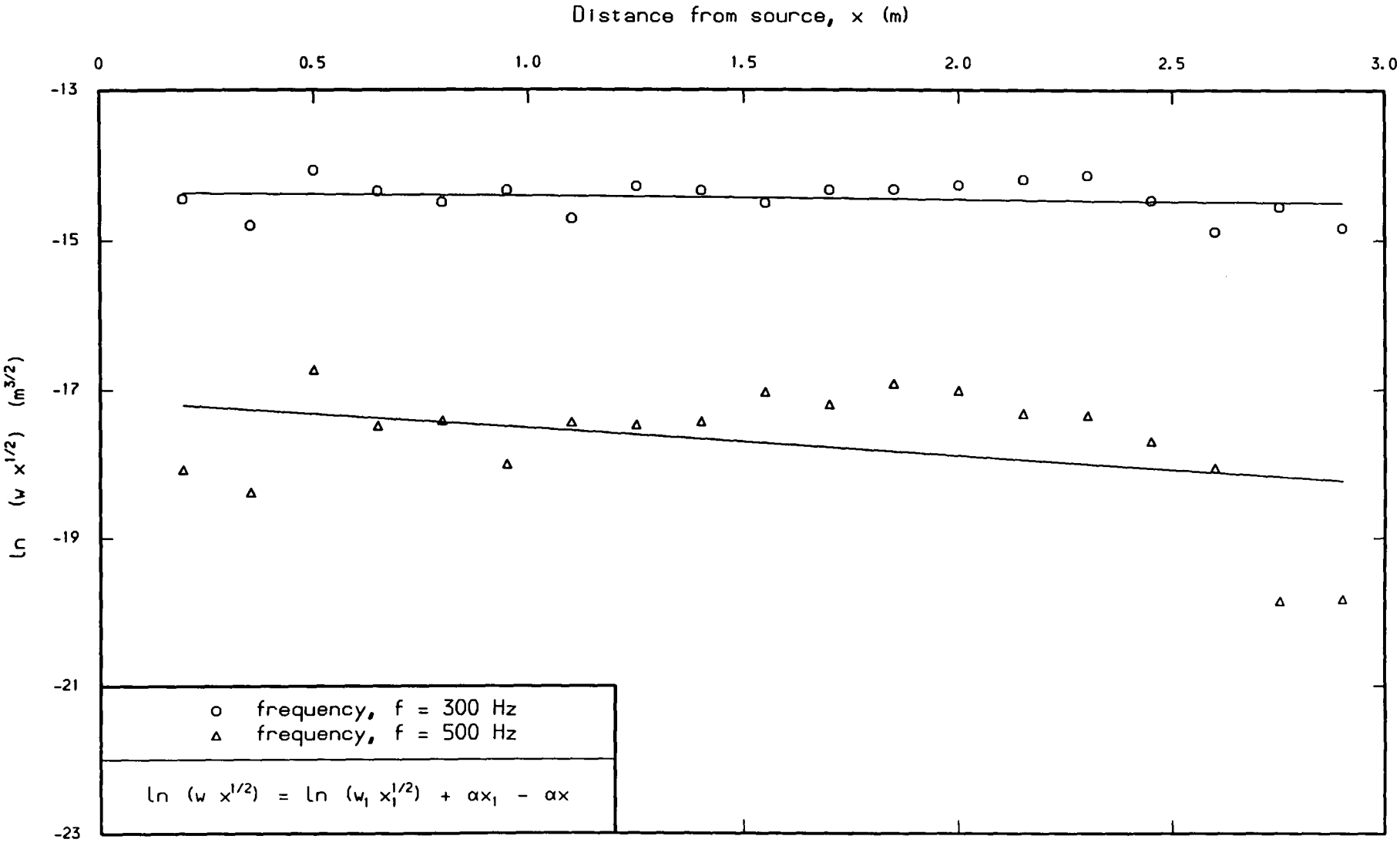

Figure 6.34 - Attenuation data for Test TSS5 (frequency, f = 300 and 500 Hz).

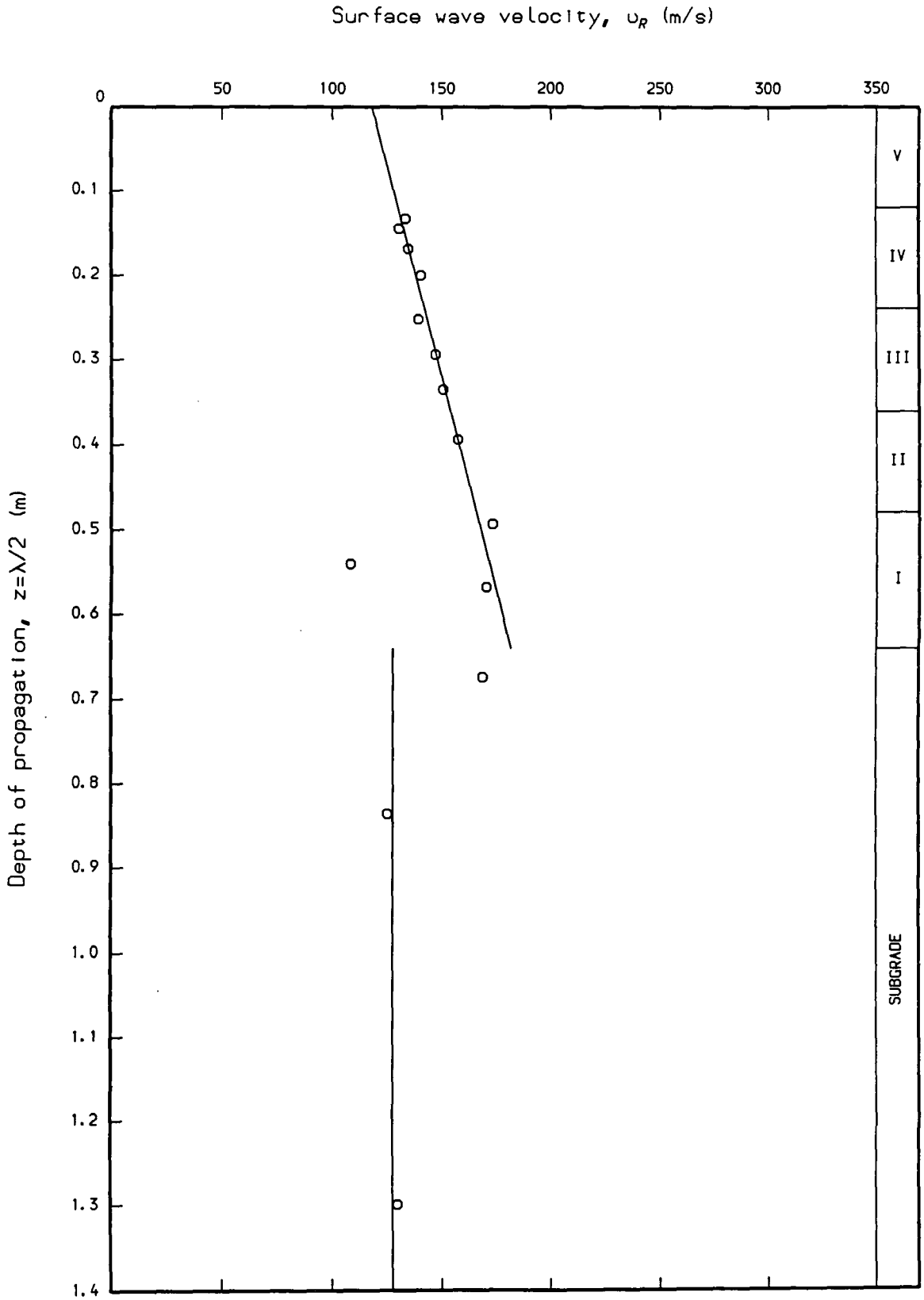

Figure 6.35 - Surface wave velocity-depth profile for Test WMM1.

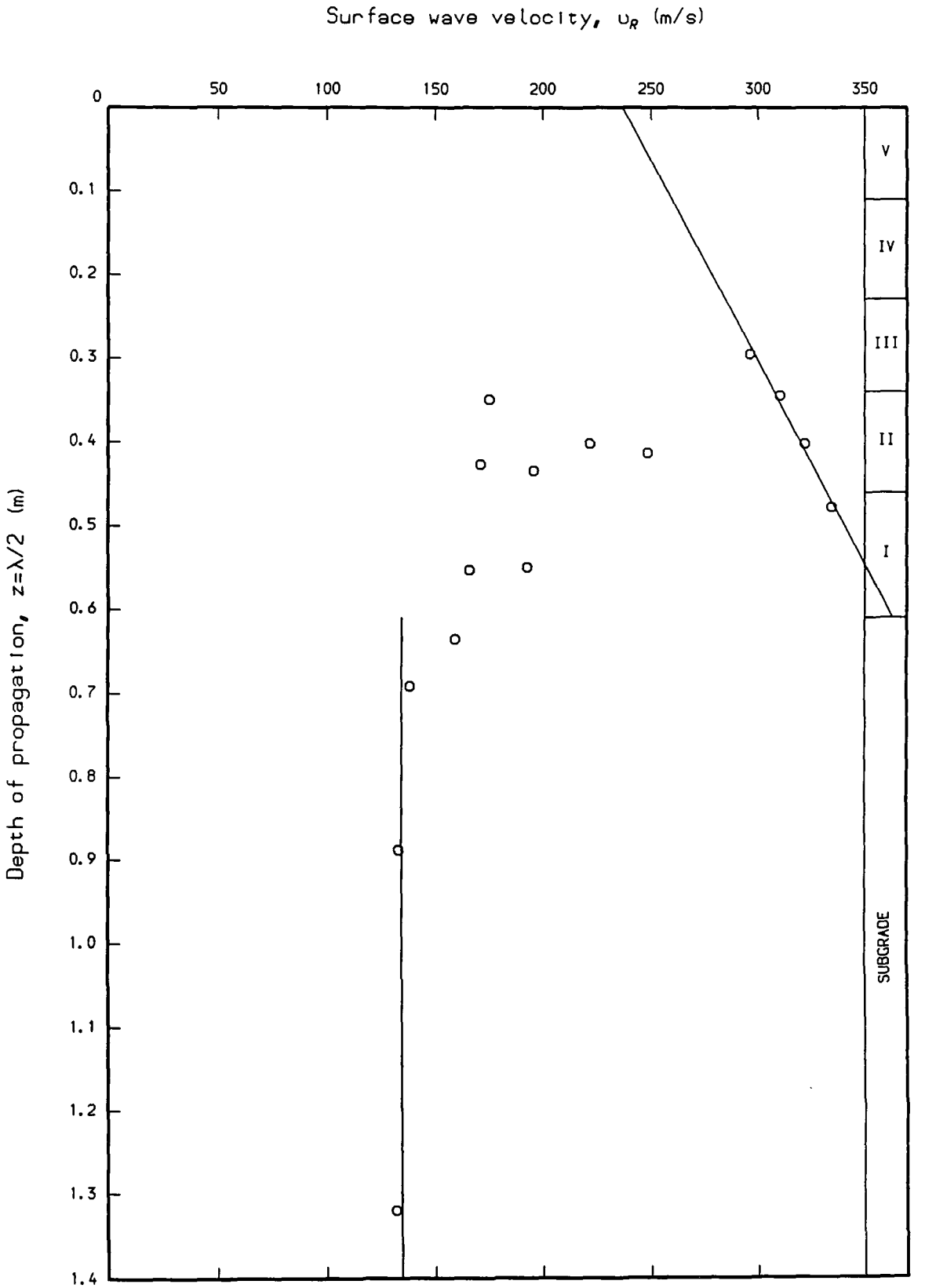

Figure 6.36 - Surface wave velocity-depth profile for Test WMM2.

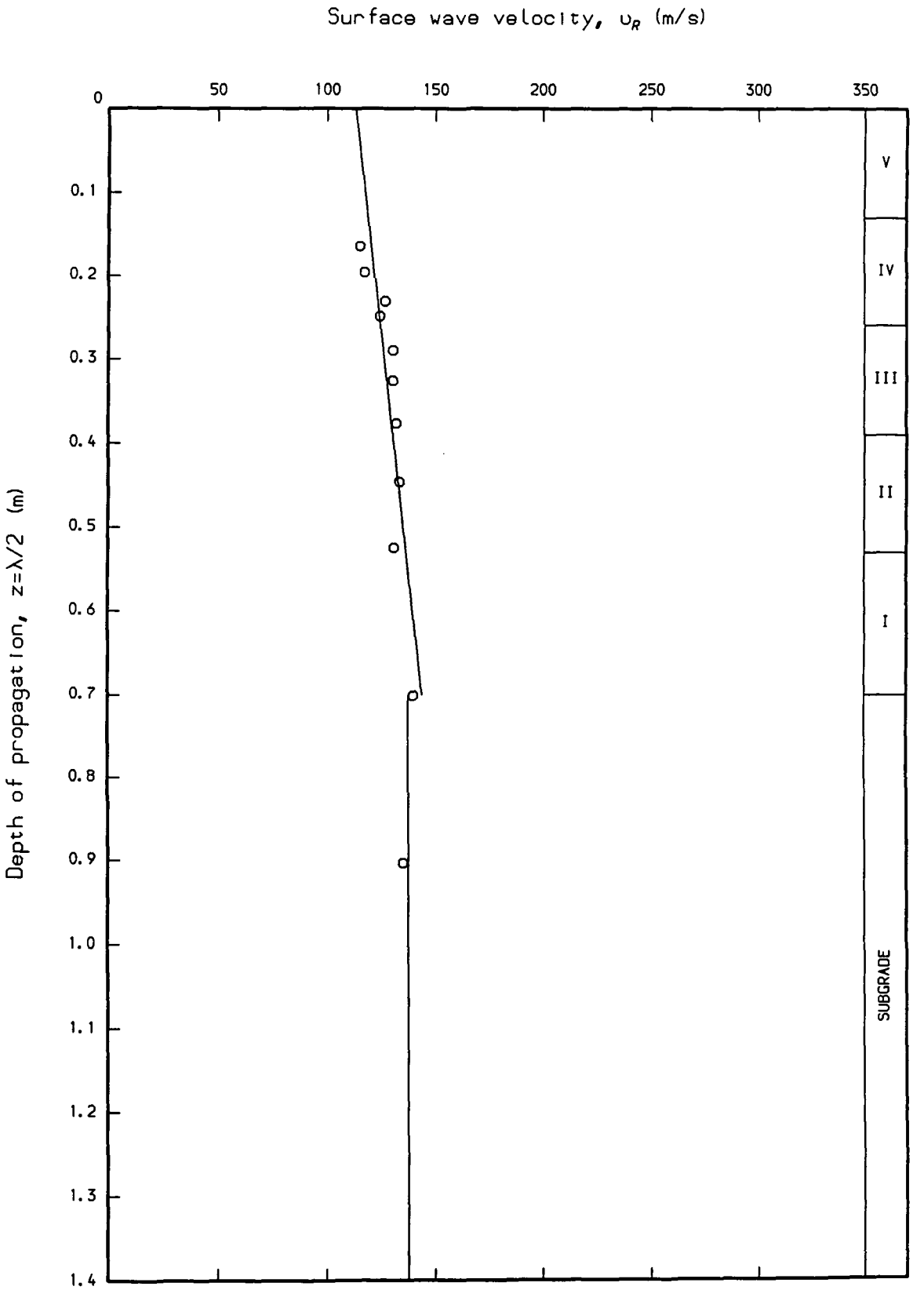

Figure 6.37 - Surface wave velocity-depth profile for Test WMM3.

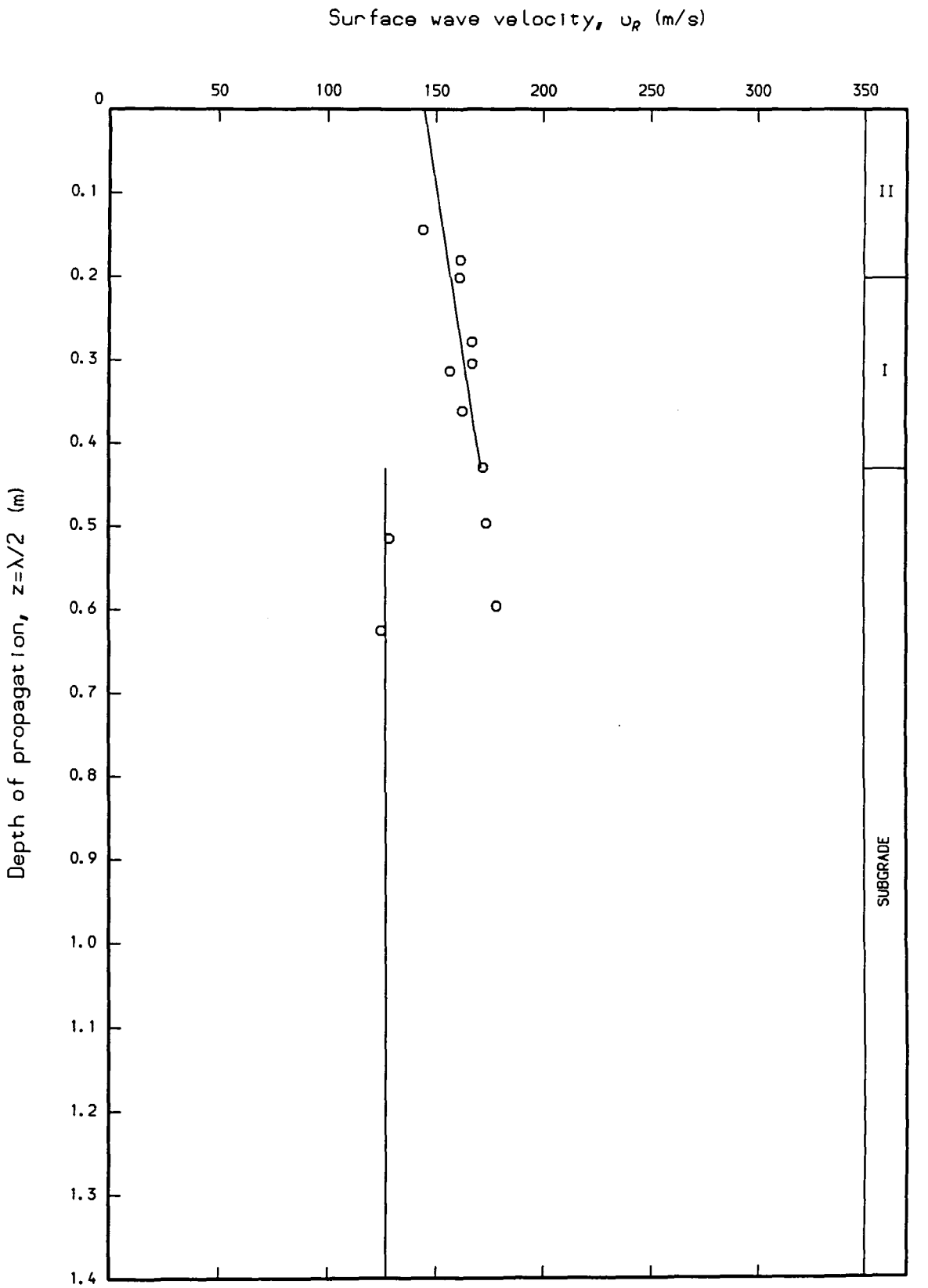

Figure 6.38 - Surface wave velocity-depth profile for Test WMM4.

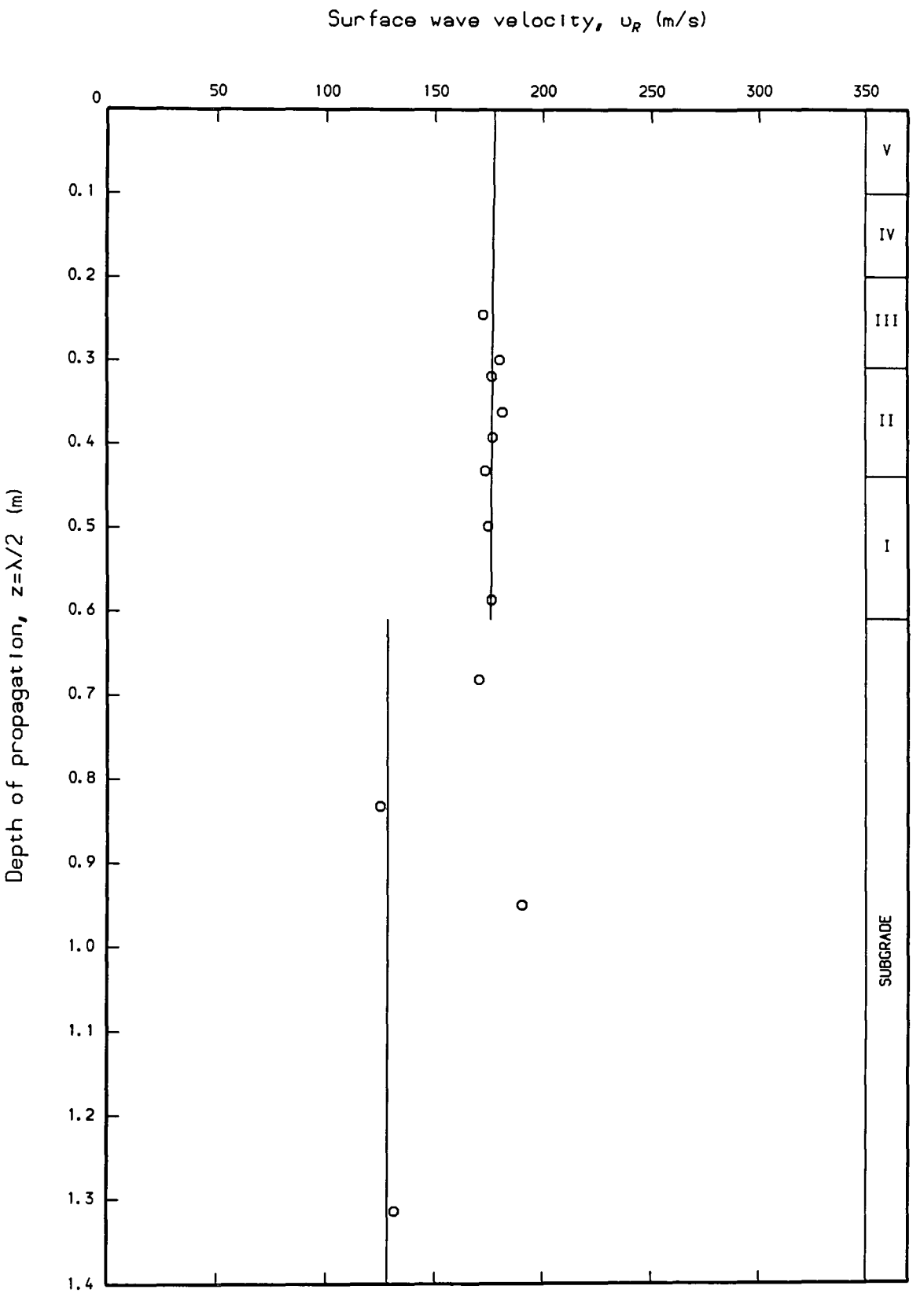

Figure 6.39 - Surface wave velocity-depth profile for Test WMM5.

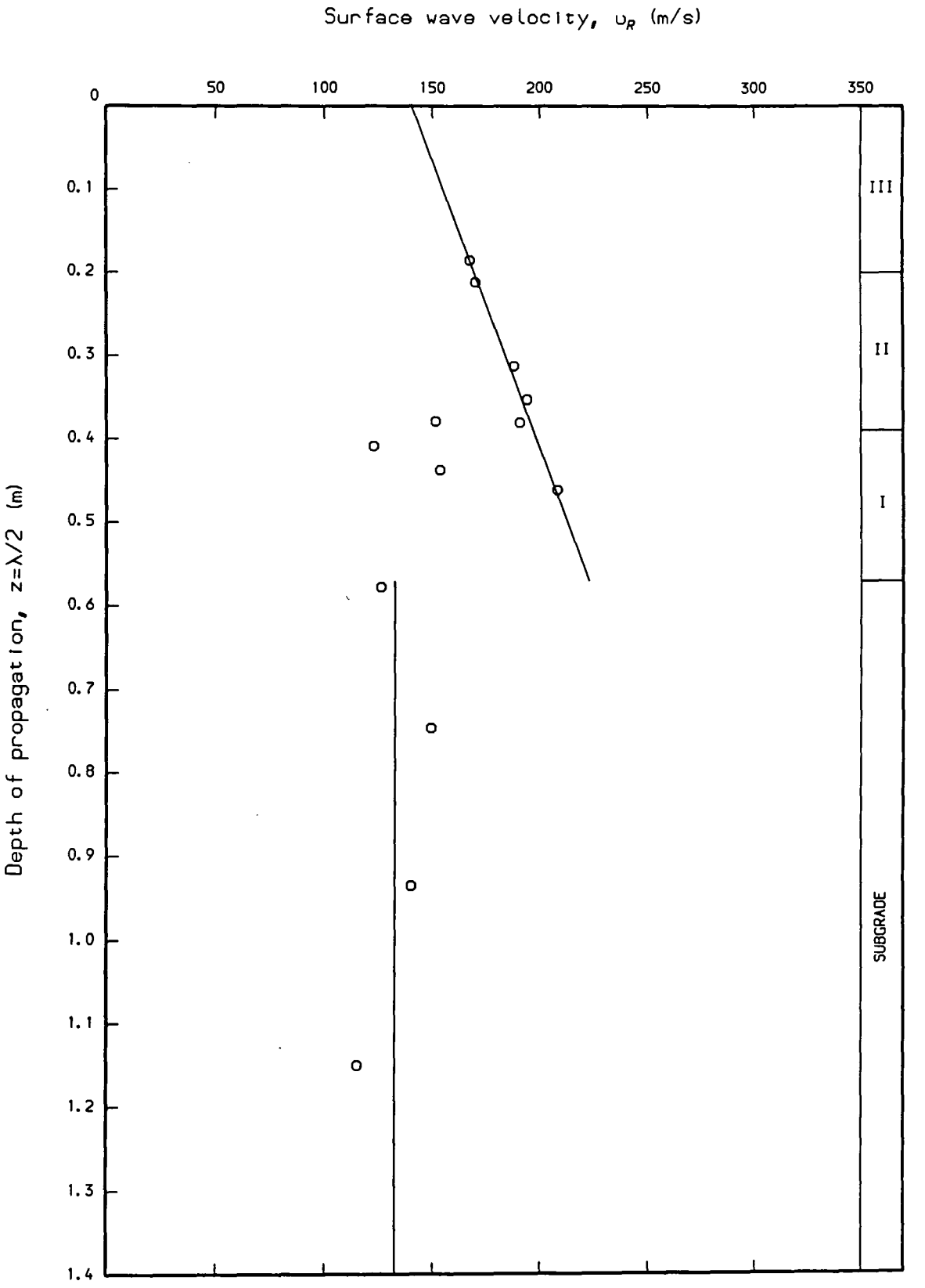

Figure 6.40 - Surface wave velocity-depth profile for Test WMM6.

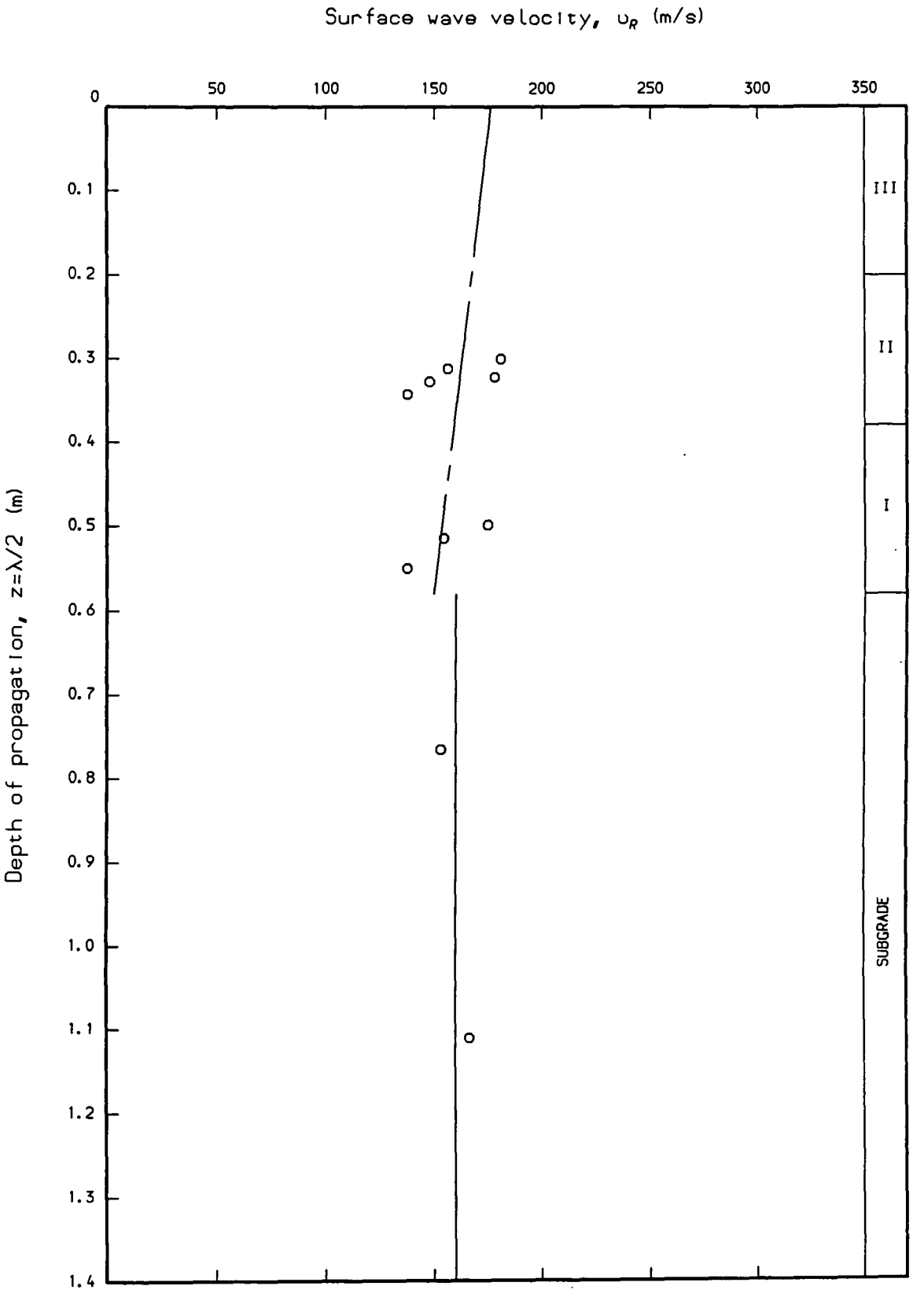

Figure 6.41 - Surface wave velocity-depth profile for Test WMM10.

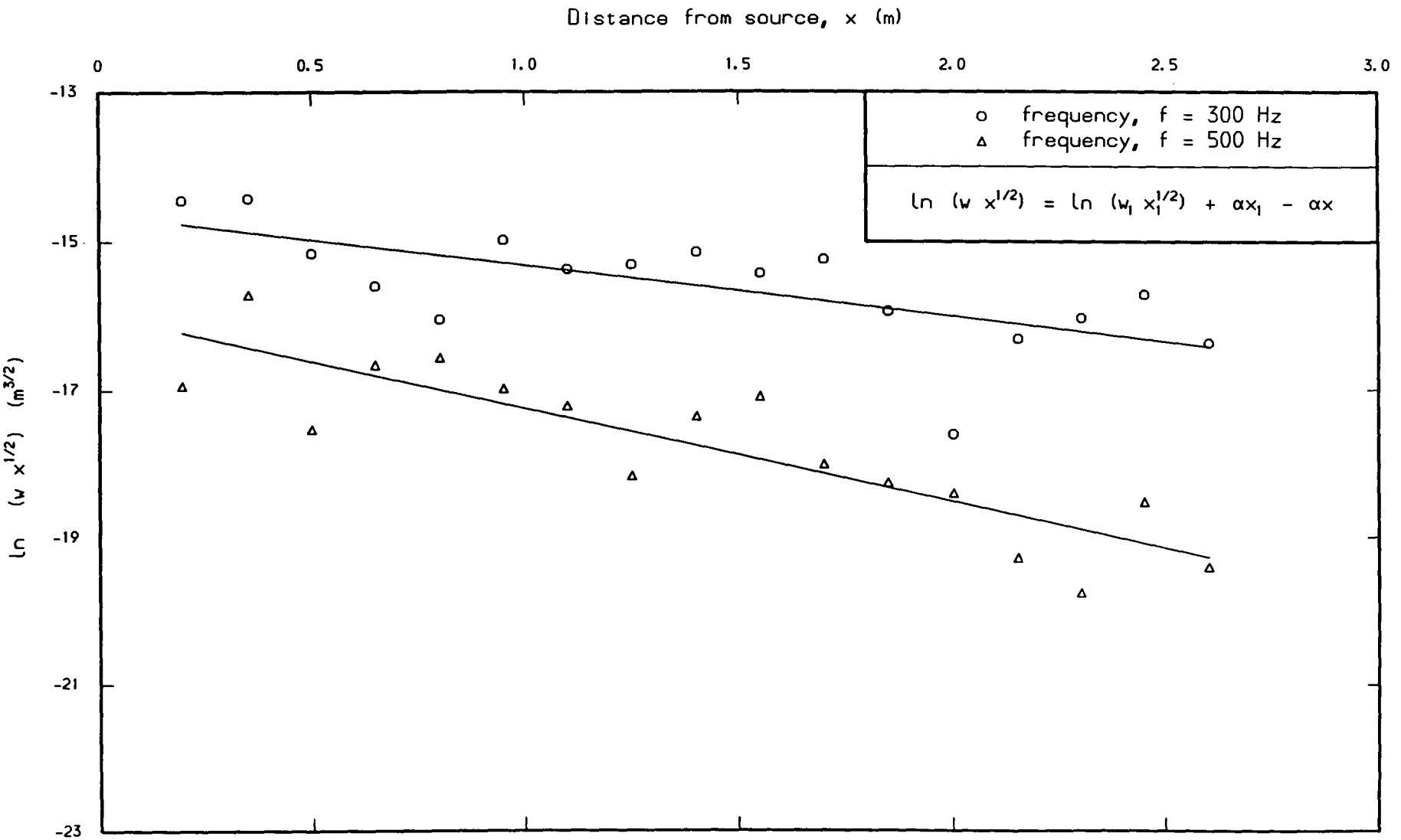

Figure 6.42 - Attenuation data for Test WMM1 (frequency, f = 300 and 500 Hz).

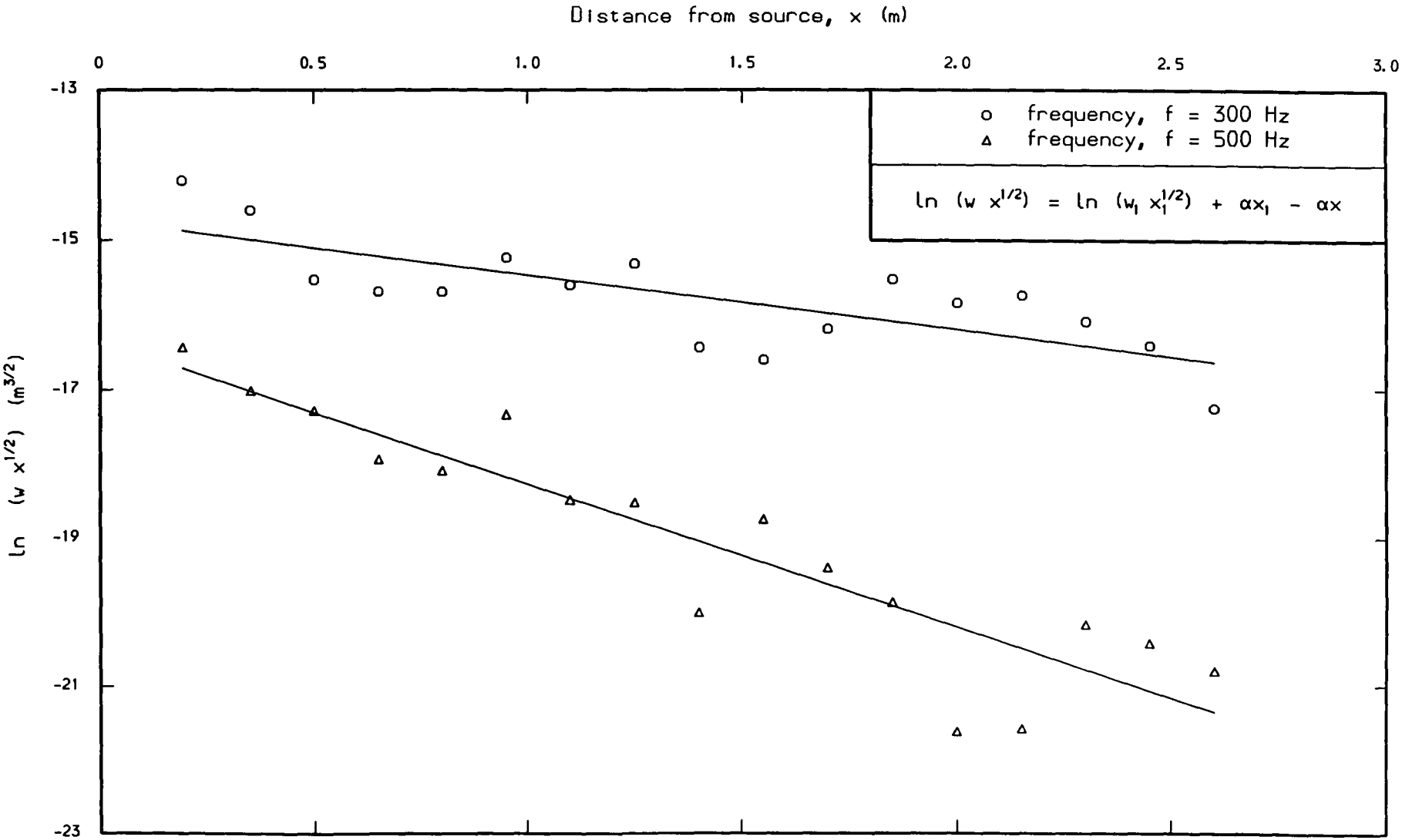

Figure 6.43 - Attenuation data for Test WMM2 (frequency, f = 300 and 500 Hz).

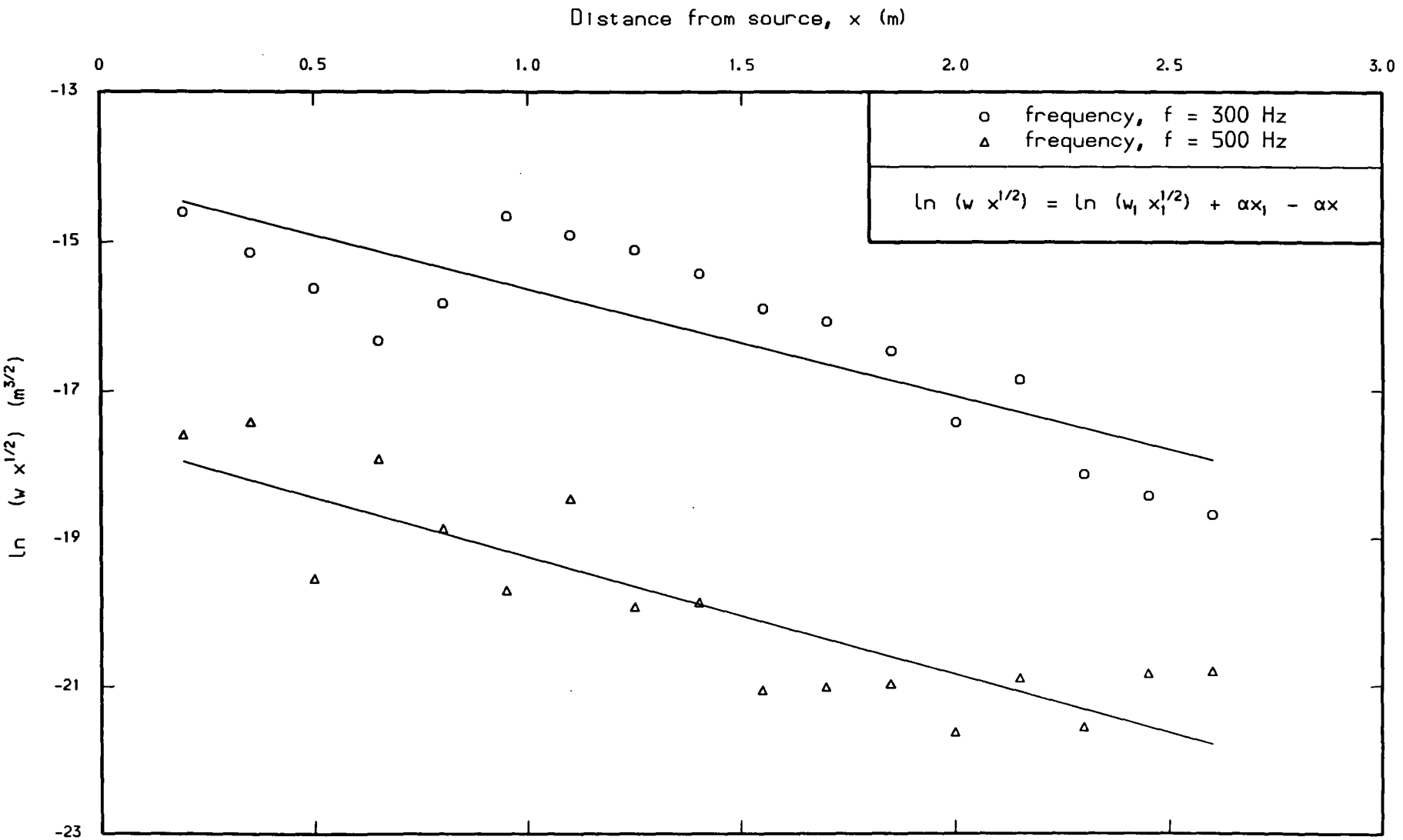

Figure 6.44 - Attenuation data for Test WMM3 (frequency, f = 300 and 500 Hz).

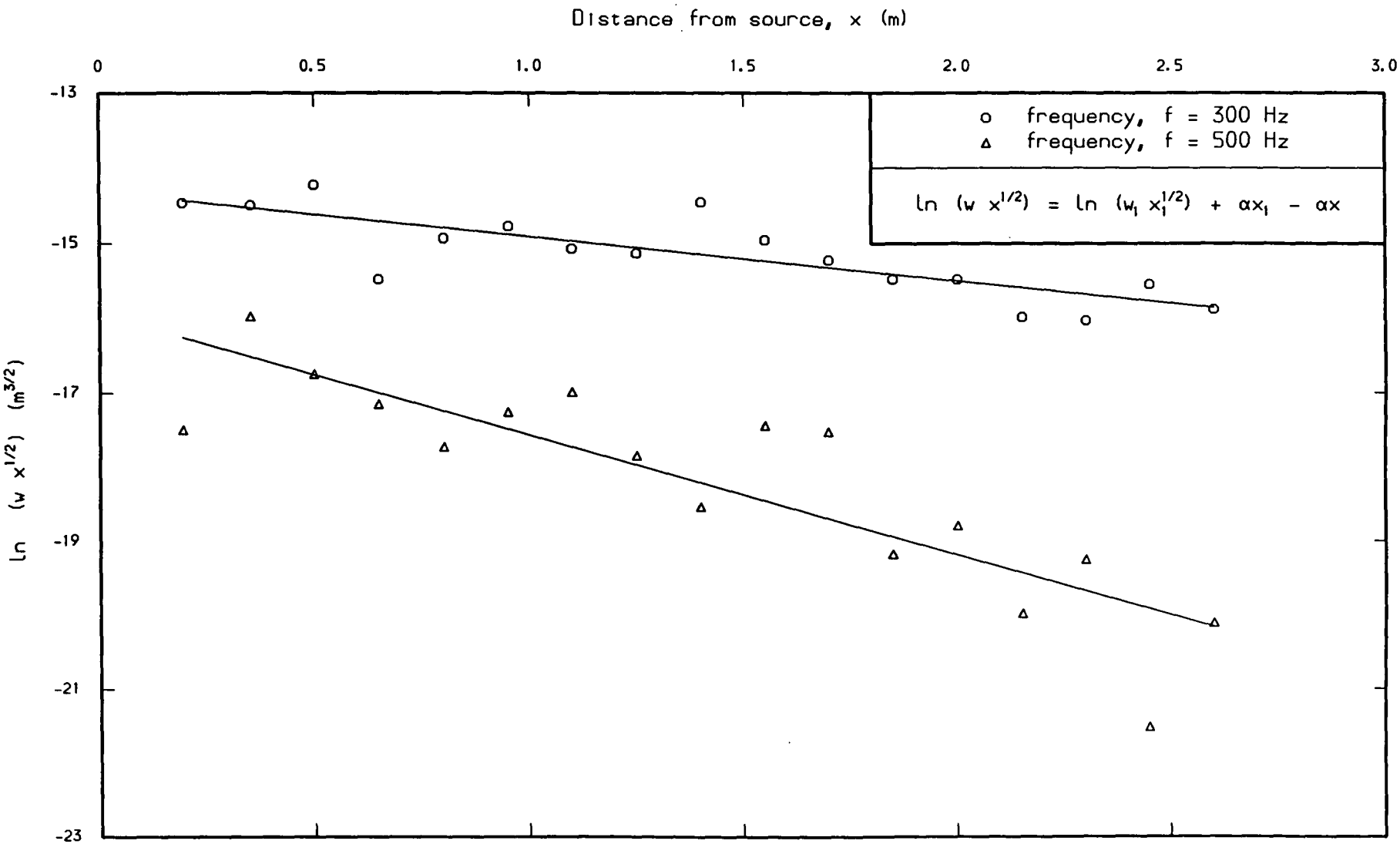

Figure 6.45 - Attenuation data for Test WMM4 (frequency, f = 300 and 500 Hz).

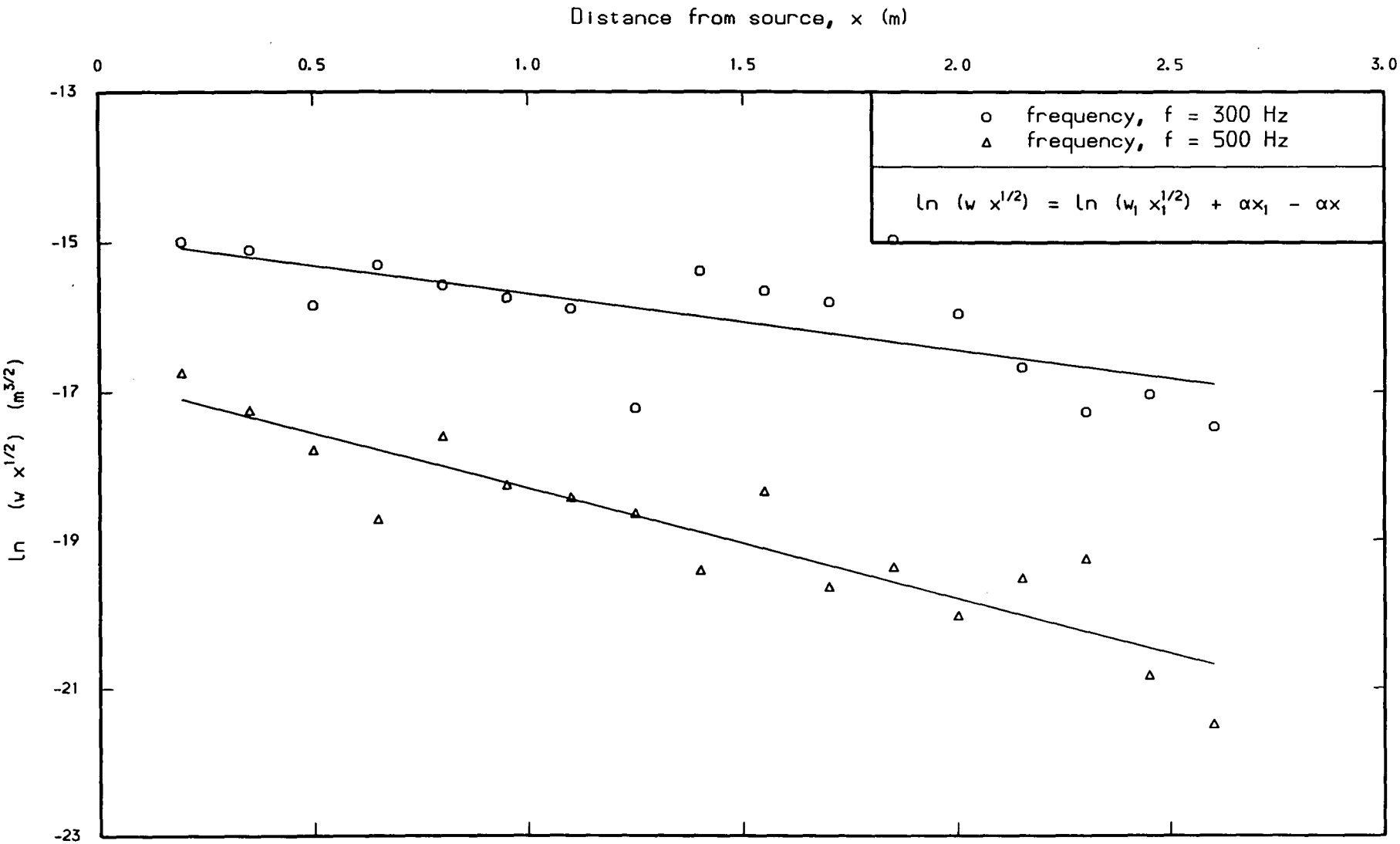

Figure 6.46 - Attenuation data for Test WMM5 (frequency, f = 300 and 500 Hz).

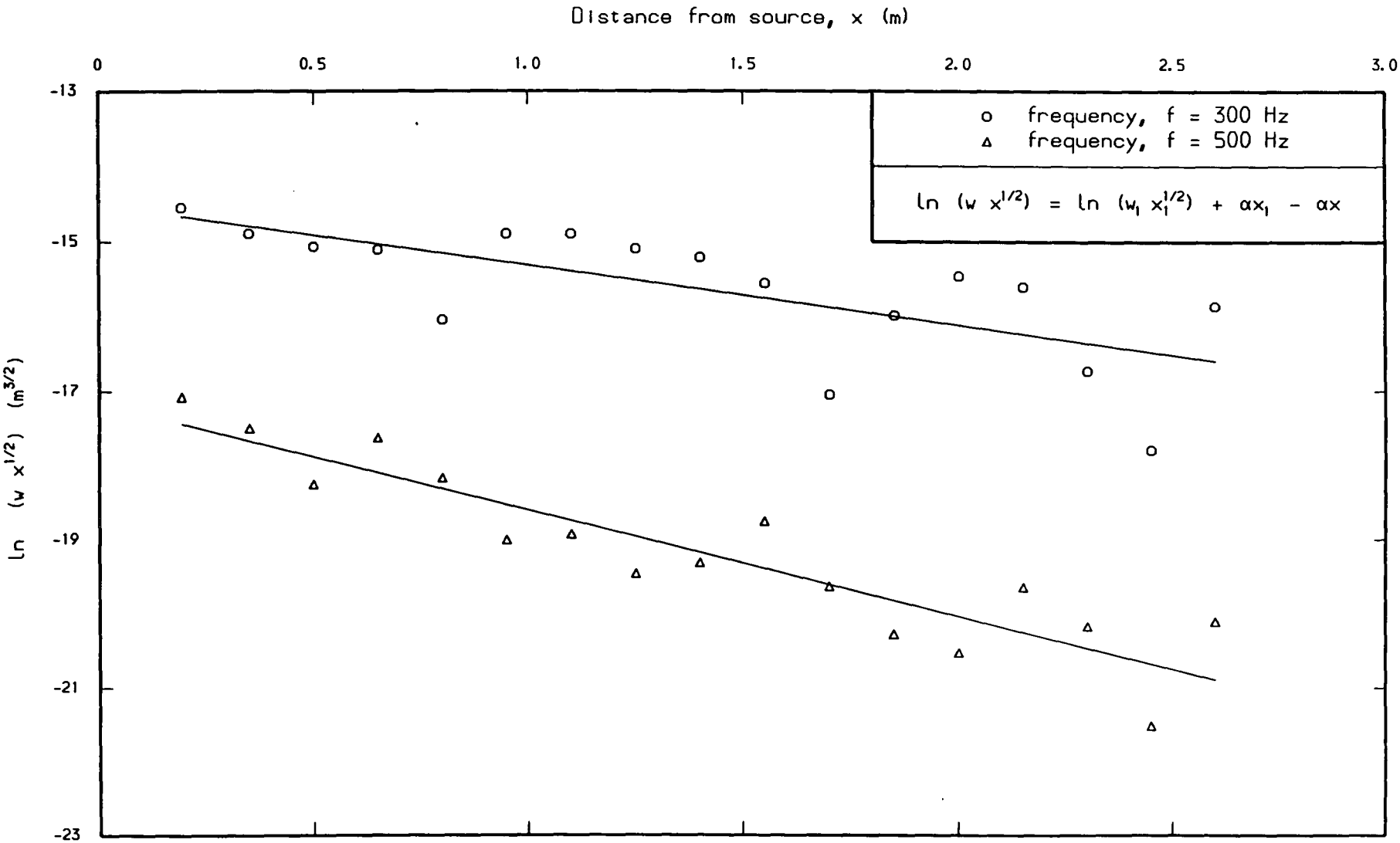

Figure 6.47 - Attenuation data for Test WMM6 (frequency, f = 300 and 500 Hz).

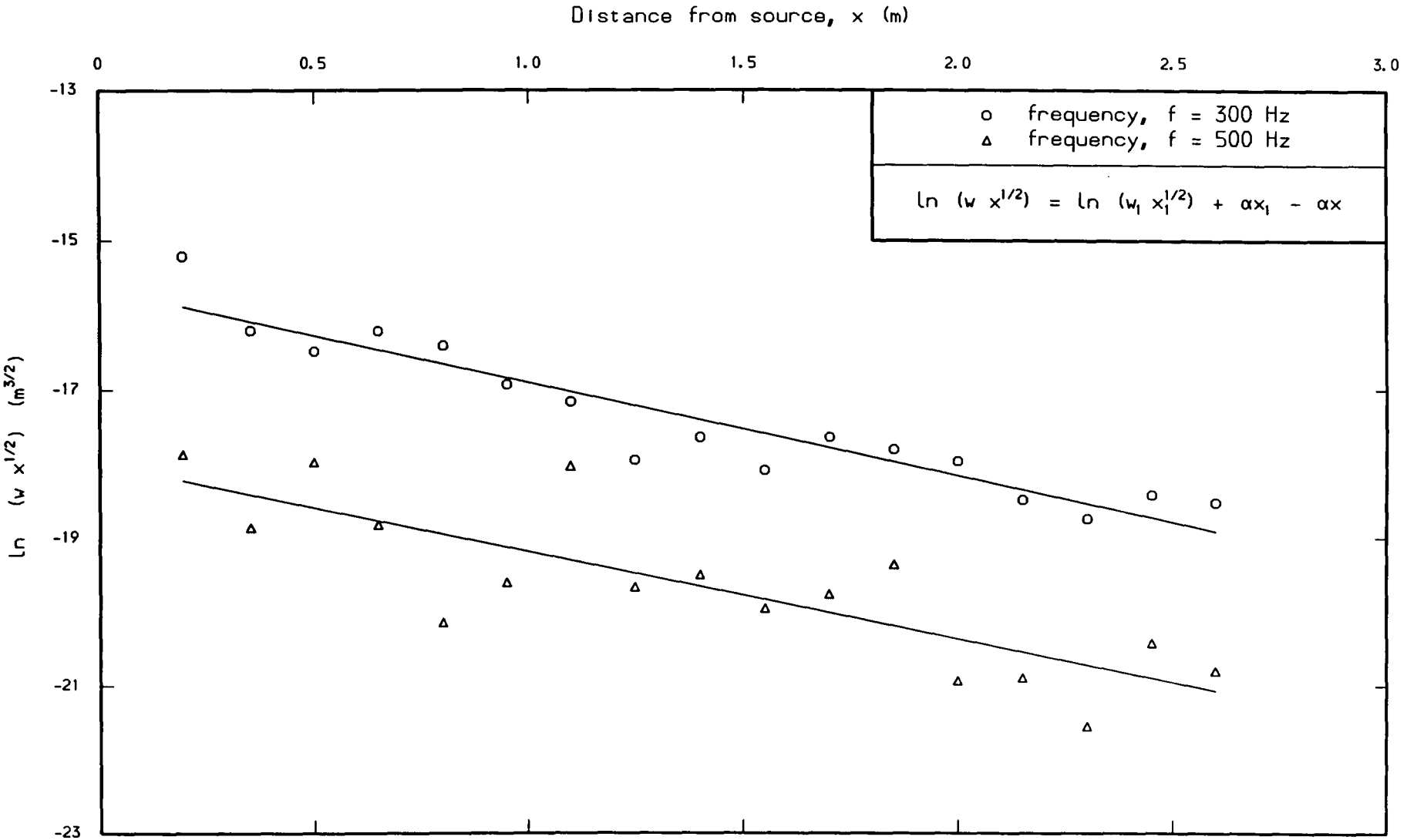

Figure 6.48 - Attenuation data for Test WMM10 (frequency, f = 300 and 500 Hz).

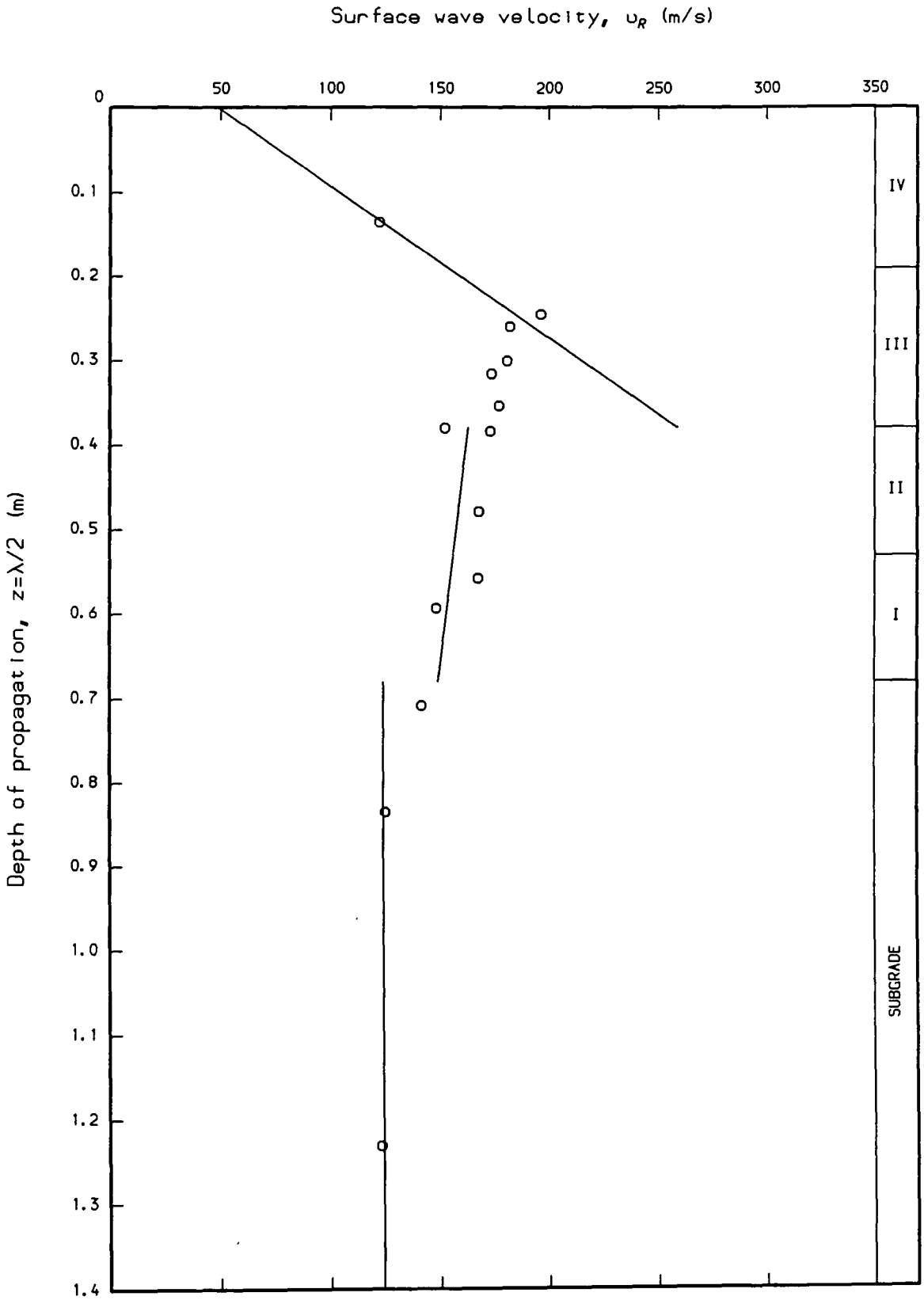

Figure 6.49 - Surface wave velocity-depth profile for Test WMM7.

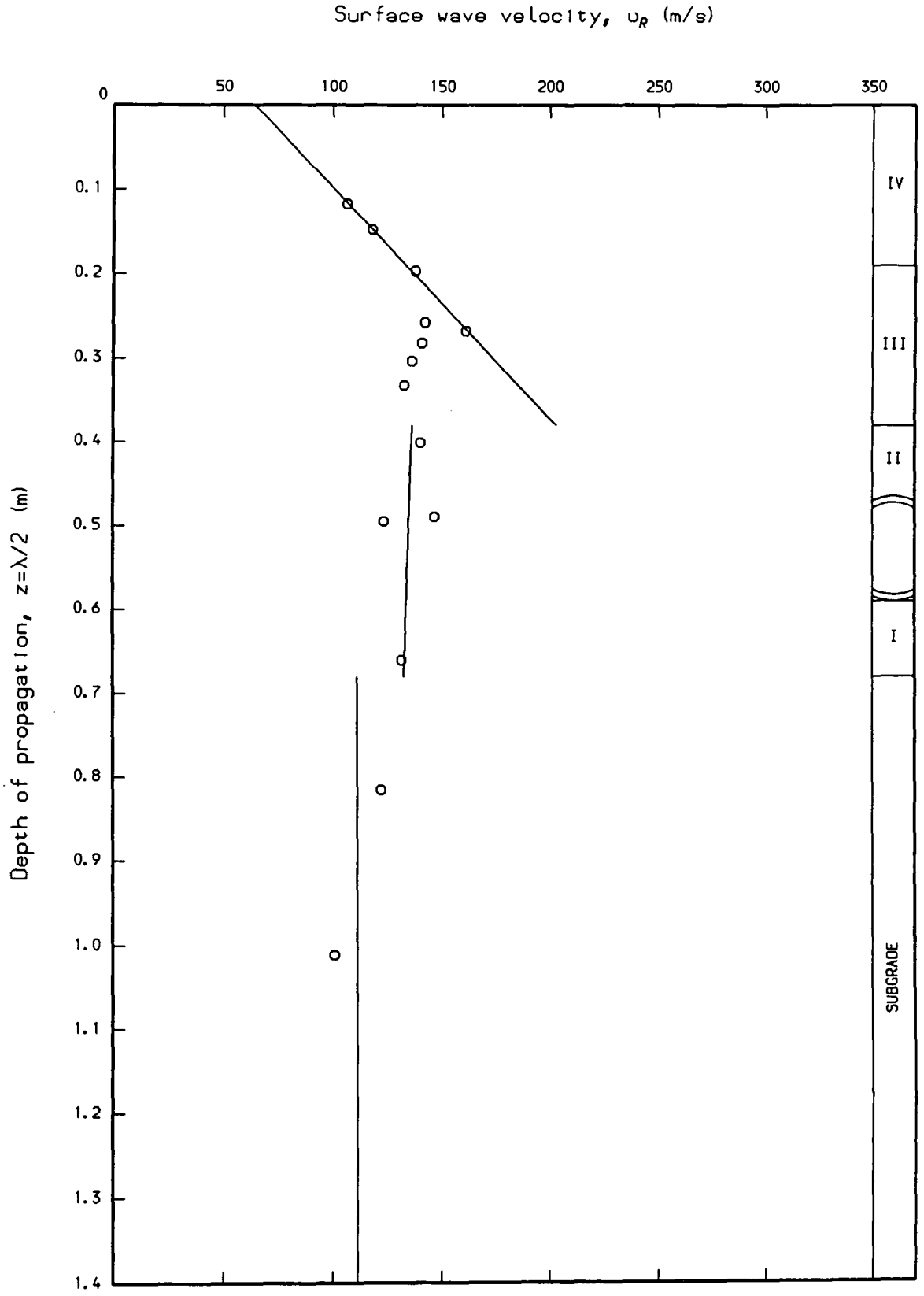

Figure 6.50 - Surface wave velocity-depth profile for Test WMM8.

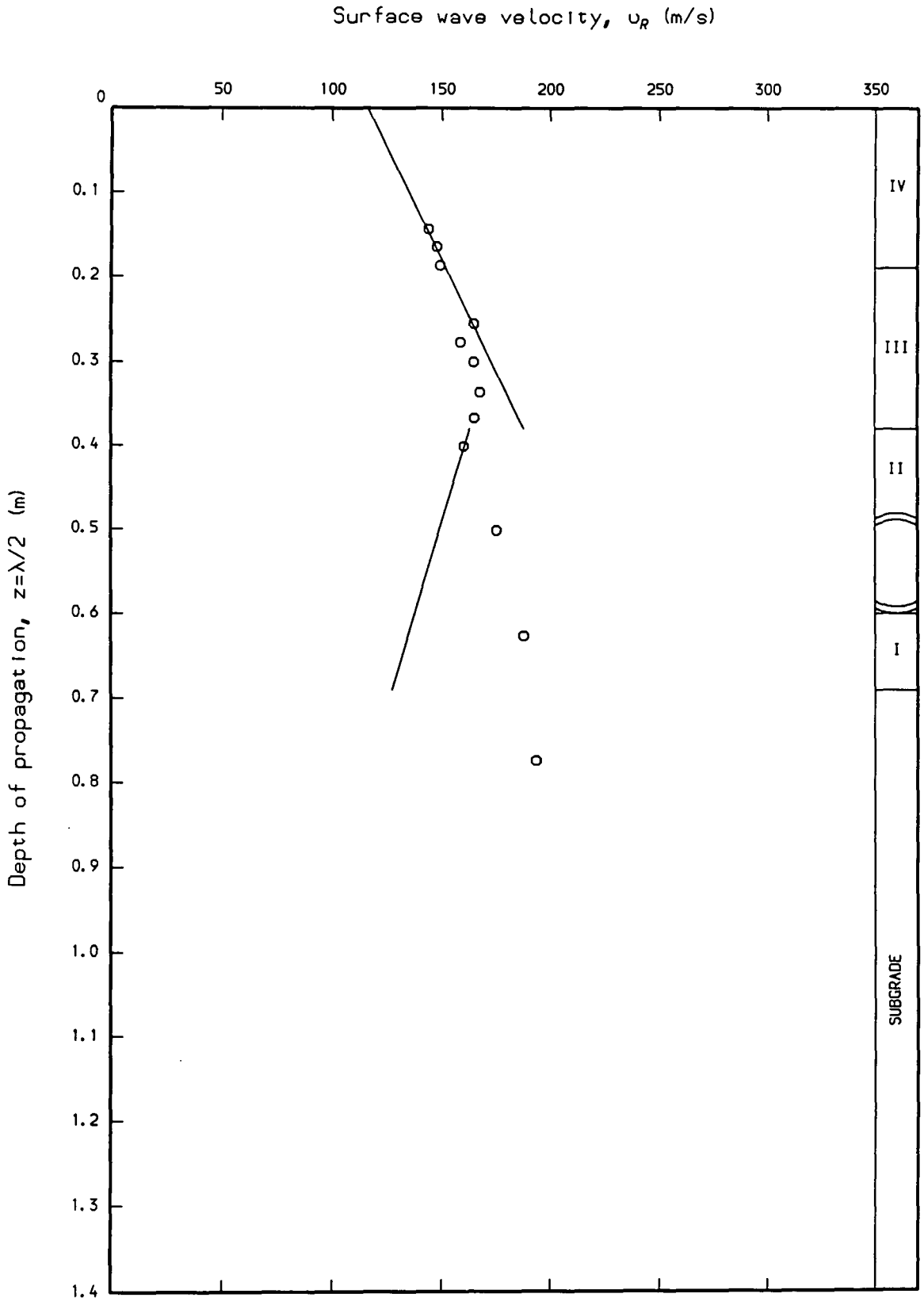

Figure 6.51 - Surface wave velocity-depth profile for Test WMM9.

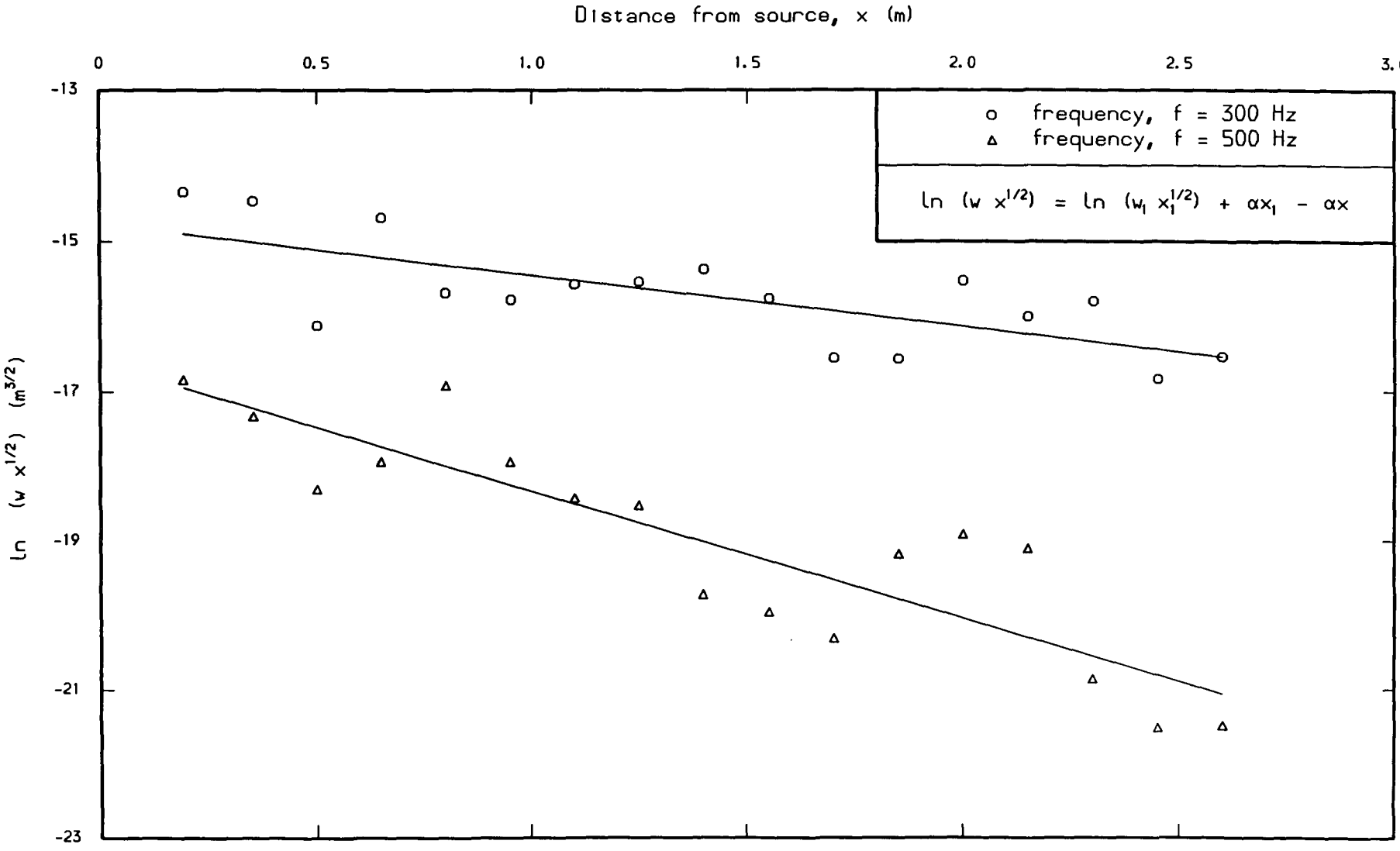

Figure 6.52 - Attenuation data for Test WMM7 (frequency, f = 300 and 500 Hz).

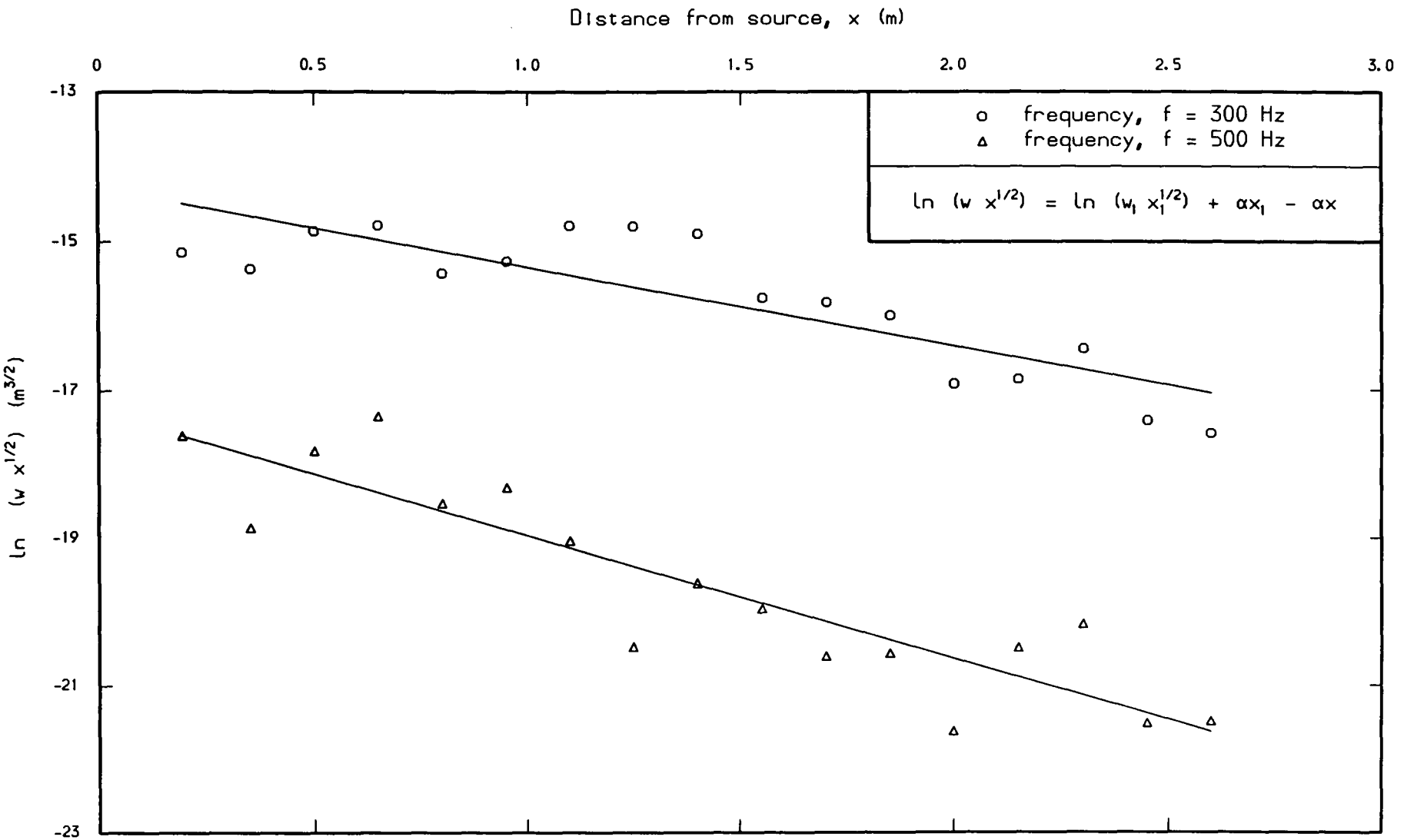

Figure 6.53 - Attenuation data for Test WMM8 (frequency, f = 300 and 500 Hz).

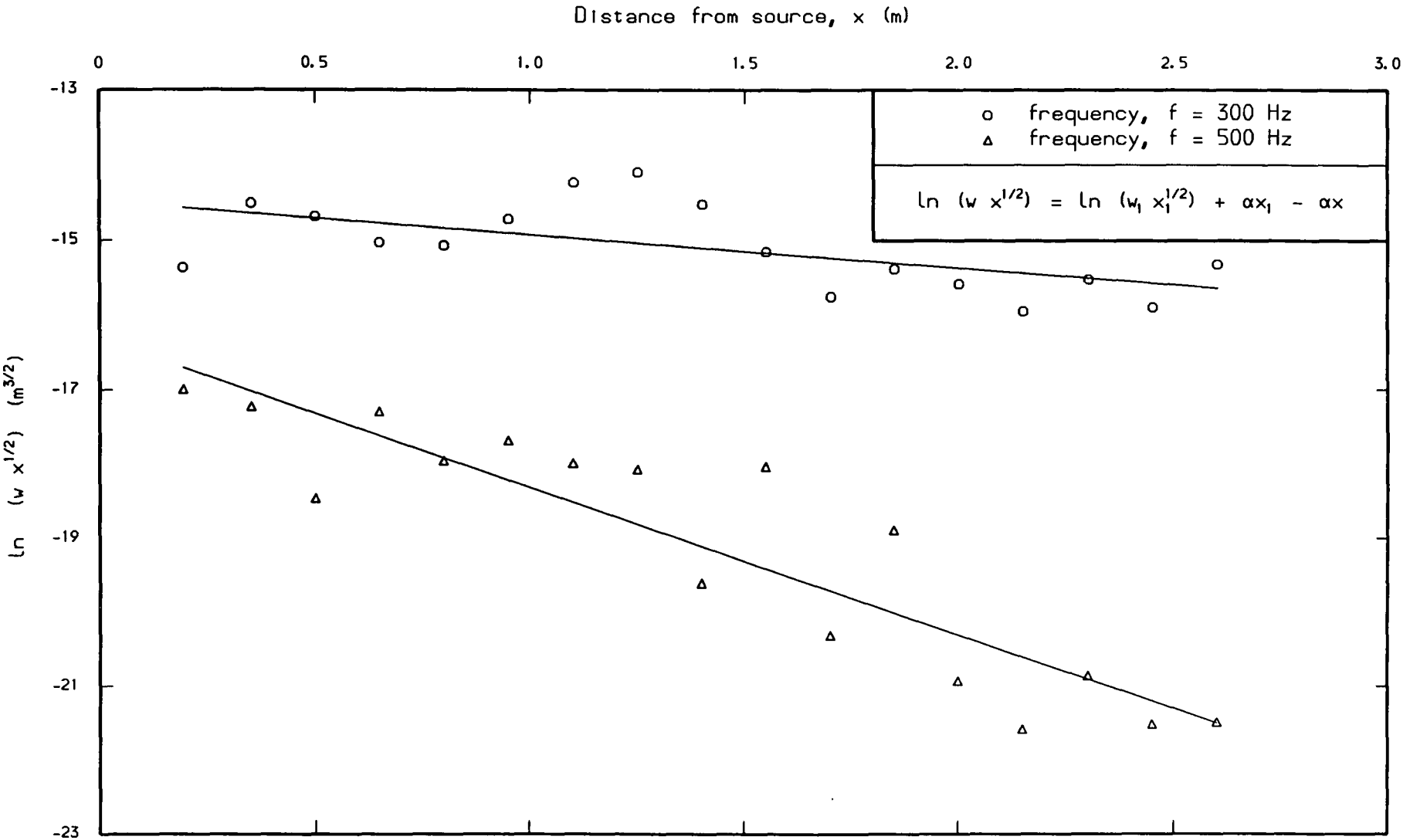

Figure 6.54 - Attenuation data for Test WMM9 (frequency, f = 300 and 500 Hz).

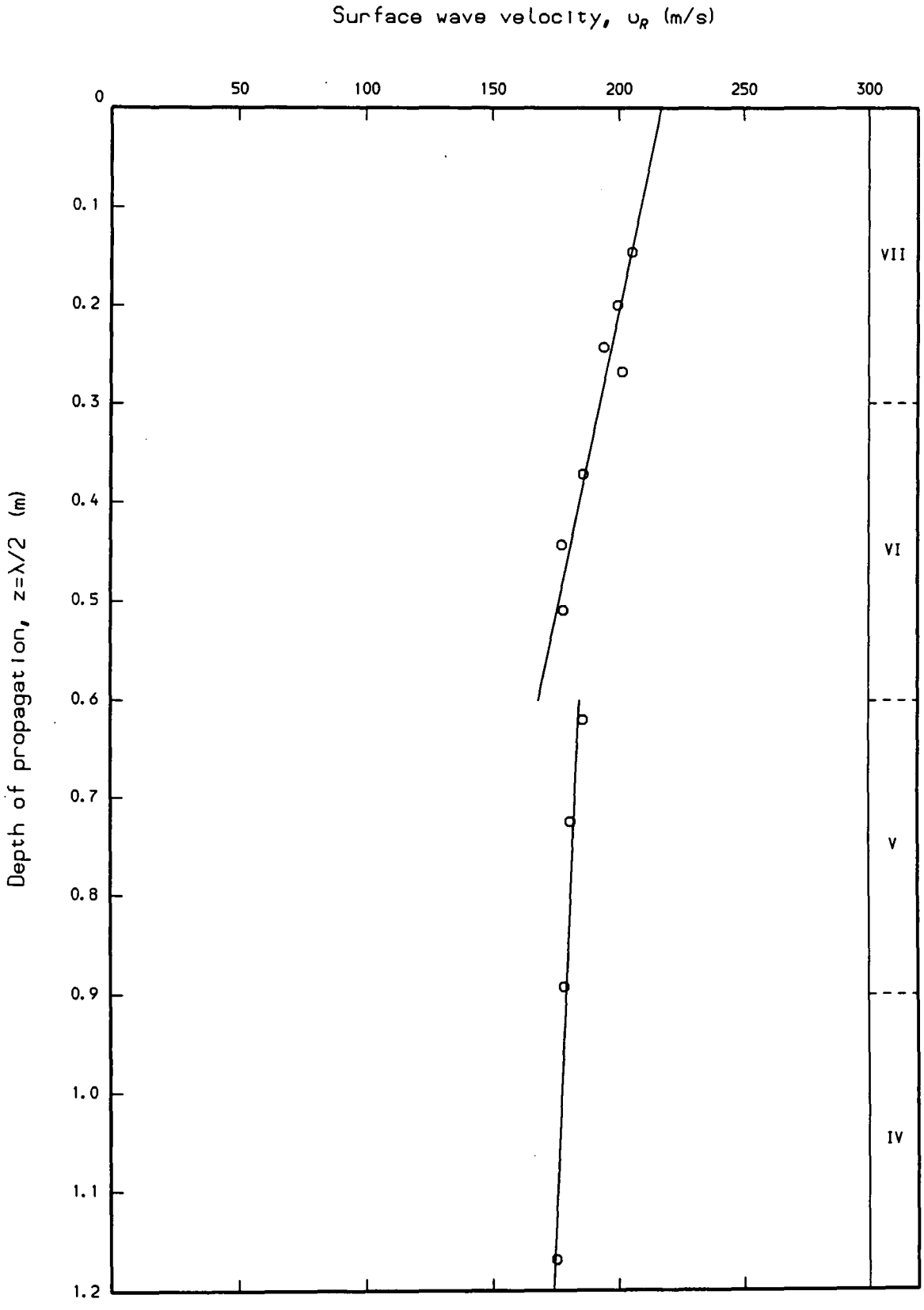

Figure 6.55 - Surface wave velocity-depth profile for Test NSSEAS.

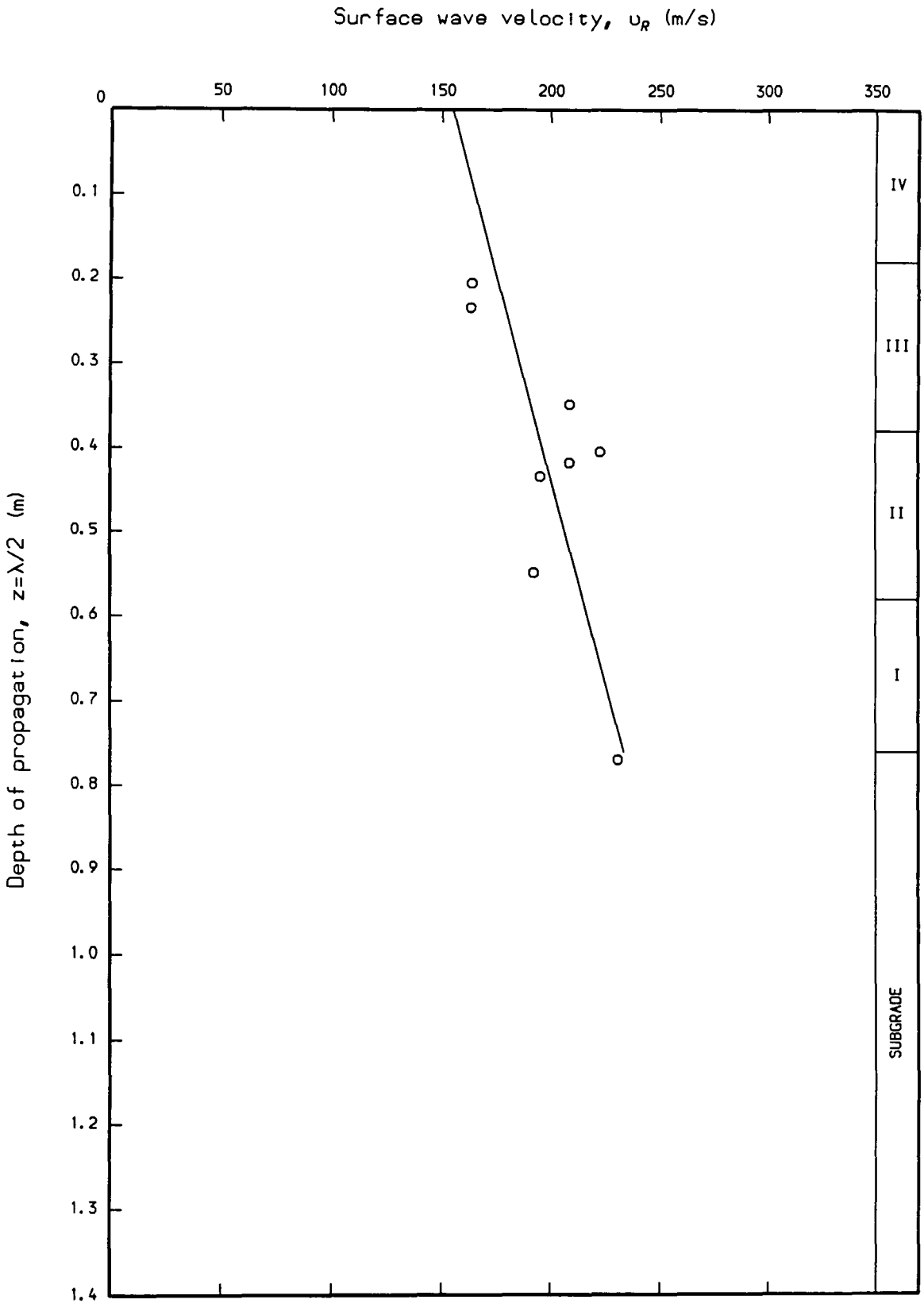

Figure 6.56 - Surface wave velocity-depth profile for Test SL1.

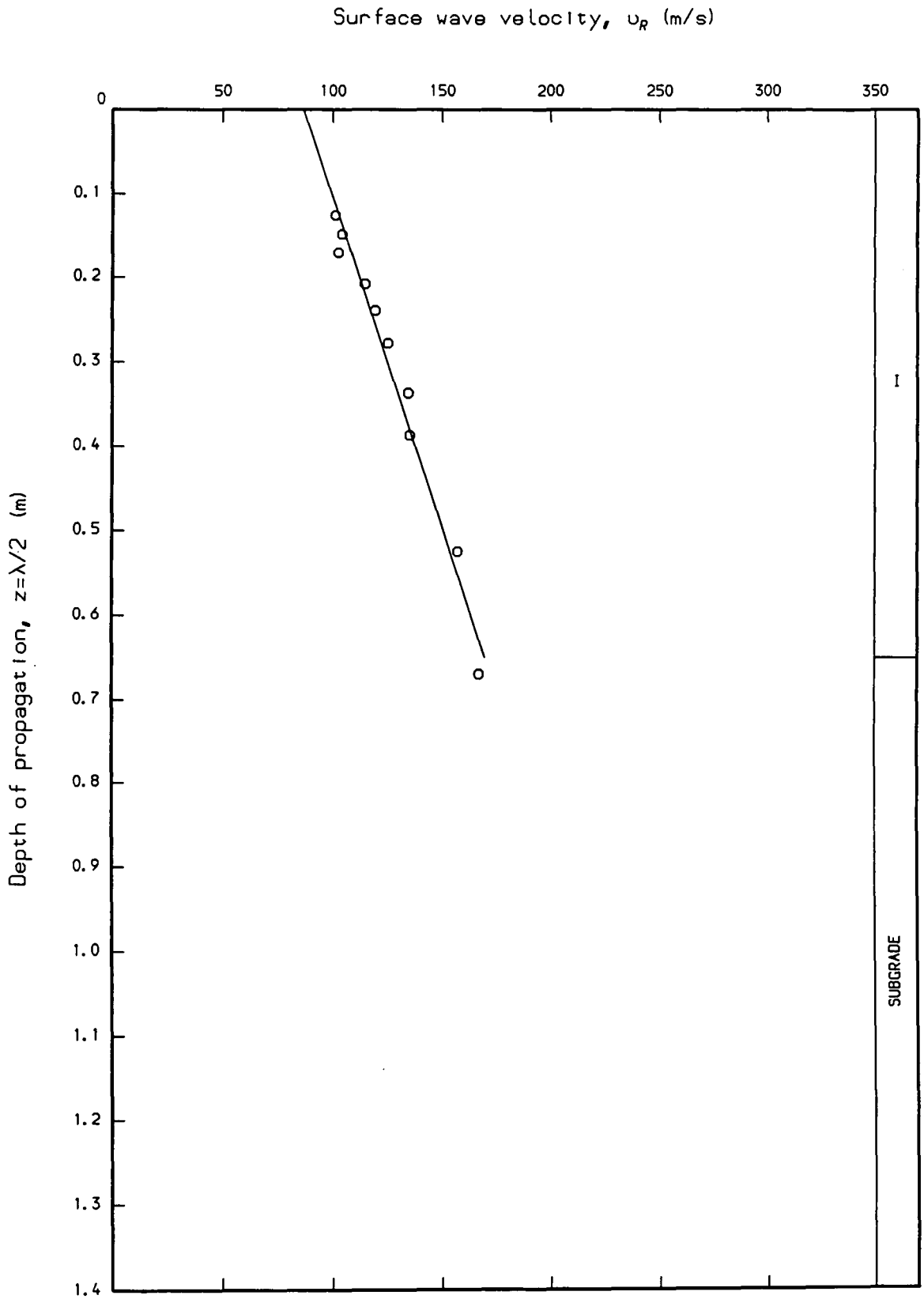

Figure 6.57 - Surface wave velocity-depth profile for Test SL2.

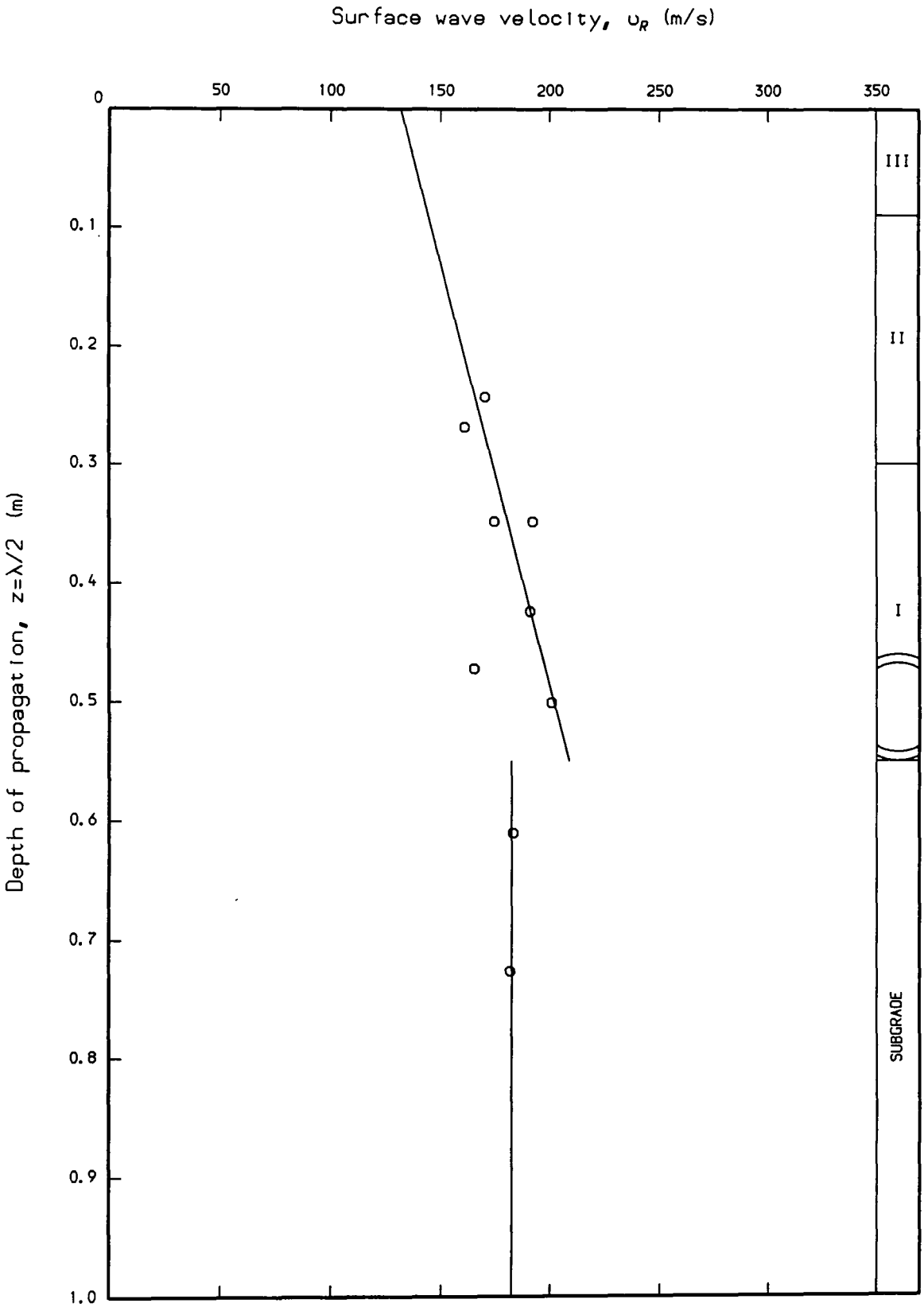

Figure 6.58 - Surface wave velocity-depth profile for the case study at Acton Dean, Stanley, County Durham.

Plate 6.1 - The Bomag BG 100 vibratory roller narrow trench compactor.

CHAPTER 7

INTERPRETATION AND DISCUSSION OF RESULTS

7.1 Introduction

In this chapter the results presented in Chapter 6 are discussed and more detailed analyses performed on the data. The layout of this chapter has been constrained to be broadly similar to that of the previous chapter in order to enable direct comparisons to be made.

Numerical values of the mean and sample standard deviation (x and $\sigma_{x_{n-1}}$) were given in the tabulated data summaries presented in Chapter 6. These could be used to show error bars in graphical presentations of experimental (*e.g.* error bars of magnitude $\overline{x} \pm \sigma_{x_{n-1}}$ include approximately 68% of the experimental data). This form of presentation was used in early reports of the work presented here (Winter and Selby, 1988 and 1989). The addition of further data since the time of writing these papers has meant that plots with error bars obscure the clarity of the information conveyed. Consequently, for the sake of clarity and ease of understanding, error bars are not generally shown on the figures presented in this chapter.

Regression analyses presented in this chapter were performed using the Casio *fx*-6000G programmable calculator described in Section 5.1.

Reinstatement backfill quality has been assessed using five different parameters. Density measurements have been made using either density rings (laboratory tests) or using the sand replacement method described in BS 1377 (1975): Test 15(A) (field tests). A limited number of California Bearing Ratio tests were also carried out on the Permian Sand and the Sharp Sand compacted in the laboratory based trench. These two tests, which are traditional methods of compaction control, involve considerable disturbance to the reinstated material, are slow and cumbersome (both in operation and interpretation) and require the testing of each compacted layer prior to the placement of the subsequent layer to obtain an evaluation of the variation of properites with depth. It should be noted that California Bearing Ratio tests conducted much below ground level are extremely difficult and certainly not appropriate on a cost basis for reinstatement works. Density and *CBR* value measurements do not conform in any way to the four points which describe the

ideal characteristics of a test, for use as the basis of a performance specification for reinstatement backfill, which were identified in Section 2.5. The Impact Value, as measured using the Clegg meter, may be seen as something of an improvement over the density and *CBR* value approaches. The test is simple and quick providing a simple digital readout of the Impact Value. However, the volume of material which influences the Impact Value is almost certainly small and testing must be carried out on each compacted layer prior to the placement of the subsequent layer to obtain an evaluation of the variation of properties with depth. There also exists some doubt as to precisely what the Impact Value is a measure of (*i.e.* stiffness or strength—see Section 2.4.1). In contrast, surface wave velocity measurements satisfy all of the ideal test characteristics that were identified in Section 2.5 with the notable exception that the test method is neither quick nor simple. There does exist, however, some potential for simplifying both the test procedures and the test equipment as is discussed in Section 8.2. Surface wave velocity data may also be converted, when density measurements are available, to shear modulus data giving reinstatement backfill properties in terms of a true elastic deformation parameter as a function of depth.

Traditionally, *'compaction is measured quantitatively in terms of the dry density of the soil'*, (Road Research Laboratory, 1952) the resultant dry density increasing with compactive effort. From consideration of the packing of single sized particulate media, ranging from cubic packing in the loosest state to tetrahedral packing in the densest state (Barnes, 1987) it is plain that a simple linear relationship will not exist between the compactive effort and resultant dry density. Hogentogler (1938) demonstrated the existence of a semi-logarithmic relationship between static compaction pressure and maximum dry density. Consequently, the logarithm of the number of passes ($\log N_p$) applied to each layer of compacted material placed in each test is taken as the parameter of compactive effort. Linear regression analyses of the form:

$$y = c + m \log x \qquad (7.1),$$

are performed on the data, where x is the parameter of compactive effort, m is the slope of the regression line, c is the intercept of the regression line (at $x = 1$) and y is the measurement parameter under consideration (*i.e.* ρ_d, *IV*, etc.). A new parameter of compactive effort, the logarithm of the number of passes per layer

divided by the mean compacted layer thickness ($\log N_p/\overline{h}$) is also investigated using Equation 7.1.

In Section 4.4.6 the level of compactive effort applied to material compacted for British Standard tests to determine the dry density-moisture content relationship using vibrating hammer methods (BS 1377, 1975: Test 14 and BS 5835: Part 1, 1980) was defined as:

$$CE = \frac{Pt}{V} \qquad (4.12\text{bis})$$

where:

P is the power output of the compaction machine,

t is the time for which the compactive effort is applied, and

V is the volume of the compacted material.

In each of the laboratory and field tests (TPS, TSS and WMM) the trench width and length were 0.30 m and 4.60 m, respectively. Thus, it is simply the layer thickness which determines the relative magnitude of the volume component of Equation 4.12. The Pt component may be assumed to be approximately constant for each pass of the Wacker BS45Y vibratory rammer as the power output (P) is non-variable and the constant surface area (0.30 × 4.60 m) constrains the time taken to compact a layer (t) to be constant (*i.e.* the travel speed is assumed to be constant). The number of passes applied to each layer (N_p) and the mean layer thickness ($\overline{h}$) completely describes the mean energy applied to each layer during compaction:

$$CE = \frac{N_p Pt}{\overline{h} \times 0.30 \times 4.60} \qquad (7.2)$$

and P is taken to be 615 W (the actual power transmitted to the ground surface) from Table A5.1 and t can be calculated as the maximum travel speed of the BS45Y at 15 m/min ($t = 4.60^{60}/_{15} = 18.4$ seconds). The average compactive effort (or energy), CE, applied to each layer is thus:

$$CE = \frac{N_p}{\overline{h}} . \frac{615 \times 18.4 \times 10^{-3}}{0.30 \times 4.60} = 8.2 \times \frac{N_p}{\overline{h}} \text{ kJ/m}^3 \text{ for each layer} \qquad (7.3)$$

Thus, this parameter which takes account of the thickness of the placed layers is believed to provide a more complete representation of compactive effort and also allows the direct comparison of data from tests of differing nominal layer thicknesses since it may be viewed as a measure of the compactive energy applied per cubic metre of compacted material.

The surface wave velocity-depth profiles individually presented in Chapter 6 are combined on the same axes in this chapter so that the change in the profiles under increasing compactive effort may be studied. For tests conducte d in the laboratory based trench (Sections 7.2 and 7.3) in the half-full and full conditions the surface wave velocity-depth profiles are plotted on the same axes to aid comparisons.

7.2 Measurements on Permian Sand

Due to trials of different types of velocity and acceleration transducers for wave velocity measurements a long time delay occurred (*circa* 106 days) between the placing of the layers for Test TPS1 and the final excavation and determination of the dry density, *CBR* and Impact Values. This led to concern as to whether the results derived from this test should be compared with the results from the other tests (Tests TPS2 to TPS5). The time delays between placement and subsequent excavation for Tests TPS2 to TPS5 were much shorter (between 24 and 64 days). The use of a petrol driven vibratory rammer prior to the introduction of the standard usual electrically driven device was another possible source of experimental error. Logarithmic regression analyses of the form of Equation 2.1 were thus performed on data both including and excluding Test TPS1 in order quantitatively to assess the importance of the factors described above. In this chapter the regression lines plotted for Permian Sand are those which exclude from the calculation the data obtained from Test TPS1.

7.2.1 Density, moisture content, Impact Value and CBR results

Detailed data for these parameters are presented in Section 6.2.1 and the particular data used in the analyses presented here are detailed in Table 6.7, for results obtained at the time of compaction, and Table 6.8, for results obtained at the time of excavation.

The moisture content during the compaction of the Permian Sand in the laboratory based trench was carefully controlled using the procedure described in Section 5.3.1 and Appendix 4. It was observed in Section 4.4.6 (Table 4.3) that the optimum moisture content varied with compactive effort. The moisture content data achieved immediately after compaction (Table 6.7) was generally within the range $10.20 \leq w \leq 12.20\%$; *i.e.* $w_{opt} \pm 1.0\%$ where w_{opt} is determined from the standard BS 1377 (1975): Test 12, with the number of blows per layer, $N_b = 27$.

Taking the number of passes per layer (N_p) as the compactive effort parameter and fitting dry density data to the corresponding values of log N_p yields:

$$\rho_d = 1.757 + 0.104 \log N_p \quad (r = 0.763) \tag{7.4}$$

for data excluding Test TPS1, and

$$\rho_d = 1.743 + 0.108 \log N_p \quad (r = 0.690) \tag{7.5}$$

for data including Test TPS1. The relationship defined by Equation 7.4 is illustrated in Figure 7.1. Taking $N_p/\overline{h}$ as the compactive effort parameter yields:

$$\rho_d = 1.759 + 0.051 \log \left(N_p/\overline{h}\right) \quad (r = 0.433) \tag{7.6}$$

for data excluding Test TPS1, and

$$\rho_d = 1.759 + 0.044 \log \left(N_p/\overline{h}\right) \quad (r = 0.317) \tag{7.7}$$

for data including Test TPS1. The relationship defined by Equation 7.6 is illustrated in Figure 7.2. The low values of regression correlation coefficient for the data with the compactive effort parameter taken as $N_p/\overline{h}$ may be explained by consideration of Test TPS4 in which the layer thickness was approximately two-times that of the other tests. D'Appolonia *et al* (1969) showed that for sand compacted using a single drum vibratory roller the dry density increased rapidly from the surface of the layer to within around $1/5h$ of the base of the layer before decreasing towards the interface with the underlying layer. This is qualitatively supported by the work of Moorhouse and Baker (1969). As the density rings were placed prior to compaction each successive pass of the vibratory rammer forced the density rings slightly deeper within the layer. Thus for the two data points with $N_p/\overline{h} \approx 18\ \mathrm{m}^{-1}$, one compacted with $N_p = 2$ and the other compacted with $N_p = 5$ it is likely that, all other factors being constant, the latter test would yield a higher value of dry density as the density ring had been forced further down the curve of increasing dry density with depth. This explanation is qualitatively supported by the data presented in Figure 7.2.

Taking a similar approach for the interpretation of the Impact Value data, obtained at the time of compaction, yields:

$$IV = 2.12 + 4.04 \log N_p \quad (r = 0.968) \tag{7.8}$$

for data excluding Test TPS1, and

$$IV = 2.73 + 3.86 \log N_p \quad (r = 0.760) \tag{7.9}$$

for data including Test TPS1. Data obtained as the laboratory trench reinstatements were excavated yields:

$$IV = 7.34 + 3.85 \log N_p \quad (r = 1.000) \tag{7.10}$$

for data excluding Test TPS1, and

$$IV = 8.47 + 3.52 \log N_p \quad (r = 0.521) \tag{7.11}$$

for data including Test TPS1. The relationships defined by Equations 7.8 and 7.10 are illustrated in Figure 7.3. Plainly the relationships between IV and the logarithm of the number of passes per layer are significant, with high values of the regression correlation coefficient, for the regression lines ignoring data from Test TPS1. The seeming lack of fit of the Test TPS1 data to the rest of the data lends further weight to the earlier indications that these data are anomalous due either to the time delay between compaction and subsequent excavation and/or the different compaction plant used in that test.

Taking the compactive effort parameter to be $N_p/\overline{h}$ for data at the time of compaction yields:

$$IV = -2.30 + 4.32 \log \left(N_p/\overline{h}\right) \quad (r = 0.983) \tag{7.12}$$

for data excluding Test TPS1, and

$$IV = -2.27 + 4.56 \log \left(N_p/\overline{h}\right) \quad (r = 0.845) \tag{7.13}$$

for data including Test TPS1. Data similarly obtained at the time of excavation yields:

$$IV = 0.88 + 5.29 \log \left(N_p/\overline{h}\right) \quad (r = 0.931) \tag{7.14}$$

for data excluding Test TPS1, and

$$IV = 0.93 + 5.76 \log \left(N_p/\overline{h}\right) \quad (r = 0.704) \tag{7.15}$$

for data including Test TPS1. These data are illustrated graphically with the logarithmic regression lines defined by Equations 7.12 and 7.14 in Figure 7.4. Again significant differences are observed between the data of Test TPS1 and the remaining tests.

In general terms the Impact Value results show the Clegg meter to be an excellent device for measuring reinstatement backfill quality where measurements for each compacted layer are taken.

Careful examination of the *CBR* results yields no significant relationship with either of the two parameters of compactive effort under consideration (N_p or $N_p/\overline{h}$). For analyses performed on all data, values of the regression correlation coefficient were found to be in the range $-0.092 \leq r \leq +0.231$. The data without the linear regression lines are shown in Figures 7.5 and 7.6 for compactive effort defined as N_p and $N_p/\overline{h}$, respectively. Details of the linear regression lines are not given here. The reason for the apparent lack of a correlation betwen *CBR* and compactive effort is likely to be the differential time delay between the completion of the placement of the layers and the subsequent excavation of the layers after the *CBR* determination (between 24 and 106 days), causing the moisture content measured at the surface of the reinstatement to vary considerably ($2.77\% \leq w \leq 5.86\%$) due to drying (see Tables A6.2, A6.4, ..., A6.10). The effect of this phenomenon is to increase the strength of the reinstated surface, an effect which is particularly noticeable in Test TPS1 when the formation of a 'duri-crust' was noted, possibly due to a cementing effect caused by the calcite present in the Permian Sand (Section 4.7). To take account of this the usual *CBR* parameter is replaced by the product of the moisture content of the sand at the time of testing and the *CBR* value ($wCBR$) and thus:

$$wCBR = 39.60 + 16.02 \log N_p \quad (r = 0.881) \tag{7.16}$$

for data excluding Test TPS1, and

$$wCBR = 41.06 + 15.59 \log N_p \quad (r = 0.809) \tag{7.17}$$

for data including Test TPS1. The relationship defined by Equation 7.16 is illustrated in the inset to Figure 7.5. The alternative compactive effort parameter $N_p/\overline{h}$ yields:

$$wCBR = 3.20 + 27.02 \log \left(N_p/\overline{h}\right) \quad (r = 0.852) \tag{7.18}$$

for data excluding Test TPS1, and

$$wCBR = 3.30 + 27.21 \log \left(N_p/\overline{h}\right) \quad (r = 0.820) \tag{7.19}$$

for data including Test TPS1. The relationship defined by Equation 7.18 is illustrated in the inset to Figure 7.6. The above relationships with high values of

the regression correlation coefficient demonstrate the influence of moisture content on the strength of Permian Sand and emphasise the importance of controlling the moisture content of a material to be compacted. This effect also places considerable emphasis on the need to conduct tests on compacted materials as soon as is practical after compaction in order to avoid the effect of strength increase caused by drying out. Such effects when observed under field conditions will almost certainly be temporary as moisture ingress, due perhaps to rainfall, will soon restore the material to its original (lower) strength condition. Clegg (1985) in his 'Clegg Impact Test Guidelines' emphasises the necessity of testing to determine the Impact Value soon after compaction, so avoiding the possibility of drying out which would indicate higher, temporary strengths or falsely good compaction.

The Clegg meter has been used extensively in the experimental work detailed in this chapter, the Impact Values obtained being used as a simple and quick indicator of the degree of compaction achieved. The measurement of dry density is the traditional method used to assess the compacted state of materials, as has been observed earlier (Section 2.2.1). It is of considerable interest to examine the way in which the Impact Value varied with the dry density. Impact Values determined at the time of compaction are plotted with dry density values in Figure 7.7. Although no significant relationship could be determined for the data including Test TPS1, the exclusion of this data point yields the relationship:

$$IV = -27.59 + 17.48\rho_d \quad (r = 0.466) \qquad (7.20).$$

The anomalous data point shown for Test TPS1 gives further indication of the effect of the petrol driven BS45Y vibratory rammer used in the early stages (layers I–IV) of Test TPS1 which is believed to have applied a greater amount of compactive effort to the Permian Sand than the electrically powered device used in the remainder of that and other tests.

Clegg (1980) showed the relationship between the *CBR* and Impact Value to be given by:

$$CBR = 0.07(IV)^2 \qquad (2.1\text{bis}).$$

The validity of this relationship is tested in Figure 7.8 where the Impact Values determined for the surface of the reinstatement, immediately after the completion of the *CBR* tests, are plotted against their corresponding *CBR* value. The relationship

given by Equation 2.1 is shown for comparison and the experimental data generally show poor agreement with Equation 2.1. For a given Impact Value the *CBR* value is under-estimated. This corresponds to a 'safe' condition in the context of road design.

7.2.2 Surface wave velocity results

The surface wave velocity measurements for Tests TPS1 to TPS5 are reported in some detail in Section 6.2.2 (Table 6.9), and plotted as individual surface wave velocity-depth profiles.

The combined surface wave velocity-depth profiles for Test TPS1 are illustrated in four combinations:

Tests TPS1A and TPS1B—Figure 7.9,

Tests TPS1A and TPS1D—Figure 7.10,

Tests TPS1B and TPS1C—Figure 7.11, and

Tests TPS1C and TPS1D—Figure 7.12.

Figure 7.9 (Tests TPS1A and TPS1B) shows that an increase in the velocity of the lower layers (I–IV) occurs after the placement of the upper layers (V–VIII). This may be due to two factors; firstly additional compactive effort being transmitted to the lower layers during the compaction of the upper layers and secondly due to the stress exerted on the lower layers by the weight of the upper layers (stiffness, or velocity, being stress dependent). No increase in velocity was found by Maxwell (1960), from his tests on a road pavement at various stages of construction (*i.e.* various heights above formation level), which could be attributed to the additional compactive effort applied to the upper layers (see Figure 3.11).

In Section 7.2.1 the cementing effect caused by the calcite present in the Permian Sand, as a result of drying out was identified as the cause of the scattered *CBR* values. This effect may be observed in Figure 7.10 (Tests TPS1A and TPS1D) which show determinations of the surface wave velocity-depth profiles made on essentially the same material but with a considerable time interval of around 106 days between the two tests during which time the upper layers were placed, tested and removed. The velocity shows a marked increase (*circa* 60 m/s) from Test TPS1A to TPS1D. Increases in velocity due to drying out and consequent cementing are also observed in Figure 7.11 (Tests TPS1B and TPS1C) although the effect is not so

marked as that observed in Figure 7.10 since the time delay between Tests TPS1B and TPS1C was plainly not as long as that between Tests TPS1A and TPS1D. A slight decrease in the velocity of the lower layers of Test TPS1C (*cf.* Test TPS1B) is observed from Figure 7.11; this may be due to water migration (downwards) as the upper layers dried out. Figure 5.11 shows the surface wave velocity-depth profiles for Tests TPS1C and TPS1D (*cf.* Figure 3.6, after Jones, 1958 for tests on wet and dry clay sites). The profiles for the lower layers show good agreement, indicating that the increase in velocity of the lower layers observed in Figure 7.9, due to the placement of the upper layers was temporary, permanent increases being attributed to the effects of cementing.

The combined surface wave velocity-depth profiles for Test TPS2 are illustrated in three combinations:

Tests TPS2A and TPS2B—Figure 7.13,

Tests TPS2A and TPS2C—Figure 7.14, and

Tests TPS2B and TPS2C—Figure 7.15.

Comparison of the surface wave velocity-depth profiles for Tests TPS2A and TPS2B (Figure 7.13) shows an increase in the velocity of the lower layers (I–IV) after the placement of the upper layers (V–VIII), although this effect is not as marked as that observed in Figure 7.9 for Tests TPS1A and TPS1B. This may well indicate that for Test TPS2 (with $N_p = 10$) the scope for additional compaction of the already well compacted lower layers was less than that for Test TPS1 (with $N_p = 5$). Figures 7.14 (Tests TPS2A and TPS2C) and 7.15 (Tests TPS2B and TPS2C) indicate that the limited increase in velocity observed in the lower layers due to the placement of the upper layers was temporary, the profiles for Tests TPS2A and TPS2C being almost coincident. This observation lends weight to the assertion, made earlier, that the permanent increase in velocity observed for Test TPS1D (*cf.* Test TPS1A in Figure 7.10) was due to the drying out/cementing effect caused by the calcite present in the Permian Sand.

The combined surface wave velocity-depth profiles for Tests TPS3A and TPS3B, and TPS5A and TPS5B are illustrated in Figures 7.16 and 7.17, respectively. The test with $N_p = 2$ (Test TPS3—Figure 7.16) shows a similar relation between the half-full and full determinations as that observed for TPS1 ($N_p = 5$—Figure 7.9), a significant increase in the velocity of the lower layers (I–IV) occurring after the

placement of the upper layers (V–VIII). In contrast, the test with with $N_p = 8$ (Test TPS5—Figure 7.17) shows a similar relation between the half-full and full determinations as that observed for TPS2 ($N_p = 10$—Figure 7.13); only a limited increase in the velocity of the lower layers (I–IV) occurred after the placement of the upper layers (V–VII).

Two different effects are thus noted as a result of the placement of the upper layers. For tests with low levels of compactive effort, Tests TPS1 and TPS3 ($N_p =$ 5 and 2, respectively), significant increases in the velocity measured in the lower layers are observed as a result of the placement of the upper layers. For tests with high levels of compactive effort, Tests TPS2 and TPS5 ($N_p = 10$ and 8, respectively), the increases in the velocity measured in the lower layers as a result of the placement of the upper layers are not so marked. This would apear to indicate that a limiting state of compaction is being approached by the Permian Sand at a level of compactive effort around $N_p = 8$. This suggests that an over-compacted state may be approached as the level of compactive effort approaches $N_p = 10$ and above.

The half-depth profiles are shown for Tests TPS1A, TPS2A, TPS3A and TPS5A in Figure 7.18. The data generally show an increase in the surface wave velocity with inceasing compactive effort, although the profiles for Tests TPS2A and TPS5A ($N_p = 10$ and 8, respectively) are almost coincident. Full depth profiles for Tests TPS1B, TPS2B, TPS3B, TPS4 and TPS5B are shown in Figure 7.19. The profile for Test TPS1B may be anomalous, as described earlier, while those for Tests TPS2B and TPS5B ($N_p = 10$ and 8, respectively) lie close together, although their relative positions do not indicate that a limiting maximum increase in velocity had almost been achieved at a level of compactive effort equivalent to $N_p = 8$ passes per layer of the vibratory rammer.

The profiles for Tests TPS3B and TPS4 ($N_p = 2$ and 5 and nominal layer thickness $\leq$ 150 and $\leq$ 300 mm, respectively; *i.e.* $N_p/\overline{h} \approx 18\,\mathrm{m}^{-1}$ for both tests) are also very nearly coincident, illustrating the influence of layer thickness on the degree of compaction achieved.

In the early part of this section the various surface wave velocity-depth profiles have been compared and discussed. This method of interpretation is non-numerical. The remainder of this section is therefore devoted to a more detailed, numerical,

analysis using the mean surface wave velocity, $v_{Rz_{max}/2}$, defined as the velocity at the mid-height of the trench, calculated from the regression line:

$$v_{Rz_{max}/2} = c + m.z_{max}/2 \tag{7.21}$$

where z_{max} is the depth to the trench bottom from the surface of the final layer of compacted material. It should be noted that the variation in z_{max} from test to test implies that for any given comparison of $v_{Rz_{max}/2}$ data the depths of propagation to which the values relate will also vary, albeit slightly. The precise form of analysis is the same as that used in Section 7.2.1 (and defined by Equation 7.1) in that the two parameters of compactive effort, N_p and $N_p/\overline{h}$, are utilised.

Taking N_p as the parameter of compactive effort, and examining the data for the half-full trench, yields:

$$v_{Rz_{max}/2} = 73.85 + 119.26 \log N_p \quad (r = 0.974) \tag{7.22}$$

for data excluding Test TPS1, and

$$v_{Rz_{max}/2} = 64.51 + 121.99 \log N_p \quad (r = 0.912) \tag{7.23}$$

for data including Test TPS1. The relationship defined by Equation 7.22 is illustrated in Figure 7.20. Similarly, taking $(N_p/\overline{h})$ to be the parameter of compactive effort, yields:

$$v_{Rz_{max}/2} = -38.39 + 117.90 \log \left(N_p/\overline{h}\right) \quad (r = 0.964) \tag{7.24}$$

for data excluding Test TPS1, and

$$v_{Rz_{max}/2} = -51.02 + 121.23 \log \left(N_p/\overline{h}\right) \quad (r = 0.908) \tag{7.25}$$

for data including Test TPS1. The relationship defined by Equation 7.24 is illustrated in Figure 7.21.

Consideration of the data from tests conducted in the full trench, with N_p being taken as the parameter of compactive effort, yields:

$$v_{Rz_{max}/2} = 133.56 + 54.59 \log N_p \quad (r = 0.950) \tag{7.26}$$

for data excluding Test TPS1, and

$$v_{Rz_{max}/2} = 136.26 + 53.80 \log N_p \quad (r = 0.922) \tag{7.27}$$

for data including Test TPS1. The relationship defined by Equation 7.26 is illustrated in Figure 7.20. Similarly, taking $(N_p/\overline{h})$ to be the parameter of compactive effort, yields:

$$v_{Rz_{max}/2} = 72.02 + 59.43 \log \left(N_p/\overline{h}\right) \quad (r = 0.973) \tag{7.28}$$

for data excluding Test TPS1, and

$$v_{Rz_{max}/2} = 72.15 + 60.62 \log \left(N_p/\overline{h}\right) \quad (r = 0.951) \tag{7.29}$$

for data including Test TPS1. The relationship defined by Equation 7.28 is illustrated in Figure 7.21.

It is immediately apparent that significant relationships exist between the half-depth surface wave velocity and compactive effort for tests conducted in both the half-full and the full laboratory based trench. The regression lines for data excluding Test TPS1 are presented in Figures 7.20 and 7.21, although the omission of these data do not cause major effects on the calculated value of the regression correlation coefficient. This may be interpreted as indicating that the surface wave propagation technique is insensitive to the effects caused by the use of the petrol driven BS45Y, particularly for the results of tests in the half-full trench, and observed as apparently anomalous dry density and Impact Value results in Section 7.2.1.

7.2.3 Derived shear modulus results

The derived shear modulus results for tests on Permian Sand are reported, in detail, in Section 6.2.3 (Table 6.10).

Shear modulus-depth profiles are treated in much the same way as the surface wave velocity-depth profiles from which, along with bulk density values, they are derived. The shear modulus-depth profiles for tests on Permian Sand in the half-full trench are shown in Figure 7.22. The profiles generally show an increase in shear modulus with increasing compactive effort, although the profiles for Tests TPS2A and TPS5A (N_p = 10 and 8, respectively) are interchanged. This may well be indicative of a limiting degree of compaction being achieved at a level of compactive effort of about N_p = 8, subsequent compaction leading to a reduction in the shear modulus due to over-compaction. The profiles follow much the same form as those for the surface wave velocity (Figure 7.18).

The shear modulus-depth profiles for the full trench are shown in Figure 7.23 and again show a very similar form to those for the surface wave velocity (Figure 7.19).

The profile for Test TPS1B appears to be anomalous, as previously discussed at the beginning of Section 7.2. The profiles for Tests TPS2B and TPS5B (N_p = 10 and 8, respectively) lie close together, although their relative positions do not appear to indicate that a limiting level of shear modulus has almost been achieved at a compactive effort of $N_p \approx 8$. The profiles for Tests TPS3B and TPS4 ($N_p/\overline{h} \approx 18$ for both tests) are very nearly coincident indicating the influence of the layer thickness on the level of compaction achieved.

While the foregoing observational approach to the interpretation of the shear moduli data provides a valuable starting point, as with the surface wave velocity data, a more numerical approach yields a more rigid interpretative framework. In order to achieve this the mean shear modulus, $G_{z_{max}/2}$, is utilised. This parameter is of similar derivation to that for the mean surface wave velocity ($v_{Rz_{max}/2}$), described in Section 7.2.2 (Equation 7.21).

Taking N_p to be the parameter of compactive effort, and examining the data from tests on the half-full trench, yields:

$$G_{z_{max}/2} = 4.02 + 77.33 \log N_p \quad (r = 0.964) \tag{7.30}$$

for data excluding Test TPS1, and

$$G_{z_{max}/2} = -2.67 + 79.29 \log N_p \quad (r = 0.892) \tag{7.31}$$

for data including Test TPS1. The relationship defined by Equation 7.30 is illustrated in Figure 7.24. Similarly, taking $(N_p/\overline{h})$ to be the parameter of compactive effort, yields:

$$G_{z_{max}/2} = -68.50 + 76.31 \log \left(N_p/\overline{h}\right) \quad (r = 0.952) \tag{7.32}$$

for data excluding Test TPS1, and

$$G_{z_{max}/2} = -77.62 + 78.70 \log \left(N_p/\overline{h}\right) \quad (r = 0.887) \tag{7.33}$$

for data including Test TPS1. The relationship defined by Equation 7.32 is illustrated in Figure 7.25.

Consideration of the tests conducted in the full trench, with N_p taken as the parameter of compactive effort, yields:

$$G_{z_{max}/2} = 47.84 + 32.53 \log N_p \quad (r = 0.968) \tag{7.34}$$

for data excluding Test TPS1, and

$$G_{z_{max}/2} = 57.74 + 31.09 \log N_p \quad (r = 0.764) \tag{7.35}$$

for data including Test TPS1. The relationship defined by Equation 7.34 is illustrated in Figure 7.24. Similarly, taking $(N_p/\overline{h})$ to be the parameter of compactive effort, yields:

$$G_{z_{max}/2} = 7.00 + 37.58 \log \left(N_p/\overline{h}\right) \quad (r = 0.973) \tag{7.36}$$

for data excluding Test TPS1, and

$$G_{z_{max}/2} = 7.22 + 39.56 \log \left(N_p/\overline{h}\right) \quad (r = 0.848) \tag{7.37}$$

for data including Test TPS1. The relationship defined by Equation 7.36 is illustrated in Figure 7.25.

It is immediately apparent that, as for the equivalent surface wave velocity results, significant relationships exist between the mean shear modulus $(G_{z_{max}/2})$ and compactive effort for tests conducted in both the half-full and full trench. The values of the regression correlation coefficient (r) generally have slightly lower values than for their surface wave velocity equivalents and also show a larger decrease when the data from the potentially anomalous Test TPS1 is included. Both these effects may be attributed to the influence of the bulk density results in the calculation of the shear modulus $(G \approx \rho v_R^2)$. The bulk density results generally exhibit a higher degree of scatter (see also Section 7.2.1) than do the surface wave velocity results.

7.2.4 Surface wave attenuation results

The attenuation of a Rayleigh wave is generally considered to be described by Bornitz's (1931) equation (Equation 3.34). The evaluation of the material attenuation coefficient, α, is difficult because the derived value may be heavily dependent upon the initial selected values of the distance from the source, x_1, and the corresponding particle vertical displacement, w_1 .

The purpose of surface wave attenuation measurements is generally to describe the structural risk to buildings adjacent to sources of vibration (Forssblad, 1965; Bergström and Linderholm, 1946) and also in the assessment of potential screening structures designed to reduce the amplitude of the transmitted vibrations (Richart *et al*, 1970; Woods and Richart, 1967; Woods, 1968) so limiting the potential damage to adjacent structures.

The evaluation of the surface wave material attenuation coefficient is essential to the full description of the decay of vibration amplitudes with distance from a source of vibration. A new technique is proposed for the analysis of such data which allows the evaluation of α while obviating the need for potentially unreliable estimates of the initial conditions (x_1, w_1). It should aid significantly the reliable interpretation of surface wave attenuation data (Section 5.6.3—Equation 5.10).

Although the regression correlation coefficients (r) are low for some of the data sets, as presented in Figures 6.15, 6.16 and 6.17 and Table 6.11, this is likely to be due to the tendency of the slope (surface wave material attenuation coefficient, α) towards zero, thus causing a lower value of r than might be expected from the visual scatter of the data points (see Section 5.1).

The first steps towards illustrating the potential usefulness of this technique in terms of the frequency dependency of α were taken by Davies (1989) and the practical applications of the technique in terms of vibrational hazards due to road and rail traffic, and construction activities are illustrated by Winter and Selby (In Preparation). Further discussion of this technique is outside the scope of the work presented here.

In attempting to interpret the measured material attenuation coefficient (α) in terms of the applied compactive effort, N_p or $N_p/\overline{h}$, no consistent relations have been found. The values of the regression correlation coefficients, for interpretation of the form of Equation 7.1, vary considerably; some values are positive and some are negative (Figures 6.15, 6.16 and 6.17 and Table 6.11). These data imply that there is no obvious relationship between α and compactive effort and this avenue will not be pursued further.

7.2.5 Particle displacement at depth results

Results for the measurement of particle displacement at depth (Section 6.2.5) are presented in Figures 6.18, 6.19 and 6.20 in normalised form, displacement at depth z divided by displacement at the surface against depth divided by wavelength (*i.e.* w_z / $w_{z=0}$ against z/λ). The results are overlain on the theoretical curves, based on the factor describing the rate of attenuation of the vertical dynamic displacement with depth, described in Section 3.4.3, for the normal range of Poisson's ratio, $0 < \nu \leq 0.5$. Each of the three data sets presented form trends which tend to

conform, approximately, to the shape of the theoretical curves. Experimental observations indicate that the nature of the contact between the sand surface and the surface transducer may be different to that between the buried transducers and the surrounding sand so introducing errors to the entire data set as the surface derived value of displacement is used for normalisation (see Figure 6.19).

In theory it should be possible to estimate an approximate value for Poisson's ratio from the experimental data plotted with the normalised displacement-depth curves, although in practice this procedure is sufficient only to provide qualitative confirmation, or otherwise, for values obtained using either alternative experimental techniques or from examination of the literature. Whichever means is used to determine the Poisson's ratio it is essential to give some consideration to the strain level to which the material in the laboratory based trench is subjected. Krizek (1977) demonstrated the strain dependency of the Poisson's ratio of Kaolin. Over a range of axial strain of $0 \leq \epsilon_1 \leq 8\%$ (ϵ_1 being the axial strain measured from unconfined compression tests) the Poisson's ratio varied, approximately logarithmically, in the range $0 < \nu \leq 0.5$. In discussing the behaviour of sands subjected to low strains Hardin (1978) reports, *'the value of Poisson's ratio (ν) lies somewhere between 0 and 0.2. Any value within this range is accurate for most purposes. The author's favourite value is 0.12'.*

The experimental normalised displacement-depth curves generally confirm the low values of Poisson's ratio described by Hardin (1978), with the exception of the data illustrated in Figure 6.19 for sands subjected to low strain levels. The results are not, however, sufficiently precise to provide a quantitative estimate of the Poisson's ratio.

Perhaps an even more important consideration than the value of the Poisson's ratio to arise from the normalised displacement-depth curves is the depth of surface wave propagation approximation, $z = \lambda/2$ (Equation 3.6) noted in Section 3.3. This assumption is based on the fact that the theoretical curves taper to almost zero displacement at a depth of one wavelength, in particular at low values of Poisson's ratio; thus a depth of propagation of approximately one-half of one wavelength is indicated. The experimental results tend to confirm this assumption.

7.2.6 Summary

Logarithmic-linear least squares regression analyses have been performed on the data from tests on the Permian Sand, conducted in the laboratory based trench, to enable the interpretation of the data for dry density, Impact Value, *CBR* (corrected for moisture content), mean surface wave velocity and the mean derived shear modulus ($G \approx \rho v_R^2$) in terms of compactive effort. The compactive effort is defined in two different ways: as the number of passes applied per layer (N_p) and also as the number of passes applied per layer divided by the mean layer thickness ($N_p/\overline{h}$).

From the above mentioned analyses strong correlations of the various parameters with compactive effort are generally found. This holds true especially if the data from Test TPS1 are rejected. These data are held to be anomalous due to the long time delay between compaction and subsequent excavation allowing the limited Calcite present (Chapter 4) to act as a cement as the sand dried out. The use of a petrol driven vibratory rammer, in stead of the usual electrically driven device, is also identified as a probable source of error. Values of the regression correlation coefficient (r) derived from such analyses vary between 0.433 and 1.000; only the dry density analyses exhibiting values of $r < 0.85$ if data from Test TPS1 are excluded.

In evaluation of the suitability of a parameter for use in the assessment of reinstatement backfill quality the degree of numerical sensitivity (S) to the applied compactive effort is of great importance. Such an interpretation of the data is given in Table 7.1 for a change in compactive effort from $N_p/\overline{h} = 15\,\mathrm{m}^{-1}$ to $N_p/\overline{h} = 90\,\mathrm{m}^{-1}$. It is clear from the tests on Permian Sand that the Impact Value is most sensitive to compactive effort ($S = 75.3\%$). The mean surface wave velocity has a sensitivity of 28.0% while the dry density has a sensitivity of just 2.2%, which is, at least in part, due to the false origin inherent within the density parameter. The high value of sensitivity of the mean derived shear modulus to compactive effort ($S = 44.4\%$), compared to that for the mean surface wave velocity, is due to the shear modulus being proportional to the square of the surface wave velocity ($G \propto v_R^2$) thus making the shear modulus more sensitive to changes in compactive effort.

This simple form of analysis shows the Impact Value to be considerably more sensitive to changes in compactive effort than is the surface wave velocity which is, in turn, more sensitive than the dry density.

A tentative material-dependent relationship between the Impact Value and the dry density, with a relatively poor correlation ($r = 0.466$), has been proposed for the Permian Sand. The measured data deviated from Clegg's (1980) proposed function of Equation 2.1, albeit over a limited test range. A *CBR* value derived from Equation 2.1 would be an under estimate.

More detailed examination of the surface wave velocity-depth profiles for the individual tests tends to confirm the drying effects noted earlier. Some evidence of a limiting surface wave velocity, or shear modulus, being approached at a compactive effort equivalent to around $N_p = 8$ ($h < 150$ mm) is found from the results from tests conducted in the half-full laboratory based trench. The existence of such a phenomenon is not supported by the results from tests conducted in the full laboratory based trench; these effects are, therefore, attributable to variations in the properties of the test material and/or to experimental error. These plots also show the influence of the layer thickness on the measured properties; for the two tests with $N_p/\overline{h} \approx 18\ \mathrm{m}^{-1}$ (Tests TPS3B and TPS4) the surface wave velocity-depth profiles are very nearly coincident.

Comparison of the surface wave velocity-depth profiles from tests in the half-full and the full trench reveals distinct differences in the influence of the placement of the upper layers on the properties of the lower layers. The placement of the upper layers at low levels of compactive effort ($N_p = 2$ and 5) appears to increase the measured surface wave velocity of the lower layers. In contrast, the placement of the upper layers at high levels of compactive effort ($N_p = 8$ and 10) leads to a much smaller increase in the surface wave velocity of the lower layers. This observation may be considered to reflect the existence of a 'law of diminishing returns' with respect to the compaction process, and lends support to the use of logarithmic scales for compactive effort when interpreting measured properties in terms of the compactive effort applied.

The surface wave attenuation results have been interpreted in terms of the material absorption coefficient (α), using a new form of the Bornitz equation which allows α to be determined without the need to make potentially erroneous assumptions (albeit from the experimental data) regarding the state of the distance-displacement (attenuation) curve close to the vibratory source. Consistent relations between compactive effort and α could not be found.

The measurements of particle displacement at depth, by means of buried accelerometers, generally lend support to the basic assumption that the effective depth of propagation, z, of a Rayleigh-type surface wave is approximately equal to one-half the wavelength (*i.e.* $z = \lambda/2$).

7.3 Measurements on Sharp Sand

The format of this section largely follows that of Section 7.2, in which the results of tests conducted in the laboratory based trench on the Permian Sand were discussed. Complicating effects, such as long time delays between individual tests in a suite of tests and the use of a petrol driven vibratory rammer in place of the more usual electrically driven device (*i.e.* Test TPS1) were avoided in the tests on the Sharp Sand.

7.3.1 Density, moisture content, Impact Value and CBR results

Detailed data for these parameters are presented in Section 6.3.1 and the particular data used in the analyses presented here are detailed in Table 6.12, for results obtained at the time of compaction, and in Table 6.13, for results obtained at the time of excavation.

The moisture content during the compaction of the Sharp Sand in the laboratory based trench was carefully controlled using the procedure described in Section 5.3.1 and Appendix 4. It was observed in Section 4.4.6 (Table 4.3) that the optimum moisture content varied with compactive effort. The BS 1377 (1975): Test 12 determinations of the optimum moisture content (Table 4.3) were 13.7, 12.8 and 11.6% for $N_b = 27, 54$ and 81 blows per layer. Simple observation revealed, however, that this material at such moisture contents was too wet too handle in the large quantities needed to fill the laboratory based trench. As such a 'target' moisture content was set at 10%; at this moisture content the Sharp Sand was easily handled and very workable. This 'target' of $w = 10.0 \pm 1.0\%$ ($9.0\% \leq w \leq 11.0\%$) was achieved during the compaction process as can be seen from the moisture content data, measured immediately after compaction and presented in Table 6.12.

Taking the number of passes per layer (N_p) as the compactive effort parameter, and fitting dry density data to the corresponding values of $\log N_p$, yields:

$$\rho_d = 1.516 + 0.216 \log N_p \quad (r = 0.847) \qquad (7.38).$$

This relationship is illustrated in Figure 7.1. Taking $N_p/\overline{h}$ as the compactive effort parameter yields:

$$\rho_d = 1.450 + 0.140 \log(N_p/\overline{h}) \quad (r = 0.670) \qquad (7.39).$$

This relationship is illustrated graphically in Figure 7.2. The lower value of regression correlation coefficient for the data with the compactive effort parameter taken as $(N_p/\overline{h})$ may be explained by consideration of Test TSS4 in which the layer thickness was approximately twice that of the other tests. D' Appolonia *et al* (1969) showed that for sand compacted using a single drum vibratory roller the dry density increased rapidly from the surface of the layer to within around $1/5h$ of the base of the layer before decreasing towards the interface with the underlying layer. This is qualitatively supported by the work of Moorhouse and Baker (1969). As the density rings were placed prior to compaction, each successive pass of the vibratory rammer forced the density rings slightly deeper within the layer. Thus, for the two data points with $N_p/\overline{h} \approx 18\,\mathrm{m}^{-1}$, one representing two passes per layer and the other representing five passes per layer it is likely that, all other factors being constant, the latter test will yield a higher value of dry density because the density ring had been forced further down the curve of increasing dry density with depth. This explanation is qualitatively supported by the data presented in Figure 7.2, and the same argument has also been applied to similar data, from the tests conducted on the Permian Sand, and presented in Section 7.2.1.

Taking a similar approach for the interpretation of the Impact Value data, obtained at the time of compaction, yields:

$$IV = 2.10 + 4.48 \log N_p \quad (r = 0.996) \qquad (7.40).$$

Data obtained as the laboratory trench reinstatements were excavated yields:

$$IV = 3.58 + 7.02 \log N_p \quad (r = 0.994) \qquad (7.41).$$

These data are illustrated in Figure 7.3 with the logarithmic regression lines represented by Equations 7.40 and 7.41. Plainly the relationships between the logarithm of the number of passes per layer and the Impact Value are significant, with high values of the regression correlation coefficient.

Taking the compactive effort parameter to be $N_p/\overline{h}$ for data at the time of compaction yields:

$$IV = 0.30 + 3.15 \log(N_p/\overline{h}) \quad (r = 0.850) \qquad (7.42).$$

Data similarly obtained at the time of excavation yields:

$$IV = -1.95 + 6.39 \log(N_p/\overline{h}) \quad (r = 0.985) \qquad (7.43).$$

These data are illustrated graphically with the logarithmic regression lines described above in Figure 7.4. Plainly the relationships between the logarithm of the number of passes per layer divided by the mean layer thickness and the Impact Value are also significant, with high values of the regression correlation coefficient.

The Impact Value results show the Clegg meter to be an excellent device for measuring reinstatement backfill quality where measurement from the final surface of the completed unbound layers is not necessary, as has been previously observed from the Permian Sand data (Section 7.2.1).

California Bearing Ratio (CBR) data, with the parameter of compactive effort taken as N_p, yields:

$$CBR = 3.89 + 2.88 \log N_p \quad (r = 0.641) \qquad (7.44).$$

This relationship is illustrated in Figure 7.5. Analysis of the data with the alternative compactive effort parameter $N_p/\overline{h}$ yields:

$$CBR = 4.23 + 1.21 \log(N_p/\overline{h}) \quad (r = 0.310) \qquad (7.45).$$

This relationship is illustrated in Figure 7.6. The above relationships yield low values of the regression correlation coefficient compared to those for the Impact Value. This effect may to some degree be due to the fact that the available time permitted only one CBR determination to be made, while each data point for the IV in Figures 7.3 and 7.4 represents between 15 (Test TSS4) and 40 determinations of the Impact Value.

In Section 7.2.1 a relationship between the dry density and the Impact Value for Permian Sand was derived and although the regression correlation coefficient (r) was low (*circa* 0.47) there was some suggestion that a unique material-dependent

relationship may derived for the data achieved from tests on the Permian Sand. A similar treatment of the data achieved from tests on the Sharp Sand yields:

$$IV = -19.10 + 14.10\rho_d \quad (r = 0.826) \qquad (7.46).$$

This relationship is illustrated in Figure 7.7. Such data adds further credence to the existence of unique dry density-Impact Value relationships for each material. It should be noted, however, that attempts to incorporate the field data for the Sharp Sand layers underlying the Wet-mix macadam layers (Section 6.5.1 and Table 6.22), which was compacted at a moisture content 'dry' of the 'target' moisture content (Section 7.5), renders the relationship, as defined by Equation 7.46, intractable by virtue of a very low value of r. It is thus suggested that the unique ρ_d-IV relationships illustrated for each material in Figure 7.7 are dependent upon compaction being carried out at consistent moisture contents.

Clegg (1980) proposed a relationship between the *CBR* and Impact Values as

$$CBR = 0.07(IV)^2 \qquad (2.1\text{bis}).$$

The validity of this relationship is tested in Figure 7.8 where the Impact Values determined for the surface of the reinstatement, immediately after the completion of the *CBR* tests, are plotted against their corresponding *CBR* value. The relationship given by Equation 2.1 is shown for comparison and the fit of the data to this expression is poor for tests conducted on both the Sharp Sand and the Permian Sand (Section 7.2.1). For a given Impact Value the *CBR* value is under-estimated. This corresponds to a 'safe' condition in the context of road design.

7.3.2 Surface wave velocity results

The surface wave velocity measurements for Tests TSS1 to TSS5 are reported in some detail in Section 6.3.2 (Table 6.14), and plotted as individual surface wave velocity-depth profiles.

Combined velocity-depth profiles are presented for each test suite (TSS1, TSS2, TSS3 and TSS5) in Figures 7.26 to 7.29. While the comparison of the results obtained from tests on Permian Sand (Section 7.2.2) showed a clear division in the form of the half-full trench results compared to the full trench results dependent upon the level of compactive effort applied, there appears to be no such clear-cut

division of the results presented for Sharp Sand. All tests conducted on the Sharp Sand (half-full profiles compared to full profiles) exhibit the increase in surface wave velocity of the lower layers after compaction of the upper layers, regardless of the level of compactive effort. This may possibly be due to an effect noted during the BS 1377 (1975): Test 12 laboratory compaction tests conducted on the Sharp Sand (this effect was not noted in Chapter 4). It was observed that compaction of the first layer in the BS 1377 compaction test mould densified the material by only a very small amount and likewise for the second and third layers. The bulk of the energy applied as compactive effort appeared to be used up in simply moving the material in the compaction mould. When the compaction mould baseplate was removed it was noted that the material placed as the first layer was now much more dense than the material placed as either the second or third layers. Directly applied compactive effort appears to be much less efficient than compactive effort applied as overlying layers are compacted. It might reasonably be expected that this would be supported by the dry density and Impact Values obtained at the time of excavation (Tables A6.12, A6.14, A6.16, A6.18 and A6.20). Careful examination of the dry density results indicates that, despite some considerable scatter in the results, there is a general trend of increasing dry density with depth. The Impact Value results show no such effects but the reasons for this are simply explained. The Impact Values obtained during excavation do not represent the surface of each layer but any point at which excavation was ceased and the surface of the excavatiod levelled to obtain such data. The properties of the compacted material may be expected to vary considerably within any layer (see D' Appolonia *et al*, 1969—variation in dry density within a compacted layer; Sections 7.2.1 and 7.3.1) and as such it is unreasonable to expect to isolate effects which are a function of the depth of placement of a layer, unless data can be obtained at a predetermined point within each layer as is the case for the dry density results.

The half-full profiles for Tests TSS1A, TSS2A, TSS3A and TSS5A are combined in Figure 7.30. The profiles for Tests TSS1A, TSS3A and TSS5A are convergent at approximately the mid-height of the compacted material. The profiles show no obvious trends with compactive effort, although this will be discussed in more detail later in this section. The profiles cover an extremely narrow range of velocity, much lower than that determined from the tests on Permian Sand. Full depth profiles for Tests TSS1B, TSS2B, TSS3B, TSS4 and TSS5B are combined in Figure 7.31. Apart

from the two profiles with $N_p/\overline{h} \approx 18\,\mathrm{m}^{-1}$ (Tests TSS3B and TSS4) being almost coincident, no obvious trends are apparent from the data and as for the tests on the half-full trench the profiles cover a much smaller range of surface wave velocity than that determined from the tests on Permian Sand.

Thus far the various surface wave velocity-depth profiles have been discussed. This method of interpretation is non-numerical. The remainder of this section is devoted to a more detailed, numerical, analysis using the mean surface wave velocity, $v_{Rz_{\max}/2}$, defined as the velocity at the mid-height of the compacted material and calculated from Equation 7.21.

Taking N_p as the parameter of compactive effort, and examining the data for the half-full trench, yields:

$$v_{Rz_{\max}/2} = 108.62 + 14.26 \log N_p \quad (r = 0.504) \qquad (7.47).$$

This relationship is illustrated in Figure 7.32. Taking $N_p/\overline{h}$ as the parameter of compactive effort yields:

$$v_{Rz_{\max}/2} = 96.31 + 13.50 \log(N_p/\overline{h}) \quad (r = 0.482) \qquad (7.48).$$

This relationship is illustrated in Figure 7.33.

Data for the full trench, with N_p as the parameter of compactive effort, yields:

$$v_{Rz_{\max}/2} = 151.36 + 29.02 \log N_p \quad (r = 0.974) \qquad (7.49).$$

This relationship is illustrated in Figure 7.32. Taking $N_p/\overline{h}$ as the parameter of compactive effort yields:

$$v_{Rz_{\max}/2} = 113.82 + 34.32 \log(N_p/\overline{h}) \quad (r = 0.964) \qquad (7.50).$$

This relationship is illustrated in Figure 7.33.

It is immediately apparent that significant relationships exist between the mean surface wave velocity and compactive effort for tests conducted in both the half-full and full trench. The levels of significance for the relationships relating to data determined from tests on the half-full trench are somewhat lower than the full trench equivalents, as exemplified by the lower values of the regression correlation coefficient (r) for the half-full trench results. This may be attributed to the convergance of the

profiles for Tests TSS1A, TSS3A and TSS5A at a depth which corresponds approximately to the mean depth of the compacted material, or the depth corresponding to the mean velocity, $v_{Rz_{max}/2}$.

7.3.3 Derived shear modulus results

The derived shear modulus results for tests on Sharp Sand are reported, in detail, in Section 6.3.3 (Table 6.15).

Shear modulus-depth profiles are treated in much the same way as the surface wave velocity-depth profiles from which, along with the bulk density values, they are derived. The shear modulus-depth profiles for tests on Sharp Sand in the half-full trench are illustrated in Figure 7.34. As was also observed from the surface wave velocity results the spread of values is limited in comparison to the equivalent tests results for Permian Sand. It is interesting to note that the effect of the density on the transition of surface wave velocity to shear modulus has led to the convergence of the velocity-depth profiles, observed at around the mid-height of the compacted material (for Tests TSS1A, TSS3A and TSS5A), being effectively moved upwards to a level around 0.1 m from the surface, for the shear modulus-depth profiles.

The shear modulus profiles for tests on Sharp Sand in the full trench are shown in Figure 7.35. The profiles show a general trend of increasing shear modulus with increasing compactive effort, with the exception of Test TSS1B ($N_p = 5$).

While the foregoing observational approach to the interpretation of the shear moduli data provides a valuable starting point, as with the surface wave velocity data, a more numerical approach yields a more rigid interpretative framework. In order to achieve this the mean shear modulus, $G_{z_{max}/2}$, is utilised. This parameter is of similar derivation to the mean surface wave velocity ($v_{Rz_{max}/2}$), as described in Section 7.2.2 (Equation 7.21).

Taking N_p to be the parameter of compactive effort, and examining data from tests on the half-full trench, yields:

$$G_{z_{max}/2} = 20.66 + 15.42 \log N_p \quad (r = 0.848) \qquad (7.51).$$

This relationship is illustrated in Figure 7.36. Taking $N_p/\overline{h}$ to be the parameter of compactive effort, yields:

$$G_{z_{max}/2} = 6.69 + 14.99 \log(N_p/\overline{h}) \quad (r = 0.832) \qquad (7.52).$$

This relationship is illustrated in Figure 7.37.

Data from tests in the full trench, with N_p taken to be the parameter of compactive effort, yields:

$$G_{z_{max}/2} = 51.66 + 26.34 \log N_p \quad (r = 0.726) \qquad (7.53).$$

This relationship is illustrated in Figure 7.36. Taking $N_p/\overline{h}$ to be the parameter of compactive effort, yields:

$$G_{z_{max}/2} = 20.19 + 29.82 \log(N_p/\overline{h}) \quad (r = 0.826) \qquad (7.54).$$

This relationship is illustrated in Figure 7.37.

It is immediately apparent that significant relationships exist between the mean shear modulus ($G_{z_{max}/2}$) and compactive effort for tests conducted in both the half-full and full trench. It is of particular interest to note that the significance of the relationships for tests in the half-full trench are greater than for the equivalent surface wave velocity results due to the influence of the bulk density in the calculation of the shear modulus.

7.3.4 Surface wave attenuation

The new technique for the analysis of surface wave attenuation data was presented in Section 5.6.3 (Equation 5.10), and described further, in terms of its practical use, in Section 7.2.4. In common with the results of tests on Permian Sand the results of tests on Sharp Sand generally exhibit low values of the regression correlation coefficient (r)—see Figures 6.30, 6.31, ..., 6.34 and Table 6.16—and as previously described in Section 7.2.4 this is likely to be due to the slope of Equation 5.10 (the material attenuation coefficient, α) tending towards zero (see Section 5.1).

In common with the Permian Sand test results, interpretation in terms of compactive effort yields no consistent relations. Values of the regression correlation coefficient, for interpretation of the form of Equation 7.1, vary considerably; some values are positive and some values are negative. These data imply that there is no relationship between the material attenuation coefficient (α) and compactive effort, and this avenue will not be pursued further.

7.3.5 Summary

Logarithmic-linear least squares regression analyses have been performed on the data from tests on the Sharp Sand, conducted in the laboratory based trench, to enable the interpretation of the data for dry density, Impact Value, *CBR*, mean surface wave velocity and the mean derived shear modulus ($G \approx \rho v_R^2$) in terms of compactive effort. The compactive effort is defined in two different ways: as the number of passes applied per layer (N_p) and also as the number of passes applied per layer divided by the mean layer thickness ($N_p/\overline{h}$).

From the above-mentioned analyses strong correlations of the various parameters with compactive effort are genarally found. Values of the regression correlation coefficient (r) derived from such analyses vary between 0.310 and 0.996, only the dry density and *CBR* analyses exhibiting values of r much less than 0.50. The scatter of the data for dry density and mean surface wave velocity appear to be, to some extent, mutually compensating as the mean derived shear moduli data exhibit more significant correlations with compactive effort than do either of the two parameters from which they are derived.

In evaluation of the suitability of a parameter for use in the assessment of reinstatement backfill quality the degree of numerical sensitivity (S) to the applied compactive effort is of great importance. Such an interpretation of the data is given in Table 7.1 for a change in compactive effort from $N_p/\overline{h} = 15\,\mathrm{m}^{-1}$ to $N_p/\overline{h} = 90\,\mathrm{m}^{-1}$. It is clear from the tests on Sharp Sand that the Impact Value is most sensitive to compactive effort ($S = 47.0\%$). The mean surface wave velocity has a sensitivity of 15.9% while the dry density has a sensitivity of just 6.5%, which is, at least in part, due to the false origin inherent within the density parameter. The high value of sensitivity of the mean derived shear modulus to compactive effort ($S = 34.7\%$), compared to that for the mean surface wave velocity, is due to the shear modulus being proportional to the square of the surface wave velocity ($G \propto v_R^2$), thus making the shear modulus more sensitive to changes in compactive effort. Additionally, the sensitivity of the *CBR* to compactive effort is calculated as 16.3%.

This simple form of analysis shows the Impact Value to be considerably more sensitive to changes in compactive effort than is the surface wave velocity which is, in turn, more sensitive than the dry density.

A material dependent relationship between the Impact Value and the dry density, with a strong correlation ($r = 0.826$), has been proposed for the Sharp Sand and the *IV-CBR* data compared to Clegg's (1980) relationship indicating that the *CBR* value would be under-estimated from Equation 2.1.

Detailed examination of the surface wave velocity-depth profiles for the individual tests shows the influence of the layer thickness on the measured properties; for the two tests with $N_p/\overline{h} \approx 18\,\mathrm{m}^{-1}$ (Tests TSS3B and TSS4) the surface wave velocity-depth profiles are very nearly coincident.

A strong argument is put forward that the Sharp Sand does not densify efficiently as a result of directly applied compactive effort. Significant densification was, however, indicated due to the compactive effort applied to subsequent layers.

The surface wave attenuation results have been interpreted in terms of the material absorption coefficient (α), using a new form of the Bornitz equation which allows α to be determined without the need to make potentially erroneous assumptions (albeit from the experimental data) concerning the state of the distance-displacement (attenuation) curve close to the vibratory source. Consistent relations between compactive effort and α could not be found.

7.4 Measurements on Wet-mix macadam

The format of this section largely follows that of Sections 7.2 and 7.3, in which the results of tests conducted in the laboratory based trench on the Permian Sand and Sharp Sand were discussed. Experimental procedures for the field tests were essentially the same as those for tests conducted in the laboratory based trench. The major exception was that density measurements were achieved using the sand replacement method described in BS 1377 (1975): Test 15(A) (see Section 5.5.2).

For the single test (Test WMM10) in which the Wet-mix macadam was delivered, placed and compacted in a 'dry' condition ($w \approx 0\%$) density measurements were not possible. Excavation of the hole for sand replacement caused the collapse of the surrounding material. Consequently, the shear modulus determination for this test was also not possible (as $G \approx \rho v_R^2$). The results from Test WMM10 might reasonably be expected not to conform wth those of the other tests (in which $w \approx w_{\mathrm{opt}}$), due to the dry condition of the compacted material, and so the data are not included in analyses of the form of Equation 7.1. Data are, however, shown for comparison in the appropriate figures and appropriate comments are made regarding the relationship

of the dry soil data to the data from tests conducted on material at, or about, the optimum moisture content.

For convenience, the tests in which layers of Wet-mix macadam and Sharp Sand were combined in the same reinstatement (Tests WMM7, WMM8 and WMM9) are discussed in terms of the properties of the Wet-mix macadam in this section and only the specific effects caused by the combination of the two material types will be discussed in Section 7.5.

The lack of availability of a heavy truck, or similar vehicle, to provide the reaction to applied loads, meant that it was impossible to conduct *CBR* tests in the field trenches.

Three deliveries of Wet-mix macadam were made to the Blaydon test site, the first prior to Test WMM1, the second prior to Test WMM6 and a third of 'dry' material for Test WMM10 immediately prior to the commencement of reinstatement of that trench. The first two deliveries of Wet-mix macadam were made at a moisture content approximating to the optimum moisture content determined to BS 5835: Part 1 (1980) ($w_{\text{opt}} = 4.6\%$—see Table 4.3). Examination of the data for post-compaction moisture content (Tables 6.17 and 6.22) shows that a steady drying out of the stockpiled material occurred.

7.4.1 Density, moisture content and Impact Value results

Detailed data for these parameters are presented in Sections 6.4.1 and 6.5.1 and the particular data used in the analyses presented here are detailed in Tables 6.17 and 6.22.

The Department of Transport (1986) (see Appendix 3) specify that Wet-mix macadam should be compacted within 0.5% of the optimum moisture content, *i.e.* $w_{\text{opt}} \pm 0.5\%$, where w_{opt} is determined to BS 5835: Part 1 (1980); from Table 4.3 $w_{\text{opt}} = 4.6\%$, giving an allowable range of $4.1\% \leq w \leq 5.1\%$. Examination of the post-compaction moisture content data, given with the density data in Tables 6.17 and 6.22, indicates that on three occasions these limits were exceeded:

i)Test WMM5; $\overline{w} = 4.03\%$, $\sigma_{w_{n-1}} = 0.83\%$,

ii)Test WMM8; $\overline{w} = 4.00\%$, $\sigma_{w_{n-1}} = 0.43\%$, and

iii)Test WMM9; $\overline{w} = 3.75\%$, $\sigma_{w_{n-1}} = 0.47\%$.

In the case of Test WMM5 this effect may be attributed to the low moisture content observed for Layer I (see Table A6.25) which was found to be 2.84%. The moisture content of the stockpile, determined after the placement of Layer I was 5.36% (see Table A6.25) indicating that the density measurement may have been made in an area of low moisture content, caused by some of the dry surface material from the stockpile being placed in error. This would tend to indicate that the moisture content determined for Layer I was unrepresentative of the moisture content of the layer. This is supported by the dry density measured for Layer I being somewhat lower than that found for the lower layers. No such simple explanations are available to explain the low mean moisture contents reported for Tests WMM8 and WMM9. The 'out-of-range' moisture contents are not felt to be excessive and are, due to the general drying out effect (noted in Section 7.4), on the 'dry' side of optimum and not on the 'wet' side of optimum where very rapid decreases in strength, and stiffness, may occur with increasing moisture content. It is worth noting that the stockpile moisture contents were determined from samples taken from the excavated face after placement of each layer. These moisture contents are representative of the wettest portion of the stockpile.

In addition, the material used for Test WMM10 was delivered, placed and compacted in a condition approximating to zero moisture content (in fact $\overline{w} = 0.55\%$— Table A6.27) in order to assess the sensitivity of the various test methods to this extreme of moisture content. Although the moisture content of the material tested was slightly above zero it may be considered to behave, during compaction, as if $w = 0\%$, since the moisture content measured was somewhat lower than the absorbed moisture content, reported in Section 4.3 (Table 4.2) as $w_A = 0.8\%$, and since the material was in a surface dry condition. This was borne out by a visual examination of the 'dry' Wet-mix macadam. It had been hoped to test at a moisture content of around 2% but a supplier could not be found for such material and the controlled drying out of sufficient material was deemed impractical due to time constraints and also due to the lack of an extensive covered storage area on site.

Taking the number of passes per layer, N_p, as the parameter of compactive effort and fitting dry density data to the corresponding value of $\log N_p$, yields:

$$\rho_d = 1.765 + 0.371 \log N_p \quad (r = 0.976) \tag{7.55}$$

for test data with the nominal layer thickness < 150 mm, and

$$\rho_d = 1.803 + 0.268 \log N_p \quad (r = 0.913) \tag{7.56}$$

for test data with the nominal layer thickness < 200 mm. These relationships are illustrated in Figure 7.1.

Taking $N_p/\overline{h}$ as the parameter of compactive effort, and combining the two data sets, yields:

$$\rho_d = 1.526 + 0.318 \log(N_p/\overline{h}) \quad (r = 0.957) \tag{7.57}.$$

This relationship is illustrated in Figure 7.2. In contrast to the dry density data for the Permian Sand and the Sharp Sand, which may be seen as representative of a one-inch deep band within the layer, the dry density data for the Wet-mix macadam may be seen as representative of the average properties of the layer at the point of testing, the hole for sand replacement being around 100 mm deep. The correlations between dry density and compactive effort, given by Equations 7.55, 7.56 and 7.57, are significant, the calculated regression correlation coefficient (r) being, in all three cases, greater than 0.9.

Taking a similar interpretative approach to the Impact Value data, with N_p taken to be the parameter of compactive effort, yields:

$$IV = 7.38 + 17.42 \log N_p \quad (r = 0.999) \tag{7.58}$$

for test data with the nominal layer thickness < 150 mm, and

$$IV = 12.82 + 10.10 \log N_p \quad (r = 0.754) \tag{7.59}$$

for test data with the nominal layer thickness < 200 mm. These relationships are illustrated in Figure 7.3.

Taking $N_p/\overline{h}$ as the parameter of compactive effort, and combining the two data sets, yields:

$$IV = -2.19 + 14.44 \log(N_p/\overline{h}) \quad (r = 0.917) \tag{7.60}.$$

This relationship is ilustrated in Figure 7.4. From Figures 7.3 and 7.4 it is plain that the low moisture content of the compacted material used for Test WMM10 has a significant effect on the measured Impact Value, indicating that the Clegg meter is sensitive to extremely dry moisture contents. Clearly the relationships between compactive effort and Impact Value are significant, with generally high values of the regression correlation coefficient. These data confirm that the Clegg meter is an excellent device for the measurement of reinstatement backfill quality

when measurement from the final surface of the reinstated unbound layers is not necessary.

The existence of a unique, material-dependent, relationship between dry density and Impact Value is further suggested by the data for Wet-mix macadam as

$$IV = -69.83 + 44.58\rho_d \quad (r = 0.941) \qquad (7.61).$$

This relationship is illustrated, with the equivalent relationships for the Permian Sand and the Sharp Sand, in Figure 7.7. These material-dependent relationships are confirmed as valid only for material compacted within a narrow band of moisture contents, usually the optimum moisture content. The existence of such relationships at levels of moisture content other than the optimum moisture content is strongly suggested by the Sharp Sand data presented in Section 7.3.1.

7.4.2 Surface wave velocity results

The surface wave velocity measurements for Tests WMM1 to WMM6 and WMM10 (Figures 6.35, 6.36, ..., 6.41), and also Tests WMM7 to WMM9 (Figures 6.49, 6.50, 6.51) , are reported in some detail in Sections 6.4.2 and 6.5.2 (Tables 6.19 and 6.23), respectively. The individual surface wave velocity-depth profiles generally show a distinct break at the interface between the Wet-mix macadam and the underlying subgrade. These data, not withstanding the scatter observed in the data in the region of the interface (see Section 7.8), lend considerable weight to the fundamental assumption that the depth of propagation is equal to one-half the wavelength ($z = \lambda/2$).

The combined surface wave velocity-depth profiles for tests with nominal layer thickness < 150 mm are presented in Figure 7.38. A strong overall trend of increasing surface wave velocity with increasing compactive effort is observed from the data. The slope of the profile for Test WMM8 ($N_p = 8$) tends towards zero (slope, $m = -2.8\,\mathrm{s}^{-1}$—see Table 6.18) and it is for this reason, as discussed in Section 5.1, that the value of the regression correlation coefficient, r, is also very low ($r = -0.100$—see Table 6.18). It is possible that the low value of the slope (near vertical profile) was caused by the drawing of excess water into the lower compacted layers of Wet-mix macadam from the wet subgrade, although low Impact Values were not recorded (see Table A6.25) as was the case during case studies at Salters Lane (Test SL1—Sections 6.6.3 and 7.6.3 and Table A6.33). The profile for Test WMM2 ($N_p = 10$)

exhibits very high values of the surface wave velocity as can be seen also from the more detailed profile for this test presented in Section 6.4.2 (Figure 6.36). A considerable amount of scatter in the data is observed at the interface between the Wet-mix macadam and the underlying subgrade (see also Section 7.8). Despite repetition of the determination of the surface wave velocity-depth profile, the data, in the form of Figure 6.36, could not be refuted. However, this profile is seen as an extreme data set which bears little or no relation to data from the other tests conducted at different levels of compactive effort. Consequently the analyses, using the mean surface wave velocity ($v_{Rz_{max}/2}$), of the form of Equation 7.1 presented later in this section, are calculated excluding the data from Test WMM2. The same approach is taken to the similar analysis of the mean shear modulus presented in Section 7.4.3. It merits observation that the dry density and Impact Value data for Test WMM2 do not show any extreme values, lending further weight to the assertion that the surface wave velocity-depth profile for this test is anomalous.

The combined surface wave velocity-depth profiles for tests with nominal layer thickness < 200 mm are presented in Figure 7.39. An overall trend of increasing surface wave velocity with compactive effort is difficult to highlight from the data and will be discussed in the following paragraphs with the more detailed examination of the numerical variation of mean surface wave velocity ($v_{Rz_{max}/2}$) with compactive effort. The profile for Test WMM10 ($w \approx 0\%$) has been plotted as a broken line; interpretation of this data is nominal. The z, v_R data pairs appear to fall into two groups (this is best observed from the individual profile—Figure 6.41) at depths of approximately 0.35 m and 0.55 m. The regression correlation coefficient is low ($r = -0.274$—Table 6.18) and representative of the extremely scattered experimental data. Extreme difficulty was experienced during testing in finding the in-phase and out-of-phase Lissajous Figures as high frequency noise, most likely caused by vibration of the loose individual particles of Wet-mix macadam, interfered with the usually well-defined, inclined straight line form of the Lissajous Figures (see Plate 5.6). In terms of the compactive effort applied, the profiles for Tests WMM7 to WMM9 should coincide ($N_p/\overline{h} = 42.11$ m^{-1} for all three tests—Table 6.23). From Figure 7.39 this is plainly not the case—the reasons for this will be discussed in more detail in Section 7.5.2.

Approaching the interpretation of the various surface wave velocity-depth profiles in terms of the mean surface wave velocity ($v_{Rz_{max}/2}$) described as a function

of the logarithm of compactive effort, in the style of Equation 7.1, yields a more numerical approach to the understanding of the surface wave velocity results.

Taking N_p as the parameter of compactive effort, and examining data with nominal layer thickness < 150 mm, yields:

$$v_{Rz_{max}/2} = 103.39 + 76.10 \log N_p \quad (r = 0.967) \tag{7.62}$$

for data excluding Test WMM2 (for reasons discussed earlier in this section). Data with nominal layer thickness < 200 mm yields:

$$v_{Rz_{max}/2} = 118.11 + 42.80 \log N_p \quad (r = 0.276) \tag{7.63}.$$

Data from Test WMM10 ($w \approx 0\%$) are not included in this analysis. These relationships are illustrated in Figure 7.40.

Taking the parameter of compactive effort to be $N_p/\overline{h}$, and combining the two data sets, yields:

$$v_{Rz_{max}/2} = 61.22 + 59.44 \log(N_p/\overline{h}) \quad (r = 0.677) \tag{7.64}$$

in which data from Tests WMM2 and WMM10 have been excluded. The above relationship is illustrated in Figure 7.41.

Provided that the data from Test WMM2 ($N_p = 10; h < 150$ mm) is accepted as anomalous and excluded from the interpretation then significant correlations between the mean surface wave velocity and the logarithm of compactive effort is observed. The only exception to this is the data for Tests WMM7 to WMM9 ($N_p = 8; h < 200$ mm) which show significant variation from one test to another, as is reflected in the low value of the regression correlation coefficient for Equation 7.63. In general there do appear to be significant relationships between the mean surface wave velocity and the logarithm of compactive effort for tests conducted in the field trenches on Wet-mix macadam.

7.4.3 Derived shear modulus results

The derived shear modulus results for tests on Wet-mix macadam and Wet-mix macadam and Sharp Sand are reported, in detail, in Sections 6.4.3 and 6.5.3 (Tables 6.19 and 6.24).

The shear modulus-depth profiles for tests on Wet-mix macadam are treated in much the same way as the corresponding surface wave velocity-depth profiles, presented in Section 7.4.2. The shear modulus-depth profiles for Wet-mix macadam, with nominal layer thickness < 150 mm, are presented in Figure 7.42. These show much the same effects as do the corresponding surface wave velocity-depth profiles (Figure 7.38), having a general trend of increasing shear modulus with increasing compactive effort. The profile for Test WMM2 ($N_p = 2$) is regarded as anomalous (see Section 7.4.2) and only the upper portion of the profile is illustrated. The end position of this profile is described numerically in Figure 7.42.

The shear modulus-depth profiles for the tests on Wet-mix macadam, with nominal layer thickness < 200 mm, are illustrated in Figure 7.43. As was discussed in Section 7.4.1, dry density measurements were not possible on the Wet-mix macadam compacted at $w \approx 0\%$ (Test WMM2) and as such the shear modulus-depth profile could not be determined for that test. As was observed above, for the tests with nominal layer thickness < 150 mm the shear modulus-depth profiles show much the same effects as do the surface wave velocity-depth profiles (see Figure 7.39) with no discernible trend of increasing of shear modulus with increasing compactive effort. This will be discussed in more detail later, with the mean shear modulus being interpreted in terms of compactive effort. Figure 7.43 (and also Figure 7.39) serve as a good illustration of the value of the $G_{z_{\max}/2}$ and $v_{Rz_{\max}/2}$ parameters in terms of achieving a valid interpretation of profile data. When a number of profiles are to be compared the data soon become confused and the general trend of increasing shear modulus (or increasing surface wave velocity) becomes difficult to indentify. These comments are particularly pertinent to the case described above where there are three profiles each with $N_p/\overline{h} = 42.11$ ($N_p = 8$; $h < 200$ mm—Tests WMM7, WMM8 and WMM9).

Interpreting the shear modulus-depth profiles, for tests with nominal layer thickness < 150 mm, in terms of the mean shear modulus ($G_{z_{\max}/2}$), with N_p taken as the parameter of compactive effort, yields:

$$G_{z_{\max}/2} = 14.36 + 52.82 \log N_p \quad (r = 0.910) \tag{7.65}$$

for data excluding Test WMM2 (as discussed in Section 7.4.2). The above relationship is illustrated in Figure 7.44 and the position of the data point for Test WMM2 is illustrated numerically.

Data from tests with nominal layer thickness < 200 mm yields:

$$G_{z_{max}/2} = 3.75 + 64.07 \log N_p \quad (r = 0.549) \qquad (7.66).$$

This relationship is illustrated in Figure 7.44.

Taking the parameter of compactive effort to be $N_p/\overline{h}$, and combining the above two data sets, yields:

$$G_{z_{max}/2} = -26.70 + 52.57 \log(N_p/\overline{h}) \quad (r = 0.731) \qquad (7.67)$$

again excluding data from Test WMM2. This relationship is illustrated in Figure 7.45 and the data from Test WMM2 is illustrated numerically.

As has been previously observed, for the mean surface wave velocity data (Section 7.4.2), provided that the data from Test WMM2 ($N_p = 10$; $h < 150$ mm) is accepted as anomalous and excluded from the analysis then a strong overall trend of increasing mean shear modulus with increasing compactive effort is observed. The data from tests with $N_p/\overline{h} = 42.11$ (Tests WMM7, WMM8 and WMM9) have some noticeable variation and cause a low value of the regression correlation coefficient for Equation 7.66 ($r = 0.549$). It should, however, be noted that the fit of these data has been improved, compared to that of the surface wave velocity data (Equation 7.63), by the inclusion of the density data in the calculation of the shear modulus.

7.4.4 Surface wave attenuation results

The new technique for the analysis of surface wave attenuation data is presented in Section 5.6.3 (Equation 5.1.), and described further, in terms of its practical applications, in Section 7.2.4. In contrast to the results from tests on Permian Sand and Sharp Sand (Sections 7.2.4 and 7.3.4) the results from tests on Wet-mix macadam and Wet-mix macadam and Sharp Sand generally exhibit relatively high values of the regression correlation coefficient (r)—see Figures 6.42, 6.43, ..., 6.48 and Figures 6.52, 6.53 and 6.54 and Tables 6.20 and 6.25. In Sections 7.2.4 and 7.3.4 the low values of the slope (the material attenuation coefficient, α) were highlighted as the reason for the low values of r (see Section 5.1). Similarly, the high values of r for the tests on Wet-mix macadam are combined with higher values of the slope (α), so lending weight to the previous argument and indicating that values of r from tests on Wet-mix macadam are representative of the actual scatter of the experimental data.

It was also noted, in Sections 7.2.4 and 7.3.4, that interpretation of α in terms of compactive effort yields no consistent relations. Values of the regression correlation coefficient, for interpretation of the form of Equation 7.1, vary considerably for tests on Wet-mix macadam and Wet-mix macadam and Sharp Sand; some values are positive and some values are negative. These data imply that there is no relationship between the material attenuation coefficient (α) and compactive effort.

7.4.5 Summary

In Table 6.21 summary data relating to the subgrade properties for the field trenches (Tests WMM1 to WMM10) are presented. The data include surface wave velocities and Impact Values, both parameters being presented in mean/sample standard deviation form. The surface wave velocities are represented in this form since at the low frequencies required to propagate surface waves at these depths (generally, $f < 100$ Hz) only a limited amount of data could be obtained (*i.e.* small changes in frequency yield large changes in wavelength, or depth of propagation), and certainly not enough to justify the analysis of the data in terms of a linear regression line (surface wave velocity-depth profile). Also, the results indicate that the surface wave velocity tends not to vary greatly, with depth, for propagation within the subgrade. Significant relationships could not be found between the mean Impact Value and the mean surface wave velocity, and the analysis of this data is not pursued further.

Logarithmic-linear least squares regression analyses have been performed on the data from tests on the Wet-mix macadam, conducted in the field trenches at the British Gas plc Blaydon Depot, to enable the interpretation of dry density, Impact Value, mean surface wave velocity and the mean derived shear modulus ($G \approx \rho v_R^2$) data in terms of compactive effort. The compactive effort is defined by two different parameters as, the number of passes applied per layer (N_p) and also as the number of passes applied per layer divided by the mean layer thickness ($N_p/\overline{h}$). The analyses of both $v_{Rz_{\max}/2}$ and $G_{z_{\max}/2}$ preclude the use of data from Test WMM10 ($N_p = 10$; $h <$ 150 mm); the surface wave velocity-depth profile for this test is deemed anomalous as discussed in Section 7.4.2. This interpretation includes data from Tests WMM7, WMM8 and WMM9, which include Sharp Sand layers and, in the latter two tests, gas pipes in the trench profiles. Aspects of the experimental results specific to the aforementioned constructional differences are discussed in Section 7.5.

From the above mentioned analyses strong correlations of the various parameters with compactive effort are generally found. Values of the regression correlation coefficient derived from such analyses vary between 0.276 and 0.999; the lower value of r is for the mean surface wave velocity interpreted in terms of N_p for the tests with $h < 200$ mm for which only a small range of N_p is covered, and the three data points relating to $N_p = 8$ exhibit considerable scatter. Generally, if the data with such scatter are neglected, the values of r are around 0.7, or above. The scatter of the data for dry density and mean surface wave velocity appear to be, to some extent, mutually compensating because the mean derived shear moduli data exhibit more significant correlations with compactive effort than do either of the two parameters from which they are derived. This effect was also observed for tests on the Sharp Sand (Section 7.3.5).

In evaluation of the suitability of a parameter for use in the assessment of reinstatement backfill quality the degree of numerical sensitivity (S) to the applied compactive effort is of great importance. Such an interpretation of the data is given in Table 7.1 for a change in compactive effort from $N_p/\overline{h} = 15\,\mathrm{m}^{-1}$ to $N_p/\overline{h} = 90\,\mathrm{m}^{-1}$. It is clear from the tests on Wet-mix macadam that the Impact Value is most sensitive to compactive effort ($S = 55.1\%$). The mean surface wave velocity has a sensitivity of 30.2% while the dry density has a sensitivity of just 12.2%, which is, at least in part, due to the false origin inherent within the density parameter. The high value of sensitivity of the mean derived shear modulus to compactive effort ($S = 73.6\%$), compared to that for the mean surface wave velocity, is due to the shear modulus being proportional to the square of the surface wave velocity ($G \propto v_R^2$) thus making the shear modulus more sensitive to changes in compactive effort.

This simple form of analysis shows the Impact Value to be considerably more sensitive to changes in compactive effort than is the surface wave velocity which is, in turn, more sensitive than the dry density.

A material dependent relationship between the Impact Value and the dry density, with a strong correlation ($r = 0.941$), has been proposed for the tests on Wet-mix macadam.

Detailed examination of the surface wave velocity-depth profiles for the individual tests shows that for the test on dry material (Test WMM10) the measured surface wave velocities are open to some question as the vibration of the individual

particles caused severe difficulty in determining the points at which the in-phase and out-of-phase Lissajous Figures are found. The Impact Value measured during this test indicated that the Clegg meter is sensitive to such extremes of moisture content. It was also found that the profiles for the three tests with $N_p/\overline{h} = 42.11\ \mathrm{m}^{-1}$ did not coincide as might be expected purely on the basis of the compactive effort applied.

The individual surface wave velocity-depth profiles highlight the interface between the Wet-mix macadam and the underlying subgrade lending weight to the fundamental assumption that the depth of propagation is equal to one-half the wavelength ($z = \lambda/2$).

The surface wave attenuation results data as presented have been interpreted in terms of the material absorption coefficient (α), using a new form of the Bornitz equation which allows α to be determined without the need to make potentially erroneous assumptions (albeit from the experimental data) concerning the state of the distance-displacement (attenuation) curve close to the vibratory source. Consistent relations between compactive effort and α could not be found.

7.5 Measurements on Wet-mix macadam and Sharp Sand

Three tests which were conducted with layers of both Wet-mix macadam and Sharp Sand (Tests WMM7, WMM8 and WMM9). These tests were designed, with the guidance of the British Gas plc Engineering Research Station, to emulate aspects of British Gas reinstatement works. As such, Test WMM7 had two layers of Sharp Sand (Layers I and II) with two layers of Wet-mix macadam (Layers III and IV) placed over the Sharp Sand. This test was designed to assess the properties of a realistic reinstatement without the additional complication of the presence of a gas pipe. Tests WMM8 and WMM9 were similar to Test WMM7 but with the addition of a plastic (110 mm internal diameter pipe—see Table A6.29) and steel (103 mm internal diameter pipe—see Table A6.30) pipe, respectively. In both cases the pipes were laid after compaction of a layer of Sharp Sand ($N_p = 3$; layer thickness of 90 mm). A second layer of Sharp Sand was then carefully placed around the pipe (between the pipe and trench walls) and Sharp Sand placed on top of the pipe to a compacted thickness of 100 mm ($N_p = 4$). These three tests, described above, thus mimic, to different degrees, the real-life reinstatement. It is this rôle which will be assessed in this section.

The data for Tests WMM7, WMM8 and WMM9 have already been examined in considerable detail in Section 7.4, including the correlations of the test data with compactive effort, and only the aspects of the data which relate specifically to the presence of two materials and/or gas pipes in the reinstatement will be discussed in this section.

7.5.1 Density, moisture content and Impact Value results

The experimentally obtained values of dry density and Impact Value for the Wet-mix macadam placed on top of the Sharp Sand in Tests WMM7, WMM8 and WMM9 (see Table 6.22) should be approximately the same, since the level of compactive effort ($N_p/\overline{h} = 42.11\,\mathrm{m}^{-1}$) was the same for each test. Any differences may be attributed to one or more of the following factors:

i)experimental errors inherent in the measurement procedures,

ii)small differences in the material placement and compaction procedures, including variations in the moisture content of the compacted material,

iii)differences in the level of compaction achieved for the underlying Sharp Sand, and

iv)the presence, or otherwise, of plastic or steel, gas pipes.

In most cases it is considered that the attribution of variations in experimental data specifically to one, or more, of the above factors is impossible in such a complex environment. It is, however, possible to examine variations in specific data.

The variations in dry density for the three tests were small ($2.036\,\mathrm{Mg/m^3} \leq \rho_d \leq 2.064\,\mathrm{Mg/m^3}$) although it should be noted that the variation in bulk density was smaller still ($2.130\,\mathrm{Mg/m^3} \leq \rho \leq 2.141\,\mathrm{Mg/m^3}$) most of the variation being caused by the relatively large variation in moisture content as measured after compaction ($3.75\% \leq w \leq 4.62\%$).

The variation in the Impact Values were also relatively small, being $21.60 \leq IV \leq 23.15$, a difference of 1.55 from greatest to least which compares favourably with a typical sample standard deviation from a single test on Wet-mix macadam (see Tables 6.17 and 6.22). In general the data from the three tests under discussion here conform well to the general relationship between dry density and Impact Value described for Wet-mix macadam in Section 7.4.1 (Equation 7.61).

A precursor to an examination of the similar data for the Sharp Sand from the three tests (presented in Table 6.22) must be that the compacted moisture content of the Sharp Sand was between, approximately, 1.5% and 2.5% lower than the 'target' moisture content for tests on the Sharp Sand in the laboratory based trench ($10\% \pm 1.0\%$).

During the sand replacement density tests, conducted on the Sharp Sand, difficulties were experienced. The mass of the apparatus (*circa* 8 kg) was such that when the cone of the pouring cylinder was placed over the excavated hole significant settlement occurred, causing less sand to be poured into the excavated hole than would otherwise be the case and leading to significant doubts as to the validity of the data reported for Sharp Sand in Table 6.22. Indeed, during tests on the Sharp Sand, conducted as part of Test WMM7, the walls of the excavated holes collapsed, so rendering the density determination impossible.

Sharp Sand in Tests WMM8 and WMM9 Layers I(SS) and II(SS) were compacted with $N_p = 3$ ($h \approx 90$ mm) and $N_p = 4$ ($h \approx 210$ mm), respectively. Comparing the data with those reported for tests on Sharp Sand in the laboratory based trench (Section 7.3.1—Equation 7.38 and Figure 7.1) it can be seen that the density values for the two tests are noticeably greater than would be predicted from Equation 7.38; this is despite the lower moisture content at which the field material was compacted. These apparently high values of the measured dry density may be attributed to the settlement of the pouring cylinder.

The Impact Values determined from tests on the Sharp Sand, for Tests WMM7 ($N_p = 6$; $h < 150$ mm), WMM8 ($N_p = 3$ & 4; $h = 90$ mm and 210 mm) and WMM9 ($N_p = 3$ & 4; $h = 90$ mm and 220 mm), show a generally good agreement with the Sharp Sand compacted in the laboratory based trench (Figures 7.3 and Equation 7.40).

The apparently erroneous dry density values cause a poor agreement with the dry density-Impact Value relationship for Sharp Sand compacted in the laboratory based trench (Equation 7.46; Figure 7.7).

7.5.2 Surface wave velocity results

The combined surface wave velocity-depth profiles for Tests WMM7, WMM8 and WMM9 are illustrated in Figure 7.46 (Table 6.23). Profiles for both the Wet-mix macadam and Sharp Sand layers are shown. The profiles for the individual tests

are given in Figures 6.49, 6.50 and 6.51 for Tests WMM7, WMM9 and WMM10, respectively. The profiles for the Wet-mix macadam have been discussed previously, in Section 7.4.2, with respect to their interpretation in terms of compactive effort.

The profiles for Wet-mix macadam ($N_p/\overline{h}$ = 42.11 m^{-1}—Table 6.23) fall within a relatively wide band of surface wave velocity.

Interpretation of the surface wave velocity data was difficult due to the considerable amount of scatter introduced to the data at the interfaces between the Wet-mix macadam and the Sharp Sand. This effect is particularly noticeable for Test WMM9, in which a steel pipe was located on top of the first layer of Sharp Sand prior to the placement of the second layer of Sharp Sand. In comparison to the other two tests the velocities measured, for depths pertaining to the Sharp Sand layers, are high. This is most likely due to the steel pipe providing a preferential (faster) path along which the wave propagates. As a result the interpretation of the Sharp Sand profile for this test must be seen as doubtful. Surface wave propagation through the plastic gas pipe (Test WMM8) does not appear significantly to affect the measured surface wave velocities.

The high values of the surface wave velocity reported for the Wet-mix macadam of Test WMM7 may be due to the higher level of compactive effort applied to the underlying Sharp Sand providing a stiffer base to compact against than for the other two tests. The mean Impact Value reported for the Sharp Sand of Test WMM7 is certainly higher than that for the other two tests compacted with a lower level of compactive effort lending weight to the above argument. Dry density measurements were, of course, not possible on the Sharp Sand of Test WMM7. The surface wave velocity-depth profile for the Sharp Sand of Test WMM7 shows no notable variation from those of the other two tests and, in contrast, does not support the above argument.

The surface wave velocity-depth profiles for Tests WMM7 and WMM8 (Figures 6.49 and 6.50) are unique in that they relate to three different materials (Wet-mix macadam, Sharp Sand and subgrade). The delineation of the surface wave velocity-depth profiles between the various material types is generally good, indicating that the basic assumption that the depth of propagation is equal to one-half the wavelength ($z = \lambda/2$) holds. Also the sense of the velocity transitions between the materials indicates that the surface wave method is capable of measurement in the situation of a stiff layer overlying a less stiff layer (see Section 3.2.4).

7.5.3 Derived shear modulus results

The derived shear modulus results for tests on Wet-mix macadam and Sharp Sand are reported, in detail, in Section 6.5.3 (Table 6.24).

It was noted in Section 7.5.1 that density measurements on the Sharp Sand of Test WMM7 were not possible and as such the shear modulus-depth profile relating to the Sharp Sand placed in this test could not be determined. The three Wet-mix macadam (Tests WMM7, WMM8 and WMM9) and the two Sharp Sand (Tests WMM8 and WMM9) shear modulus-profiles are illustrated in Figure 7.47 (Table 6.24). These show very similar interelations to those already described for the equivalent surface wave velocity-depth profiles in Section 7.5.2. This is due to the very small variations in the density values that were determined and as was observed in Section 7.5.1 (for Wet-mix macadam determinations $2.130\,\mathrm{Mg/m^3} \leq \rho \leq 2.141\,\mathrm{Mg/m^3}$).

7.5.4 Surface wave attenuation results

The surface wave attenuation results from tests on Wet-mix macadam and Sharp Sand (Tests WMM7, WMM8 and WMM9) have already been discussed, for convenience, with those from tests on Wet-mix macadam only (Tests WMM1 to WMM6 and Test WMM10) in Section 7.4.4.

7.5.5 Summary

In this section the results of three tests, conducted in field trenches at the British Gas plc Blaydon Depot, have been interpreted and discussed. These trenches were each reinstated with two layers of Sharp Sand below two layers of Wet-mix macadam. Two of the tests had a gas pipe (plastic or steel) placed on top of the first layer of Sharp Sand prior to the placement of the second layer of Sharp Sand. The compactive effort applied to the two layers of Wet-mix macadam was identical in each test ($N_p/\overline{h} = 42.11\,\mathrm{m^{-1}}$). An excellent opportunity was thus afforded to evaluate the repeatability of the test methods and also to evaluate the performance of the test methods under realistic field reinstatement conditions.

The repeatability of both the dry density and Impact Value appears to be very good, as is discussed in Section 7.5.1. The surface wave velocities (Section 7.5.2) and derived shear moduli values (Section 7.5.3) do not appear to exhibit the same degree

of repeatability, although this may be attributed, at least in part, to the underlying well compacted Sharp Sand of Test WMM7 affording a stiffer base against which to compact the Wet-mix macadam. This is borne out to some extent by the Sharp Sand Impact Value results although not by the Sharp Sand surface wave velocity results, or indeed the aforementioned Wet-mix macadam dry density and Impact Value.

Surface wave propagation appears to be significantly affected by the presence of a steel gas pipe (Test WMM9) but not by the presence of a plastic gas pipe (Test WMM8). The steel pipe is believed to provide a preferential (faster) path along which the wave propagates (Section 7.5.2).

The delineation of the surface wave velocity-depth profiles between the various material types is generally good, indicating that the basic assumption that the depth of propagation is equal to one-half the wavelength ($z = \lambda/2$) holds and also that the surface wave method is capable of measurement in the situation of a stiff layer overlying a less stiff layer (see Section 3.2.4).

7.6 Case studies

In this section a series of some five case studies is reported. Two of these relate to genuine utility service trenches (Sections 7.6.1 and 7.6.4), one test simply presents data which illustrate the increase of the measured Impact Value with increased compactive effort (Section 7.6.2) and two tests were designed with the assistance of the British Gas plc Engineering Research Station, to evaluate the differences between a 'well compacted' and a 'poorly compacted' trench (Section 7.6.3).

7.6.1 SEAS service trench

The details of this test are given in Section 6.6.1. The surface wave velocity-depth profile (Figure 7.47) is divided into two distinct straight regression lines, one representing the properties of the upper two layers and the other representing the properties of the lower two layers. It is interesting to note that the slopes of both these regression lines are negative. This may well, in some instances, be a more accurate representation of the variation of stiffness properties with depth in a 'real-life' single material reinstatement environment and illustrates, albeit in a limited sense, the applicability of the surface wave method to measurement under conditions of a stiff layer overlying a less stiff layer (see Section 3.2.4).

The subjective deterioration of the waveform, noted for tests in the laboratory based trench, as the wavelength approaches the width of the trench was not observed in the tests performed on the trench between the North and South SEAS buildings.

This case study was conducted at a very early stage during the experimental work presented in this chapter (at around the same time that Test TPS2 was conducted—see Appendix 7) and provided much valuable experience of using the test methods and equipment under real-life reinstatement conditions. The experience so gained was found to be invaluable with respect to the later tests conducted at the Blaydon test site (Sections 7.4 and 7.5).

7.6.2 Blaydon demonstration trench

Details of this test are given in Section 6.6.2. The data achieved for this test consist simply of Impact Values determined at $N_p = 1, 2, 4, 7, 14$ and 20 passes per layer. These data are plotted in $\log N_p$-IV form in Figure 7.48 and the form of the least squares regression line calculated from the data is:

$$IV = 10.21 + 9.33 \log N_p \quad (r = 0.987) \qquad (7.68).$$

This supports the strong, visually observed trend of increasing Impact Value with increasing compactive effort. Throughout this chapter a uniform policy of not showing error bars on figures has been implemented, largely for the sake of clarity (see Section 7.1). Figure 7.48 is the sole exception to this rule; error bars, of magnitude $\overline{IV} \pm \sigma_{IV_{n-1}}$, to include approximately 68% of data, are shown. This form of presentation demonstrates an important point with respect to Clegg meter usage and subsequent interpretation of Impact Values. While strong overall trends of increasing Impact Value with increasing compactive effort may be observed both visually and numerically, the plotted Impact Values should be representative of the mean of a number of determinations made on an area of compacted material which has been similarly treated (*e.g.* a single layer at a given level of compactive effort as is illustrated in Figure 7.48). This is necessary because as can be observed from the error bars shown in Figure 7.48, individual determinations of the Impact Value may vary considerably.

The data from this simple case study lends weight to the assertion that the Clegg meter is an excellent device for the measurement of reinstatement backfill quality,

provided that the measurement of each individual layer prior to the placement of the subsequent layer is not precluded.

7.6.3 Salters Lane: Back-to-back tests—well/poorly compacted

Details of the two tests discussed here are given in Section 6.6.3. The two tests essentially correspond to a particular view of 'well compacted' (Test SL1) and 'poorly compacted' (Test SL2). The test material was Wet-mix macadam as used for Tests WMM1 to WMM10 (Sections 7.4 and 7.5). Compaction for Test SL1 was applied at $N_p = 8$ to four layers each of approximately 200 mm compacted thickness ($N_p/\overline{h} = 42.11\,\mathrm{m}^{-1}$), while for Test SL2 a single layer of 650 mm compacted thickness with $N_p = 12$ ($N_p/\overline{h} = 18.46\,\mathrm{m}^{-1}$).

Impact Values ($\overline{IV}/\sigma_{IV_{n-1}}$) were determined as 25.75/1.52 and 23.0/1.87 for Tests SL1 and SL2, respectively. The Impact Values for both tests compare well with data from Tests WMM7, WMM8 and WMM9 (Section 7.5.1) for which $N_p/\overline{h}$ was $42.11\,\mathrm{m}^{-1}$ (as for Test SL1). This tends to indicate a failing of the Clegg meter to determine a significant difference in the compactive effort applied to the two reinstatements. The experimentally derived data reflect, to some extent, the values which might be anticipated from a consideration of the values of N_p for the two tests regardless of the greatly differing layer thicknesses. The Clegg meter is thus shown to be essentially incapable of defining the difference between the two levels of compactive effort, when 'poorly compacted' is defined as a large number of passes applied to a very deep, single layer (*i.e.* superficial compaction).

As was observed in Section 6.6.3 the clay subgrade, prior to commencement of Test SL1, was noted to have a considerable amount of standing water at one end of the trench prior to the placement of the Wet-mix macadam. Plotting the individual Impact Values against distance from one end of the trench (Figure 7.49) the effect of the standing water on the measured Impact Values can be clearly seen for the first two layers (Layers I and II). No effects due to the standing water are apparent from the data for Layers III and IV. The mean/sample standard deviation for Layer I is based on the three high Impact Values from measurements made at the 'dry' end of the trench; measurements from the 'wet' end of the trench are deemed anomalous and neglected from the calculation. The mean/sample standard deviation for Layers II, III and IV are based on all six of the individual Impact Value measurements, the differences between the Impact Values at the 'wet' and

'dry' ends of the trench being deemed insufficient to justify neglecting the 'wet' end data.

The data from the lower layers of the well compacted reinstatement (Test SL1) indicated that the Clegg meter responds to the wet extreme of moisture content.

Individual surface wave velocity-depth profiles were presented in Section 6.6.3, Figures 6.56 and 6.57 for Tests SL1 and SL2, respectively. These profiles are combined and presented as Figure 7.50. Although there is a considerable amount of visually observed scatter in the data for Test SL1 it is clear that the surface wave method has isolated the differences between the two tests most effectively. The values of the mean surface wave velocity ($v_{Rz_{max}/2}$), calculated from Equations 6.4 and 6.5 for Tests SL1 and SL2, are 194.1 m/s and 128.2 m/s, respectively. This is plainly a significant difference and illustrates the usefulness of the surface wave method for the detection of poor compaction, at least in a back-to-back comparison.

7.6.4 Field trial: Acton Dean, Stanley, County Durham

The details of this test are given in Section 6.6.4. The test was carried out on a genuine British Gas plc footpath reinstatement in the Stanley area (Northern Region). A Model Agreement (see Chapter 1) is not operated in this area although the description contained in the Model Agreement (Department of Transport, 1974) for Suitable Excavated Material (SEM) was applied to the excavated material which was thus used for the subsequent reinstatement after placement of the gas main described in Section 6.6.4. The Department of Transport (1974) define SEM, in terms of materials which are unsuitable, as follows:

'a)Materials from swamps, marshes or bogs.

b)Peat, logs, stumps and perishable material.

c)Material susceptible to spontaneous combustion.

d)Material in a frozen condition.

e)Clay of liquid limit exceeding 80 and/or plasticity index exceeding 55.

f)Materials having moisture content not complying with the reasonable requirements of the Engineer.

Materials of class (d) if otherwise suitable shall be classified as suitable when unfrozen.'

There is no direct evidence to suggest that the excavated material could not reasonably be classified as SEM on the basis of visual observation. The only slight doubt would be with regard to the index properties of the heavy clay subgrade (see (e) above).

Compactive effort was applied ($N_p = 2$) with a Wacker BS65Y vibratory rammer, a heavier version of the BS45Y used in most of the other experimental work, to layers of 0.250 mm, 0.210 m and 0.090 m compacted thickness from the subgrade level upwards. The first layer included the plastic gas main. The Impact Values from the three layers gave $\overline{IV} = 3.00$ and $\sigma_{IV_{n-1}} = 1.30$. These values are low and reflect the visual observation that the compacted SEM was soft underfoot.

In contrast to the Impact Values the surface wave velocities, from Figure 6.58 (Equation 6.5), are high, being approximately comparable to the data from Test SL1 ('well compacted' Wet-mix macadam). Conversion to shear modulus, using density values, would almost certainly highlight the differences between these two tests. Unfortunately time constraints precluded the measurement of dry density at both test sites and so such a comparison is not possible. The surface wave velocity-depth data pinpoints the interface between the SEM and the underlying subgrade and no detrimental effects were observed due to the presence of the plastic gas pipe.

7.6.5 Summary

The results of some five case studies have been interpreted and discussed in this section.

The first case study (Section 6.6.3) lends some weight to the belief that the surface wave method is suitable for measurement in cases where a stiff layer overlies a less stiff layer, although this is more ably demonstrated by the Wet-mix macadam tests (Tests WMM1 to WMM10—Sections 7.4 and 7.5).

The second case study (Section 6.6.2) illustrates the increase of Impact Value with increasing compactive effort, progressively applied to a single layer, and also the necessity of interpreting the Impact Value as the mean of a number of individual determinations made under similar conditions.

The third and fourth case studies (Section 6.6.3) consisted of two tests on single material (Wet-mix macadam) reinstatements defined as 'well compacted' and 'poorly compacted' and showed that the Clegg meter did not clearly define the difference

between the two levels of compactive effort, when 'poorly compacted' was defined as a large number of passes applied to an extremely deep, single layer. The surface wave method, on the other hand, performed exceptionally well in this situation, clearly defining the difference between the two levels of compactive effort. The data from the lower layers of the well compacted reinstatement (Test SL1) indicated that the Clegg meter responds to the wet extreme of moisture content.

The fifth and final case study was carried out on a genuine British Gas plc footpath reinstatement; the reinstated material was Suitable Excavated Material (SEM). The surface wave velocity-depth measurements clearly defined the position of the interface between the SEM and the underlying subgrade with no detrimental effects being caused by the presence of the plastic gas pipe. Comparison of the surface wave velocity data from this test with that of Test SL1 indicates that density measurements would be a desirable addition to the Impact Value and surface wave velocity-depth profile data determined during the case studies presented here.

7.7 Comparison of laboratory and field derived dry density and moisture content data with relationships derived from British Standard tests

British Standard determinations of the dry density-moisture content relationships for the three materials under test were reported in Chapter 4 as follows:

Permian Sand; BS 1377 (1975): Test 12; Section 4.4.1 (Figure 4.4); N_b = 27, 54, 81, 108, 135.

Sharp Sand; BS 1377 (1975): Test 12; Section 4.4.2 (Figure 4.5); N_b = 27, 54, 81.

Wet-mix macadam; BS 1377 (1975): Test 12; Section 4.4.3 (Figure 4.6); N_b = 27, 54, 81.

Wet-mix macadam; BS 5835: Part 1 (1980); Section 4.4.4 (Figure 4.9).

In Figure 4.6 data were presented in forms both corrected and uncorrected for the percentage of particles retained on a 19.05 mm test sieve.

Figures 4.6, 4.5, 4.6 and 4.9 have been reproduced as Figures 7.51, 7.52, 7.53 and 7.54, respectively. The laboratory compaction data points are not shown on the latter set of figures, so allowing the clear over-plotting of mean dry density-moisture content data from the tests conducted in the laboratory based trench (Permian Sand and Sharp Sand) and also from the field tests conducted at the British Gas plc

Blaydon Depot (Wet-mix macadam). The dry density data are drawn from Tables 6.8 (Permian Sand), 6.13 (Sharp Sand), and Tables 6.17 and 6.22 (Wet-mix macadam) while the moisture content data are drawn from Tables 6.7 (Permian Sand), 6.12 (Sharp Sand), and Tables 6.17 and 6.22 (Wet-mix macadam). In all cases the moisture content data that are plotted are post-compaction values; *i.e.* the moisture content measured from samples taken immediately after the completion of compaction.

Careful examination of Figures 7.51 and 7.52, the plots for the two fine-grained materials, reveals that the dry densities show equivalence to compactive efforts between $N_b < 27$ and $N_b \approx 108$, for the Permian Sand, and between $N_b \ll 27$ and $N_b \approx 54$, for the Sharp Sand.

The Permian Sand was compacted at moisture contents which approximate to $w_{\text{opt}} \pm 1.0\%$ for the determination of w_{opt} with $N_b = 27$ (see Section 7.2.1 and Figure 7.51). The Sharp Sand was found to be difficult to work, even at optimum moisture contents derived from higher levels of compactive effort than the standard $N_b = 27$, and as such a 'target' moisture content was set at $10\% \pm 1.0\%$ (see Section 7.3.1 and Figure 7.52).

The increase of dry density with compactive effort, with approximately constant moisture content, has been discussed in terms of the compactive effort applied to the material in the laboratory based trench (Section 7.2.1 and 7.3.1). Figures 7.51 and 7.52 compare the same data with the levels of compactive effort applied during British Standard (modified and unmodified) compaction tests.

The compactive efforts applied to the Permian Sand and the Sharp Sand in the laboratory based trench may be defined either in terms of the number of passes per layer (N_p) or the ratio of the number of passes per layer to the mean layer thickness ($N_p/\overline{h}$). The range of compactive effort applied to the Permian Sand in tests in the laboratory based trench was $18.32\,\text{m}^{-1} \leq N_p/\overline{h} \leq 94.34\,\text{m}^{-1}$ (Table 6.7), while for the Sharp Sand it was $17.54\,\text{m}^{-1} \leq N_p/\overline{h} \leq 88.50\,\text{m}^{-1}$ (Table 6.12).

As the data were achieved in a trench of standard horizontal dimensions, the $N_p/\overline{h}$ data may be simply converted to an equivalent compactive effort, CE (in kJ/m^3), from Equation 7.3 giving $152\,\text{kJ/m}^3 \leq CE \leq 774\,\text{kJ/m}^3$, for the Permian Sand, and $144\,\text{kJ/m}^3 \leq CE \leq 726\,\text{kJ/m}^3$, for the Sharp Sand. These values may be compared to the equivalent British Standard compactive efforts applied to the

same materials, as quoted in Table 4.4. For Permian Sand the compactive efforts used to achieve the dry density-moisture content relationships shown in Figure 7.51 were $631\,\mathrm{kJ/m^3} \leq CE \leq 3157\,\mathrm{kJ/m^3}$, and for Sharp Sand the compactive efforts used to achieve the dry density-moisture content relationships shown in Figure 7.52 were $631\,\mathrm{kJ/m^3} \leq CE \leq 1894\,\mathrm{kJ/m^3}$.

Plainly, the higher levels of compactive effort applied to the material in the laboratory based trench are comparable to the lower levels of compactive effort applied to the materials in the British Standard compaction tests. Also the disposition of the individual points with regard to the British Standard dry density-moisture content relationships indicates the existence of a strong argument for the varying of the moisture content with the compactive effort applied under field conditions (or the psuedo-field conditions of the laboratory based trench) so as to achieve an improved comparison with optimum moisture content and, as a result, improved dry densities. This should also prevent field dry densities from falling within the 'wet of optimum' range for any given level of compactive effort. In this range there is potential for rapid strength loss on wetting of the compacted material as may occur under field conditions.

A similar examination of the data from the field tests on Wet-mix macadam, which are plotted with the laboratory dry density-moisture content relationship in Figures 7.53 (BS 1377, 1975: Test 12) and 7.54 (BS 5835: Part 1, 1980), immediately highlights the difference in the optimum moisture contents achieved from the two British Standard tests. As was discussed in Section 4.4.5, the BS 5835 test is specifically designed for the testing of aggregates and much more credence is placed upon the results from this test. As such, further discussion of the relationships between field dry density-moisture content and the British Standard curves will be confined to the BS 5835 test data (Figure 7.54).

In all cases the field moisture content data compared well with the optimum moisture content (Figure 7.54), as is discussed in Section 7.4.1. The dry density values are, in contrast, considerably lower than might be anticipated from the laboratory derived compaction curve. The level of compactive effort applied at the optimum moisture content is given in Table 4.4 as $CE = 18664\,\mathrm{kJ/m^3}$. Evaluation of the field compactive efforts ($14.29\,\mathrm{m^{-1}} \leq N_p/\overline{h} \leq 81.97\,\mathrm{m^{-1}}$—from Tables 7.17 and 7.22) using Equation 7.3 gives a range of compactive effort, applied in the field, of $117\,\mathrm{kJ/m^3} \leq CE \leq 672\,\mathrm{kJ/m^3}$. In short, purely on the basis of the applied

compactive effort one would not expect field dry densities to compare well with the maximum dry density obtained from the BS 5835: Part 1 (1980). Emphasising a previous observation it may be advisable, in future work, to vary the moisture content with compactive effort in order to achieve an approximation of the optimum moisture content at each level of compactive effort applied in the field. It is, however, difficult to envisage a reliable method by which this may be achieved other than by conducting full scale trials to determine the relationships between field and laboratory (British Standard) compactive efforts.

The data from tests on the Sharp Sand and the Wet-mix macadam all indicate that the compacted materials had an air voids content of less than 10%. This indicates that under field conditions a potential exists for strength reduction due to the ingress of water to the air voids. Somewhat lower levels of air voids are exhibited by the Permian Sand indicating a lesser potential for strength reduction due to moisture ingress.

7.8 Additional comments on surface wave velocity measurements

In the early stages of Test TPS1, waveforms with a sawtooth shape were noted when high vibration amplitudes were used; experimental observations indicated that this corresponded to a setting greater then 'four' on the 'Gain' control of the Ling Dynamics power amplifier (see Section 5.3.3). This had the effect, when combining the signals using an oscillope in X-Y mode, of distorting the resulting Lissajous Figure. Frederick (1965) described this effect in terms of the elementary theory of sound wave propagation which assumes that the individual particle velocities are much smaller than the velocity of propagation of the wave in the medium (*i.e.* strain levels are small—see Section 7.8.1). High amplitude sources may exceed the above restriction, causing alternate compressions and rarefactions of the medium which have higher and lower velocities than the average propagation velocity for the material and so causing a 'piling-up' which appears as a sawtooth waveform. Such a waveform can be shown, by Fourier analysis, to have many harmonics. The harmonics are, however, short lived as higher frequencies are more efficiently damped, causing the waveform to revert to its normal sinusoidal shape after propagating a relatively short distance. The foregoing relates to sound waves in which the difference between the density in a zone of compression and a zone of rarefaction will be high compared

to those in Rayleigh-type surface waves. This effect has been eliminated by the appropriate setting of the power amplifier gain control, as noted above.

Kolsky (1963) notes that waves propagated in a bounded medium will be subject to interference as the wavelength approaches the dimension of the medium—this effect has been observed as a subjective deterioration of the waveform as the wavelength approaches the width of the laboratory based trench (0.300 m). A similar effect was not observed during work carried out under field conditions as described in Sections 7.4, 7.5 and 7.6.

Of some interest is the boundary effect where the Rayleigh-type surface wave is incident to the trench walls. Stoneley (1924) suggested that waves analagous to Rayleigh waves may be propagated in the areas close to the boundary, with the maximum amplitude of vibration at the surface of separation. This leads to the tentative conclusion that reflections from the trench walls may be minimal; an assertion which is qualitatively supported by experimental observation—no identifiable distortion, or interference, effects being detectable.

In tests on Wet-mix macadam (Tests WMM1 to WMM10), at the British Gas plc Blaydon Depot, scatter was, in most instances, observed as the depth of propagation ($z = \lambda/2$) approached the depth of the interface between the Wet-mix macadam and the subgrade as described by Abbiss (1981) (Section 3.3). This scatter appears to be most pronounced in tests where the level of compactive effort was greatest, *i.e.* Tests WMM2 ($N_p = 10$) and WMM5 ($N_p = 8$), and thus the difference in stiffness between the two material was most pronounced. Likewise, the scatter appears to be least pronouced in tests where the level of compactive effort was least, *i.e.* Tests WMM1 ($N_p = 5$) and WMM3 ($N_p = 2$), in which the difference in stiffness between the two materials was a minimum.

7.8.1 Shear strains due to surface waves

It was observed in Section 3.5 that the shear strain, γ, due to the vertical component of deformation of a propagated Rayleigh-type surface wave is given by:

$$\gamma = \dot{w}/v_R \qquad (3.38\text{bis})$$

where $\dot{w}$ is the peak particle velocity in the z-direction (vertical) and v_R is the velocity of propagation of the surface wave.

Taking maximum (peak-to-peak) values of particle displacement (w) from the surface wave attenuation data presented in Appendix 8, values of particle velocity (peak) may be calculated, as $\dot{w} = \pi f w$[1], for the two frequencies for which attenuation measurements were made (*i.e.* frequency, $f = 300$ Hz and 500 Hz). Selecting the surface wave velocities for these frequencies from the data presented in Appendix 7, allows the simple calculation of shear strain from Equation 3.38. Selection of the maximum values of peak-to-peak particle displacement gives an estimate of shear strain which approximates to the maximum strain induced in the compacted material due to the propagation of a surface wave. Determination of the shear strain induced in the Sharp Sand was not possible for a frequency of 500 Hz due to the lack of surface wave velocity data at this frequency.

The overall range of shear strain calculated is $0.09 \times 10^{-3}\%$ to $2.49 \times 10^{-3}\%$ for all tests on the Permian Sand, Sharp Sand and the Wet-mix macadam at frequencies of 300 Hz and 500 Hz. More detailed ranges, relating to individual materials and frequencies are given in Table 7.2 from which it is clear that the strains induced in the Wet-mix macadam are somewhat lower than those induced in the Permian Sand. As the calculated values of shear modulus (see Sections 7.2.3 and 7.4.3) for the two materials were broadly similar it is implied that the shear stresses generated in the Permian Sand were somewhat higher than those generated in the Wet-mix macadam. This could well be due to a better contact being formed between the oscillator baseplate and the compacted material under laboratory conditions.

The range of shear strain induced in the test materials encompasses the estimate made by Seed and Idriss (1970) of $\gamma = 5 \times 10^{-4}\%$ (or $0.5 \times 10^{-3}\%$) and reported in Section 3.5.

7.9 Summary

In this chapter a very detailed interpretation and discussion of the experimental results from tests on Permian Sand, Sharp Sand, Wet-mix macadam and Wet-mix macadam and Sharp Sand (Sections 7.2, 7.3, 7.4 and 7.5, respectively) has been presented. The results of some five case studies (Section 7.6), a comparison of the dry density-moisture content data from the above tests with British Standard

[1]Note that $\dot{w} = 2\pi f w$ where values of both $\dot{w}$ and w are either peak-to-peak or peak values. In this case w is the peak-to-peak particle displacement and $\dot{w}$ is the peak particle velocity, so we have $\dot{w} = \pi f w$.

relationships (Section 7.7) and further observations on surface wave propagation (Section 7.8) are also presented.

Experimental results are generally interpreted by means of linear regression analyses of the form of:

$$y = c + m \log x \qquad (7.1\text{bis}).$$

where x is the applied compactive effort. The compactive effort is defined in two ways:

i)the number of passes applied to each layer (N_p), and

ii)the number of passes applied to each layer divided by the mean layer thickness ($N_p/\overline{h}$).

Most of the experimental work was conducted in trenches of standard dimensions and as a result $N_p/\overline{h}$ may be approximated to the compactive effort (energy in kJ/m^3) using Equation 7.3 (Section 7.1).

The experimental results from Test TPS1 are excluded from the analyses to determine the linear regression lines (of the form of Equation 7.1) shown in the figures, although calculated linear regression lines for data both including and excluding Test TPS1 are given in the text. The long period (*circa* 106 days) for which the compacted material of Test TPS1 stood drying is believed to have caused a cementing effect due to the 2% Calcite found to be present in the Permian Sand (Section 4.7). Also, the use of a petrol driven Wacker BS45Y vibratory rammer to apply compactive effort to the first four layers of this test, as opposed to the electrically driven device described in Appendix 5, is believed to be a potential source of error.

Data from Test WMM10, the test conducted on surface dry Wet-mix macadam, is also excluded from analyses in terms of compactive effort.

The surface wave velocity-depth profile (and also the derived shear modulus-depth profile) for Test WMM2 is deemed anomalous (see Section 7.4.2) and is excluded from analyses of mean surface wave velocity ($v_{Rz_{max}/2}$) and mean shear moduli data ($G_{z_{max}/2}$) in terms of compactive effort.

The three materials were each compacted at a consistent level of moisture content, optimum moisture content in the case of the Permian Sand and the Wet-mix macadam and a 'target' moisture content in the case of the Sharp Sand. The Sharp Sand which was used in Tests WMM7, WMM8 and WMM9 was, however, delivered

to site and compacted at a moisture content some 1.5% to 2.5% below the 10.0% 'target' moisture content specified for work in the laboratory based trench. Additionally, the determination of the dry density of the Sharp Sand, using the sand replacement method (Section 7.5.1), was largely unsuccessful and as such Sharp Sand data from these tests is not directly compared to that from tests conducted in the laboratory based trench.

The dry density results for the three materials generally show good, positive correlations with compactive effort (Figures 7.1 and 7.2). The dry density measurements conducted on the Permian Sand and the Sharp Sand in the laboratory based trench were made using buried density rings which were subsequently excavated. Some doubt inevitably exists regarding the precise location of the rings within each layer. There is, however, some indication that this may be related to the number of passes applied to the layer, each pass forcing the density rings deeper within the compacted material. This is indicated by consideration of the dry density results for Tests TPS3 and TPS4 and Tests TSS3 and TSS4; $N_p/\overline{h} \approx 18$ with $N_p = 2$ and 5 for Tests 3 and 4, respectively.

Analysis of the Impact Value data generally yields strong correlations with compactive effort. For the plotted linear regression lines, of the form of Equation 7.1, the regression correlation coefficient, r, is generally greater than 0.75 (Figures 7.3 and 7.4). Case studies (Section 7.6) illustrate two important points regarding the Clegg meter derived Impact Value. Firstly, the Impact Value does not differentiate between material which is well compacted and material that is superficially compacted by a large number of passes per layer applied to a very thick, single layer (Section 7.6.3). Secondly, it is necessary for reported Impact Values to represent the mean of a number of separate determinations (*e.g.* five or six determinations for each layer of compacted material in a reinstatement; Section 7.6.2).

The Impact Value measured during Test WMM10 indicates that the Clegg meter is sensitive to the dry extreme of moisture content while the data from the lower layers of the well compacted reinstatement at the Salters Lane test site (Section 7.6.3) indicated that the Clegg meter responds to the wet extreme of moisture content.

The foregoing illustrates that the Clegg meter is an excellent device for the measurement of reinstatement backfill quality provided that there is adequate supervision of the compaction process and that measurements immediately after the compaction of each layer are undertaken.

As the three materials were each compacted at moisture contents within a band around either an optimum or 'target' moisture content it has been possible to explore the dependency of the Impact Value on the dry density (Figure 7.7). In general a strong dependence of the Impact Value on dry density is found. This is particularly so for the Sharp Sand and the Wet-mix macadam results.

California Bearing Ratio (*CBR*) determinations were made during tests conducted on the Permian Sand and the Sharp Sand in the laboratory based trench. A general trend of increasing *CBR* with increasing compactive effort is observed for tests on the Sharp Sand (Figures 7.5 and 7.6). No such correlation is observed for the Permian Sand data. Correction of the *CBR* value for moisture content indicates that the above lack of correlation is most likely due to varying degrees of the drying/Calcite cementing effect noted in Section 7.2.1.

Comparison of *IV*, *CBR* data with Clegg's (1980) relationship (Equation 2.1) indicates that the estimated values of *CBR* from Impact Value results would be under-estimated. This corresponds to a 'safe' condition in the context of road design. It should be appreciated, however, that this observation is based on limited data from tests on just two materials the results of which cover a very narrow range of Impact Value. A considerable amount of further work is required before sound conclusions may be drawn regarding the validity, or otherwise, of Clegg's relationship.

The individual surface wave velocity-depth profiles from tests, conducted in the half-full and the full laboratory based trench, on Permian Sand and Sharp Sand are compared in Sections 7.2.2 and 7.3.2.

Such comparisons from tests on the Permian Sand, in addition to highlighting permanent increases in the surface wave velocity due to the previously noted drying/Calcite cementing effect, reveal distinct differences in the influence of the placement of the upper layers on the measured properties of the lower layers. The placement of the upper layers at low levels of compactive effort (N_p = 2 and 5) appears to increase the measured surface wave velocity of the lower layers. In contrast, the placement of the upper layers at high levels of compactive effort (N_p = 8 and 10) leads to a significantly less marked increase in the surface wave velocity of the lower layers. This observation may be considered to reflect the existence of a 'law of diminishing returns' with respect to the compaction process, and supports the use of logarithmic scales for compactive effort when interpreting measured properties in terms of the compactive effort applied.

A similar comparison of test data derived from tests on the Sharp Sand does not reveal a similar effect. However, a strong argument is put forward that the Sharp Sand does not densify efficiently as a result of directly applied compactive effort. Significant densification was, however, indicated due to the compactive effort applied to subsequent layers.

Examination of the combined surface wave velocity-depth profiles for tests on the Permian Sand and Sharp Sand (all tests in the half-full trench and all tests in the full trench) reveals the influence of the layer thickness on the measured properties. For tests on both materials the profiles for the two tests with $N_p/\overline{h} \approx 18\,\mathrm{m}^{-1}$ (Tests TPS3B and TPS4 and Tests TSS3B and TSS4) are almost coincident, as would be expected from consideration of the applied compactive effort.

For similar tests on Wet-mix macadam, which are combined on the basis of layer thickness, a detailed examination of the surface wave velocity-depth profiles for the individual tests shows that for the test on dry material (Test WMM10) the measured surface wave velocities are open to some question as the vibration of the individual particles caused severe difficulty in determining the points at which the in-phase and out-of-phase Lissajous Figures are found. It was also found that the profiles for the three tests with $N_p/\overline{h} = 42.11\,\mathrm{m}^{-1}$ did not coincide as might be expected purely on the basis of the compactive effort applied.

Surface wave propagation appears to be significantly affected by the presence of a steel gas pipe (Test WMM9) but not by the presence of a plastic gas pipe (Test WMM8). The steel pipe is believed to provide a preferential (faster) path along which the wave propagates (Section 7.5.2).

The individual surface wave velocity-depth profiles highlight the interfaces between different material types, lending weight to the fundamental assumption that the depth of propagation is equal to one-half the wavelength ($z = \lambda/2$). The measurements of particle displacement at depth by means of buried accelerometers also lend support to this basic assumption (Section 7.2.5).

The sense of the changes in surface wave velocity at the above mentioned interfaces indicate that the surface wave method is capable of measurement in the situation of a stiff layer overlying a less stiff layer (see Section 3.2.4).

Tests conducted on the Wet-mix macadam at the British Gas plc Salters Lane test site (Section 7.6.3) indicate that the surface wave method is capable of clearly

defining the differences between well compacted and poorly compacted (defined as a large amount of superficial compactive effort applied to a single very deep layer) reinstatements at least in a back-to-back test. This is in contrast to the almost complete failure of the Clegg meter to indicate any quantifiable difference between the two reinstatements.

The plotted linear regression lines correlating the mean surface wave velocity (Equation 7.21) and the mean shear modulus with the applied compactive effort generally yield high values of the regression correlation coefficient with $0.67 \leq r \leq 0.97$, with the exceptions of the analyses of the mean surface wave velocity data for tests on the Sharp Sand in the half-full laboratory based trench and both the mean surface wave velocity and the mean shear moduli data for tests on the Wet-mix macadam having a nominal layer thickness < 200 mm. This latter data relates to a very limited range of compactive effort and includes three tests with an identical level of compactive effort. Considerable scatter was observed in the $v_{Rz_{\max}/2}$ and $G_{z_{\max}/2}$ values and is most likely the root cause of the low values of the regression correlation coefficient.

In general, it is noted that the use of density measurements to convert the surface wave velocities to shear modulus values leads to an improvement in the regression correlation coefficient. On the basis of this factor alone one might justify the provision of density measurements in a future measurement programme. When combined with the fact that the shear modulus is a more appropriate measure of deformational properties, than is the surface wave velocity, such a requirement would seem wholly justified. It has also been observed that surface wave velocity measurements from tests on two entirely different materials (Section 7.6.4), one of which is visually observed as very soft and the other as very stiff, may be comparable. Density measurements and conversion to shear moduli values should highlight the differences in the elastic deformation properties of such materials.

In evaluation of a suitable parameter for use in the assessment of reinstatement backfill quality the degree of numerical sensitivity to the applied compactive effort is of great importance. Such an interpretation of the data is given in Table 7.1 for a change in compactive effort from $N_p/\overline{h} = 15\,\mathrm{m}^{-1}$ to $N_p/\overline{h} = 90\,\mathrm{m}^{-1}$. For all three materials the Impact Value is more sensitive to the applied compactive effort than is the mean surface wave velocity. The mean surface wave velocity is, in turn, more sensitive to the applied compactive effort than is the dry density. The sensitivity

of the mean shear modulus to the applied compactive effort is generally somewhat lower than that of the Impact Value, but higher than that of the mean surface wave velocity (inevitably as $G \propto v_R^2$). As has been previously noted, the shear modulus is a more appropriate measure of reinstatement backfill quality than is the surface wave velocity. The high sensitivity of the mean shear modulus to the applied compactive effort simply serves to reinforce this observation.

Although a high sensitivity to compactive effort is without doubt a highly desirable feature of a parameter which is to be used for the measurement of reinstatement backfill quality, a high level of sensitivity is of little use if the scatter in the experimental data is expected to be great (*i.e.* low values of the regression correlation coefficient, r). This factor is allowed for by re-evaluating the numerical sensitivity as a 'correlation sensitivity', defined as the product of the regression correlation coefficient and the numerical sensitivity (rS). Such an analysis is shown in Table 7.1. The essential relationships between the parameters, as determined from the numerical sensitivity analysis, remain largely unaltered. The Impact Value has a higher value of 'correlation sensitivity' than has the mean surface wave velocity which, in turn, has a higher 'correlation sensitivity' than was the dry density. The mean shear modulus has a 'correlation sensitivity' intermediate between that of the mean surface wave velocity and of the Impact Value, as for the numerical sensitivity.

A series of some five case studies has also been interpreted and discussed in this chapter and the major observations drawn from these tests being combined with observations from the test series on Permian Sand, Sharp Sand and Wet-mix macadam earlier in this section.

Comparisons between laboratory and field derived values of dry density and moisture content with the dry density-moisture content relationships determined from British Standard tests (Chapter 4) are made in Section 7.7. The major observation from this section is that it may well be advisable in future work to vary the moisture content of field compacted material with the level of applied compactive effort in order to ensure that the field moisture content approximates to the optimum moisture content at each level of compactive effort. This should prevent field dry densities from falling within the 'wet of optimum' range for any given level of compactive effort. In this range there is a potential for rapid strength loss on wetting of the compacted material as may occur under field conditions.

Section 7.8 highlights a number of experimental observations concerning the surface wave velocity propagation technique including the tentative conclusion that reflections fron the trench sides are minimal, both in the field trenches and in the laboratory based trench. Maximum shear strains due to surface wave propagation are also calculated (Section 7.8.1) and the measured values are shown to encompass the estimate made by Seed and Idriss (1970).

Surface wave attenuation measurements have been made as part of the test programme on Permian Sand, Sharp Sand and Wet-mix macadam (not Tests TPS1 and TPS2). These facilitated the calculation of the shear strains (see above) and also of the material attenuation coefficient (α). The calculation of α was achieved using a new, straight line form of the Bornitz equation which eliminates the need to make potentially erroneous assumptions regarding the state of the attenuation curve close to the source of vibration. Consistent relations between α and the applied compactive effort could not be found. The potential use of this technique in improving the reliability and ease of calculation of the material attenuation coefficient and, therefore, vibration amplitude predictions due to construction activities is significant (see Section 7.2.4).

Table 7.1 - Numerical sensitivities (S) and 'correlation sensitivities' (rS) of the parameters ρ_d, IV, CBR, $v_{Rz_{max}/2}$ and $G_{z_{max}/2}$ to compactive effort.

Parameter	Material	Value at $N_p/\overline{h} = 15\,\mathrm{m}^{-1}$	Value at $N_p/\overline{h} = 90\,\mathrm{m}^{-1}$	$S^{\dagger}$ (%)	r	rS (%)	Based on Equation
ρ_d	TPS‡	1.819	1.859	2.2	0.433	1.0	(7.6)
($\mathrm{Mg/m^3}$)	TSS	1.615	1.724	6.5	0.670	4.4	(7.39)
	WMM	1.900	2.147	12.2	0.957	11.7	(7.57)
IV	TPS‡	2.78	6.14	75.3	0.983	74.0	(7.12)
	TSS	4.00	6.46	47.0	0.850	40.0	(7.42)
	WMM	14.79	26.03	55.1	0.917	50.5	(7.60)
CBR (%)	TSS	5.56	6.60	16.3	0.310	5.1	(7.45)
$v_{Rz_{max}/2}$*	TPS‡	141.92	188.16	28.0	0.973	27.2	(7.28)
(m/s)	TSS	154.18	180.89	15.9	0.964	15.3	(7.50)
	WMM	130.13	176.38	30.2	0.677	20.4	(7.64)
$G_{z_{max}/2}$*	TPS‡	51.20	80.44	44.4	0.973	43.2	(7.36)
(MPa)	TSS	55.26	78.47	34.7	0.826	28.7	(7.54)
	WMM	35.13	76.04	73.6	0.731	53.8	(7.67)

† Sensitivity, $S = \dfrac{(\text{Value at } N_p/\overline{h} = 90\,\mathrm{m}^{-1} - \text{ Value at } N_p/\overline{h} = 15\,\mathrm{m}^{-1})}{1/2\,(\text{Value at } N_p/\overline{h} = 90\,\mathrm{m}^{-1} + \text{ Value at } N_p/\overline{h} = 15\,\mathrm{m}^{-1})}$.

‡Permian Sand (TPS) sensitivities are calculated from the equations excluding data from Test TPS1.

*TPS and TSS data for $v_{Rz_{max}/2}$ and $G_{z_{max}/2}$ are for tests conducted in the full laboratory based trench.

Table 7.2 - Ranges for maximum shear strains induced by surface wave propagation for tests on Permian Sand, Sharp Sand and Wet-mix macadam.

Material	Range of shear strain, γ (10^{-3}%)	
	frequency, f = 500 Hz	frequency, f = 300 Hz
Permian Sand	1.00 to 1.59	1.08 to 2.49
Sharp Sand	— to —	0.59 to 1.10
Wet-mix macadam	0.09 to 0.30	0.30 to 0.84

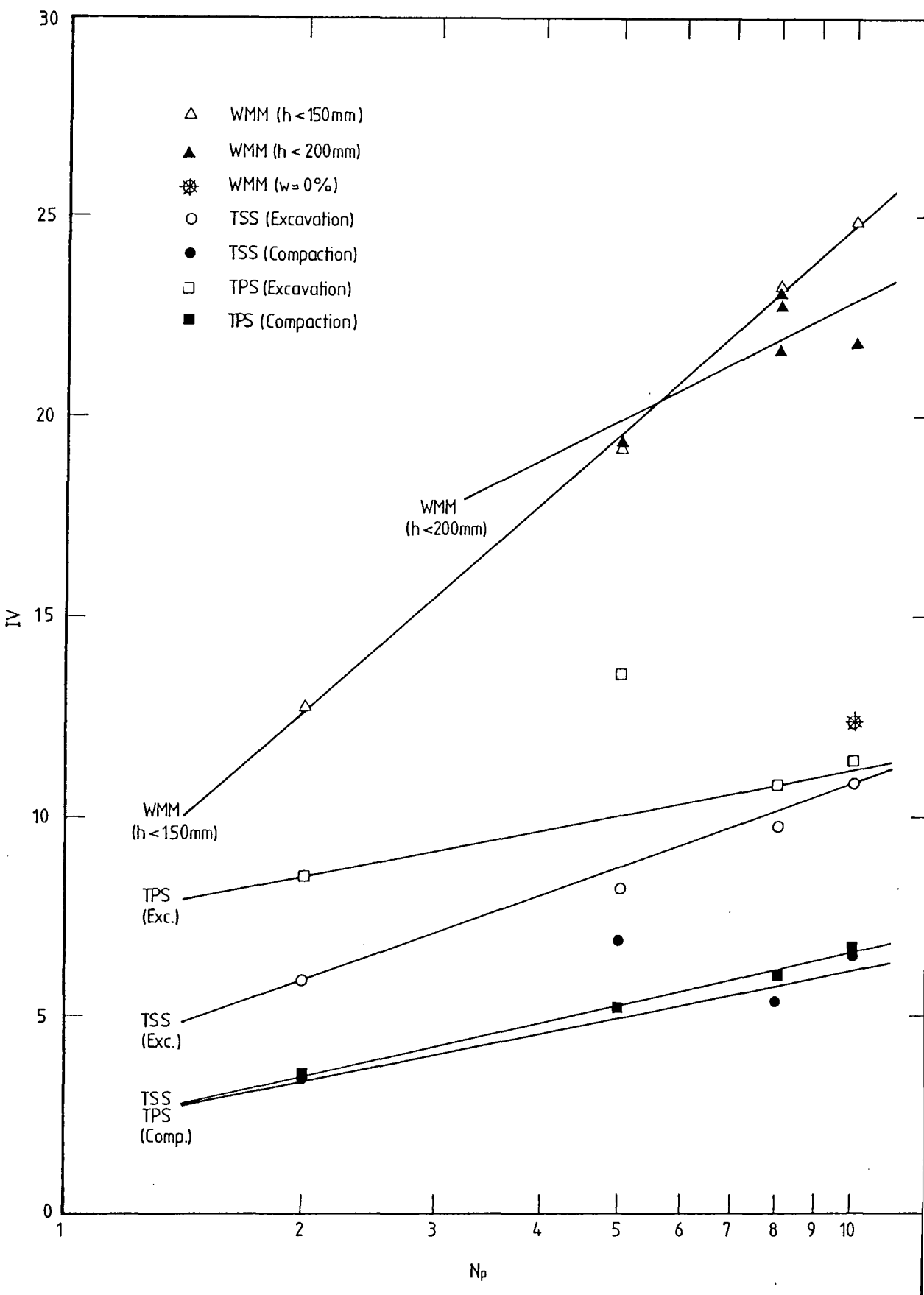

Figure 7.3 - Plot of the number of passes per layer (N_p) (logarithmic scale) against Impact Value (IV) for tests on Permian Sand, Sharp Sand and Wet-mix macadam.

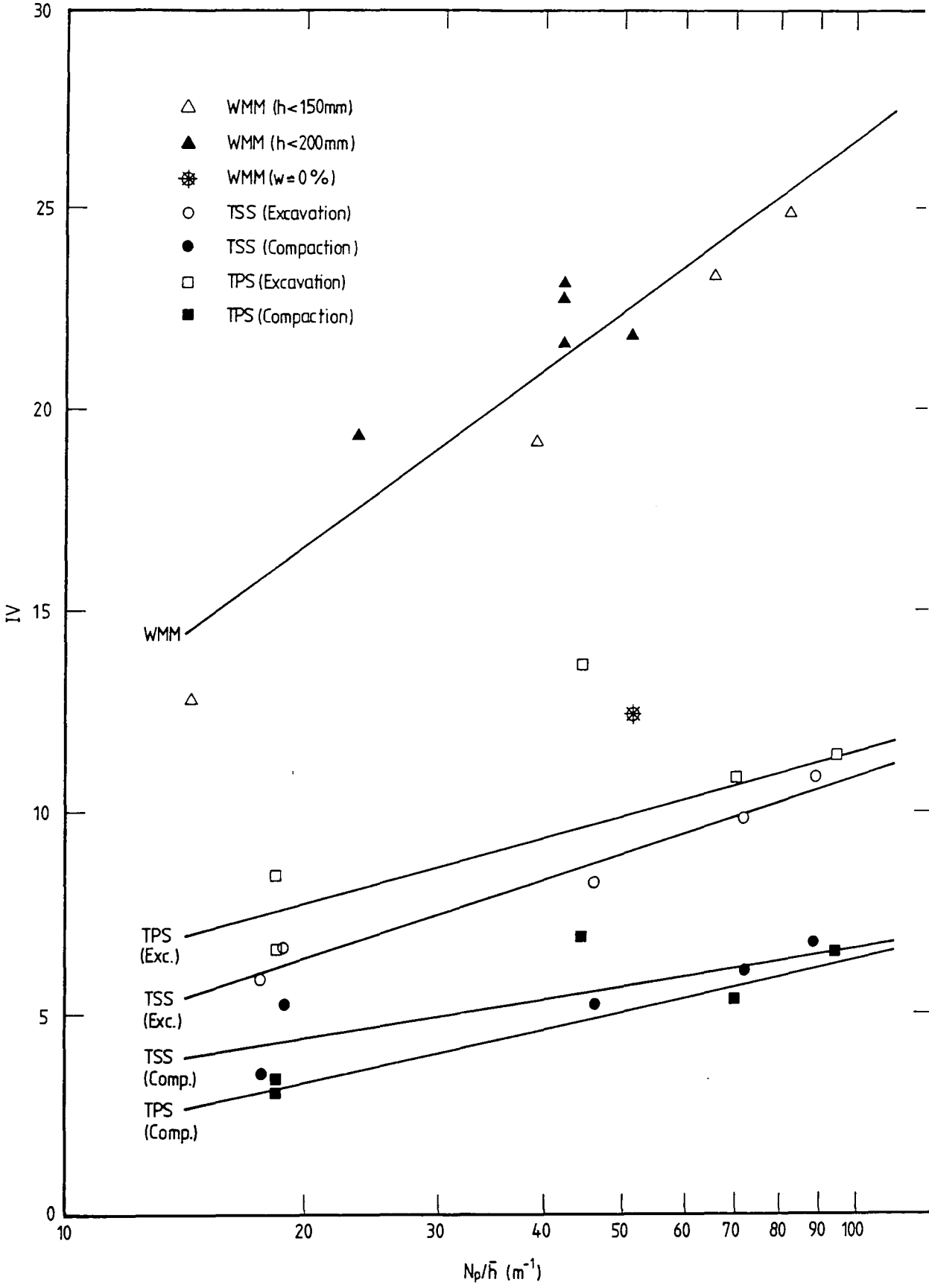

Figure 7.4 - Plot of the ratio of the number passes per layer to the mean layer thickness ($N_p/\bar{h}$) (logarithmic scale) against Impact Value (IV) for tests on Permian Sand, Sharp Sand and Wet-mix macadam.

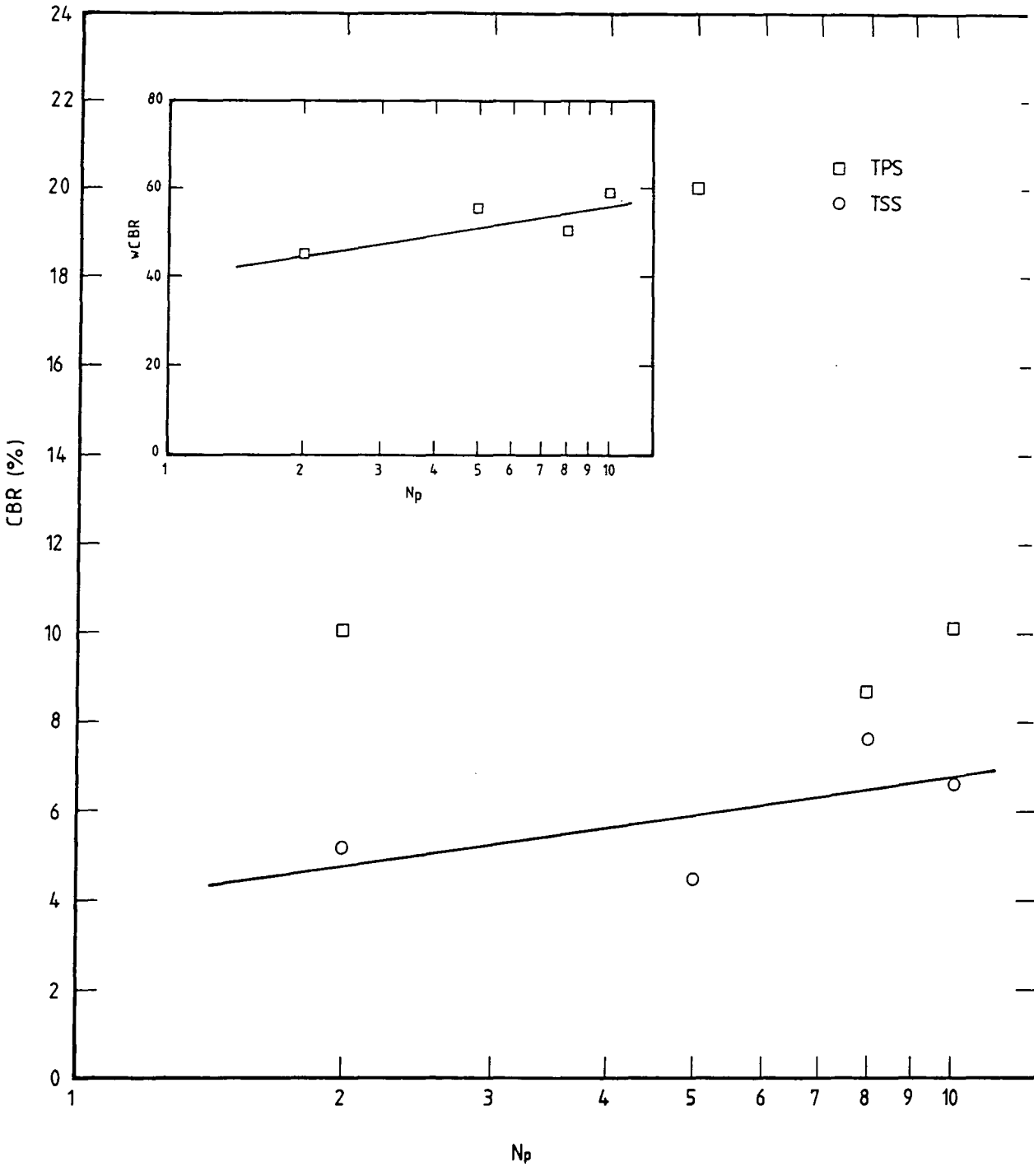

Figure 7.5 - Plot of the number passes per layer (N_p) (logarithmic scale) against CBR for tests on Permian Sand and Sharp Sand. Also shown (inset) is the relationship between log N_p and the product of CBR and moisture content ($wCBR$) for tests on Permian Sand.

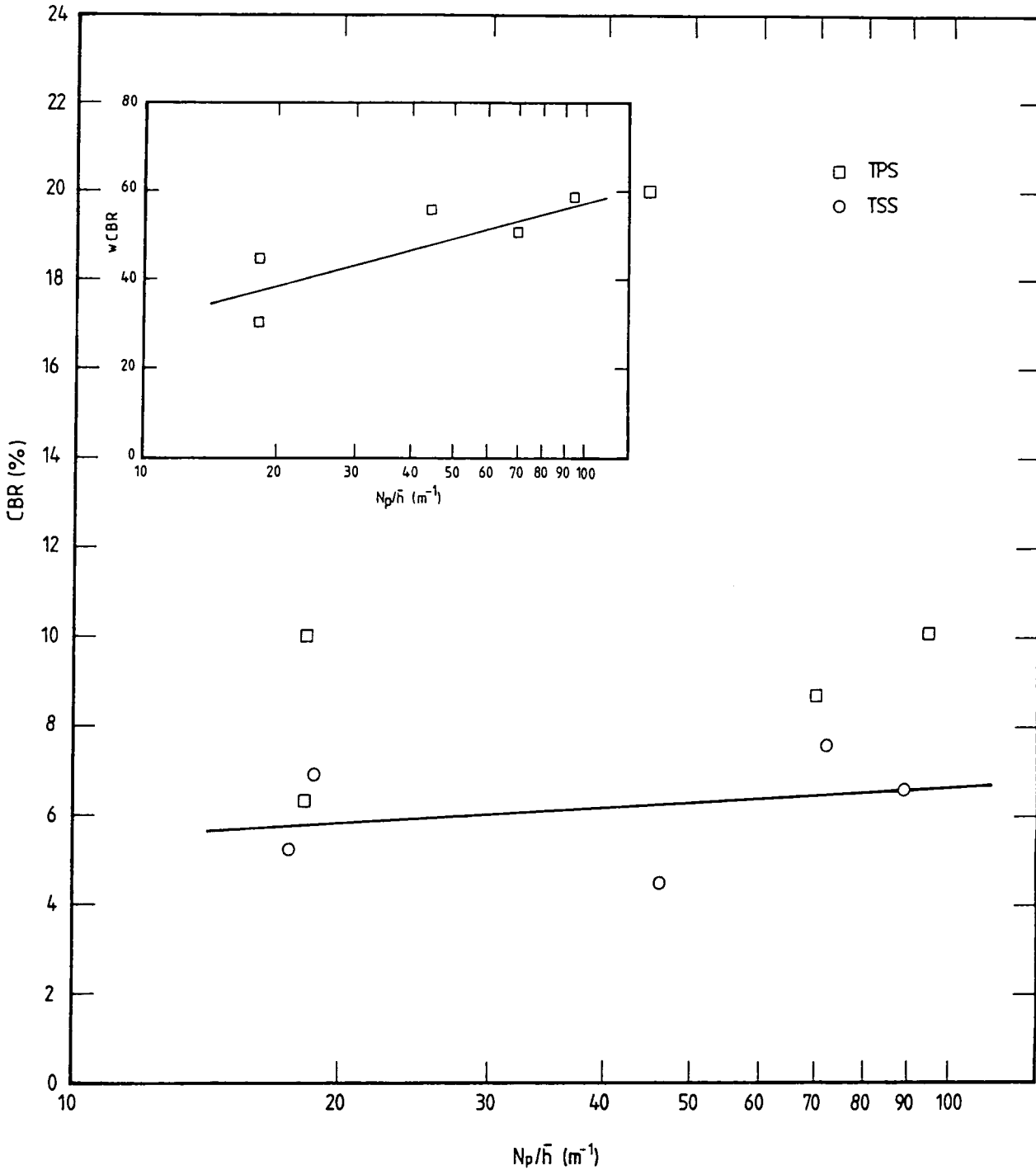

Figure 7.6 - Plot of the ratio of the number passes per layer to the mean layer **thickness** ($N_p/\overline{h}$) (logarithmic scale) against CBR for tests on Permian Sand **and Sharp** Sand. Also shown is the relationship between $\log(N_p/\overline{h})$ and the product **of** CBR and moisture content ($wCBR$) for tests on Permian Sand.

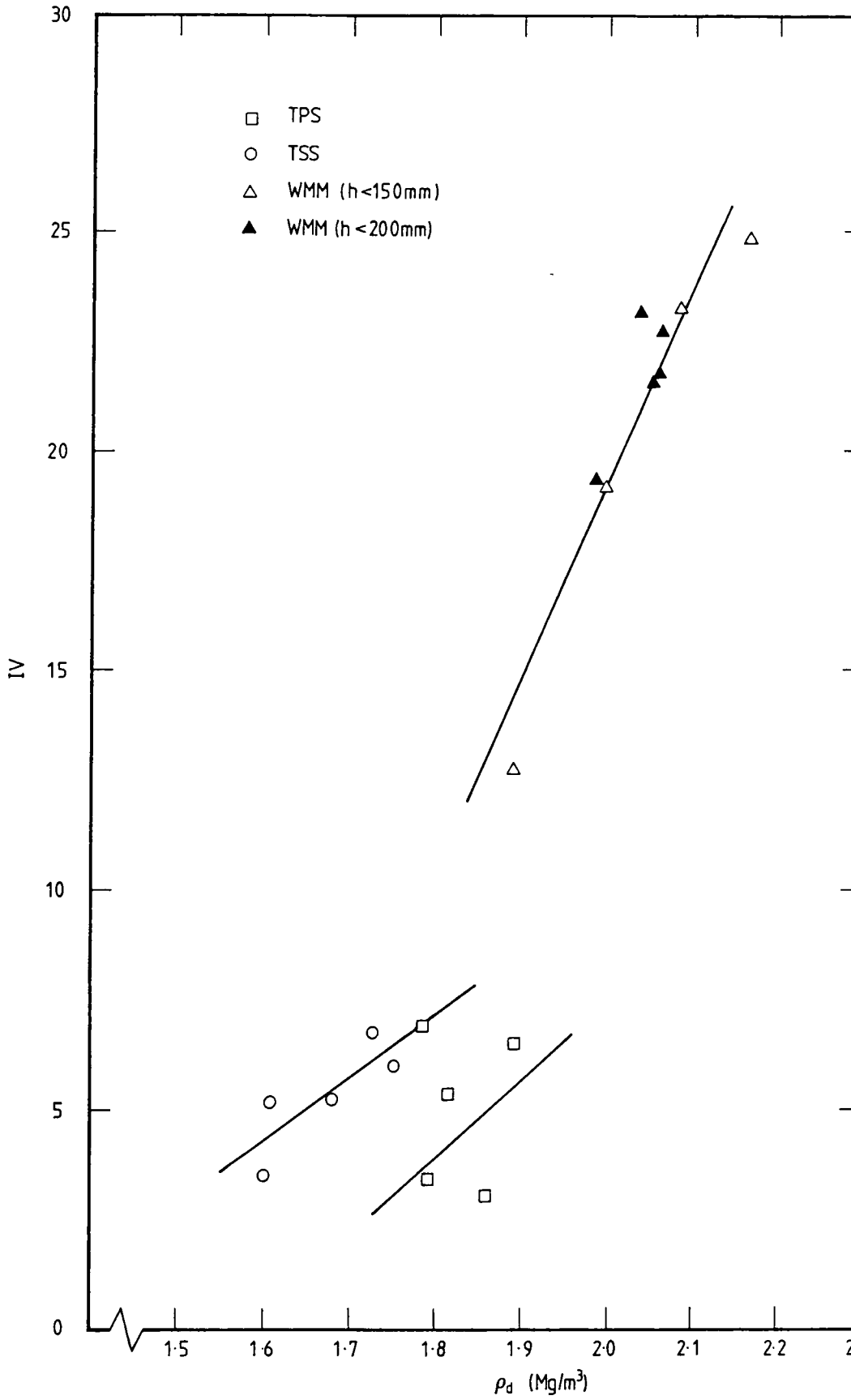

Figure 7.7 - Plot of dry density (ρ_d) against IV for tests on Permian Sand, Sharp Sand and Wet-mix macadam.

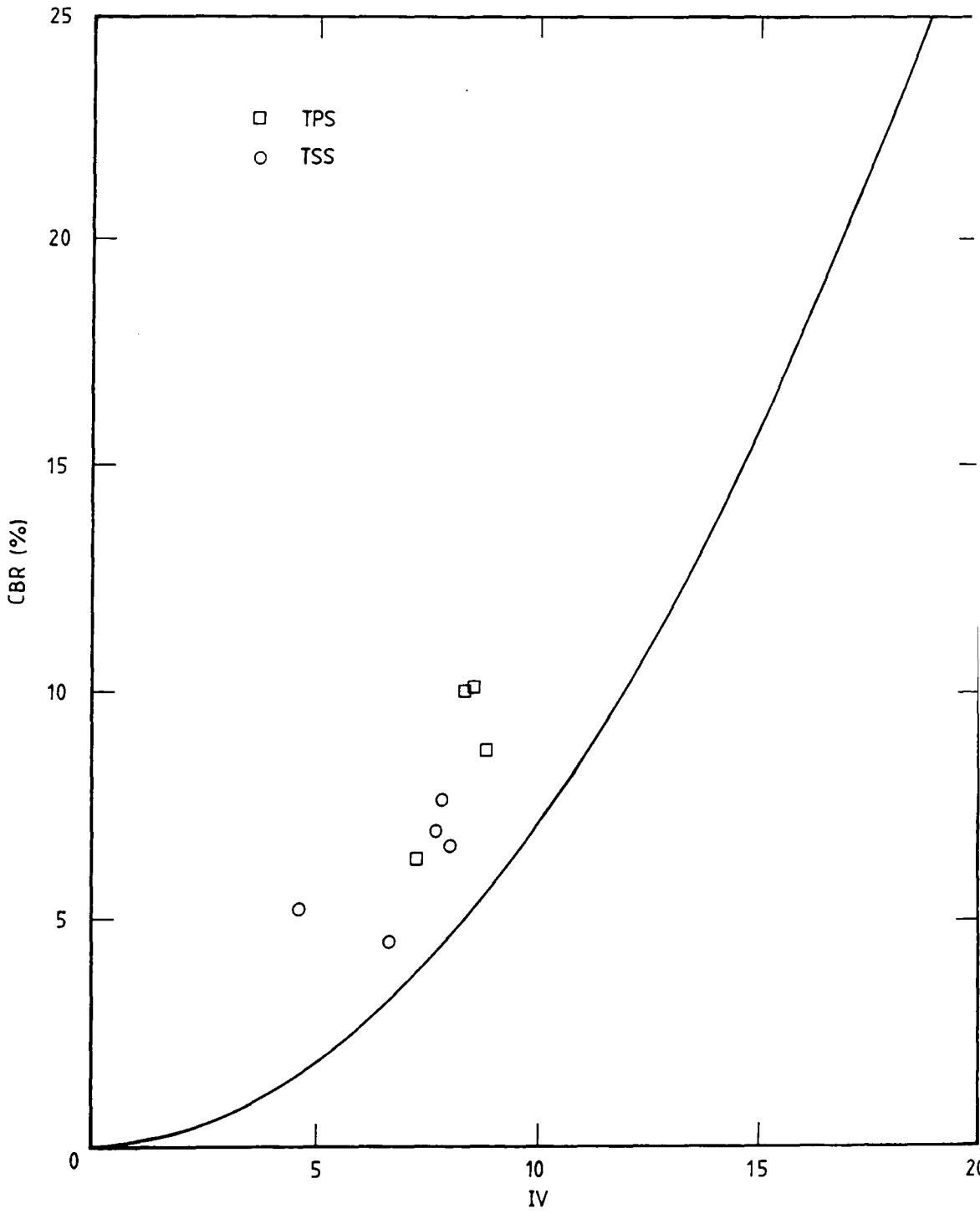

Figure 7.8 - Plot of Impact Value (IV) against CBR for tests on Permian Sand a
Sharp Sand. Clegg's (1980) relationship [$CBR = 0.07(IV)^2$] is shown for compa
son.

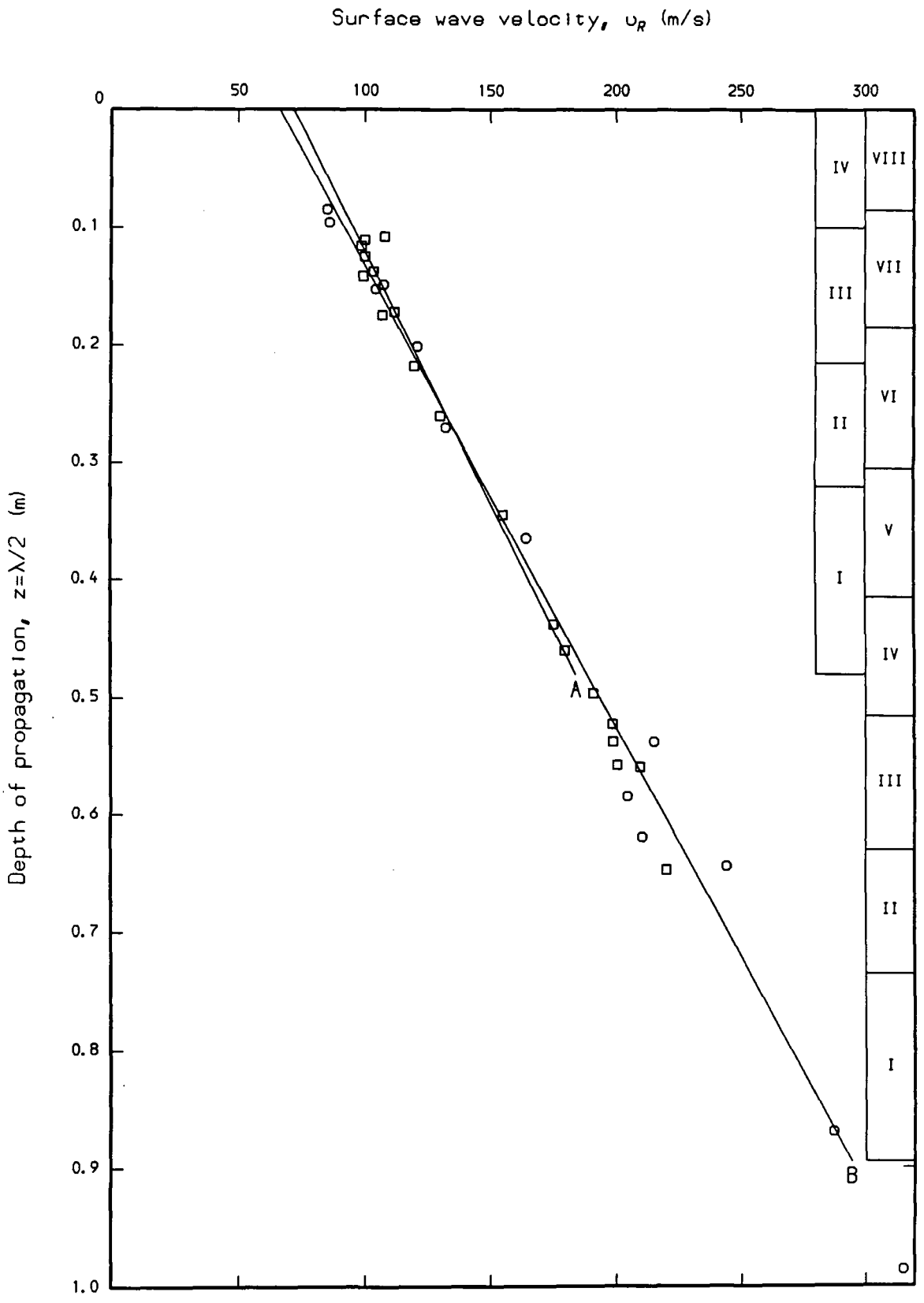

Figure 7.9 - Surface wave velocity-depth profiles for Tests TPS1A and TPS1B. Layer logs are shown for the two tests.

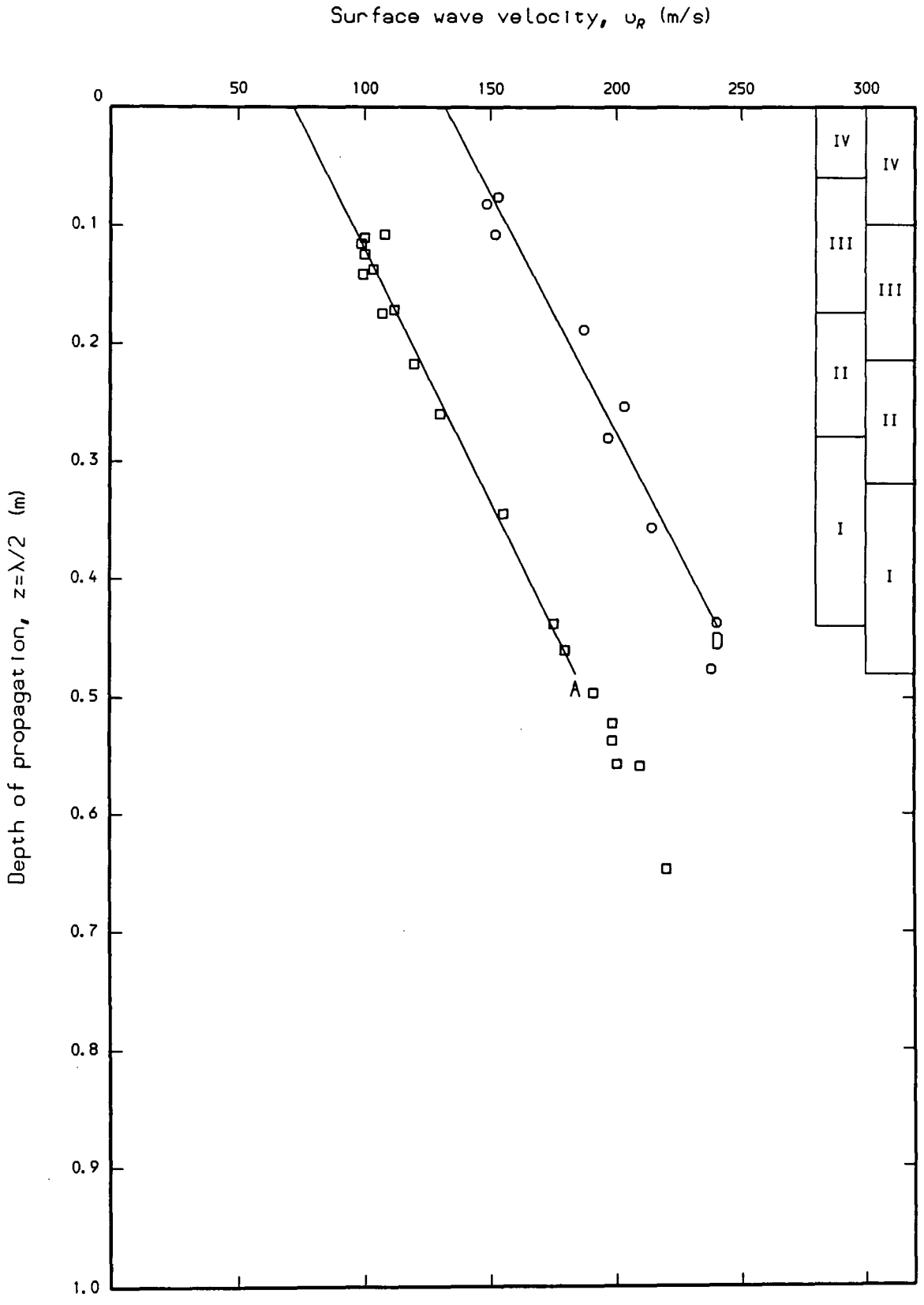

Figure 7.10 - Surface wave velocity-depth profiles for Tests TPS1A and TPS1D. Layer logs are shown for the two tests.

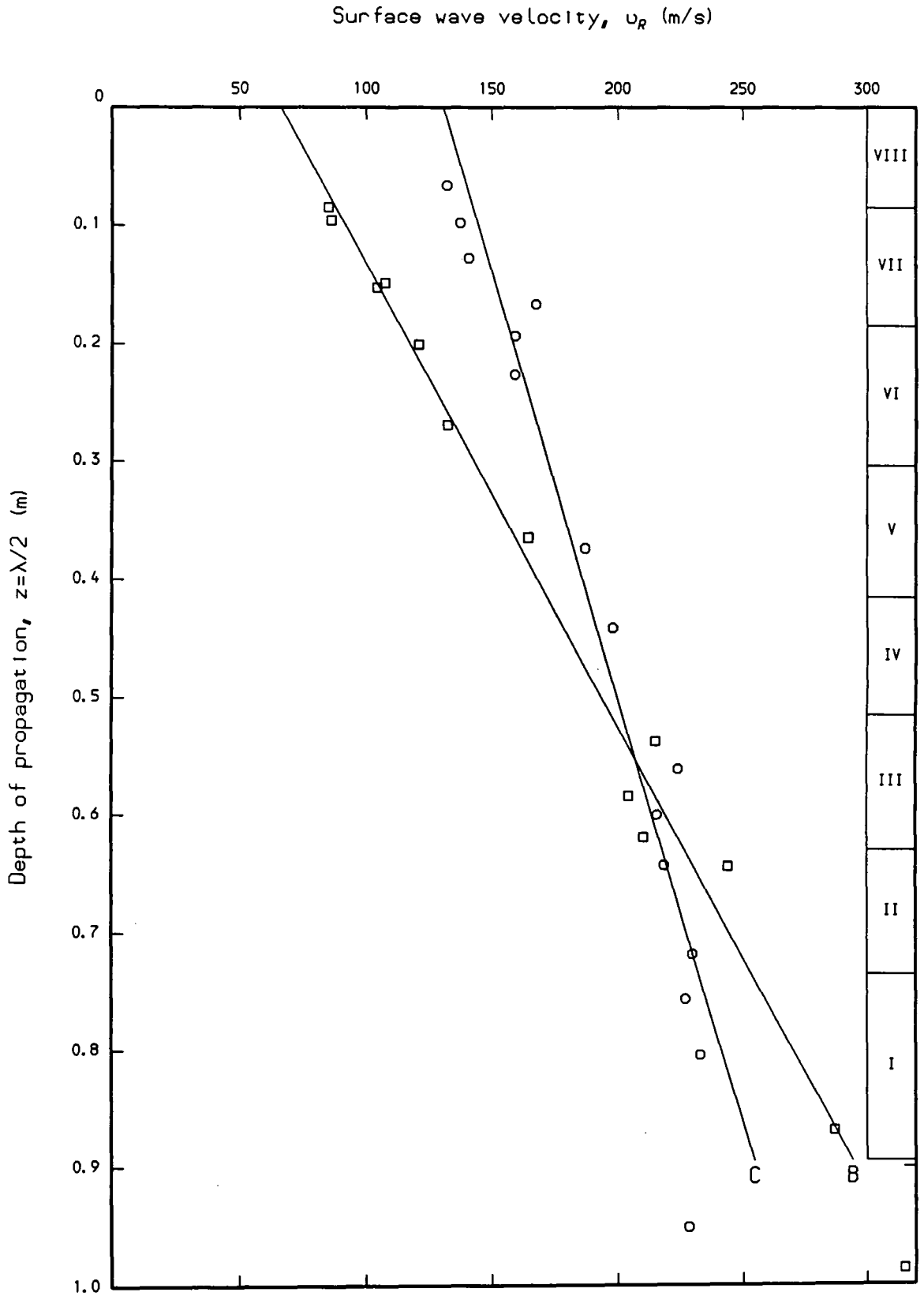

Figure 7.11 - Surface wave velocity-depth profiles for Tests TPS1B and TPS1C. The layer log shown is for both tests.

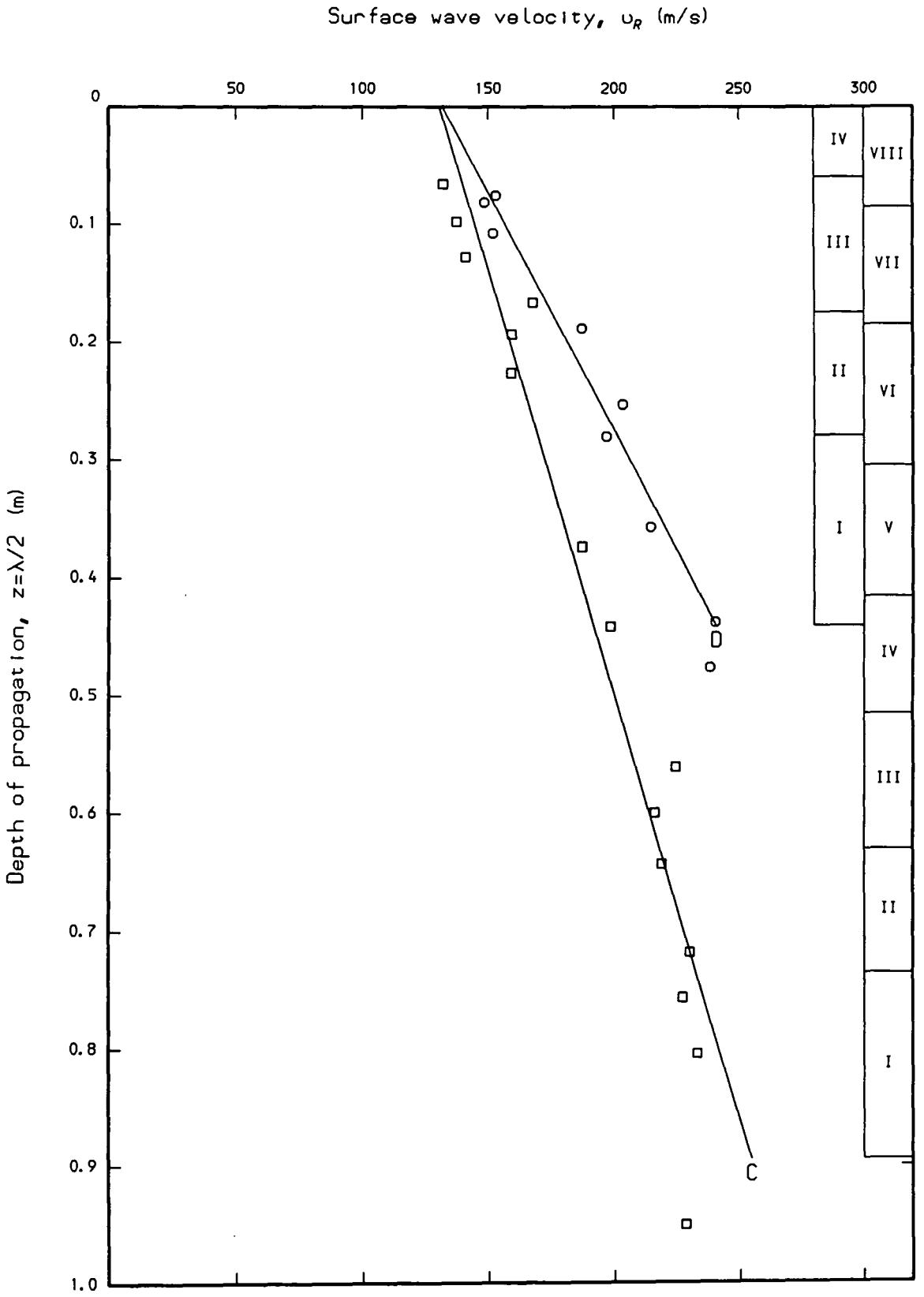

Figure 7.12 - Surface wave velocity-depth profiles for Tests TPS1C and TPS1D. Layer logs are shown for the two tests.

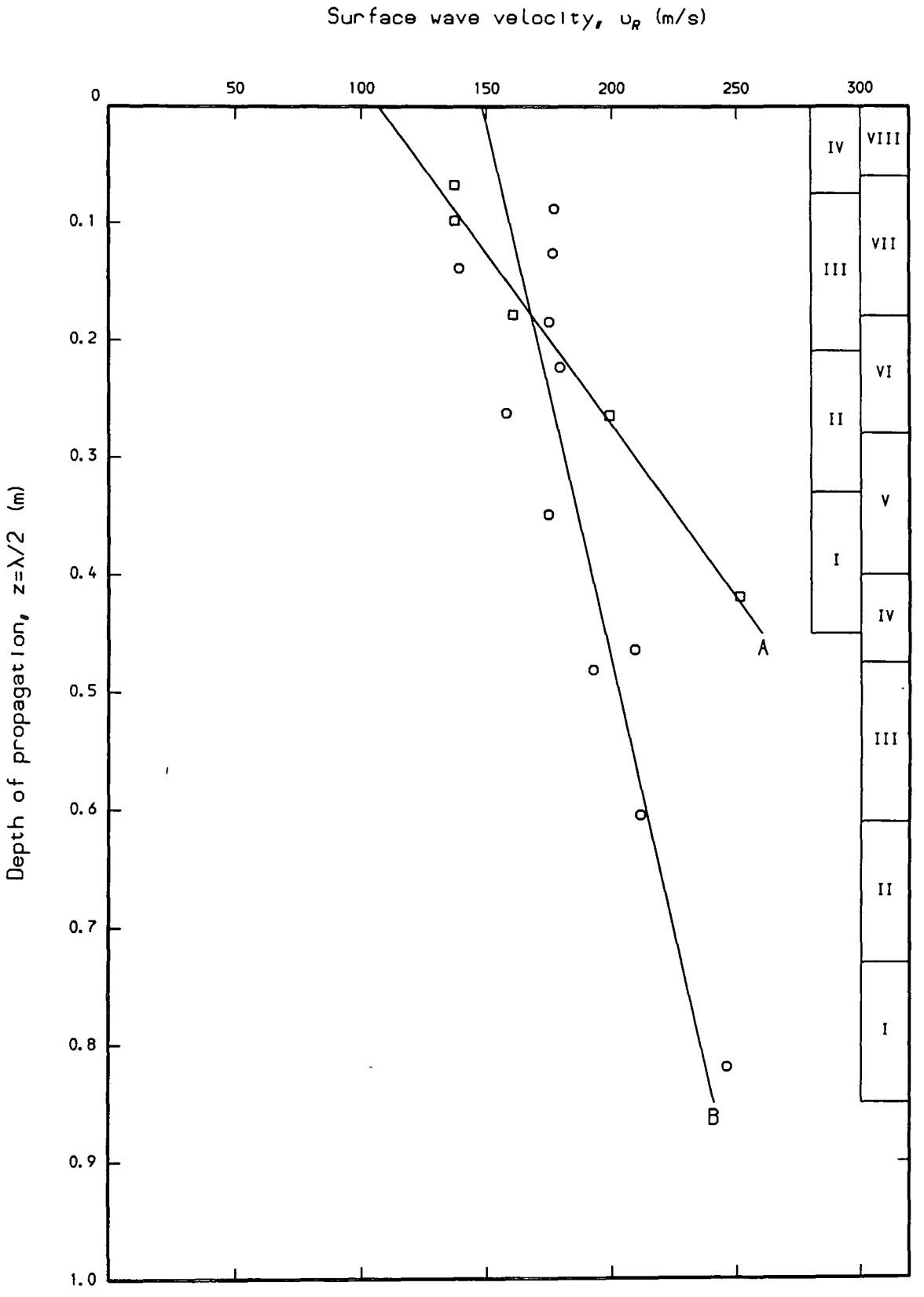

Figure 7.13 - Surface wave velocity-depth profiles for Tests TPS2A and TPS2B. Layer logs are shown for the two tests.

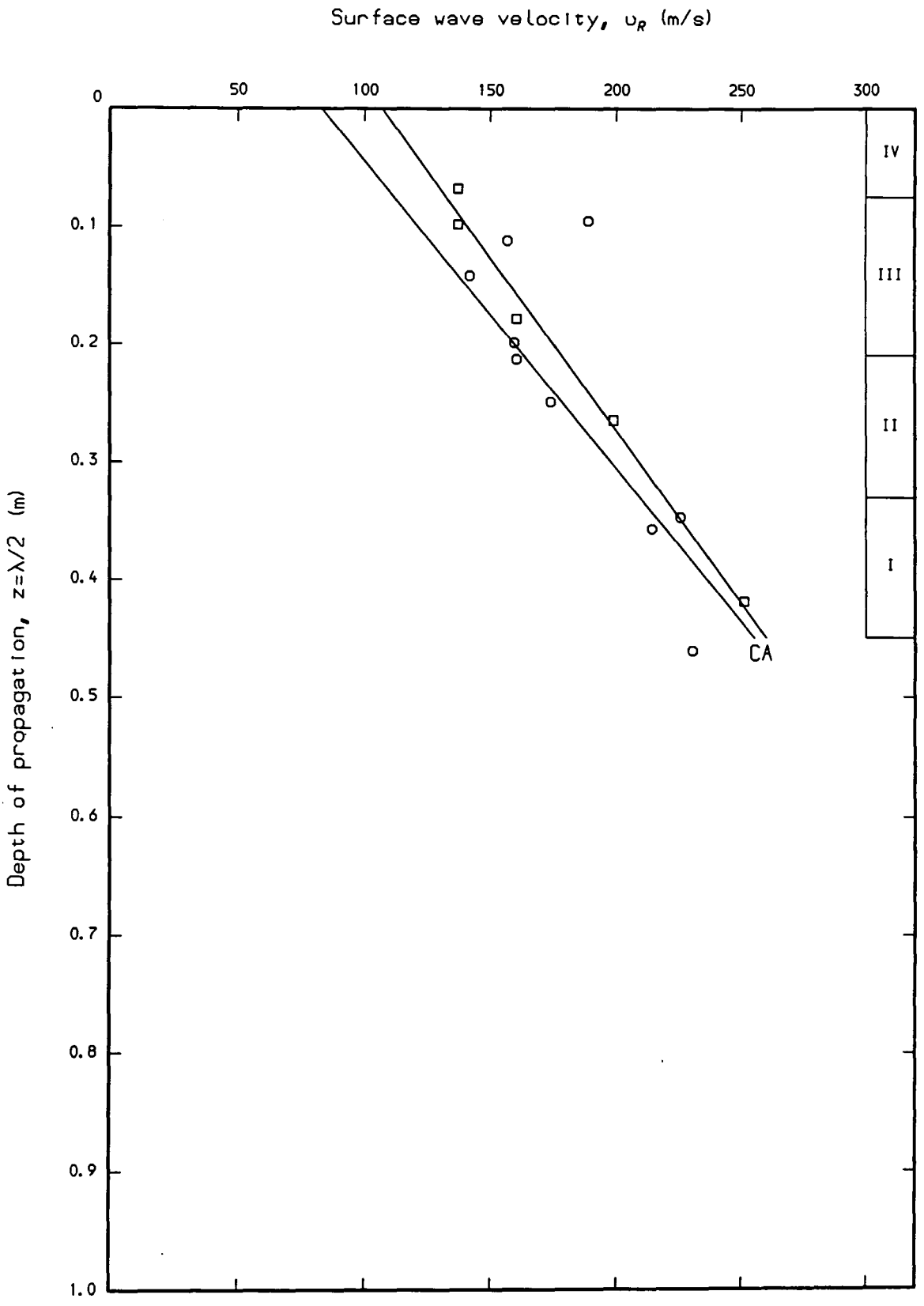

Figure 7.14 - Surface wave velocity-depth profiles for Tests TPS2A and TPS2C. The layer log shown is for both tests.

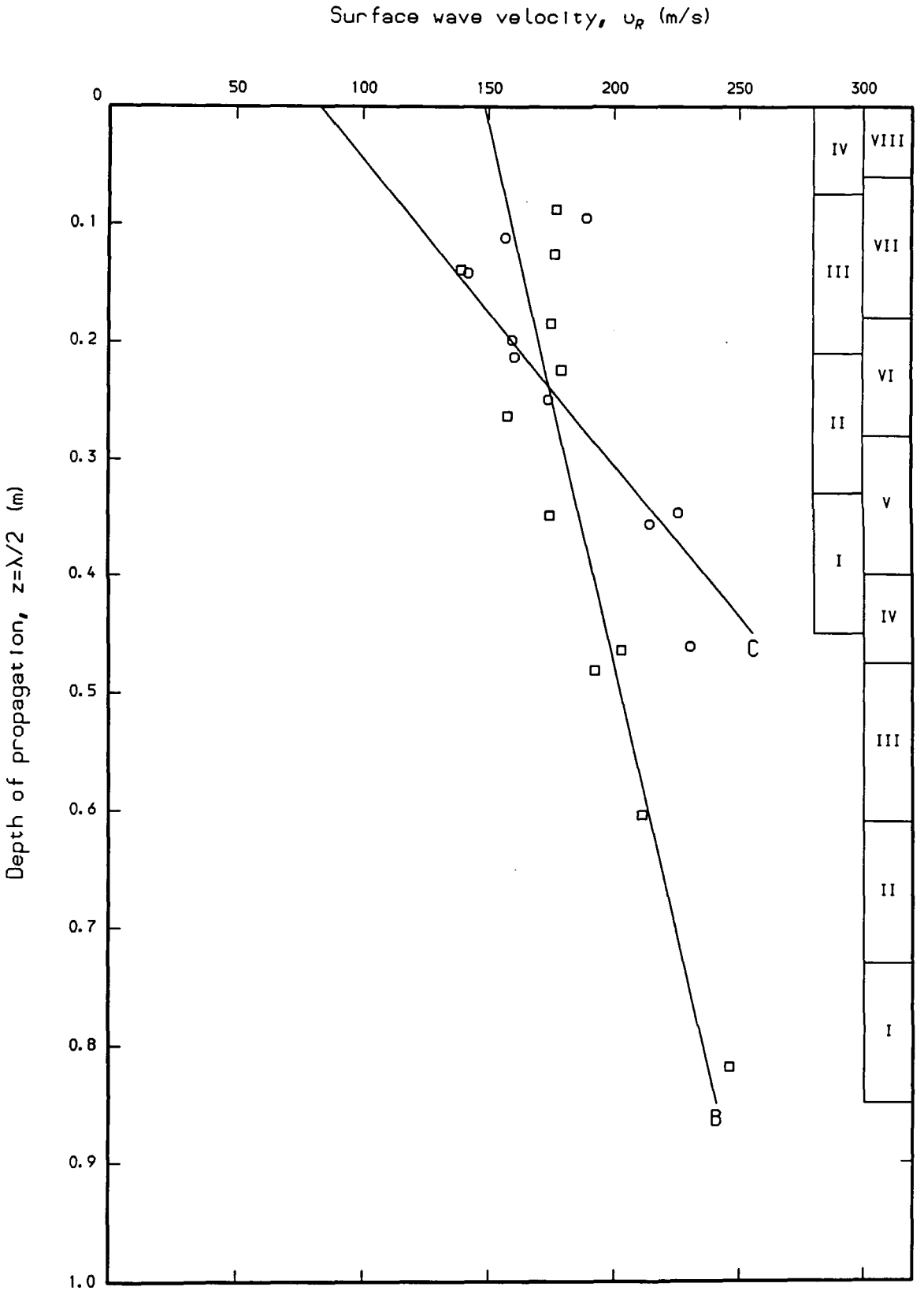

Figure 7.15 - Surface wave velocity-depth profiles for Tests TPS2B and TPS2C. Layer logs are shown for the two tests.

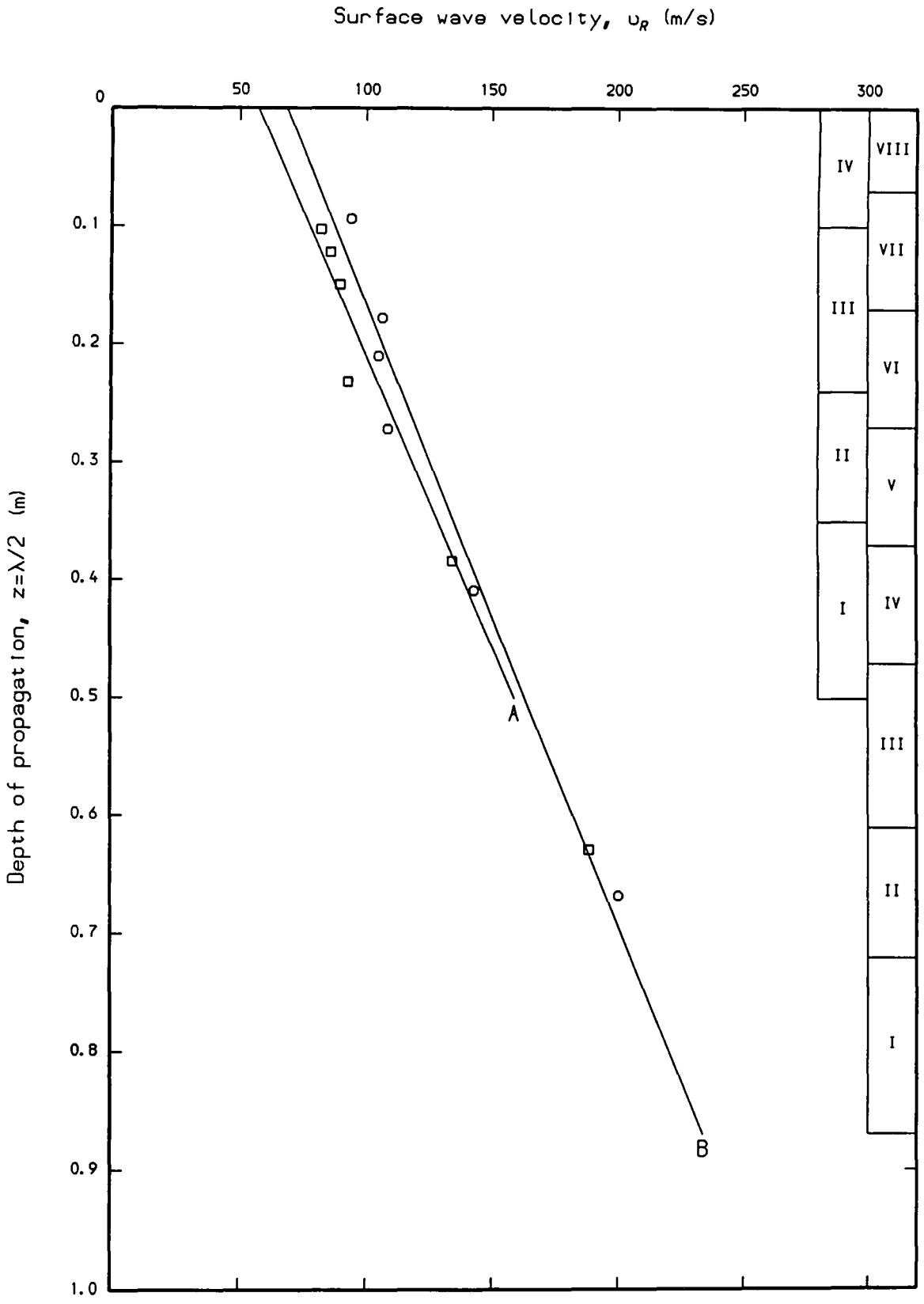

Figure 7.16 - Surface wave velocity-depth profiles for Tests TPS3A and TPS3B. Layer logs are shown for the two tests.

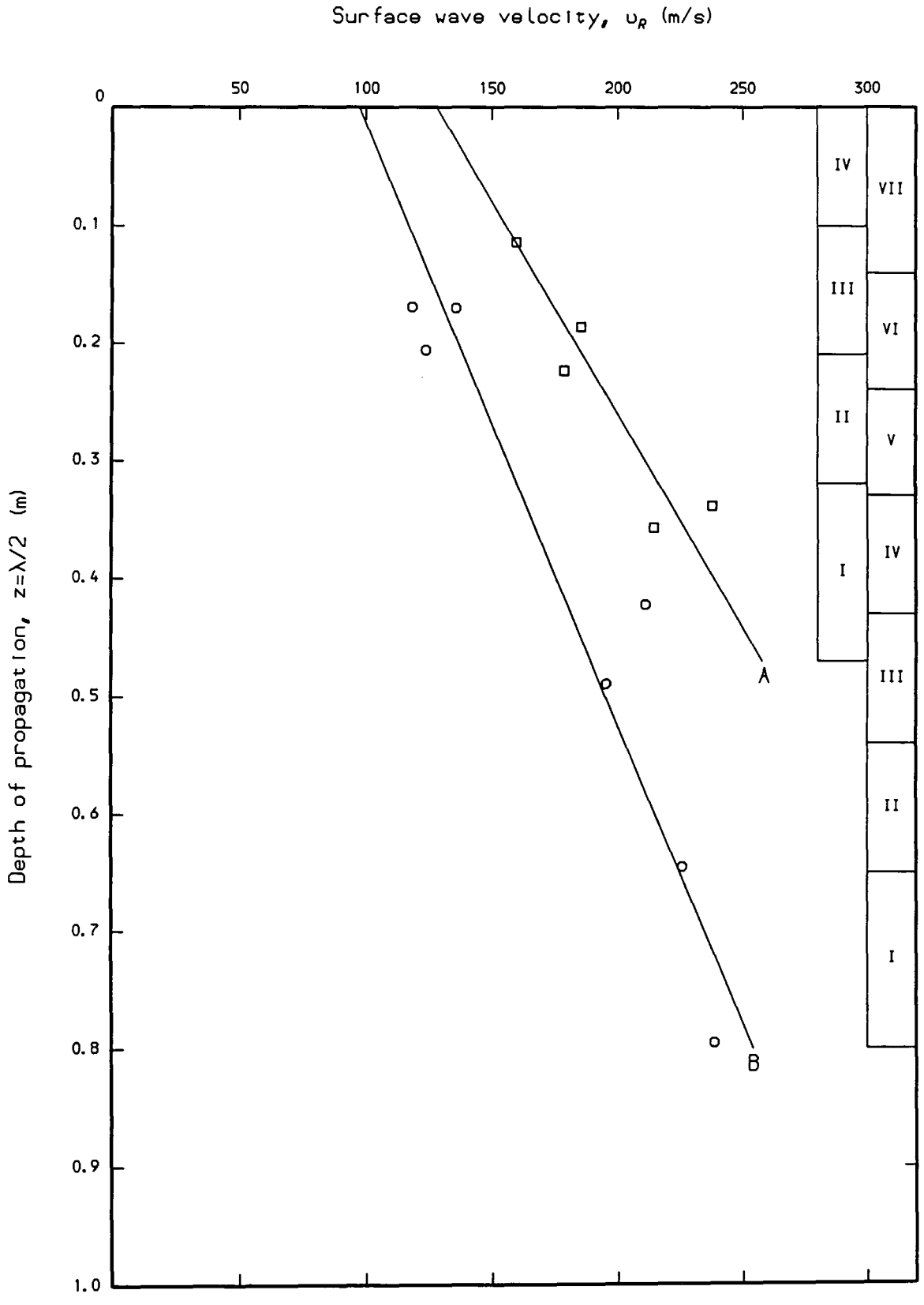

Figure 7.17 - Surface wave velocity-depth profiles for Tests TPS5A and TPS5B. Layer logs are shown for the two tests.

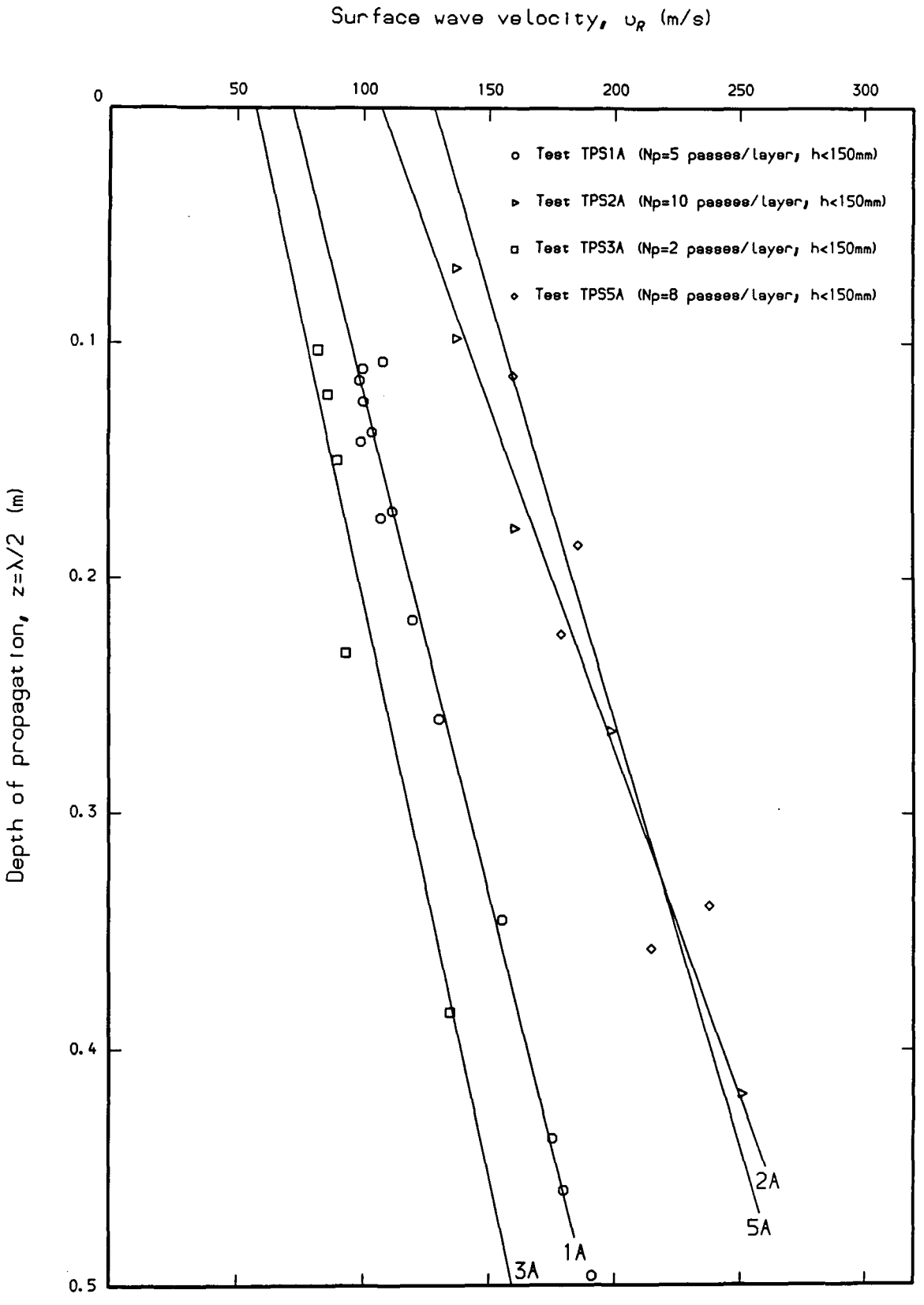

Figure 7.18 - Surface wave velocity depth-profiles for Tests TPS1A, TPS2A, TPS3A and TPS5A (half depth).

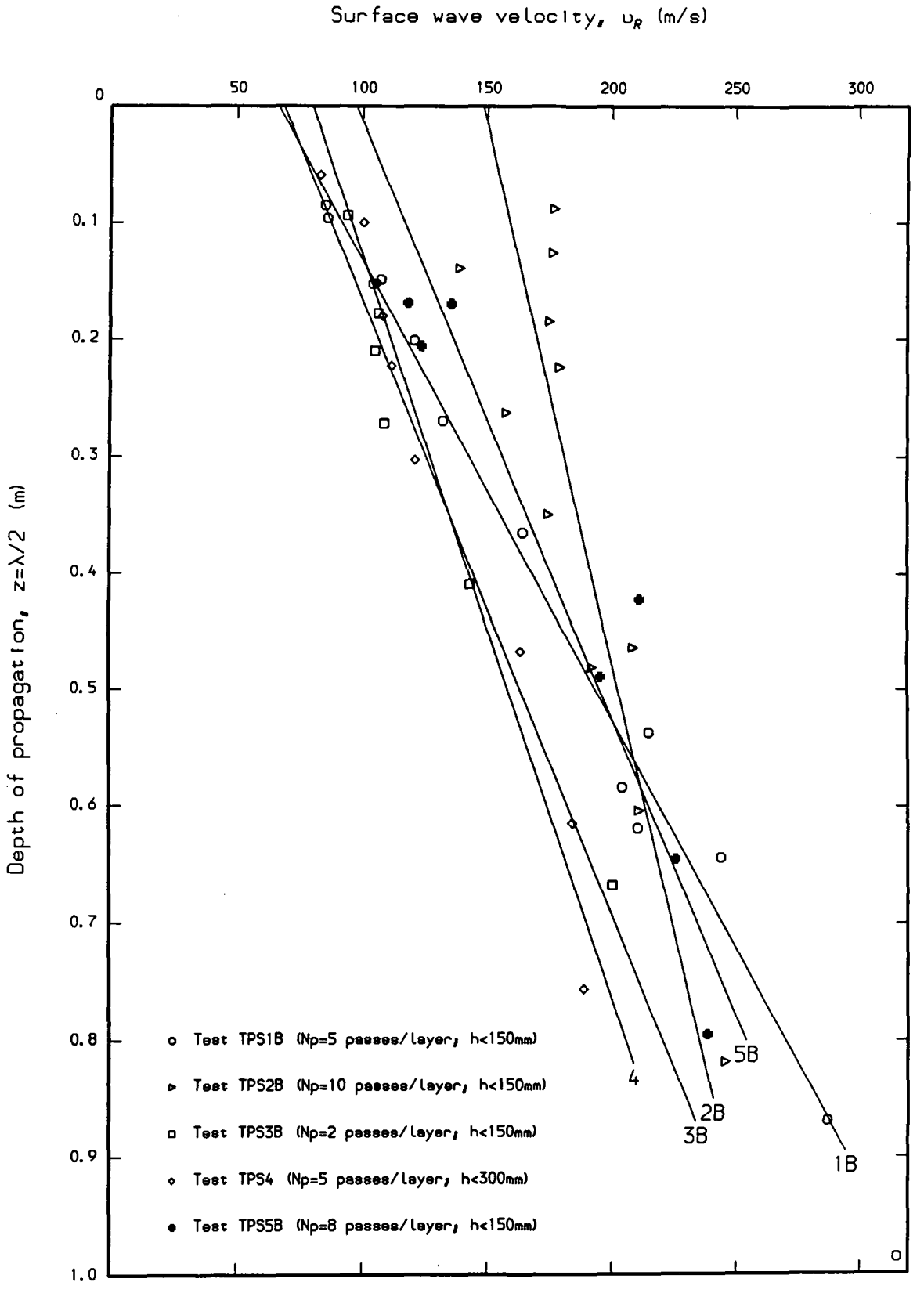

Figure 7.19 - Surface wave velocity-depth profiles for Tests TPS1B, TPS2B, TPS3B, TPS4 and TPS5B (full depth).

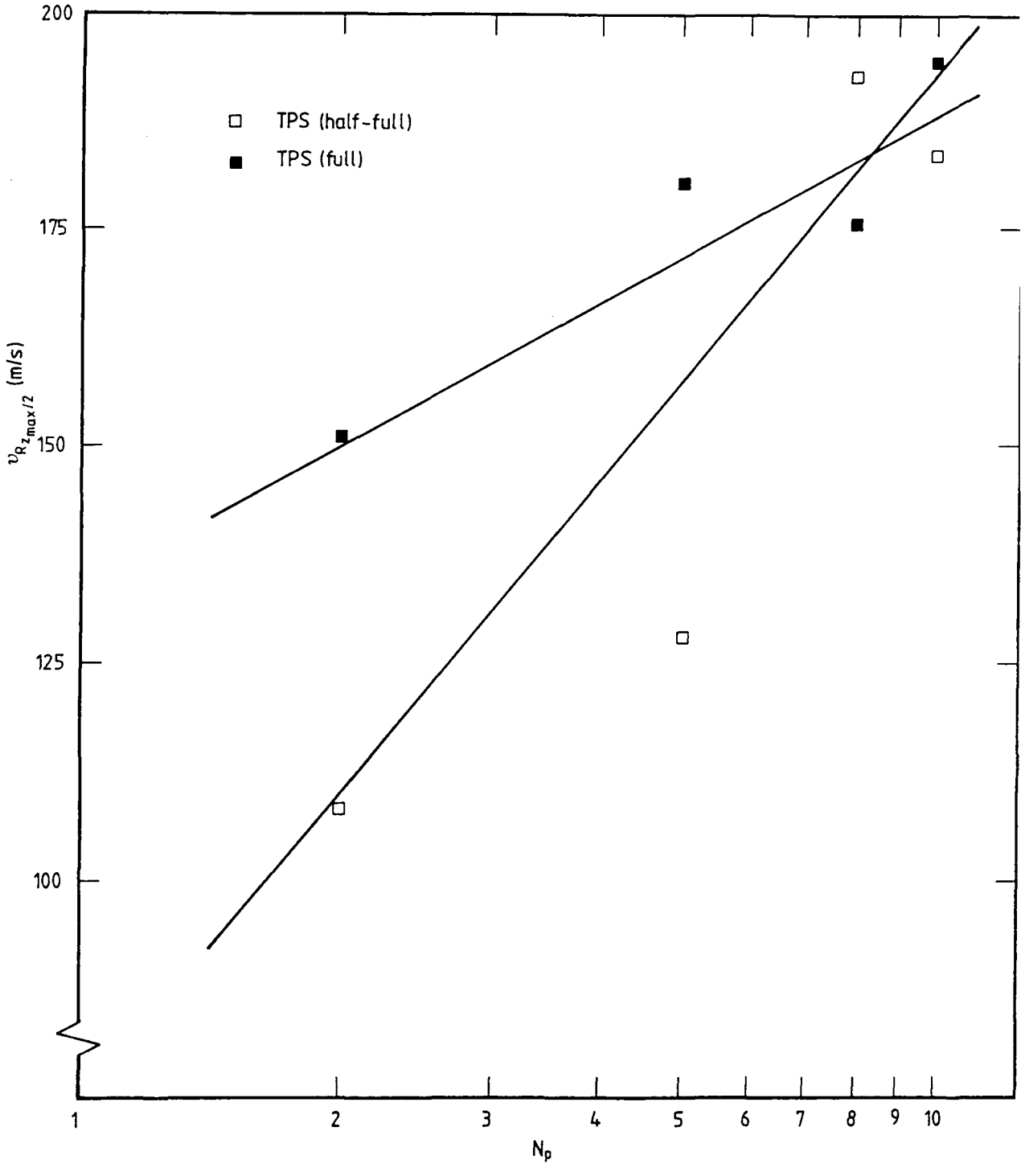

Figure 7.20 - Plot of the number of passes per layer (N_p) (logarithmic scale) against the mean surface wave velocity ($v_{Rz_{max}/2}$) for tests on the Permian Sand in both the half-full and the full trench.

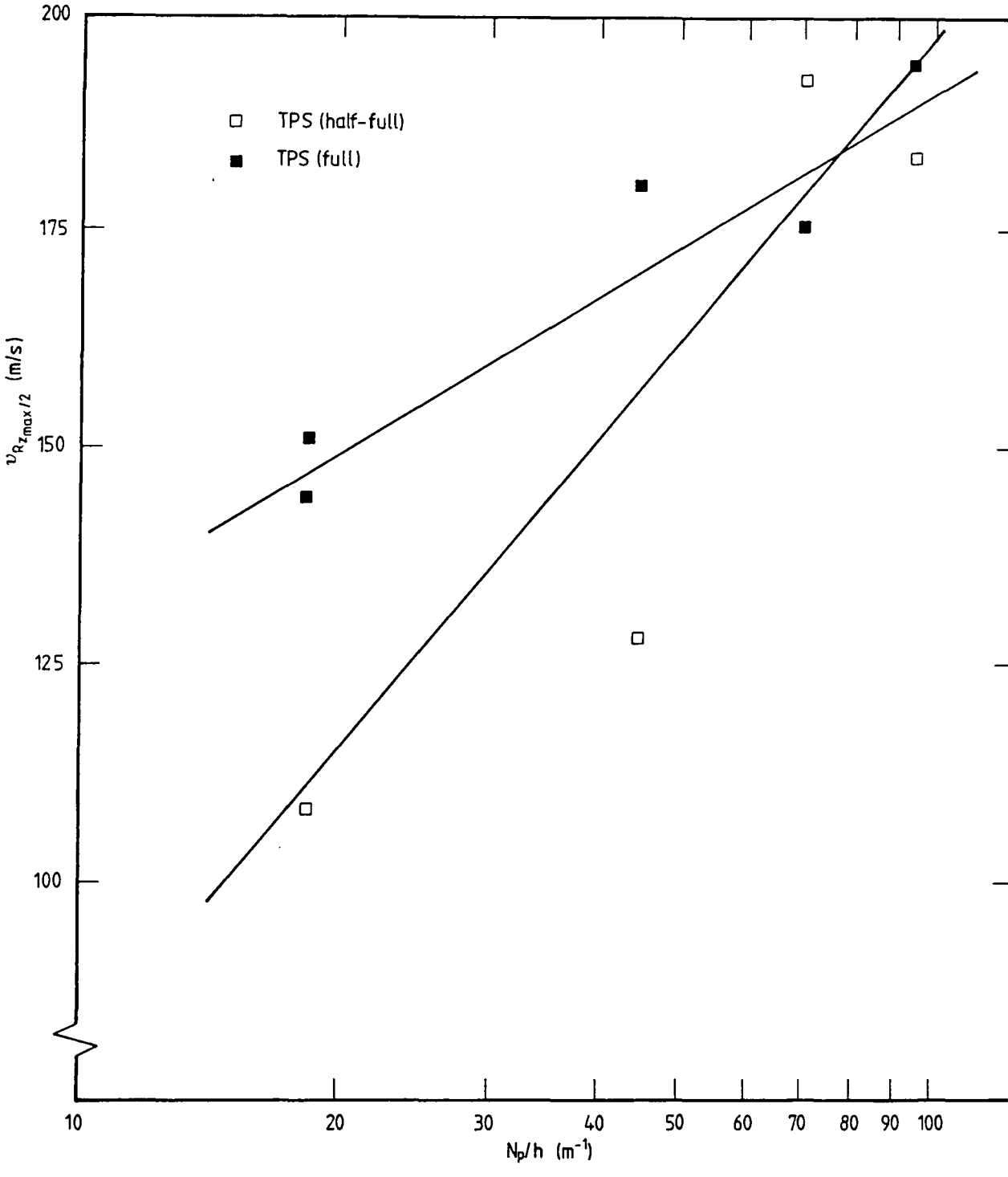

Figure 7.21 - Plot of the ratio of the number of passes per layer to the mean layer thickness ($N_p/\overline{h}$) (logarithmic scale) against the mean surface wave velocity ($v_{Rz_{max}/2}$) for tests on the Permian Sand in both the half-full and the full trench.

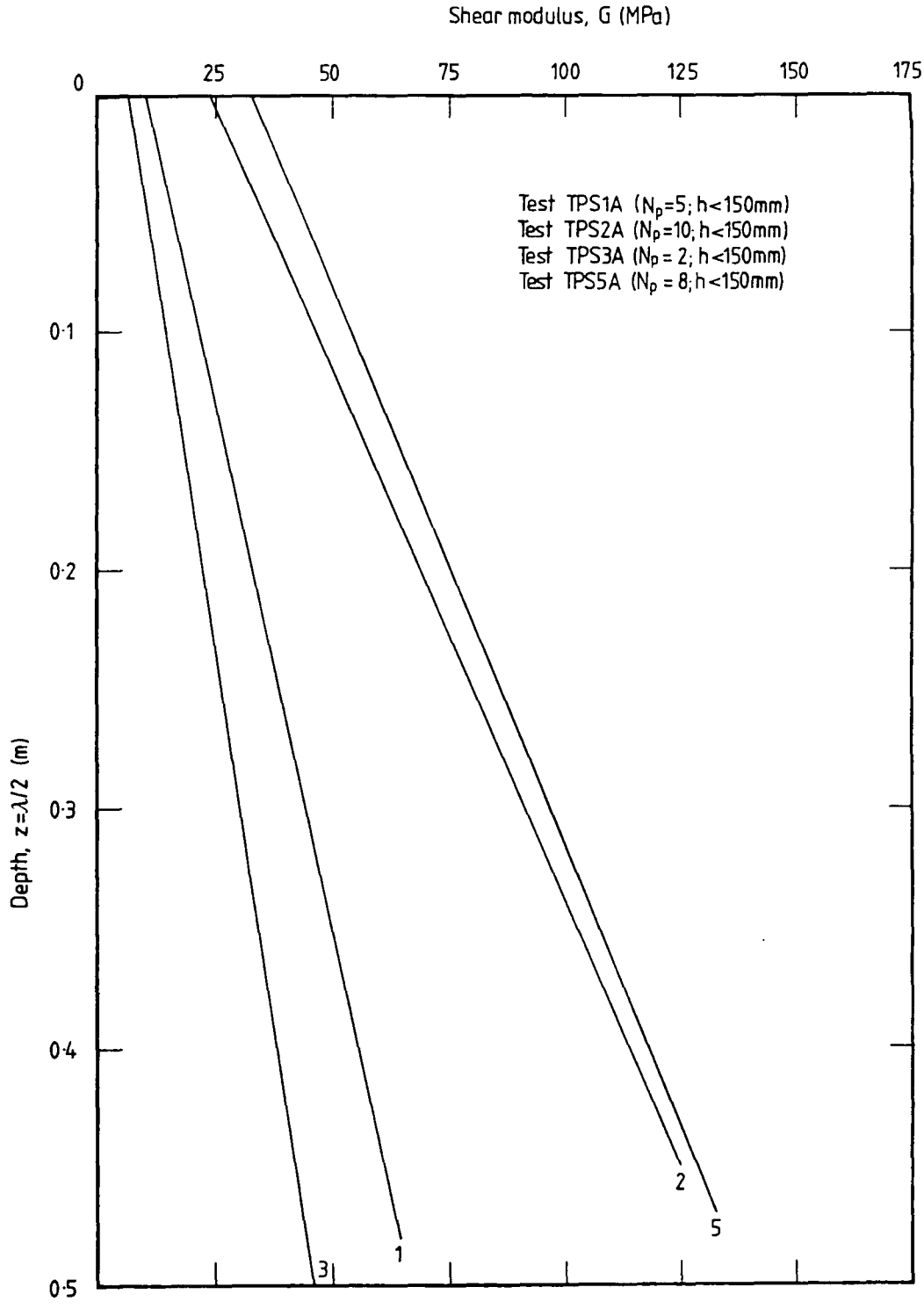

Figure 7.22 - Shear modulus-depth profiles for Tests TPS1A, TPS2A, TPS3A and TPS5A (half depth).

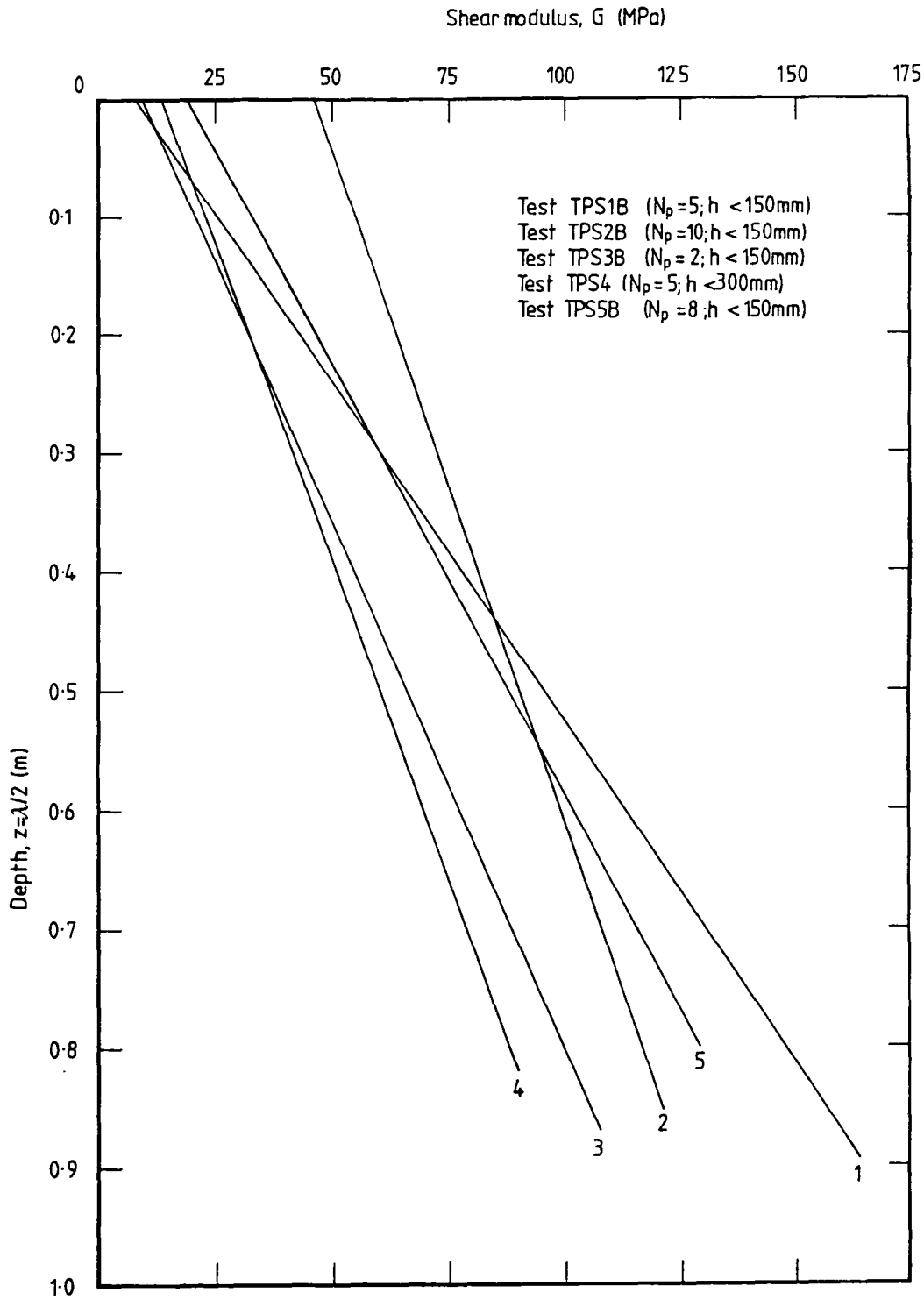

Figure 7.23 - Shear modulus-depth profiles for Tests TPS1B, TPS2B, TPS3B, TPS4 and TPS5B (full depth).

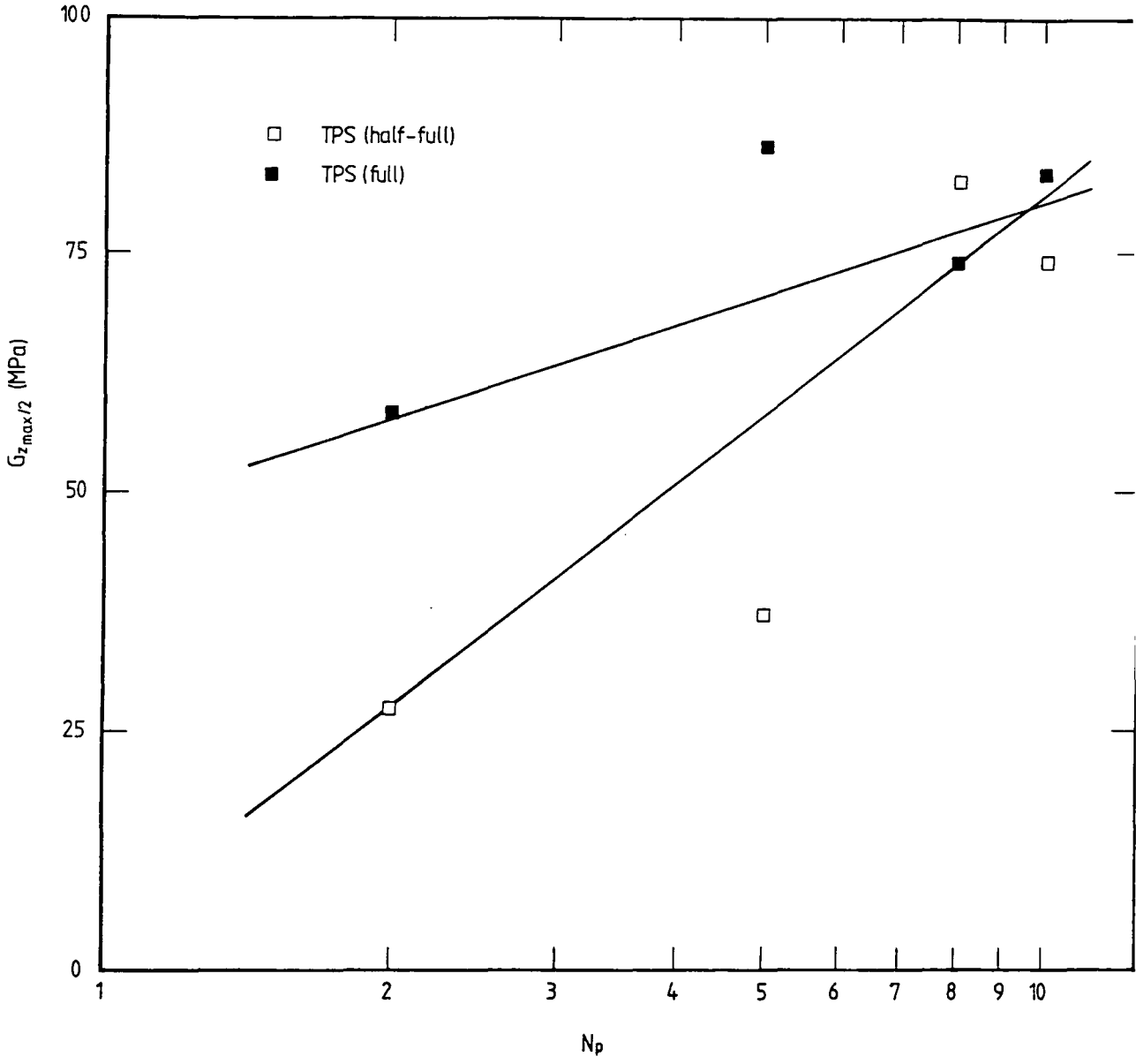

Figure 7.24 - Plot of the number of passes per layer (N_p) (logarithmic scale) against the mean shear modulus ($G_{z_{max}/2}$) for tests on the Permian Sand in both the half-full and the full trench.

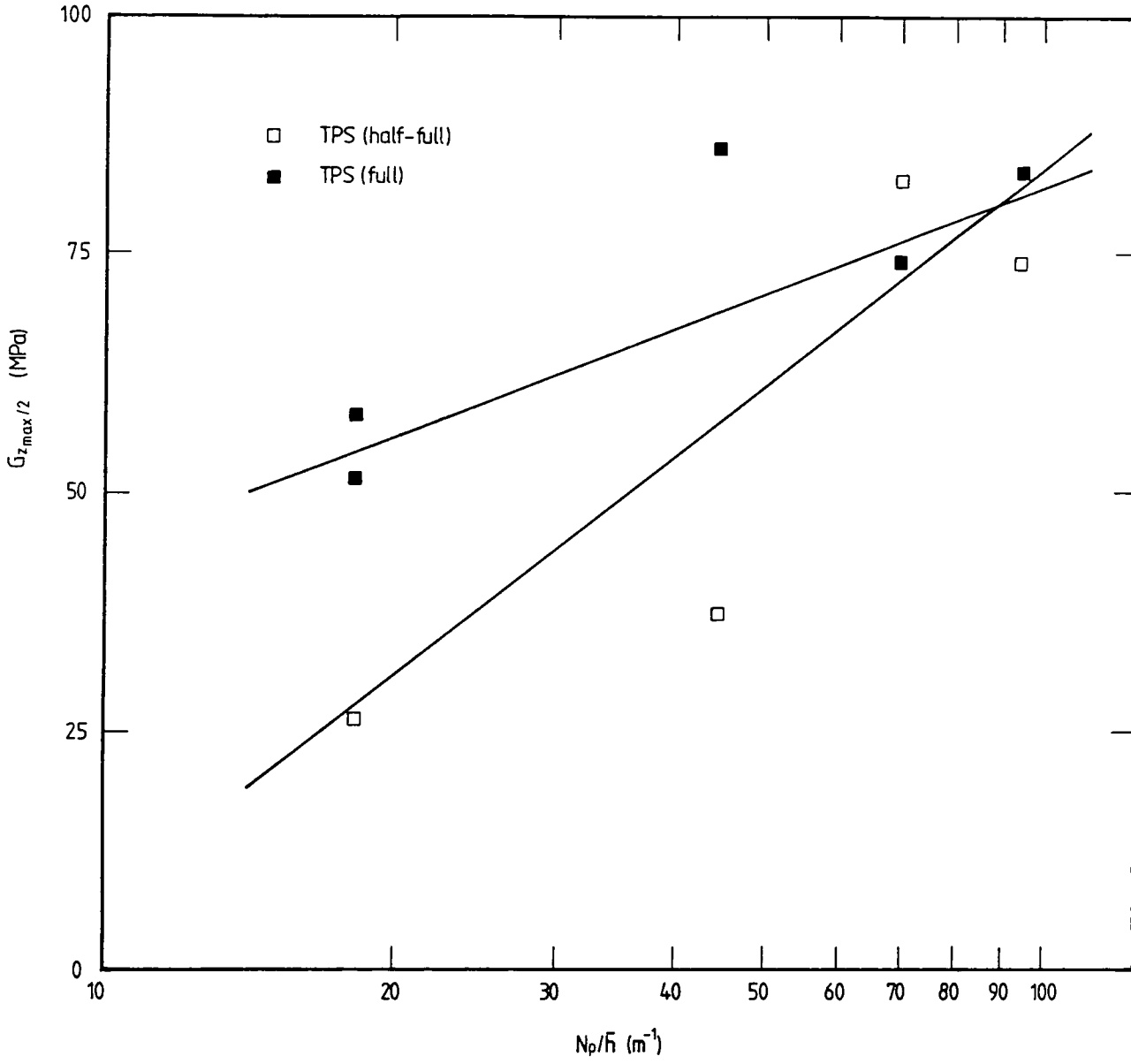

Figure 7.25 - Plot of the ratio of the number of passes per layer to the mean layer thickness ($N_p/\bar{h}$) (logarithmic scale) against the mean shear modulus ($G_{z_{max}/2}$) for tests on the Permian Sand in both the half-full and the full trench.

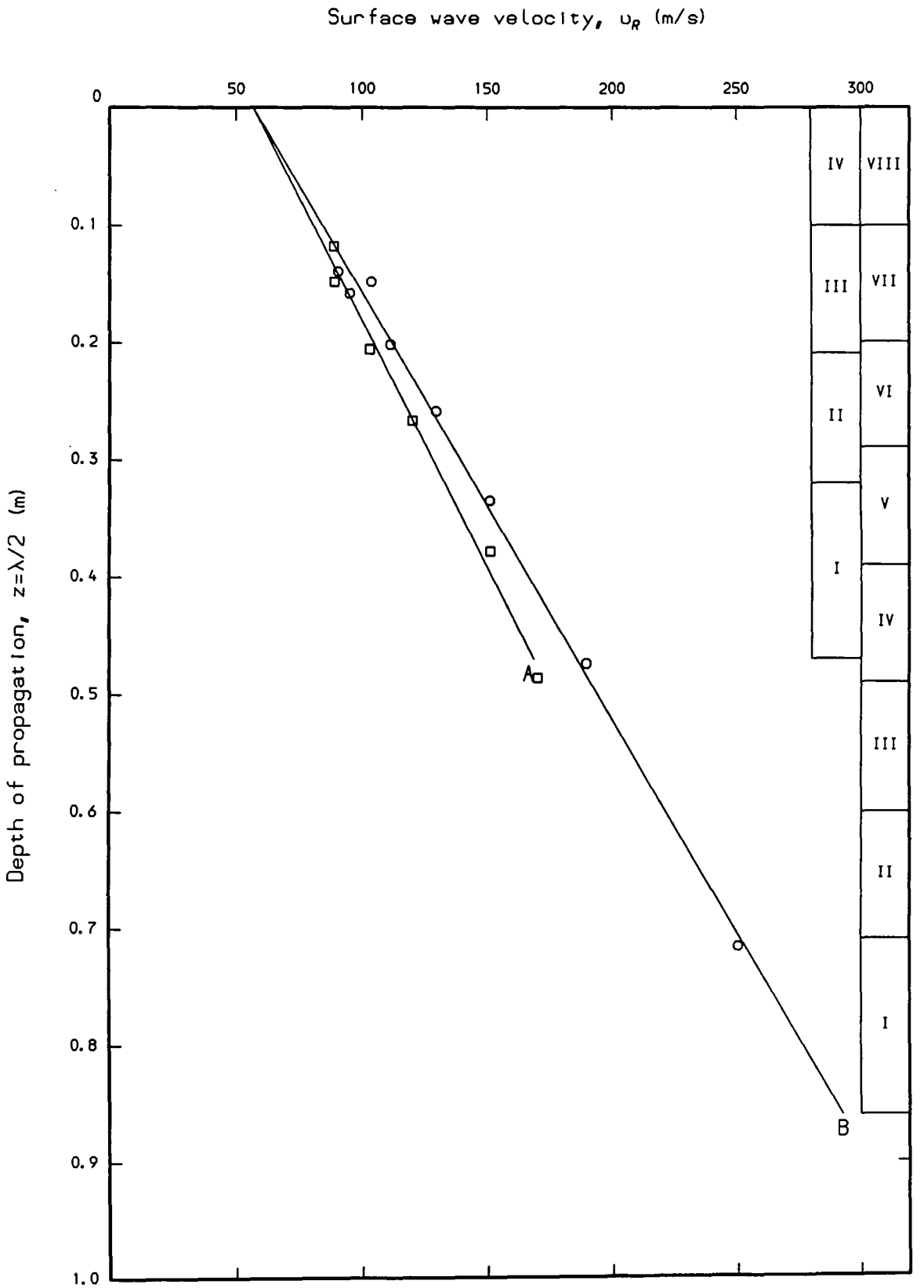

Figure 7.26 - Surface wave velocity-depth profiles for Tests TSS1A and TSS1B. Layer logs are shown for the two tests.

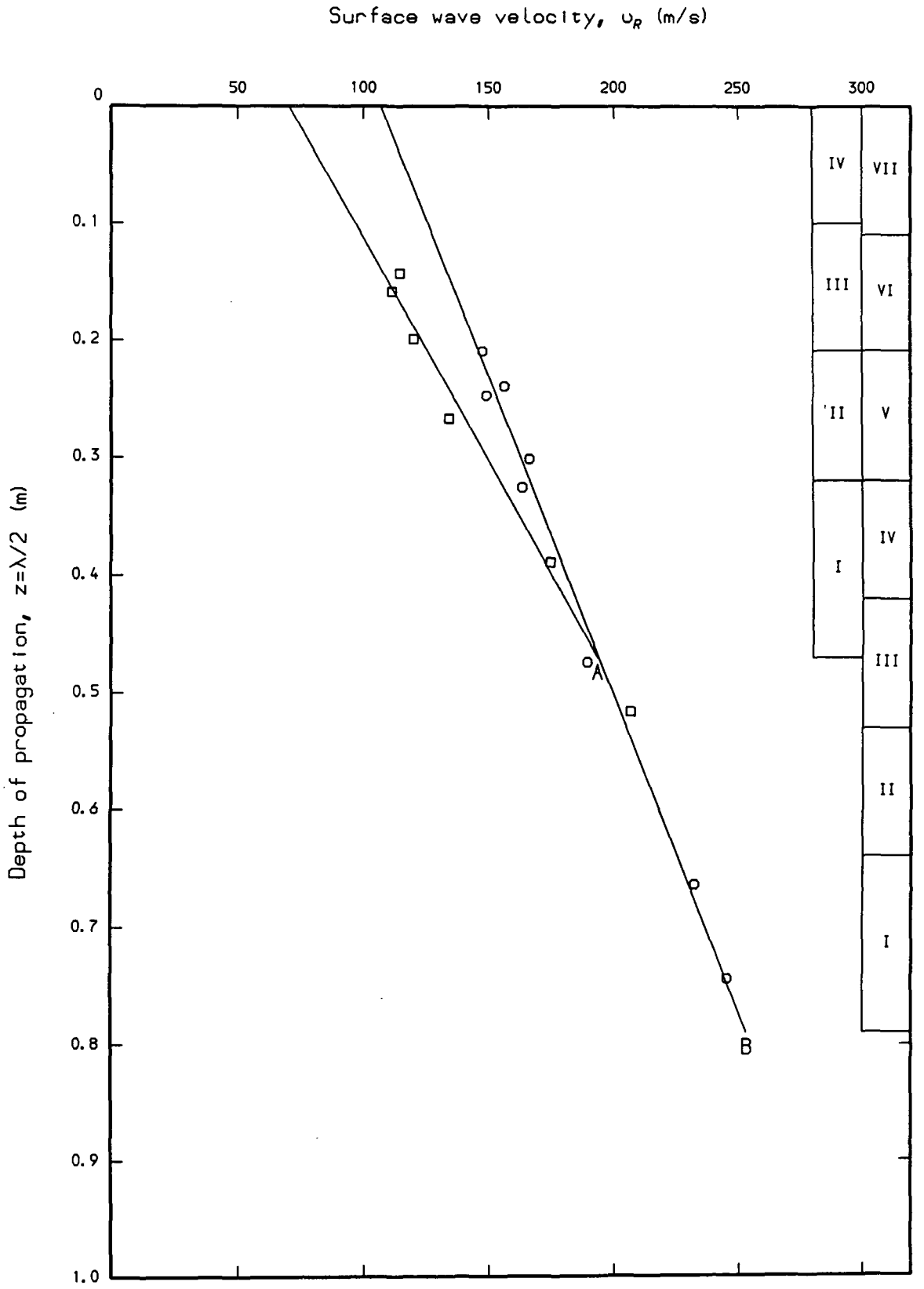

Figure 7.27 - Surface wave velocity-depth profiles for Tests TSS2A and TSS2B. Layer logs are shown for the two tests.

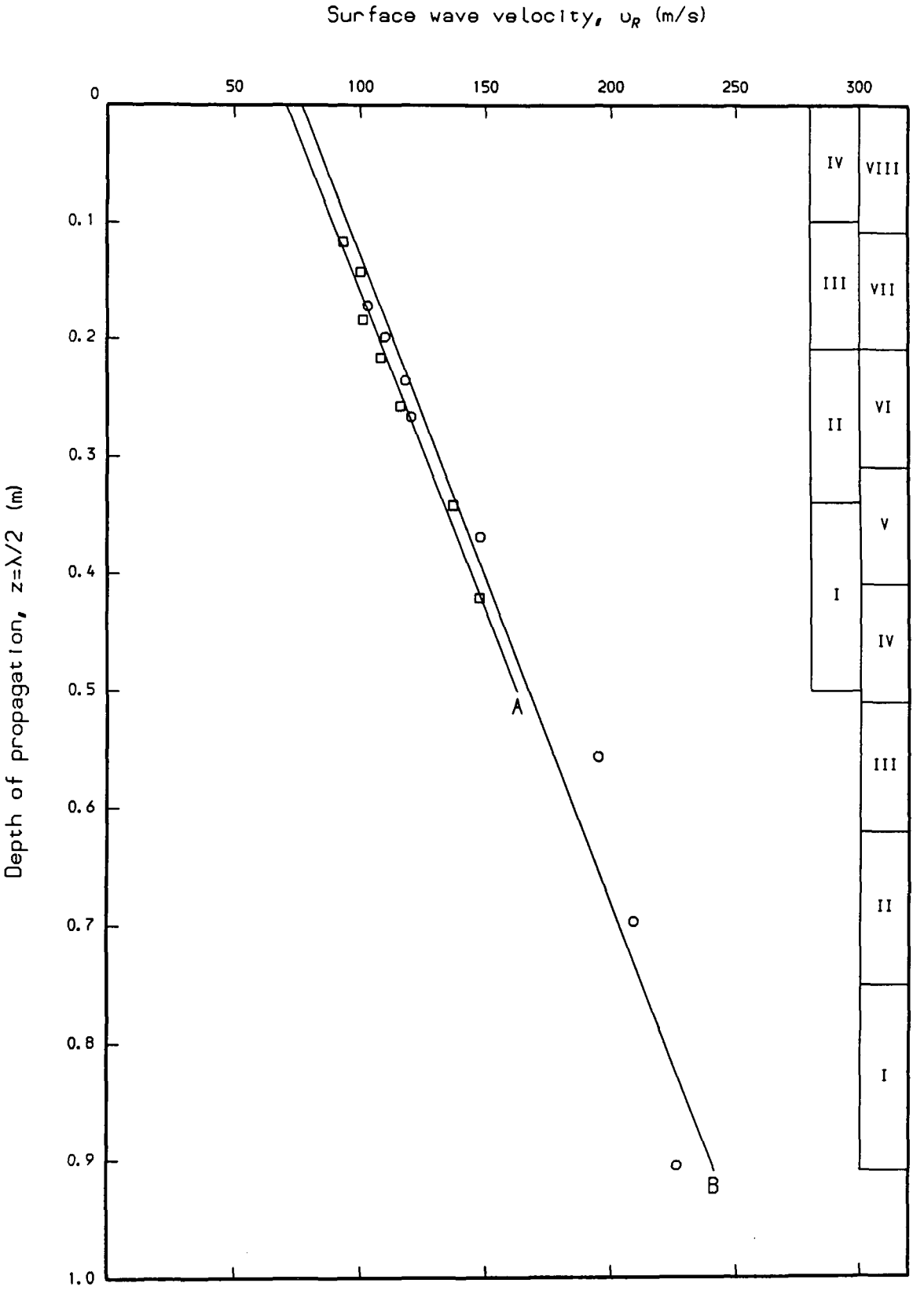

Figure 7.28 - Surface wave velocity-depth profiles for Tests TSS3A and TSS3B. Layer logs are shown for the two tests.

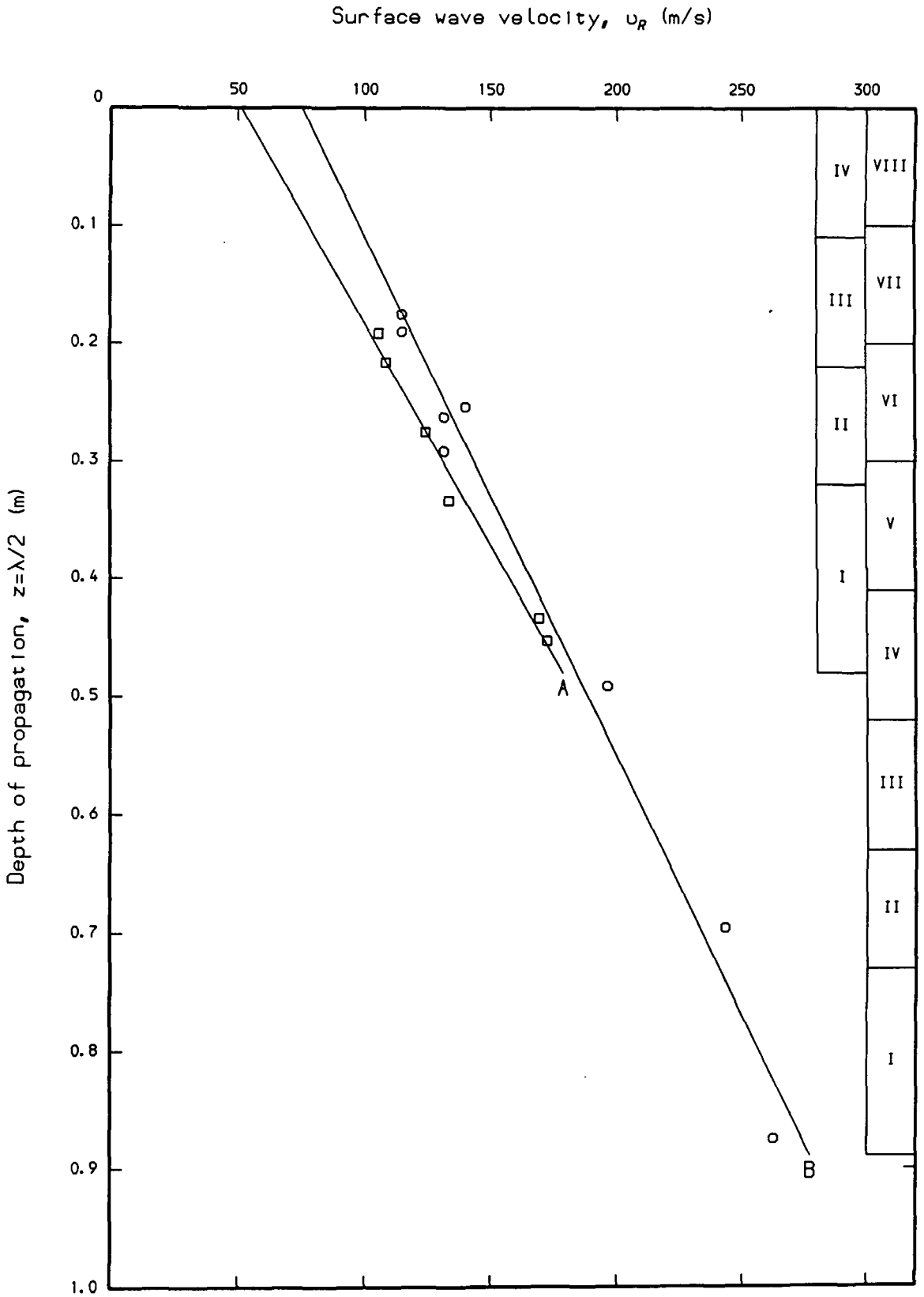

Figure 7.29 - Surface wave velocity-depth profiles for Tests TSS5A and TSS5B. Layer logs are shown for the two tests.

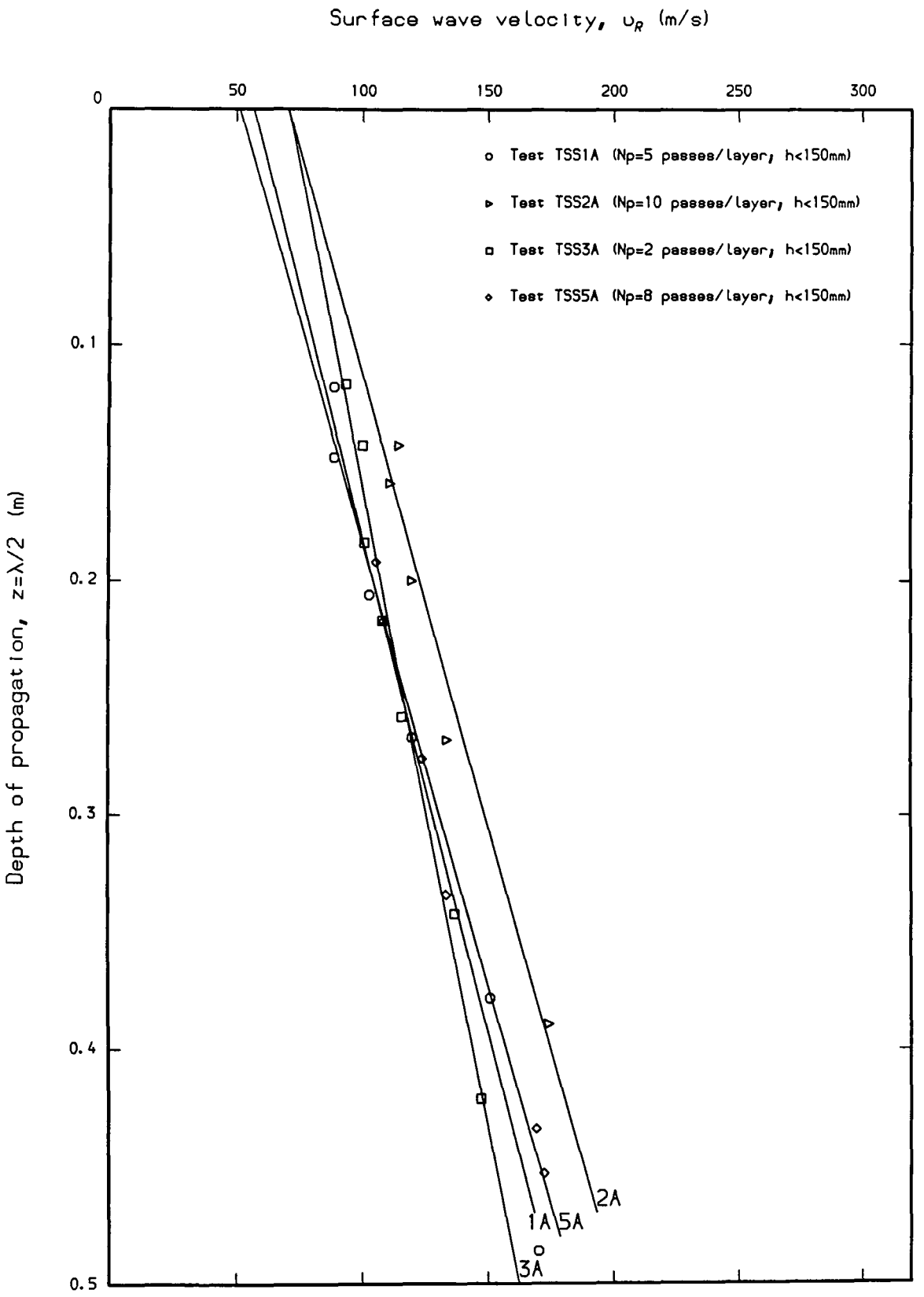

Figure 7.30 - Surface wave velocity-depth profiles for Tests TSS1A, TSS2A, TSS3A and TSS5A (half depth).

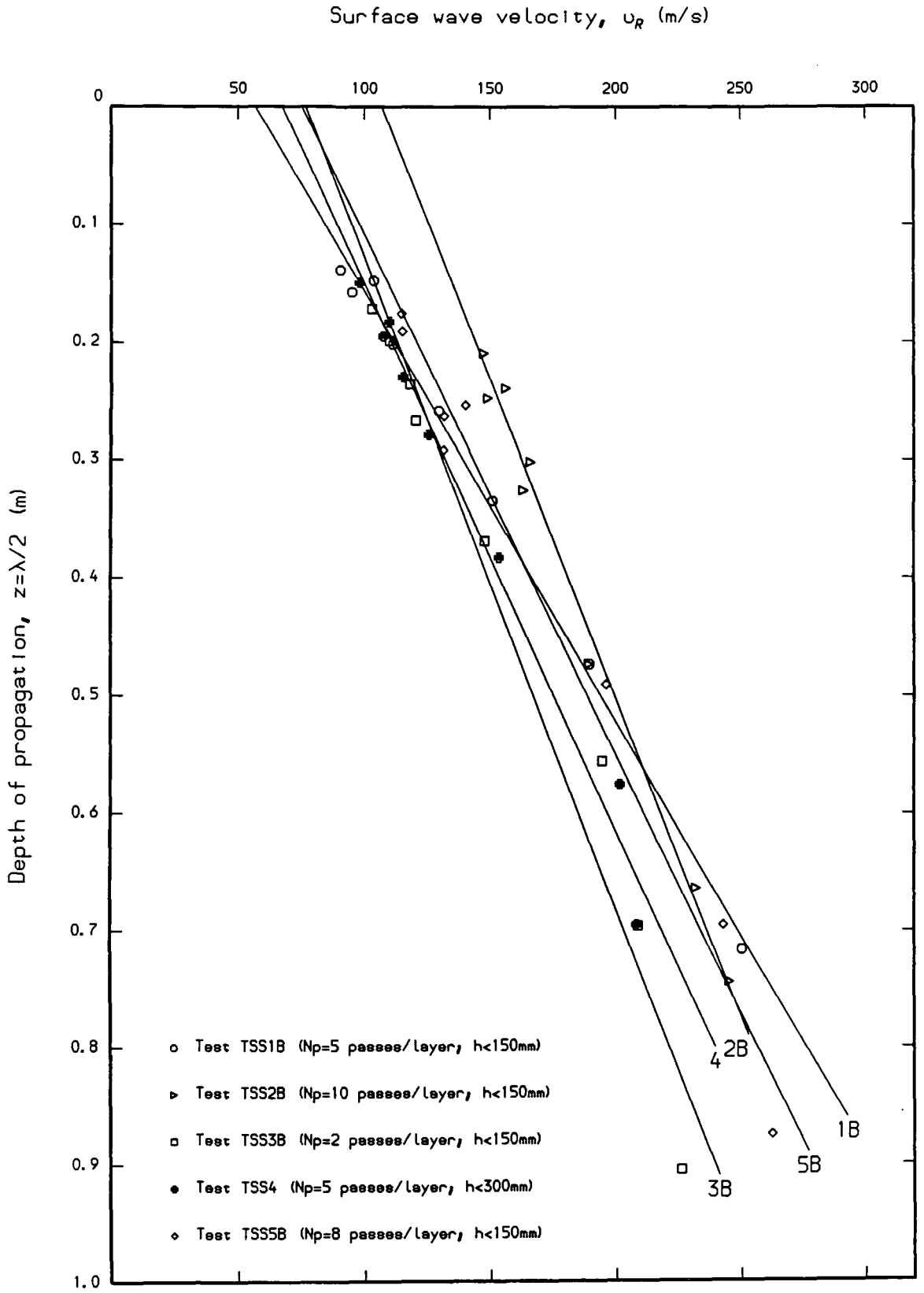

Figure 7.31 - Surface wave velocity-depth profiles for Tests TSS1B, TSS2B, TSS3B, TSS4 and TSS5B (full depth).

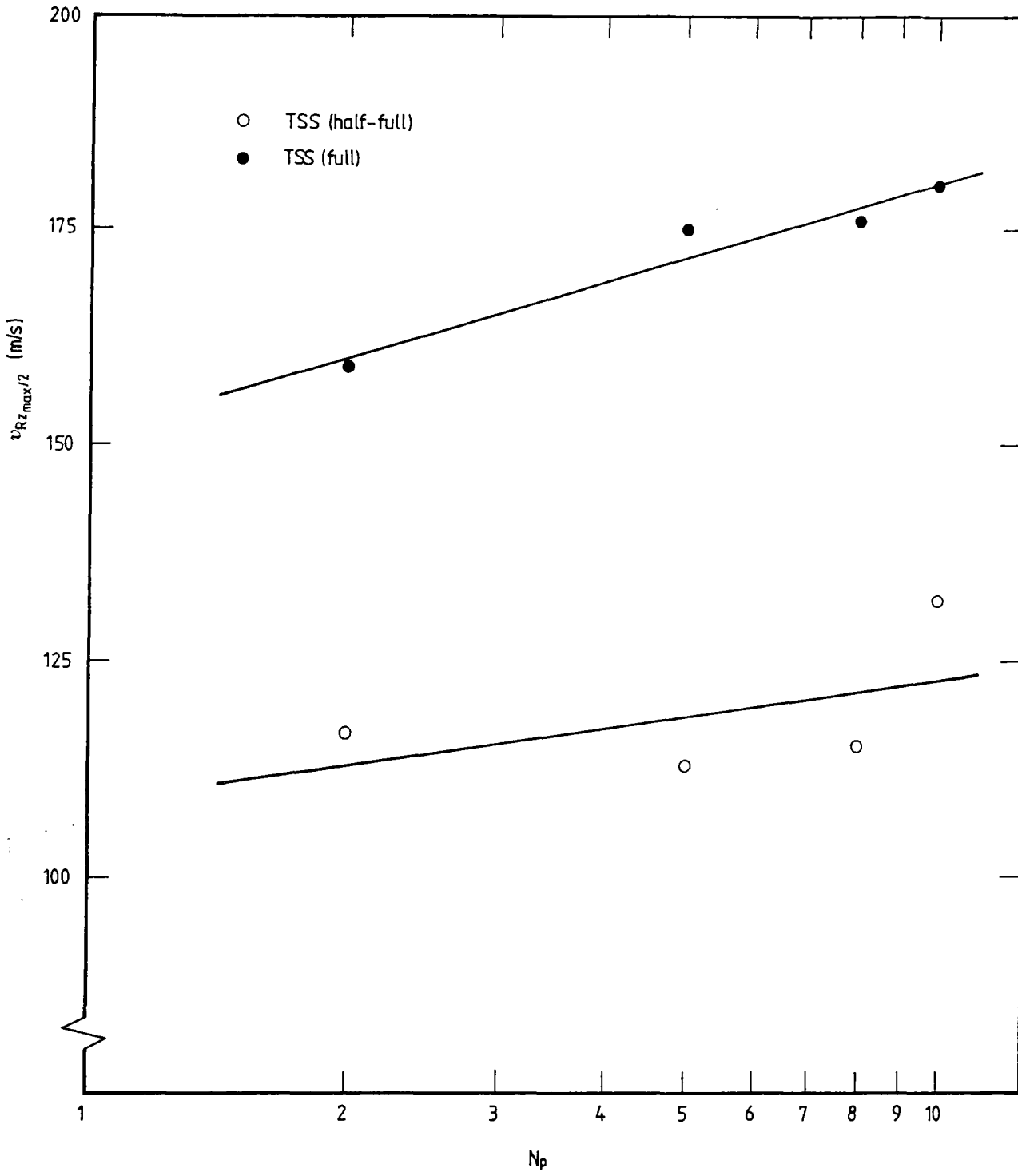

Figure 7.32 - Plot of the number of passes per layer (N_p) (logarithmic scale) against the mean surface wave velocity ($v_{Rz_{max}/2}$) for tests on the Sharp Sand in both the half-full and the full trench.

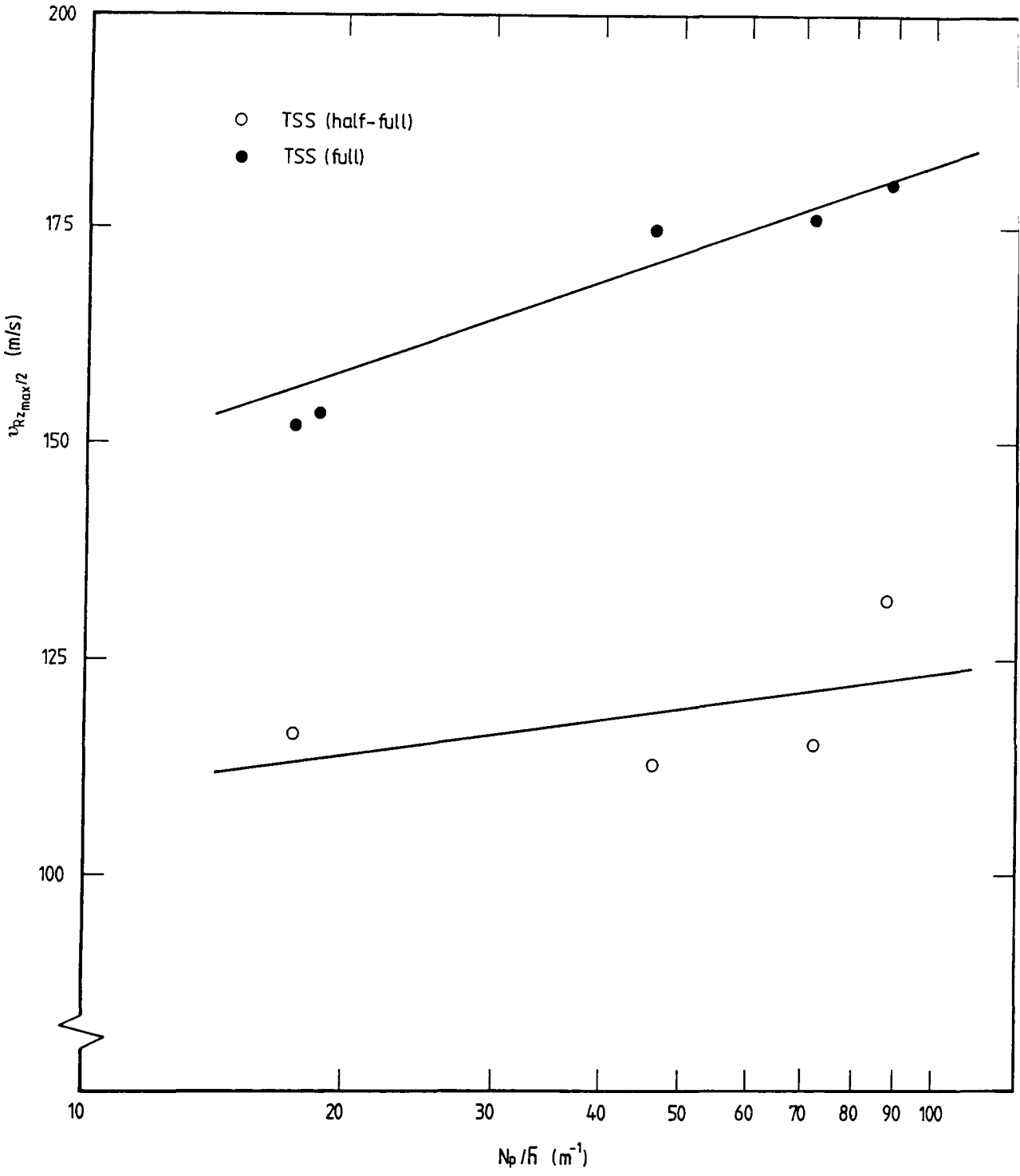

Figure 7.33 - Plot of the ratio of the number of passes per layer to the mean layer thickness ($N_p/\bar{h}$) (logarithmic scale) against the mean surface wave velocity ($v_{Rz_{max}/2}$) for tests on the Sharp Sand in both the half-full and the full trench.

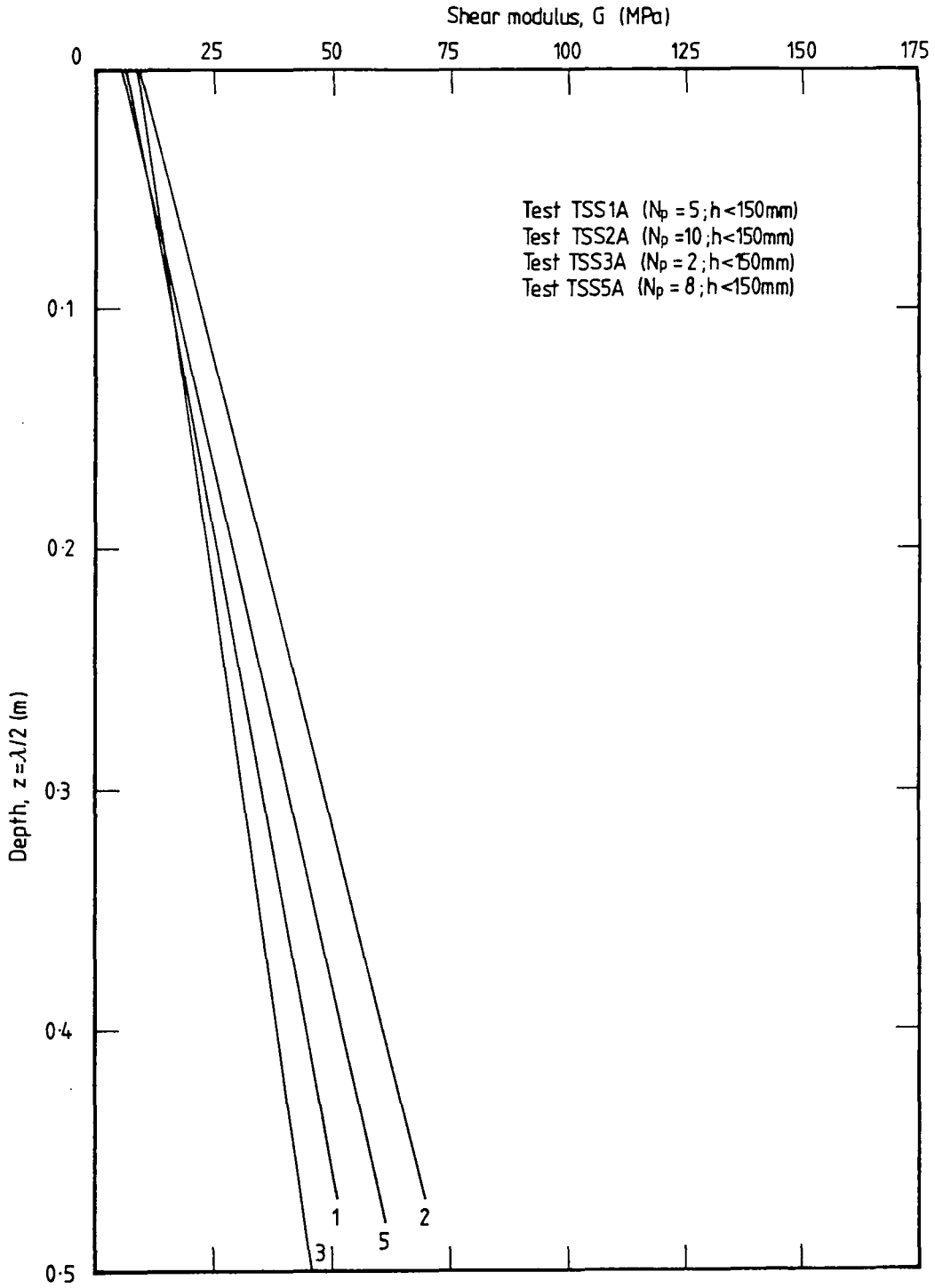

Figure 7.34 - Shear modulus-depth profiles for Tests TSS1A, TSS2A, TSS3A and TSS5A (half depth).

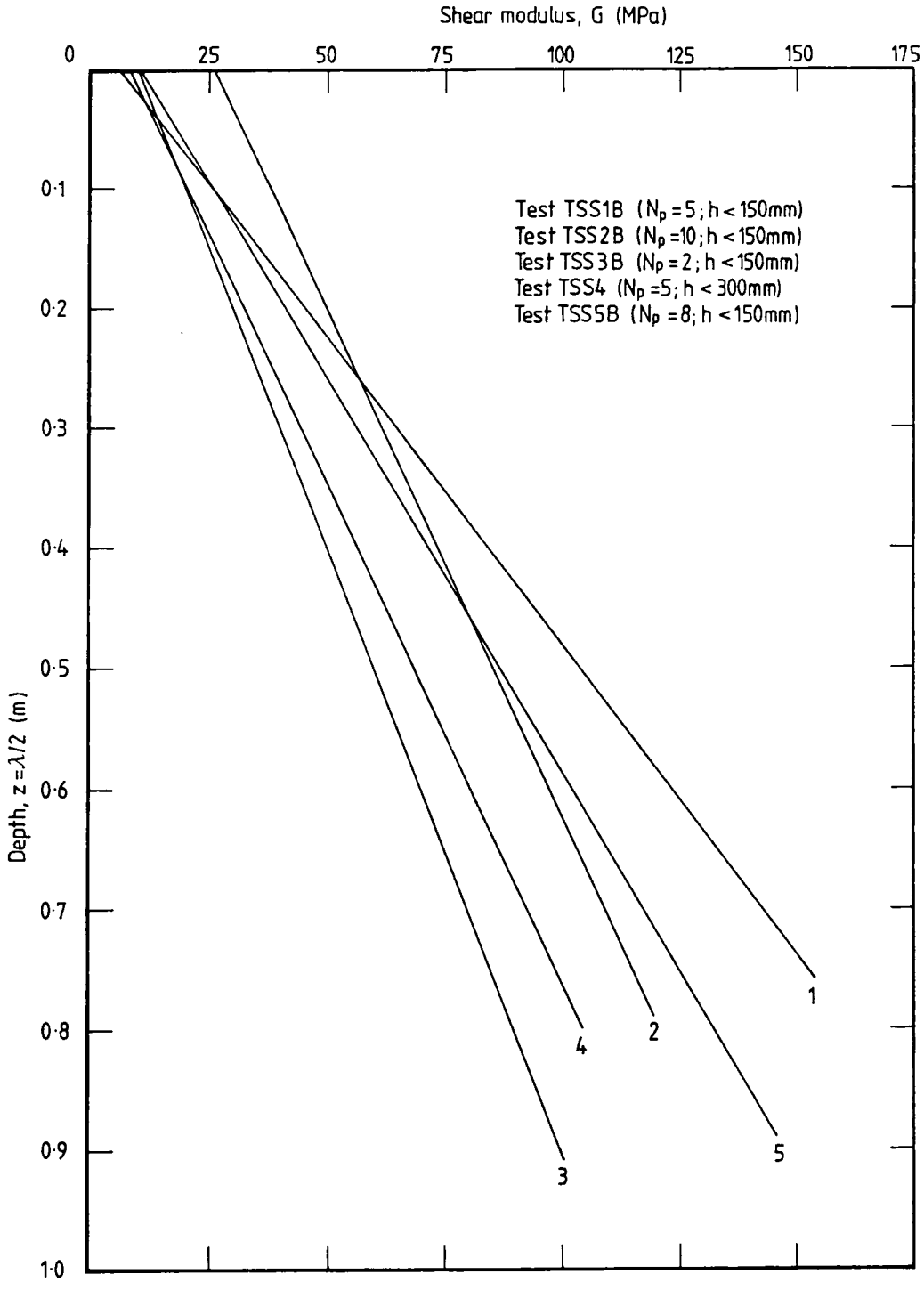

Figure 7.35 - Shear modulus-depth profiles for Tests TSS1B, TSS2B, TSS3B, TSS4 and TSS5B (full depth).

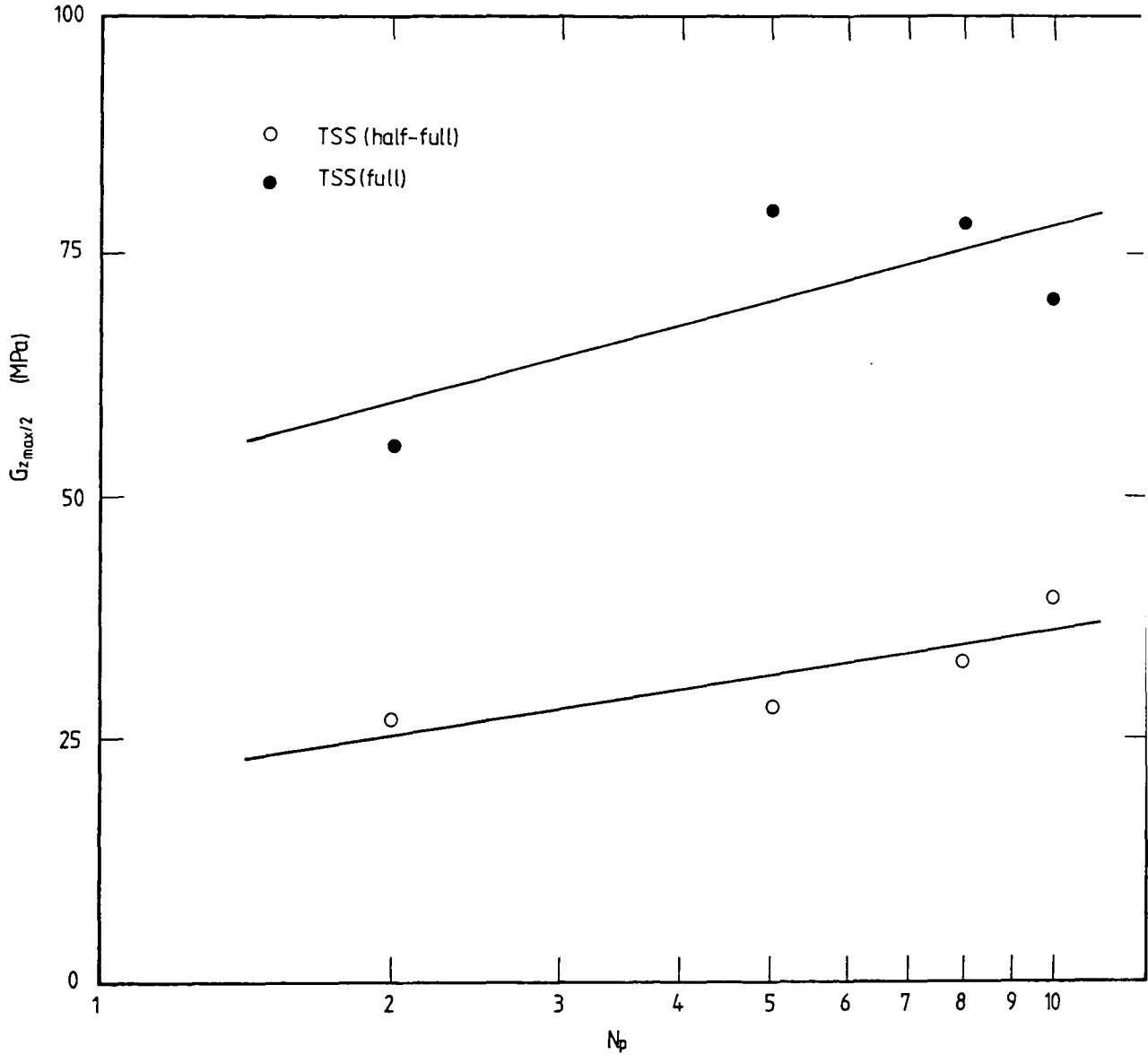

Figure 7.36 - Plot of the number of passes per layer (N_p) (logarithmic scale) against the mean shear modulus ($G_{z_{max}/2}$) for tests on the Sharp Sand in both the half-full and the full trench.

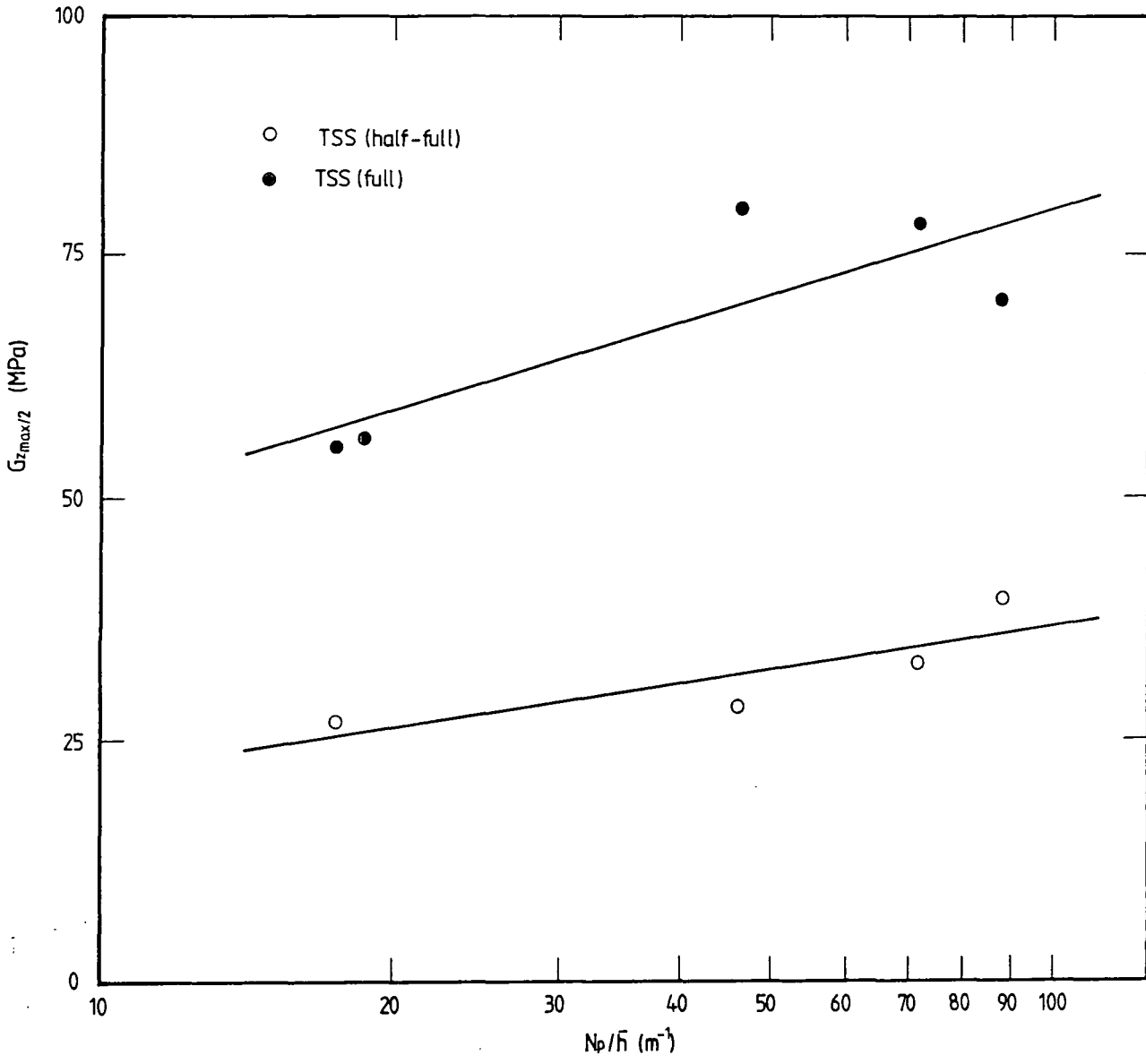

Figure 7.37 - Plot of the ratio of the number of passes per layer to the mean layer thickness ($N_p/\bar{h}$) (logarithmic scale) against the mean shear modulus ($G_{z_{max/2}}$) for tests on the Sharp Sand in both the half-full and the full trench.

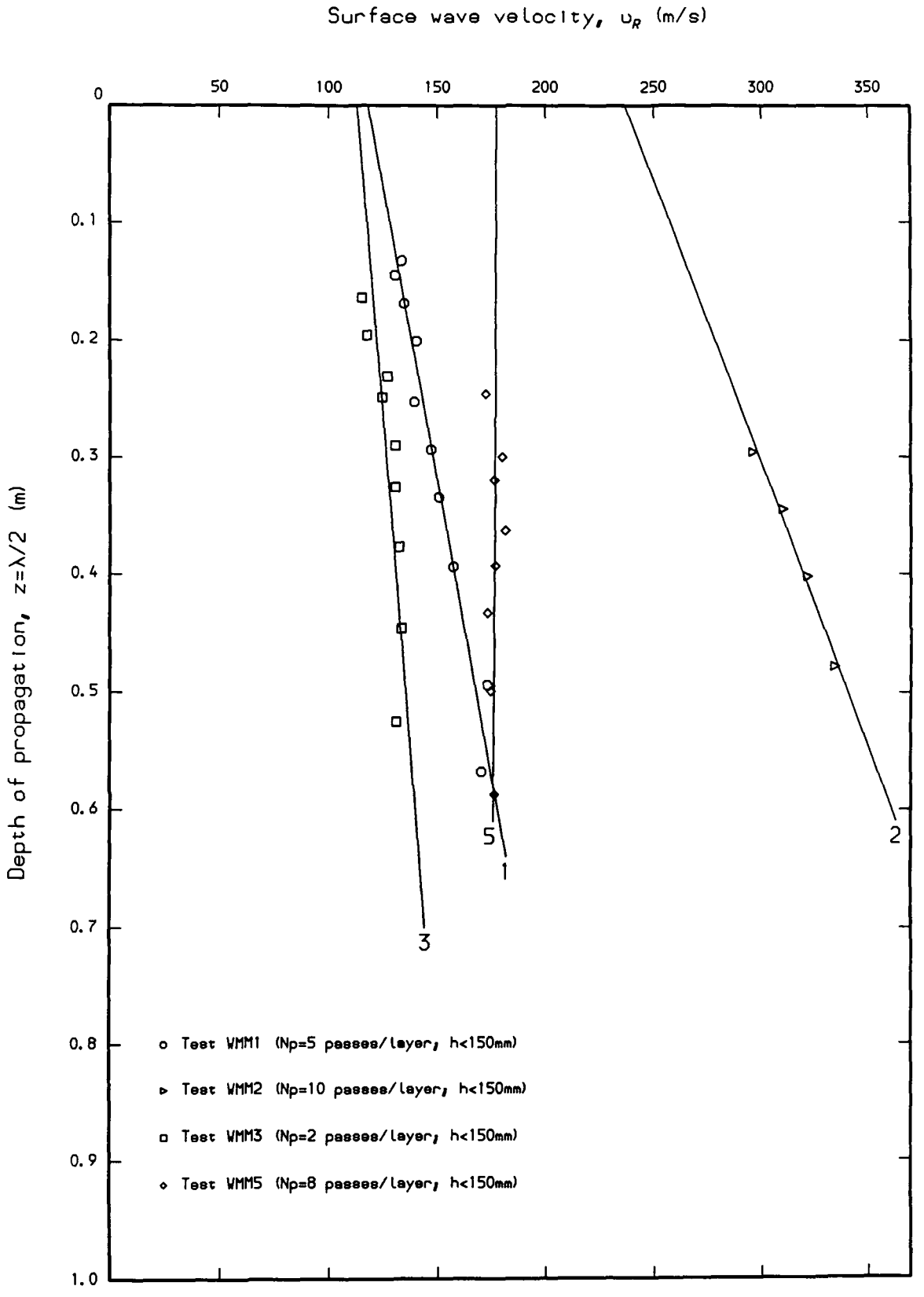

Figure 7.38 - Surface wave velocity-depth profiles for Tests WMM1, WMM2, WMM3 and WMM5 (nominal layer thickness, h<150mm).

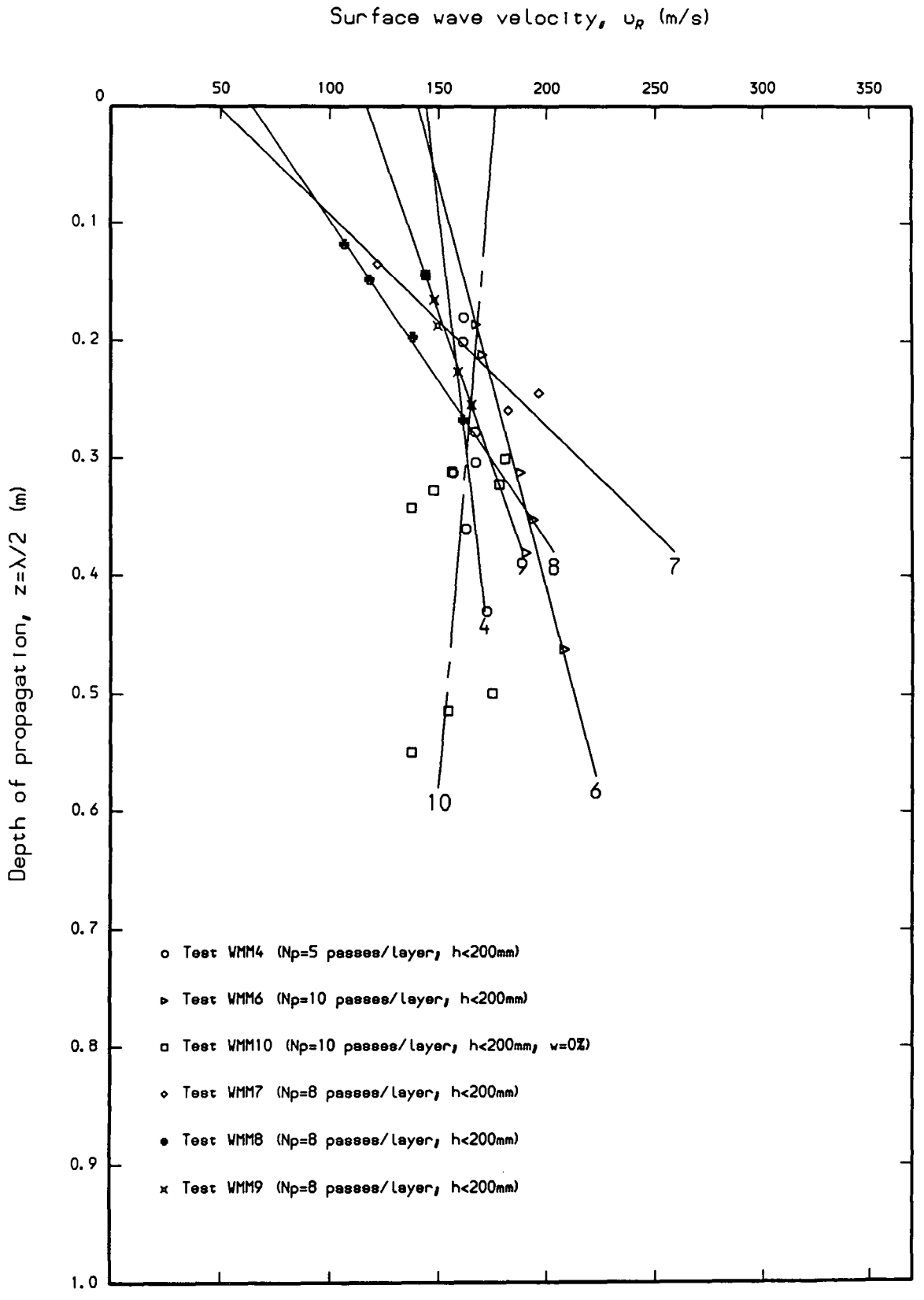

Figure 7.39 - Surface wave velocity-depth profiles for Tests WMM4, WMM6, WMM10 and Tests WMM7, WMM8 amd WMM9 (nominal layer thickness, h<200mm).

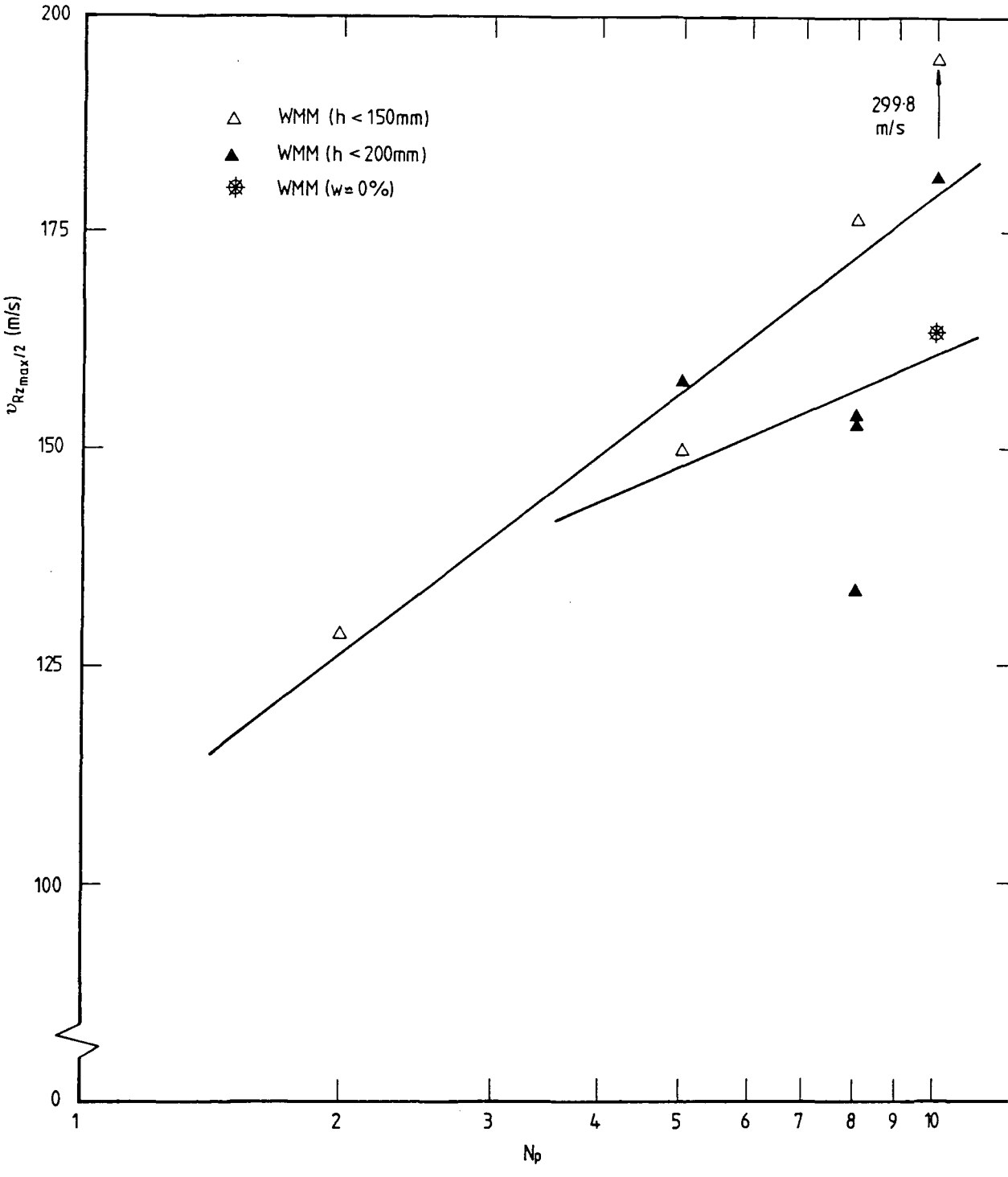

Figure 7.40 - Plot of the number of passes per layer (N_p) (logarithmic scale) against the mean surface wave velocity ($v_{Rz_{max}/2}$) for tests on the Wet-mix macadam.

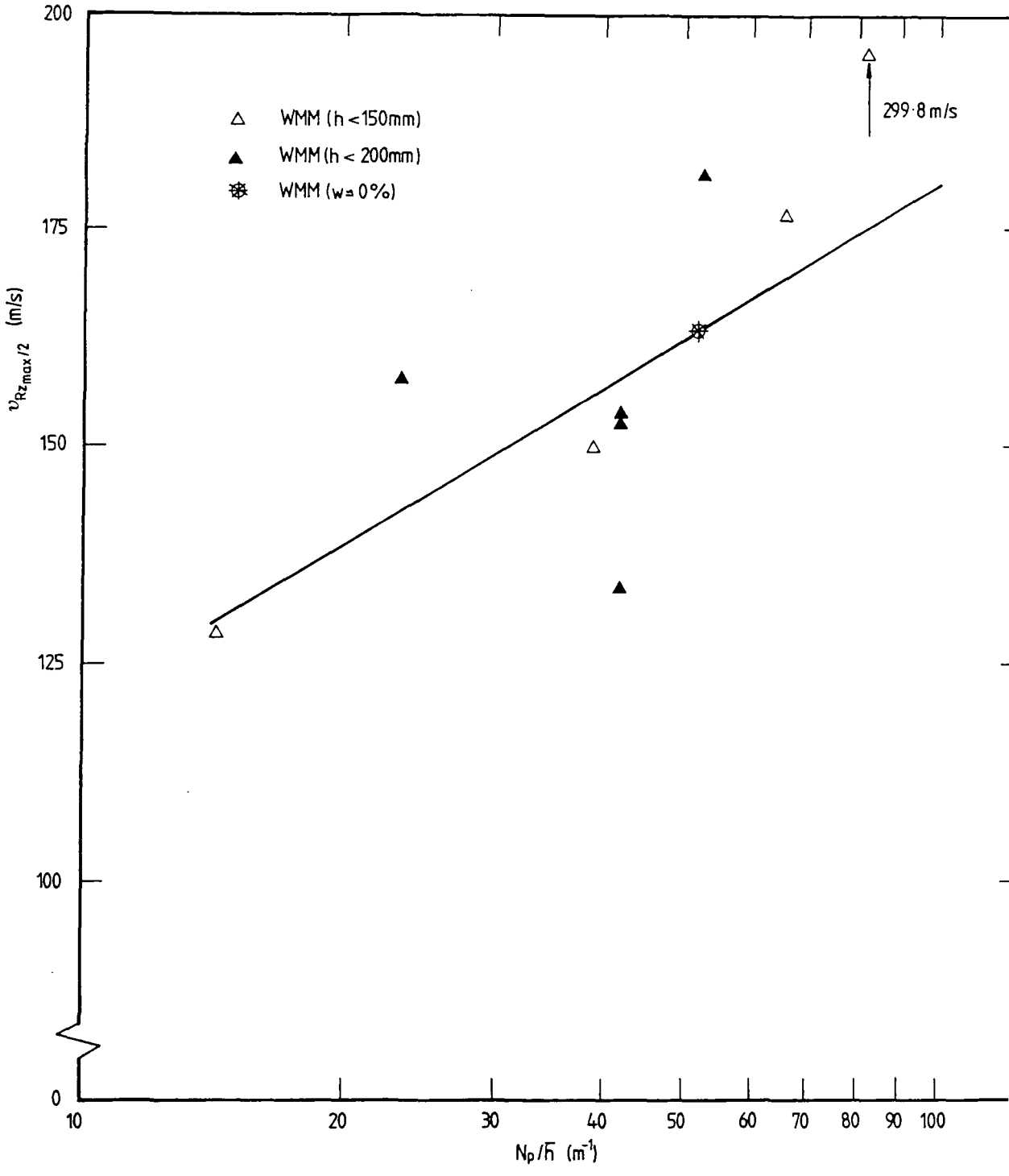

Figure 7.41 - Plot of the ratio of the number of passes per layer to the mean layer thickness ($N_p/\bar{h}$) (logarithmic scale) against the mean surface wave velocity ($v_{Rz_{max}/2}$) for tests on the Wet-mix macadam.

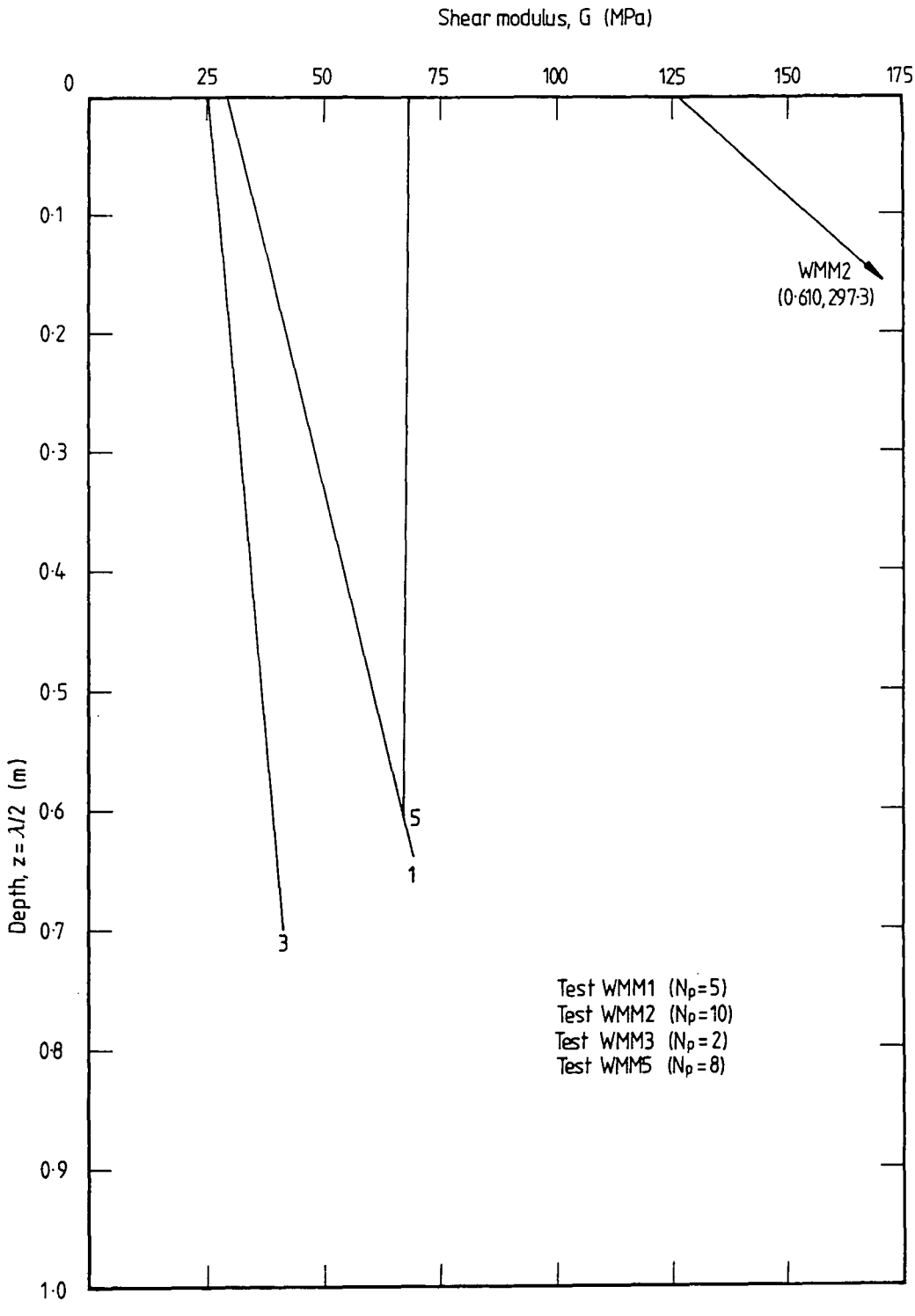

Figure 7.42 - Shear modulus-depth profiles for Tests WMM1, WMM2, WMM3 and WMM5 (nominal layer thickness, $h < 150$ mm).

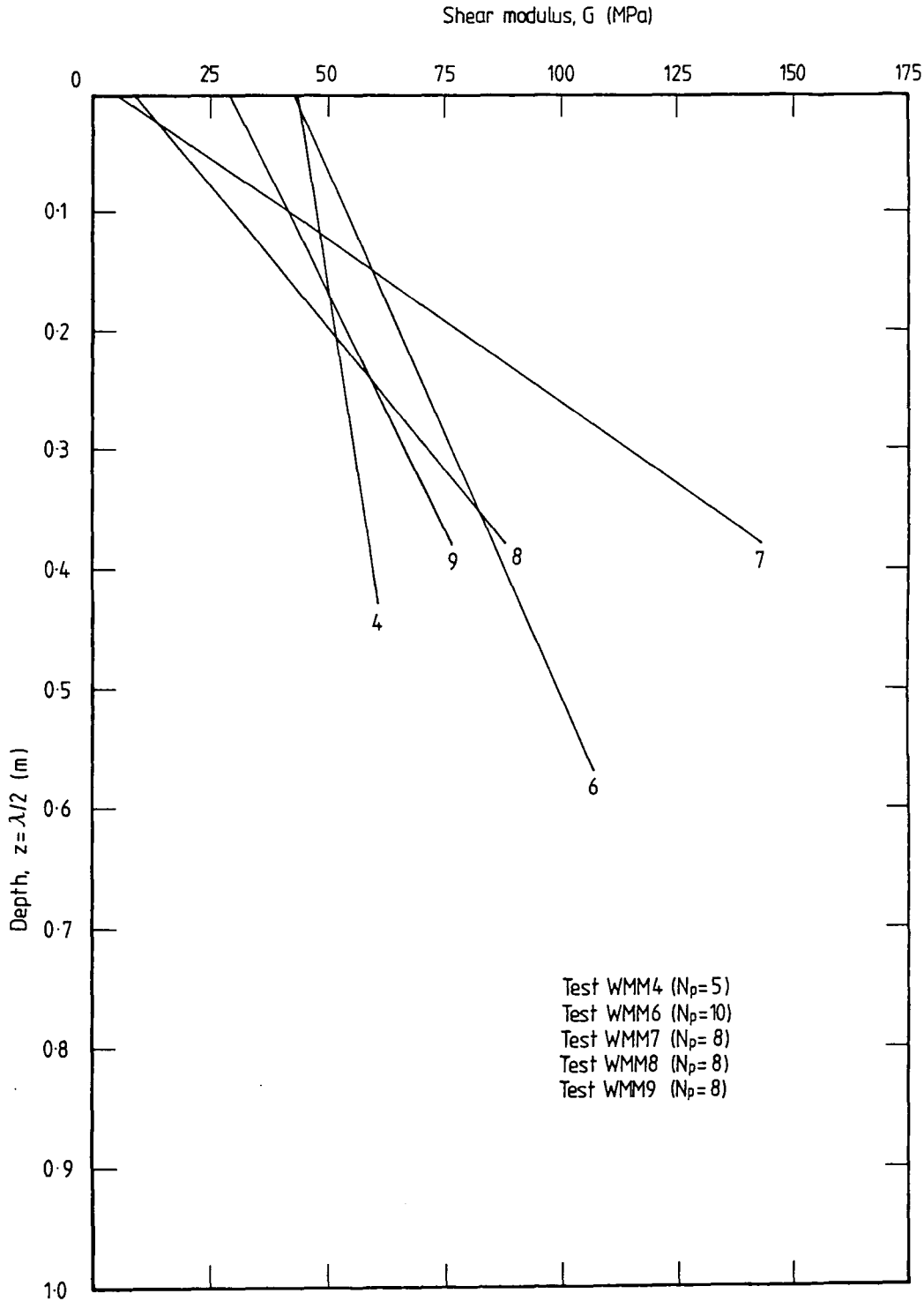

Figure 7.43 - Shear modulus-depth profiles for Tests WMM4 and WMM6 and WMM7, WMM8 and WMM9 (nominal layer thickness, $h < 200$ mm).

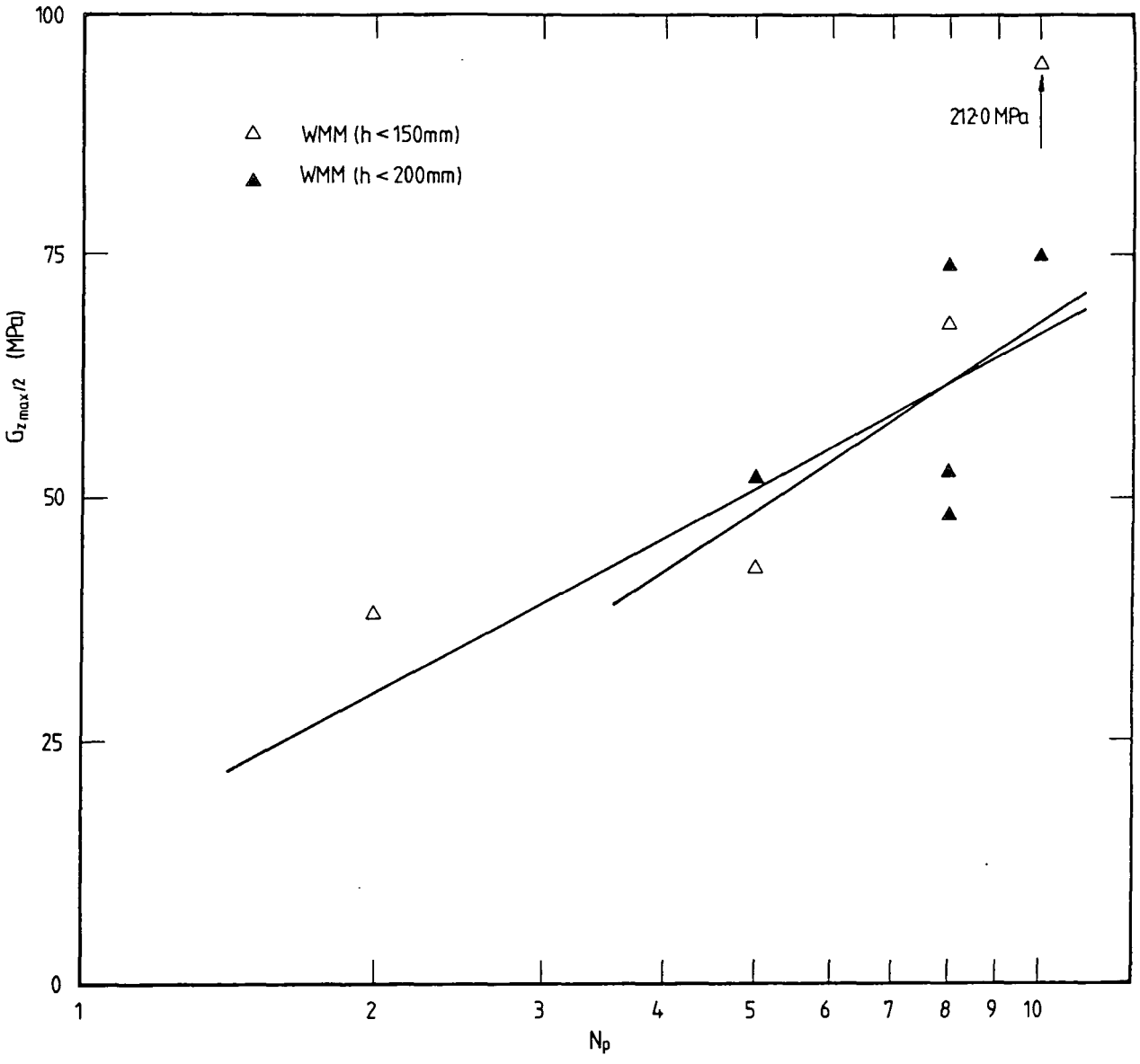

Figure 7.44 - Plot of the number of passes per layer (N_p) (logarithmic scale) against the mean shear modulus ($G_{z_{max}/2}$) for tests on the Wet-mix macadam.

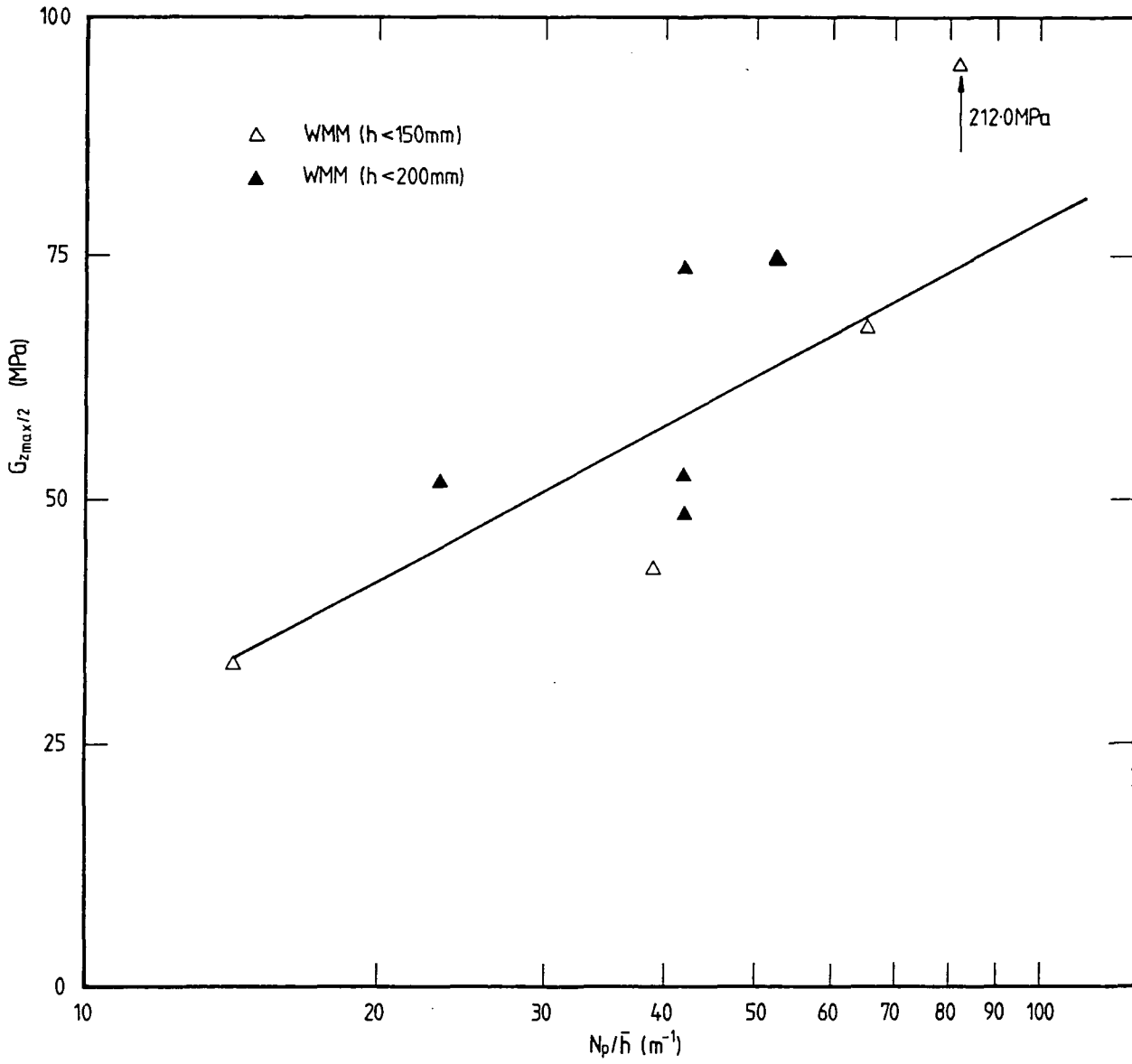

Figure 7.45 - Plot of the ratio of the number of passes per layer to the mean layer thickness ($N_p/\bar{h}$) (logarithmic scale) against the mean shear modulus ($G_{z_{max}/2}$) for tests on the Wet-mix macadam.

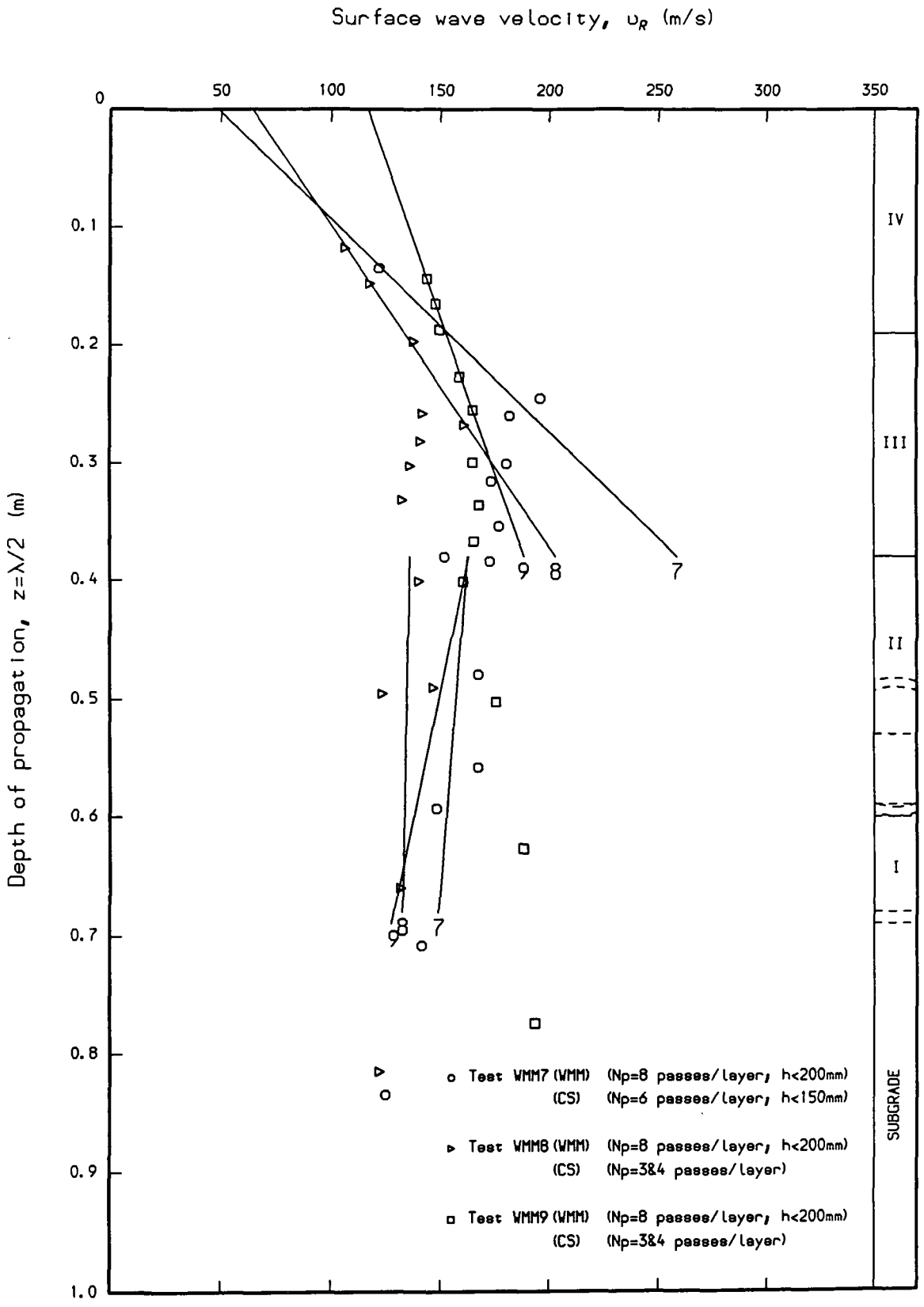

Figure 7.46 - Surface wave velocity-depth profiles for Tests WMM7, WMM8 and WMM9 (tests with Wet-mix macadam and Sharp Sand).

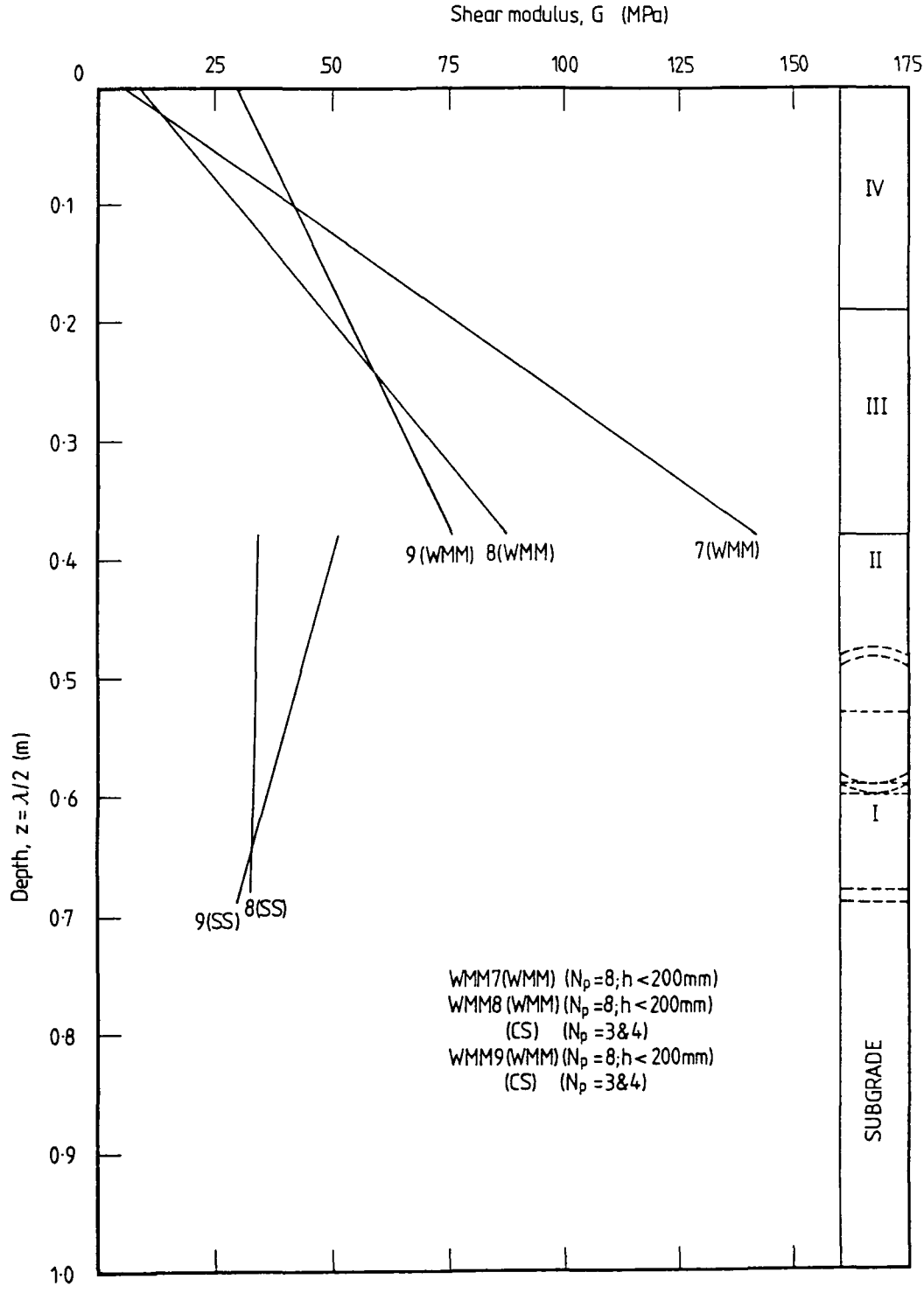

Figure 7.47 - Shear modulus-depth profiles for Tests WMM7, WMM8 and WMM9 (tests with Wet-mix macadam and Sharp Sand layers).

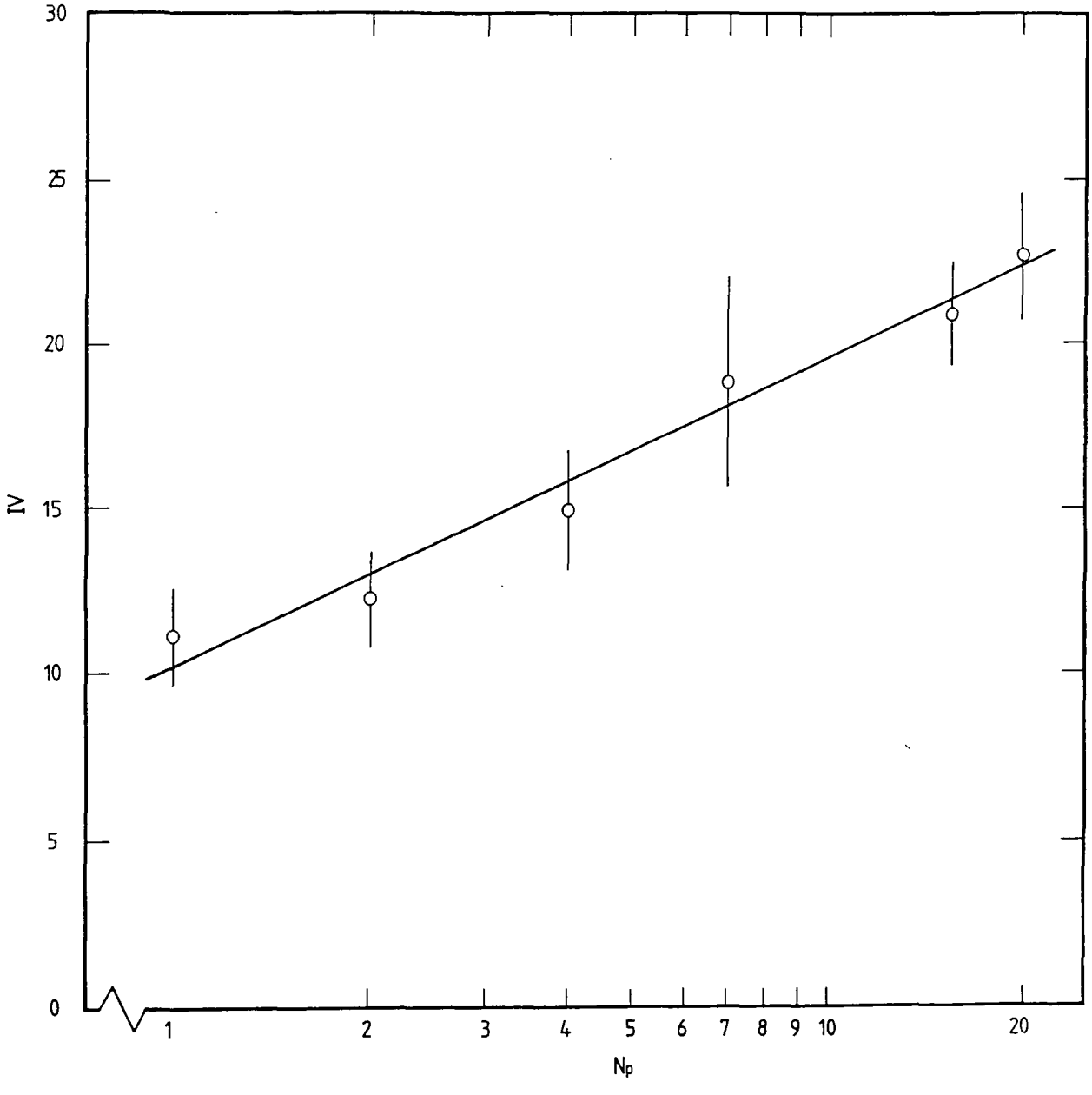

Figure 7.48 - The increase of Impact Value (IV) with applied compactive effort (N_p) (Blaydon demonstration trench).

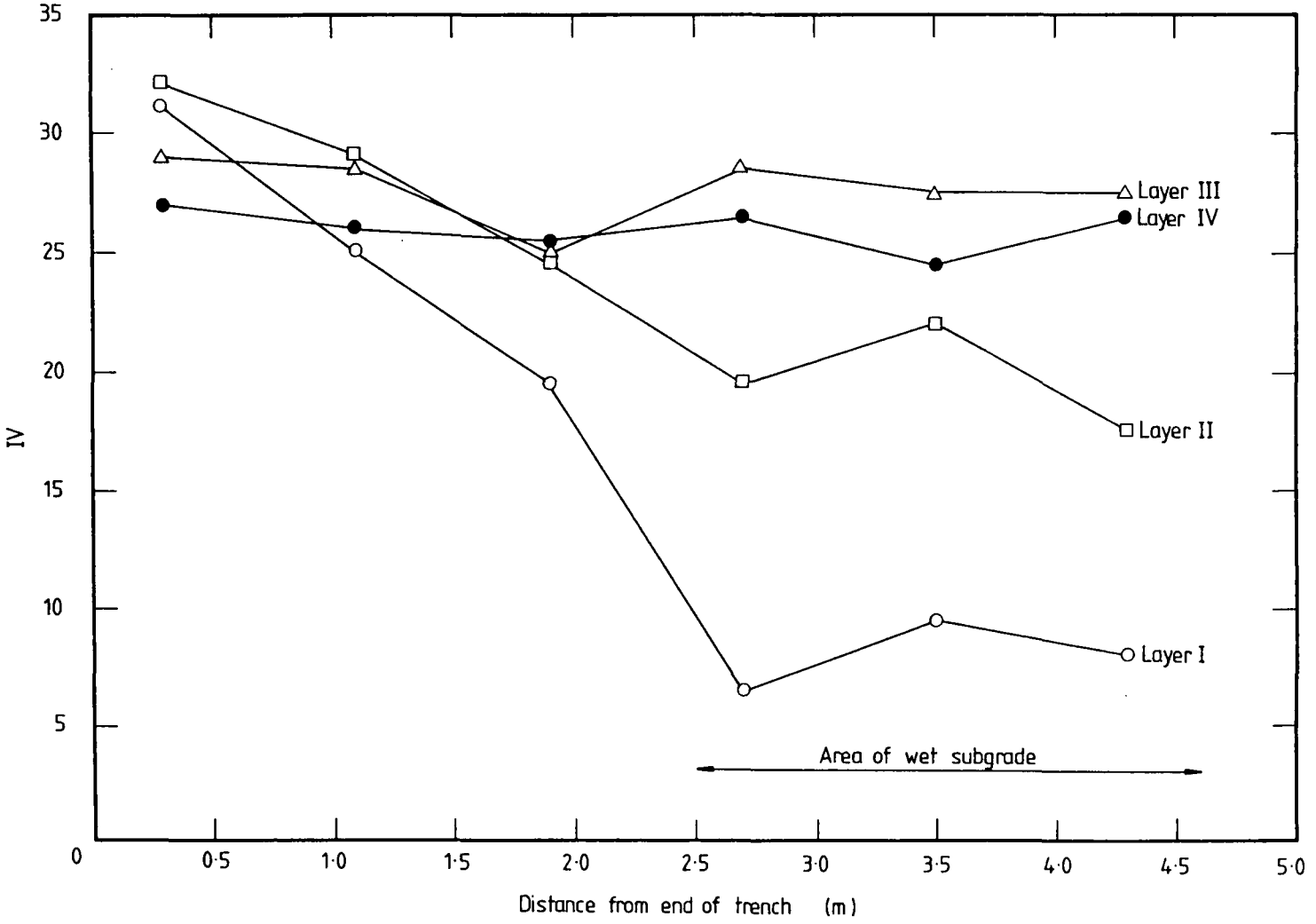

Figure 7.49 - The variation of Impact Value (IV) along the length of the trench for Test SL1 (Salters Lane).

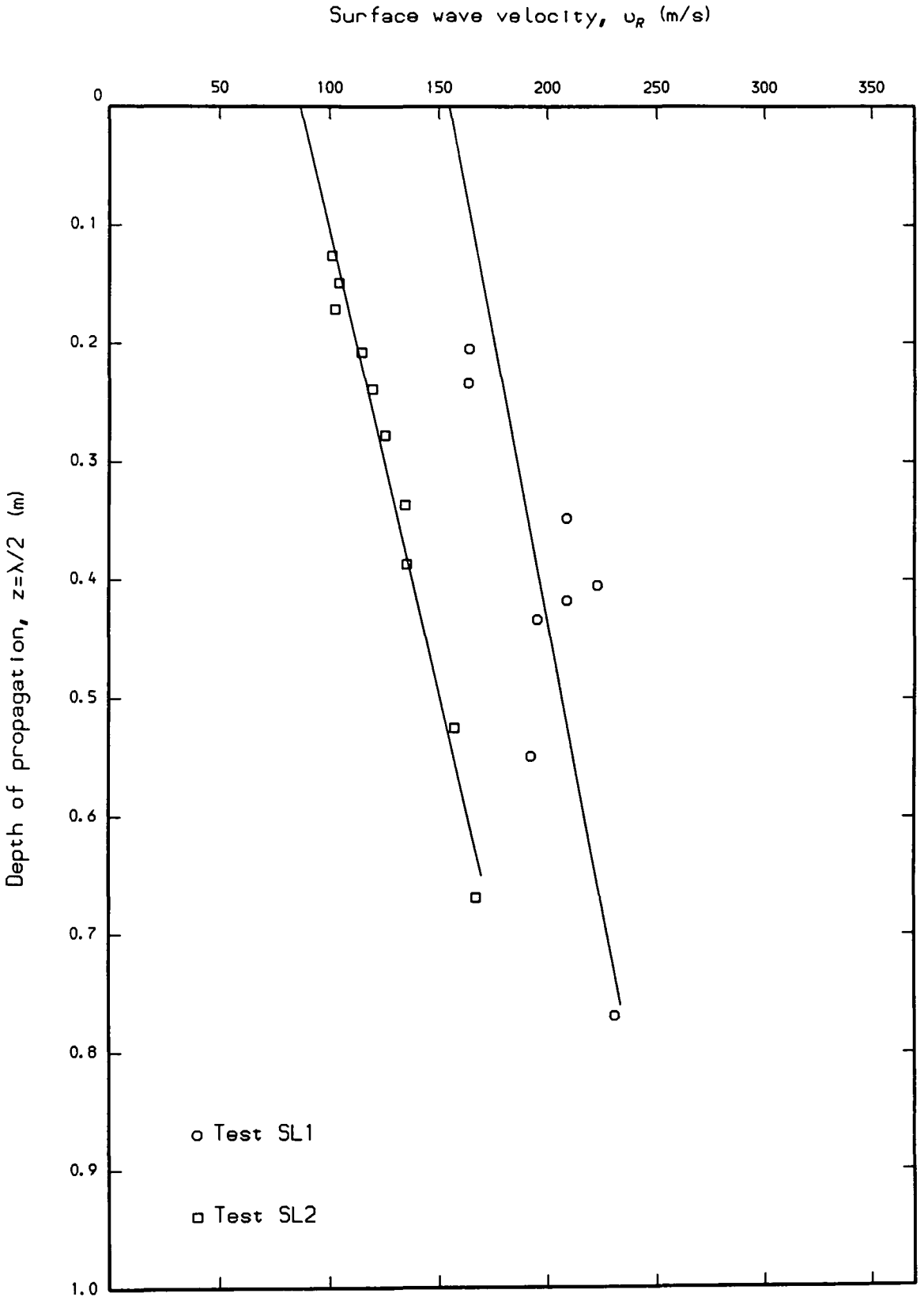

Figure 7.50 - Surface wave velocity-depth profile for Tests SL1 and SL2.

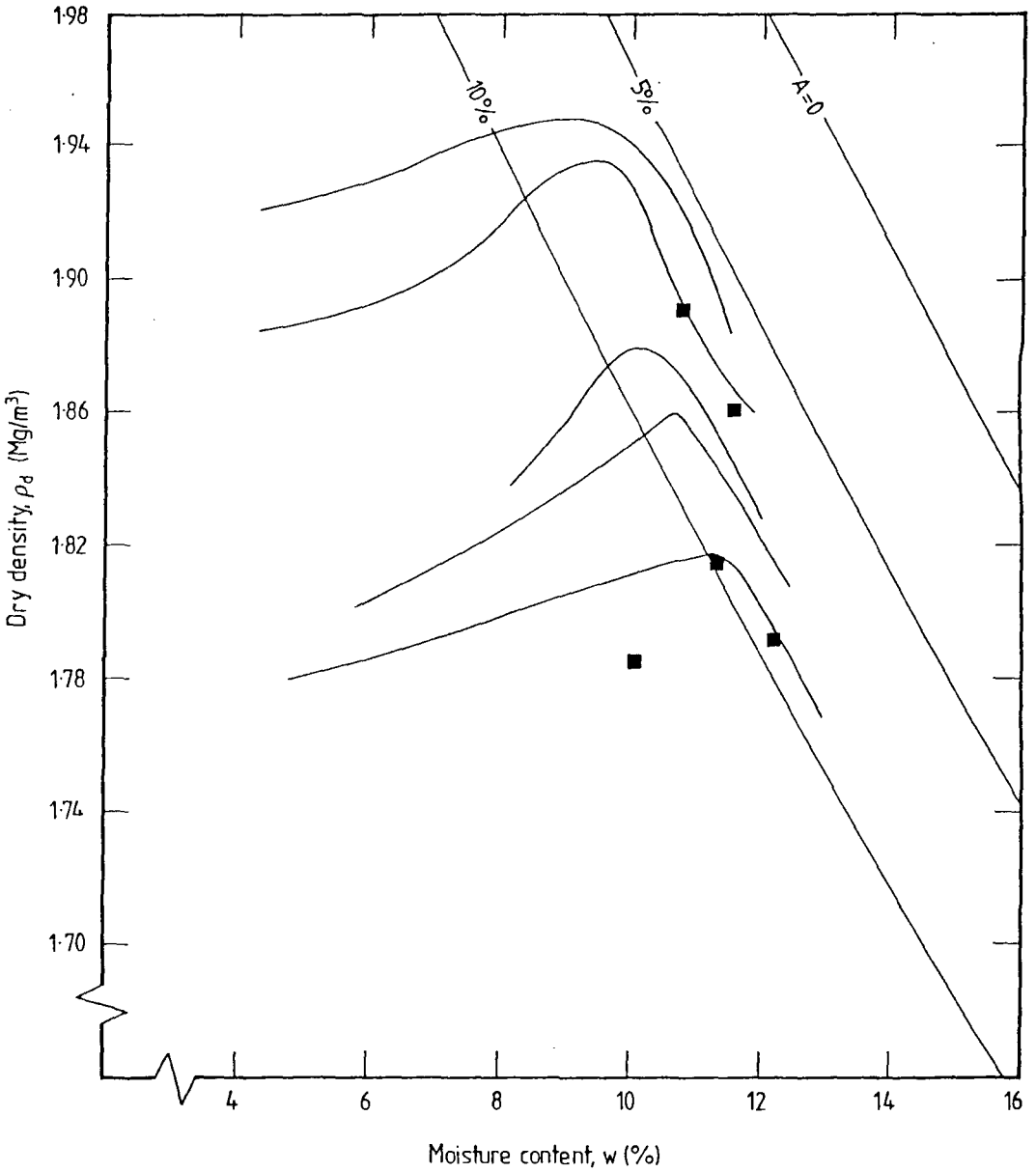

Figure 7.51 - Dry density-moisture content relationships for Permian Sand co
pacted at 27, 54, 81, 108 and 135 blows/layer to BS 1377 (1975): Test 12. Field d
density-moisture content data are plotted for comparison. Curves of constant
voids ($A = 0,\ 5$ and 10%) are also shown.

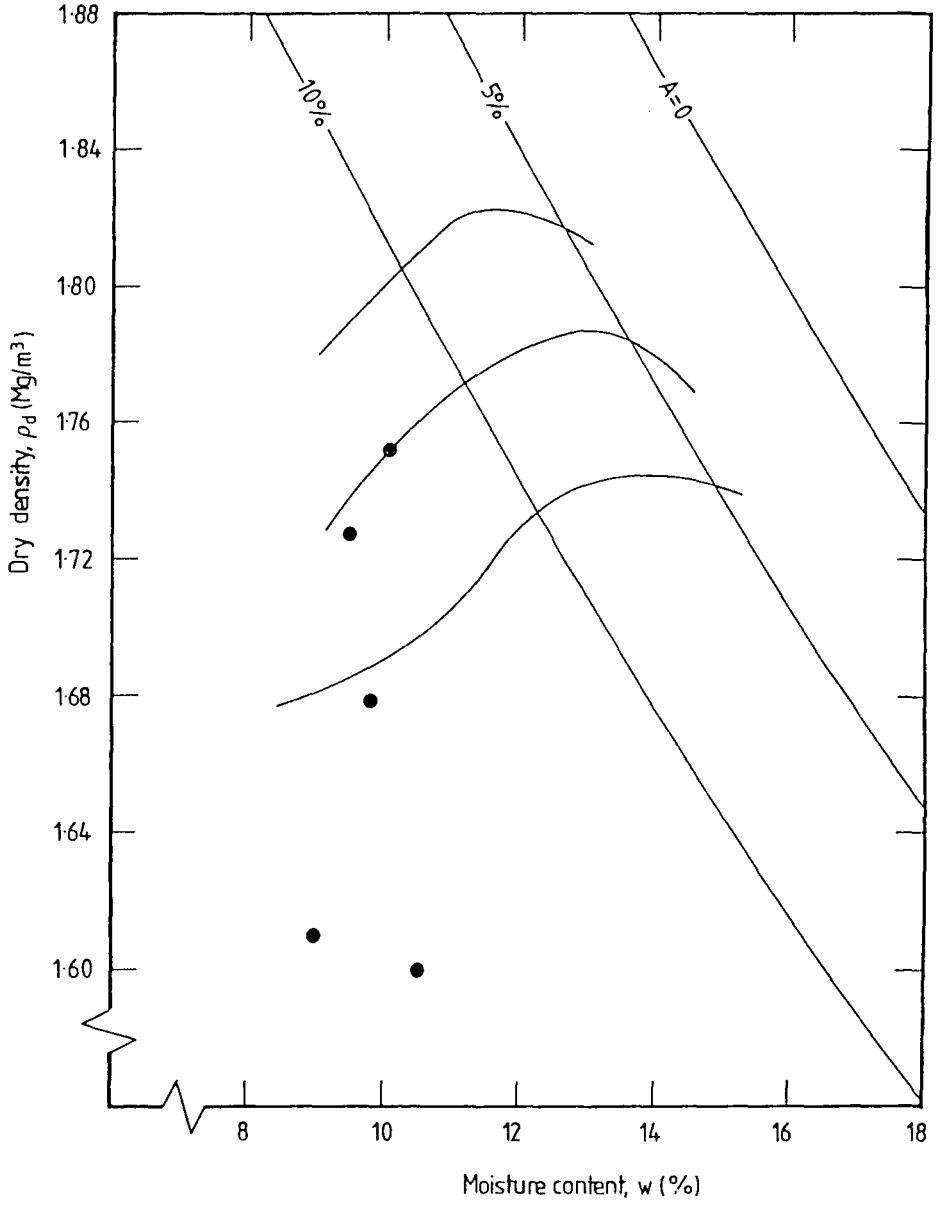

Figure 7.52 - Dry density-moisture content relationships for Sharp Sand compacted at 27, 54 and 81 blows/layer to BS 1377 (1975): Test 12. Field dry density-moisture content data are plotted for comparison. Curves of constant air voids (A = 0, 5 and 10%) are also shown.

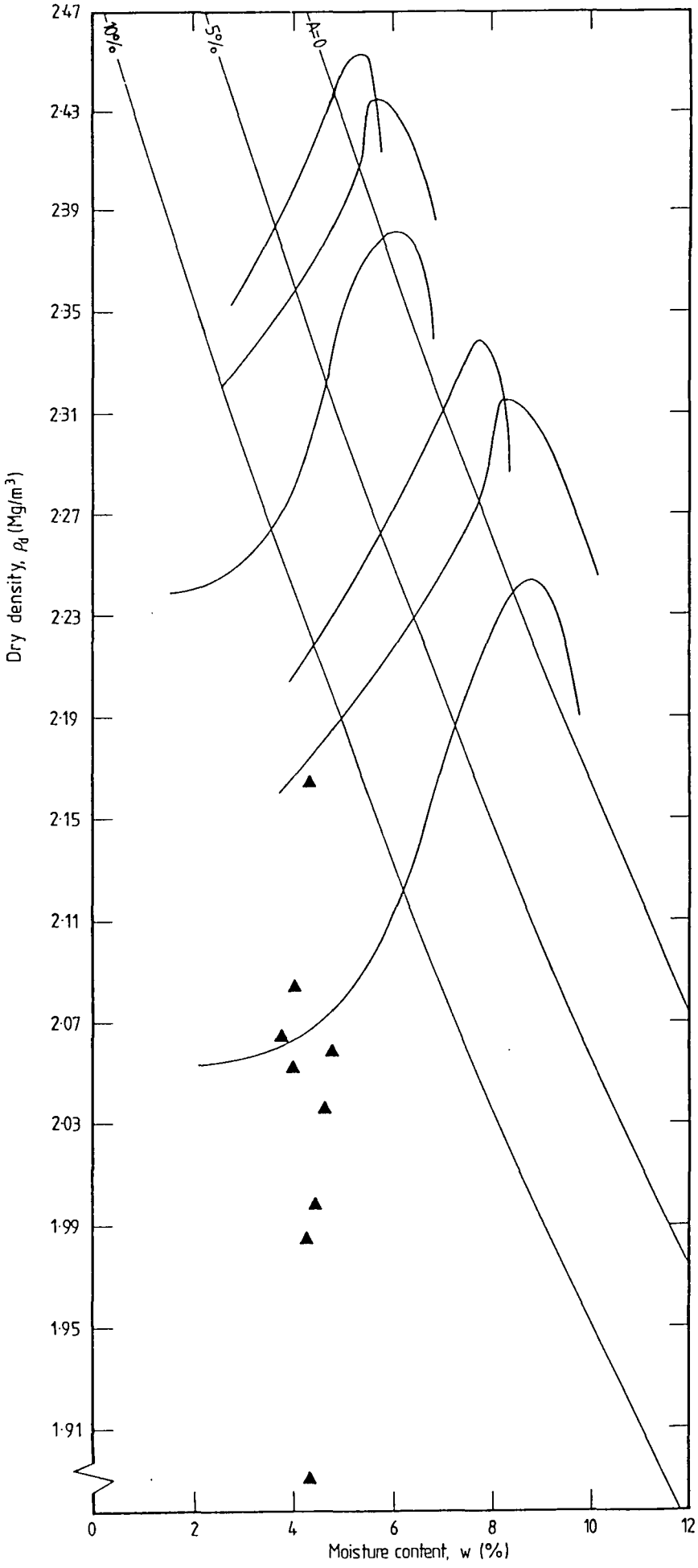

Figure 7.53 - Dry density-moisture content relationships for Wet-mix macadam compacted at 27, 54 and 81 blows/layer to BS 1377 (1975): Test 12. The curves are shown both corrected (top three curves) and uncorrected (lower three curves) for the stone content of the material. Field dry density-moisture content data are plotted for comparison. Curves of constant air voids (A = 0, 5 and 10%) are also shown.

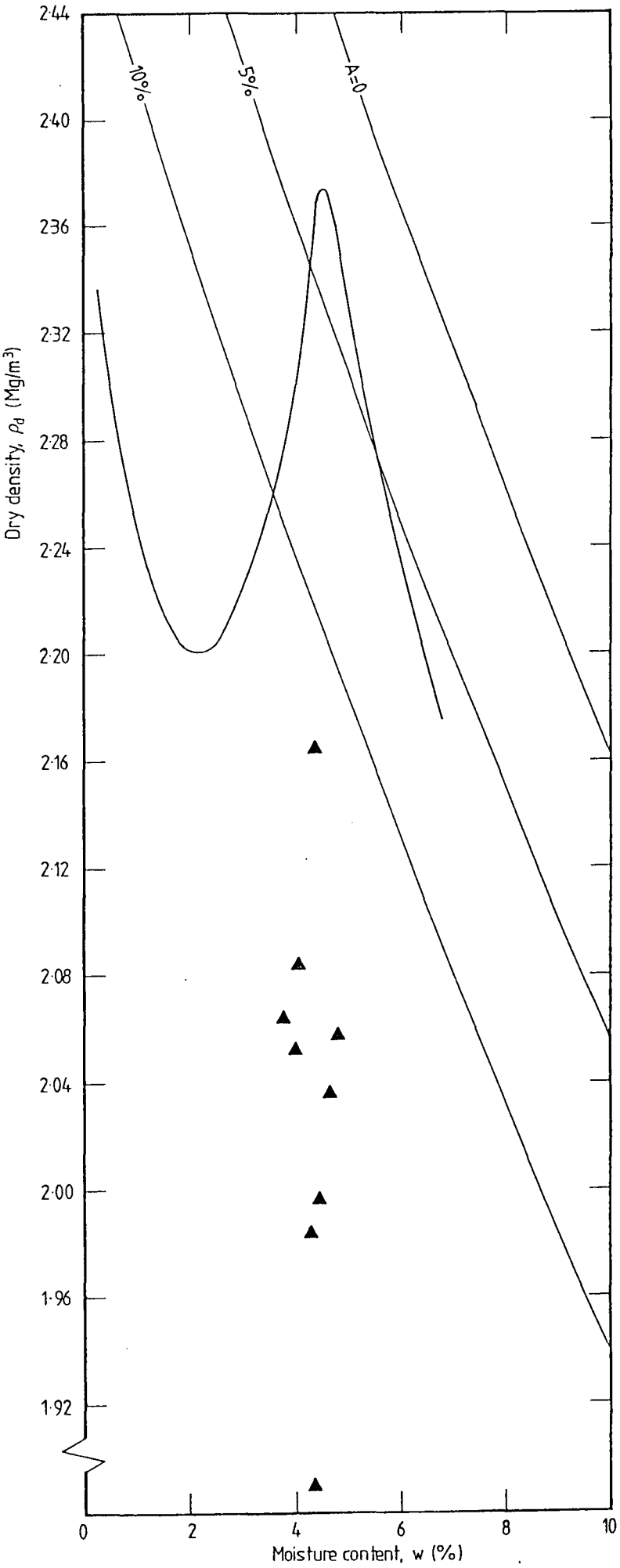

Figure 7.54 - Dry density-moisture content relationship for Wet-mix macadam co
pacted to BS 5835: Part 1 (1980). Field density-moisture content data are plot
for comparison. Curves of constant air voids (A = 0, 5 and 10%) are also show

CHAPTER 8

CONCLUSIONS AND RECOMMENDATIONS FOR FURTHER WORK

8.1 Conclusions

In Chapter 1 the current administrative methods of reinstatement works, which are a result of the need to service and develop the utilities' buried plant (replacement cost £117,000 m), were examined. The current Public Utilities Street Works Act of 1950 is scheduled for replacement by a new Parliamentary Act which is not expected to be fully operational, complete with a national specification for reinstatements, until late 1990 at the earliest possible date.

The purpose of the work presented here was to identify and evaluate a potential testing technique, based on the propagation of seismic waves, on which a performance specification for unbound reinstatement backfill quality might be based. Ideally the technique was to be operated from the completed surface of the unbound backfill. The generally small scale nature of reinstatement works means that the test should be simple and quick to operate.

The sinusoidal propagation of Rayleigh-type surface waves was identified, in Chapter 3, as a potential measurement technique. This technique allowed the wave velocity of the compacted materials to be determined as a function of depth by making the classical assumption that the depth of propagation is equal to one-half the wavelength ($z = \lambda/2$).

The form of the theoretical vertical displacement-depth curves is generally supported by measurements of the displacement due to a surface wave, and a simple analysis to find the centroid of the area under the curves indicates that the depth to the centroid is $0.406 < \overline{z/\lambda} \leq 0.609$ for the normal range of Poisson's ratio; $0 < \nu \leq 0.5$.

A body of experimental evidence presented by previous authors also goes some way towards confirming the validity of this assumption and experimental data from field trials (Sections 7.4, 7.5 and 7.6), involving the measurement of surface wave velocities of one or two compacted materials and the underlying subgrade, also

indicates the validity of this assumption. Each data set was thus plotted as a surface wave velocity-depth profile of the straight line form.

Theoretical considerations also indicate that the Rayleigh wave velocity is only slightly lower than the shear wave velocity and thus it may be assumed that the shear modulus, $G \approx \rho v_R^2$.

A short review of currently available test methods for compacted materials is presented in Chapter 2. These test methods relate to both bound and unbound materials and are generally found to be geometrically unsuitable for use in the reinstatement environment. Two devices do, however, bear further investigation with respect to their potential application to reinstatements. Firstly, *'La Dynaplaque'*, which measures the coefficient of restitution of a mass in collision with a plate bearing on the ground surface *via* a set of springs, could possibly be scaled down to a size suitable for the reinstatement environment. This device is currently used in France for the evaluation of compacted earthworks. Secondly, a device developed jointly by Loughborough University and Geotechnics Ltd shows some promise. This device is similar in principle to the Clegg meter but as well as measuring the maximum deceleration (Impact Value) the time period of the impact is also measured.

As implied in the previous paragraph the Clegg meter (Section 2.4.1) consists of a drop-weight (or drop-hammer) of mass 4.5 kg with an internally mounted accelerometer which is dropped, from a height of 450 mm on to the test material and the peak deceleration is measured and characterised in terms of an Impact Value ($1IV = -10\,\mathrm{g}$).

Experimental results were obtained from tests conducted on Permian Sand (Section 7.2) and Sharp Sand (Section 7.3) in a purpose built laboratory based trench, for density, Impact Value, *CBR*, surface wave velocity and derived shear modulus. The moisture content was generally controlled to within $\pm 1\%$ of the optimum moisture content for the Permian Sand and a 'target' moisture content for the Sharp Sand. Experimental results were also obtained from tests conducted on Wet-mix macadam (Section 7.4) and Wet-mix macadam over Sharp Sand (Section 7.5) during field trials, for density, Impact Value, surface wave velocity and derived shear modulus. The moisture content was generally controlled to within $\pm 1\%$ of the optimum moisture content for the Wet-mix macadam while for the Sharp Sand the moisture content, as delivered and compacted, was between 1.5% and 2.5% below the 'target' moisture content set for tests conducted in the laboratory based trench.

The test materials were classified and optimum moisture contents determined using British Standard test methods as described in Chapter 4. A series of some five case studies were also presented in Section 7.6.

The British Standard compaction tests which were conducted on the Wet-mix macadam led to the conclusion that the BS 5835: Part 1 (1980) test is more suitable for the determination of the dry density-moisture content relationship of aggregates than is the conventional drop-mass BS 1377 (1975): Test 12, not least because the former test allows particles up to 37.5 mm to be included in the test specimen which is therefore more representative of the material compacted under field conditions. The type of compactive effort applied (vibrating hammer) is also of a similar nature to the compactive effort applied in the field using the Wacker BS45Y vibratory-rammer.

The experimental results were interpreted in terms of the logarithm of compactive effort, defined in two ways:

i)the number of passes applied per layer (N_p), using the Wacker BS45Y vibratory-rammer described in Appendix 5, and

ii)the number of passes applied per layer divided by the mean layer thickness ($N_p/\overline{h}$). As most of the tests were conducted in trenches of similar horizontal dimensions then this parameter may be converted to an equivalent compactive energy (in kJ/m^3) as described in Section 7.1.

Interpretation of this form, using a linear regression program, generally gave strong correlations for dry density, Impact Value, mean surface wave velocity ($v_{Rz_{max}/2}$) and mean shear modulus ($G_{z_{max}/2}$) with either N_p or $N_p/\overline{h}$ taken as the parameter of compactive effort. There was, however, some evidence to suggest that the measured properties of the Permian Sand were to some extent dependent upon the time for which the compacted material was left to dry prior to testing. The drying out process is believed to have caused the small amount (2%) of Calcite in the Permian Sand to act as a cement (Sections 4.7 and 7.2.1).

In addition to the interpretation of the data in terms of the applied compactive effort, relationships between the dry density and Impact Value are reported for each material. Plainly these relationships may only be applied over the limited range of moisture contents at which the materials were compacted, as is evidenced by the lack of fit of the field compacted Sharp Sand data with the data from tests conducted

in the laboratory based trench on the same material, but at moisture contents some 1.5% to 2.5% higher.

Comparison of the Impact Value and *CBR* data indicates that Clegg's (1980) relationship (Equation 2.1) may lead to an under-estimate of the *CBR* from measured Impact Values. This observation is, however, based on limited data covering a very narrow range of Impact Values and a considerable amount of further testing is required before firm conclusions can be drawn regarding the validity, or otherwise, of Clegg's relationship.

In the evaluation of a suitable parameter for use in the assessment of reinstatement backfill quality the degree of numerical sensitivity to the applied compactive effort is of great importance. Such an interpretation is presented in Chapter 7 for a change in compactive from $N_p/\overline{h} = 15\,\mathrm{m}^{-1}$ to $N_p/\overline{h} = 90\,\mathrm{m}^{-1}$. For all three materials the Impact Value is more sensitive to the applied compactive effort than is the mean surface wave velocity which is, in turn, more sensitive to the applied compactive effort than the dry density. The sensitivity of the mean shear modulus to the applied compactive effort is generally somewhat lower than that of the Impact Value but higher than that of the mean surface wave velocity. A similar interpretation in terms of the 'correlation sensitivity' (defined as the product of the regression correlation coefficient and the numerical sensitivity—rS) which takes account of the potential scatter of the experimental data is perhaps a more representative measure of the suitability of a parameter for the measurement of reinstatement backfill quality. The essential relationships between the parameters remain as described above for the numerical sensitivity.

Being a parameter of elastic deformation the shear modulus is a highly appropriate measure for reinstatement backfill quality. It may therefore be concluded that density measurements should, in future work, be specified as part of a surface wave velocity testing programme. This point is reinforced by the observation made in Section 7.6.4 that the surface wave velocity-depth profiles for tests on two materials, one well compacted with a high density and the other poorly compacted with a low density, may coincide. Measurement of the density and conversion to shear modulus-depth profiles would isolate the difference between materials in compacted states such as these.

With respect to the general suitability of the surface wave method for use in the reinstatement environment, experimental procedures may be simplified and the

time taken to establish a surface wave velocity-depth profile reduced, as is discussed in Section 8.2. The considerable weight of evidence in favour of the classical assumption that the depth of propagation of a Rayleigh-type surface wave is equal to one-half the wavelength has already been discussed and this enables the interface between layers of different materials to be identified. The presence of gas pipes within the reinstatement profile appears to have a variable effect dependent upon the pipe material. Steel pipes appear to provide a preferential (faster) path for the transmitted wave, while plastic pipes appear to have no identifiable effect upon the wave transmission (Section 7.5.2).

In general it may be observed that the surface wave method isolates the differences between 'well' compacted and 'poorly' compacted materials. Certainly in a back-to-back test, where 'poorly' compacted was defined as a large number of passes applied to a single very deep layer, the surface wave method yielded significantly different surface wave velocity-depth profiles for the two tests. In contrast, the Impact Values for the two tests were broadly comparable, indicating that the Clegg meter cannot identify superficially compacted material as being 'poorly' compacted. The surface wave method did, however, yield results which were considered anomalous for Test WMM2 ($N_p = 10$) and considerable difficulty was experienced during testing the dry Wet-mix macadam (Test WMM10) due to the accelerometers picking up high frequency 'chatter' between the loose, individual particles. The Clegg meter identified this material as being very poorly compacted compared to similar tests on the Wet-mix macadam compacted at the optimum moisture content.

The tentative conclusion was drawn, in Section 7.8, that reflections from the trench walls were minimal, both in the laboratory and field trenches. Maximum shear strains were calculated and these compared well with values quoted by Seed and Idriss (1970).

It is concluded that the Clegg meter is a useful device for the measurement of reinstatement backfill quality provided that there is adequate supervision of the compaction process and that measurement immediately after the compaction of each layer presents no logistical problems.

The determination of the shear modulus-depth profile from density measurements and the measured surface wave velocity-depth profile would appear to be

a viable alternative to the Clegg meter. However, both the density and the surface wave velocity-depth profile take a relatively long time to determine. Means of accelerating and simplifying these processes are discussed in Section 8.2.

In addition to the surface wave velocity determinations surface wave attenuation measurements have been made as part of the test programme conducted on the Permian Sand (not Tests TPS1 and TPS2), Sharp Sand and Wet-mix macadam. These facilitated the calculation of shear strains and also of the material attenuation coefficient (α). The calculation of α was achieved using a new, straight line form of the Bornitz equation (Section 5.6.3) which eliminates the need to make potentially erroneous assumptions regarding the state of the attenuation curve close to the source of vibration. Consistent relations between α and the applied compactive effort could not be found. The potential use of this technique for improving the reliability and ease of the calculation of the material attenuation coefficient and, therefore, vibration amplitude predictions due to construction activity is considerable.

8.2 Recommendations for further work

The test programme to determine the dynamic displacement-depth profiles was, of necessity, limited and although the data indicated a reasonable agreement with theory further confirmation is desirable. Ideal test conditions would involve burying accelerometers at different depths and distances from a vibrating source and some degree of redundancy in the measurements might be introduced by repeating the measurements on more than one radial axis. Such a test programme would require a cylindrical excavation of a minimum 5 m diameter and a large number of accelerometers. Plainly this would require a considerable investment in terms of time, equipment resources and capital expenditure. It is debatable whether such an investment is justifiable in terms of the anticipated results. If such a project were to proceed, however, particular attention should be paid to the nature of the contact between the surface accelerometers and the host material, ensuring that the contact is comparable to that of the buried accelerometers and the host material. If such a test facility were to be constructed then the three-dimensional displacements due not only to Rayleigh-type surface waves but also to surface generated SH- and SV-waves and due to P-waves and S-waves generated at depth, in boreholes, could be undertaken.

Further work on the technique presented for the determination of the material attenuation coefficient (α) has already been instigated (Davies, 1989). This work is primarly concerned with the assessment of the frequency dependency of α.

Further tests, conducted over a wide range of Impact Value, are necessary before sound conclusions can be drawn concerning the validity of Clegg's (1980) relationship for obtaining *CBR* values from measured Impact Values.

Further work is also required to determine the sensitivity of the reported material dependent dry density-Impact Value relationships to moisture content for the materials tested and also for other materials relevant to the reinstatement environment. If reliable estimates of the dry density can be achieved from measured Impact Values then the Clegg meter would appear to be a most reliable test method around which the acceptance testing of reinstatement backfill quality could be based.

If the surface wave method is to be used for a significant amount of further work in the reinstatement environment then a number of modifications to the equipment and experimental procedures might be envisaged.

The use of variable frequency band-pass filters to remove unwanted signal frequencies prior to processing by the CRO (or other phase measurement device) and digital counter would be of advantage in removing the effects of particle 'chatter' from dry material (see Test WMM10), traffic and construction induced vibrations. Design principles for band-pass filters are given by both Diefenderfer (1979) and Millman (1979). These devices would ideally be linked to the frequency control of the variable frequency power amplifier (Section 5.3.2). A variable frequency band-pass filter would be required for each accelerometer used.

The procedure of stepping-out one accelerometer from another to identify successive in-phase and out-of-phase separations (*i.e.* $\phi = 0, \pi, 2\pi, 3\pi, \ldots, n\pi$) is repeated for every measurement frequency and is extremely slow and laborious. Although reservations have been expressed regarding the measurement of absolute phase angles (Section 3.3) the use of a number of accelerometers at fixed separation distances which correspond to less than the maximum anticipated wavelength and an appropriate method to correct for the number of wavelengths separating the first and current measurement transducer (j—a counter) may well overcome these reservations. When measurements are to be made at n transducer locations,

i.e. $(d_1, \phi_1), (d_2, \phi_2), (d_3, \phi_3), \ldots, (d_n, \phi_n)$ and $d_2 - d_1 = d_3 - d_2 =, \ldots, = d_n - d_{n-1}$ etc, such a technique may be presented in the elegant form of a computer algorithm:

let $j := 1$

for $i := 1$ **step until** n **do**

read $\phi[i]$

if $\phi[i] < \phi[i-1]$ **then** $\phi[i] = \phi[i] + j2\pi$ **and** $j = j + 1$

write $\phi[i]$

end.

The setting-up of the experimental apparatus on site is a very time consuming task. The mounting of the components in a modular rack system, which could be loaded into a vehicle as a single unit, such that the various electrical and power connections need not be made and un-made on each site, would significantly reduce the total time required for testing.

The above mentioned modifications to the surface wave method would considerably improve the simplicity and time taken to establish a surface wave velocity-depth profile. If the shear modulus-depth profile is to be determined then density measurements are also required. As bulk densities (*i.e.* not dry densities) are required, then removal of material for testing to determine the moisture content is not required. However, the sand replacement methods described in BS 1377 (1975) require the excavation of a hole, and testing would need be carried out on each layer after compaction. Consideration of the use of a Nuclear Density Gauge for density measurement might be considered, despite the problems associated with this device, as outlined in Chapter 2.

On balance, given the complexity of the surface wave method, even after appropriate modifications, the author would suggest that this method is best suited to a research rôle in terms of reinstatement works while the Clegg meter is perhaps the most suitable of the currently available devices for routine testing. Disadvantages of the Clegg meter include the requirement for testing after the compaction of each layer and the quest for a more suitable test method, or device, should not end here as none of the test methods have proved to be ideal. In the interim (at least) a method specification would appear to be the most logical approach to be adopted for a future code of practice for reinstatement works.

References

ABBISS, CP (1981). 'Shear wave measurements of the elasticity of the ground'. *Géotechnique,* Vol. 31, No. 1, pp. 91–104.

ABBISS, CP (1983). *'Shear wave measurements of deformation properties of soils'.* PhD Thesis, University of London.

ANDERSSON, O (1975). 'Measurement of the bearing capacity of roads—A comparison between four methods'. *National Swedish Road and Traffic Research Institute, Report No. 61A,* Stockholm.

ANON (1987a). 'Compaction update needs new thinking'. *New Civil Engineer,* 29th October 1987, pp. 19–20.

ANON (1987b). 'Gauge assesses asphalt accuracy'. *New Civil Engineer,* 19th November 1987, pp. 40.

ANON (1988a). 'The hole truth'. *The Independent Magazine,* 17th September 1988, pp. 14–15.

ANON (1988b). 'Trench warfare'. *New Civil Engineer,* 19th June 1988, pp. 20–21.

ANON (1988c). 'Road opening code compromise close'. *New Civil Engineer,* 22nd September 1988, pp. 8.

ANON (1988d). 'Soothing out streetworks'. *New Civil Engineer,* 22nd September 1988, pp. 28, 30.

ANON (1988e). 'Fast compactor comes of age'. *New Civil Engineer,* 9th June 1988, pp. 28–30.

ANON (1988f). 'Joint venture seeks new soils test'. *New Civil Engineer,* 3rd March 1988, pp. 21.

ANON (1988g). 'Engineering geophysics'. Report by the Geological Society Engineering Group Working Party, *Quarterly Journal of Engineering Geology,* London, Vol. 21, pp. 207–271.

ANON (1989a). '"Needless" road repairs cost £220m a year'. *The Daily Telegraph,* 2nd January 1989.

ANON (1989b). 'Street wise'. *New Civil Engineer,* 15th June 1989, pp. 40.

ANON (1989c). 'Huge growth in streetworks to follow new law'. *New Civil Engineer,* 22nd June 1989, pp. 7.

ANON (1989d). 'Hole lotta shaking'. *Evening Chronicle,* 15th June 1989, pp. 3.

ASAI, S (1960). 'Measurements of bearing capacity of subgrade by drop impact method'. *Soils and Foundations, Japanese Society of Soil Mechanics and Foundation Engineering,* Vol. 1, Part 1, pp. 42–52.

BALLARD, RF (1963). 'Nondestructive dynamic testing of proposed radar sites: White Sands Missile Range, New Mexico'. *US Army Engineer Waterways Experiment Station, Miscellaneous Paper No. 4-584,* Corps of Engineers, Vicksburg, Mississippi.

BALLARD, RF and McLEAN, FG (1975). 'Seismic field methods for in situ moduli'. *US Army Engineer Waterways Experiment Station, Miscellaneous Paper No. S-75-10,* Corps of Engineers, Vicksburg, Mississippi.

BARKAN, DD (1962). *'Dynamics of bases and foundations'.* McGraw-Hill, New York.

BARNES, GE (1987). 'The Moisture Condition Value and compaction of stony clays'. *Proceedings, New Civil Engineer Conference, 'Compaction Technology 87',* pp. 79–90. October 29th 1987, Institution of Civil Engineers, London.

BENOIST, J and SCHAEFFNER, M (1982). 'La Dynaplaque'. *Road Earthworks—Liason Bulletin of the "Laboratores Ponts et Chaussées 122"* . Nov.–Dec. 1982, pp. 61–72. (English translation from the original French.)

BENTLEY, SP and CARTER, M (1987). 'A microwave drying time chart'. *The Journal of the Institution of Highways and Transportation and HTTA, 'Highways and Transportation',* March 1987, Vol. 34, No. 3, pp. 36–37.

BERGSTRÖM, SG and LINDERHOLM, S (1946). 'A dynamic method for determining average elastic properties of surface soil layers'. *Proceedings, Handlingar,* Svenska Forskningsinstitutet för Cement och Betong vid Kungl, Techniska Högskolan i Stockholm, N:R. 7, pp. 1–47.

BORNITZ, G (1931). *'Über die ausbreitung der von groszkolbenmaschinen erzeugten bodenschwingungen in die tiefe'.* J. Springer, Berlin.

BOYCE, JR, COBBE, MI and FLEMING, PR (1989). 'Development of a prototype variable impact testing apparatus'. *Proceedings, 3rd Conference on Unbound Road Aggregates, 'Unbar 3'.* Edited by RH Jones and AR Dawson. University of Nottingham. Butterworths.

BOYES, D and ROBINSON, AJ (1987). 'The Clegg impact meter—Its relevance and use for the assessment of compaction'. *British Gas Engineering Research Station Report No. ERS R.3785 87/1215 RSC,* Killingworth. British Gas Confidential Report.

BS 410 (1986). 'British Standard specification for test sieves'. *British Standards Institution,* London.

BS 812: Part 1 (1975). 'Methods of testing and sampling of mineral aggregates, sands and fillers: Part 1. Sampling, size shape and classification'. *British Standards Institution,* London.

BS 812: Part 2 (1975). 'Methods of testing and sampling of mineral aggregates, sands and fillers: Part 2. Physical properties'. *British Standards Institution,* London.

BS 812: Part 3 (1975). 'Methods of testing and sampling of mineral aggregates, sands and fillers: Part 3. Mechanical properties'. *British Standards Institution,* London.

BS 812: Part 102 (1984). 'British Standard testing aggregates: Part 102. Methods for sampling'. *British Standards Institution,* London.

BS 812: Part 103 (1985). 'British Standard testing aggregates: Part 103. Methods for determination of particle size distribution'. *British Standards Institution,* London.

BS 812: Section 105.1 (1985). 'British Standard testing aggregates: Section 101. Flakiness index'. *British Standards Institution,* London.

BS 882 (1983). 'Aggregates from natural sources for concrete'. *British Standards Institution,* London.

BS 1305 (1974). 'British Standard batch type concrete mixers'. *British Standards Institution,* London.

BS 1377 (1967). 'Methods of testing soils for civil engineering purposes'. *British Standards Institution,* London.

BS 1377 (1975). 'Methods of test for soils for civil engineering purposes'. *British Standards Institution,* London.

BS 1377: Part 4 (1988). 'Methods of test for soils for civil engineering purposes: Part 4. Compaction related tests'. Draft for Comment Document *British Standards Institution,* London.

BS 5835: Part 1 (1980). 'Recommendations for testing of aggregates: Part 1. Compactability test for graded aggregates'. *British Standards Institution,* London.

BS 5930 (1981). 'Code of parctice for site investigations (Formerly CP 2001). *British Standards Institution,* London.

CLEGG, B (1976). 'An impact testing device for in situ base course evaluation'. *Proceedings, 8th Australian Road Research Board Conference,* Session 8, pp. 1–6. Perth.

CLEGG, B (1977). 'Field assessment of the impact soil tester'. *Australian Road Research Board, Research Report, ARR No. 76.*

CLEGG, B (1980). 'Impact test as alternative to California Bearing Ratio'. *Proceedings, 3rd Australia-New Zealand Conference on Geomechanics,* Vol. VI, pp. 1225–1230. Wellington, New Zealand, May 12th–16th 1980.

CLEGG, B (1983a). 'Application of an impact test to field evaluation of marginal base course materials'. *Transportation Research Record 898,* pp. 174–181. Transportation Research Board, National Research Council, Washington DC.

CLEGG, B (1983b). 'Design compatible control of basecourse construction'. *Australian Road Research,* Vol. 13. No. 2, pp. 112–122.

CLEGG, B (1985). 'Clegg impact test guidelines'. *Report of the Department of Civil Engineering, University of Western Australia,* Nedlands, Western Australia 6009.

COGHILL, WH (1967). 'The design and evaluation of asphalt concrete pavements using continuous waves'. *Proceedings, 2nd International Conference on Structural Design of Asphalt Pavements,* pp. 367–371. August 7th–11th 1967, University of Michigan, Ann Arbor.

D'APPOLONIA, DJ, WHITMAN, RV and D'APPOLONIA, ED (1969). 'Sand compaction with vibratory rollers'. *Journal of the Soil Mechanics and Foundations Division,* ASCE, Vol. 95, SM1, pp. 263–284.

DAS, BM (1983). *'Fundamentals of soil dynamics'.* Elsevier, Oxford.

DAVIES, P (1989). *'The frequency dependency of the attenuation/absorption coefficient of Rayleigh-type surface waves'.* MSc Advanced Course in Engineering Geology Dissertation, University of Durham.

DAWSON, AR and THOM, NH (1988). 'Field tests on pavement foundations'. *Preprints, 24th Annual Conference of the Engineering Group of the Geological Society, 'Field Testing in Engineering Geology'*, Edited by FG Bell, MG Culshaw and JC Cripps, pp. 177–190. September 4th–8th 1988, Sunderland Polytechnic.

DEPARTMENT OF TRANSPORT (1973). *'Guide to the Public Utilities Street Works Act'*. HMSO, London.

DEPARTMENT OF TRANSPORT (1974). *'Reinstatements under the Public Utilities Street Works Act 1950: A model agreement and specifications'*. HMSO, London.

DEPARTMENT OF TRANSPORT (1976). *'Specification for road and bridge works'* and *'Notes for guidance on the specification for road and bridge works'*. Department of Transport, Scottish Development Department, Welsh Office, HMSO, London.

DEPARTMENT OF TRANSPORT (1986). *'Specification for highways works: Parts 1–7'* and *'Notes for guidance on the specification for highways works: Parts 1–6.'* Department of Transport, Scottish Development Department, Welsh Office, Department of the Environment for Northern Ireland, HMSO, London.

DEPARTMENT OF TRANSPORT (1987). 'Structural design of new road pavements'. *Highways and Transport, Departmental Standard HD14/87,* also *Amendment No. 1 to HD14/87, Highways and Transport, Advice Note HA35/87* and *Amendment No. 1 to HA35/87,* Department of Transport.

DIEFENDERFER, AJ (1979). *'Principles of electronic instrumentation'*, 2nd Edition. WB Saunders, London.

DJÄRF, L (1982). 'The wave propagation method—A reliability study'. *Proceedings, International Symposium on 'Bearing Capacity of Roads and Airfields'*, Vol. II, pp. 543–548. June 23rd–25th 1982, Norwegian Institute of Technology, Trondheim, Norway.

DOWDING, CH (1985). *'Blast vibration monitoring and control'*. Prentice-Hall, New Jersey.

EWING, WM, JARDETSKY, WS and PRESS, F (1957). *'Elastic waves in layered media'*. McGraw-Hill, New York.

FERRIS, AJ (1987). 'Review of plant'. *Proceedings, New Civil Engineer Conference, 'Compaction Technology 87'*, pp. 75–77. October 29th 1987, Institution of Civil Engineers, London.

FILIPCZYNSKI, L, PAWLOWSKI, Z and WEHR, J (1966). *'Ultrasonic methods of testing materials'*. Butterworths, London.

FORSSBLAD, L (1965). 'Investigations of soil compaction by vibration'. *Acta Polytechnica Scandinavica, Civil Engineering and Building Series No. 34,* Stockholm.

FORSSBLAD, L (1982). 'Control of bearing capacity by means of compaction meter'. *Proceedings, International Symposium on 'Bearing Capacity of Roads and Airfields'*, Vol. I, pp. 501–509. June 23rd–25th 1982, Norwegian Institute of Technology, Trondheim, Norway.

FREDERICK, JR (1965). *'Ultrasonic engineering'*. J Wiley and Sons, London.

FREER-HEWISH, RJ (1982). 'Developments in field control of earthworks compaction'. *Proceedings, 11th Australian Road Research Board Conference,* Volume 11, Part 3, pp. 1–10. Melbourne, Australia.

FRY, ZB (1963). 'A procedure for determining elastic moduli of soils by field vibratory techniques'. *US Army Engineer Waterways Experiment Station, Miscellaneous Paper No. 4-577,* Corps of Engineers, Vicksburg, Mississippi.

FRY, ZB (1965). 'Dynamic soils investigations: Project Buggy, Buckboard Mesa, Nevada Test Site, Mercury, Nevada'. *US Army Engineer Waterways Experiment Station, Miscellaneous Paper No. 4-666,* Corps of Engineers, Vicksburg, Mississippi.

GAZETAS, G and YEGIAN, MK (1979). 'Shear and Rayleigh waves in soil dynamics'. *Journal of the Geotechnical Division,* ASCE, Vol. 105, GT12, pp. 1455–1470.

GRIM, RE (1968). *'Clay mineralogy'*, 2nd Edition. McGraw-Hill, New York.

GUILLEMIN, R and GRAMSAMMER, JC (1972). 'Dynamic non-destructive testing of pavements in France'. *Proceedings, 3rd International Conference on Structural Design of Asphalt Pavements,* Vol I, pp. 1167–1177. September 11th–15th 1972, London.

GENT, DW (1985). *'The application of surface acoustic waves in the measurement of ground structure and compaction profiles'.* BSc Project Report, Department of Engineering, Cambridge University.

HARDIN, BO (1978). 'The nature of stress-strain behaviour for soils'. *Proceedings, ASCE Geotechnical Engineering Division Speciality Conference, 'Earthquake Engineering and Soil Dynamics'*, Vol. I, pp. 3–90, June 19th–21st. Pasadena, California.

HEAD, KH (1980). *'Manual of soil laboratory testing: Volume 1, Soil classification and compaction tests'.* Pentech Press, London: Plymouth.

HEUKELOM, W and FOSTER, CR (1960). 'Dynamic testing of pavements'. *Journal of the Structural Division,* ASCE, SD1, pp. 1–28.

HOADLEY, PJ (1985). 'Measurement of dynamic soil properties'. In: *Analysis and Design of Foundations for Vibrations,* Edited by PJ Moore, pp. 349–419. AA Balkema, Rotterdam.

HODGE, MB (1932). 'The Permian yellow sands of north-east England'. *Proceedings, University of Durham Philosophical Society,* Vol. 8, No. 5, pp. 410–458.

HOGENTOGLER, CA (1938). 'Developments in soil stabilization'. *Proceedings, 38th Annual Convention of the American Road Builders' Association,* January 17th–21st 1938, Cleveland, Ohio. Washington DC undated (American Road Building Association), pp. 71–75.

HORNE COMMITTEE (1985). 'Roads and the Utilities: Review of the Public Utilities Street Works Act 1950'. *Report to the Secretary of State for Transport of a Committee chaired by MR Horne,* Department of Transport, HMSO, London.

HORNE, MR (1986). 'The review of the Public Utilities Street Works Act'. *Proceedings, 38th Annual Conference of the Institute of Works and Highways Management,* pp. 33–37. October 28th–31st 1986, Harrogate.

JONES, R (1958). 'In-situ measurement of the dynamic properties of soil by vibration methods'. *Géotechnique,* Vol. 8, No. 1, pp. 1–21.

JONES, R (1960). 'Measurement and interpretation of surface vibrations on soil and roads'. *Highway Research Board, Bulletin 277 and National Research Council Publication 815: 39th Annual Meeting,* pp. 8–29. January 11th–15th 1960, Washington DC.

JONES, R and WHIFFEN, AC (1960). 'A survey of dynamic methods of testing roads and runways'. *Highways Research Board Bulletin 227* and *National Research Council Publication 815: 39th Annual Meeting,* pp. 1–7. January 11th–15th 1960, Washington, DC.

JONES, R (1962). 'Surface wave technique for measuring the elastic properties and thickness of roads: Theoretical development'. *British Journal of Applied Physics,* Vol. 13, pp. 21–29.

JONES, R (1963). 'Following changes in the properties of road bases and sub-bases by the surface wave propagation method'. *Civil Engineering and Public Works Review,* May 1963, pp. 613–617.

JONES, R, THROWER, EN and GATFIELD, EN (1967). 'Surface wave method'. *Proceedings, 2nd International Conference on Structural Design of Asphalt Pavements,* pp. 505–519. August 7th–11th 1967, University of Michigan, Ann Arbor.

KASIANCHUK, DA and ARGUE, GH (1972). 'A comparison of plate load testing with the wave propagation technique'. *Proceedings, 3rd International Conference on Structural Design of Asphalt Pavements,* Vol I, pp. 444–454. September 11th–15th 1972, London.

KELSO, AE (1934–35). 'The construction of Silvan Dam, Melbourne Water Supply'. *Minutes of Proceedings, Institution of Civil Engineers,* Vol. 239, Part 1, p. 403.

KENNEDY, CK (1982). 'Equipment for assessing the structural strength of road pavements'. *Proceedings, International Symposium on 'Bearing Capacity of Roads and Airfields',* Vol. I, pp. 421–434. June 23rd–25th 1982, Norwegian Institute of Technology, Trondheim, Norway.

KLOMP, AGJ and DORMAN, GM (1964). 'Stress distribution and dynamic testing in relation to road design'. *Proceedings, 2nd Conference of the Australian Road Research Board,* Vol. II, pp. 701–728. (Also published as *Shell Bitumen Reprint No. 18.)*

KNOPOFF, L (1952). 'On Rayleigh wave velocities'. *Bulletin of the Seismological Society of America,* Vol. 42, pp. 307–308.

KOLSKY, H (1963). *'Stress waves in solids'.* Dover Publications, New York.

KREYSZIG, E (1983). *'Advanced engineering mathematics',* 5th Edition, John Wiley and Sons, New York.

KRIZEK, RJ (1977). 'Fabric effects on strength and deformation of Kaolin clay'. *Proceedings, 9th International Conference on Soil Mechanics and Foundation Engineering,* Vol. I, pp. 169–176. Tokyo.

KURZEME, M (1972). 'The in situ determination of the elastic moduli of layered pavements using SH-wave propagation'. *Proceedings, 3rd International Conference on Structural Design of Asphalt Pavements,* Vol I, pp. 468–475. September 11th–15th 1972, London. Also corrections to paper in Vol. II, pp. 422–424.

LAMB, H (1917). 'On waves in an elastic plate'. *Proceedings, Royal Society of London, Series A*, Vol. 93, pp. 114–128.

LAMBE, TW and WHITMAN, RV (1979). *'Soil mechanics*, SI Version. J Wiley and Sons, New York.

LEES, G and BINDRA, S (1982). 'A comprehensive evaluation of unbound granular material response for its use in pavement design and evaluation studies'. *Proceedings, International Symposium on 'Bearing Capacity of Roads and Airfields'*, Vol. II, pp. 670–683. June 23rd–25th 1982, Norwegian Institute of Technology, Trondheim, Norway.

LOVEDAY, CA (1987). 'End result compaction and the blacktop contractor'. *Proceedings, New Civil Engineer Conference, 'Compaction Technology 87'*, pp. 47–61. October 29th 1987, Institution of Civil Engineers, London.

LUTTON, RJ (1974). 'Use of Loess soil for modelling rock mechanics'. *US Army Engineer Waterways Experiment Station, Miscellaneous Paper No. S-74-28*, Corps of Engineers, Vicksburg, Mississippi.

MARKWICK, AHD (1945). 'The basic principles of soil compaction and their application'. *Engineering Division Paper, Institution of Civil Engineers*, 3, Road Engineering Division Paper No. 16. Also in: *'A century of soil mechanics'*, Edited by LF Cooling, AW Skempton and AL Little, pp. 333–378. Institution of Civil Engineers, 1969.

MARTINČEK, G and KADLEČIK, T (1982). 'The use of wave propagation method in evaluation of road pavement stiffness'. *Proceedings, International Conference on 'Bearing Capacity of Roads and Airfields'*, Vol. I, pp. 119–127. June 23rd–25th 1982, Institute of Technology, Trondheim, Norway.

MATHUR, TS and COGHLAN, GT (1987). 'The use of the Clegg impact test in managing and designing aggregate-surfaced roads'. *Proceedings, 4th International Conference on Low-Volume Roads, Transportation Research Record 1106*, Vol. I, pp. 232–236. Transportation Research Board, National Research Council, Washington DC.

MAXWELL, AA (1960). 'Non-destructive testing of pavements'. *Highway Research Board, Bulletin 277 and National Research Council Publication 815: 39th Annual Meeting*, pp. 30–36. January 11th–15th 1960, Washington DC.

MAXWELL, AA and FRY, ZB (1967). 'A procedure for determining elastic moduli of in situ soils by dynamic techniques'. *Proceedings, International Symposium on Wave Propagation and Dynamic Properties of Earth Materials*, pp. 913–919. University of New Mexico Press.

MAXWELL, AA and JOSEPH, AH (1967). 'Vibratory study of stabilized layers of pavement in runway at Randolph Air Force Base'. *Proceedings, 2nd International Conference on Structural Design of Asphalt Pavements*, pp. 547–552. August 7th–11th 1967, University of Michigan, Ann Arbor.

McCULLOCH, IR (1987). *'Cyclic loading on confined samples of sand'*. MSc Advanced Course in Engineering Geology Dissertation, University of Durham.

MEEHAN, RI (1967). 'The uselessness of elephants in compacting fill'. *Canadian Geotechnical Journal*, Vol. 4, No. 3, pp. 358–360.

METCALF, CT (1967). 'Field measurement of dynamic elastic moduli of materials in flexible pavement structures'. *Proceedings, 2nd International Conference on Structural Design of Asphalt Pavements,* pp. 521–535. August 7th–11th 1967, University of Michigan, Ann Arbor.

MILLER, CH and ODUM, JK (1986). 'A review of concepts and techniques for obtaining shear wave velocities from measured Rayleigh and compressional wave velocities at engineering sites'. *Bulletin of the Association of Engineering Geologists,* Vol. XXIII, No. 3, pp. 317–327.

MILLER, GF and PURSEY, H (1955). 'On the partition of energy between elastic waves in a semi-infinite solid'. *Proceedings, of the Royal Society of London, Series A, Mathematical and Physical Sciences,* Vol. 233, No. 1192, pp. 55–69.

MILLMAN, J (1979). *'Microlectronics: Digital and analog circuits and systems'.* McGraw-Hill, International Student Edition, London.

MOORHOUSE, DC and BAKER, GL (1969). 'Sand densification by heavy vibratory compactor'. *Journal of the Soil Mechanics and Foundations Division,* ASCE, Vol. 95, SM4, pp. 985–994.

MURDOCH, J and BARNES, JA (1970). *'Statistical tables for science, engineering, management and business studies',* 2nd Edition, Revised and expanded. MacMillan, London.

NETTLETON, LL (1940). *'Geophysical prospecting for oil'.* McGraw-Hill, London.

NIJBOER, LW (1967). 'New developments in vibration techniques'. *Proceedings, 2nd International Conference on Structural Design of Asphalt Pavements,* pp. 537–546. August 7th–11th 1967, University of Michigan, Ann Arbor.

NIJBOER, LW and VAN DER POEL, C (1953). 'A study of vibration phenomena in asphaltic road construction'. *Proceedings, American Association of Asphalt Paving Technologists,* Vol. 22, pp. 197–231.

NITZE, RJ (1986). 'Dudley digital records trial'. *Proceedings, 38th Annual Conference of the Institute of Works and Highways Management,* pp. 41–55. October 28th–31st 1986, Harrogate.

NUTT, PE (1987). 'Compaction and the new specification for highways works'. *Proceedings, New Civil Engineer Conference, 'Compaction Technology 87',* pp. 1–14. October 29th 1987, Institution of Civil Engineers, London.

ORRJE, O and BROMS, B (1970). 'Strength and deformation properties of soils as determined by a free falling weight'. *Proceedings, Swedish Geotechnical Institute No. 23.* Stockholm.

ØVERBY, C (1982). 'A comparison between Benkelman Beam, DCP and Clegg-Hammer measurements for pavement strength evaluation'. *Proceedings, International Symposium on 'Bearing Capacity of Roads and Airfields',* Vol. I, pp. 138–147. June 23rd–25th 1982, Norwegian Institute of Technology, Trondheim, Norway.

PARSONS, AW and BODEN, JB (1979). 'The moisture condition test and its potential applications in earthworks'. *Transport and Road Research Laboratory, Supplementary Report 552,* Department of the Environment, Department of Transport, Crowthorne, Berkshire.

PETERS, G (1984). 'Economics of reinstatement works'. *British Gas Engineering Research Station Report No. ERS P. 27,* Killingworth. British Gas Confidential Report.

PIKE, DC (1972). 'Compactability of graded aggregates: 1. Standard laboratory tests'. *Transport and Road Research Laboratory, Laboratory Report 447,* Department of the Environment, Crowthorne, Berkshire.

PIKE, DC and ACOTT, SM (1975). 'A vibrating hammer test for compactability of aggregates'. *Transport and Road Research Laboratory, Supplementary Report 140UC,* Department of the Environment, Crowthorne, Berkshire.

POWELL, WD, POTTER, JF, MAYHEW, HC and NUNN, ME (1984). 'The structural design of bituminous roads'. *Transport and Road Research Laboratory, Laboratory Report 1132,* Department of Transport, Crowthorne, Berkshire.

POWELL, WD and LEECH, D (1987). 'Compaction and performance of dense roadbase macadam'. *Proceedings, New Civil Engineer Conference, 'Compaction Technology 87'*, pp. 15–32. October 29th 1987, Institution of Civil Engineers, London.

PRAKASH, S (1981). *'Soil dynamics'.* McGraw-Hill, New York.

PROCTOR, RR (1933). 'Fundamental principles of soil compaction'. *Engineering News Record,* Vol. 111, pp. 245, 286, 348, 372.

RAO, HAB (1972). 'Evaluation of flexible pavements by nondestructive tests'. *Proceedings, 3rd International Conference on Structural Design of Asphalt Pavements,* Vol I, pp. 903–910. September 11th–15th 1972, London.

RAY, NP and CHAPMAN, TG (1954). 'The British Standard compaction test for soils: A study of some factors affecting the test results'. *Géotechnique,* Vol. 4, No. 4, pp. 169–177.

RAYLEIGH, LORD (1885). 'On waves propagated along the plane surface of an elastic solid'. *Proceedings, London Mathematical Society,* Vol. 17, pp. 4–11.

REID, DJ (1983). 'Compaction equipment and its use'. *British Gas Engineering Research Station Report No. ERS P. 23,* Killingworth. British Gas Confidential Report.

RHODES, AH, ADAMSON, P, STAFFORD, A and SMITH, BJ (1987). 'The Horne Report—Can we afford not to reinstate highway's properly?' *Talk presented to the Institution of Civil Engineers, Northern Counties Association,* 17th November 1987, Blackwell Grange, Darlington.

RICHART, FE, WOODS, RD and HALL, JR (1970). *'Vibrations of soils and foundations'.* Prentice-Hall, New Jersey.

ROAD RESEARCH LABORATORY (1952). *'Soil mechanics for road engineers'.* Department of the Environment, HMSO, London.

ROAD RESEARCH LABORATORY (1970). *'A guide to the structural design of pavements for new roads',* Third Edition. Department of the Environment, Road Note 29, HMSO, London.

ROBERTSON, JK (1954). *'Introduction to optics: Geometrical and physical',* 4th Edition. University Physics Series, D Van Nostrand Company, New York.

SAVAGE, PF (1963). 'A preliminary investigation into the impact value/CBR relationship for compacted soils'. *Proceedings, 3rd International Conference for Africa on Soil Mechanics and Foundation Engineering,* Vol. 1, pp. 201–205.

SCOTTISH DEVELOPMENT DEPARTMENT (1987). 'Structural design of new road pavements'. *Chief Road Engineer, Technical Memorandum SH6/87,* Scottish Development Department, also *Amendment No. 1 (April 1988).*

SEED, HB and IDRISS, IM (1970). 'Soil moduli and damping factors of dynamic response analyses'. *Earthquake Engineering Research Centre, Report No. EERC-70-10,* University of California, Berkeley.

SHERWOOD, PT (1970). 'The reproducibility of the results of soil classification and compaction tests'. *Road Research Laboratory, Laboratory Report 339,* Ministry of Transport, Crowthorne, Berkshire.

SMITH, BJ (1983). 'Developments in trench excavation and reinstatement'. *Journal of the Institute of Highways and Transportation, 'Highways and Transportation',* November 1983, Vol. 30, No. 11, pp. 2–12.

SMITH, DB and PATTISON, J (1970). 'Permian and Triass'. In: *'Geology of Durham County',* Edited by GAL Johnson and G Hickling. *Transactions, Natural History Society of Northumberland, Durham and Newcastle Upon Tyne,* Vol. 41, No. 1, pp. 66–91.

STOKOE, KH and NAZARIAN, S (1985). 'Use of Rayleigh waves in liquefaction studies'. *Proceedings of a Session Sponsored by the Geotechnical Engineering Division; 'Measurement and use of shear wave velocity for evaluating soil properties'.* Edited by RD Woods, pp. 1–17. ASCE Convention, May 1st 1985, Denver, Colarado.

STONELEY, R (1924). 'Elastic waves at the surface of separation of two solids'. *Proceedings, Royal Society of London, Series A,* Vol. 106, pp. 416–428.

SOUTH, DW (1986). 'Development in surface treatment systems'. *Proceedings, 38th Annual Conference of the Institute of Works and Highways Management,* pp. 69–78. October 28th–31st 1986, Harrogate.

TILL, R (1974). *'Statistical methods for the earth scientist'.* MacMillan, London.

TIMOSHENKO, SP and GOODIER, JN (1970). *'Theory of elasticity',* Third Edition. J Wiley and Sons, London.

TOLL, DG, HIGHT, DW and SHAW, HF (1987). 'The rôle of soil fabric in determining the engineering behaviour of compacted lateritic and quartzitic gravels'. *Zeitschrift für Geomorphologie,* Suppl-Bd, Berlin-Stuttgart, June, pp. 133–144.

WHITE, JE (1965). *'Seismic waves: Radiation, transmission and attenuation'.* International Series in the Earth Sciences, McGraw-Hill, New York.

WINTER, MG and SELBY, AR (1988). 'The measurement of reinstatement backfill quality by a non-intrusive method'. *Preprints, 24th Annual Conference of the Engineering Group of the Geological Society, 'Field Testing in Engineering Geology',* Edited by FG Bell, MG Culshaw and JC Cripps, pp. 411–437. September 4th–8th 1988, Sunderland Polytechnic.

WINTER, MG and SELBY, AR (1989). 'The measurement of reinstatement backfill quality by means of the Clegg Meter'. *Proceedings, Foundations and Tunnels-89: The 2nd International Conference,* pp. 367–372. September 19th–21st 1989, University of London.

WINTER, MG and SELBY, AR (In Preparation). 'A technique for the analysis of Rayleigh-type surface wave attenuation data with potential applications'.

WOODS, RD (1968). 'Screening of surface waves in soils'. *Journal, Soil Mechanics and Foundations Division,* ASCE, Vol. 94, SM4, pp. 951–979.

WOODS, RD and RICHART, FE, (1967). 'Screening of elastic surface waves by trenches'. *Proceedings, International Symposium on Wave Propagation and Dynamic Properties of Earth Materials,* pp. 275–284. University of New Mexico Press.

YODER, EJ, SHURIG, DG and COLUCCI-RIOS, B (1982). 'Evaluation of existing aggregate roads to determine suitability for resurfacing'. *Transportation Research Record 875,* pp. 1–7. Transportation Research Board, National Academy of Science, Washington DC.

APPENDIX 1

INTEGRATION TO FIND THE EFFECTIVE DEPTH OF PROPAGATION FOR RAYLEIGH-TYPE SURFACE WAVES

A1.1 Introduction

The measurement of the transmission velocity of sinusoidally excited Rayleigh-type surface waves was identified as a potential means of assessing the quality of the unbound layers of utility reinstatement works in Chapter 3 (Section 3.3). Ideally, properties should be determined as a function of depth. A classical empirical form exists; effective depth of propagation is equal to one-half the wavelength:

$$z = \lambda/2 \qquad \text{(3.6bis)}.$$

This approximation has been used by a number of previous workers (Huekelom and Foster, 1960; Maxwell and Fry, 1967; Abbiss, 1983) and was based upon the matching of experimental wave velocity-depth data to core logs by means of a general form of Equation 3.6, $z = k\lambda$, where k is a constant.

Displacements due to the horizontal and vertical component of Rayleigh-type surface waves are presented, in normalised form, in Figure 3.5 based on the equations for the horizontal vertical displacement factors U (horizontal) and W (vertical):

$$\mathrm{U} = -e^{-\mathrm{a}(pz)} + \mathrm{b}\, e^{-\mathrm{c}(pz)} \qquad \text{(3.31bis)}$$

and

$$\mathrm{W} = -e^{-\mathrm{a}(pz)} + \mathrm{d}\, e^{-\mathrm{c}(pz)} \qquad \text{(3.32bis)}$$

where a, b, c and d are constants dependent upon the Poisson's ratio. Putting $p = 2\pi/\lambda$ Equation 3.32 becomes:

$$\mathrm{W} = -e^{-2\pi\,\mathrm{a}(z/\lambda)} + \mathrm{d}\, e^{-2\pi\,\mathrm{c}(z/\lambda)} \qquad \text{(A1.1)}.$$

The experimental technique used to obtain Rayleigh-type surface wave velocities involves the measurement of the vertical component induced in the ground by vertical oscillations. Integration of Equation 3.32 to find the position of the centroid of the area under this curve in the z/λ direction (over the range $0 \leq z/\lambda \leq \infty$), should yield an estimate for the effective depth of propagation z in terms of the wavelength λ.

A1.2 Centroid of the area under the W function

The centroid of an area under a curve ($\overline{x}$) defined by an equation $f(x)$ is:

$$\overline{x} = \frac{\int x f(x) dx}{\int f(x) dx} \qquad \text{(A1.2).}$$

Using basic relations[1], the solution for the centroid of the area under Equation 3.32 becomes a simple matter:

$$\overline{z/\lambda} = \frac{\int_0^\infty \left(-(z/\lambda)e^{-2\pi\, a(z/\lambda)} + d(z/\lambda)e^{-2\pi\, c(z/\lambda)}\right) d(z/\lambda)}{\int_0^\infty \left(-e^{-2\pi\, a(z/\lambda)} + d\, e^{-2\pi\, c(z/\lambda)}\right) d(z/\lambda)} \qquad \text{(A1.3).}$$

For convenience and clarity it is sensible to put $x = z/\lambda$ so Equation A1.3 becomes:

$$\begin{aligned} \overline{x} &= \frac{\int_0^\infty \left(-xe^{-2\pi\, a\, x} + d\, xe^{-2\pi\, c\, x}\right) dx}{\int_0^\infty \left(-e^{-2\pi\, a\, x} + d\, e^{-2\pi\, c\, x}\right) dx} \\ &= \frac{I_1}{I_2} \end{aligned} \qquad \text{(A1.4).}$$

Integrating,

$$I_1 = \left[\frac{1}{2\pi\, a} e^{-2\pi\, a\, x}\left(x + \frac{1}{2\pi\, a}\right) - \frac{d}{2\pi\, c} e^{-2\pi\, c\, x}\left(x + \frac{1}{2\pi\, c\, x}\right)\right]_0^\infty$$

and applying the limits gives

$$\begin{aligned} I_1 &= -\frac{1}{4\pi^2\, a^2} + \frac{d}{4\pi^2\, c^2} \\ I_1 &= \frac{1}{4\pi^2}\left(\frac{d}{c^2} - \frac{1}{a^2}\right) \end{aligned} \qquad \text{(A1.5).}$$

Similarly, integrating I_2 gives

$$I_2 = \left[\frac{1}{2\pi\, a} e^{-2\pi\, a\, x} - \frac{d}{2\pi\, c} e^{-2\pi\, c\, x}\right]_0^\infty$$

and applying the limits gives

---

[1]

$$\int u\frac{dv}{dx}dx = uv - \int v\frac{du}{dx}dx \quad \text{and} \quad \int e^{kv}dv = \frac{1}{k}e^{kv}$$

gives

$$\int xe^{-kx}dx = \left[x\left(-\frac{1}{k}\right)e^{-kx} - \left(-\frac{1}{k}\right)\int 1 \times e^{-kx}dx\right]$$

$$= \left[-\frac{x}{k}e^{-kx} - \frac{1}{k^2}e^{-kx}\right]$$

and similarly

$$-\int xe^{-kx}dx = \left[\frac{x}{k}e^{-kx} + \frac{1}{k^2}e^{-kx}\right]$$

$$I_2 = -\frac{1}{2\pi\, a} + \frac{d}{2\pi\, c}$$

$$I_2 = \frac{1}{2\pi}\left(\frac{d}{2\pi\, c} - \frac{1}{2\pi\, a}\right) \qquad \text{(A1.6)}.$$

Now, because $\overline{x} = I_1 / I_2 = \overline{z/\lambda}$

$$\overline{z/\lambda} = \frac{1}{2\pi}\frac{(d/c^2 - 1/a^2)}{(d/c - 1/a)} \qquad \text{(A1.7)}.$$

Plainly, Equation A1.7 is dependent only upon the value of Poisson's Ratio. Thus, applying the Poisson's ratio-dependent values of a, c and d given in Table 3.4, the centroid $\overline{z/\lambda}$ can be calculated such that for the normal range $0 < \nu \leq 0.5$ the centroid is $0.406 < \overline{z/\lambda} \leq 0.609$ (or $0.406\lambda < \overline{z} \leq 0.609\lambda$). Detailed values are given in Table A1.1 and the relationship between Poisson's ratio and the centroid $(\overline{z/\lambda})$ is illustrated in Figure A1.1.

Table A1.1 - Values of the centroid, $\overline{z/\lambda}$, corresponding to values of Poisson's ratio.

Poisson's ratio ν	Centroid $\overline{z/\lambda}$
0	0.406
0.1	0.433
0.2	0.468
0.3	0.506
0.4	0.555
0.5	0.609

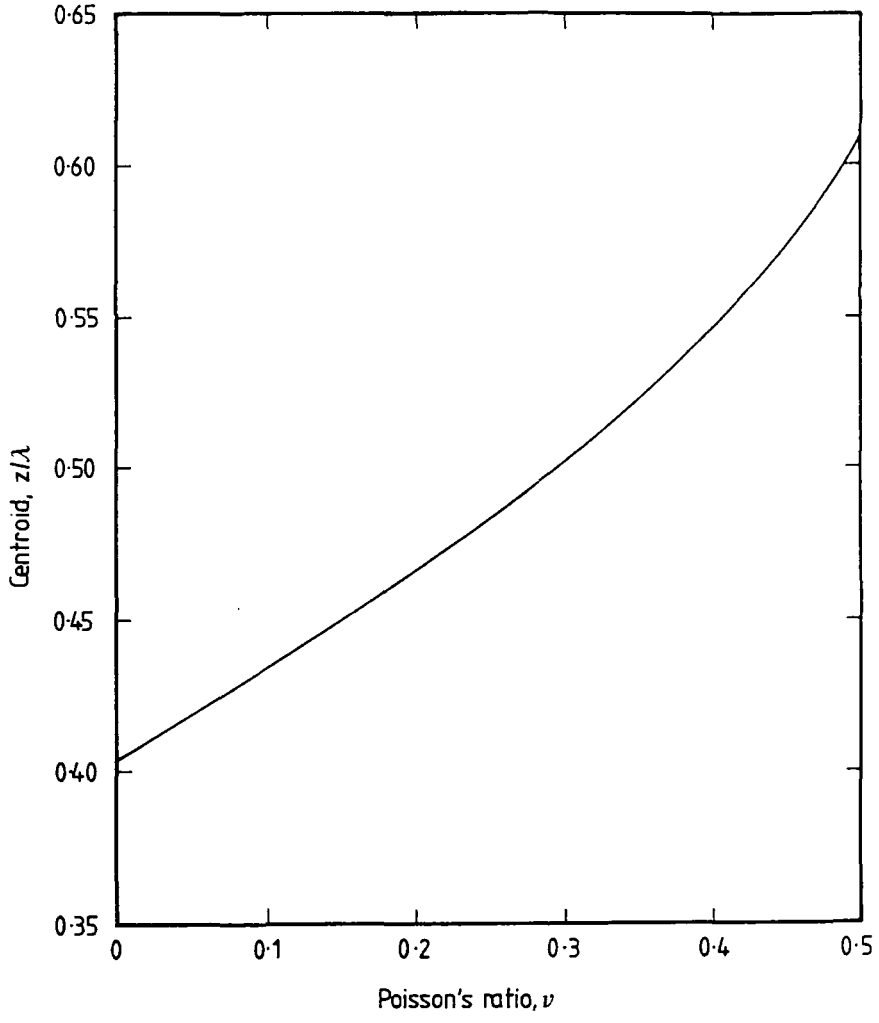

Figure A1.1 - Centroid of the area under the W function, $\overline{z/\lambda}$, plotted as a function of Poisson's ratio.

APPENDIX 2

SOIL CLASSIFICATION AND COMPACTION TESTS: DETAILED DATA

A2.1 Particle size distribution

Table A2.1 - Particle size distributions for Permian Sand, Sharp Sand and Wet-mix macadam.

BS sieve size	PERCENTAGE BY MASS PASSING BS SIEVE			
	Permian Sand	Sharp Sand	Wet-mix macadam	
			Before Scalping	After Scalping
38.10 mm	—	—	100.0	—
19.05	—	—	65.1	100.0
12.70	—	—	51.0	78.3
9.53	—	—	42.0	64.5
6.35	—	—	37.8	58.1
5.00	100	100	—	—
4.76	—	—	35.2	54.1
4.00	—	95.6	33.8	51.9
3.35	—	—	31.4	48.2
2.80	99.8	83.0	28.7	44.1
2.40	—	—	26.6	40.9
1.40	99.0	63.0	20.0	30.7
850 μm	—	—	16.0	24.6
710	—	47.6	14.7	22.6
600	81.0	—	—	—
500	—	—	12.9	19.8
425	65.6	35.6	—	—
420	—	—	12.0	18.4
300	53.8	24.8	10.8	16.6
212	—	—	9.8	15.1
150	—	—	8.9	13.7
125	29.2	5.2	—	—
90	—	—	8.4	12.9
75	12.2	2.4	7.6	11.7

A2.2 Dry density moisture content relationships

Table A2.2 - Dry density-moisture content data for Permian Sand; BS 1377 (1975): Test 12.

Number of blows per layer	Moisture content w (%)	Bulk density ρ (Mg/m^3)	Dry density ρ_d (Mg/m^3)	Degree of Compaction D_c
27	4.75	1.866	1.781	0.980
	7.05	1.920	1.792	0.986
	8.23	1.950	1.802	0.991
	9.96	1.990	1.810	0.996
	11.22	2.021	1.817	1.000
	11.79	2.015	1.803	0.992
	11.81	2.020	1.806	0.994
	12.79	2.000	1.773	0.976
	12.86	1.996	1.768	0.973
54	5.82	1.906	1.801	0.969
	9.23	2.008	1.839	0.989
	9.75	2.026	1.846	0.993
	10.65	2.057	1.859	1.000
	10.74	2.056	1.857	0.999
	11.20	2.051	1.845	0.992
	11.42	2.037	1.828	0.983
	12.41	2.031	1.807	0.972
81	8.10	1.987	1.838	0.978
	9.02	2.023	1.856	0.988
	9.10	2.021	1.852	0.986
	9.25	2.023	1.866	0.993
	10.03	2.074	1.879	1.000
	10.22	2.065	1.873	0.997
	10.80	2.071	1.869	0.995
	11.42	2.057	1.846	0.982
	11.91	2.051	1.833	0.976
	11.95	2.047	1.828	0.973

Table A2.2 (Continued) - Dry density-moisture content data for Permian Sand; BS 1377 (1975): Test 12.

Number of blows per layer	Moisture content w (%)	Bulk density ρ (Mg/m^3)	Dry density ρ_d (Mg/m^3)	Degree of Compaction D_c
108	4.28	1.967	1.886	0.975
	5.47	1.992	1.889	0.976
	6.33	2.010	1.890	0.977
	6.55	2.026	1.901	0.982
	7.21	2.042	1.905	0.984
	8.37	2.085	1.924	0.994
	9.44	2.118	1.935	1.000
	10.20	2.111	1.916	0.990
	10.82	2.093	1.889	0.976
	11.87	2.082	1.861	0.962
135	4.33	2.005	1.922	0.987
	5.77	2.039	1.928	0.990
	6.46	2.057	1.932	0.992
	7.58	2.089	1.942	0.997
	9.03	2.124	1.948	1.000
	9.76	2.134	1.944	0.999
	10.42	2.130	1.929	0.990
	11.24	2.125	1.910	0.980
	11.52	2.101	1.884	0.967

Table A2.3 - Dry density-moisture content data for Sharp Sand; BS 1377 (1975): Test 12.

Number of blows per layer	Moisture content w (%)	Bulk density ρ (Mg/m^3)	Dry density ρ_d (Mg/m^3)	Degree of Compaction D_c
27	8.43	1.817	1.676	0.960
	9.34	1.845	1.687	0.967
	10.32	1.866	1.691	0.969
	11.12	1.886	1.697	0.972
	11.22	1.890	1.699	0.974
	11.69	1.917	1.716	0.983
	11.95	1.937	1.730	0.991
	12.41	1.950	1.735	0.994
	13.17	1.973	1.743	0.999
	14.27	1.993	1.744	0.999
	15.21	2.002	1.738	0.996
54	9.12	1.886	1.728	0.968
	9.46	1.895	1.731	0.969
	9.52	1.899	1.734	0.971
	9.92	1.925	1.751	0.980
	10.45	1.933	1.750	0.980
	11.06	1.966	1.770	0 991
	11.80	1.986	1.776	0 994
	13.02	2.019	1.786	1.000
	14.50	2.024	1.768	0.990
81	9.03	1.940	1.780	0.977
	9.43	1.958	1.789	0.982
	10.81	2.012	1.816	0.997
	11.05	2.020	1.819	0.998
	12.41	2.042	1.817	0.997
	13.00	2.048	1.812	0 995

Table A2.4 - Dry density-moisture content data for Wet-mix macadam; BS 1377 (1975): Test 12. Data prior to the application of the correction for stone content.

Number of blows per layer	Moisture content w (%)	Bulk density ρ (Mg/m^3)	Dry density ρ_d (Mg/m^3)	Degree of Compaction D_c
27	2.12	2.098	2.054	0.915
	4.03	2.141	2.058	0.917
	6.80	2.308	2.161	0.963
	7.46	2.377	2.212	0.986
	8.99	2.444	2.242	0.999
	9.77	2.404	2.190	0.976
54	3.64	2.239	2.160	0.933
	6.20	2.361	2.224	0.960
	7.49	2.436	2.267	0.979
	7.90	2.461	2.281	0.985
	8.04	2.487	2.302	0.994
	8.23	2.506	2.316	1.000
	10.05	2.472	2.246	0.970
81	3.99	2.292	2.204	0.942
	5.69	2.424	2.293	0.980
	6.40	2.444	2.297	0.982
	7.04	2.477	2.314	0.989
	7.73	2.520	2.339	1.000
	8.34	2.478	2.287	0.978

Table A2.5 - Dry density-moisture content data for Wet-mix macadam; BS 1377 (1975): Test 12. Data after the application of the correction for stone content.

Number of blows per layer	Moisture content w (%)	Bulk density ρ (Mg/m^3)	Dry density ρ_d (Mg/m^3)	Degree of Compaction D_c
27	1.57	—	2.238	0.940
	2.83	—	2.241	0.941
	4.66	—	2.321	0.974
	5.09	—	2.359	0.990
	6.10	—	2.382	1.000
	6.62	—	2.343	0.984
54	2.57	—	2.320	0.952
	4.26	—	2.368	0.972
	5.11	—	2.400	0.985
	5.38	—	2.411	0.990
	5.48	—	2.426	0.996
	5.60	—	2.436	1.000
	6.80	—	2.385	0.979
81	2.80	—	2.353	0.960
	3.93	—	2.420	0.988
	4.39	—	2.423	0.989
	4.82	—	2.435	0.994
	5.27	—	2.453	1.000
	5.67	—	2.415	0.986

Table A2.6 - Dry density-moisture content data for Wet-mix macadam; BS 5835: Part 1 (1980).

Initial moisture content w_i (%)	Residual moisture content w_r (%)	Dry density ρ_d (Mg/m^3)	
		BS 5835†	BS 1377‡
0.15	0.26/0.03*	2.336/0.029	2.318/0.036
1.12	1.20/0.03	2.233/0.029	2.233/0.030
2.12	2.23/0.06	2.198/0.019	2.197/0.018
3.08	3.06/0.10	2.232/0.028	2.231/0.029
4.13	4.14/0.07	2.306/0.025	2.309/0.023
5.00	4.40/0.16	2.373/0.009	2.388/0.009
5.88	5.06/0.13	2.319/0.017	2.352/0.018
6.94	5.84/0.14	2.250/0.016	2.287/0.024
7.78	6.76/0.29	2.175/0.038	2.207/0.038

†These data are analysed using the style of analysis described in BS 5835: Part 1 (1980) and Section 4.4.4 of this thesis.

‡These data are analysed using the style of analysis described in BS 1377 (1975) and Section 4.4.4 of this thesis.

*Data referring to tests carried out on five samples prepared at the same initial moisture content are given as Mean/Sample standard deviation ($\overline{x}/\sigma_{x_{n-1}}$).

APPENDIX 3

MATERIAL SPECIFICATIONS

In this Appendix, material specifications are reproduced from the appropriate document for Concrete Sand (Section A3.1) and Wet-mix macadam (Section A3.2). Table numbers are altered from those used in the original specifications in order that they fit into the general numbering scheme; references are also modified to conform with the style of this thesis. Where appropriate, references to British Standards have been modified to cater for the most recent editions of that standard.

A3.1 Concrete Sand: BS 882 (1983)

The following specification for Concrete Sand (fine aggregate) is reproduced from BS 882 (1983). The grading envelopes given in Table A3.1 for Concrete Sand, Gradings C, M amd F, are compared graphically in Figure A3.1.

5.2 Fine aggregate

5.2.1 *General:* When determined in accordance with BS 812: Part 1 (1975), using test sieves of the sizes given in Table A3.1 complying with BS 410 (1986), full tolerance, the grading of the fine aggregate shall comply with the overall limits given in Table A3.1. Additionally, not more than one in ten consectutive samples shall have a grading outside the limits for any one of the gradings C, M or F, given in Table A3.1.

5.2.2 *Heavy duty concrete floor finishes:* For heavy duty concrete floor finishes, the fine aggregate shall comply with C or M given in Table A3.1.

A3.2 Wet-mix Macadam: Department of Transport (1986)

The following specification for Wet-mix macadam is reproduced from Department of Transport (1986). The grading envelopes given in Table A3.2 for Types 1 and 2 granular sub-base material and Wet-mix macadam are compared graphically in Figure A3.2.

805 Wet-mix Macadam

1 Wet-mix macadam shall be made and constructed in the following manner.

Aggregate

2 The coarse and fine aggregate shall consist of crushed rock or crushed slag and the aggregate shall have the grading shown in Table A3.2.

3 The material shall have a 10% fines value of 50 kN or more when tested in compliance with BS 812: Part 3 (1975) except that the samples shall be tested in a saturated and surface dried condition. Prior to testing the selected test portions shall be soaked in water at room temperature for 24 hours without having previously having been oven dried.

4 The flakiness index shall be less than 35 when determined in accordance with BS 812: Section 105.1 (1985).

Mixing

5 The material shall be mixed in a mixer complying with BS 1305 (1974) or approved by the Engineer.

Laying and Compacting

6 The wet-mix macadam shall be laid and compacted at the optimum moisture content ±0.5% as determined in compliance with BS 5835: Part 1 (1980).

7 The compacted thickness of each layer shall not be more than 200 mm. Any areas of compacted material having a loose surface deficient in fines shall be removed and replaced with properly graded material.

Table A3.1 - Concrete Sand range of grading (from BS 882, 1983: Table 5).

Sieve size	PERCENTAGE BY MASS PASSING BS TEST SIEVE			
	Overall limits	ADDITIONAL LIMITS FOR GRADING		
		C	M	F
10.00 mm	100	—	—	—
5.00	89–100	—	—	—
2.36	60–100	60–100	65–100	80–100
1.18	30–100	30–90	45–100	70–100
600 μm	15–100	15–54	25–80	55–100
300	5–70	5–40	5–48	5–70
150	0–15*	—	—	—

*Increased to 20% for crushed rock fines, except when they are used for heavy duty floors.

NOTE. Fine aggregate not complying with Table 5 may also be used provided that the supplier can satisfy the purchaser that such materials can produce concrete of the required quality.

Table A3.2 - Wet-mix macadam range of grading. Also shown are the gradings for Types 1 and 2 granular sub-base materials (from Department of Transport, 1986: Tables 8/2, 8/3 and 8/4).

BS sieve size	PERCENTAGE BY MASS PASSING BS TEST SIEVE		
	Type 1 (Clause 803)	Type 2 (Clause 804)	Wet-mix macadam (Clause 805)
75 mm	100	100	—
50	—	—	100
37.5	85–100	85–100	95–100
20	—	—	60–80
10	40–70	45–100	40–60
5	25–45	25–85	25–40
2.36	—	—	15–30
600 μm	8–22	8–45	8–22
75	0–10	0–10	0–8

The particle size shall be determined by the washing and sieving method of BS 812: Part 103 (1983).

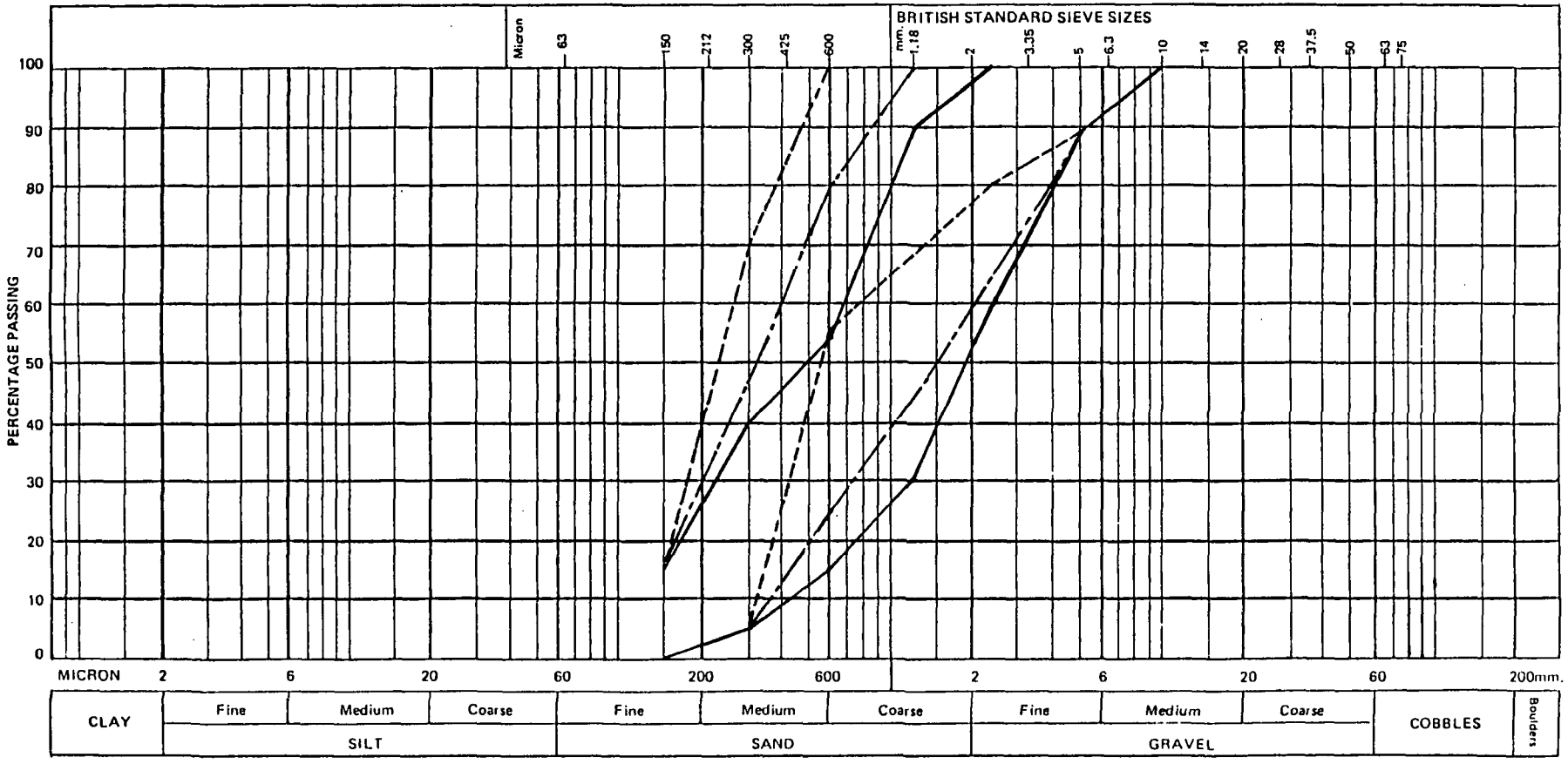

Figure A3.1 - BS 882 (1983) grading envelopes for Concrete Sand Gradings C, M and F.

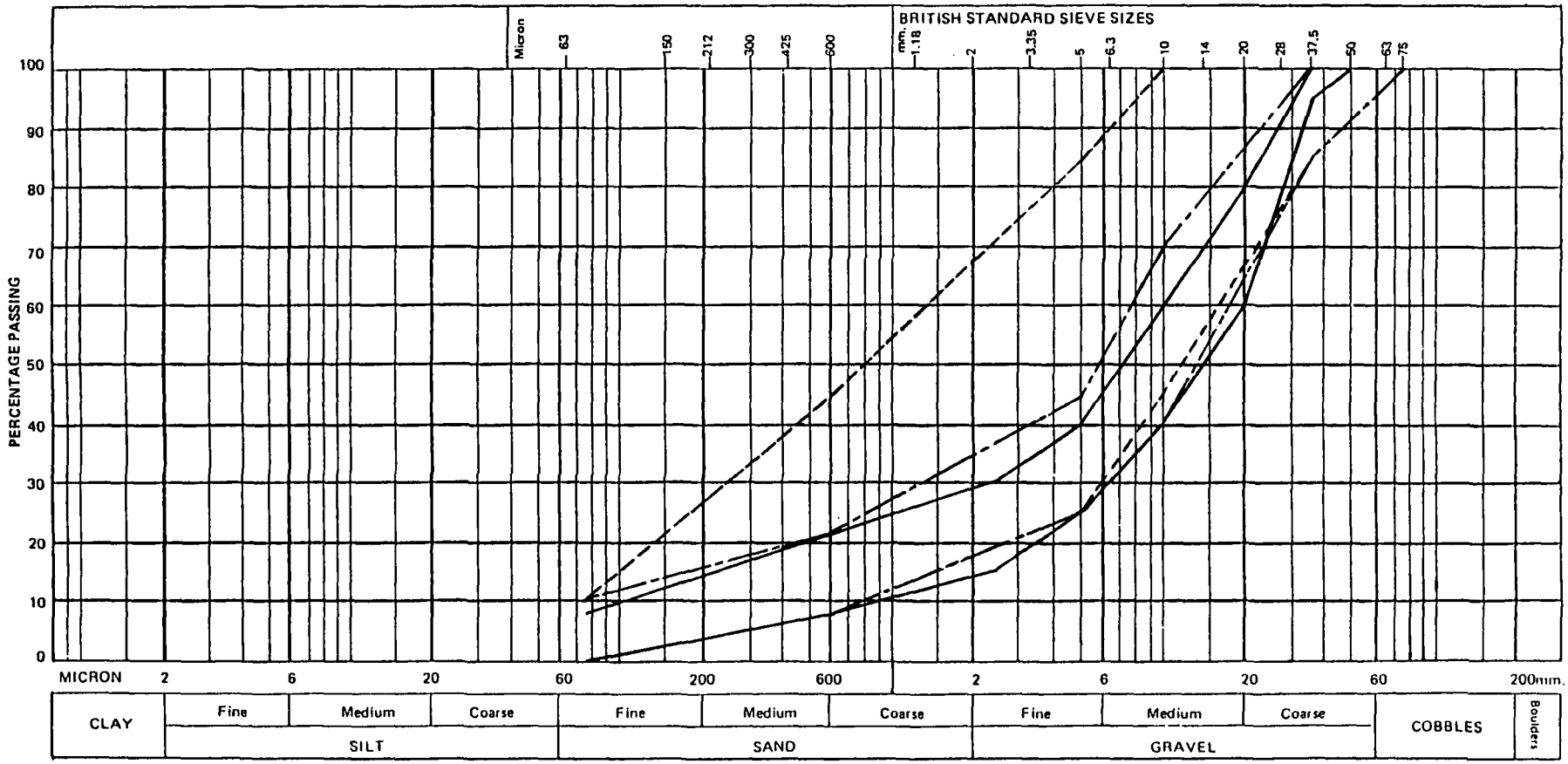

Figure A3.2 - Department of Transport (1986) grading envelopes for Type 2 (Clause 803), Type 1 (Clause 804) and Wet-mix macadam (Clause 805).

APPENDIX 4

MOISTURE CONTENT DETERMINATION AND CONTROL

A4.1 Moisture content determination by the microwave method

A4.1.1 General

With the exception of moisture content determinations made on samples obtained using metal density rings, a microwave oven has been used throughout the testing to determine the moisture content of reinstatement materials. This test is currently subject to no known standard although a number of authors, including Bentley and Carter (1987), have written on the subject of microwave drying of soils. The detailed method presented here follows the essential principles outlined in the Bentley and Carter paper.

A4.1.2 Apparatus

i)Microwave oven.

ii)Desiccator.

iii)Ceramic dishes.

iv)Balance of 500 g capacity accurate to 0.1 g.

A4.1.3 Procedure

i)Clean and dry container in oven, cool in desiccator and weigh (m_1).

ii)Place soil in container (at least 100 g) replace lid and weigh (m_2).

iii)Place container in microwave oven at high power setting.

iv)After 5 minutes remove the sample and weigh (m_n).

v)Repeat (iv) at one minute intervals until there is no reduction in the value of m_n for three consecutive weighings.

vi)Remove container from microwave oven and place in desiccator to cool.

vii)Remove from desiccator and weigh (m_3).

A4.1.4 Results

The moisture content, w is calculated from

$$w = \frac{m_2 - m_3}{m_3 - m_1} \times 100\% \tag{A4.1}$$

The values should shall be reported to the nearest whole number, except that values up to 10% shall be reported to two significant figures.

Note: Do not under any circumstances attempt to dry organic soils in the microwave oven.

Note: Do not place any metal objects, or objects with even small metal contents, in the microwave oven.

A4.2 Moisture content control

In this section an equation is developed to enable the simple calculation of the mass of water to be added (m_{H_2O}) to a known mass of soil (m_{wet_i}) at a known moisture content (w_i) in order to achieve a required moisture content (w_{req})[1], where $w_{req} > w_i$.

Initially the moisture content w_i is given by

$$w_i = \frac{m_{wet_i} - m_{dry}}{m_{dry}} \tag{A4.2}$$

where:

m_{wet_i} is the initial mass of the soil and

m_{dry} is the dry mass of the soil.

Re-arranging we have

$$m_{dry} = \frac{m_{wet_i}}{w_i + 1} \tag{A4.3}$$

For the soil at its required moisture content w_{req} we have

$$m_{wet_r} = m_{dry}\,(w_{req} + 1) \tag{A4.4}$$

substituting A4.3 into A4.4 we have

$$m_{wet_r} = \frac{m_{wet_i}}{(w_i + 1)}\,(w_{req} + 1) \tag{A4.5}$$

[1]In this section the moisture content w is treated as a ratio and not as a percentage as is more usual.

The mass of water to be added is $m_{H_2O} = m_{wet_r} - m_{wet_i}$, so

$$m_{H_2O} = \frac{m_{wet_i}}{(w_i + 1)} (w_{req} + 1) - m_{wet_i} \qquad \text{(A4.6)}$$

and re-arranging we have

$$m_{H_2O} = m_{wet_i} \left[\frac{(w_{req} + +1)}{(w_i + 1)} - 1 \right] \qquad \text{(5.2bis).}$$

APPENDIX 5

THE ELECTRICALLY POWERED WACKER BS45Y VIBRATORY RAMMER

The compaction plant used during the bulk of the testing carried out in the laboratory based trench is non-standard and as such bears detailed description. The standard Wacker BS45Y is fitted with a 2.2 kW two-stroke petrol engine which gives a claimed compaction rate of 150 m^2/h. Early testing (Test TPS1—layers I to IV) using such a standard machine, fitted with a proprietory 'leak-proof' exhaust hose, led to extreme operator discomfort due to excessive exhaust fume leakage, mainly at the junction between the hose and the exhaust pipe. Although Wacker do supply a version of the larger BS65Y vibratory rammer fitted with a three-phase (380 V) electric motor to special order, this device was felt to be too powerful for the laboratory work. Also the laboratory in which the trench was located was supplied with single-phase electrics only. A modified version of the BS45Y fitted with a 2.3 kW single-phase (11 A; 240 V) electric motor has been supplied by Wacker for use in this work.

Wacker describe the suitable applications of the standard petrol driven BS45Y as *'the compaction of granular, mixed and cohesive soils in confined areas'.*

The annotated photograph (Plate A5.1) shows the essential features of the modified BS45Y. Wacker claim that the detailed specifications of the modified BS45Y match those of the standard petrol driven model (Table A5.1). A 400 mm long extension leg is also used to extend the reach of the device to facilitate compaction of the lower layers in the laboratory based trench adding 5 kg to the normal weight of 50 kg. Thus the method specification for the compaction of granular materials (Department of Transport, 1986: Clause 612, sub-Clauses 4–10, Table 6/4) is unchanged by the use of an extension leg.

Table A5.1 - Specifications for the Wacker BS45Y electrically powered vibratory rammer (source: Wacker Great Britain Ltd).

Property	Units	BS45Y
Length × width × height	mm	665 × 360 × 960
Width × length of ramming shoe	mm	250 × 330
Weight	kg	50
Compaction depth	cm	up to 50
Stroke length	mm	up to 65
Percussion performance	W	615
Single stroke impact	J	48
Percussion rate	1/min	650–770
Travel speed	m/min	up to 15
Compaction rate	m^2/h	up to 232

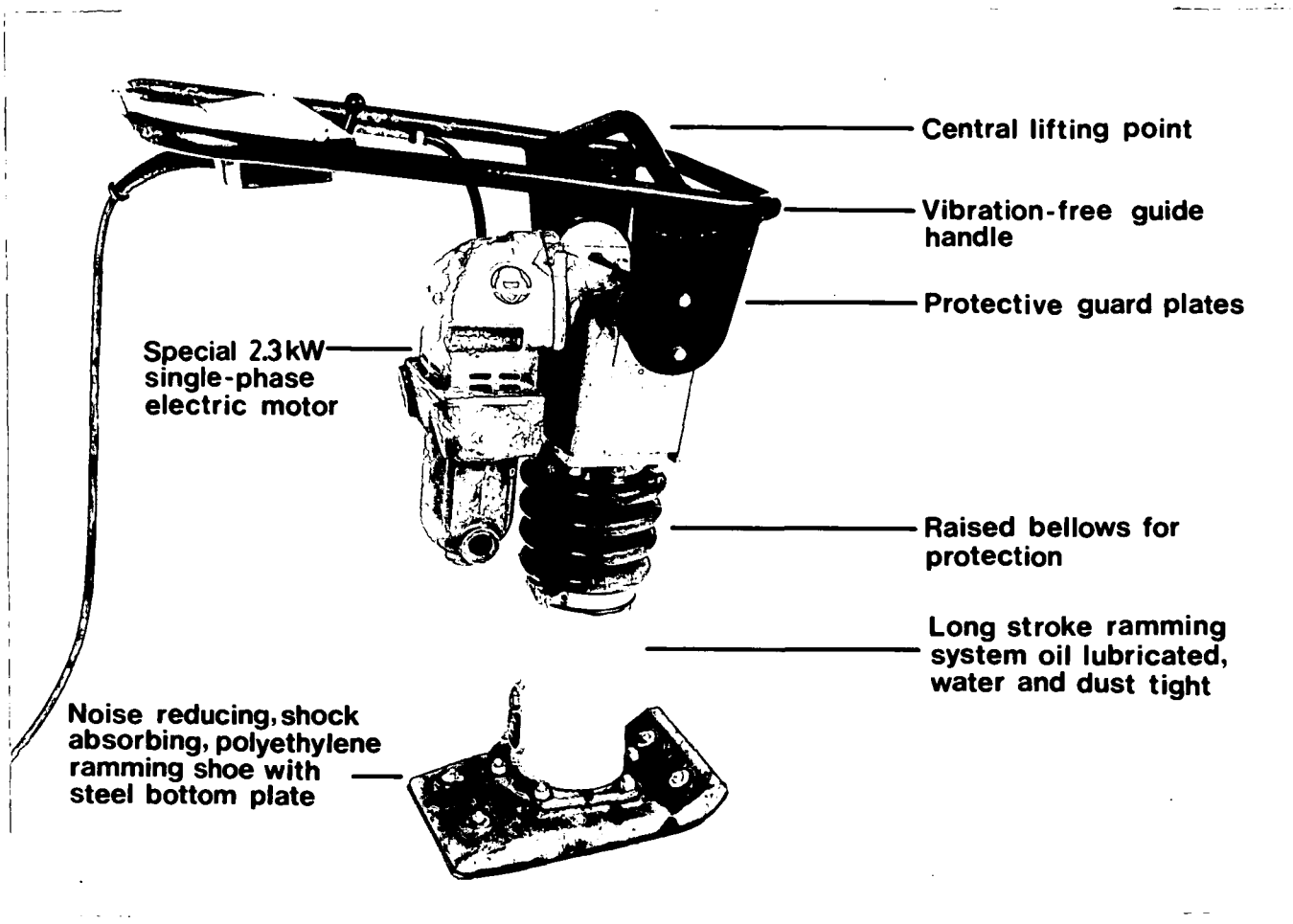

Plate A5.1 - The specially modified Wacker BS45Y electrically powered vibratory rammer.

APPENDIX 6

DENSITY, MOISTURE CONTENT AND IMPACT VALUE MEASUREMENTS: DETAILED DATA

A6.1 Permian Sand: Tests TPS1 to TPS5

Table A6.1 - Compaction data for Test TPS1 (6–30/3/87).

Layer No (Material)	h (m)	Surcharge (%)	z (m)	w (%)	$\overline{IV}/\sigma_{IV_{n-1}}$	Compaction plant
VIII(PS)	0.085	39.3	0	8.25	7.6/0.22	BS45Y(electric)
VII(PS)	0.100	23.1	0.085	9.38	7.0/0.50	BS45Y(electric)
VI(PS)	0.120	33.3	0.185	12.86	6.3/0.27	BS45Y(electric)
V(PS)	0.110	35.3	0.305	11.82	7.8/0.45	BS45Y(electric)
IV(PS)	0.100	16.7	0.415	9.10	7.7/0.45	BS45Y(petrol)+leg
III(PS)	0.115	17.9	0.515	9.09	6.9/0.22	BS45Y(petrol)+leg
II(PS)	0.105	25.0	0.630	11.68	6.0/0.50	BS45Y(petrol)+leg
I(PS)	0.160	17.9	0.735	8.26	5.7/0.98	BS45Y(petrol)+leg
Mean/SD	0.112/0.022	26.06/8.81	—	10.06/1.79	6.88/0.81	—
Total depth	—	—	0.895	—	—	—

Table A6.2 - Excavation data for Test TPS1 (9–20/6/87).

z (m)	Density data			$\overline{IV}/\sigma_{IV_{n-1}}$
	w (%)	ρ (Mg/m^3)	ρ_d (Mg/m^3)	
0	2.77	1.821	1.791	—/—
0.085	4.78	1.857	1.773	—/—
0.185	5.98	1.964	1.854	—/—
0.305	7.53	1.993	1.854	—/—
0.335	—	—	—	15.3/1.72
0.415	6.96	1.852	1.732	—/
0.455	—	—	—	13.4/1.19
0.515	6.02	1.856	1.751	—/—
0.540	—	—	—	14.5/0.87
0.630	8.35	1.928	1.779	—/—
0.680	—	—	—	11.2/0.98
0.735	7.25	1.870	1.744	—/—
Mean/SD	6.20/1.77	1.893/0.061	1.785/0.047	13.60/1.78

Table A6.3 - Compaction data for Test TPS2 (2-23/7/87).

Layer No (Material)	h (m)	Surcharge (%)	z (m)	w (%)	$\overline{IV}/\sigma_{IV_{n-1}}$	Compaction plant
VIII(PS)	0.060	40.0	0	7.68	5.8/0.22	BS45Y(electric)
VII(PS)	0.120	20.0	0.060	10.03	5.5/0.50	BS45Y(electric)
VI(PS)	0.100	33.0	0.180	11.96	5.1/0.27	BS45Y(electric)
V(PS)	0.120	25.0	0.280	12.91	6.8/0.45	BS45Y(electric)
IV(PS)	0.075	40.0	0.400	10.58	6.9/0.45	BS45Y(electric)+leg
III(PS)	0.135	36.0	0.475	11.65	6.0/0.22	BS45Y(electric)+leg
II(PS)	0.120	37.0	0.610	12.19	4.5/0.50	BS45Y(electric)+leg
I(PS)	0.120	40.0	0.730	9.33	3.6/0.98	BS45Y(electric)+leg
Mean/SD	0.106/0.026	33.88/7.55	—	10.79/1.73	6.52/1.12	—
Total depth	—	—	0.850	—	—	—

Table A6.4 - Excavation data for Test TPS2 (26/8-3/9/87).

z (m)	Density data			$\overline{IV}/\sigma_{IV_{n-1}}$
	w (%)	ρ (Mg/m^3)	ρ_d (Mg/m^3)	
0	5.86	1.911	1.805	8.5/0.41
0.060	9.86	2.096	1.908	—/—
0.120	—	—	—	12.6/1.60
0.180	12.32	2.102	1.871	—/—
0.280	10.88	2.142	1.932	—/—
0.340	—	—	—	15.8/0.65
0.400	9.58	2.099	1.916	14.1/1.14
0.475	11.24	2.112	1.899	—/—
0.500	—	—	—	10.9/1.64
0.610	10.44	2.116	1.936	—/—
0.650	—	—	—	9.8/0.76
0.730	11.74	2.118	1.864	—/—
0.750	—	—	—	8.2/1.64
Mean/SD	10.24/1.99	2.087/0.073	1.891/0.043	11.41/2.87

Table A6.5 - Compaction data for Test TPS3 (22/9-5/10/87).

Layer No (Material)	h (m)	Surcharge (%)	z (m)	w (%)	$\overline{IV}/\sigma_{IV_{n-1}}$	Compaction plant
VIII(PS)	0.070	30.0	0	9.96	4.3/0.27	BS45Y(electric)
VII(PS)	0.100	33.3	0.070	12.79	3.4/0.22	BS45Y(electric)
VI(PS)	0.100	33.3	0.170	13.12	3.5/0.79	BS45Y(electric)
V(PS)	0.100	33.3	0.270	13.95	3.4/0.42	BS45Y(electric)
IV(PS)	0.100	33.3	0.370	10.44	3.5/0.50	BS45Y(electric)+leg
III(PS)	0.140	22.2	0.470	12.21	3.2/0.57	BS45Y(electric)+leg
II(PS)	0.110	26.7	0.610	12.65	3.1/0.55	BS45Y(electric)+leg
I(PS)	0.150	25.0	0.720	12.48	2.7/1.26	BS45Y(electric)+leg
Mean/SD	0.109/0.025	26.64/4.46	—	12.20/1.34	3.39/0.46	—
Total depth	—	—	0.870	—	—	—

Table A6.6 - Excavation data for Test TPS3 (6–12/11/87).

z (m)	Density data			$\overline{IV}/\sigma_{IV_{n-1}}$
	w (%)	ρ (Mg/m^3)	ρ_d (Mg/m^3)	
0	4.49	1.798	1.721	8.3/0.58
0.070	7.79	1.943	1.802	—/—
0.120	—	—	—	7.8/0.29
0.170	10.03	1.979	1.798	—/—
0.220	—	—	—	9.8/0.96
0.270	10.36	1.950	1.767	—/—
0.320	—	—	—	8.1/0.63
0.370	10.81	2.030	1.831	—/—
0.470	10.42	1.991	1.803	9.1/0.75
0.590	—	—	—	8.9/0.63
0.610	9.90	—	—	—/—
0.720	11.06	2.032	1.829	—/—
0.740	—	—	—	7.4/0.65
Mean/SD	9.36/2.21	1.960/0.080	1.793/0.038	8.49/0.83

Table A6.7 - Compaction data for Test TPS4 (17–18/11/87).

Layer No (Material)	h (m)	Surcharge (%)	z (m)	w (%)	$\overline{IV}/\sigma_{IV_{n-1}}$	Compaction plant
III(PS)	0.260	35.0	0	9.70	2.9/0.65	BS45Y(electric)
II(PS)	0.260	35.0	0.260	11.12	3.8/0.76	BS45Y(electric)
I(PS)	0.300	25.0	0.520	13.91	2.3/0.45	BS45Y(electric)+leg
Mean/SD	0.273/0.023	31.67/5.77	—	11.58/2.14	3.00/0.76	—
Total depth	—	—	0.820	—	—	—

Table A6.8 - Excavation data for Test TPS4 (10-11/12/87).

z (m)	Density data			$\overline{IV}/\sigma_{IV_{n-1}}$
	w (%)	ρ (Mg/m^3)	ρ_d (Mg/m^3)	
0	5.04	1.911	1.819	7.2/0.65
0.170	6.33	—	—	5.4/0.22
0.260	11.95	2.125	1.898	—/—
0.300	—	—	—	7.4/0.42
0.460	7.34	—	—	6.7/0.57
0.520	13.30	2.114	1.866	—/—
0.540	—	—	—	7.6/0.55
0.670	7.63	—	—	5.0/0.00
Mean/SD	8.60/3.28	2.050/0.098	1.861/0.040	6.55/1.10

Table A6.9 - Compaction data for Test TPS5 (4-16/1/88).

Layer No (Material)	h (m)	Surcharge (%)	z (m)	w (%)	$\overline{IV}/\sigma_{IV_{n-1}}$	Compaction plant
VII(PS)	0.140	41.7	0.	9.81	5.9/0.89	BS45Y(electric)
VI(PS)	0.100	37.5	0.140	10.95	6.1/0.42	BS45Y(electric)
V(PS)	0.090	40.0	0.240	13.98	5.7/0.57	BS45Y(electric)
IV(PS)	0.100	33.3	0.330	10.00	6.5/0.50	BS45Y(electric)+leg
III(PS)	0.110	26.7	0.430	11.25	4.9/0.65	BS45Y(electric)+leg
II(PS)	0.110	26.7	0.540	12.11	4.7/1.20	BS45Y(electric)+leg
I(PS)	0.150	25.0	0.650	10.80	3.6/0.65	BS45Y(electric)+leg
Mean/SD	0.114/0.022	32.99/6.39	—	11.27/1.42	5.34/1.00	—
Total depth	—	—	0.800	—	—	—

Table A6.10 - Excavation data for Test TPS5 (25–27/1/88).

z (m)	Density data			$\overline{IV}/\sigma_{IV_{n-1}}$
	w (%)	ρ (Mg/m^3)	ρ_d (Mg/m^3)	
0	5.62	1.854	1.756	8.8/1.44
0.140	11.66	2.123	1.902	12.1/0.22
0.240	11.48	2.072	1.859	—/—
0.280	—	—	—	12.2/0.76
0.330	8.44	1.894	1.746	—/—
0.400	—	—	—	12.9/0.82
0.430	10.29	1.990	1.816	—/—
0.520	—	—	—	11.8/0.57
0.540	10.25	1.972	1.778	—/—
0.620	—	—	—	10.7/0.84
0.650	11.38	2.055	1.845	—/—
0.680	—	—	—	7.4/1.60
Mean/SD	9.27/2.18	1.994/0.120	1.815/0.058	10.84/2.03

A6.2 Sharp Sand: Tests TSS1 to TSS5

Table A6.11 - Compaction data for Test TSS1 (8-17/2/88).

Layer No (Material)	h (m)	Surcharge (%)	z (m)	w (%)	$\overline{IV}/\sigma_{IV_{n-1}}$	Compaction plant
VIII(SS)	0.100	33.3	0	9.56	5.8/0.27	BS45Y(electric)
VII(SS)	0.100	33.3	0.100	8.70	5.8/0.91	BS45Y(electric)
VI(SS)	0.090	35.7	0.200	9.50	5.6/0.74	BS45Y(electric)
V(SS)	0.100	33.3	0.290	7.88	4.5/0.50	BS45Y(electric)
IV(SS)	0.100	33.3	0.390	8.38	5.0/0.35	BS45Y(electric)+leg
III(SS)	0.110	26.7	0.490	9.04	5.0/0.35	BS45Y(electric)+leg
II(SS)	0.110	26.7	0.600	9.68	5.2/0.76	BS45Y(electric)+leg
I(SS)	0.150	25.0	0.710	9.08	4.7/0.84	BS45Y(electric)+leg
Mean/SD	0.108/0.018	30.91/4.07	—	8.98/0.63	5.20/0.49	—
Total depth	—	—	0.860	—	—	—

Table A6.12 - Excavation data for Test TSS1 (22/2/88).

z (m)	Density data			$\overline{IV}/\sigma_{IV_{n-1}}$
	w (%)	ρ (Mg/m^3)	ρ_d (Mg/m^3)	
0	8.17	1.680	1.554	6.6/1.12
0.100	10.42	1.752	1.587	—/—
0.160	—	—	—	10.6/0.96
0.200	9.32	1.797	1.643	—/—
0.290	11.20	1.795	1.591	—/—
0.310	—	—	—	9.7/0.57
0.390	11.08	1.798	1.619	—/—
0.460	—	—	—	8.3/0.45
0.490	11.05	1.784	1.606	—/—
0.580	—	—	—	8.7/0.98
0.600	10.78	1.798	1.624	—/—
0.710	15.57	1.917	1.659	—/—
0.760	—	—	—	5.4/1.67
Mean/SD	10.95/2.14	1.790/0.065	1.610/0.033	8.22/1.93

Table A6.13 - Compaction data for Test TSS2 (25/2-15/3/88).

Layer No (Material)	h (m)	Surcharge (%)	z (m)	w (%)	$\overline{IV}/\sigma_{IV_{n-1}}$	Compaction plant
VII(SS)	0.110	35.3	0	9.71	6.8/0.91	BS45Y(electric)
VI(SS)	0.100	33.3	0.110	10.09	7.3/0.74	BS45Y(electric)
V(SS)	0.110	26.7	0.210	9.01	7.2/0.50	BS45Y(electric)
IV(SS)	0.100	33.3	0.320	9.49	6.7/0.35	BS45Y(electric)+leg
III(SS)	0.110	26.7	0.420	9.20	6.8/0.35	BS45Y(electric)+leg
II(SS)	0.110	26.7	0.530	8.65	6.5/0.76	BS45Y(electric)+leg
I(SS)	0.150	25.0	0.640	9.92	5.9/0.84	BS45Y(electric)+leg
Mean/SD	0.113/0.017	29.57/4.21	—	9.44/0.52	6.74/0.46	—
Total depth	—	—	0.790	—	—	—

Table A6.14 - Excavation data for Test TSS2 (24/3/88).

z (m)	Density data			$\overline{IV}/\sigma_{IV_{n-1}}$
	w (%)	ρ (Mg/m^3)	ρ_d (Mg/m^3)	
0	4.45	1.766	1.691	8.0/0.71
0.110	6.70	1.878	1.760	—/—
0.210	7.14	1.891	1.765	14.4/2.18
0.320	7.84	1.842	1.708	—/—
0.390	—	—	—	11.1/0.96
0.420	7.39	1.861	1.733	—/—
0.530	8.86	1.841	1.691	—/—
0.550	—	—	—	9.9/0.65
0.640	12.10	1.953	1.742	—/—
Mean/SD	7.78/2.16	1.862/0.057	1.727/0.031	10.85/2.69

Table A6.15 - Compaction data for Test TSS3 (13–21/4/88).

Layer No (Material)	h (m)	Surcharge (%)	z (m)	w (%)	$\overline{IV}/\sigma_{IV_{n-1}}$	Compaction plant
VIII(SS)	0.110	21.4	0	9.98	4.1/0.42	BS45Y(electric)
VII(SS)	0.100	28.6	0.110	10.10	3.8/0.27	BS45Y(electric)
VI(SS)	0.100	28.6	0.210	11.81	4.2/0.27	BS45Y(electric)
V(SS)	0.100	28.6	0.310	10.84	4.4/0.42	BS45Y(electric)
IV(SS)	0.100	33.3	0.410	10.09	2.5/0.50	BS45Y(electric)+leg
III(SS)	0.110	26.7	0.510	10.72	2.6/0.65	BS45Y(electric)+leg
II(SS)	0.130	13.3	0.620	11.27	2.9/0.42	BS45Y(electric)+leg
I(SS)	0.160	20.0	0.750	9.48	3.4/0.42	BS45Y(electric)+leg
Mean/SD	0.114/0.021	25.06/6.39	—	10.54/0.77	3.49/0.75	—
Total depth	—	—	0.910	—	—	—

Table A6.16 - Excavation data for Test TSS3 (29/4-4/5/88).

z (m)	Density data			$\overline{IV}/\sigma_{IV_{n-1}}$
	w (%)	ρ (Mg/m^3)	ρ_d (Mg/m^3)	
0	4.20	1.652	1.585	4.6/0.25
0.110	5.62	1.721	1.629	—/—
0.160	—	—	—	7.7/0.27
0.210	6.75	1.631	1.528	—/—
0.310	7.78	1.772	1.644	—/—
0.330	—	—	—	7.1/0.89
0.410	7.62	1.702	1.581	—/—
0.510	8.22	1.743	1.611	5.4/0.82
0.620	8.44	1.671	1.541	—/—
0.660	—	—	—	4.3/0.45
0.750	11.56	1.849	1.678	—/—
Mean/SD	7.52/2.17	1.718/0.071	1.600/0.051	5.82/1.51

Table A6.17 - Compaction data for Test TSS4 (9/5/88).

Layer No (Material)	h (m)	Surcharge (%)	z (m)	w (%)	$\overline{IV}/\sigma_{IV_{n-1}}$	Compaction plant
III(SS)	0.260	25.7	0	11.36	5.5/0.35	BS45Y(electric)
II(SS)	0.250	28.6	0.260	9.90	5.3/0.45	BS45Y(electric)
I(SS)	0.290	21.6	0.510	8.17	4.9/0.74	BS45Y(electric)+leg
Mean/SD	0.267/0.021	25.30/3.52	—	9.81/1.60	5.23/0.31	—
Total depth	—	—	0.800	—	—	—

Table A6.20 - Excavation data for Test TSS5 (8-9/6/88).

z (m)	Density data			$\overline{IV}/\sigma_{IV_{n-1}}$
	w (%)	ρ (Mg/m^3)	ρ_d (Mg/m^3)	
0	6.12	1.852	1.746	7.8/0.29
0.100	7.73	1.868	1.734	—/ —
0.200	8.65	1.906	1.754	13.8/1.26
0.300	8.02	1.908	1.766	—/ —
0.380	—	—	—	11.2/0.91
0.410	8.12	1.871	1.730	—/ —
0.520	8.15	1.881	1.740	—/ —
0.570	—	—	—	8.9/1.14
0.630	9.12	1.924	1.764	—/ —
0.730	11.16	1.988	1.781	—/ —
0.750	—	—	—	7.3/1.40
Mean/SD	8.38/1.42	1.900/0.043	1.752/0.018	9.80/2.69

A6.3 Wet-mix macadam: Tests WMM1 to WMM6 and WMM10

Table A6.21 - Compaction data for Test WMM1 (13–15/9/88).

Layer No (Material)	h (m)	Surcharge (%)	z (m)	w (%)	$\overline{IV}/\sigma_{IV_{n-1}}$	Compaction plant	Density data ρ (Mg/m^3)	w (%)	ρ_d (Mg/m^3)
V(WMM)	0.120	20.0	0	5.46	19.5/1.94	BS45Y(electric)	2.202	4.54	2.106
IV(WMM)	0.120	20.0	0.120	5.45	22.4/0.75	BS45Y(electric)	2.041	3.87	1.965
III(WMM)	0.120	20.0	0.240	5.60	19.7/2.25	BS45Y(electric)+leg	2.098	4.34	2.011
II(WMM)	0.120	20.0	0.360	4.58	18.4/2.70	BS45Y(electric)+leg	2.046	4.86	1.951
I(WMM)	0.160	20.0	0.480	5.46	15.9/1.71	BS45Y(electric)+leg	2.043	4.65	1.952
Mean/SD	0.128/0.018	20.00/0.00	—	5.31/0.41	19.18/2.35	—	2.086/0.069	4.45/0.38	1.997/0.066
Subgrade	—	—	0.640	34.10	0.6/0.89	—	—	—	—

Table A6.22 - Compaction data for Test WMM2 (29–30/9/88).

Layer No (Material)	h (m)	Surcharge (%)	z (m)	w (%)	$\overline{IV}/\sigma_{IV_{n-1}}$	Compaction plant	Density data ρ (Mg/m^3)	w (%)	ρ_d (Mg/m^3)
V(WMM)	0.110	26.7	0	5.13	28.2/2.12	BS45Y(electric)	2.211	5.02	2.105
IV(WMM)	0.120	20.0	0.110	5.23	28.1/3.49	BS45Y(electric)	2.285	4.41	2.188
III(WMM)	0.110	21.4	0.230	4.56	24.0/1.22	BS45Y(electric)+leg	2.300	4.36	2.204
II(WMM)	0.120	20.0	0.340	4.96	23.4/1.64	BS45Y(electric)+leg	2.226	3.86	2.143
I(WMM)	0.150	25.0	0.460	5.12	20.6/2.33	BS45Y(electric)+leg	2.271	4.16	2.180
Mean/SD	0.122/0.016	22.62/3.06	—	5.00/0.26	24.86/3.27	—	2.258/0.039	4.36/0.43	2.164/0.040
Subgrade	—	—	0.610	—	1.9/1.56	—	—	—	—

Table A6.23 - Compaction data for Test WMM3 (7–14/10/88).

Layer No (Material)	h (m)	Surcharge (%)	z (m)	w (%)	$\overline{IV}/\sigma_{IV_{n-1}}$	Compaction plant	Density data ρ (Mg/m^3)	w (%)	ρ_d (Mg/m^3)
V(WMM)	0.130	13.3	0	3.91	12.7/1.26	BS45Y(electric)	1.897	4.65	1.813
IV(WMM)	0.130	13.3	0.130	4.96	12.7/0.76	BS45Y(electric)	1.858	3.58	1.794
III(WMM)	0.130	13.3	0.260	5.93	11.9/1.75	BS45Y(electric)+leg	1.888	4.54	1.806
II(WMM)	0.140	6.7	0.390	5.24	12.6/0.74	BS45Y(electric)+leg	2.206	4.74	2.106
I(WMM)	0.170	15.0	0.530	4.18	13.9/1.38	BS45Y(electric)+leg	2.012	4.23	1.930
Mean/SD	0.140/0.017	12.32/3.23	—	4.84/0.82	12.76/0.72	—	1.972/0.143	4.35/0.47	1.890/0.133
Subgrade	—	—	0.700	—	5.1/0.55	—	—	—	—

Table A6.24 - Compaction data for Test WMM4 (28–31/10/88).

Layer No (Material)	h (m)	Surcharge (%)	z (m)	w (%)	$\overline{IV}/\sigma_{IV_{n-1}}$	Compaction plant	Density data ρ (Mg/m^3)	w (%)	ρ_d (Mg/m^3)
II(WMM)	0.200	13.0	0	5.31	21.9/1.64	BS45Y(electric)+leg	2.029	3.98	1.951
I(WMM)	0.230	8.0	0.200	5.78	16.8/1.04	BS45Y(electric)+leg	2.109	4.60	2.016
Mean/SD	0.215/0.021	10.50/3.54	—	5.54/0.33	19.35/3.61	—	2.069/0.057	4.29/0.44	1.984/0.046
Subgrade	—	—	0.430	—	7.9/1.14	—	—	—	—

Table A6.25 - Compaction data for Test WMM5 (8–10/11/88).

Layer No (Material)	h (m)	Surcharge (%)	z (m)	w (%)	$\overline{IV}/\sigma_{IV_{n-1}}$	Compaction plant	Density data ρ (Mg/m^3)	w (%)	ρ_d (Mg/m^3)
V(WMM)	0.100	28.6	0	5.37	23.9/1.78	BS45Y(electric)	2.103	3.71	2.028
IV(WMM)	0.100	28.6	0.100	4.85	24.4/1.92	BS45Y(electric)	2.249	4.29	2.156
III(WMM)	0.110	21.4	0.200	4.80	23.3/1.44	BS45Y(electric)+leg	2.209	4.26	2.119
II(WMM)	0.130	13.3	0.310	4.80	22.4/1.82	BS45Y(electric)+leg	2.219	5.07	2.112
I(WMM)	0.170	15.0	0.440	5.36	22.4/2.43	BS45Y(electric)+leg	2.062	2.84	2.005
Mean/SD	0.122/0.030	21.38/7.25	—	5.04/0.30	23.28/0.89	—	2.168/0.081	4.03/0.83	2.084/0.064
Subgrade	—	—	0.610	—	—/—	—	—	—	—

Table A6.26 - Compaction data for Test WMM6 (25–28/11/88).

Layer No (Material)	h (m)	Surcharge (%)	z (m)	w (%)	$\overline{IV}/\sigma_{IV_{n-1}}$	Compaction plant	Density data ρ (Mg/m^3)	w (%)	ρ_d (Mg/m^3)
III(WMM)	0.200	16.7	0	6.32	23.3/0.98	BS45Y(electric)+leg	2.264	4.91	2.158
II(WMM)	0.190	20.8	0.200	5.73	20.9/1.34	BS45Y(electric)+leg	2.021	5.37	1.918
I(WMM)	0.180	25.0	0.390	6.38	21.2/1.21	BS45Y(electric)+leg	2.183	4.11	2.097
Mean/SD	0.190/0.010	20.83/4.15	—	6.14/0.36	21.80/1.31	—	2.156/0.124	4.80/0.64	2.058/0.125
Subgrade	—	—	0.570	—	5.1/0.82	—	—	—	—

Table A6.27 - Compaction data for Test WMM10 (18/1/89).

Layer No (Material)	h (m)	Surcharge (%)	z (m)	w (%)	$\overline{IV}/\sigma_{IV_{n-1}}$	Compaction plant	Density data ρ (Mg/m^3)	w (%)	ρ_d (Mg/m^3)
III(WMM)	0.200	9.1	0	0.55	13.2/2.20	BS45Y(electric)+leg	—	—	—
II(WMM)	0.180	14.3	0.200	—	13.7/2.64	BS45Y(electric)+leg	—	—	—
I(WMM)	0.200	9.1	0.380	—	10.2/1.44	BS45Y(electric)+leg	—	—	—
Mean/SD	0.193/0.012	10.83/3.00	—	0.55/0.00	12.37/1.89	—	—/—	—/—	—/—
Subgrade	—	—	0.580	—	—/—	—	—	—	—

A6.4 Wet-mix macadam and Sharp Sand: Tests WMM7 to WMM9

Table A6.28 - Compaction data for Test WMM7 (7-8/12/88).

Layer No (Material)	h (m)	Surcharge (%)	z (m)	w (%)	$\overline{IV}/\sigma_{IV_{n-1}}$	Compaction plant	Density data ρ (Mg/m^3)	w (%)	ρ_d (Mg/m^3)
IV(WMM)	0.190	20.8	0	4.20	21.9/1.02	BS45Y(electric)	2.046	4.27	1.962
III(WMM)	0.190	20.8	0.190	5.70	24.4/1.02	BS45Y(electric)	2.214	4.96	2.109
Mean/SD	0.190/0.000	20.80/0.00	—	4.95/1.06	23.15/1.77	—	2.130/0.119	4.62/0.49	2.036/0.104
II(SS)	0.150	16.7	0.380	7.54	6.1/0.42	BS45Y(electric)+leg	—	7.86	—
I(SS)	0.150	16.7	0.530	7.86	5.6/0.74	BS45Y(electric)+leg	—	9.12	—
Mean/SD	0.150/0.000	16.70/0.00	—	7.70/0.23	5.85/0.35	—	—/—	8.49/0.89	—/—
Subgrade	—	—	0.680	—	2.9/1.52	—	—	—	—

Table A6.29 - Compaction data for Test WMM8 (14/12/88).

Layer No (Material)	h (m)	Surcharge (%)	z (m)	w (%)	$\overline{IV}/\sigma_{IV_{n-1}}$	Compaction plant	Density data ρ (Mg/m^3)	w (%)	ρ_d (Mg/m^3)
IV(WMM)	0.190	20.8	0	5.02	21.5/2.06	BS45Y(electric)	2.116	3.70	2.040
III(WMM)	0.190	20.8	0.190	5.50	21.7/1.99	BS45Y(electric)	2.152	4.31	2.063
Mean/SD	0.190/0.000	20.80/0.00	—	5.23/0.34	21.60/0.14	—	2.134/0.026	4.00/0.43	2.052/0.016
II(SS)†	0.210	19.2	0.380	7.68	3.5/0.35	BS45Y(electric)+leg	1.957	7.01	1.831
I(SS)	0.090	18.2	0.590	7.76	3.6/0.55	BS45Y(electric)+leg	1.726	8.74	1.587
Mean/SD	0.150/0.085	18.70/0.71	—	7.72/0.06	3.55/0.07	—	1.842/0.163	7.78/1.22	1.709/0.172
Subgrade	—	—	0.680	—	2.9/1.60	—	—	—	—

†In this test a 125 mm external diameter (110 mm internal diameter) yellow plastic gas pipe (PLASTRON GAS PE.X 125MM SDR17.6 88254D) was placed after the compaction of Layer I ($N_p = 3$). The material for Layer II was then placed, on top of the pipe, and compacted ($N_p = 4$).

Table A6.30 - Compaction data for Test WMM9 (21/12/88).

Layer No (Material)	h (m)	Surcharge (%)	z (m)	w (%)	$\overline{IV}/\sigma_{IV_{n-1}}$	Compaction plant	Density data ρ (Mg/m^3)	w (%)	ρ_d (Mg/m^3)
IV(WMM)	0.190	20.8	0	3.89	23.8/0.57	BS45Y(electric)	2.122	3.42	2.052
III(WMM)	0.190	20.8	0.190	5.34	21.7/1.48	BS45Y(electric)	2.160	4.08	2.075
Mean/SD	0.190/0.000	20.80/0.00	—	4.62/1.03	22.75/1.48	—	2.141/0.027	3.75/0.47	2.064/0.016
II(SS)†	0.220	15.4	0.380	7.52	5.3/0.91	BS45Y(electric)+leg	1.713	7.18	1.598
I(SS)	0.090	18.2	0.600	7.12	3.7/0.45	BS45Y(electric)+leg	1.924	7.65	1.787
Mean/SD	0.155/0.092	16.80/1.98	—	7.32/0.28	4.50/1.13	—	1.819/0.149	7.42/0.33	1.692/0.134
Subgrade	—	—	0.690	—	4.8/0.76	—	—	—	—

†In this test a 118 mm external diameter (103 mm internal diameter) yellow plastic coated steel gas pipe (CHK 527290. REF 2000216/ESP/4.114.3.X. 6.02MM. HFS TUBE API 5L GRADE8: BSC GAS L.1.486 114.3) was placed after the compaction of Layer I ($N_p = 3$). The uncoated external diameter of the pipe was 114.3 mm. The material for Layer II was then placed, on top of the pipe, and compacted ($N_p = 4$).

A6.5 Case study data

Table A6.31 - Impact Value data for the Blaydon demonstration trench.

Number of passes per layer N_p	Impact Value $\overline{IV}/\sigma_{IV_{n-1}}$
1	11.1/1.43
2	12.2/1.44
4	14.9/1.82
7	18.8/3.17
14	20.8/1.48
20	22.6/1.92

Table A6.32 - Compaction data for tests at Salters Lane (Tests SL1 and SL2).

Layer No Test Code	h (m)	Surcharge (%)	z (m)	w (%)	$\overline{IV}/\sigma_{IV_{n-1}}$	Compaction plant
IV(SL1)	0.180	25.0	0	—	26.0/0.89	BS45Y(petrol)+leg
III(SL1)	0.200	20.0	0.180	—	27.7/1.44	BS45Y(petrol)+leg
II(SL1)	0.200	20.0	0.380	—	24.1/5.58	BS45Y(petrol)+leg
I(SL1)	0.180	25.0	0.580	—	25.2/5.75	BS45Y(petrol)+leg
Mean/SD	0.190/0.012	22.5/2.89	—	3.74/0.13	25.75/1.52	
Total depth	—	—	0.760	—	—	
I(SL2)	0.650	13.3	0	3.74/0.13	23.0/1.87	BS45Y(petrol)+leg
Total depth	—	—	0.650	—	—	

Table A6.33 - Additional (detailed) Impact Value data for Test SL1.

Layer I		Layer II		Layer III		Layer IV	
Depth from trench end (m)	*IV*	Depth from trench end (m)	*IV*	Depth from trench end (m)	*IV*	Depth from trench end (m)	*IV*
0.3	31.0	0.3	32.0	0.3	29.0	0.3	27.0
1.1	25.0	1.1	29.0	1.1	28.5	1.1	26.0
1.9	19.5	1.9	24.5	1.9	25.0	1.9	25.5
2.7	6.5	2.7	19.5	2.7	28.5	2.7	26.5
3.5	9.5	3.5	22.0	3.5	27.5	3.5	24.5
4.3	8.0	4.3	17.5	4.3	27.5	4.3	26.5

Table A6.34 - Compaction data for the case study at Acton Dean, Stanley, County Durham.

Layer No Material	h (m)	Surcharge (%)	z (m)	$\overline{IV}/\sigma_{IV_{n-1}}$	Compaction plant
III(SEM)	0.090	35.7	0	3.7/1.37	BS65Y(petrol)
II(SEM)	0.210	19.2	0.090	3.8/1.81	BS65Y(petrol)
I(SEM)	0.250	16.7	0.300	1.5/0.41	BS65Y(petrol)
Mean/SD	0.183/0.083	23.87/10.32	—	3.00/1.30	
Total depth	—	—	0.550	—	

APPENDIX 7

SURFACE WAVE VELOCITY MEASUREMENTS: DETAILED DATA

A7.1 Permian Sand: Tests TPS1 to TPS5

Table A7.1 - Surface wave velocity data for Test TPS1A (test completed 30/3/87).

Frequency f (Hz)	Correlation coefficient r	Intercept (π radians)	Slope (π radians/m)	Wavelength λ (m)	Depth z (m)	Velocity v_R (m/s)
500	0.999	0.0016	9.2748	0.216	0.108	107.8
450	0.998	−0.5400	9.0129	0.222	0.111	99.9
425	1.000	−0.4104	8.6044	0.232	0.116	98.6
400	0.998	1.5746	7.9859	0.250	0.125	100.0
375	0.999	−0.4803	7.3233	0.276	0.138	103.5
350	1.000	1.1212	7.0345	0.284	0.142	99.4
325	0.999	−0.6066	5.8162	0.344	0.172	111.8
306	0.999	0.2438	5.7144	0.350	0.175	107.1
275	0.999	−0.8861	4.5958	0.435	0.218	119.6
250	0.999	−0.8021	3.8455	0.520	0.260	130.0
225	1.000	−0.8639	2.9003	0.690	0.345	155.2
200	0.998	−1.0475	2.2813	0.877	0.438	175.4
195	1.000	−1.0957	2.1713	0.921	0.460	179.6
192.6	0.996	−1.1447	2.0176	0.991	0.496	190.9
190	0.998	−1.0630	1.9139	1.045	0.522	198.6
185	1.000	−1.0998	1.8616	1.074	0.537	198.7
180	0.999	−1.0127	1.7948	1.114	0.557	200.5
175	1.000	−0.9725	1.6696	1.198	0.599	209.6
170	0.998	−0.9604	1.5454	1.294	0.647	220.0

Table A7.2 - Surface wave velocity data for Test TPS1B (test completed 29/4/87).

Frequency f (Hz)	Correlation coefficient r	Intercept (π radians)	Slope (π radians/m)	Wavelength λ (m)	Depth z (m)	Velocity v_R (m/s)
500	0.996	0.3463	11.7479	0.170	0.085	85.1
450	0.999	-0.4037	10.4510	0.191	0.096	86.1
410	0.999	-0.4426	6.7033	0.298	0.149	107.4
340	0.998	-0.3725	6.5220	0.307	0.153	104.3
300	0.995	-0.5036	4.9646	0.403	0.201	120.9
244.5	0.997	-0.9982	3.7102	0.539	0.270	132.3
225	0.996	1.1361	2.7370	0.731	0.365	164.4
200	0.998	0.1858	1.8612	1.075	0.537	215.0
189.5	0.998	0.1686	1.5526	1.288	0.644	244.1
175	0.998	0.2379	1.7118	1.168	0.584	204.4
170	0.999	0.1168	1.6154	1.238	0.619	210.5
165	0.998	0.5941	1.1503	1.739	0.869	286.9
160	1.000	0.1072	1.0145	1.971	0.986	315.4

Table A7.3 - Surface wave velocity data for Test TPS1C (test completed 21/5/87).

Frequency f (Hz)	Correlation coefficient r	Intercept (π radians)	Slope (π radians/m)	Wavelength λ (m)	Depth z (m)	Velocity v_R (m/s)
1000	0.997	−0.4337	15.1418	0.132	0.066	132.0
700	1.000	0.2451	10.2137	0.196	0.098	137.2
550	0.990	0.2674	7.8227	0.256	0.128	140.8
500	0.996	0.1593	5.9773	0.335	0.167	167.5
410	0.996	0.4630	5.1476	0.388	0.194	159.1
350	0.999	0.1469	4.4082	0.454	0.227	158.9
250	0.998	0.0574	2.6744	0.748	0.374	187.0
225	1.000	0.0070	2.2699	0.881	0.441	198.2
200	0.998	0.0651	1.7836	1.121	0.561	224.2
180	0.999	−0.0238	1.6676	1.199	0.600	215.8
170	0.999	−0.0392	1.5548	1.286	0.643	218.6
160	0.998	0.0131	1.3929	1.436	0.718	229.8
150	1.000	−0.0186	1.3220	1.513	0.756	227.0
145	1.000	0.0050	1.2445	1.607	0.804	233.0
120	1.000	0.0184	1.0517	1.902	0.951	228.2

Table A7.4 - Surface wave velocity data for Test TPS1D (test completed 17/6/87).

Frequency f (Hz)	Correlation coefficient r	Intercept (π radians)	Slope (π radians/m)	Wavelength λ (m)	Depth z (m)	Velocity v_R (m/s)
1000	0.998	0.1396	13.1047	0.153	0.076	153.0
900	0.994	0.0109	12.1495	0.165	0.082	148.5
700	0.999	0.1343	9.2307	0.217	0.108	151.9
495	0.993	−0.0194	5.2951	0.378	0.189	187.1
400	0.999	0.0335	3.9392	0.508	0.254	203.2
350	0.998	−0.0237	3.5587	0.562	0.281	196.7
300	0.998	−0.0390	2.8000	0.714	0.357	214.2
275	0.998	0.0258	2.2903	0.873	0.437	240.1
250	0.999	0.0241	2.1009	0.952	0.476	238.0

Table A7.5 - Surface wave velocity data for Test TPS2A (test completed 10/7/87).

Frequency f (Hz)	Correlation coefficient r	Intercept (π radians)	Slope (π radians/m)	Wavelength λ (m)	Depth z (m)	Velocity v_R (m/s)
1000	1.000	−0.7657	14.6433	0.137	0.068	137.0
700	0.998	−0.3219	10.1861	0.196	0.098	137.2
450	0.998	−0.4247	5.5993	0.357	0.179	160.6
375	0.979	1.3586	3.7734	0.530	0.265	198.8
300	0.998	−0.2611	2.3888	0.837	0.419	251.1

Table A7.6 - Surface wave velocity data for Test TPS2B (test completed 25/7/87).

Frequency f (Hz)	Correlation coefficient r	Intercept (π radians)	Slope (π radians/m)	Wavelength λ (m)	Depth z (m)	Velocity v_R (m/s)
1000	0.999	0.1107	11.3307	0.177	0.088	177.0
700	0.996	−0.0808	7.9206	0.252	0.126	176.4
500	0.993	−0.5716	7.1976	0.278	0.139	139.0
450	0.996	−0.0001	5.4210	0.389	0.185	175.0
400	0.999	0.0901	4.4620	0.448	0.224	179.2
300	0.999	0.0131	3.8004	0.526	0.263	157.8
250	1.000	0.1666	2.8691	0.698	0.349	174.5
225	0.996	0.3769	2.1554	0.928	0.464	208.8
200	0.989	0.3486	2.0786	0.962	0.481	192.4
175	0.999	0.2210	1.6564	1.207	0.604	211.2
150	1.000	0.1956	1.2205	1.639	0.819	245.8

Table A7.7 - Surface wave velocity data for Test TPS2C (test completed 1/9/87).

Frequency f (Hz)	Correlation coefficient r	Intercept (π radians)	Slope (π radians/m)	Wavelength λ (m)	Depth z (m)	Velocity v_R (m/s)
1000	0.993	0.2019	10.5751	0.189	0.095	189.0
700	0.983	0.5351	8.9335	0.224	0.112	156.8
500	0.996	0.6379	7.0451	0.284	0.142	142.0
400	0.999	0.1595	5.0147	0.399	0.199	159.6
375	0.998	0.0365	4.6861	0.427	0.213	160.6
350	0.998	0.0859	4.0213	0.497	0.249	174.0
325	0.996	0.6672	2.8806	0.694	0.347	225.6
300	0.998	0.0571	2.8018	0.714	0.357	214.2
250	0.998	0.2719	2.1708	0.921	0.461	230.2

Table A7.8 - Surface wave velocity data for Test TPS3A (test completed 5/10/87).

Frequency f (Hz)	Correlation coefficient r	Intercept (π radians)	Slope (π radians/m)	Wavelength λ (m)	Depth z (m)	Velocity v_R (m/s)
400	0.994	−0.3965	9.7365	0.205	0.103	82.0
350	0.998	−0.0757	8.1731	0.245	0.122	85.8
300	0.996	−0.1053	6.6804	0.299	0.150	89.7
200	0.995	0.3500	4.3044	0.465	0.232	93.0
175	0.999	0.0067	2.6056	0.768	0.384	134.4
150	0.998	0.0289	1.5904	1.258	0.629	188.7

Table A7.9 - Surface wave velocity data for Test TPS3B (test completed 15/10/87).

Frequency f (Hz)	Correlation coefficient r	Intercept (π radians)	Slope (π radians/m)	Wavelength λ (m)	Depth z (m)	Velocity v_R (m/s)
500	0.995	0.0602	10.6195	0.188	0.094	94.0
300	0.996	0.2579	5.6306	0.335	0.178	106.5
250	0.987	0.2749	4.7586	0.420	0.210	105.0
200	0.993	0.4286	3.6772	0.544	0.272	108.8
175	0.999	0.0443	2.4455	0.818	0.409	143.2
150	1.000	0.0106	1.4969	1.336	0.668	200.4

Table A7.10 - Surface wave velocity data for Test TPS4 (test completed 8/12/87).

Frequency f (Hz)	Correlation coefficient r	Intercept (π radians)	Slope (π radians/m)	Wavelength λ (m)	Depth z (m)	Velocity v_R (m/s)
700	0.999	0.2386	16.8270	0.119	0.059	83.3
500	0.996	0.0320	9.9697	0.201	0.100	100.5
350	0.987	0.1190	6.5999	0.303	0.152	106.0
300	0.996	−0.1055	5.5601	0.360	0.180	108.0
250	0.997	0.0261	4.4758	0.447	0.223	111.8
200	0.996	−0.0499	3.3008	0.606	0.303	121.2
175	1.000	0.0221	2.1380	0.935	0.468	163.7
150	1.000	0.0168	1.6251	1.230	0.615	184.5
125	1.000	−0.0169	1.3236	1.511	0.756	188.9

Table A7.11 - Surface wave velocity data for Test TPS5A (test completed 9/1/88).

Frequency f (Hz)	Correlation coefficient r	Intercept (π radians)	Slope (π radians/m)	Wavelength λ (m)	Depth z (m)	Velocity v_R (m/s)
700	0.992	0.0435	8.7796	0.228	0.114	159.6
500	0.998	0.2480	5.3917	0.371	0.186	185.5
400	0.995	0.0824	4.4719	0.447	0.224	178.8
350	0.998	0.1497	2.9471	0.679	0.339	237.6
300	0.989	0.6020	2.7977	0.715	0.357	214.5

Table A7.12 - Surface wave velocity data for Test TPS5B (test completed 20/1/88).

Frequency f (Hz)	Correlation coefficient r	Intercept (π radians)	Slope (π radians/m)	Wavelength λ (m)	Depth z (m)	Velocity v_R (m/s)
400	0.994	0.7381	5.8924	0.339	0.170	135.6
350	0.991	0.4354	5.9163	0.338	0.169	118.3
300	0.996	0.0686	4.8587	0.412	0.206	123.6
250	1.000	0.0461	2.3684	0.844	0.422	211.0
200	1.000	−0.0272	2.0456	0.978	0.489	195.6
175	0.999	0.0654	1.5509	1.290	0.645	225.8
150	1.000	0.0021	1.2578	1.590	0.795	238.5

A7.2 Sharp Sand: Tests TSS1 to TSS5

Table A7.13 - Surface wave velocity data for Test TSS1A (test completed 12/2/88).

Frequency f (Hz)	Correlation coefficient r	Intercept (π radians)	Slope (π radians/m)	Wavelength λ (m)	Depth z (m)	Velocity v_R (m/s)
375	0.998	0.5042	8.4629	0.236	0.118	88.6
300	0.999	−0.2071	6.7494	0.296	0.148	88.9
250	0.999	0.0890	4.8646	0.411	0.206	102.8
225	0.999	0.1655	3.7501	0.533	0.267	120.0
200	0.999	−0.5891	2.6473	0.755	0.378	151.1
175	0.996	0.1909	2.0558	0.973	0.486	170.2

Table A7.14 - Surface wave velocity data for Test TSS1B (test completed 21/2/88).

Frequency f (Hz)	Correlation coefficient r	Intercept (π radians)	Slope (π radians/m)	Wavelength λ (m)	Depth z (m)	Velocity v_R (m/s)
350	0.994	0.2005	6.7640	0.296	0.148	103.5
325	0.999	−0.1237	7.1852	0.276	0.139	90.5
300	0.999	−0.1943	6.3244	0.316	0.158	94.9
275	0.998	0.6292	4.9490	0.404	0.202	111.1
250	0.997	0.3328	3.8643	0.518	0.259	129.4
225	0.996	−0.0426	2.9826	0.671	0.335	150.9
200	0.993	−0.0531	2.1095	0.948	0.474	189.6
175	0.998	0.0015	1.3972	1.431	0.716	250.5

Table A7.15 - Surface wave velocity data for Test TSS2A (test completed 14/3/88).

Frequency f (Hz)	Correlation coefficient r	Intercept (π radians)	Slope (π radians/m)	Wavelength λ (m)	Depth z (m)	Velocity v_R (m/s)
400	0.999	0.2704	6.9874	0.286	0.143	114.5
350	1.000	−0.1590	6.2951	0.318	0.159	111.2
300	0.999	0.0984	5.0047	0.400	0.200	119.9
250	0.999	0.0748	3.7303	0.536	0.268	134.0
225	1.000	0.0204	2.5784	0.776	0.389	174.5
200	1.000	0.0416	1.9371	1.032	0.516	206.5

Table A7.16 - Surface wave velocity data for Test TSS2B (test completed 23/3/88).

Frequency f (Hz)	Correlation coefficient r	Intercept (π radians)	Slope (π radians/m)	Wavelength λ (m)	Depth z (m)	Velocity v_R (m/s)
350	0.999	−0.2880	4.7548	0.421	0.210	147.4
325	0.998	−0.1800	4.1694	0.480	0.240	156.0
300	0.987	−0.1020	4.0296	0.496	0.248	148.8
275	0.994	0.3995	3.3116	0.604	0.302	166.1
250	0.992	0.3170	3.0630	0.653	0.326	163.2
200	0.999	−0.0431	2.1119	0.947	0.474	189.4
175	1.000	−0.0050	1.5068	1.327	0.664	232.2
165	0.999	−0.0129	1.3448	1.487	0.744	245.4

Table A7.17 - Surface wave velocity data for Test TSS3A (test completed 19/4/88).

Frequency f (Hz)	Correlation coefficient r	Intercept (π radians)	Slope (π radians/m)	Wavelength λ (m)	Depth z (m)	Velocity v_R (m/s)
400	0.998	0.1206	8.5680	0.233	0.117	93.2
350	0.999	0.1674	6.9981	0.286	0.143	100.1
275	0.997	0.1889	5.4488	0.367	0.184	100.9
250	0.996	0.2200	4.6168	0.433	0.217	108.2
225	1.000	0.0671	3.8813	0.515	0.258	115.9
200	0.992	0.3230	2.9254	0.684	0.342	136.8
175	0.993	0.2483	2.3764	0.842	0.421	147.4

Table A7.18 - Surface wave velocity data for Test TSS3B (test completed 24/4/88).

Frequency f (Hz)	Correlation coefficient r	Intercept (π radians)	Slope (π radians/m)	Wavelength λ (m)	Depth z (m)	Velocity v_R (m/s)
300	0.995	−0.5347	5.8262	0.343	0.172	102.9
275	0.999	−0.2744	5.0155	0.399	0.199	109.7
250	0.995	−0.0620	4.2468	0.471	0.236	117.8
225	0.998	0.0181	3.7441	0.534	0.267	120.2
200	0.998	0.2018	2.7118	0.738	0.369	147.6
175	0.999	−0.0526	1.7974	1.113	0.556	194.8
150	0.999	−0.0384	1.4358	1.393	0.696	209.0
125	1.000	0.0037	1.1049	1.810	0.905	226.2

Table A7.19 - Surface wave velocity data for Test TSS4 (test completed 16/5/88).

Frequency f (Hz)	Correlation coefficient r	Intercept (π radians)	Slope (π radians/m)	Wavelength λ (m)	Depth z (m)	Velocity v_R (m/s)
325	0.999	−0.1223	6.6532	0.301	0.150	97.8
300	0.983	−0.0783	5.4622	0.366	0.183	109.8
275	0.999	0.1038	5.1266	0.390	0.195	107.2
250	0.999	−0.0226	4.3389	0.461	0.230	115.2
225	0.995	−0.1477	3.5901	0.557	0.279	125.3
200	0.998	−0.0279	2.6086	0.767	0.383	153.4
175	1.000	−0.0019	1.7348	1.153	0.576	201.8
150	1.000	−0.0334	1.4398	1.389	0.695	208.4

Table A7.20 - Surface wave velocity data for Test TSS5A (test completed 27/5/88).

Frequency f (Hz)	Correlation coefficient r	Intercept (π radians)	Slope (π radians/m)	Wavelength λ (m)	Depth z (m)	Velocity v_R (m/s)
275	0.995	−0.2202	5.2102	0.384	0.192	105.6
250	0.995	−0.2787	4.6052	0.434	0.217	108.5
225	0.998	0.3204	3.6253	0.552	0.276	124.2
200	0.998	0.9546	2.9961	0.668	0.334	133.6
195	0.998	0.0142	2.3017	0.869	0.434	169.5
190	0.998	−0.0525	2.2088	0.906	0.453	172.4

Table A7.21 - Surface wave velocity data for Test TSS5B (test completed 7/6/88).

Frequency f (Hz)	Correlation coefficient r	Intercept (π radians)	Slope (π radians/m)	Wavelength λ (m)	Depth z (m)	Velocity v_R (m/s)
325	0.998	0.0050	5.6684	0.353	0.176	114.7
300	0.999	−0.1509	5.2261	0.383	0.191	114.9
275	0.984	0.1120	3.9308	0.509	0.254	140.0
250	0.999	0.0282	3.8028	0.526	0.263	131.5
225	0.999	−0.1082	3.4237	0.584	0.292	131.4
200	1.000	−0.0227	2.0369	0.982	0.491	196.4
175	1.000	−0.0028	1.4398	1.389	0.695	243.1
150	1.000	−0.0092	1.1426	1.750	0.875	262.5

A7.3 Wet-mix macadam: Tests WMM1 to WMM6 and Test WMM10

Table A7.22 - Surface wave velocity data for Test WMM1 (test completed 16/9/88).

Frequency f (Hz)	Correlation coefficient r	Intercept (π radians)	Slope (π radians/m)	Wavelength λ (m)	Depth z (m)	Velocity v_R (m/s)
500	0.999	−0.0492	7.5002	0.267	0.133	133.5
450	0.999	−0.2784	6.9203	0.289	0.145	130.5
400	0.999	−0.2458	5.9334	0.337	0.169	134.8
350	0.997	−0.3846	4.9857	0.401	0.201	140.4
275	0.995	−0.0890	3.9548	0.506	0.253	139.2
250	0.999	−0.0191	3.4001	0.588	0.294	147.0
225	0.996	0.1220	2.9894	0.669	0.335	150.5
200	0.999	0.0828	2.5406	0.787	0.394	157.4
175	0.989	0.1827	2.0227	0.989	0.494	173.1
150	0.996	0.2617	1.7601	1.136	0.568	170.4
125	1.000	0.0222	1.4826	1.349	0.674	168.6
100	0.986	−0.2349	1.8501	1.081	0.541	108.1
75	0.998	−0.0605	1.1970	1.671	0.836	125.3
50	1.000	0.0075	0.7691	2.600	1.300	130.0

Table A7.23 - Surface wave velocity data for Test WMM2 (test completed 4/10/88).

Frequency f (Hz)	Correlation coefficient r	Intercept (π radians)	Slope (π radians/m)	Wavelength λ (m)	Depth z (m)	Velocity v_R (m/s)
500	1.000	−0.0922	3.3789	0.592	0.296	296.0
450	0.999	0.1771	2.9021	0.689	0.345	310.0
400	1.000	0.0065	2.4880	0.804	0.402	321.6
350	0.999	0.0647	2.0934	0.955	0.478	334.2
300	0.955	−0.2221	2.4187	0.827	0.413	248.1
275	1.000	−0.0363	2.4858	0.805	0.402	221.4
250	0.998	−0.1616	2.8578	0.700	0.350	175.0
225	0.998	−0.0284	2.3020	0.869	0.434	195.5
200	0.997	−0.0847	2.3409	0.854	0.427	170.8
175	1.000	−0.1387	1.8171	1.101	0.550	192.7
150	0.999	−0.1074	1.8074	1.107	0.553	166.0
125	1.000	0.0071	1.5715	1.273	0.636	159.1
100	1.000	0.0212	1.4463	1.383	0.691	138.3
75	0.999	−0.0308	1.1266	1.775	0.888	133.1
50	0.998	0.0255	0.7574	2.641	1.320	132.0

Table A7.24 - Surface wave velocity data for Test WMM3 (test completed 17/10/88).

Frequency f (Hz)	Correlation coefficient r	Intercept (π radians)	Slope (π radians/m)	Wavelength λ (m)	Depth z (m)	Velocity v_R (m/s)
350	0.993	−0.3475	6.0879	0.329	0.164	115.2
300	0.996	−0.3369	5.1022	0.392	0.196	117.6
275	0.999	−0.0346	4.3369	0.461	0.231	126.8
250	0.998	−0.0133	4.0133	0.498	0.249	124.5
225	0.999	0.0793	3.4466	0.580	0.290	130.5
200	0.999	0.1289	3.0646	0.653	0.326	130.6
175	0.999	0.0668	2.6496	0.755	0.377	132.1
150	0.999	0.0456	2.2448	0.891	0.446	133.6
125	0.999	−0.0508	1.9059	1.049	0.525	131.1
100	1.000	0.0014	1.4265	1.402	0.701	140.2
75	1.000	0.0232	1.1080	1.805	0.903	135.4

Table A7.25 - Surface wave velocity data for Test WMM4 (test completed 2/11/88).

Frequency f (Hz)	Correlation coefficient r	Intercept (π radians)	Slope (π radians/m)	Wavelength λ (m)	Depth z (m)	Velocity v_R (m/s)
500	0.997	−0.3475	6.9521	0.288	0.144	144.0
450	1.000	−0.3475	5.5687	0.359	0.180	161.6
400	0.998	−0.3475	4.9679	0.403	0.201	161.2
300	1.000	−0.3369	3.5951	0.556	0.278	166.8
275	1.000	0.0346	3.2901	0.608	0.304	167.2
250	0.998	−0.0133	3.1912	0.627	0.313	156.8
225	0.999	−0.0793	2.7672	0.723	0.361	162.7
200	1.000	0.1289	2.3239	0.861	0.430	172.2
175	0.998	0.0668	2.0134	0.993	0.497	173.8
150	1.000	−0.0456	1.6794	1.191	0.596	178.6
125	1.000	−0.0508	1.9425	1.030	0.515	128.8
100	1.000	−0.0014	1.5997	1.250	0.625	125.0

Table A7.26 - Surface wave velocity data for Test WMM5 (test completed 11/11/88).

Frequency f (Hz)	Correlation coefficient r	Intercept (π radians)	Slope (π radians/m)	Wavelength λ (m)	Depth z (m)	Velocity v_R (m/s)
350	0.999	−0.4612	4.0618	0.492	0.246	172.2
300	0.999	−0.2839	3.3315	0.600	0.300	180.0
275	0.998	−0.2152	3.1204	0.641	0.320	176.3
250	0.999	−0.0393	2.7576	0.752	0.363	181.2
225	0.999	−0.0665	2.5433	0.786	0.393	176.8
200	0.999	−0.0630	2.3090	0.866	0.433	173.2
175	1.000	−0.0623	2.0057	0.997	0.499	174.5
150	0.999	−0.0617	1.7039	1.174	0.587	176.1
125	0.999	−0.0552	1.4672	1.363	0.682	170.4
100	1.000	−0.0102	1.0523	1.901	0.950	190.1
75	0.996	−0.0496	1.2012	1.665	0.832	124.9
50	1.000	0.0013	0.7605	2.630	1.315	131.5

Table A7.27 - Surface wave velocity data for Test WMM6 (test completed 6/12/88).

Frequency f (Hz)	Correlation coefficient r	Intercept (π radians)	Slope (π radians/m)	Wavelength λ (m)	Depth z (m)	Velocity v_R (m/s)
450	1.000	0.0434	5.3726	0.372	0.186	167.4
400	0.998	0.2442	4.7111	0.425	0.212	170.0
300	0.999	−0.0152	3.1972	0.626	0.313	187.8
275	0.999	0.0639	2.8354	0.705	0.353	193.9
250	0.998	0.1692	2.6262	0.762	0.381	190.5
225	0.999	0.1213	2.1641	0.924	0.462	207.9
200	0.999	−0.1211	2.6409	0.757	0.379	151.4
175	1.000	0.1296	2.2810	0.877	0.438	153.5
150	0.997	−0.0574	2.4434	0.819	0.409	122.8
125	0.998	0.0821	1.7291	1.157	0.578	126.2
100	1.000	−0.0013	1.3405	1.492	0.746	149.2
75	1.000	−0.0018	1.0695	1.870	0.935	140.2
50	1.000	−0.0029	0.8695	2.300	1.150	115.2

Table A7.28 - Surface wave velocity data for Test WMM10 (test completed 20/1/89).

Frequency f (Hz)	Correlation coefficient r	Intercept (π radians)	Slope (π radians/m)	Wavelength λ (m)	Depth z (m)	Velocity v_R (m/s)
300	0.998	0.8792	3.3200	0.602	0.301	180.6
275	0.997	0.3342	3.0926	0.647	0.323	177.9
250	0.995	0.2023	3.2000	0.625	0.312	156.2
225	0.998	0.2484	3.0496	0.656	0.328	147.6
200	0.998	−0.0511	2.9128	0.687	0.343	137.4
175	1.000	0.0405	2.0037	0.998	0.499	174.6
150	1.000	0.0207	1.9443	1.029	0.514	154.4
125	1.000	0.0000	1.8182	1.100	0.550	137.5
100	1.000	0.0007	1.3066	1.531	0.765	153.1
75	1.000	0.0077	0.9010	2.220	1.110	166.5

A7.4 Wet-mix macadam and Sharp Sand: Tests WMM7 to WMM9

Table A7.29 - Surface wave velocity data for Test WMM7 (test completed 12/12/88).

Frequency f (Hz)	Correlation coefficient r	Intercept (π radians)	Slope (π radians/m)	Wavelength λ (m)	Depth z (m)	Velocity v_R (m/s)
450	0.997	0.2800	7.3918	0.271	0.135	122.0
400	0.996	0.0785	4.0793	0.490	0.245	196.0
350	0.998	0.1681	3.8436	0.520	0.260	182.0
300	0.996	0.2302	3.3217	0.602	0.301	180.6
275	1.000	0.0345	3.1692	0.631	0.316	173.5
250	1.000	0.0542	2.8266	0.708	0.354	177.0
225	1.000	0.0203	2.6057	0.768	0.384	172.8
200	0.997	−0.0052	2.6324	0.760	0.380	152.0
175	0.999	0.1794	2.0878	0.958	0.479	167.6
150	0.998	0.1219	1.7921	1.116	0.558	167.4
125	1.000	0.0761	1.6861	1.186	0.593	148.2
100	1.000	0.0102	1.4121	1.416	0.708	141.6
75	1.000	0.1058	1.1976	1.670	0.835	125.2
50	0.997	−0.0036	0.8126	2.461	1.231	123.0

Table A7.30 - Surface wave velocity data for Test WMM8 (test completed 15/12/88).

Frequency f (Hz)	Correlation coefficient r	Intercept (π radians)	Slope (π radians/m)	Wavelength λ (m)	Depth z (m)	Velocity v_R (m/s)
450	0.999	−0.0817	8.4546	0.237	0.118	106.6
400	0.999	0.0690	6.7773	0.295	0.148	118.0
350	0.999	0.1974	5.0809	0.394	0.197	137.9
300	0.998	0.1932	3.7260	0.537	0.268	161.1
275	0.997	0.2104	3.8702	0.517	0.258	142.2
250	0.999	0.1148	3.5493	0.564	0.282	141.0
225	0.999	0.1090	3.2983	0.606	0.303	136.4
200	0.999	0.1112	3.0106	0.664	0.332	132.8
175	0.998	0.1927	2.4954	0.802	0.401	140.4
150	0.997	0.1970	2.0411	0.980	0.490	147.0
125	0.999	−0.0827	2.0204	0.990	0.495	123.8
100	0.999	0.0671	1.5148	1.320	0.660	132.0
75	1.000	−0.0178	1.2265	1.631	0.815	122.3
50	1.000	−0.0127	0.9896	2.021	1.011	101.0

Table A7.31 - Surface wave velocity data for Test WMM9 (test completed 21/12/88).

Frequency f (Hz)	Correlation coefficient r	Intercept (π radians)	Slope (π radians/m)	Wavelength λ (m)	Depth z (m)	Velocity v_R (m/s)
500	0.999	−0.0247	6.9324	0.288	0.144	144.0
450	1.000	−0.1078	6.0756	0.329	0.165	148.0
400	0.999	−0.0797	5.3445	0.374	0.187	149.6
350	0.996	−0.1165	4.4028	0.454	0.227	158.9
300	0.985	−0.0135	3.6342	0.550	0.255	165.0
275	0.998	−0.2682	3.3352	0.600	0.300	165.0
250	0.999	−0.1963	2.9792	0.671	0.336	167.8
225	1.000	−0.0678	2.7218	0.735	0.367	165.4
200	1.000	0.0109	2.4924	0.802	0.401	160.4
175	0.999	0.0628	1.9937	1.003	0.502	175.5
150	0.999	0.0629	1.5957	1.253	0.627	188.0
125	0.998	0.0707	1.2920	1.548	0.774	193.5

A7.5 Case study data

Table A7.32 - Surface wave velocity data for the SEAS service trench: Test NSSEAS (test completed 30/8/87).

Frequency f (Hz)	Correlation coefficient r	Intercept (π radians)	Slope (π radians/m)	Wavelength λ (m)	Depth z (m)	Velocity v_R (m/s)
700	0.999	−0.0101	6.8323	0.293	0.146	205.1
500	1.000	−0.1288	5.0080	0.399	0.200	199.5
400	0.997	0.1450	4.1230	0.485	0.243	194.0
375	0.997	0.1736	3.7250	0.537	0.268	201.4
250	0.997	0.0539	2.6864	0.744	0.372	186.0
200	0.996	−0.1648	2.2551	0.887	0.443	177.4
175	0.996	0.0358	1.9649	1.018	0.509	178.2
150	0.994	0.1558	1.6134	1.240	0.620	186.0
125	0.996	0.1097	1.3810	1.448	0.724	181.0
100	0.965	0.0970	1.1205	1.785	0.892	178.5
75	0.998	0.0413	0.8555	2.338	1.169	175.4

Table A7.33 - Surface wave velocity data for Test SL1 (test completed 13/6/89).

Frequency f (Hz)	Correlation coefficient r	Intercept (π radians)	Slope (π radians/m)	Wavelength λ (m)	Depth z (m)	Velocity v_R (m/s)
400	0.998	0.1907	4.8788	0.410	0.205	164.0
350	0.998	−0.0036	4.2792	0.467	0.234	163.4
300	0.998	−0.0032	2.8720	0.696	0.348	208.8
275	0.998	0.2145	2.4682	0.810	0.405	222.8
250	0.999	0.1550	2.3933	0.836	0.418	209.0
225	1.000	0.0660	2.3025	0.869	0.434	195.5
175	0.999	−0.0595	1.8225	1.100	0.549	192.5
150	0.999	−0.0142	1.2997	1.539	0.769	230.8

Table A7.34 - Surface wave velocity data for Test SL2 (test completed 14/6/89).

Frequency f (Hz)	Correlation coefficient r	Intercept (π radians)	Slope (π radians/m)	Wavelength λ (m)	Depth z (m)	Velocity v_R (m/s)
400	0.980	0.4335	7.9060	0.253	0.126	101.2
350	0.995	0.1577	6.6951	0.299	0.149	104.6
300	0.998	−0.1294	5.8415	0.342	0.171	102.6
275	0.999	−0.0760	4.8000	0.417	0.208	114.7
250	1.000	−0.0027	4.1870	0.478	0.239	119.5
225	1.000	−0.0525	3.5912	0.557	0.278	125.3
200	0.998	0.0930	2.9716	0.673	0.337	134.6
175	1.000	0.0006	2.5832	0.774	0.387	135.4
150	1.000	−0.0111	1.9062	1.049	0.525	157.4
125	1.000	−0.0014	1.4958	1.337	0.669	167.1

Table A7.35 - Surface wave velocity data for the case study at Acton Dean, Stanley, County Durham (test completed 8/8/89).

Frequency f (Hz)	Correlation coefficient r	Intercept (π radians)	Slope (π radians/m)	Wavelength λ (m)	Depth z (m)	Velocity v_R (m/s)
350	0.999	0.0442	4.1044	0.487	0.244	170.4
300	0.999	−0.5084	3.7216	0.537	0.269	161.1
275	1.000	−0.0450	2.8641	0.698	0.349	192.0
250	0.998	−0.4202	2.8675	0.698	0.349	174.5
225	1.000	−0.5627	2.3574	0.848	0.424	190.8
200	1.000	−0.4298	1.9946	1.003	0.501	200.6
175	0.995	−0.2420	2.1180	0.944	0.472	165.2
150	1.000	−0.1198	1.6388	1.220	0.610	183.0
125	0.999	−0.3950	1.3767	1.435	0.726	181.6

APPENDIX 8

SURFACE WAVE ATTENUATION MEASUREMENTS: DETAILED DATA

A8.1 Permiam Sand: Tests TPS3 to TPS5

Table A8.1 - Attenuation data for Permian Sand (Test TPS3) at frequencies of 300 *and* 500 Hz.

Distance from oscillator x (m)	Peak to peak particle displacement w (10^{-9} m)	
	Frequency = 500 Hz	Frequency = 300 Hz
0.190	386.33	2602.54
0.350	598.58	2731.06
0.500	422.19	2795.32
0.650	252.45	1365.53
0.800	387.49	1486.02
0.950	242.90	1124.55
1.100	226.00	1751.09
1.250	277.32	755.06
1.400	94.27	931.77
1.550	115.38	1718.96
1.700	6.94	747.02
1.850	49.74	345.40
2.000	74.03	128.52
2.150	131.86	979.67
2.300	91.38	658.67
2.450	50.32	763.09
2.600	52.92	538.18
2.750	90.22	369.50
2.900	58.70	538.18

Table A8.2 - Attenuation data for Permian Sand (Test TPS4) at frequencies of 300 *and* 500 Hz.

Distance from oscillator x (m)	Peak to peak particle displacement w (10^{-9} m)	
	Frequency = 500 Hz	Frequency = 300 Hz
0.190	101.79	1241.02
0.350	9.25	779.15
0.500	53.21	642.60
0.650	54.94	743.01
0.800	36.44	409.66
0.950	61.88	530.15
1.100	6.07	293.19
1.250	18.51	334.96
1.400	25.74	99.60
1.550	2.60	353.43
1.700	19.09	345.40
1.850	4.63	180.73
2.000	4.05	44.98
2.150	0.87	126.11
2.300	6.36	116.47
2.450	5.78	337.37
2.600	3.47	293.19
2.750	7.81	159.04
2.900	7.52	258.65

Table A8.3 - Attenuation data for Permian Sand (Test TPS5) at frequencies of 300 *and* 500 Hz.

Distance from oscillator x (m)	Peak to peak particle displacement w (10^{-9} m)	
	Frequency = 500 Hz	Frequency = 300 Hz
0.190	15.04	1010.49
0.350	56.10	578.34
0.500	19.09	1590.44
0.650	52.34	867.51
0.800	17.93	452.23
0.950	8.68	898.84
1.100	18.22	204.03
1.250	11.57	349.42
1.400	8.39	187.16
1.550	15.04	522.11
1.700	9.54	327.73
1.850	12.15	217.68
2.000	11.57	502.03
2.150	8.68	169.49
2.300	15.90	64.26
2.450	6.94	322.91
2.600	4.05	148.60
2.750	4.63	638.59
2.900	7.52	66.67

A8.2 Sharp Sand: Tests TSS1 to TSS5

Table A8.4 - Attenuation data for Sharp Sand (Test TSS1) at frequencies of 300 *and* 500 Hz.

Distance from oscillator x (m)	Peak to peak particle displacement w (10^{-9} m)	
	Frequency = 500 Hz	Frequency = 300 Hz
0.190	52.05	522.11
0.350	66.51	992.37
0.500	59.28	1108.49
0.650	32.68	811.28
0.800	33.54	381.54
0.950	17.35	422.51
1.100	32.39	506.05
1.250	38.75	538.18
1.400	24.58	264.27
1.550	22.27	424.92
1.700	15.90	530.15
1.850	11.57	166.27
2.000	11.57	207.24
2.150	15.04	332.55
2.300	7.23	305.24
2.450	10.70	281.14
2.600	8.68	120.49
2.750	12.15	354.23
2.900	11.86	81.13

Table A8.5 - Attenuation data for Sharp Sand (Test TSS2) at frequencies of 300 *and* 500 Hz.

Distance from oscillator x (m)	Peak to peak particle displacement w (10^{-9} m)	
	Frequency = 500 Hz	Frequency = 300 Hz
0.190	53.21	528.54
0.350	36.44	795.22
0.500	30.65	893.22
0.650	15.90	430.54
0.800	16.77	560.67
0.950	22.84	302.02
1.100	9.25	560.67
1.250	19.95	599.23
1.400	13.30	526.13
1.550	4.05	196.80
1.700	9.54	430.54
1.850	27.76	536.57
2.000	9.25	175.11
2.150	3.47	478.74
2.300	9.25	369.50
2.450	16.48	89.96
2.600	7.81	200.81
2.750	4.05	120.49
2.900	10.41	168.68

Table A8.6 - Attenuation data for Sharp Sand (Test TSS3) at frequencies of 300 *and* 500 Hz.

Distance from oscillator x (m)	Peak to peak particle displacement w (10^{-9} m)	
	Frequency = 500 Hz	Frequency = 300 Hz
0.190	31.52	642.60
0.350	40.48	737.39
0.500	12.15	880.36
0.650	44.82	988.00
0.800	29.78	198.40
0.950	30.07	345.40
1.100	33.83	409.66
1.250	32.39	184.75
1.400	15.90	528.54
1.550	16.77	231.34
1.700	15.62	273.11
1.850	2.89	453.84
2.000	12.43	72.29
2.150	16.19	192.78
2.300	6.07	212.86
2.450	11.86	60.24
2.600	3.76	580.75
2.750	15.90	193.58
2.900	16.19	152.62

Table A8.7 - Attenuation data for Sharp Sand (Test TSS4) at frequencies of 300 *and* 500 Hz.

Distance from oscillator x (m)	Peak to peak particle displacement w (10^{-9} m)	
	Frequency = 500 Hz	Frequency = 300 Hz
0.190	64.77	1036.20
0.350	64.77	423.31
0.500	30.07	687.58
0.650	20.24	875.54
0.800	27.47	583.16
0.950	24.29	565.49
1.100	14.46	396.81
1.250	14.46	397.61
1.400	13.30	277.12
1.550	13.59	353.43
1.700	8.10	494.00
1.850	11.86	409.66
2.000	25.16	192.78
2.150	14.46	262.66
2.300	12.43	194.39
2.450	14.75	337.37
2.600	9.25	56.23
2.750	18.80	162.26
2.900	8.10	32.13

Table A8.8 - Attenuation data for Sharp Sand (Test TSS5) at frequencies of 300 *and* 500 Hz.

Distance from oscillator x (m)	Peak to peak particle displacement w (10^{-9} m)	
	Frequency = 500 Hz	Frequency = 300 Hz
0.190	32.39	1220.94
0.350	17.64	634.57
0.500	76.63	1096.44
0.650	31.52	730.96
0.800	30.65	569.51
0.950	15.62	610.47
1.100	25.45	389.58
1.250	23.13	562.28
1.400	22.84	502.03
1.550	32.10	403.23
1.700	26.03	457.85
1.850	32.97	442.59
2.000	28.92	449.82
2.150	20.53	469.10
2.300	19.37	478.74
2.450	13.30	333.35
2.600	8.96	212.86
2.750	1.45	289.17
2.900	1.45	212.86

A8.3 Wet-mix macadam: Tests WMM1 to WMM6 and WMM10

Table A8.9 - Attenuation data for Wet-mix macadam (Test WMM1) at frequencies of 300 *and* 500 Hz.

Distance from oscillator x (m)	Peak to peak particle displacement w (10^{-9} m)	
	Frequency = 500 Hz	Frequency = 300 Hz
0.190	101.21	1220.94
0.350	254.47	923.74
0.500	34.70	369.50
0.650	72.29	208.85
0.800	72.29	120.49
0.950	43.38	321.30
1.100	31.81	200.81
1.250	11.57	200.81
1.400	24.58	224.91
1.550	30.36	160.65
1.700	11.57	184.75
1.850	8.68	88.36
2.000	7.23	16.07
2.150	2.89	56.23
2.300	1.74	72.29
2.450	5.78	96.39
2.600	2.31	48.20

Table A8.10 - Attenuation data for Wet-mix macadam (Test WMM2) at frequencies of 300 *and* 500 Hz.

Distance from oscillator x (m)	Peak to peak particle displacement w (10^{-9} m)	
	Frequency = 500 Hz	Frequency = 300 Hz
0.190	167.14	1542.24
0.350	69.40	772.73
0.500	44.53	257.04
0.650	20.24	192.78
0.800	15.62	172.70
0.950	30.65	249.01
1.100	8.96	160.65
1.250	8.10	200.81
1.400	1.74	61.85
1.550	5.78	49.80
1.700	2.89	72.29
1.850	1.74	134.14
2.000	0.29	93.98
2.150	0.29	100.41
2.300	1.16	68.28
2.450	0.87	48.20
2.600	0.58	20.08

Table A8.11 - Attenuation data for Wet-mix macadam (Test WMM3) at frequencies of 300 *and* 500 Hz.

Distance from oscillator x (m)	Peak to peak particle displacement w (10^{-9} m)	
	Frequency = 500 Hz	Frequency = 300 Hz
0.190	52.63	1045.83
0.350	46.27	449.82
0.500	4.63	232.94
0.650	20.53	101.42
0.800	7.23	151.01
0.950	2.89	443.40
1.100	9.25	321.30
1.250	2.02	248.20
1.400	2.02	170.29
1.550	0.58	100.41
1.700	0.58	81.13
1.850	0.58	52.21
2.000	0.29	19.28
2.150	0.58	32.93
2.300	0.29	8.84
2.450	0.58	6.43
2.600	0.58	4.82

Table A8.12 - Attenuation data for Wet-mix macadam (Test WMM4) at frequencies of 300 *and* 500 Hz.

Distance from oscillator x (m)	Peak to peak particle displacement w (10^{-9} m)	
	Frequency = 500 Hz	Frequency = 300 Hz
0.190	58.12	1208.09
0.350	196.35	862.69
0.500	76.05	944.62
0.650	44.53	236.96
0.800	22.56	365.48
0.950	32.97	393.59
1.100	39.91	271.50
1.250	15.90	239.37
1.400	7.52	447.41
1.550	21.40	256.24
1.700	18.80	187.16
1.850	3.47	139.77
2.000	4.92	134.14
2.150	1.45	77.92
2.300	2.89	72.29
2.450	0.29	113.26
2.600	1.16	78.72

Table A8.13 - Attenuation data for Wet-mix macadam (Test WMM5) at frequencies of 300 *and* 500 Hz.

Distance from oscillator x (m)	Peak to peak particle displacement w (10^{-9} m)	
	Frequency = 500 Hz	Frequency = 300 Hz
0.190	124.05	706.86
0.350	54.94	468.89
0.500	26.89	187.16
0.650	9.25	281.14
0.800	25.45	192.78
0.950	12.15	149.40
1.100	9.54	120.49
1.250	7.23	29.72
1.400	3.18	176.72
1.550	8.68	128.52
1.700	2.31	106.03
1.850	2.89	232.94
2.000	1.45	83.54
2.150	2.31	39.36
2.300	2.89	20.88
2.450	0.58	25.70
2.600	0.29	16.07

Table A8.14 - Attenuation data for Wet-mix macadam (Test WMM6) at frequencies of 300 *and* 500 Hz.

Distance from oscillator x (m)	Peak to peak particle displacement w (10^{-9} m)	
	Frequency = 500 Hz	Frequency = 300 Hz
0.190	88.49	1104.47
0.350	42.80	578.34
0.500	16.77	405.64
0.650	27.47	341.38
0.800	14.46	120.49
0.950	5.78	348.61
1.100	5.78	322.91
1.250	3.18	249.01
1.400	3.47	208.85
1.550	5.78	140.57
1.700	2.31	30.52
1.850	1.16	84.34
2.000	0.87	136.55
2.150	2.02	114.06
2.300	1.16	36.15
2.450	0.29	12.05
2.600	1.16	80.33

Table A8.15 - Attenuation data for Wet-mix macadam (Test WMM10) at frequencies of 300 *and* 500 Hz.

Distance from oscillator x (m)	Peak to peak particle displacement w (10^{-9} m)	
	Frequency = 500 Hz	Frequency = 300 Hz
0.190	39.91	570.31
0.350	10.99	155.83
0.500	22.27	98.80
0.650	8.39	114.06
0.800	2.02	84.34
0.950	3.18	45.79
1.100	14.17	33.74
1.250	2.60	14.46
1.400	2.89	18.48
1.550	1.74	11.25
1.700	2.02	16.87
1.850	2.89	13.66
2.000	0.58	11.25
2.150	0.58	6.43
2.300	0.29	4.82
2.450	0.87	6.43
2.600	0.58	5.62

A8.4 Wet-mix macadam and Sharp Sand: Tests WMM7 to WMM9

Table A8.16 - Attenuation data for Wet-mix macadam (Test WMM7) at frequencies of 300 *and* 500 Hz.

Distance from oscillator x (m)	Peak to peak particle displacement w (10^{-9} m)	
	Frequency = 500 Hz	Frequency = 300 Hz
0.190	111.33	1343.04
0.350	50.60	881.97
0.500	15.90	142.18
0.650	20.24	420.90
0.800	50.60	173.50
0.950	16.77	145.39
1.100	9.54	164.67
1.250	8.10	160.65
1.400	2.31	178.32
1.550	1.74	115.67
1.700	1.16	49.80
1.850	3.47	47.39
2.000	4.34	128.52
2.150	3.47	77.11
2.300	0.58	91.57
2.450	0.29	31.33
2.600	0.29	40.97

Table A8.17 - Attenuation data for Wet-mix macadam (Test WMM8) at frequencies of 300 *and* 500 Hz.

Distance from oscillator x (m)	Peak to peak particle displacement w (10^{-9} m)	
	Frequency = 500 Hz	Frequency = 300 Hz
0.190	52.05	610.47
0.350	10.99	361.46
0.500	26.02	498.02
0.650	36.44	473.92
0.800	10.12	224.91
0.950	11.57	241.78
1.100	5.20	361.46
1.250	1.16	337.37
1.400	2.60	289.17
1.550	1.74	115.67
1.700	0.87	104.42
1.850	0.87	83.54
2.000	0.29	32.13
2.150	0.87	32.93
2.300	1.16	48.20
2.450	0.29	17.67
2.600	0.29	14.46

Table A8.18 - Attenuation data for Wet-mix macadam (Test WMM9) at frequencies of 300 *and* 500 Hz.

Distance from oscillator x (m)	Peak to peak particle displacement w (10^{-9} m)	
	Frequency = 500 Hz	Frequency = 300 Hz
0.190	96.00	489.98
0.350	56.39	851.45
0.500	13.59	594.41
0.650	38.46	369.50
0.800	17.93	319.69
0.950	21.69	417.69
1.100	14.75	628.14
1.250	12.72	677.94
1.400	2.60	417.69
1.550	11.86	210.45
1.700	1.16	110.85
1.850	4.63	154.22
2.000	0.58	121.29
2.150	0.29	81.13
2.300	0.58	120.49
2.450	0.29	80.33
2.600	0.29	138.16

APPENDIX 9

PARTICLE DISPLACEMENT AT DEPTH MEASUREMENTS: DETAILED DATA FOR PERMIAN SAND TESTS TPS2 AND TPS3

Table A9.1 - Particle displacement at depth data for Test TPS2B at 450 Hz (λ = 0.388 m).

Depth z (m)	z/λ	Acceleration $\ddot{w}$ (g)	Displacement w ($\times 10^{-8}$ m)	w_z / $w_{z=0}$
0	0	0.076	9.326	1.000
0.060	0.155	0.050	6.136	0.658
0.180	0.464	0.033	4.050	0.434
0.280	0.722	0.020	2.454	0.263
0.400	1.031	0.007	0.859	0.092

Table A9.2 - Particle displacement at depth data for Test TPS3B at 300 Hz (λ = 0.280 m).

Depth z (m)	z/λ	Acceleration $\ddot{w}$ (g)	Displacement w ($\times 10^{-8}$ m)	w_z / $w_{z=0}$
0	0	0.201	55.496	1.000
0.070	0.250	0.145	40.035	0.721
0.170	0.607	0.150	41.415	0.746
0.270	0.964	0.120	33.132	0.597
0.370	1.321	0.068	18.775	0.338
0.470	1.679	0.015	4.142	0.075
0.610	2.179	0.027	7.455	0.134
0.720	2.571	0.056	15.462	0.279

Table A9.3 - Particle displacement at depth data for Test TPS3B at 150 Hz (λ = 0.810 m).

Depth z (m)	z/λ	Acceleration $\ddot{w}$ (g)	Displacement w ($\times 10^{-8}$ m)	w_z / $w_{z=0}$
0	0	0.285	314.75	1.000
0.070	0.086	0.244	269.47	0.856
0.170	0.210	0.211	233.03	0.740
0.270	0.333	0.162	178.91	0.568
0.370	0.457	0.132	145.78	0.463
0.470	0.580	0.113	124.80	0.397
0.610	0.753	0.113	124.80	0.397
0.720	0.889	0.103	113.75	0.361